The copyright of this thesis vests in the author. No quotation from it or information derived from it is to be published without full acknowledgement of the source. The thesis is to be used for private study or non-commercial research purposes only.

Published by the University of Cape Town (UCT) in terms of the non-exclusive license granted to UCT by the author.

University of Cape Town

16

Retention of Fermentation Biomass for Extended L-Lysine Fermentations

Thomas Potgieter

Thesis Presented for the Degree of
DOCTOR OF PHILOSOPHY
In the Department of Chemical Engineering
UNIVERSITY OF CAPE TOWN
March 2002

Bioprocess Research Group
Department of Chemical Engineering
University of Cape Town
Rondebosch
Cape Town
South Africa

University of Cape Town

To my father:

TIJ Potgieter

Retention of Fermentation Biomass for Extended L-Lysine Fermentations

Thomas Potgieter

Chemical Engineering Department, University of Cape Town

March 2002

Synopsis

In this thesis it was demonstrated that the current L-lysine fermentation technology can be enhanced by continuously withdrawing spent medium while recycling the biomass in the culture suspension to the bioreactor. The biomass in the reactor outlet stream is separated from the spent medium using cross-flow filtration. The objective of this thesis was to study, understand, model and optimise the performance of the L-Lysine fermentation with biomass retention using cross flow filtration.

Following a review of the factors affecting cross-flow filtration and modelling approaches available, the most suitable filtration flux estimation equation was selected. The impact of filtration on microbial performance was assessed and approaches to modelling the lysine fermentation overviewed, leading to the selection of an appropriate model. Thereafter a rigorous approach to the optimisation of the biomass recycling system for lysine production was conducted and experimentally validated.

A generic form of Hermia's blocking laws was found to be well suited to the description of the initial stages of cross-flow microfiltration. A constant term (the pseudo steady state flux) has been included to provide a semi-empirical correlation of the cross flow filtration flux. The pseudo steady state flux is based on Darcy's law and a combination of the shear induced diffusion and surface transport models. The presented model adequately described the experimental data.

The qualitative effects of the increased hydrodynamic shear stress experienced in the filtration recycling loop on the growth, metabolism and morphology of *Corynebacterium glutamicum* cells have been investigated. It was found that the cell volume increases under increased hydrodynamic shear although increased shear does not alter the cell shape. The apparent specific growth rate, the yield of biomass from threonine and the specific lysine productivity of the cells exposed to hydrodynamic shear in the filtration system decreases at increased hydrodynamic shear. Using a bioreaction network (BRN) model, it was postulated that increased hydrodynamic shear causes a shift in cellular metabolism from oxidative phosphorylation to substrate level phosphorylation and glycolysis. Furthermore it

is postulated that increased hydrodynamic shear causes an increase in the flux of carbon towards the cell wall to either repair or strengthen the cell wall.

Fermentation models were developed based on mass and volume balances coupled to either a set of empirical correlations of the cellular metabolism developed from experimental data or a bioreaction network. The impact of filtration-associated hydrodynamic stress on the cellular metabolism was modelled based on a linear relationship between the metabolic impact and the average energy dissipation rate per unit cell mass. A critical average energy dissipation rate was identified below which no impact on the fermentation performance relative to conventional batch fermentations was detected.

The fed batch fermentation with biomass recycling using cross flow filtration was optimised using an equation-based dynamic simulation package (gPROMS). The predicted optimum represented a 26% reduction in variable cost of production compared to the conventional fed-batch fermentation technology (R14.50/kg vs. R10.65/kg). The predicted optimum was physically achievable and the experimental results obtained when a fermentation was conducted at the optimal conditions corresponded well with that predicted by the proposed model.

The model parameters were re-established for the industrial lysine producing strain (AEC94). At the optimum conditions the model predicted a 12% improvement in variable cost of production while a 14% improvement was realised from experimental data.

Retention of Fermentation Biomass for Extended L-Lysine Fermentations

L-lysine is an essential amino acid in monogastric animal nutrition. The bulk of L-lysine production throughout the world depends on the direct fermentation of carbohydrates by auxotrophic and regulatory mutants of *Corynebacteria* and *Brevibacteria* species. Amino acid fermentations are intensive in raw material usage. Hence the process yield and productivity are critical measures of performance and economic viability (Kiss & Stephanopoulos, 1991).

The overall fermentation performance have been improved by using fed-batch strategies whereby the cells are maintained in the L-Lysine overproduction metabolic state by continuously feeding the substrate to the reactor (Hadj *et al.* 1988; Rutkov, 1984, Hirao *et al.* 1989; Kiss & Stephanopoulus, 1991). The fermentation is stopped when the bioreactor reaches the maximum volume. A large portion of the production cost contributes to establishing a viable biomass population. To maximise the volumetric productivity and reduce production costs, feed and bleed strategies are often employed. However, since L-lysine is predominantly a secondary metabolite, the maximum yield of L-lysine from carbohydrates is achieved at very low growth rates. This implies that viable biomass, still capable of L-lysine production is lost in bleed. The reactor volume as well as the inability of the process to retain the microbial population limits the productivity and conversion of carbohydrates to L-Lysine.

In this thesis it was demonstrated that the L-Lysine fermentation performance can be enhanced by continuously withdrawing spent medium while recycling the biomass in the culture suspension to the bioreactor. The biomass in the reactor outlet stream was separated from the spent medium using cross-flow filtration. The objective of this thesis was to study, understand, model and optimise the performance of the L-Lysine fermentation with biomass retention using cross flow filtration.

Following a review of the factors affecting cross-flow filtration and modelling approaches available, the most suitable filtration flux estimation equation was selected. The impact of filtration on microbial performance was assessed and approaches to modelling the lysine fermentation overviewed, leading to the selection of an appropriate model. Thereafter a rigorous approach to the optimisation of the biomass recycling system for lysine production was conducted and experimentally validated.

Two L-Lysine producing strains (ATCC 21253 and AEC 94), two ultrafiltration (150 kD and 300 kD) and two microfiltration (0.22 μm & 0.45 μm) tubular ceramic membranes were used. Fermentations were conducted on 10-litre scale using both a chemically defined and an industrial fermentation media composition.

Following an overview of lysine production by *Corynebacterium glutamicum and Brevibacterium* sp., the factors that influence the cross flow filtration flux of suspensions of *C. glutamicum* were investigated. It was found that the pseudo-steady state flux decreases as the complexity of the solvent increases. The flux increases with increasing trans-membrane pressure drop (ΔP) until a critical value is reached beyond which an increase in the pressure drop does not result in a proportional increase in the flux. An increase in flux was also reported on increasing cross-flow velocity.

Membrane fouling can be divided into internal and external fouling phenomena. The hydraulic resistance that results from pore plugging (internal fouling) was found to depend on the membrane pore size and the fraction of near sized particles. External fouling is mainly due to the build-up of a fouling cake layer on the membrane surface. The hydraulic resistance caused by the cake layer increases with increasing complexity of the feed suspension and increasing trans-membrane pressure drop. A decrease in the cake resistance was found with increasing cross-flow velocity that could be attributed to a decrease in cake weight.

The understanding of the fouling phenomena encountered during cross-flow filtration of *C. glutamicum* suspensions served as a basis for the development of a semi-empirical model describing the system's behaviour. A generic form of Hermia's (1982) blocking laws (Equation 3-90) was found to be well suited to the description of the initial stages of cross-flow microfiltration. A constant term (the pseudo steady state flux) was included to provide a semi-empirical correlation of the cross flow filtration flux (Equation 3-91). The pseudo steady state flux is based on Darcy's law (Equation 3-92) and a combination of the shear induced diffusion and surface transport models. Darcy's law divides the total hydraulic resistance into the membrane resistance (or the impact of the membrane on the filtration flux), the pore plugging resistance (or the interaction between the feed suspension and the membrane) and the cake resistance (or the impact of the feed suspension on the filtration flux). The model presented adequately described the experimental data. Bayesian analysis was used to illustrate that the "hybrid model" developed exhibited the highest probability of predicting the cross flow filtration flux of suspensions of *C. glutamicum* when compared to some previously developed models.

Although these mathematical models can provide useful descriptions of the decline in flux observed during membrane filtration, it is not currently possible to obtain, *a priori*, estimates of the key parameters in these equations. In addition, these models do not provide a quantitative basis for understanding the effects of solution properties or membrane characteristics on the flux decline. These models also provide little insight into the actual physical and chemical mechanisms by which the filtration flux declines during the filtration process.

The qualitative effects of the increased hydrodynamic shear stress on the growth, metabolism and morphology of *Corynebacterium glutamicum* cells have been investigated. It was found that the cell volume increases under increased hydrodynamic shear although increased shear does not alter the cell shape. It was also found that the effects of

hydrodynamic shear stress on the cell's morphology were reduced at increased biomass concentrations.

The apparent specific growth rate, the yield of biomass from threonine and the specific lysine productivity of the cells exposed to hydrodynamic shear in the filtration system decreases at increased hydrodynamic shear. The reduced specific lysine productivity and the increased glucose uptake rate of the cells exposed to increased shear in the filtration loop implies a reduced cumulative yield of lysine from glucose. These effects were less pronounced at the higher biomass concentrations (25 g/l DCW).

The fermentation data provided convenient sets of extracellular flux to elucidate the impact of increased hydrodynamic stress caused by biomass recycling on the biochemistry of L-lysine synthesis through intracellular flux analysis (BRN). The excess ATP (ATP produced above the consumption level accounted for by the BRN) for cells exposed to increased hydrodynamic stress due to cell recycle was reduced relative to that found in the "conventional batch" process. The reduction in ATP formation is postulated to be a result of a shift in cellular metabolism from oxidative phosphorylation to substrate level phosphorylation and glycolysis.

The flux of carbon through PPP was reduced at increased hydrodynamic shear due to a reduction in the requirement for NADPH of the cells exposed to hydrodynamic shear in the filtration module. Exposure to hydrodynamic shear in the membrane unit did not have an impact on the split of carbon at the PEP or OaA nodes. At the Pyr node the flux of carbon to lysine and the flux of Pyr to AcCoA were reduced at increased hydrodynamic shear, while the flux of pyruvate into other amino acids increased. Thus, under increased shear conditions the total flux of carbon toward the TCA cycle decreased.

From the qualitative analysis presented it was postulated that increased hydrodynamic shear causes an increase in the flux of carbon towards the cell wall to either repair or strengthen the cell wall.

The effect of exposing the cells to increased hydrodynamic shear in the cross flow filtration system was quantified in Chapter 6. Two fermentation models were developed to predict the fermentation performance as a function of the controllable variables. The models consist of a mass and volume balance coupled to two sets of metabolic equations. In the first approach, the cellular metabolism is modelled by approximating the cell as a "black box" and using empirical correlations developed from experimental data to depict the cells' response to changes in the extracellular environment. In the alternative approach the metabolism is modelled based on a bioreaction network of the intracellular central carbon distribution. Some critical nodes within this network were identified and the carbon split ratios around these nodes were fixed or modelled based on extracellular conditions. From this information the cells response to changes in the extracellular environment could be predicted.

The impact of filtration associated hydrodynamic stress on the cellular metabolism was modelled based on a linear relationship between the metabolic impact and the average energy dissipation rate per unit cell mass. A critical average energy dissipation rate was identified below which no impact on the fermentation performance relative to conventional batch fermentations were detected. Above this critical energy dissipation rate, a reduction in growth rate and specific productivity and an increase in the yield of biomass from threonine were modelled as linear functions of the turbulent energy dissipation divided by the biomass concentration.

The Bayesian approach was used to illustrate that the model using empirical correlations to estimate the metabolic behaviour of the cell exhibits a higher probability of predicting the system's performance. The model with the empirically estimated metabolism was used to optimise the entire system's performance.

The fed batch fermentation with biomass recycling using cross flow filtration for the production of L-lysine was optimised using an equation-based dynamic simulation package (gPROMS). The variable cost of production (VCOP), defined as the cost to produce a kilogram of lysine, was used as the objective function for the optimisation process. The predicted optimum represented a 26% reduction in variable cost compared to the conventional fed-batch fermentation technology (R14.50/kg vs. R10.65/kg).

The predicted optimum was physically achievable and the experimental results obtained when a fermentation was conducted at the optimal conditions corresponded with that predicted by the proposed model (Figure 7-4 to 7-9). This indicated that the fermentation model as proposed was sufficiently accurate, with enough resolution for optimisation of the fermentation process.

The VCOP of the lysine fermentation can be minimised by maximising the biomass in the bioreactor and retaining all the biomass produced in the bioreactor, while feeding glucose at a rate close to the maximum glucose uptake rate. The specific sugar feed rate represents a trade-off between increased yield at lower feed rates and increased productivity at higher feed rates. None of the auxotrophic amino acids are to be included in the feed during the fed-batch operation for minimal VCOP.

The permeate flow rate from the cross flow filtration system matched the total feed rate, thus maintaining a zero or minimal bleed rate. Furthermore, it was evident that at optimal conditions the fermentation is to be conducted at residual sugars concentration approaching zero. Since spent medium is continuously withdrawn from the bioreactor, a residual sugar concentration of zero maximises the yield of lysine from the sugar fed. The duration of the fermentation process is limited by the strain's ability to sustain its performance and not by the residence time of the biomass in the bioreactor as found in the feed and bleed system.

The model parameters were re-established for the industrial lysine-producing strain (AEC94). The model was then used to optimise the fermentation performance of a

conventional fed-batch process with a feed and bleed strategy as well as that of a fed-batch process with biomass recycling using cross flow filtration. The model predicted a 12% improvement in VCOP while a 14% improvement was realised from experimental data.

The linear approximation used to model the impact of filtration on fermentation performance is limited to application of hydrodynamic shear experienced in cross flow filtration systems and cannot be transferred to other hydrodynamic stress impacts. The model parameters are empirical in nature and must therefore be redeveloped for each strain. Although this is a tedious process, the methodology allows for process optimisation that produces a physically realisable optimum. Biomass recycling using cross flow filtration improves the variable cost of production of the lysine fermentation process by at least 12% compared to the current fed-batch technology.

Acknowledgements

This study could not have been achieved without the support of my wife, my parents, friends, colleagues at AECI Bioproducts, and the Bioprocess Engineering group at UCT.

Firstly, I would like to thank my wife, Liana, for her everlasting love and support. Her smile and the many-many cups of coffee (281.2 litres thereof) dragged me through the long nights. Her incredible patients allowed my working hours to extent well into hours that should have been spent on housekeeping.

I would like to thank my parents, for their unconditional support and encouragement. Apparently, as an infant I used to spent my nights on my father's lap while he was studying. Although, today I do not fit onto his lap any more, his encouragement and critical review is still of great value. He opened the book of science for me, so that I can appreciate the wonder of God's creation.

I would like to express my sincere thanks to my supervisors, Dr. Sue Harrison and Dr. Chris Swartz for their guidance, training and encouragement over the past four years.

The original idea for the thesis originated from Johan van Walsem from AECI Bioproducts, who not only arranged the financial support for work but also contributed significantly to the content thereof. I am most grateful to Elizma Parry for allowing me to use the laboratory at AECI Bioproducts for a large portion of the experimental work. Special thanks to Gerrit van de Pypekamp for his support and mentoring during the past three years at AECI Bioproducts. His endless efforts to convert a graduate into a process engineer allowed this work to be focussed and applicable in the real world.

I have received endless wishes of good luck, support, help with the garden and sympathy from my friends in Amanzimtoti. I would especially like to thank Andrew Robinson and Jo-Ann Moon, from the Bioprocess research group at UCT, for their moral support, their peer review, the many trips to and from the airport as well as the accompanying pizzas and cokes.

Last, but by no means least I would like to thank our heavenly Father, for the privilege to study and report on the grandeur of his creation.

Nomenclature

1. ABBREVIATIONS

Ac	Acetate
AcCoA	Acetyl-coenzyme A
AEC	S-(2-aminoethyl)-L-cysteine
aKG	α-Ketogluteraldehyde
Ala	Alanine
Asp	Aspartate
ATCC	American Type culture collection
ATP	Adenosine tri-phosphate
BSA	Bovine Serum Albumin
CCRD	Central Composite Rotational Experimental Design
DCW	Dry Cell Weight
E4P	Erytrose-4-phosphate
EMP	Embden Meyerhof Parnas Pathway (Glycolysis)
FAD	Flavin adenine dinucleotide
Fru6P	Fructose-6-phosphate
G3P	3-Phosphoglycerate
GaP	Glyceraldehyde-3-phosphate
Glc6P	Glucose-6-phosphate
Glum	Glutamine
Glut	Glutamate
IsoCit	Isocitrate
Lac	Lactate
LysE	Extracellular lysine
LysI	Entracellular lysine
Mal	Malate
MF	Microfiltration
NAD	Nicotinamide adenine dinucleotide
NF	Nanofiltration
NMR	Nuclear magnetic resonance

OaA	Oxaloacetate
PEP	Phosphoenolpyruvate
PPC	Phosphoenolpyruvate carboxylase
Pyr	Pyruvate
Rib5P	Ribose-5-phosphate
Ribu5P	Ribulose-5-phosphate
RO	Reverse Osmosis
Sed7P	Sedoheptulose-7-phosphate
SEM	Scanning electron microscope
Suc	Succinate
SucCoa	Succinyl-coenzyme A
TCA	Tri-carbocylic acid cycle
Trehal	Trehalose
t-RNA	Transfer Ribonucleic acid
UF	Ultrafiltration
Val	Valine

2. SYMBOLS

a	[m]	Particle radius
α		Empirical factor for electricity usage in membrane unit
A	[m^2]	Membrane area
A	[-]	m × n matrix of stoichiometric coefficient
A'	[-]	Constant in Eq. 5-12
A_7	[-]	Function of impeller geometry
a_{block}	[m^{-3}]	Number of pores that are blocked per unit filtrate volume
$a_{deposit}$	[m^{-3}]	Fraction of particles convected to the membrane that actually adds to the deposit
Air	[m^3/s]	Air flow rate
a_{media}	[mmol l^{-1} h^{-1}]	Constant in mass transfer correlation
a_n	[-]	Coefficients in Eq. 3-1
A_o	[m^2]	Clean membrane area
a_{pore}	[m^3/m3]	Pore volume of foulant that deposits on the interior pore

		walls per unit of filtrate volume
b	[-]	Dimensionless distance from the wall. Eq. 3-49
b'	[m^2 N^{-1}]	Constant in Eq. 3-19
b_e	[m]	Short ellipsoidal semi-axis
Bleed	[l/h]	Bleed rate
BDF		Backwards difference formula
b_{sf}	[h^{-1}]	Constant in solids flux model
c_1 to c_3		Constants in the specific lysine productivity equation Eq. 6-30
C_{AS}	[g/l]	Ammonium sulphate concentration in the AS feed stream
C_b	[g/l]	Concentration of foulant species in the feed
C_c	[g/l]	Solids concentration of foulant species in the cake layer
c_e	[m]	Long ellipsoidal semi-axis
C_e	[g/l]	Permeate concentration
C_F	[g/l]	Fouling layer concentration
C_{Gluc}	[g/l]	Glucose concentration in the glucose feed stream
C_n	[-]	Hydrodynamic correction factor to Stokes law
C_{O2}	[mMol/l]	Dissolved oxygen concentration
$C_{O2,sat}$	[mMol/l]	Saturation dissolved oxygen concentration
C_t	[-]	Correction factor to Stokes law
$C_{T,Mg}$	[mol/l]	Total Mg^{2+} ion concentration
$C_{T,NH4}$	[mol/l]	Total NH_4^+ ion concentration
$C_{T,PO4}$	[mol/l]	Total PO_4^{3-} ion concentration
C_{Thr}	[g/l]	Threonine concentration in the threonine feed stream
C_w	[g/l]	Concentration of foulant in the boundary layer above the fouling layer
d	[m]	Turbulent eddy size
D	[cm^2 s^{-1}]	Diffusivity
D_{mem}	[m]	Membrane cross sectional diameter
D		Vector of specific design variables
D_{Bo}	[cm^2 s^{-1}]	Brownian diffusivity
d_{eq}	[m]	Equivalent sphere diameter
d_h	[m]	Height of protrusion in surface transport model

d_{hyd}	[cm]	Hydraulic diameter of the channel
D_{imp}	[m]	Impeller diameter
DO	[%]	Percentage of the saturation dissolved oxygen concentration
DP	[Pa]	Pipe pressure drop
d_{pipe}	[m]	Pipe diameter
DP_v	[Pa]	Pressure drop across needle valve
d_s	[m]	Characteristic separation between the bulk protein and the deposit at which the process are just able to overcome the repulsive interactions
D_s	[cm^2/s]	Shear induced diffusivity
e	[m^2/s^3]	Energy dissipation rate per unit mass
$\bar{e}$	[m^2/s^3]	Rate of energy dissipation due to the mean velocity gradients
e_{ave}	[m^2/s^3]	Average energy dissipated in the bioreactor system including the recycle loop
$E_{c,50}$	[J/m^3]	Total viscous energy dissipation per unit volume at which 50% of the original biological activity are maintained
E_k	[m^2/s^2]	Total kinetic energy per unit mass
E_L	[m^2/s^2]	Energy dissipated in the laminar sublayer
e_{mem}	[m^2/s^3]	Average energy dissipation rate in the membrane module
e_{react}	[m^2/s^3]	Average energy dissipated in the bioreactor
e_t	[m^2/s^3]	Turbulent energy dissipation rate
E_T	[m^3/s]	Total energy dissipation rate
e_v	[m^2/s^3]	Viscous energy dissipation rate
e_{valve}	[m^2/s^3]	Average energy dissipation rate in the needle valve
e_w	[m^2/s^3]	Maximum energy dissipation rate
f	[kg / mol s]	Frictional coefficient
F	[-]	Dimensionless Perrin shape factor
f_{app}	[-]	Apparent friction factor
F_{AS}	[l/h]	AS feed rate
F_{Gluc}	[l/h]	Glucose feed rate
F_n	[N]	Normal drag force

f_{PPP}	[m/m]	Fraction of glucose that enters the PPP
f_{sph}	[kg/mol s]	Frictional coefficient for sphere
f		System vector continuously differentiable in all arguments
F_t	[N]	Tangential drag force
F_{Thr}	[l/h]	Threonine feed rate
G	[s^2/m]	Defined in Eq. 2-14
G_{ij}	[-]	Combined growth effect of limiting substrates
Gluc	[g/l]	Glucose concentration in the bioreactor
$Gluc_o$	[g/l]	Initial glucose concentration in the bioreactor
H	[mmol/l/Pa]	Henry's Constant
H'	[-]	Shape function for ellipsoid
H_o	[m]	Half height of split or radius of tubular conduit
I	[-]	Constant in X_{cr} correlation
i	[#]	Number of absorbed layers inside membrane pores
J	[m/s]	Permate flux
$j(r_p)$	[m/s]	Local flow rate through pore of size r
J'	[m/s]	Modified flux as defined in Eq. 3-16
J_1'/J_2'	[-]	Ratio of clean membrane and fouled membrane modified fluxes
J_l	[m/s]	Permeate flux after cleaning
J_o	[m/s]	Flux through membrane at t=0
J_o	[m/s]	Clean membrane flux
$J_{o,w}$	[m/s]	Pure water flux
J_{ss}	[m/s]	Pseudo steady state flux
J_{ss}	[m/s]	Pseudo steady state flux
$J_{ss,\ iso}$	[m/s]	Pseudo steady state flux at the iso-electric point
k		Stages of the optimization problem
K'	[-]	Constant in Eq. 2-11 and 3-9
k'_la	[mmol/h/kPa]	Volumetric mass transfer coefficient
k_1	[g/l]	Saturation constant in growth rate equation
k_2	[g/l]	Saturation constant in growth rate equation
k_B	[J / mol K]	Boltzman constant

k_{BL}	[-]	Constant in Eq. 2-13
k_c	[-]	Constant in Eq 3-82
K_c	[-]	Adjustable parameters in Eq. 3-89
k_{clean}	[h^{-1}]	Membrane cleaning constant
k_d	[h^{-1}]	Death constant
$k_{decline}$	[h^{-1}]	Flux decline constant
k_F	[-]	Constant in Eq. 3-56
k_{fl}	[-]	Constant in Eq. 4-24
k_i	[-]	Constant in Eq. 4-21
K_i	[-]	Adjustable parameters in Eq. 3-89
k_{IL}	[-]	Inertial lift proportionality constant
k_l	[cm s^{-1}]	Local mass transfer coefficient (Eq. 3-34)
k_l'a	[mmol h^{-1} kPa^{-1}]	Volumetric mass transfer coefficient
$k_l a$	[h^{-1}]	Liquid interface mass transfer coefficient
K_{lam}	[-]	Empirical constant in Eq. 3-51
k_{Lys}	[-]	Constant in Eq 6-30
k_m	[g/l]	Saturation constant in Monod kinetics (Eq. 5-35)
K_m	[mMol]	Michalis Menten kinetics constant
km_1	[g/l]	Saturation constant for cell growth under threonine limited conditions
k_p	[m^{-1}]	Permeability of the porous medium
k_{pd}	[-]	Constant in Eq. 3-81
k_{pd}	[-]	Constant in Eq. 3-81
K_{rate}	[s^{-1}]	Empirical constant describing the rate of cake formation
K_s	[-]	Adjustable parameters in Eq. 3-89
k_{si}	[-]	Constant in Eq. 4-22
k_{sp}	[-]	Constant in Eq. 4-25
k_t	[m]	Constant in Eq. 3-99
k_{thick}	[m]	Thickness of an absorbed multilayer inside a pore
K_{tur}	[-]	Empirical constant in Eq. 3-52
k_{vl}	[-]	Constant in Eq. 4-23
$\#_n$	[-]	Constant in Eq. 3-87
L_{mem}	[m]	Membrane length

LMH	[l m^{-2} h^{-1}]	Filtration flux
LMOPP	[kPa]	Log mean oxygen partial pressure
$LMOPP_o$	[kPa]	Log mean oxygen partial pressure at the time when the DO probe was calibrated
l_n	[-]	Exponent in Eq. 3-87
L		Scalar function – Lagrangian loss function
L_p	[m]	Pore length
L_{pipe}	[m]	Pipe length
L_{RES}	[m]	Resultant turbulent macroscale
Lys	[g/l]	Lysine concentration
$m_0 \ldots m_3$	[-]	Empirical constants used to estimate $k_{decline}$ as a function of J_o, v and X
m_c	[kg m^{-2}]	Mass of cake formed on membrane surface
m_c^{max}	[kg m^{-2}]	Maximum cake mass at steady state
m_j		Polynomial order for approximation of control variable j
m_{sp}	[-]	Constant in Eq. 4-25
m_{vl}	[-]	Constant in Eq. 4-23
$n(r_p)$	[-]	Log normal pore size distribution
N*	[#]	Number of pores
n_c	[-]	Exponent in cake compressibility equation (Eq. 2-12)
n_{DE}	[-]	Constant in Eq. 2-13
$n_{decline}$	[-]	Constant in Eq. 3-86
n_{fl}	[-]	Constant in Eq. 4-24
n_{IL}	[-]	Exponent in Eq. 3-48
N_p	[m^{-2}]	Number of pores per unit area
n_{pd}	[-]	Order of the polymerisation reaction in Eq. 3-81
N_{Power}	[-]	Power number
NS		Number of stages in optimal control problem
$n_{s,n}$	[-]	Constant in Eq. 3-53
n_{si}	[-]	Constant in Eq. 4-22
n_{sp}	[-]	Constant in Eq. 4-25
n_v	[-]	Exponent in J vs. v relationship (Eq. 2-2)
n_{vl}	[-]	Constant in Eq. 4-23

o_{sp}	[-]	Constant in Eq. 4-25
OTR	[mMol/l/h]	Oxygen transfer rate
OUR	[mmol/l/h]	Oxygen uptake rate
p(A)	[-]	Probability of event A
p_1	[-]	Constant that compensate for concentration profiles in broth (Eq. 3-99)
p_1		Constant in cake resistance estimation
p_2	[-]	Constant that compensate for the stickiness of the particles in the cake layer (Eq. 3-99)
p_e	[-]	Ellipsoidal shape factor
P		Vector of explicit algebraic variables
Perm	[m^3/s]	Volumetric permeate flow rate
Perm'	[l/h]	Permeate flow rate
$Perm_o$	[m^3/s]	Volumetric permeate flow rate at t=0
$Perm_t$	[l/h]	Volumetric permeate flow rate at t=t
P_g	[W]	Gassed power input into the bioreactor
P_o	[W]	Ungassed power input into bioreactor
P_{O2}	[Pa]	Oxygen partial pressure
P_{perm}	[$C^2\ J^{-1}$]	Permittivity of the solvent
P_s	[-]	Solubility product Eq. 2-4
$Q_{chilling}$	[W]	Heat to be removed from bioreactor
q_{Gluc}	[g/g/h]	Specific glucose feed rate
Q_L	[m^3/s]	Volumetric flow rate through recycle system
q_{Lys}	[g/g/h]	Specific lysine productivity for unstressed conditions
$q_{Lys,obs}$	[g/g/h]	Observed specific lysine productivity
Q_o	[-]	Dimensionless constant in Eq. 3-55
q_{o2}	[mmol/g/h]	Specific oxygen uptake rate
q_{pore}	[m]	Pore size distribution
Q_s	[-]	Solubility quotient Eq. 2-4
q_{Thr}	[g/g/h]	Specific threonine feed rate
$\bar{R}_c$	[m^{-2}]	Specific cake resistance per unit cake thickness
r(t)	[mol/h]	m-dimensional metabolite accumulation rate vector
r*	[m]	Mean membrane pore radius

R^2	[-]	Correlation coefficient
R_c	[m^{-1}]	Cake resistance
R_c'	[m^{-1} kg^{-1}]	Hydraulic cake resistance per unit cake mass per unit area
$\mathbf{r}_E$	[mol/h]	Extracellular metabolite accumulation rate
Re	[-]	Pipe flow Reynolds number
Rev	[s^{-1}]	Impeller speed
Re_w	[]	Wall Reynolds number
r_i	[mol C/h]	Accumulation rate of metabolite i
$\mathbf{r}_i$	[mol/h]	Intracellular metabolite accumulation rate
R_m	[m^{-1}]	Intrinsic membrane resistance
r_p	[m]	Membrane pore radius
R_p	[m^{-1}]	Pore plugging resistance
r_p^*	[m]	Mean membrane pore size
$r_{p,STDEV}$	[m]	Membrane pore radius standard deviation
r_{po}	[m]	Clean membrane pore radius
RQ	[]	Respiration quotient (Ratio of carbon dioxide evolution rate to oxygen uptake rate)
R_t	[m^{-1}]	Total hydraulic resistance
Rugosity	[μm]	Height difference between the deepest troughs and highest peaks on a surface
s	[-]	Solids fraction in the feed suspension
S		Surface in phase space
S1 and S2	[g/g]	Stoichiometric constant in AS feed rate
S_c	[m^2/m]	Specific surface area of the cake layer
S_f	[$kg/s/m^2$]	Solids flux
S_m	[m^2/m^3]	Specific surface area of membrane
Sub_1	[g/l]	Limiting substrate concentration
Sub_2	[g/l]	Limiting substrate concentration
t	[s]	Time
T	[K]	Temperature
T	[-]	Time space
t'	[h]	Time

$t_{f,\ Ferment}$	[h]	Final fermentation time
$t_{f,\ Permt}$	[h]	Total recycle time
t_{clean}	[h]	Duration of the membrane cleaning process
Thr	[g/l]	L-Threonine concentration (All the other auxotropic amino acids will be in present in the stream in stoichiometric amounts as calculated for *C. glutamicum* ATCC 21253)
Thr_o	[g/l]	Initial L-Threonine concentration
t_{perm}	[h]	Duration of the filtration process in the cell recycling
$t_{ferment}$	[h]	Fermentation time
Tdur	[h]	Membrane cleaning frequency
u	[m/s]	Linear velocity
$\overline{u^2}_i$	[m/s]	Mean square turbulent velocity at a point
$\bar{u}_1(d)$	[m/s]	Root mean square velocity difference for eddies of diameter d in the viscous dissipation range
$\bar{u}_2(d)$	[m/s]	Root mean square velocity difference for eddies of diameter d in the inertial convection subrange
$\bar{U}$	[m/s]	Mean velocity
u_c	[-]	Input control vector
$u_{c,i,j,k}$		Control variable j, parameter i, for stage k
$u_{cj}^{(k)}$	[-]	Control variable j during stage k
u_{c^*}		Allowable control function
U_c	[-]	Subset of input functions
$\bar{U}_i$	[m/s]	Average velocity at a point
$\bar{U}_{RMS}$	[m/s]	Root mean square turbulent velocity
u^*	[m/s]	Parameter in Eq. 5-29
u_l	[m/s]	Fluctuating velocity at a point
U_i	[m/s]	Instantaneous velocity at a point
U_{max}	[m/s]	Maximum linear velocity in flow profile
v	[m/s]	Average cross flow velocity
v	[m/s]	Cross flow velocity through membrane module
v_t		Time invariant parameters
V	[litre]	Broth volume

V_c		Cost function
VCOP	[R/kg]	Variable cost of production
V_o	[litre]	Initial bioreactor volume
V'_f	[litre]	Volume of filtrate collected
v_{actual}	[m/s]	Measured cross flow velocity
V_b	[m/s]	Back flow velocity
V_f	[m^3]	Volume of filtrate collected
V_L	[m^3]	Volume of laminar sublayer
$v_{l.o}$	[m/s]	Inertial lift velocity
V_{max}	[nmol.min^{-1}.mg DCW^{-1}]	Michalis Menten kinetics constant
V^{max}	[litre]	Maximum bioreactor volume
V_{mem}	[m^3]	Membrane volume
V_{react}	[m^3]	Bioreactor volume
V_{valve}	[m^3]	Valve volume
w		Constraints of the system
x	[cm]	Axial coordinate along channel length
X	[g/l DCW]	Biomass concentration
$\bar{x}_n$	[-]	Variables in stepwise multiple regression Eq. 3-1
x(t)	[mol/h]	n-dimensional flux vector
x	[-]	State vector of the system
X	[-]	State space
X		Vector of explicit algebraic variables
X_{cr}	[cm]	Critical distance from filter exit where cake formation starts
x_i	[mol C/h]	Rate of flux through reaction i
y		Algebraic variables in the model
y	[m]	Distance from centre of tube Eq. 3-30
Y		Vector of differential variables
$Y_{x/Thr}$	[g/g]	Yield of biomass on threonine for unstressed conditions
$Y_{X/Thr,obs}$	[g/g]	Observed yield of biomass on threonine
z	[-]	Empirical constant in Eq. 3-52 and Eq 3-53
Z_n	[-]	Variable combinations in stepwise multiple regression Eq. 3-1

3. GREEK SYMBOLS

α_o	[-]	Constant in mass transfer correlation
α_l	[-]	Stoichiometric coefficient
α_{o2}	[-]	Variable in mass transfer equation
β_{o2}	[-]	Variable in mass transfer equation
β	[m^{-2}]	Cake compressibility constant, (Eq 2-12)
β_o	[-]	Constant in mass transfer correlation
β'	[m^{-1} kg^{-1}]	Cake compressibility constant, (Eq. 3-11)
δ_a	[m]	Thickness of monolayer absorbed inside membrane pores
δ_c	[m]	Thickness of the cake layer on the membrane surface
δ_m	[m]	Membrane thickness
δ_t	[m]	Thickness of laminar sublayer
Δ	[s^{-1}]	Components if the mean rate of deformation tensor for compressible flows
$\Delta\pi$	[Pa]	Osmotic pressure difference across the membrane
ΔP	[Pa]	Trans-membrane pressure drop
ΔP_{actual}	[Pa]	Trans-membrane pressure drop
ΔP_{crit}	[Pa]	Critical trans-membrane pressure drop
ε_m	[-]	Void fraction of the membrane
ε_c	[-]	Void fraction of the cake layer
ϕ_b	[-]	Solids volume fraction of the feed
ϕ_c	[-]	Solids volume fraction of the cake
ϕ_w	[-]	Solids volume fraction of the boundary layer
$\Phi_i^{(m)}$		Lagrange polynomials of order m
$\overset{o}{\gamma}_o$	[s^{-1}]	Shear rate at the wall
$\overset{o}{\gamma}$	[s^{-1}]	Local shear rate
η		State of the system
$\eta(t)$		Function of t from adjustable input variables
$\eta_u(t, x_o$		Motion of system state passing through x_o at time t_o under

t_o)		action of control u_c
η_o	[-]	Probability density of radius r_p
η_v	[-]	Probability density of radius r
κ_1	[-]	Constant in Eq. 3-66
κ_2	[-]	Constant in Eq. 3-67
κ^{-1}	[m]	Debye length
λ	[m]	Kolmogorov length
μ	[h^{-1}]	Specific growth rate
μ_{max}	[h^{-1}]	Maximum specific growth rate
μ_{obs}	h^{-1}	Observed specific growth rate
θ	[deg]	Angle between normal drag force and the tangent to the protrusion. Fig. 3-3
ρ	[kg/m^3]	Density
ρ_F	[kg/m^3]	Feed density
ρ_s	[kg/m^3]	Solids density of the particles comprising the cake
ρ_p	[kg/m^3]	Filtrate density
σ	[m^2/m^3]	Blocked permeate area per unit permeate volume
σ_o	[Pa]	Osmotic reflection coefficient
σ_{STDEV}	[-]	Standard deviation of measured data
k_τ	[s/m]	Time constant
τ	[s]	Time constant
$\tau_n^{(k)}$		Normalised time of stage k
τ'	[Pa]	Reynolds shear stress
τ_o	[Pa]	Wall shear stress
τ_{ij}	[Pa]	Newtonian viscous stress tensor
τ_w	[Pa]	Wall shear stress
υ	[Pa s]	Permeate viscosity
υ_F	[Pa s]	Feed viscosity
υ'	[$cm^2\ s^{-1}$]	Kinematic viscosity
υ'	[$cm^2\ s^{-1}$]	Kinematic viscosity
φ		Scalar function of terminal cost

φ	[-]	Particle shape factor
ψ	[-]	Parameter in Bayesian inference
Ψ		Measurement noise covariance matrix associated with **r**
ζ_s	[mV]	Zeta potential / Surface Charge
$\zeta(t)$		Moving target
ζ	[Cm^{-2}]	Surface charge density

Table of Contents

Chapter 3. Modelling of the Cross-Flow Filtration Flux of Suspensions of *Corynebacterium glutamicum* Cells

List of Figures

List of Tables

Retention of Fermentation Biomass for Extended L-Lysine Fermentations

L-lysine is an essential amino acid in mono gastric animal nutrition. Many plant products used as livestock feeds are deficient in L-lysine. L-lysine is therefore added as supplement to the feed (Hopwood 1981). The world market for L-lysine of 436 000 ton L-lysine per annum (2000) is currently growing at a rate of between 5 and 10% each year (Weuster-Botz *et al.* 1997; BBC, 2000). The bulk of L-lysine production throughout the world depends on the direct fermentation of carbohydrates by auxotrophic and regulatory mutants of *Corynebacteria* and *Brevibacteria* species.

Amino acid fermentations are intensive in raw material usage. This means that the process yield and productivity are critical measures of performance and economic viability (Kiss & Stephanopoulos 1991). Previous research activities, aimed at improving the performance of the L-lysine fermentation processes with respect to L-lysine yield, volumetric productivity and L-lysine concentration have focussed primarily on strain manipulation (Shimazaki *et al.* 1983; Matsumoto 1985; Nakayama 1985; Beppu 1986; Nakanishi *et al.* 1987; Yokata & Shiio 1988; Hirao *et al.* 1989; Schrumpf *et al.* 1992; Yoshihara *et al.* 1993; Oh *et al.* 1993a; Nakano *et al.* 1994; Nakayama 1985; Sano *et al.* 1987; Cremer *et al.* 1988; Menkel *et al.* 1989; Eikmanns 1992; Gubler *et al.* 1994; Sahm 1995; Eggeling 1994). Several investigators attempted to improve amino acid fermentation performance, by process manipulations (Akashi *et al.* 1979; Hilliger & Hanel 1981; Radjai *et al.* 1984; Hilliger *et al.* 1984).

The overall fermentation performance have been improved by using fed-batch strategies whereby the cells are maintained in the L-Lysine overproduction metabolic state by continuously feeding the substrate to the reactor (Hadj *et al.* 1988; Rutkov 1984, Hirao *et al.* 1989; Kiss & Stephanopoulus 1991). The fermentation is stopped when the bioreactor reaches the maximum volume.

A large portion of the production cost is spent to establish a viable biomass population. To maximise the volumetric productivity and reduce production costs, feed and bleed strategies are often employed. However, since L-lysine is predominantly a secondary metabolite, the maximum yield of L-lysine from carbohydrates is achieved at very low growth rates. This implies that viable biomass, still capable of L-lysine production are lost in bleed. The reactor volume as well as the inability of the process to retain the microbial population limits the productivity and conversion of carbohydrates to L-Lysine.

Biomass re-use, recycling or retention offer important advantages when the process micro-organisms are either slow growing or strongly affected by product inhibition (Hammer 1982; Karel *et al.* 1985;Kargupta *et al.* 1998). In an effort to extend the productive life span

of the biomass, Sweeting *et al.* (1990) re-used *Corynebacterium,* biomass for 6 Leucine production cycles in the presence of the auxotrophic amino acids.

In this thesis it was demonstrated that the L-Lysine fermentation performance can be enhanced by continuously withdrawing spent medium and recycling of the biomass in the culture suspension to the bioreactor. The biomass in the reactor outlet was separated from the spent medium using cross-flow filtration before being recycled to the reactor. The objective of this thesis was to study, understand, model and optimise the performance of the L-Lysine fermentation with biomass retention using cross flow filtration.

Two L-Lysine producing strains (ATCC 21253 and AEC 94) have been used in this study. The ATCC 21253 strain is auxothropic for L-Threonine, L-Methionine and L-Leucine. The metabolism and biochemistry of ATCC 21253 have been intensively studied (Vallino & Stephanopoulos 1993). The AEC 94 strain is an industrial strain developed by AECI (Pty) Ltd. The characterisation of this strain is confidential and all performance variables related to this strain are reported in a normalised manner.

Two ultrafiltration (150 kD and 300 kD) and two microfiltration (0.22 μm & 0.45 μm) tubular ceramic membranes were used. These membranes are steam sterilisable, a requirement of the monoseptic process conditions. Fermentations were conducted on 10-litre scale using both a chemically defined and an industrial medium composition.

Chapter 1 of this thesis provides an overview of the published approaches to improve the L-Lysine fermentation performance. The factors that influence the cross-flow filtration flux through the ceramic membranes were studied and reported in Chapter 2. This is followed by the development of fundamental and empirical filtration models in Chapter 3. The most suitable filtration model is selected in Chapter 4, based on Bayesian inference.

In Chapter 5, the qualitative impact of cross-flow filtration on the L-Lysine fermentation performance is described, followed by the development of a mathematical model that predicts the fermentation performance of a L-Lysine producing bioreactor with biomass recycling in Chapter 6. Chapter 7 reports on the mathematical optimisation of the process model and illustrates that the predicted optimum can be realised experimentally using the two strains.

References

Akashi, K. Shibai, H. and Hirose, Y. (1979), Effect of oxygen supply on L-Lysine, L-Threonine and L-Isoleucine fermentations, *Agric. Biol. Chem.,* **43**, 2087-2092

Beppu, T. (1986), In "Biotechnology of Amino Acid Production" (Aida, K. Chibata, J. Nakayama, K. Takinami, K. and Yamada, H., Eds.), Elsevier, NY, pp 24-35

Business Communications Company, August 2000

Cremer, J. Treptow, C. Eggling, L. and Sahm, H. (1988), Regulation of enzymes of L-Lysine biosynthesis in *Corynebacterium glutamicum*, *J. Gen. Microbiol.*, **134**, 3221-3229

Eggeling, L. (1994), Biology of L-Lysine overproduction by *Corynebacterium glutamicum*, *Amino Acids*, **6**, 261-272

Eikmanns, B. (1992), Identification, sequence analysis and expression of a *Corynebacterium glutamicum* gene cluster encoding the three glycolytic enzymes: glyceraldehyde-3-phosphate dehydrogenase, 3-phosphoglycerate kinase and triosephosphate isomerase, *J. Bacteriol.*, **174**, 6067-6086

Gubler, M. Jetten, M. Lee, S. H. and Sinskey, A. J. (1994), Cloning of the pyruvate kinase gene (pyk) of *Corynebacterium glutamicum* and site specific inactivation of pyk in a lysine producing *Corynebacterium lactofermentum* strain, *Appl. Environ. Microbiol.*, **60**, 2494-2500

Hadj Sassi, A. Queric, M. P. Deschamps, A. M. and Lebeault, J. M. (1988), *Biotechnology Letters*, **10**(3), 583-586

Hammer, G. (1982), Recycle in fermentation processes, *Biotechnology and Bioengineering*, **24**, 511

Hilliger, M and Hanel, F. (1981), Process analysis of L-Lysine fermentation under different oxygen supply, *Biotechnology Letters*, **3**(5), 219-224

Hilliger, M. Möckel, H. –O. and Forberg, W. (1984), The optimisation of L-lysine fermentation and a mass transfer model, *Acta Biotechnol.*, **4**(4), 355-360

Hirao, T. Nakano, T. Azuma, T. Sugimoto, M and Nakanishi, T. (1989), L-Lysine production in a continuous culture of an L-Lysine hyperproducing mutant of *Corynebacterium glutamicum*, *Appl. Microbiol. Biotechnol.*, **32**, 269-273

Hopwood, D. A. (1981), The genetic programming of industrial microorganisms, *Sci. Am.*, **245**(3), 30-42

Karel, S. F. Libicki, S. B. and Robertson, C. R. (1985), *Chem. Eng. Sci.*, **40**, 1321

Kargupta, K. Datta, S. and Sanyal, S. K. (1998), Analysis of the performance of a continuous membrane bioreactor with cell recycling during ethanol fermentation, *Biochemical Engineering Journal*, **1**, 31-37

Kiss, R. D. and Stephanopoulos, G. (1991), Metabolic activity control of the L-lysine fermentation by restrained growth fed-batch strategies. *Biotechnology Progress*, **7**, 501-509

Matsumoto, S. (1985), A method for producing L-lysine, EP 0 175 309 A2

Menkel, E. Thierback, G. Eggling, L. and Sahm, H. (1989), Influence of increased aspartate availability on lysine formation by a recombinant strain of *Corynebacterium glutamicum* and utilisation of fumarate. *Appl. Environ. Microbiol.*, **55**(3), 684-688

Nakanishi, T. Hirao, T. and Sakurai, M. (1987), Process for producing L-lysine by fermentation, US Patent 4,657,860

Nakano, T. Azuma, T. and Kuratsu, Y. (1994), Process for producing L-Lysine by iodothyrosine resistant strains of *Mucorynebacterium glutamicum,* US Patent 5,302,521

Nakayama, K. (1985), Lysine, In "Comprehensive Biotechnology" (H. W. Blanch, S. Drew, D. I. C. Wang, Eds.), Vol. 3, Pergamon Press, New York, pp 607-620

Oh, J. W. Kim, S. J. Cho, Y. J. Park, N. H. and Lee, J. H. (1993a), Strain of *Corynebacterium glutamicum* and method for producing L-lysine, US Patent 5,268,293

Oh, N. S. and Sernetz, M. (1993b), Turnover characteristics in continuous L-lysine fermentation. *Appl. Microbiol. Biotechnol.,* **39,** 691-695

Radjai, M. K. Hatch, R. T. and Cadman, T. W. (1984), Optimisation of amino acid production by self-tuning digital control of redox potential, *Biotechnology and Bioengineering Symposium,* **14**, 657-679

Rutkov, A. B. (1984), Microbiological Production of L-Lysine by Employing Feed Batch Cultivation, *Bulg. Akad. Nauk.*, **37**(12), 1677-1680

Sahm, H. (1995), Metabolic design in the amino acid producing bacterium *Corynebacterium glutamicum*, *Folia Microbiol.*, **40**(1), 23-30

Sano, K. Ito, K. Miwa, K. and Nakamori, S. (1987), Amplification of the phosphoenolpyruvate carboxylase gene of *Brevibacterium lactofermentum* to improve amino acid production, *Agric. Biol. Chem.,* **51**(2), 597-599

Schrumpf, B. Eggling, L. and Sahm, H. (1992), Isolation and prominent characteristics of an L-Lysine hyperproducing strain of *Corynebacterium glutamicum. Appl. Microbiol. Biotechnol.*, **37**, 566-571

Shimazaki, K. Nakamura, Y. and Yamada, Y. (1983), Method for producing L-lysine by fermentation, US Patent 4,411,997

Sweeting, K. B. Sauer, E. C. Chotani, G. Smith, C. and LaDuca, J. (1990), Strategies for reuse of bacteria for the production of amino acids, *Acta Biotechnol.,* **4**(4), 983-986

Vallino, J. J. and Stephanopoulos, G. (1993), Metabolic flux distributions in *Corynebacterium glutamicum* during growth and lysine overproduction, *Biotechnology and Bioengineering,* **41**, 633-646

Weuster-Botz, D. Kelle, R. Frantzen, M. and Wandrey, C. (1997), Substrate controlled fed-batch production of L-lysine with *Corynebacterium glutamicum, Biotechnol. Prog.,* **13,** 387-393

Yokata, A. and Shiio, I. (1988), Effects of reduced citrate synthase activity and feedback-resistant phosphoenolpyruvate carboxylase on lysine productivities of *Brevibacterium flavum. Agric. Biol. Chem.,* **52**(2), 455-463

Yoshihara, Y. Kawahara, Y. and Ikeda, S. (1993), Fermentation process for producing L-lysine, Us Patent 5,179,010

The Production of L-Lysine via a Fermentation Route

1 Introduction

L-lysine is a limiting amino acid in monogastric animal nutrition. L-lysine is produced by the direct fermentation of carbohydrates by auxotrophic and regulatory mutants of *Corynebacteria* and *Brevibacteria* species.

Amino acid fermentations are intensive in raw material usage. This means that the process yield and productivity are critical measures of performance and economic viability (Kiss & Stephanopoulos 1991). Previous research activities to improve the performance of L-lysine fermentation processes with respect to L-lysine yield, volumetric productivity and L-lysine concentration have focussed primarily on strain manipulation by mutation and selection for regulatory deficient mutants (Shimazaki *et al.* 1983; Matsumoto 1985; Nakayama 1985; Beppu 1986; Nakanishi *et al.* 1987; Yokata & Shiio 1988; Hirao *et al.* 1989; Schrumpf *et al.* 1992; Yoshihara *et al.* 1993; Oh *et al.* 1993b; Nakano *et al.* 1994) and recombinant genetic technology for the amplification of key enzymes (Nakayama 1985; Beppu 1986, Sano *et al.* 1987; Cremer *et al.* 1988; Menkel *et al.* 1989, Eikmanns 1992; Gubler *et al.* 1994; Sahm *1995*; Eggeling 1994). Although these approaches have produced mutants exhibiting increased rates of product formation, they do not necessarily improve the fermentation yield. Increasing the yield of L-lysine from sugar requires redirecting the cellular metabolism in favour of the desired product as opposed to biomass or other side product formation (Kiss & Stephanopoulos 1991).

Several investigators attempted to improve amino acid fermentation performance, by process manipulations. These studies have examined the effects of the environmental and process parameters on the yield, specific productivity of the cells and volumetric productivity of the bioreactor. Parameters such as initial medium composition, dissolved oxygen concentration, culture redox potential, power input and aeration rates have been studied in batch cultures (Akashi *et al.* 1979; Hilliger & Hanel 1981; Radjai *et al.* 1984; Hilliger *et al.* 1984).

The overall fermentation performance have been improved by using fed-batch strategies whereby the cells are maintained in the L-lysine overproduction metabolic state while substrate is continuously fed to the reactor. These strategies have been further improved by studies on the effects of sugar concentrations, optimal feed rates, aeration and dilution rates (Hadj *et al.* 1988; Rutkov 1984; Hirao *et al.* 1989; Kiss & Stephanopoulos 1991). Researchers have applied metabolic activity control with respiratory measurements and feed rate manipulation to achieve optimal yield and volumetric productivities (Kiss & Stephanopoulos 1991). Continuous fermentations have been used to research process kinetics with very little industrial application (Oh & Sernetz 1993a).

The impact of biomass recycling on the overall L-lysine fermentation process performance and economic viability was investigated in this study. This chapter provides an overview of the L-lysine production metabolism. The metabolic stages of *Corynebacterium glutamicum* during the L-lysine fermentation will be described followed by a discussion of the major metabolic and process improvements of the L-lysine fermentation that have been published.

2 Metabolism of *Corynebacterium glutamicum*

The yield and productivity of L-lysine fermentation can be improved by strain manipulation. These techniques have traditionally been very empirical and iterative. Quantitative measures have focussed primarily on final titres, yields and average volumetric productivities (Tosaka *et al.* 1978; Nakayama 1985; Beppu 1986; Yokata & Shiio 1988). With the advent of genetic engineering techniques, it became possible to achieve a better understanding of the physiology on the molecular level. New characteristics of *C. glutamicum* were discovered and quantified by biochemical work. This section will review the metabolism of *C. glutamicum* leading to L-lysine excretion to allow a better understanding of the mutated strain behaviour and impact of process parameters on the fermentation performance.

2.1 Energy generation in C. glutamicum

The metabolic pathways responsible for energy generation in the cell as described by Prescott *et al.* (1996) is discussed below. *C. glutamicum* utilises the Embden-Meyerhof-Parnas (EMP) pathway (glycolysis) to break glucose down to pyruvate. The catabolic pathways of *C. glutamicum* are illustrated in Figure 1-1. Stored energy and reducing power in the form of 2 molecules of ATP and 2 molecules of NADH result from a single pass through the overall EMP pathway. The pathway also provides carbon skeletons as starting materials in cellular biosynthetic reactions.

Respiration is the energy producing process in which pyruvate is oxidised by oxygen. The reactions peculiar to respiration start with pyruvate. Additional reducing power is generated from pyruvate by converting it to acetyl co-enzyme A. The first phase of the oxidation is carried out in the tri-carboxylic acid cycle (TCA) cycle. Acetyl-CoA is oxidised to CO_2. In each pass around the TCA cycle, four pairs of hydrogen atoms are liberated. Three pairs are transferred to NAD and the fourth to FAD. The TCA cycle serves an important function in providing a pool of precursors for biosynthetic reactions.

In the second phase of respiration, the hydrogen atoms are passed through a sequence of reactions in the respiratory chain, during which ATP is generated, from ADP. At the end, the hydrogen atom combines with O_2 to give H_2O. Respiration potentially makes available to the cell 30 molecules of ATP compared to 8 molecules of ATP made available during glycolysis on a single pass through these pathways respectively.

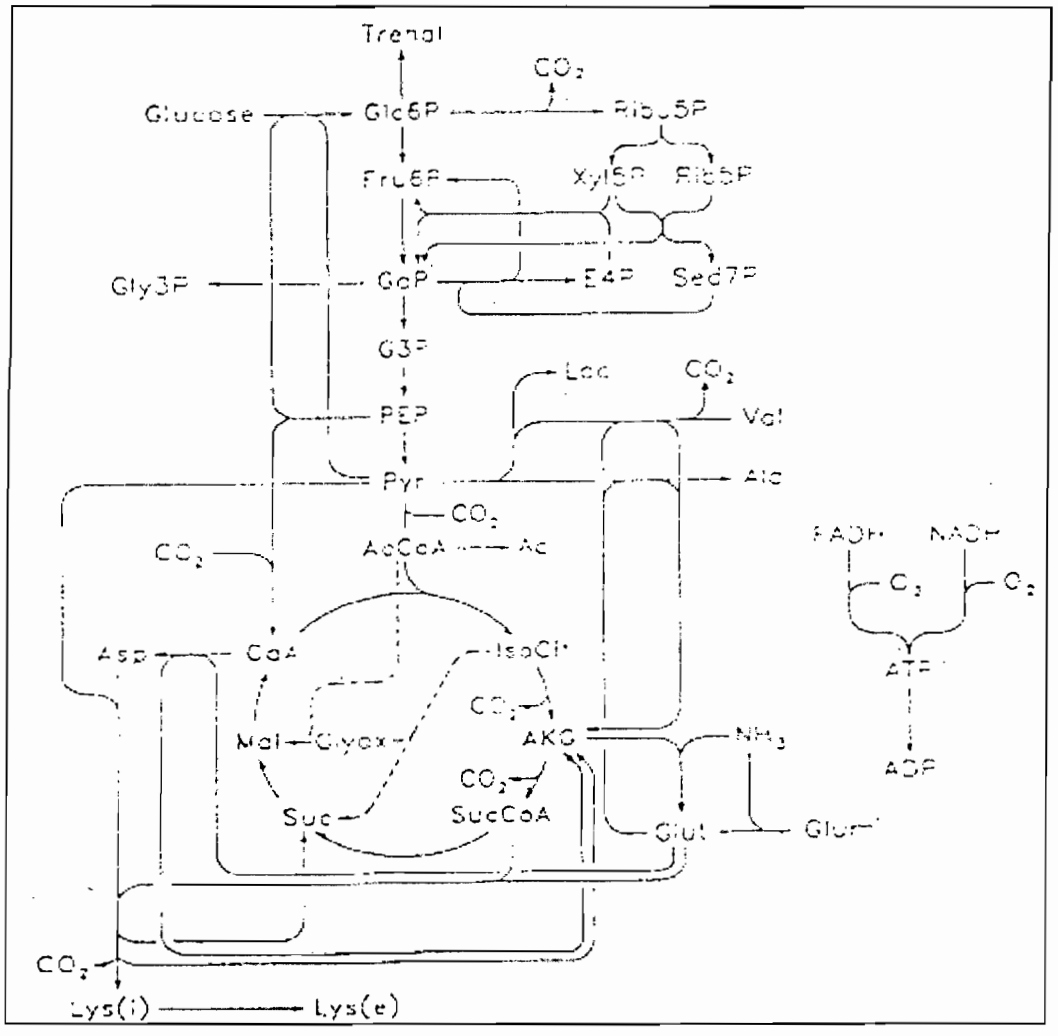

Figure 1-1. Primary metabolism of *C. glutamicum* (Adapted from Vallino 1991)

2.2 Metabolic pathways for L-lysine production

The bacterial synthesis of L-lysine starts from the central metabolite L-aspartate, which is derived from the tricarboxilic acid cycle (TCA) intermediate, oxaloacetate by transamination. Aspartate is activated via phosphorylation by aspartate kinase and reduced to give aspartate semialdehyde. This intermediate is an important branch point to L-threonine, L-methionine and L-isoleucine synthesis or the further reactions of L-lysine synthesis. The latter are the condensation of aspartate semialdehyde with pyruvate by dihydrodipicolinate synthase and its reduction to piperideine-2, 6-dicarboxilate.

At this step, the bacterial diaminopimelate pathway of L-lysine synthesis is at variance. *E. coli* and other bacteria (Weinberger & Gilvarg 1970) use the succinylase variant with its four specific reactions to make the ultimate L-lysine precursor D, L diaminopimelate (Figure 1-2). The second variant, known as the acetylase variant is a minor modification

where an acetyl group replaces the succinyl group. This is used, for example in *Bacillus subtilis* (Eggeling 1994). In the dehydrogenase variant, D, L-diaminopimelate is synthesised in one single step by the action of D-diaminopimelate dehydrogenase (Misono & Soda 1980), as is the case *in Bacillus sphaericus*.

The metabolic pathways of the three variants rejoin at D, L-diaminopimelate. This metabolite is another branch point since it is used either for cell wall synthesis or decarboxylated to L-lysine. This process is depicted in Figure 1-2.

The peculiarity of *C. glutamicum* is that both the succinylase and the dehydrogenase variants are used (Schrumpf *et al.* 1991). Gene-directed inactivation of dehydrogenase by integration of vector sequences (Schrumpf *et al.* 1991) verified that the dehydrogenase variant is dispensable. Corresponding genes have not yet been cloned to enable gene-directed mutagenesis to ascertain the necessity of the active succinylase variant (Eggeling 1994). In different attempts to clone genes of the split pathway by the use of an appropriate *E. coli* mutant, the gene encoding D-diaminopimelate dehydrogenase was always isolated (Ishino *et al.* 1988, Yeh *et al.* 1988). This is probably due to specific promoter structures of the genes of *C. glutamicum* opposed to those used in *E. coli* (Eikmanns 1992).

Sonntag *et al.* (1993) found that 30% of the L-lysine finally accumulated is synthesised over the dehydrogenase variant. The succinylase variant was found to be the dominant pathway for both the wild type and the investigated mutant over-producers. Since strains with widely different L-lysine production rates were analysed, it might be suggested that the flux ratio is independent of the total flux. However, the instantaneous partition coefficient determined at various cultivation times showed that at the beginning of cultivation the flux partition coefficient over the dehydrogenase variant is 72% decreasing to 0% at the end of cultivation (Sonntag *et al.* 1993). Use of varying initial ammonium concentrations and replacement of free ammonium with an organic nitrogen source verified that the dynamic changes of this ratio during cultivation are due to a decrease in the ammonium concentration (Sonntag *et al.* 1993).

Misono *et al.* (1979) have shown that D-aminopimelate dehydrogenase has a weak affinity for ammonium. It thus follows that the *in vivo* activity of the dehydrogenase enzyme is directly linked to the flux distribution. It was therefore postulated that the use of the dehydrogenase variant of L-lysine synthase is kinetically controlled by the availability of ammonium. In contrast to the well known control of enzymes of nitrogen metabolism in *C. glutamicum* at the genetic level (Sung *et al.* 1995) this is thus an example of flux variation in direct response to changing environmental conditions (Cremer *et al.* 1988; Schrumpf *et al.* 1991).

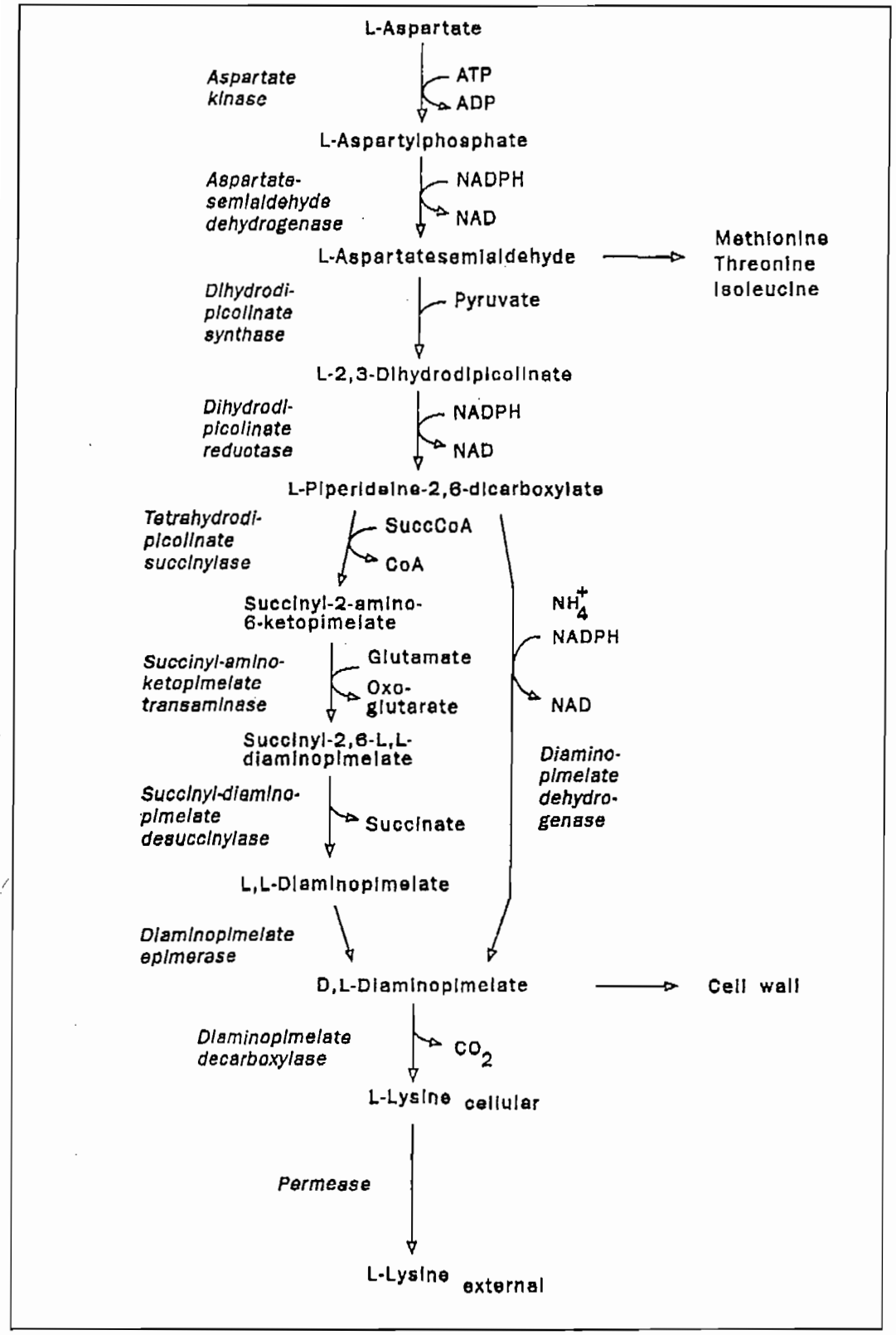

Figure 1-2. Biochemistry of L-lysine overproduction by *Corynebacterium glutamicum* (Adapted from Eggeling 1994)

The Production of L-lysine via a Fermentation Route

2.3 The lysine excretion system

C. glutamicum effectively excretes L-lysine when the internal L-lysine concentration is elevated. Bröer & Kramer (1991) investigated L-lysine efflux using selected mutants, which were not able to regulate L-lysine biosynthesis by feedback inhibition. Secretion of L-lysine was not the consequence of unspecific permeability of the plasma membrane but was mediated by a secretion carrier, specific for L-lysine. This carrier function according to a secondary transport mechanism, the driving force being the membrane potential, the L-lysine gradient and the proton gradient. At low external L-lysine concentrations, the total export activity is mainly dependent on the membrane potential. L-Lysine and proton gradients come into play at high external L-lysine concentrations. This is due to the mechanistically different steps of binding, release and reorientation of the carrier, influenced differently by the three forces.

Bröer and Kramer (1991) characterised the L-lysine export of *C. glutamicum* ATCC 13032 (wild type) as having a high activation energy, followed by Michaelis-Menten type kinetics with an internal K_m of 20 mM and V_{max} of 12 nmol.min^{-1}.mg dry cells^{-1}. Excretion can proceed against a pre-existing chemical gradient and against the electrical potential. L-Lysine excretion was also observed in the wild type strain, especially under conditions of peptide up-take. The possible physiological function of L-lysine excretion may be related to regulation of internal amino acid concentrations under special growth conditions (Bröer & Kramer 1991).

3 Batch fermentation profile of a typical L-lysine overproducing strain of *Corynebacterium glutamicum*

The fermentation profile depends on the nature of the specific strain. For this study *C. glutamicum* (ATCC 21253) auxotrophic for L-leucine and L-homoserine without the feedback kinase modification, was used. A typical media formulation as reported by Kiss & Stephanopoulos (1991) was used. The details of the media formulations used in this study are discussed in Appendix A.2. A typical fed-batch fermentation profile for *C. glutamicum* (ATCC 21253) is presented in Figure 1-3 below. The data was obtained from experimental work conducted by Kiss & Stephanopoulos (1991).

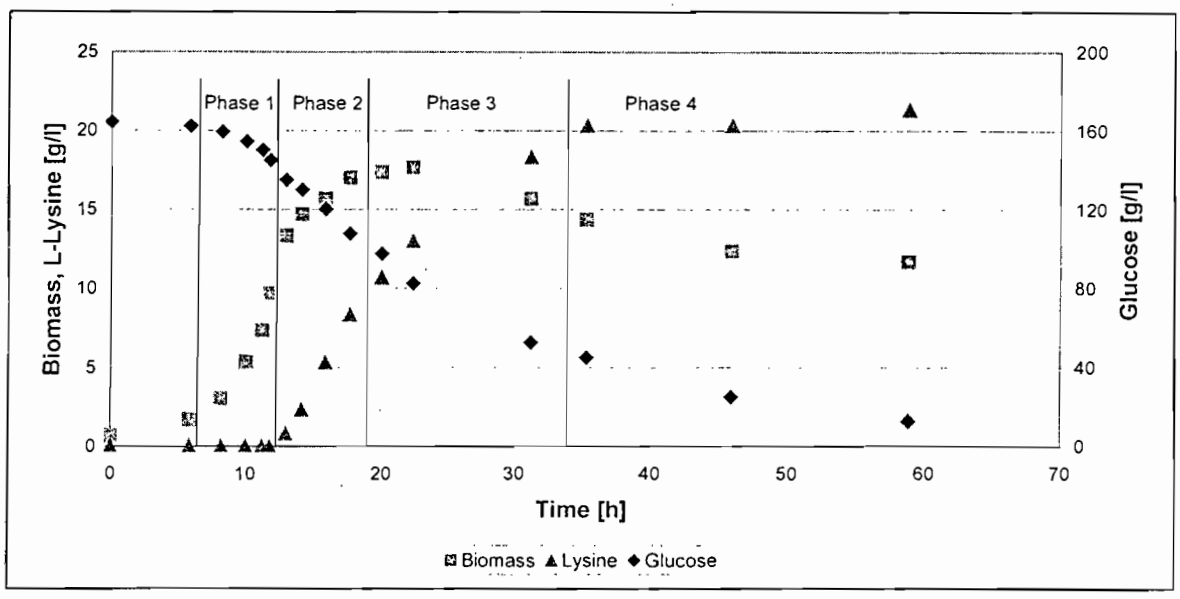

Figure 1-3. Typical batch fermentation profile for *C. glutamicum* (ATCC 21253) as reported by Kiss & Stephanopoulos (1991)

The fermentation can be broken down into four separate phases as shown in Figure 1-3. Phase 1 of the fermentation is marked by balanced (exponential) growth with no or little byproduct accumulation (except CO_2). The duration of phase 1, and the biomass concentration attained during this phase is governed by the initial supply of the auxotrophic amino acids which, in concert with L-lysine, inhibit aspartate kinase and prevent the overproduction of L-lysine.

Phase 2 commences at the depletion of L-threonine, as evident by the increase in the respiration quotient (carbon dioxide release / oxygen uptake) and is marked by high L-lysine and low biomass production rates. The duration of phase 2 depends on the extracellular environmental conditions in the bioreactor. Various feed strategies have been suggested to maintain the L-lysine overproduction state in fed-batch operated fermentations (Kiss & Stephanopoulos 1991). The slight increase in biomass during this phase is probably due to either scavenging of L-threonine reserves or the accretion of cellular constituents including total protein. Changes in cellular morphology that accompany extracellular L-threonine depletion are quite complex and very important in L-lysine synthesis but has not been investigated.

Phase 3 of the culture commences as growth plateau's and is marked by high lysine production rates and decreasing respiration and respiration quotient (RQ).

Phase 4 of the culture represents the death phase. This is evident from the gradual reduction in L-lysine production, a decrease in biomass concentration and a redirection of glucose metabolism to byproduct formation. Byproducts such as pyruvate, acetate, alanine and valine as well as small amounts of a few unidentified metabolites have been found (Kiss & Stephanopoulos 1991). It is believed that the decrease in L-lysine synthesis in this

phase results from the decay of primary enzymes such as phosphoenolpyruvate carboxylase (PPC), that can no longer be regenerated due to the lack of L-threonine and the loss of protein turnover (Kiss & Stephanopoulos 1991).

4 Enhancement of L-lysine production

To increase L-lysine fermentation performance, essentially two approaches can be followed:

- manipulation of the strain to improve single cell yield and productivity or
- process manipulation to allow for the extracellular conditions that will maximise yield and productivity of the cell population.

In the next section a review of the improvements of the L-lysine fermentation performance is discussed, superficially classified as explained above.

4.1 Increase in the L-lysine flux by strain improvement

Since the wildtype of *Corynebacterium glutamicum* does not overproduce or excrete L-lysine under normal fermentation conditions, some metabolic mutation is required. Previously random mutagenesis was the standard practice for strain improvement. Even though this technique yielded various strains with industrial application, recombinant genetic technology allowed a more fundamental approach to strain manipulations. The three most basic and major L-lysine producing strain improvements with regard to the wildtype, *C. glutamicum* will be discussed in the next sections.

4.1.1 Flux increase by deregulated aspartate kinase

The aspartate kinase reaction handles 25% of the total carbon incorporated into cellular material (Neidhardt 1990). Four amino acids arise from the activated aspartate molecule. The large flux and the localisation of the kinase at the entry of the C4 unit into the highly branched pathway suggest a sensitive control of the overall activity of the enzyme. In *C. glutamicum* the enzyme activity is allosterically controlled by the combined presence of L-threonine plus L-lysine (Shiio & Miyajima 1969b), whose concentrations in the cell control the availability of these amino acids in the two major branches of the pathway.

The tight control of the kinase activity can be overcome by using the general procedure of isolation of mutants, which are resistant towards an analogue of a regulatory amino acid. Mutants of *C. glutamicum* resistant to the L-lysine analogue, S-(2-aminoethyl)-L-cysteine (AEC) have been obtained (Sano & Shiio 1970). These clones included those that are impaired in the uptake of S-(2-aminoethyl)-L-cysteine by the L-lysine import system (Seep-Feldhaus *et al.* 1991), and those with increased

availability to degrade the analogue (Rossol & Puhler 1992). The important clones are however those with the mutated aspartate kinase gene, rendering the protein insensitive to allosteric control by L-lysine plus L-threonine. Bröer *et al.* (1993) found that the strain with the adapted aspartate kinase produced 29 mM of L-lysine and no L-threonine. This shows the sufficient, but simple control of L-lysine synthesis in the wild type of *C. glutamicum*, whereas more than one enzyme tightly controls the flux of the C-4 unit, aspartate, towards L-threonine or iso-leucine.

These strains can be used profitably to produce L-lysine when the L-threonine concentration is low (Shiio & Sano 1969b). The L-threonine limitation can be introduced into the fermentation by chemical engineering techniques (Kiss & Stephanopoulos 1991).

It also has to be considered that a general limitation might be advantageous for overproduction as has long been known for *Klebsiella pneumoniae*, which can excrete pyruvate, oxoglutarate or acetate depending on the kind of growth limitations (Tempest & Neijssel 1992). Patek *et al.* (1994) found that strains with reduced L-leucine production accumulated higher quantities of L-lysine. This is in accord with the idea that a general limitation is advantageous for overproduction.

4.1.2 Flux increase by increasing the dihydrodipicolinate synthase activity

Within the pathway of L-lysine synthesis, there are two split nodes to other amino acids (Figure 1-2). One is the branch point at the level of D, L-diaminopimelate to cell wall synthesis. Little is known on the regulation of this branch point in *C. glutamicum*, except that diaminopimelate decarboxylase and arginyl t-RNA synthetase forms an operon (Marcel *et al.* 1990; Sharp & Mitchell 1993). A biological role for this connection is unclear, but the gene arrangement is suggestive for an interconnection of amino acid synthesis at a different level than carbon flux.

The second branch point is at the level of aspartate semialdehyde where it has long been known that L-homoserine dehydrogenase is inhibited in its activity by L-threonine and repressed in its synthesis by L-methionine (Miyajima *et al.* 1968; Follettie *et al.* 1988). Recently it has been shown that dihydrodipicolinate synthase is also involved in flux control (Eggeling 1994), since over-synthesis of the wild type enzyme resulted in L-lysine excretion in the wild type background (Cremer *et al.* 1991). It must therefore be concluded that the total amount of enzyme is critical.

If a stationary picture of flow can be drawn at all, then the synthase could function as a kind of barrier. The homoserine dehydrogenase has a high affinity towards the aldehyde, but the synthase a low one (Tosaka *et al.* 1979). The dehydrogenase therefore preferentially converts the aldehyde to L-threonine. When the dehydrogenase activity decreases in response to L-threonine, an increased aspartate semialdehyde concentration becomes available to the synthase to be converted to L-

lysine. In accord with this critical control of the synthase, the amplitude of its variations is at best threefold (Cremer *et al.* 1988). Also the structural elements in front of the gene point to a tight control mechanism (Bonnassie *et al.* 1990; Pisabarro *et al.* 1993). This renders the aldehyde branch point as a very good candidate for manipulation. Synthase over-expression also results in increased L-lysine yields in strains with feedback resistant aspartate kinase (Cremer *et al.* 1991).

4.1.3 Attempts to quantify and optimise the total metabolite flux

Deregulation of the L-lysine synthesis, however, does not result in the maximum yield of lysine on glucose (75% molar) (Kiss & Stephanopoulos 1991). Although these previously discussed approaches have produced mutants exhibiting increased rates of product formation, they do not necessarily improve the fermentation yield. Increasing fermentation yield presents additional difficulties, for it requires redirecting the cellular metabolism in favour of the desired product, opposed to biomass or other side product formation. This required analysis of the entire flux in the cell from the glucose substrate to the amino acid product.

Ishino *et al.* (1991) compared glutamate and L-lysine excreted by mutants of *C. glutamicum* by the use of 13-C labelled glucose. From the finally accumulated label in L-lysine, it was estimated that 60-70% of the carbon flux is via the pentose phosphate pathway while only 20% of the flux proceeds to glutamate formation.

In an entirely different approach, Vallino & Stephanopoulos (1993) used metabolite balances to calculate the absolute flux rates through the main biochemical pathways by assuming a simplified metabolism. The data are in accord with the general view that the pentose phosphate pathway (Yamaguchi *et al.* 1986) and phosphoenolpyruvate carboxylase (O'Reagan *et al.* 1989) may support significant fluxes for L-lysine synthesis.

Peters *et al.* (1993) showed that phosphoenolpyruvate carboxylase inactivation does not effect L-lysine or glutamate secretion. This implies either that the previous assumptions used for modelling were incorrect or the cell has an enormous flexibility, which still has to be discovered.

Flux analysis techniques primed work for the modification of enzymes of the primary metabolism such as citrate synthase (Shiio *et al.* 1959), the pyruvate dehydrogenase complex (Ozaki & Shiio 1983; Tosaka *et al.* 1985), pyruvate kinase (Shiio *et al.* 1990; Shiio *et al.* 1987) and phosphoenolpyruvate carboxylase (Yokota & Shiio 1988). These modifications have resulted in a strain that produces L-lysine at a 55% molar yield (Shiio *et al.* 1984b) although it is not known in what respect this strain differs from the parent strain.

4.2 Increase in the lysine production through process manipulation

The volumetric productivity and process yield of the L-lysine fermentation can also be improved by manipulation of the process parameters. Knowledge of the impact of process parameters on cell metabolism allows optimal operation of the fermentation process. In this section, the effect of the environmental and process variables on the microbial metabolism with regard to L-lysine production will be discussed followed by some fed-batch operational strategies. Lastly biomass recycling, a relatively new technique for improvement of the fermentation performance, will be discussed.

4.2.1 Effects of environmental and process variables

The major environmental and process variables that influence the fermentation performance relate to the medium composition and the availability of oxygen.

4.2.1.1 Oxygen availability

Oxygen is required in large quantities by the microbial catabolism or energy generation metabolism in *C. glutamicum.* In most amino acid fermentations, the high metabolic requirement for oxygen, rendered oxygen mass transfer the single most limiting process variable (Akashi *et al.* 1979). Oxygen is transferred from the gaseous phase to the liquid phase where it can be utilised by the cells. The rate of mass transfer to the liquid phase can be described by:

$$OTR = k_l a(C_{o2,sat} - C_{o2}) \qquad (1\text{-}1)$$

where k_la is the liquid interface mass transfer coefficient (h^{-1}), $C_{o2,sat}$ is the dissolved oxygen saturation concentration (mmol/l) and C_{o2} the actual dissolved oxygen concentration (mmol/l).

The volumetric liquid interface mass transfer coefficient (k_la) depends on the medium composition, viscosity and the hydrodynamic conditions in the bioreactor. The impact of various variables, relating to the availability of oxygen to the cell, such as dissolved oxygen concentrations (Akashi *et al.* 1979; Hilliger & Hanel 1981), redox potential (Radjai *et al.* 1984) and power input (Hilliger *et al.* 1984) on the L-lysine fermentation performance have been studied extensively.

Radjaj *et al.* (1984) found that the amino acid productivity can be influenced by the availability of oxygen in the fermenter. Low oxygen availability generally favours lactate formation while higher oxygen availability leads to L-lysine production. Since it was not possible to measure the low dissolved oxygen levels of the fermentation medium, redox potential was used as indirect measurement of the dissolved oxygen concentration (DO). Radjaj *et al.* (1984) developed a control algorithm to maintain the DO at a level ideal for L-lysine production.

The magnitude of the impact of oxygen availability is strain specific. Generally however, oxygen limitation causes a decrease in biomass yields, substrate consumption and L-lysine production, concomitant with the formation of by-products such as acetate, L-alanine and L-valine (Hilliger *et al.* 1984).

4.2.1.2 The impact of media composition on fermentation performance

It is well established that the external environment of the cell influences the cell's metabolism. This environment is made up of the hydrodynamic conditions as well as the chemical composition of the surrounding media. The effect of a specific substrate on the cell depends on the metabolic state of the cell, the concentrations of various other substrates present at that point in time as well as the history of the cell and its surroundings. The large number of interacting variables cannot be regarded as a simple system and any discussion with regard to the manipulation of the extracellular environment must be seen in this context. The following discussion therefore only gives a very general description of the impact of each of the major external metabolites.

- Carbohydrate

  In most of the published experimental work, glucose has been used as carbon source. Glucose can however, be substituted by sucrose or even a combination of sugars such as that found in molasses (Hadj Sassi *et al* 1988; Lee *et al.* 1995). Gluconate (Lee *et al.* 1995) lactic acid and acetic acid (Cocaign *et al.* 1993) have been used as secondary carbon sources with different impacts on the cellular metabolism.

  In batch fermentations Hadj Sassi *et al.* (1988) found that at low glucose concentrations (50-60 g/l) biomass production was favoured over L-lysine formation. The biomass yield decreased while the L-lysine yield increased with increasing glucose concentration. In continuous cultures, the same but more marked effect was reported. No L-lysine formation was seen under glucose limited conditions (Hadj Sassi *et al.* 1988; Coello *et al.* 1992). When glucose was limited, the carbohydrates were converted mainly to biomass and both product and by-product formation was minimised.

  Weuster-Botz *et al.* (1997), however, showed that in fed-batch cultures a constant set-point of 2-20 g/l glucose as well as a variable setpoint within this range had no effect on the specific L-lysine production rate and differential L-lysine selectivity. This was confirmed by Kelle *et al.* (1996). It is suggested that as long as glucose remains available for L-lysine synthesis there is not an optimum carbohydrate concentration that will allow maximal productivity and product yields (Weuster-Botz *et al.* 1997). The availability of glucose to the cell would however depend on the bioreactor configuration and the nature of the feed (Lee *et al.* 1995).

- Auxotrophic amino acids
  Due to strain manipulation, most of the industrial strains used for L-lysine production are auxotrophic for some amino acids (L-threonine, L-methionine and L-leucine). As the cell has lost the ability to produce the specific amino acids, these must be supplemented to allow functioning of the cell's metabolism for biomass production. Upon depletion, cell growth generally seizes and viability is lost soon after (Lee *et al.* 1995).

  Most L-lysine producing auxotrophic strains are susceptible to back-mutation or reversion (Kiss & Stephanopoulos 1992b). The revertant cells no longer overproduce the desired product (L-lysine), and are also not limited in their growth by the low levels of the auxotrophic amino acid. Kiss & Stephanopoulos (1992b) have shown that, although long-term culture demise is inevitable, the dimensionless ratio of two limiting substrates controls the rate of take-over by the non-productive cells. Their analysis demonstrated the importance of proper medium design in delaying the onset of take-over.

- Nitrogen sources
  The internal pathway followed for lysine production depends on the nature and the availability of the nitrogen source (Eggeling 1994). Hadj Sassi *et al.* (1990) evaluated different inorganic nitrogen sources. They found that ammonium sulphate gave the highest L-lysine productivity when compared to ammonium chloride, tri-ammonium phosphate, di-ammonium hydrogenphosphate, di-ammonium hydrogencitrate and urea.

- Phosphates
  Phosphate is an important metabolite in the catabolism of microbial cells. Despite being present in the cell wall, it also plays an important role in the chemistry of ATP, the cell's universal energy carrier.

  Büchs *et al.* (1988) showed that the phosphorus content of *C. glutamicum* has a distinct influence on the cell wall properties of the cell, resulting in a variation on the flocculation and adsorption behaviour. The cell wall of gram-positive cells such as *C. glutamicum,* consists of teichoic acids in non-limiting phosphate conditions. Under phosphorus deprived conditions the teichoic acids can be almost completely replaced by teichuronic acids (Ellwood & Tempest 1972).

  The phosphate content of the medium determines to a large extent the surface properties of *C. glutamicum* cells. Cells saturated with phosphate are hydrophobic and show a high tendency to flocculate and adsorb onto treated glass surfaces due to hydrophobic interactions. Phosphate depletion of the cells led to a more hydrophilic surface character and a comparatively low ability to flocculate and to adhere. (Büchs *et al.* 1988)

Besides the effect on surface properties, phosphate depletion down to 20% of saturation was shown to have no effect on growth rate and on amino acid productivity (Büchs *et al.* 1988). In phosphate limiting conditions at low growth rates, L-lysine production can be favoured (Coello *et al.* 1992).

4.2.1.3 Optimal media compositions

Various investigators used empirical approaches to optimise the media composition for a specific strain (Hadj Sassi *et al.* 1988; 1990; Sweeting *et al.* 1990; Weuster-Botz *et al.* 1997). Genetic algorithms, statistical surface response methods and other statistical methods gave an optimum composition based on the experimenters definition of optimality (Weuster-Botz *et al.* 1997). Truly optimal medium compositions may vary with time during the course of the fermentation. Such operating procedures can be realised by using fed-batch or continuously operated fermentations.

4.2.2 Fed-batch fermentation techniques

Lysine overproduction is associated with a specific metabolic state of the cell (Kiss & Stephanopoulos 1991; Kwong & Rao 1991; Rutkov 1984; Modak *et al.* 1986; Liu *et al.* 1993). L-lysine productivity can be dramatically improved if the cells can be maintained in the metabolic state of overproduction for longer periods.

Control of metabolic activity through manipulation of the environment is a useful feedback controlled method of addressing the time varying nature of the optimal fermentation rate. The most representative example of control of metabolic activity is fed batch fermentation of baker's yeast. Overfeeding of sugars results in ethanol formation and poor biomass yield, even under aerobic conditions (Crabtree effect), while underfeeding causes starvation, deterioration of specific growth rate, leading to low volumetric productivities. These opposing effects are optimally balanced by regulating the sugar feed rate to maintain the optimal sugar concentration for growth.

Various restrained growth fed-batch fermentation techniques have been suggested to maintain the L-lysine overproduction metabolic state. These are described below:

4.2.2.1 Fed-batch configuration at constant feed rate

The bioreactor is operated in batch model until L-lysine overproduction starts. At that point the fed-batch configuration may be assumed at a constant feed rate. The composition and feeding rates are calculated to correspond to the substrate consumption rate for maximum L-lysine production. No measurements are taken and the feed is normally initiated based on previous batch data. This approach is very susceptible to process disturbances and the true optimum is never reached due to inherent process variations (Weuster-Botz 1997).

4.2.2.2 Substrate controlled fed-batch technique

In the substrate controlled fed-batch technique, a specific substrate (such as the carbon source (Weuster-Botz *et al.* 1997)) concentration in the bioreactor is controlled at a constant concentration. This concentration is selected from previous optimisation experiments and economical considerations. A feedback control algorithm is normally used to maintain this concentration. The substrate concentration can either be measured (Weuster-Botz *et al.* 1997) directly or inferred from a process model predicting the substrate concentration in the bioreactor based on more accessible measurements (Yet-Pole *et al.* 1996; Linko *et al.* 1995).

4.2.2.3 Feed rate profiles – optimal control theory

Optimal control theory involves setting up a model to predict the fermentation performance. Based on some easy measurements of some process variables, the process performance is predicted. The manipulated variables are then adjusted according to model predictions to allow for optimal operation (Ohno & Nakanishi 1976; Modak *et al.* 1986).

This type of approach depends critically on the quality of the mathematical model used to describe the fermentation dynamics. In addition, the open loop structure of optimal control is usually inadequate for biological processes due to the large variability in inoculum quality, nature of the medium, and even bioreactor operation (Kiss & Stephanopoulos 1991).

Formulation of the optimisation problem with a feedback structure would address such inherent problems associated with open loop control but may require extensive on-line bioreactor measurements. These measurements, such as biomass, substrate, and product concentrations, are still largely unavailable online. Estimation algorithms can reduce the number of required measurements but are complex and subject to sensitivity and error propagation (Grosz *et al.* 1984).

4.2.2.4 Direct metabolic activity control

In this approach, key environmental parameters are manipulated to maintain a specific metabolic activity. Direct approaches to metabolic activity control include the use of the respiratory quotient as an indirect measure of metabolic activity (Kiss & Stephanopoulos 1991; Wang *et al.* 1977; Spruytenberg *et al.* 1979).

Kiss & Stephanopoulos (1991) manipulated the metabolism to favour the desired pathway for L-lysine production through control of the microbial environment. The control strategy aimed to provide an environment, which maximised the L-lysine yield and specific productivity and maintained the cell population for extended fermentation times. Because of the difficulty in finding a complete on-line bioreactor

state estimate, respiratory measurements were used as an indirect indicator of metabolic activity.

4.2.3 Biomass recycling

Biomass re-use, recycling or retention offer important advantages when the process micro-organisms are slow growing or strongly affected by product inhibition (Hammer 1982). Besides the wastewater industry, cell recycling has been applied successfully to ethanol production (Kargupta *et al.* 1998).

Since L-lysine is predominately a secondary metabolite, maximum L-lysine yields from carbohydrates are achieved at very low growth rates. To maximise the volumetric productivity of fed-batch bioreactors, feed and bleed strategies are often employed. Alternatively the fermentation is stopped when the bioreactor reaches the maximum volume. Either way biomass discarded from the reactor is still capable of L-lysine production. In an effort to extend the productive life span of the biomass, Sweeting *et al.* (1990) re-used the biomass for 6 production cycles in the presence of the auxotrophic amino acids.

In this thesis biomass recycling using cross flow filtration was studied to understand, model and optimise the performance of the L-lysine fermentation.

5 References

Akashi, K., Shibai, H. and Hirose Y. (1979), Effect of oxygen supply on L-lysine, L-Threonine and L-Isoleucine Fermentations, *Agric. Biol. Chem.* **43**, 2087-2092

Beppu, T. (1986), "Biotechnology of Amino Acid Production"; Aida, K. Chibata, J. Nakayama, K. Takinami, K. and Yamada, H. Eds. Elsevier, NY, pp 24-35

Bonnassie, S., Oreglia, A. M. and Sicard, J. (1990), Nucleotide sequence of the dapA gene from *Corynebacterium glutamicum*, *Nucleic Acids Res.* **18**, 6421

Bröer, S. and Kramer, R. (1991), Lysine excretion by *Corynebacterium glutamicum*_2. Energetics and mechanism of the transport System, *Eur. J. Biochem.* **202**, 137-143

Bröer, S., Eggling, L. and Kramer, R. (1993), Strains of *Corynebacterium glutamicum* with different lysine productivities may have different lysine excretion systems, *Appl. Environ. Microbiol.* **59**, 316-321

Büchs, J., Mozes, N., Wandrey, C. and Rouxhet, P. G. (1988), Cell adsorption control by culture conditions, *Appl. Microbiol. Biotechnol.* **29**, 119-128

Business Communications Company, August 2000, Section B, pp 45

Cocaign, M., Monnet, C. and Lindley, N. D. (1993), Batch kinetics of *Corynebacterium glutamicum* during growth on various carbon substrates: use of substrate mixtures to localise metabolic bottlenecks. *Appl. Microbiol Biotechnol.* **40,** 526-530

Coello, N., Pan, J. G. and Lebeault, J. M. (1992), Physiological aspects of L-lysine production: effect of nutritional limitations on a producing strain of *Corynebacterium glutamicum, Appl. Microbiol. Biotechnol.* **38,** 259-262

Cremer, J., Eggeling, L. and Sahm, H. (1991), Control of the lysine biosynthetic sequence in *Corynebacterium glutamicum* as analysed by over-expression of the individual corresponding genes, *Appl. Environ. Microbiol..* **57**, 1746-1752

Cremer, J., Treptow, C., Eggling, L. and Sahm, H. (1988), Regulation of enzymes of lysine biosynthesis in *Corynebacterium glutamicum*, *J. Gen. Microbiol.* **134**, 3221-3229

Crueger, W. and Crueger, A. (1984), Strain development, In "Biotechnology: A textbook of industrial microbiology", T. D. Brock (ed.), Sinauer Associates, Sunderland, MA, pp 9-48

Dairaku, K., Izumoto, E., Morikawa, H., Shioya, S. and Takamatsu, T. (1983), An advanced microcomputer coupled control system in a bakers yeast fed-batch culture using a tubing Method, *J. Ferment. Technol.* **61**(2), 189-196

Eggeling, L. (1994), Biology of L-lysine overproduction by *Corynebacterium glutamicum*, *Amino Acids*, **6**, 261-272

Eikmanns, B. (1992), Identification, sequence analysis and expression of a *Corynebacterium glutamicum* gene cluster encoding the three glycolytic enzymes: glyceraldehyde-3-phosphate dehydrogenase, 3-phosphoglycerate kinase and triosephosphate isomerase, *J. Bacteriol.* **174**, 6067-6086

Ellwood, D. C. and Tempest, D. W. (1972), Effects of environment on bacterial wall content and composition, *Adv. Microbiol Physiol.* **7**, 83-117

Follettie, M. T., Shin, H. K. and Sinskey, J. A. (1988), Organisation and regulation of the *Corynebacterium glutamicum hom-thrB* and *thrC* loci, *Mol. Microbiol.* **2**, 53-62

Grosz, R., Stephanopoulos, G. and San, K. -Y. (1984), Studies on on-line bioreactor identification. III. Sensitivity problems with respiratory and heat evolution measurements. *Biotechnology and Bioengineering,* **26,** 1198-1208

Gubler, M., Jetten, M., Lee, S. H. and Sinskey, A. J. (1994), Cloning of the pyruvate kinase gene (pyk) of *Corynebacterium glutamicum* and site specific inactivation of *pyk* in a lysine

producing *Corynebacterium lactofermentum* strain, *Appl. Environ. Microbiol.* **60,** 2494-2500

Hadj Sassi, A., Queric, M. P., Deschamps, A. M. and Lebeault, J. M. (1988), Optimisation of L-lysine production by *Corynebacterium sp.* in fed batch cultures, *Biotechnology Letters,* **10**(3), 583-586

Hadj Sassi, A., Coello, N., Deschamps, A. M. and Lebeault, J. M. (1990), Effect of medium composition on L-lysine production by a variant strain of *Corynebacterium glutamicum* ATCC 21513, *Biotechnology Letters*, **12**(4), 295-298

Hammer, G. (1982), Recycle in fermentation processes, *Biotechnology and Bioengineering*, **24**, 511

Hilliger, M and Hanel, F. (1981), Process analysis of L-lysine fermentation under different oxygen supply, *Biotechnology Letters*, **3**(5), 219-224

Hilliger, M. Möckel, H. –O. and Forberg, W. (1984), The optimisation of L-lysine fermentation and a mass transfer model, *Acta Biotechnol.* **4**(4), 355-360

Hirao, T., Nakano, T., Azuma, T., Sugimoto, M and Nakanishi, T. (1989), L-Lysine production in a continuous culture of an L-lysine hyperproducing mutant of *Corynebacterium glutamicum, Appl. Microbiol. Biotechnol.* **32**, 269-273

Hopwood, D. A. (1981), The genetic programming of industrial microorganisms, *Sci. Am.* **245**(3), 30-42

Hsiao, T-Y. and Glatz, C. E. (1996), Water reuse in the L-lysine fermentation process, *Biotechnology and Bioengineering*, **49**, 341-347

Ishino, S., Muzikami, T., Yamaguchi, K., Katsumata, R. and Araki, K. (1988), Cloning and sequencing of the meso-diaminopimelate-D-dehydrogenase (ddh) gene of *Corynebacterium glutamicum*, *Agric. Biol. Chem. Tokyo*, **48**, 2557-2560

Ishino, S., Shimomura-Nishimuta, J., Yamaguchi, K., Shirahata K. and Araki, K. (1991), 13C Nuclear magnetic resonance studies of glucose metabolism in L-glutamic acid and L-lysine fermentation by *Corynebacterium glutamicum*, *J. Gen. Appl. Microbiol Tokyo*, **37**, 157-165

Kargupta, K., Datta, S. and Sanyal, S. K. (1998), Analysis of the performance of a continuous membrane bioreactor with cell recycling during ethanol fermentation, *Biochemical Engineering Journal*, **1,** 31-37

Kelle, R., Laufer, B., Brunzema, C., Weuster-Botz, D., Krämer, R. and Wandrey, C. (1996), Reaction engineering analysis of L-lysine transport by *Corynebacterium glutamicum. Biotechnology and Bioengineering,* **51,** 40-50

Kiss, R. D. and Stephanopoulos, G. (1991), Metabolic activity control of the L-lysine fermentation by restrained growth fed-batch strategies. *Biotechnol. Prog.* **7**, 501-509

Kiss, R. D. and Stephanopoulos, G. (1992a), Metabolic characterisation of an L-lysine producing strain by continuous culture, *Biotechnology and Bioengineering*, ***39, 565-574***

Kiss, R. D. and Stephanopoulos, G. (1992b), Culture instability of auxotrophic amino acid producers, *Biotechnology and Bioengineering,* **40**, 75-85

Kwong, S. C. W. and Rao, G. (1991), Utility of culture redox potential for identifying metabolic state changes in amino acid fermentation, *Biotechnology and Bioengineering*, **38**, 1034-1040

Lee, H. W., Pan, J. G. and Lebeault, M. (1995), Characterisation of kinetic parameters and metabolic transitions of *Corynebacterium glutamicum* on L-lysine production on continuous culture, *Appl. Microbiol. Biot.* **43**, 1019-1027

Linko, S., Rajalathi, T. and Zhu, Y. –H. (1995), Neural state estimation and prediction in amino acid fermentation, *Biotechnology Techniques,* **9**(8), 607-612

Lui, Y. C., Wu, W. T. and Tsao, J. H. (1993), Fed-batch culture for L-lysine production via on-line state estimation. *Bioprocess Eng.* **9**(4), 135-139

Marcel, T., Archer, J. A. C., Mengin-Lecreulx, D. and Sinskey, A. J. (1990), Nucleotide sequence and organisation of the upstream region of the *Corynebacterium glutamicum lysA* gene, *Mol. Microbiol.* **4**, 1819-1830

Matsumoto, S. (1985), A method for producing L-lysine, EP 0 175 309 A2

Menkel, E., Thierback, G., Eggling, L. and Sahm, H. (1989), Influence of increased aspartate availability on lysine formation by a recombinant strain of *Corynebacterium glutamicum* and utilisation of fumarate, *Appl. Environ. Microbiol.* **55**(3), 684-688

Misono, H. and Soda, K. (1980), Properties of meso-diaminopimelate D-hydrogenase from *Bacillus sphaericus sp*, *J. Biol Chem.* **255**, 10599-10605

Misono, H., Togawa, K., Yamamoto H. and Soda, T. (1979), Meso-Diaminopimelate D-dehydrogenase: Distribution and the reaction product, *J. Bacteriol.* **137**, 22-27

Miyajima R., Otsuka, S. and , I. (1968), Regulation of aspartate family amino acid biosynthesis in *Brevibacterium flavum*. Inhibition by amino acids of enzymes in threonine Biosynthesis, *J. Biochem (Tokyo)*, **63**, 139-148

Modak, J. M., Lim, H. C. and Tayeb, Y. J. (1986), General characteristics of optimal feed rate profiles for various fed-batch fermentation processes. *Biotechnology and Bioengineering,* **28,** 1396-1407

Nakanishi, T., Hirao, T. and Sakurai, M. (1987), Process for producing L-lysine by fermentation, US Patent 4,657,860

Nakayama, K. (1985), Lysine, In "Comprehensive biotechnology", H. W. Blanch, S. Drew, D. I. C. Wang (eds.), Vol 3, Pergamon Press, New York, pp 607-620

Nakano, T., Azuma, T. and Kuratsu, Y. (1994), Process for producing L-lysine by iodothyrosine resistant strains of *Corynebacterium glutamicum,* US Patent 5,302,521

Neidhardt, F. C. (1990), "Physiological of the bacterial cell: A molecular approach", Sinauer Associates, Sunderland MA

Oh, N. S. and Sernetz, M. (1993a), Turnover characteristics in continuous L-lysine fermentation, *Appl. Microbiol. Biotechnol.* **39,** 691-695

Oh, J. W., Kim, S. J., Cho, Y. J., Park, N. H. and Lee, J. H. (1993b), Strains of *Corynebacterium glutamicum* and method for producing L-lysine, US Patent 5,268,293

Ohno, H. and Nakanishi, E. (1976), Optimal control of a semibatch fermentation. *Biotechnology and Bioengineering,* **18,** 847-864

O'Reagan, M., Thierbach, G., Bachmann, B., Villeval, V., Lepage, P., Viret, J. and Lemoine, Y. (1989), Cloning and nucleotide sequence of the phosphoenolpyruvate carboxylase coding gene of *Corynebacterium glutamicum* ATCC 13032, *Gene,* **77**, 237-251

Ozaki, H. and Shiio, I. (1983), Production of lysine by pyruvate kinase mutants of *Brevibacterium flavum, Agric. Biol. Chem.* **47,** 1569-1576

Patek, M., Krumbach, K., Eggling, L. and Sahm, H. (1994), Leucine synthesis in *Corynebacterium glutamicum* enzyme activities, structure of *leuA*, and effect of *leuA* inactivation on lysine synthesis, *Appl. Environ. Microbiol.* **60**, 133-140

Peters, P., Eikmans, B. J., Thierbach, G. and Sahm, H. (1993), Phosphoenolpyruvate carboxylase in *Corynebacterium glutamicum* is dispensable for growth and lysine production, *FEMS Microbiol. Lett.* **112**, 269-274

Pisabarro, A., Malumbres, M., Mateos, L. M., Oguiza, J. A. and Martin, J. F. (1993), A cluster of three genes (*dapA, orf2* and *dapB*) of *Brevibacterium lactofermentum* encodes dihydrodipicolinate synthase, dihydrodipicolinate reductase, and a third polypeptide of unknown function, *J. Bacteriol.* **175**, 2743-2749

Presscott, L. M., Harley, J. P. and Klein, D. A. (1996), "Microbiology", WCB Publishers

Radjai, M. K., Hatch, R. T. and Cadman, T. W. (1984), Optimisation of amino acid production by self-tuning digital control of redox potential, *Biotechnology and Bioengineering Symposium*, **14**, 657-679

Rossol, I. and Puhler, A. (1992), The *Corynebacterium glutamicum aecD* gene encodes a C-S lyase with a,b-elimination activity that degrades aminoethylcysteine, *J. Bacteriol.* **174**, 2968-2977

Rutkov, A. B. (1984), Microbiological production of L-lysine by employing fed batch cultivation, *Bulg. Akad. Nauk.* **37**(12), 1677-1680

Sahm, H. (1995), Metabolic design in the amino acid producing bacterium *Corynebacterium glutamicum*, *Folia Microbiol.* **40**(1), 23-30

Sano, K. and Shiio, I. (1970), Microbial production of L-lysine III. production by mutants resistant to S-(2-aminoethyl)-L-cysteine, *J. Gen. Appl. Microbiol.* **16**, 373-391

Sano, K., Ito, K., Miwa, K. and Nakamori, S. (1987), Amplification of the phosphoenolpyruvate carboxylase gene of *Brevibacterium lactofermentum* to improve amino acid production, *Agric. Biol. Chem.* **51**(2), 597-599

Schrumpf, B., Eggling, L. and Sahm, H. (1992), Isolation and prominent characteristics of a L-lysine hyperproducing strain of *Corynebacterium glutamicum*, *Appl. Microbiol. Biotechnol.* **37**, 566-571

Schrumpf, B., Schwarzer, A., Kalinowski, J., Puhler, A., Eggling, L. and Sahm, H. (1991), A functionality split pathway for lysine synthesis in *Corynebacterium glutamicum*, *J. Bacteriol.* **173**, 4510-4516

Seep-Feldhaus, A. H., Kalinowski, J. and Pühler, A. (1991), Molecular analysis of the *Corynebacterium glutamicum lysI* gene involved in lysine uptake, *Mol. Microbiol.* **5,** 2995-3005

Sharp, P. M. and Mitchell, K. J. (1993), *Corynebacterium glutamicum* Arginyl-tRNA Synthase. *Mol. Microbiol.* **8**, 200-205

Shiio, I., Otsuka, S. –I. and Tsunoda, T. (1959), Glutamic acid formation from glucose by bacteria. I. Enzymes of the Embden-Meyerhof-Parnas pathway, the Krebs cycle and the glyoxylate bypass in cell extracts of *Brevibacterium flavum, J. Biochem.* **46,** 1303-1311

Shiio, I., Sugimoto, S. –I. and Kawamura, K. (1990), Effects of carbon source sugars on the yield of amino acid production and sucrose metabolism in *Brevibacterium flavum, Agric. Biol. Chem.* **54,** 1513-1519

Shiio, I. and Miyajima, R. (1969a), Concerted inhibition and its reversal by end products of aspartate kinase in *Brevibacterium flavum, J. Biol. Chem. (Tokyo)*, **65**, 849-859

Shiio, I. and Sano, K. (1969b), Microbial production of l-lysine II. Production by mutants sensitive to threonine or methionine, *J. Gen. Appl. Microbiol.* **15**, 267-287

Shiio, I., Ozaki, H., Ujigawa-Takeda, K. (1982), Production of aspartic acid and L-lysine by citrate synthase mutants of *Brevibacterium flavum, Agric. Biol. Chem.* **46,** 101-107

Shiio, I., Sugimoto, S. –I., and Toride, Y. (1984a), Studies on mechanisms for lysine production by pyruvate kinase-deficient mutants of *Brevibacterium flavum, Agric. Biol. Chem.* **48,** 1551-1558

Shiio, I., Toride, Y. and Sugimoto, S. –I. (1984b), Production of lysine by pyruvate dehydrogenase mutants of *Brevibacterium flavum. Agric. Biol. Chem.* **48,** 3091-3093

Shiio, I., Yokota, A. and Sugimoto, S. –I. (1987), Effects of pyruvate kinase deficiency on L-lysine productivities of mutants with feedback resistant aspartokinases, *Agric. Biol. Chem.* **51,** 2485-2493

Shimazaki, K., Nakamura, Y. and Yamada, Y. (1983), Method for producing L-lysine by fermentation, US Patent 4,411,997

Sonntag, K., Eggeling, L., De Graaf, A. A. and Sahm, H. (1993), Flux partitioning in the split pathway of lysine synthesis in *Corynebacterium glutamicum*. Quantification by 13C- and 1H-NMR spectroscopy, *Eur. J. Biochem.* **213**, 1325-1331

Spruytenberg, R., Dunn, I. J. and Bourne, J. R. (1979), Computer control of a glucose feed to a continuous aerobic culture of *Saccharomyces cerevisae* using the respiratory quotient, *Biotechnology and Bioengineering Symposium,* **9,** 359-368

Stephanopoulos, G. and Vallino, J. J. (1991), Network rigidity and metabolic engineering in metabolite overproduction, *Science*, **252**, 1675-1681

Sung, H-C., Takahasi, M., Tamaki, H., Tachiki, T., Kumagai, H. and Tochikura, T. (1985), Ammonia assimilation by glutamine synthetase/glutamate synthase system in *Brevibacterium flavum, J. Ferment. Technol.* **63**, 5-19

Sweeting, K. B., Sauer, E. C., Chotani, G., Smith, C. and LaDuca, J. (1990), Strategies for reuse of bacteria for the production of amino acids, *Acta Biotechnol.* **4**(4) 983-986

Tempest, D. W. and Neijssel, O. M. (1992), Physiological and energetic aspects of bacterial metabolite overproduction, *FEMS Microbiol. Lett.* **100,** 169-176

Tosaka, O., Takinami, K. and Hirose, V. (1978), L-Lysine production by S-(2-aminoethyl)-L-cysteine and a-amino- b-hydroxyvaleric acid resistant mutants of *Brevibacterium lactofermentum, Agric. Biol. Chem.* **42**, 745-752

Tosaka, O., Ishihara, M., Morinaga, Y. and Takinami, M. (1979), Mode of conversion of Asparto semialdehyde to L-threonine and L-lysine in *Brevibacterium lactofermentum, Agric. Biol. Chem.* **43,** 265-270

Tosaka, O., Yoshihara, Y., Ikeda, S., and Takinami, K. (1985), Production of L-lysine by fluoropyruvate-sensitive mutants of *Brevibacterium flavum, Agric. Biol. Chem.* **49,** 1305-1312

Vallino, J. J. and Stephanopoulos, G. (1993), Metabolic flux distributions in *Corynebacterium glutamicum* during growth and lysine overproduction, *Biotechnology and Bioengineering,* **41**, 633-646

Vallino, J. J. (1991), Identification of branch-point restrictions in microbial metabolism through metabolic flux analysis and local network perturbations, PhD Thesis, Massachusetts Institute of Technology, Cambridge, MA, USA

Wang, H., Cooney, C. L. and Wang D. I. C. (1977), Computer aided baker's yeast fermentations, *Biotechnology and Bioengineering 19*, 69-86

Weinberger, S. and Gilvarg, C. (1970), Bacterial distribution of the use of succinyl and acetyl blocking groups in diaminopimelic acid biosynthesis, *J. Bacteriol.* **101**, 323-324

Weuster-Botz, D., Kelle, R., Frantzen, M. and Wandrey, C. (1997), Substrate controlled fed-batch production of L-lysine with *Corynebacterium glutcamicum, Biotechnol. Prog.* **13,** 387-393

Yamaguchi, K., Ishino, S., Araki, K. and Shirahata, K. (1986), 13-NMR Studies of the lysine fermentarion with*Corynebacterium glutamicum* mutant, *Agric. Biol. Chem.* **50**, 2453-2459

Yeh, P., Sicard, A. M. and Sinskey, A. J. (1988), General organisation of the genes specifically involved in the diaminopimelate-lysine biosynthetic pathway of *Corynebacterium glutamicum, Mol. Gen. Genet.* **212**, 105-111

Yet-Pole, I., Wu, W-T. and Liu, Y-C. (1996), Neural network modelling for on-line state estimation in fed-batch culture of l-lysine production, *Chemical Engineering Journal*, **61**, 35-40

Yokata, A. and Shiio, I. (1988), Effects of reduced citrate synthase activity and feedback-resistant phosphoenolpyruvate carboxylase on lysine productivities of *Brevibacterium flavum, Agric. Biol. Chem.* **52**(2), 455-463

Yoshihara, Y., Kawahara, Y. and Ikeda, S. (1993), Fermentation process for producing L-lysine, Us Patent 5,179,010

Factors Affecting the Cross-Flow Filtration Flux of Suspensions of *Corynebacterium glutamicum* Cells

1 Introduction

The L-lysine fermentation performance can be enhanced by continuously withdrawing broth and recycling the biomass to the reactor. The biomass in the reactor outlet can be separated from the spent medium using cross-flow filtration before being recycled to the reactor.

Cross-flow filtration is a pressure driven membrane separation process characterised by the perpendicular flow of the feed suspension to the permeate flow. The filtration process is based on a size exclusion mechanism whereby the solvent is forced through the membrane (driven by the pressure difference across the membrane) while the larger solutes (or suspended particles) are retained by the membrane.

Even though micro-filtration was commercialised as early as 1929 by Sartorius Werke (GmbH) in Gottingen, Germany (Belfort *et al.*1994), the principles governing the behaviour of cross-flow filtration of microbial suspensions are as yet not clearly understood. Experimental research programmes have often used ill-characterised, complex feed streams containing mixtures of molecules and particles, either or both of which may be membrane foulants. As a consequence the published literature is often conflicting to the extent that understanding the effects of even simple parameters such as the cross-flow velocity and trans-membrane pressure drop remains largely unresolved (Tarleton & Wakeman 1993). Theoretical work has been hampered by conflicting experimental data. The models produced whilst attempting to solve an inherently complex problem seem to be evaluated by their ability to interpret flux decline data and not on their description of particle and deposit dynamics (Tarleton & Wakeman 1993). Previous work has shown that the experimental data can be described by empirically derived relations between the flux and process parameters (Tarleton & Wakeman 1993).

The objective of this investigation was to review previous cross-flow filtration data to obtain an understanding of the published membrane fouling mechanisms and their reported impact on the filtration flux. This was followed by an experimental investigation of the factors that influence the cross-flow filtration flux of suspensions of *C. glutamicum* cells. Based on the impact of these factors, fouling mechanisms could be inferred. These formed the basis for a semi-empirical model to predict the filtration flux as a function of the operating parameters.

2 Review of current knowledge base

In this section a review of the current understanding of the cross-flow filtration fouling phenomena is presented. These include a review of filtration processes (2.1), and filtration membranes (2.2). Applications of cross-flow filtration are discussed (2.3) with emphasis on the use of cross-flow filtration in the separation of microbial suspensions. This is followed by a discussion of the factors that influence the cross-flow filtration flux (2.5) including membrane properties (2.5.1), feed stream properties (2.5.2) and operational parameters (2.5.3). Some fundamental approaches to flux decline and fouling mechanisms are discussed in the last section (2.6).

2.1 Membrane separation processes

A membrane is a thin layer of material that is capable of separating species as a function of their physical and/or chemical properties when a driving force is applied across it. Membranes may be classified by the range of materials separated and the driving forces employed. Pressure-driven membrane separation processes can be subdivided according to the size of species retained by the membrane. Table 2-1 summarises the various pressure-driven membrane separation processes. Technically relevant parameters such as the magnitude of the driving force, the mechanism of separation and the membrane structure are used to further classify the membrane separation processes.

Table 2-1. Classification of pressure driven membrane separation processes

Membrane Operation	Driving Force	Mechanism of Separation	Smallest particles retained	Membrane structure
Reverse Osmosis (RO)	Pressure 5-8 MPa	Differences in solubility and diffusivity of materials in the membrane (solution-diffusion mechanism)	Monovalent and multivalent ions such as Na^+, Cl^-, Mg^{2+} and Ca^{2+}	Dense
Nanofiltration (NF)	Pressure 0.5-1.5 MPa	Differences in size (sieving)	Molecules in the 200-500 kD range	Micropores
Ultrafiltration (UF)	Pressure 50-500 kPa	Differences in size (sieving)	Molecules in the 1000 – 80000 kD	Mesopores
Microfiltration (MF)	Pressure <500 kPa	Differences in size (sieving)	Particles and colloids greater than 0.1 μm	Macropores

2.2 Filtration membranes

Various materials are used in membrane manufacturing and can be best classified according to the manufacturing process and application.

2.2.1 Manufacturing processes

Zsigmondy's original microporous membrane was solvent cast from cellulose nitrate and cellulose acetate (Zsigmondy 1922). Depending on the application newer polymers and inorganic membranes are available with wider pH and temperature operational ranges. Typical membrane manufacturing processes are discussed by Aptel and Buckley (1996).

The membranes used in this thesis are produced from ceramic pastes derived from alumina (Al_2O_3) and zircona (ZrO_2). These pastes are extruded and then sintered at high temperatures to give macroporous supports with pore diameters larger than 1 μm. Suspensions of submicron powders are then laid on the supports in successive layers to obtain microfiltration membranes with smaller pore diameters (Aptel & Buckley 1996).

2.2.2 Membrane Structure

Since membrane filtration is a pressure-driven process, high mechanical stability is required to withstand the forces involved. An increase in the membrane thickness provides the added strength but also results in an increase in the resistance to permeate flow through the membrane. Reduced hydraulic resistance and increased mechanical stability can be obtained from membranes with a thin layer responsible for the separation properties of the membrane on a thick macroporous support to increase membrane strength (Aptel & Buckley 1996). This structure is schematically displayed in Figure 2-1.

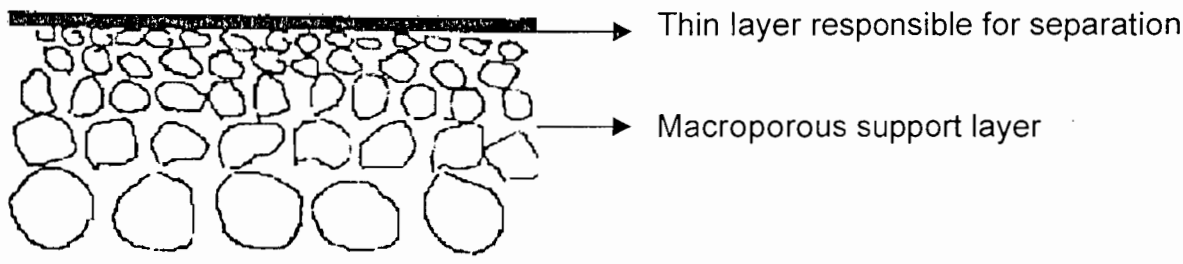

Figure 2-1. Schematic cross section of a membrane, with a thin layer responsible for the separation properties of the membrane supported on a macroporous structure.

2.2.3 Membrane Modules

The main requirements of a membrane module are to separate the feed suspension from the permeate solution or suspension and to maintain sufficient pressure drop across the membrane to obtain the desired flux and selectivity.

If the feed suspension flow is directed perpendicular to the membrane, usually with one inlet port, dead-end filtration or impact flow filtration result. It is most often used for laboratory applications or where the solid (or gel) cake formed on the membrane is the desired product. The main advantage of dead-end filtration is simplicity. The feed suspension is not recycled or passed across the membrane through costly inlet and outlet ports. The permeation flux drags all the solutes, suspended and dissolved, towards the membrane resulting in solute intrusion and adsorption into and/or deposition onto the membrane surface. A fouling cake of solutes thus forms on the membrane surface that increases in thickness with the volume of permeate flux collected. This cake offers additional resistance to flow. A point is reached at which the cake thickness has increased such that the permeation rate is no longer economical.

It was realised in the 1960's with reverse osmosis (RO), that moving the suspension tangentially to the membrane surface resulted in much higher permeation fluxes (Sieveka 1966). Re-entrainment of deposited solutes by wall shear stresses has been used to explain this improved performance. This type of flow arrangement is referred to as cross-flow filtration or tangential flow filtration. It is most often used for industrial applications where the permeate is the desired product or where the unit operation objective is to concentrate a process stream by solvent removal. The conceptual difference between dead-end and cross flow filtration is illustrated in Figure 2-2.

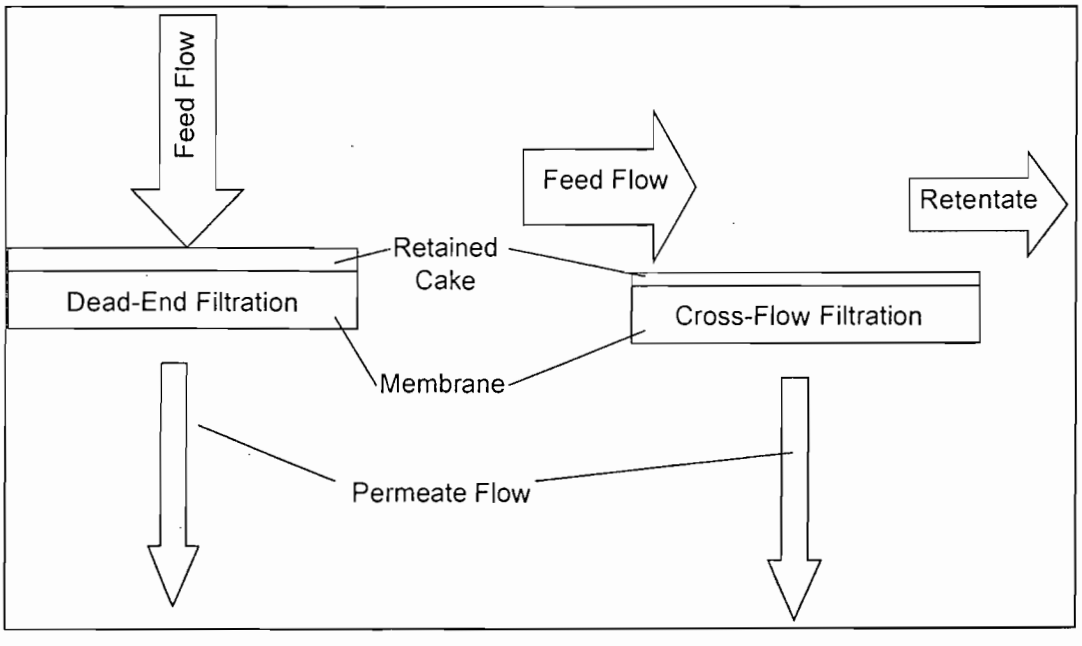

Figure 2-2. Difference between cross-flow and dead-end filtration

2.3 *Applications of cross-flow filtration*

Although there are some applications of cross-flow filtration using organic solvents, most are with aqueous suspensions containing dissolved or suspended solutes. Common variants from aqueous solvents include milk, blood, fermentation broth, paints and effluents. The solutes can vary from macromolecular molecules such as proteins or polysaccharides to particles ranging from less than 1 μm to 20 mm. Table 2-2 summarised the composition of the various streams treated by membrane cross-flow filtration techniques.

Table 2-2. Solutes and colloids in industrial fluids most relevant to microfiltration

Industrial fluid	Sizes of solutes, colloids and particles (m)					
	10^{-10} (A)	10^{-9} (nm)	10^{-8}	10^{-7} (μm)	10^{-6} (μm)	10^{-5} (μm)
					Microfiltration	
Whole milk	Lactose salts		Proteins	Fat globulets		Casein micelles
Whole Blood	Salts	Amino acids	Peptides and proteins	Platelets		Erythrocytes
Cell Culture Broth	Salts, glucose, vitamins and antibiotics	Amino acids and lipids	Proteins			Bacteria and Mammalian cells
Paints	Surfactants		Organic macromolecules			Latices
Effluents	Salts and humic and fulvic acids		Viruses			Particles

(Adapted from Aimar *et al.* 1994)

2.3.1 Cross-flow filtration of microbial suspensions

Some common applications for microfiltration of microbial suspensions are given in Table 2-3. It is important to notice that under normal operating conditions most workers, including Grabler & Ryan (1985b), Hoffman *et al.* (1987), Le and Atkinson (1985), Ryder *et al.* (1988) and Taddei & Howel (1989) have found that there is generally no significant loss of viability during cross-flow filtration. Some viability loss has been reported under high shear conditions (Nagata *et al.* 1989; Rebsamen *et al.* 1987; Tanny *et al.* 1980).

Table 2-3. Microfiltration of microbial suspensions

Application		*Reference*
Treatment of waste waters		Cheryan 1986
Continuous product removal and cell recycle during fermentation		Grabler 1985a
Downstream processing of fermentation broth		
	Cell harvesting or broth clarification	Grabler & Ryan 1985b
	Cell washing	Grabler & Ryan 1985b
	Removal of debris after cell disruption	Datar 1984; Quirck & Woodrow 1984
	Product recovery, e.g. affinity filtration	Herak & Merrill 1989; Mattiasson & Ramstrop 1984; Michales & Matson 1985

(Adapted from Lojinke *et al.*1992)

2.4 Flux decline in cross-flow filtration

The standard term for filtration rate is flux, expressed in volume of permeate per unit area of membrane per unit time (generally in l/m^2h or LMH). The filtration rate may also be expressed as a permeate velocity (in m/s). The filtration flux typically declines sharply over the first 10-30 minutes, generally to a flux of 10-50 LMH, followed by an ongoing gradual decline. This behaviour was noticed, for example by Gatenholm *et al.* (1988a), Le (1987), Le *et al.* (1984a), Matsumoto *et al.* (1987) and Reismeier *et al.* (1987). In addition, a pseudo-steady state may be reached, but some time may elapse before this happens (Bauser *et al.* 1982; Hoffman *et al.* 1987; Le & Billiet 1984; Nagata *et al.* 1989; Patel *et al.* 1987; Scott 1988; Taddei *et al.* 1990). Henry & Allfred (1972) found that up to 18 hours could be required to reach the pseudo-steady state.

It is generally believed that the flux decreases due to concentration polarisation, which is an inevitable consequence of the filtration process. The water, salts, macromolecules and the suspended material are convected towards the membrane surface where some or all of the suspended material and some macromolecules are rejected depending on the membrane pore size. The rejected material accumulates at the membrane surface, giving rise to a local concentration, substantially greater than the bulk concentration. As the concentration increases, a close packed cake forms on the membrane surface. The presence of this particulate cake at the membrane surface increases the hydraulic resistance to permeate flow, and consequently decreases the permeate flux.

Factors affecting the cross-flow filtration flux

Another source of increased permeation resistance and hence flux decline is fouling. Fouling is a blanket term used to cover the physicochemical causes of flux decline, which are not reversed when the trans-membrane pressure drop (ΔP) is relaxed. Fouling phenomena include:

- Adsorption of solutes on the membrane, both within the pores and onto the membrane surface
- Partial and complete plugging of the pores.
- Deposition of suspended material onto the membrane surface, followed by adhesion
- Consolidation of the concentration polarisation layer by chemical or physical compaction.

2.5 Factors affecting the cross-flow filtration flux

The factors that influence the flux decline rate and the pseudo-steady state flux as well as the decline rate have been classified according to the impact of the membrane properties, the feed stream properties as well as the operational parameters. These factors and their impact have been classified according to the structure depicted in Figure 2-3 for the purposes of this discussion.

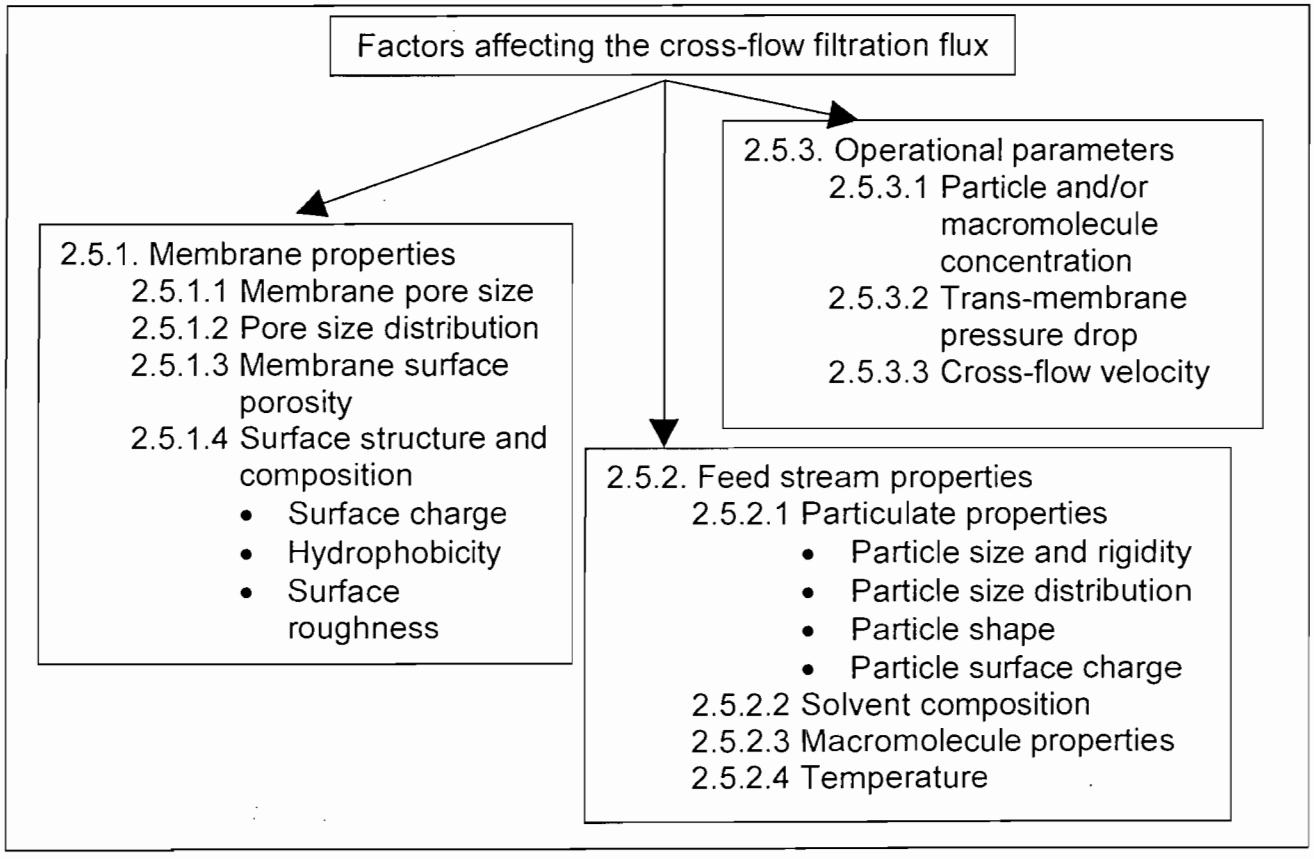

Figure 2-3. Classification of the factors that influence the cross flow filtration flux

2.5.1 Membrane Properties

The permeate flow through the membrane can be modelled by Darcy's law (Equation 2-1), which states that the flow through the membrane is proportional to the driving force (trans-membrane pressure drop) and inversely proportional to some resistance. The resistance to permeate flow is the product of the permeate viscosity and the hydraulic resistance of the membrane. The hydraulic resistance on its part is the sum of the intrinsic membrane resistance, the pore plugging resistance and the cake resistance (See Figure 2-4).

$$J = \frac{\Delta P}{\upsilon R_t} \qquad R_t = R_m + R_p + R_c \tag{2-1}$$

where J is the permeate flux (m/s), υ is the permeate viscosity (Pas), R_t is the total hydraulic resistance (m^{-1}), R_c is the cake resistance (m^{-1}), R_p is the pore plugging resistance (m^{-1}) and R_m is the intrinsic membrane resistance (m^{-1}).

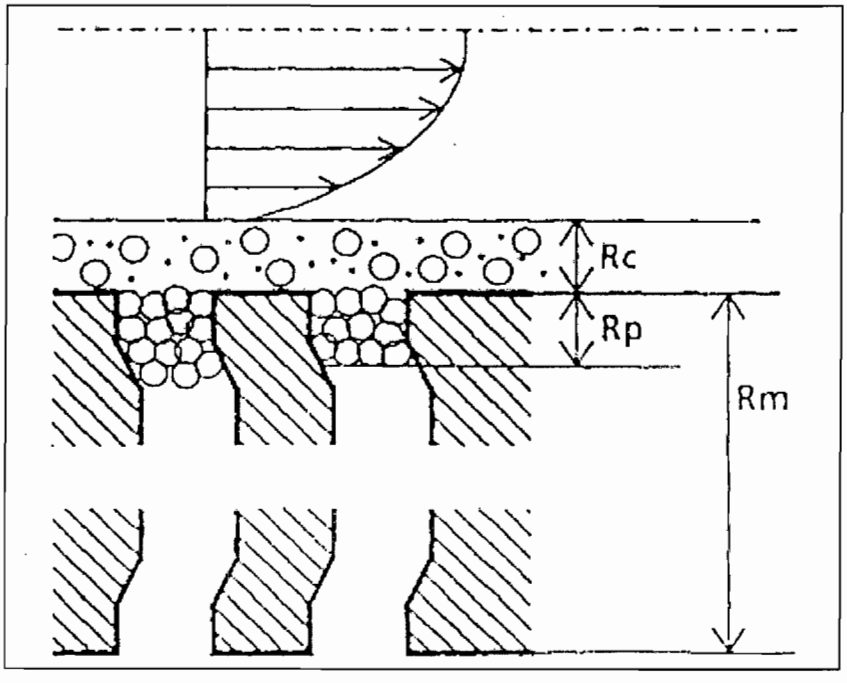

Figure 2-4. Hydraulic resistances to permeate flow through a fouled membrane

The impact of the membrane properties on the permeate flux depends on the magnitude of the hydraulic resistance of the cake layer relative to the magnitude of the intrinsic membrane resistance. The resistance of the cake layer can be more than two orders of magnitude larger than the intrinsic membrane resistance in which case the effect of the membrane would be insignificant (Lojinke *et al.* 1992). However, for some

low fouling applications the cake resistance and the membrane resistance have the same order of magnitude. For such cases, several investigators have reported a relationship between membrane properties and flux behaviour. These cases are reviewed in the next section based on the impact of the membrane pore size, the pore size distribution, the surface porosity and the membrane surface structure and composition.

2.5.1.1 Membrane Pore size

The effect of membrane pore size appears to be system specific according to Table 2-4.

Table 2-4. The effect of membrane pore size

Impact of pore size on flux	Particles		Membrane		Reference
	Nature	Size (μm)	Pore size (μm)	Material	
Flux increase with increasing pore size	*Eschericia Coli*		0.22		Reismeier (1989)
Flux increases with pore diameter below 1μm but plateau at this value	Blood		0.8-1.1	Glass	Sakai *et al.* (1989)
Flux: 0.45μm > 0.2μm	*Saccaromyces cerevisiae* in cider	5	0.2 and 0.45		Scott (1988)
Flux: 0.45μm < 0.2μm	*Saccaromyces cerevisiae* in beer	5	0.2 and 0.45		Le (1987)
Flux: 0.45μm > 0.6μm > 0.2μm	*Ps. fluorescens*		0.2, 0.45 and 0.6		Le *et al.* (1984)
Steady state reached with 0.45μm pore size membrane but not with 1.0μm.	Filamentous fungus: *Schizophyllum commune*		0.45 and 1.0		Haarstrick *et al.* (1991)

There are two possible phenomena that can account for the apparently random behaviour of permeate flux with changes in membrane pore size:

- During the initial period of filtration, before the cake layer is established, smaller particles may be trapped inside the membrane pores causing irreversible fouling. These particles effectively reduce the total area available for permeate

flow, resulting in a significant increase in the total hydraulic resistance and subsequently a decrease in the flux. This means that the impact of the pore size depends on the fraction of particles that are of the same order of magnitude as the membrane pores. The flux would be most favourable if the membrane pores are significantly smaller than the smallest particles present in the feed stream (Tarleton & Wakeman 1993, Lojinke *et al.* 1992, Le 1987, Haarstrick *et al.* 1991 Tarleton & Wakeman 1993).

- Reismeier *et al.* (1990), filtering *E. coli* and *S. cerevisiae*, found that the specific resistance of the cell layers deposited onto the membrane surface decreased markedly as the pore size of the membranes increased. This led to the conclusion that the membrane pore size determines the nature of the particles that are retained. The retained particles then act as a dynamic membrane that determined the rejection as well as the permeate flux.

2.5.1.2 Pore Size Distribution

The mean membrane pore size does not fully characterise the membrane pores with respect to their impact on membrane fouling. For UF membranes, it was found by Fane *et al.* (1981) that 50% of the flow passes through only 20% of the pores. The larger pores contribute significantly more to the permeate flux compared to the smaller ones (Michaels 1968). Generally, the larger pores are constricted by the smaller particles in the feed. Fane *et al.* (1981) proposed that the ratio of the 95% percentile of pore sizes to the 5% percentile of particle sizes can be used to predict the internal fouling probability of the feed suspension and membrane combination.

2.5.1.3 Membrane Surface Porosity

Fane *et al.* (1981) used Poiseuille flow to estimate the surface porosity of two commercial UF membranes (Amicon XM100A and XM300). They found that the membrane surface for many of the commercially available membranes couldn't be estimated as being a continuum of pores. For the track-etched membranes they found that the average space between two pores were between 6 and 15 pore diameters. This indicates that there are severe differences in the surface porosities of different membranes.

The membrane porosity may have an influence on the permeate flux. Fane *et al.* (1990) found that the specific resistance of the cake layer appeared greater for less porous membranes. They suggested that sparse porosity implies that the permeate must flow laterally through the cake to reach a pore and the longer flow path is responsible for the apparently greater specific resistance.

Fane *et al.* (1981) found that 50% of the flux flowed through the upper 20% of the pores. From this conclusion, it can be inferred that blocking of the upper 10% of the

membrane pores would result in a larger decrease in the flux. This effect is exaggerated by sparse membrane porosity.

Membrane porosity not only influences the fouling behaviour of the membrane but also the nature of the cake formed on the membrane surface. The nature of the cake depends to some extent on the number of particles competing to enter a single pore. When each pore is approached by a small number of particles penetration of the fines into the pores are more likely than when a large number of particles all compete to enter the same opening in the membrane surface. Thus, when the number of particles approaching each opening increases the penetration of the pores may be prevented by particles forming bridges over the membrane pores. These properties are however also dependent on the feed composition. (Tarleton & Wakeman 1993)

Pores that are far apart may also cause inhomogeneous cakes to form on the membrane surface. Particles will tend to deposit over the area of greatest suction. If these points of suction are significantly removed from each other, particles may clump or deposit primarily around these regions. This results in higher surface roughness, which again might affect the deposition of particles comprising the cake layer, as described in the next section. (Tarleton & Wakeman 1993)

2.5.1.4 Surface Structure and Composition

The chemical composition of the membrane can influence the sorption properties of macromolecules as well as the affinity of the membrane for particles in the feed. The chemical composition of the membrane also influence properties such as surface charge, hydrophobicity and the surface roughness of the membranes which, will on their part influence the filtrate flux.

- Surface charge

  Membrane surface charge can be determined by streaming potential or electro-osmotic flow techniques which measure the zeta potential of membranes in contact with solutions of known ionic composition and pH. The zeta potential of membranes varies with pH to a degree dependant on the properties of the membrane material and the solution in which they are immersed. (Tarleton and Wakeman 1994a)

  A charged membrane surface with a similar charge to the foulants in the feed stream could prevent cake formation and fouling by electrostatic interactions. Only minor differences in the flux performance over the range of membrane surface charges have been observed experimentally for microfiltration applications (Tarleton & Wakeman 1994b).

- Hydrophobicity

  The hydrophobicity or wettability of the membrane is a measure of the surface energy of the membrane as well as the affinity of the membrane for water. Membrane wettability is an intrinsic property of a membrane and is not influenced by pH, or the presence of solids in the feed stream (Tarleton & Wakeman 1993).

  Membrane hydrophobicity can influence the pure water flux as well as the interaction between the particles or macromolecules in the feed stream and the membrane surface. Pure water fluxes of hydrophilic UF membranes are generally higher than that of hydrophobic membranes. Furthermore, hydrophobic particles tend to adhere to hydrophobic surfaces and vice versa. Therefore the affinity between hydrophobic particles and a hydrophobic membrane surface would be more severe that that between hydrophobic particles and a hydrophilic membrane. It has also been suggested that hydrophilic particles form a water layer around them that could act as a buffer between the particle and the hydrophobic membrane to prevent cake formation or fouling. (Tarleton & Wakeman 1993; Fane *et al.* 1990; Gatenholm *et al.* 1988b; Defrise & Gekas 1988)

  Various investigators (Tarleton & Wakeman 1994b) found that hydrophobic UF membranes generally produce higher fluxes during the initial period of microfiltration of hydrophilic particles (such as microbial suspensions) (Tarleton & Wakeman 1994a; Fane *et al.* 1990; Gatenholm *et al.* 1988b; Defrise & Gekas 1988).

  It has however been observed that for microfiltration membranes these effects disappear and both hydrophobic and hydrophilic membranes exhibit the same fluxes under the same operating conditions (Tarleton and Wakeman 1994b).

- Surface roughness

  The membrane structure might give an indication of the primary mechanisms by which the flux declines (Tarleton & Wakeman 1993). Depending on the manufacturing process, membrane surfaces can have a variety of surface rugosities. Nucleopore membranes are generally smooth while cast membranes have a very tortuous uneven surface. Inorganic membrane surfaces generally have a rugosity between 5 and 40 microns (Liberge *et al.* 1994).

  Liberge *et al.* (1994) observed pseudo steady-state flux differences between inorganic membranes with the same pore size rating and different rugosities, filtering yeast suspensions. They reported easier particle deposition on membranes with more uneven surface structures. Stamatakis & Tien (1993)

developed a model emphasising the role of rugosity on particle deposition. The model calculated the probability of particle deposition based on the availability of a constriction extending high enough above the membrane surface. These constrictions can either be particles deposited earlier or membrane surface irregularities.

The surface rugosity effects have only been reported for microfiltration membranes although various investigators (Tarleton & Wakeman 1994b; Stamatakis & Tien 1993; Liberge *et al.* 1994) suggested that it might also apply to ultrafiltation.

2.5.2 Feed stream Properties

The feed stream can contain any combination of particulate matter, macromolecules or dissolved salts in both aqueous and other solvent mediums. The impact of the feed stream properties on the filtration flux would be discussed under the following headings:

- particulate properties
- solvent composition
- macromolecular properties
- temperature

2.5.2.1 Particulate Properties

The nature of the particles and/or colloids in the feed stream can influence the nature of the cake that forms on the membrane surface (Tarleton & Wakeman 1993; Belfort *et al.* 1994; Lojinke *et al.* 1992). Factors such as the particle size, size distribution, shape and surface charge can have an impact on the permeate flux.

- Particle size and rigidity (Tarleton & Wakeman 1993).

  According to Tarleton and Wakeman (1993) the particle size determines the extent of internal fouling as well as the cake properties. Internal fouling will occur if the particle size corresponds to that of the membrane pore size. This will allow the particles to enter the pores and be trapped inside the membrane to decrease the area available for permeate flow.

  The size and the elasticity of the particles comprising the cake influences the resistance of the cake formed on the membrane surface (Tarleton & Wakeman 1993; Belfort *et al.* 1994). According to the Carman-Kozeny equation, the specific hydraulic cake resistance is inversely proportional to the square of the rigid particle diameter. Reduced particle size will therefore result in lower overall fluxes.

The cake resistance increases as the rigidity decreases (Tarleton & Wakeman 1993). Less rigid particles will deform easily to reduce the void space in the cake and subsequently reduce the permeability of the cake.

These effects are less significant at higher cross-flow velocities and concentrations (Tarleton & Wakeman 1993; Belfort *et al.* 1994; Lojinke *et al.* 1992).

- Particle size distribution

  Various investigators (Tarleton & Wakeman (1993); Romeo & Davis (1991); Fischer and Raasch (1986); Lu and Ju (1989)) found that the mean particle size of the cake is less than that of the feed. Furthermore, the cake particle size decreases as the cross-flow velocity increases leading to thinner cakes with generally higher resistances (Fischer *et al.* 1985). The smaller particles in the feed are therefore predominantly responsible for the formation of the cake or fouling layer. It therefore follows that some size fraction less than the mean should be used to characterise the feed, as this is more indicative of the fouling potential of the feed.

  Tarleton & Wakeman (1993) also found that a wider particle size distribution leads to reduced cake voidage and therefore a higher hydraulic resistance. This effect was most pronounced at low cross-flow velocities and concentrations.

- Particle shape

  Tarleton & Wakeman (1993) investigated the effect of particle shape on the flux decline pattern. They used platelet shaped china clay suspensions and found that irregularly shaped particles could have a significant impact on filtration flux. The cake formed during filtration was predominantly composed of particles lying with their faces parallel to the membrane surface. This apparent uniform orientation of the particles comprising the cake resulted in cakes with higher hydraulic resistances and subsequently lower filtration fluxes when compared to cakes formed from apparently randomly orientated particles.

  Tanaka *et al.* (1994) found that rod shaped (*Bacillus*) cells in the cake layer were orientated towards the direction of circulation flow compared to the almost random packing of ellipsoidal cells (*C. glutamicum*). The parallel arrangement of the cells resulted in a cake layer with increased hydraulic resistance compared to the randomly packed cell layer.

  Although the influence of the particle shape can be demonstrated, Tarleton & Wakeman (1994a) reports that it is difficult to predict its effects a priory. For example Tarleton and Wakeman (1994a) found that suspensions of irregularly

shaped aragonite particles exhibited very similar filtration performance to its polymorph calcite which has a rhomboidal shape.

- Particle surface charge

  Similar to membrane surface charge, particle surface charge can be determined by streaming potential or electro-osmotic flow techniques which measure the zeta potential (ζ_s) of the particle surface in contact with solutions of known ionic composition and pH (Tarleton and Wakeman 1994a).

  Suspensions of "stable" particles or macromolecules, with high ζ_s-potential values, are invariably more difficult to filter than suspensions containing "unstable" particles or macromolecules with low ζ_s-potential values (Baker *et al.* 1985; Bowen & Clark 1984). Tarleton and Wakeman (1994a) suggested that these highly charged foulants are well dispersed by mutually repulsive electrostatic forces. For the initial period of the filtration process, any foulant which are discrete due to high surface charge and within the immediate vicinity of the membrane will tend to move with the permeate flow toward the membrane pore throats. These particles and/or macromolecules are likely to penetrate the relatively open pore entrances on the membrane surface, leading to irreversible fouling due to pore blocking and/or constriction. Suspensions containing low ζ_s-potential particles or macromolecules tend to agglomerate, due to mainly attractive van der Waals forces. The fouling deposit thus formed has a lower overall resistance due to the larger effective size (Bansal *et al.* 1991; Palacek & Zydney 1994b).

2.5.2.2 Solvent Composition

During cross-flow filtration of microbial suspensions, the flux is influenced by the composition of the medium used to suspend the cells. Cells suspended in cultivation media are more difficult to filter than cells re-suspended in buffers (Hoffman *et al.* 1987; Patel *et al.* 1987). Furthermore Nipkow *et al.* (1989), have shown that complex fermentation media exhibited lower fluxes than minimal media. These effects can be ascribed to the presence and interaction among macromolecules and salts within the media (solvent) that can also contribute to the fouling nature of the feed stream.

2.5.2.3 Macromolecule Properties

Most feed streams encountered in the filtration of microbial suspensions contain large amounts of proteins and other macromolecules. Ofsthun *et al.* (1990) obtained data for the filtrate flux as a function of time during cross-flow filtration of yeast cells suspended in bovine serum albumin (BSA) through different polymeric membranes. Although cakes of yeast cells formed on the membrane surface, the flux decline was essentially the same as that obtained during a cell free BSA filtration under

identical conditions. This suggests that much of the flux decline observed was the result of some type of protein-membrane interaction. Generally, the size and shape of these macromolecules did not play a significant role in the permeation flux (Belfort *et al.* 1994).

2.5.2.4 Suspension temperature

As noted by Gabler & Ryan (1985); Henry & Alfred (1972); Schutte *et al.* (1983) and Scott (1988); flux increases with increasing temperature. This increase is attributed primarily to the decrease in fluid viscosity with increasing temperature.

2.5.3 Operational parameters

The operational parameters used in most cross-flow filtration applications include the particle and/or macromolecule concentrations, the trans-membrane pressure drop and the cross-flow velocity. The impact of these operating parameters on the cross flow filtration flux would be discussed in the following sections.

2.5.3.1 Particle and/or macromolecule concentration

The filtration flux generally decreases as concentration of foulants increases (Henry & Alfred 1972; Hoffman *et al.* 1987; Kroner & Nissinen 1988; Le *et al.* 1984b; Mateus & Gabral 1989; Matsumoto *et al.* 1987; Nagata *et al.* 1989; Patel *et al.* 1987; Schutte *et al.* 1983). Plots of the permeate flux versus the feed concentration for batch experiments are often sigmoidal (Hoffman *et al.* 1987; Schutte *et al.* 1983) or concave upward (Kroner & Nissinen 1988; Le *et al.* 1984b; Matsumoto *et al.* 1987). A fast initial decline in flux with increasing feed concentration is followed by a period of gradually declining flux, which may be followed, by a second sharp decline (Lojinke *et al.* 1992). Typical curves as shown in Figure 2-5.

Lojinke *et al.* (1992) reports that most of the investigators agree that the initial decline in flux with increased concentration can be explained by the higher solid flux toward the membrane wall at higher bulk concentrations, if there is no significant change in the feed viscosity. According to Lojinke *et al.* (1992), no explanation for the intermediate plateau was offered by any of the investigators who reported the effect.

Scott (1988) reported an increase in the flux after the plateau, which can be attributed to a rise in the trans-membrane pressure drop as the viscosity of the suspension increased with increasing concentration.

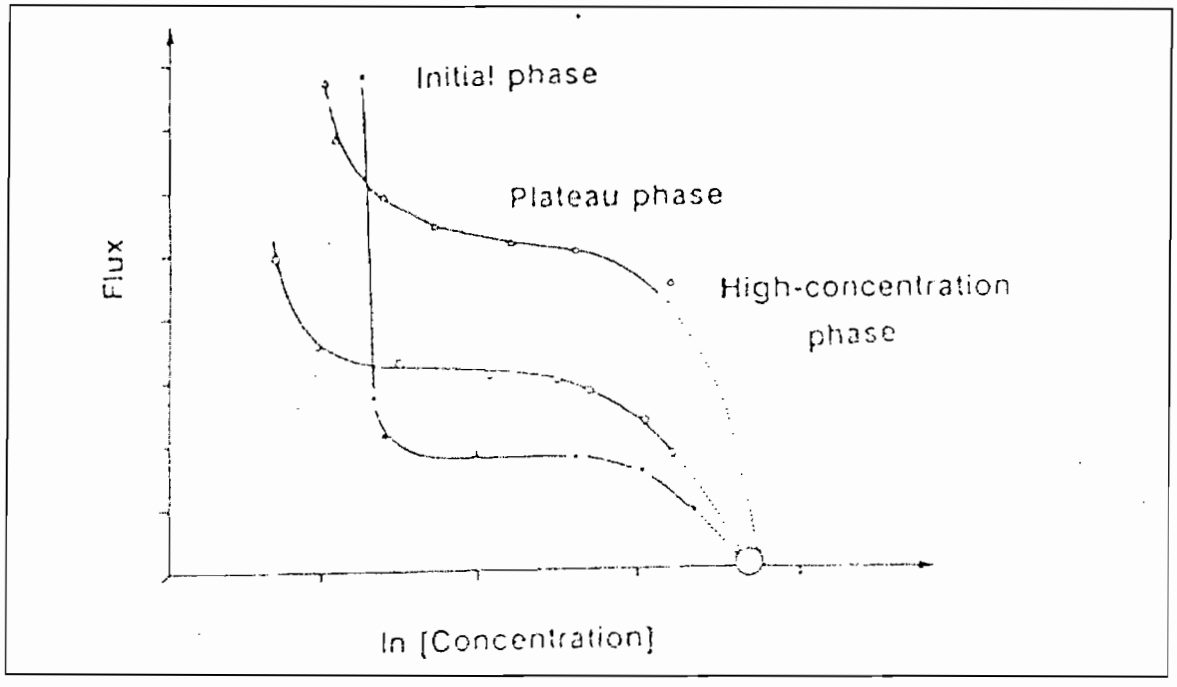

Figure 2-5. Typical flux vs. feed concentration plots for microbial suspensions. Adapted from Lojinke *et al.* (1992) based on the data of Kröner *et al.* (1984)

Pritchard (1991) reported that at very high concentrations the increased shear stress (due to higher viscosity because of increased concentration) could be sufficient to induce an increase in the flux. Pritchard (1991) compared the effect of increased concentration on the filtration flux of baker's yeast in a tubular module with data for the same suspension in a flat sheet module. The flux declined during the first 30 min and reached a region where the flux was virtually independent of concentration. It extended up to a point where the flux sharply decreased for the tubular module and increased for the flat sheet module. The concentration at which this occurred varied with the cross-flow velocity. For the tubular module, the Reynolds number at the point of transition was always around 2300. According to Pritchard (1991) the decline in flux for the tubular module can be attributed to the transition from turbulent to laminar flow. This transition was attributable to the increase in viscosity with increasing concentration. The data for the flat sheet module (in which conditions were always laminar) showed an increase in flux at the end of the plateau region. The increase corresponded with a wall stress of 50 Pa. The increase in the laminar shear rate was attributable to the increase in concentration. Thus, for this particular system there is a marked increase in flux when the wall stress exceeds a threshold value. Presumably, the upper layers of the cell cake are sheared away. Similar results were not obtained with cider lees, which is shear thinning. Similar results (Pritchard *et al.* 1992) were however obtained in an ultra-filtration module during the processing of xanthan gum and pectin solutions.

2.5.3.2 Trans membrane pressure drop (ΔP)

Although the trans-membrane pressure drop (ΔP) provides the driving force for filtration, increases in ΔP do not always result in increased flux. Generally, the flux increases linearly with increasing ΔP at low pressures up to a critical or limiting pressure (Belfort *et al.* 1984; Lojinke *et al.* 1991) after which conflicting behaviour has been reported. Above the critical pressure drop:

- the rate of increase may decrease (Forman *et al.* 1990; Grabler & Ryan 1985b; Henry & Allfred 1972; Kroner & Nissinen 1988; Le *et al.* 1984a; Patel *et al.* 1987; Reismeier *et al.* 1987 and Tanny *et al.* 1980),
- the flux may be independent of pressure drop (Le *et al.* 1984; Ofsthun & Colton 1987; Sakai *et al.* 1989 and Taddei *et al.* 1990) or
- the flux may decrease with increasing pressure drop (Forman *et al.* 1990; Sakai *et al.* 1989).

The value of the critical pressure drop depends on cross-flow velocity (Le *et al.* 1984), the membrane pore size (Forman *et al.* 1990; Le 1987) and concentration of foulants in the suspension (Forman *et al.* 1990; Patel *et al.* 1987). Table 2-5 summarises some values of critical trans-membrane pressure drops for microbial suspensions.

Table 2-5. Critical values of the trans-membrane pressure drop (ΔP) for the filtration of microbial suspensions

Organism	Membrane pore size (μm)	Critical ΔP (kPa)	Reference
E. coli	0.2	>250	Gatenholm *et al.* (1988b)
E. coli	0.2	70-140	Tanny *et al.* (1980)
E. coli	0.2	40-60	Reismeier *et al.* (1987)
Disrupted *E. coli*	0.45	>400	Grabler & Ryan (1985b)
Disrupted *E. coli*	0.45-0.65	25	Forman *et al.* (1990)
Micrococcus sp.	0.22	60	Henry & Allred (1972)
Disrupted *Ps. fluorescens*	0.45	100-250	Le *et al.* (1984a)
S. cerevisae	0.2	20+	Kröner & Nissenen (1988)
S. cerevisae	0.2	50-150	Patel *et al.* (1987)
S. cerevisae	0.22	600	Taddei *et al.* (1990)
Blood	0.35	4-8	Ofsthun & Colton (1987)
Bovine blood	0.8-1.1	4	Sakai *et al.* (1989)

(Adapted from Lojinke *et al.* 1992)

The most common explanation of the flux behaviour above the critical trans-membrane pressure drop, as reported in various review papers (Belfort *et al.* 1984; Lojinke *et al.* 1991) is that at low trans-membrane pressure-drops the flux increases due to the increasing driving force. Beyond the critical pressure-drop an increase in the driving force does not only increase the solid flux towards the membrane surface but also serves to compress the cake layer. The higher solid flux then serves to increase the cake thickness while the compression causes an increase in the specific cake resistance. Both these effects will reduce the permeate flux. The relative magnitude of the increased driving force, the compressed cake and the increased cake thickness can explain the flux behaviour above the critical pressure drop.

2.5.3.3 Cross-flow velocity

The cross flow velocity is the average linear velocity of the bulk flow in the filtration module. Different effects of cross-flow velocity on the permeate flux have been reported for different feed streams (Belfort *et al.* 1984; Romero & Davis 1991; Lojinke *et al.* 1991). According to Tarleton & Wakeman (1993) feed streams containing a higher proportion of "larger" particles, will result in decreased cross-flow filtration flux when the cross-flow velocity is increased. If the portion of fines are however increased higher cross-flow velocities results in improved filtration fluxes. In this context, "large" means more than an order of magnitude larger than the membrane pores, while fines are particles within the size range of the membrane pores.

Tarleton and Wakeman (1993) suggested that the effect of cross-flow velocity can be best explained by considering "large" and "small" feed suspensions separately.

- "Larger particle" feed suspensions:

  It has been reported that the mean particle size of the cake decreases with increasing cross-flow velocity (Tarleton & Wakeman 1993; Romeo & Davis 1991; Fischer and Raasch 1986; Lu and Ju 1989). Zydney and Colton (1986) explained this phenomenon in terms of hydrodynamic diffusion or "particle classification". It is known that the cake layer is formed from the finer particles in the feed stream (Tarleton & Wakeman 1993; Lu & Ju 1989). The axial velocity gradient generated across the flow channel, causes the larger particles to migrate away from the membrane surface at a faster rate than the smaller ones. As the cross-flow velocity increases, more of the larger particles, which were potential foulants, remain in the retentate stream. Another explanation, as proposed by Green and Belfort (1984) and supported by the observations of Wakeman (1994) is that larger particles may be removed from the foulant layer by the scouring action of the cross-flow stream. Irrespective of the mechanism(s) responsible for the classification, at higher cross-flow velocities, the cake layer is

composed of progressively finer particles, which results in higher hydraulic resistances and lower filtration rates.

- "Smaller particle" feed suspensions:
  A large number of workers have reported that an increase in cross-flow velocity leads to an increase in the filtration flux (Bauser *et al.* 1982; Datar 1984; Forman *et al.* 1990; Harris *et al.* 1988; Le & Billet 1984; Le *et al.* 1984a; Le *et al.* 1984b; Nagata *et al.* 1989; Sakai *et al.* 1989; Scott 1988, Taddei *et al.* 1990; Tanny *et al.* 1980).

  Several of these workers have suggested a power law relationship between the cross-flow velocity and the flux:

$$J \propto v^{n_v} \qquad (2\text{-}2)$$

  where J is the permeate flux (m/s), v is the average cross flow velocity (m/s) and n_v is the exponential parameter.

  The values of the exponent n_v, for some microbial suspensions are summarised in Table 2-6.

Table 2-6. Power law dependence of flux on cross-flow velocity for microbial suspensions.

Organism or cell	Membrane pore size (μm)	Exponent in power law relationship (n_v)	Reference
Micrococcus sp.	0.22	0.5; 0.75[2]	Henry & Alfred (1972)
Ps. fluorescens[3]	0.45	0.5	Le *et al.* (1984a)
S. Cerevisiae	0.2-1.2	0.4; 0.7[1]	Taddei *et al.* (1990)
S. Cerevisiae	0.22	1.1	Le (1987)
Bovine blood	0.8-1.1	0.9	Sakai *et al.* (1989)

[1]Two different feeds same module
[2]Same feed, two different modules
[3]Lysate, i.e. cells were disrupted prior to processing
(Adapted from Lojinke *et al.* 1992)

Wakeman (1994) explained the increase in flux with increasing cross-flow velocity by the increased shear rate caused by higher cross-flow velocities. The higher shear forces decreased the cake thickness and subsequently the hydrodynamic resistance of this layer. Since the hydraulic resistance of the smaller particles are already at a maximum value due to the high packing density of the fines the reduction in cake thickness leads to an increased flux.

Based on the reduction in cake thickness by increased cross-flow velocity, Green & Belfort (1980) suggested that for fine particles or macromolecular suspensions there is a cross-flow velocity beyond which fouling could be avoided. This velocity would correspond with the shear rate required to remove the entire cake layer from the membrane surface. Evidence of such velocities has been found for non-interacting fine particles (Green & Belfort 1980; Tarleton & Wakeman 1994a).

2.6 Fundamental approaches to flux decline and fouling mechanisms

Various investigators attempted to describe the fundamental processes governing the filtration flux decline pattern and to predict the value of the pseudo-steady state flux. Flux decline is thought to be caused by concentration polarisation and fouling, while the steady-state flux is influenced by the relative motion of foulants towards and away from the membrane surface.

2.6.1 Concentration polarisation and fouling

Concentration polarisation is the reversible build-up of dissolved or suspended solutes in the solution phase near the membrane-solution interface (Wankat 1990; Belfort *et al.* 1984; Lojinke *et al.* 1991; Aptel & Buckley 1992; Howell *et al.* 1993; Mulder 1991; Rautenbach & Albrecht 1989). This layer of increased concentration is established due to an imbalance between the convective drag force towards the membrane and the back transport away or along the membrane surface. The concentrated layer acts as a barrier to the filtration flux that increases the hydraulic resistance.

On the other hand solute and particle deposition onto and into the porous membrane is likely to occur when the permeate flux is high relative to the back transport mechanisms. This phenomenon together with macromolecular adsorption onto the membrane is termed membrane fouling. Various investigators (Belfort *et al.* 1984; Lojinke *et al.* 1991; Aptel & Buckley 1992; Tarleton & Wakeman 1993) characterised the two phenomena by defining concentration polarisation as a reversible- and fouling as an irreversible process.

2.6.2 Mechanisms explaining concentration polarisation and fouling

The mechanism of fouling can be explained by differentiating between the role of the particulate and the macromolecular components in the feed suspension. Particulate fouling mechanisms include deposition and intrusion of the particles into and onto the membrane surface. Particle deposition is the process by which particles are being trapped onto the membrane surface leading to cake formation. Intrusion effects refer

to pore narrowing and pore plugging due to some of the smaller particles being trapped inside the membrane pores.

Filtration flux decline caused by the macromolecules present in the feed stream can be attributed to one or more of the following phenomena:

- Macromolecule adsorption, which involves a specific interaction between the macromolecule and the membrane, occurs in the absence of any convective flow through the membrane.
- Macromolecule deposition, which refers to any additional macromolecules that become associated with the membrane (either the outer surface or internally in the membrane pores) during filtration over and above that which would be adsorbed to the membrane in a static system
- Macromolecule deposition on an already established particulate cake layer. (Arora & Davis 1994; Mochizuki & Zydney 1993 and Bowen & Gan 1991)
- Macromolecule mass transfer limitations (often referred to as concentration polarisation or boundary layer effects), which refers to the accumulation of retained macromolecules or particulate matter at the upper surface of the membrane.

2.6.2.1 The physical phenomena associated with flux decline

Nagata & Herouvis (1989) described the physical phenomenon associated with each period of flux decline as observed in experimental literature.

- *Rapid internal fouling*
  Fast internal sorption of macromolecules, and pore constriction due to pore plugging and constriction by smaller particles and colloids causes the permeate flux to decline very rapidly during the initial stages of the filtration process (Opong & Zydney 1991; Bowen & Gan 1991; Clark *et al.* 1991; Bansal *et al.* 1991; Persson *et al.* 1993; Belfort *et al.* 1994). Tanaka (1993) described this process as irreversible and stochastic in nature.

- *Initial foulant build-up on the membrane surface*
  As the permeation flux drags suspended particles and/or macromolecules towards the membrane surface these particles and/or macromolecules begin to deposit onto the membrane surface. Various single particle models using a force and momentum balance on a single particle in a tangential flow field has been used to explain the deposition of this layer (Stamatakis & Tien 1993; Davis & Birdsell 1987; Leonard & Vassilieff 1984; Lu & Ju 1989).

- *Build-up of multi-layers – Cake formation*
  During this period, particles are dragged towards the membrane surface by the convective forces of the permeate flux where particles larger than the effective

membrane pore size are retained. The particles accumulate on the membrane surface in a growing cake layer.

The cake formed on the membrane surface acts in itself as a membrane with most frequently a cut-off much smaller than that of the clean membrane. This leads to the accumulation of smaller particles on the cake surface during the quasi-steady state period, since these particles would have passed through the membrane during the earlier stages of the filtration process. (Shimizu *et al.* 1989; Tanaka *et al.* 1998). This implies that the rejection coefficient of the system increases with time. Arora and Davis (1994) demonstrated that yeast cakes formed on macroporous supports by either gravity settling or vacuum filtration are able to retain proteins during subsequent dead-end filtration. This effect has also been reported experimentally by Tanaka *et al.* (1998) for the cross-flow filtration cakes formed by C*orynebacterium glutamicum* cultivated in a complex, protein-containing medium. They found a gel layer of most likely proteins and polysaccharides on a cake that caused the increased hydraulic resistance and the subsequent flux decline.

Although these cakes (deposits) formed by flocculated colloids and particles remain permeable, a distinct drop in permeation flux is seen during this period. Various investigators believed that the flux decline pattern observed during this phase corresponds to that of conventional dead-end filtration (Belfort *et al.* 1994; Davis 1992).

- *Reaching the pseudo-steady state flux*

  During conventional dead-end filtration the cake continues to grow until the resistance is so high that it is virtually impermeable. During cross-flow filtration the tangential flow arrests the formation of the cake layer due to either back transport mechanisms or preventing the further growth of the cake due to hydraulic shear forces acting on the cake surface. At this point the pseudo-steady state flux is reached. The exact reason for the establishment of steady state cake thickness is not yet fully understood (Belfort *et al.* 1994).

  Traditionally it was believed that the rate of deposition of particles dragged to the cake interface was balanced by the rate of particle removal from the cake layer. Various back transport mechanisms have been suggested including; Brownian diffusion, inertial lift, shear-induced diffusion and erosion mechanisms (Belfort *et al.* 1994). Most of these theories have been evaluated experimentally with varying degrees of success.

  To oppose the particle back transport explanations for the steady state flux it is argued that the rate of deposition decreases as the cake thickness increases (Belfort *et al.* 1994; Tarleton & Wakeman 1993 1994a 1994b). Based on visual observations of particles in cross-flow filtration modules, various mechanisms

have been used to explain this phenomenon (Wakeman 1994). These include particle trajectory (Stamatakis & Tien 1993; Davis & Birdsell 1987; Leonard & Vassilieff 1984; Lu & Ju 1989; Mackley 1992) mechanisms whereby the forces acting on a single particle in the cross-flow filtration hydraulic regime have been used to determine the trajectory of the particle as it flows through the membrane module. As with the back transport mechanisms mathematical models based on these mechanisms do not predict the filtration flux behaviour observed experimentally (Belfort *et al.* 1994; Tarleton & Wakeman 1994b).

- *Densification of sub-layers*

  During the pseudo steady state period, the flux declines slowly. This may be due to a combination of a slower growing cake layer and the compression of the formed cake layer due to the applied pressure (Nagata & Herouvis 1989). Both these mechanisms would cause a subsequent increase in the specific hydraulic resistance, leading to the slow flux decline observed.

3 Membrane selection

The criteria used in selection of the most appropriate membrane for the recycling of *C. glutamicum* for extended L-lysine fermentations are summarised below:

- The L-lysine fermentation is operated monoseptically to prevent foreign organisms from competing for the carbohydrate source. Therefore, it is a prerequisite that the membrane should be easily sterilisable and capable of operating aseptically. Sterilisation using ethanol or peroxide solutions is feasible for some polymeric membranes but are rather expensive in terms of industrial operating costs when compared to heat sterilisation using low-pressure steam (> 2 bar). Most polymeric membranes can only sustain temperatures up to 80 °C, compared to inorganic membranes that can withstand temperatures up to 250 °C. This implies that the most suitable membrane would most probably be inorganic in nature.
- The membrane should be capable of delivering a high flux (>30 LMH), under a low (<150 kPa) trans-membrane pressure drop. The trans membrane pressure drop is generated by maintaining a positive pressure in the bioreactor. Large bioreactor back-pressures would increase the dissolved CO_2 concentration in the fermentation broth that is toxic to the cells (Hadj Sassi *et al.* 1996). High permeate fluxes would minimise membrane area and subsequently capital cost. Inorganic microfiltration membranes are generally operated at lower trans-membrane pressure drops when compared to organic membranes at similar permeation rates (Aptel & Buckley 1996).
- To allow for easy cleaning during the short turn around times available, fouling should be limited and irreversible internal fouling should be avoided. Inorganic membranes can be cleaned with aggressive cleaning solutions ranging from pH 1 to 14 at high temperatures (>100°C). Most organic membranes will decompose at these extreme conditions (Aptel & Buckley 1996).

- The membrane module should allow for easy scale-up and should therefore be representative of actual industrial applications. Tubular membranes are most readily scaled-up since large scale hydrodynamic conditions can easily be reproduced on laboratory scale (Aptel & Buckley 1996).

Based on the criteria as explained above it was decided to evaluate tubular ceramic membranes. These membranes are constructed from titanium oxide, supported on macroporous aluminium oxide. Both ultrafiltration and microfiltration membranes were evaluated. The exact details of the membranes are summarised in Tables 2-7 and 2-8 below.

Table 2-7. Physical properties of the tubular ceramic membranes

Support	
Material	Alumina
Burst Pressure	>60 bar
Average pore diameter	3.5 μm
Max operating pressure	10 bar
pH range	0-14
Temp	<350 °C
Active Membrane	
Material	Titanium
Area	95.2 cm^2
Channels	3
Diameter	3.6 mm

The membranes were housed in a cross-flow filtration rig. The cross-flow filtration set-up was designed to evaluate the impact of the operating parameters on the filtration flux. The design of the system is described in Appendix B-1.

4 Experimental Design

The experimental design was done according to a central composite rotational design (CCRD) (Haaland 1989; Khuri & Cornell 1987). This statistical experimental design fits a quadratic model to the measured data where each variable are evaluated on essentially five levels. From the fitted equation, the linear and the extent of non-linear dependence of the measured variable on the manipulated variables as well as the degree of interaction can be determined. A few repeated mid point experiments were performed to determine the intrinsic experimental variability.

5 The factors that influence the pseudo-steady state cross-flow filtration flux of *Corynebacterium glutamicum* suspensions.

The effect of the membrane pore size, the solvent and the operating parameters on the cross-flow filtration flux of *C. glutamicum* suspensions, were evaluated experimentally using the cross-flow filtration rig.

5.1 Effect of the solvent and the membrane pore size

Two micro-filtration (0.22 μm & 0.45 μm) and two ultra-filtration (150 kD & 300 kD) tubular ceramic membranes were evaluated. The filtration flux at a cross-flow velocity of 2 m/s, a trans-membrane pressure drop of 100 kPa and 35 g/l dry cell weight suspended in:

1) a 0.9% saline solution
2) a defined minimal media formulation and
3) a typical industrial media formulation

are illustrated in Figure 2-6. Details of the media composition are given in Appendix A-2.

The following exponential function was used to estimate the pseudo steady state flux from the experimental results (Liberge *et al.* 1994).

$$J = J_{ss} + (J(t_1) - J_{ss}) \exp\left(\frac{t - t_1}{J(t_1) - J_{ss}}\right)\left(\frac{dJ}{dt}\Big|_{t=t_1}\right) \qquad (2\text{-}3)$$

where $J(t_1)$ is the flux value at time, t_1 when the modelling begins with the exponential function (dJ/dt) is the slope value at t_1 and J_{ss} is the adjustable parameter (limit of the function when $t \rightarrow \infty$). The experiments were continued until no visible change in the flux was observed. The last data points were then modelled with Equation 2-3 to determine the value of J_{ss} – the steady state flux – by using a least squares fit.

Each data point represents the average of the results obtained in 5 experiments. The membranes were cleaned in between runs, using 5% nitric acid and a 10% caustic solution at elevated temperatures (60°C) as described by the supplier (Appendix B-6). The pure water flux of each of the membranes evaluated at 100 kPa and 2 m/s are summarised in Table 2-8

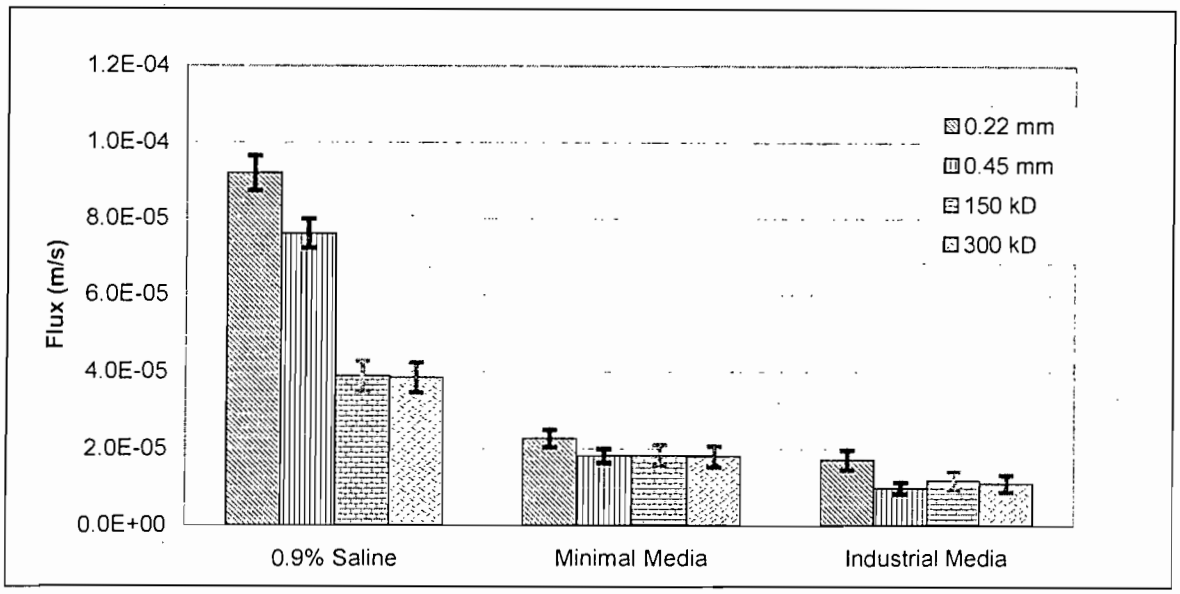

Figure 2-6. The effect of the membrane pore size on the permeate flux evaluated at 2m/s cross-flow velocity, 100 kPa and 35 g/l DCW suspended in 1) a 0.9% saline solution, 2) a minimal media formulation and 3) an industrial media formulation. Each data point represents the average pseudo-steady state flux obtained using Equation 2-3 of five experiments.

Table 2-8. Pure water flux ($J_{o,w}$) at 100 kPa

Pure Water Flux at 100 kPa		
300 kD	[m/s]	1.11×10^{-4}
150 kD	[m/s]	1.09×10^{-4}
0.45 micron	[m/s]	1.23×10^{-3}
0.22 micron	[m/s]	1.09×10^{-3}

The feed suspension for the filtration trials contained cells that were cultivated in either a minimal or an industrial media formulation. A generalised composition of the cultivation media is given in Table 2-9. The cells suspended in the 0.9% saline solution was cultivated in the minimal media formulation, removed by centrifugation and re-suspended in the saline solution. The composition of the solvent for the filtration feed suspensions in minimal and industrial media formulations correspond to that given in Table 2-9 except that the carbohydrates would have been consumed and lysine (10-15 g/l) would have been produced.

Table 2-9. Solvent composition

Component	Unit	0.9 % Saline	Minimal Media	Industrial Media
Ammonium Sulfate	[g/l]		5	40
Antifoam	[g/l]		0.12	0.12
Biotin	[g/l]		0.0005	0.001
$CaCl_2$	[g/l]		0.055	
Citric acid	[g/l]		1.14	
CSL	[g/l]			50
FeSO4.7H2O	[g/l]		0.02	
Glucose	[g/l]		20	
HTM	[g/l]			700
K_2HPO4	[g/l]		8	4
KH2PO4	[g/l]		1	2
Leucine	[g/l]		0.1	1.5
Methionine	[g/l]		0.04	0.6
MgSO4.7H2O	[g/l]		0.2	
Mineral salts	[g/l]			
NaCl	[g/l]	9	1	
Thiamine	[g/l]		0.001	0.002
Threonine	[g/l]		0.15	0.7

The feed suspension was further qualified by measuring the mean particle size in each of the suspensions. The particle size distribution as measured in each of the feed suspensions by the Malvern particle sizer (Method described in Appendix C-1) is displayed in Table 2-10. The size of a single *Corynebacterium glutamicum* cell in the stationary growth phase as measured under a light microscope at 1000 times magnification was approximately 0.7 by 1.2-μm. During the early growth phase, these cells are rod-shaped (Figure 2-7) but as the fermentation progresses, the cells become increasingly circular (Figure 2-8). The cells are often seen in v-shaped pairs.

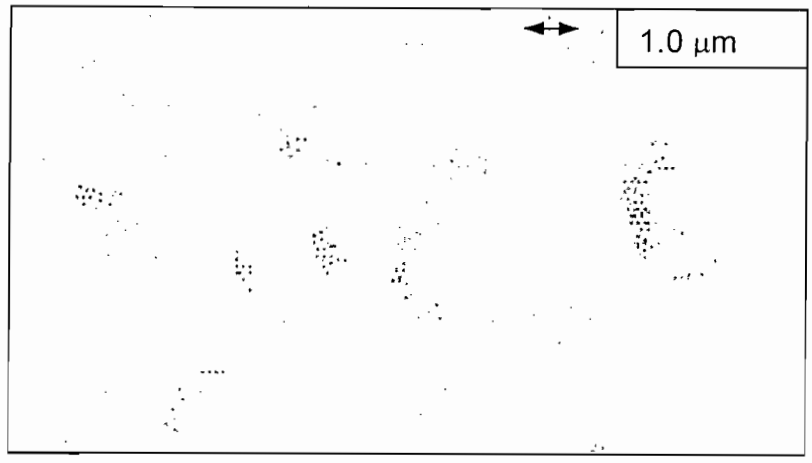

Figure 2-7 *Corynebacterium glutamicum* cells suspended in 0.9% saline solution in growth phase

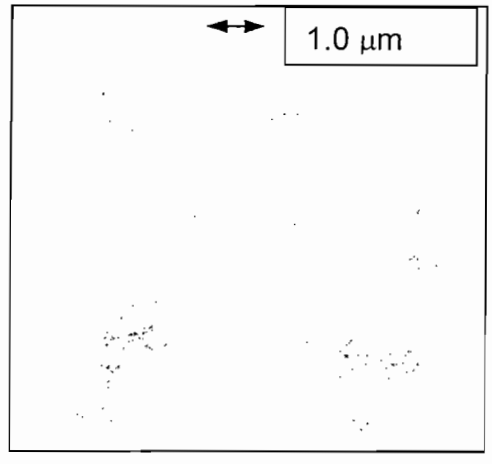

Figure 2-8 *Corynebacterium glutamicum* cells suspended in 0.9% saline solution in stationary phase

Table 2-10. Particle Size analysis of stationary phase cells suspended in various solvents

	D(n,0.1)	D(n,0.5)	D(n,0.9)
0.9% Saline	0.71	1.08	1.97
Minimal Media	0.70	1.07	1.95
Industrial Media	0.49	1.38	3.25

5.1.1 Cells suspended in 0.9% saline

The cells suspended in 0.9% saline solution were cultivated in the minimal media and separated from the spent medium by using centrifugation prior to re-suspension. The effective median size as measured by the Malvern particle sizer was 1.08 micron. This compared well with the size of single cells as measured under the light microscope.

This indicates that the re-suspension of the cells after centrifugation was sufficient to mimic the clumping behaviour of the cells during the cultivation process. This was confirmed by the similar median particle size of the cells cultivated in minimal media as measured by the Malvern particle sizer (1.07-micron). No morphological changes were observed microscopically during the first two hours after re-suspension. After roughly two hours, the cells became elliptical with a single swollen end. No cell lysis was seen microscopically.

From Figure 2-6 it is clear that when the cells are suspended in the saline solution, the micro-filtration membranes exhibits a much larger steady state flux compared to the ultra-filtration membranes. No difference could be noted between the steady state fluxes measured for the 150 kD and 300 kD, UF membranes although for the MF membranes, the 0.22 micron membrane exhibits a larger flux than the 0.45 micron membrane.

5.1.2 Cells suspended in the spent minimal media

The cell size measured in the spent minimal media agreed with that measured in the saline solution (Table 2-10). The fluxes however, for both UF and MF membranes were lower for cells cultivated in minimal media compared to the cells re-suspended in saline. The 0.22-micron membrane exhibited the highest flux, while the other membrane allowed a lower flux. There was very little difference in the flux between the other membranes (0.45 μm 150 kD and 300 kD).

5.1.3 Cells suspended in the spent industrial media

The industrial media formulation contains a large portion of foreign particles causing a wider particle size distribution. All the steady state, fluxes measured for cells suspended in industrial spent medium were lower than that of any of the other suspensions. The effect of the membrane pore size at 100 kPa and 2 m/s was less apparent when compared to cells suspended in either saline solution or minimal media. An 8% difference between the flux through the 150 kD and 300 kD UF membrane and a 30% difference in flux between the 0.22 and 0.45-micron MF membrane were detected. The 0.45-micron MF membrane exhibited the lowest flux almost 30% less than that of the 0.22-micron membrane. There was however only a 5% difference between the fluxes through the 0.22 micron and the 150 kD membranes.

5.1.4 Discussion

The pseudo steady state flux decreases as the complexity of the solvent increases. The effect of the membrane pore size can largely be ignored for the more complex

solutions. It is therefore clear that it is not only the cells that influence the fouling behaviour of the membranes. The minimal media components as well as the macromolecules and other particulate matter present in the industrial media have a significant impact on the cross-flow filtration flux.

It has been reported that a particulate cake formed from a wider size distribution would form a less permeable fouling layer due to the denser packing thereof (Tarleton & Wakeman 1993). Tanaka *et al.* (1998) observed a macromolecular gel layer on a layer of *C. glutamicum* cells during cross-flow filtration trials. Although the gel layer was only a few micro-meter thick, the hydraulic resistance was orders of magnitude higher than that of the cell layer. It was postulated that the gel layer consisted of proteins and macromolecules associated with the complex spent media composition. This could explain the reduction in flux with increasing solvent complexity.

Choo and Lee (1996) identified struvite ($MgNH_4PO_4.6H_2O$) as the major inorganic foulant in microbial systems. The conditional solubility product of struvite as a function of pH was calculated by Stum & Morgan (1981) and is plotted in Figure 2-9. The ionic strength and activity coefficient in aqueous solutions was calculated based on Russel's derivation and the extended Debye-Hückel approximation respectively (Snoeyink & Jenkins 1980). Using the composition displayed in Table 2-9 the solubility quotient (Q_s) for the actual concentration of struvite is obtained:

$$Q_s = C_{T,Mg} \times C_{T,NH4} \times C_{T,PO4} \qquad (2\text{-}4)$$

Where $C_{T,Mg}$, $C_{T,NH4}$ and $C_{T,PO4}$ are the total concentrations of magnesium, ammonium and orthophosphate ions respectively.

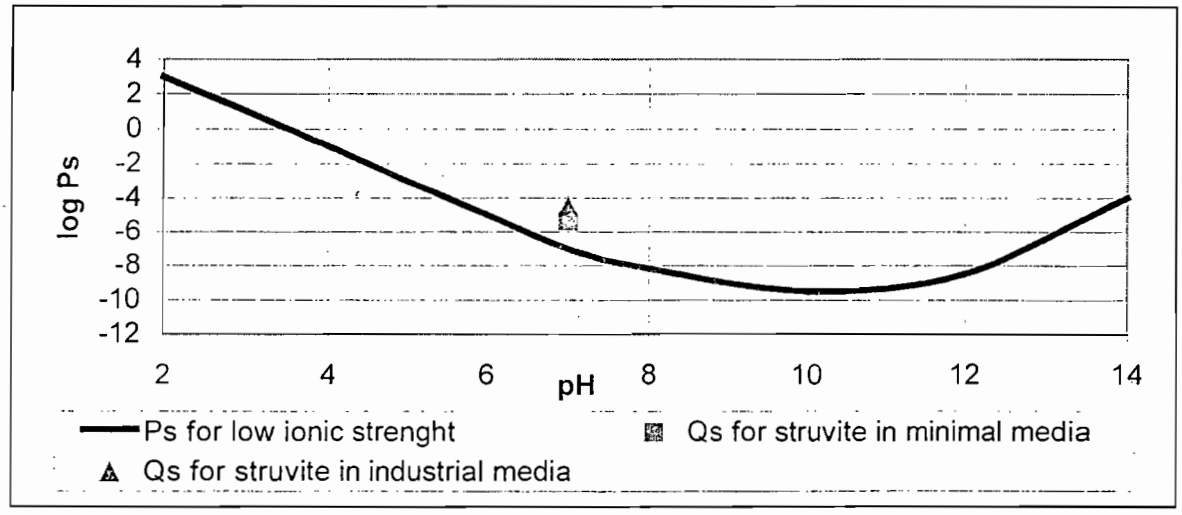

Figure 2-9. Conditional solubility product of struvite at the ionic strength of 0.1 and products of the actual concentrations of ammonium, magnesium and orthophosphate in minimal and industrial media formulations

The predicted solubility quotient (Q_s) for both the minimal and industrial media formulations significantly exceeded the conditional solubility product (P_s). The difference between Q_s and P_s can be assumed to precipitate out as struvite. The minimal and industrial media have an increased fouling potential due to the possibility of inorganic precipitation leading to the reduced filtration flux observed.

The membrane with the largest pore diameter (0.45-micron) exhibited the highest reduction in flux due to the presence of foreign matter in the feed suspension. This is consistent with the findings of Tarleton & Wakeman (1993); Lojinke *et al.* (1992); Le (1987) and Haarstrick, *et al.* (1991). Micro-filtration membranes are more susceptible to internal fouling by particulate matter compared to UF membranes (Tarleton & Wakeman 1993). Although the UF membranes exhibit a lower pure water flux than the MF membranes, the steady state flux for the cells suspended in the industrial media formulation is nearly 30% higher through the UF membranes due to the differences in internal fouling.

5.2 Effect of operating parameters on the steady state flux

The effect of the trans-membrane pressure drop and the cross-flow velocity on the filtration flux of cells suspended in the industrial media formulation was determined using the CCRD experimental design. The steady state flux, surface response for 150 kD and 0.45 μm cut-off membranes as predicted by the fit are illustrated in Figures 2-10 and 2-11 respectively.

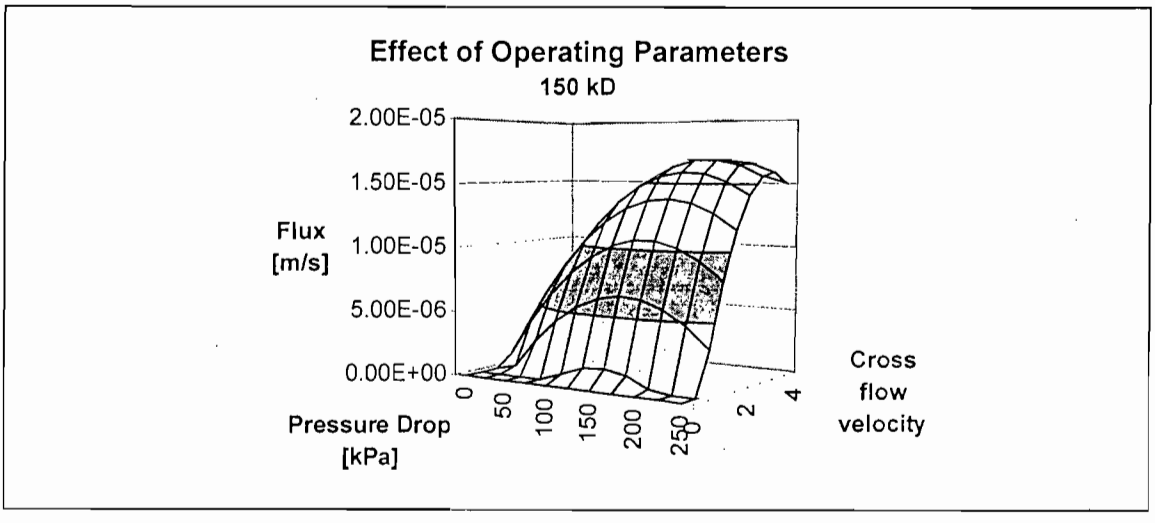

Figure 2-10. Surface response of the pseudo-steady state flux of cells suspended in industrial media through a 150 kD UF membrane under different cross-flow velocities and trans-membrane pressure drops as predicted by the CCRD fit.

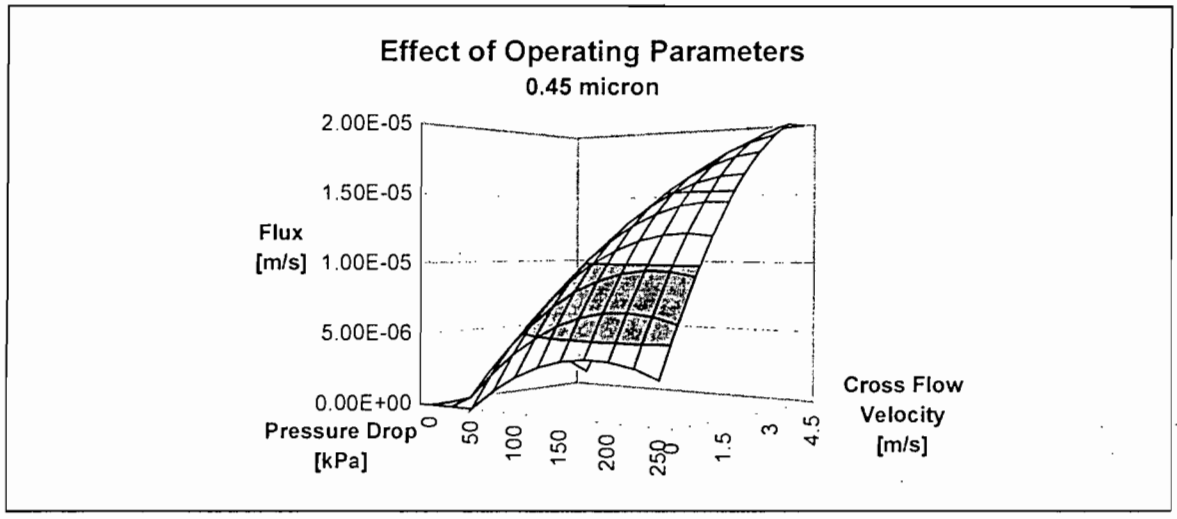

Figure 2-11. Surface response of the pseudo-steady state flux of cells suspended in industrial media through a 0.45-micron MF membrane under different cross-flow velocities and trans-membrane pressure drops as predicted by the CCRD fit.

The quadratic CCRD model for each of the membranes is given below.

$$\begin{aligned}\text{Flux (150 kD)} = & -3.55 \times 10^{-6} \\ & + 2.17 \times 10^{-8}\ \Delta P_{actual} \\ & +8.86 \times 10^{-6}\ v_{actual} \\ & - 1.96 \times 10^{-10}\ \Delta P_{actual}^{2} \\ & - 1.45 \times 10^{-6}\ v_{actual}^{2} \\ & + 1.75 \times 10^{-8}\ \Delta P_{actual} \cdot v_{actual}\end{aligned} \quad (2\text{-}5)$$

$$\begin{aligned}\text{Flux (0.45 } \mu\text{m)} = & +2.86 \times 10^{-6} \\ & + 3.31 \times 10^{-8}\ \Delta P_{actual} \\ & + 1.34 \times 10^{-6}\ v_{actual} \\ & - 8.77 \times 10^{-11}\ \Delta P_{actual}^{2} \\ & - 9.54 \times 10^{-8}\ v_{actual}^{2} \\ & + 9.46 \times 10^{-9}\ \Delta P_{actual} \cdot v_{actual}\end{aligned} \quad (2\text{-}6)$$

If the pressure drop and the cross-flow velocity are scaled to a number between –1.41 to +1.41 using a linear conversion the relative values of the quotients can be compared (Khuri & Cornell 1987). These equations are depicted below.

$$\text{Now} \quad \Delta P_{conv} = 70.7\ \Delta P_{actual} + 100 \quad (2\text{-}7)$$

$$v_{conv} = 1.41\ v_{actual} + 2.0 \quad (2\text{-}8)$$

with ΔP_{actual} in [kPa], and v_{actual} in m/s

$$\text{Flux (150 kD)} = 1.21 \times 10^{-5} + 1.24 \times 10^{-6}\,\Delta P_{conv} + 6.81 \times 10^{-6}\,v_{conv} - 9.82 \times 10^{-7}\,\Delta P_{conv}^{\,2} - 2.89 \times 10^{-6}\,v_{conv}^{\,2} + 1.75 \times 10^{-6}\,\Delta P_{conv}\,.v_{conv} \quad (2\text{-}9)$$

$$\text{Flux (0.45 } \mu\text{m)} = 9.49 \times 10^{-6} + 2.44 \times 10^{-6}\,\Delta P_{conv} + 2.70 \times 10^{-6}\,v_{conv} - 4.38 \times 10^{-7}\,\Delta P_{conv}^{\,2} - 1.91 \times 10^{-7}\,v_{conv}^{\,2} + 9.46 \times 10^{-7}\,\Delta P_{conv}\,.v_{conv} \quad (2\text{-}10)$$

The percentage error of each of the two fits is depicted in Figures 2-12 and 2-13. From these graphs, it can be seen that the model fits the experimental data within 5% over most of the tested range.

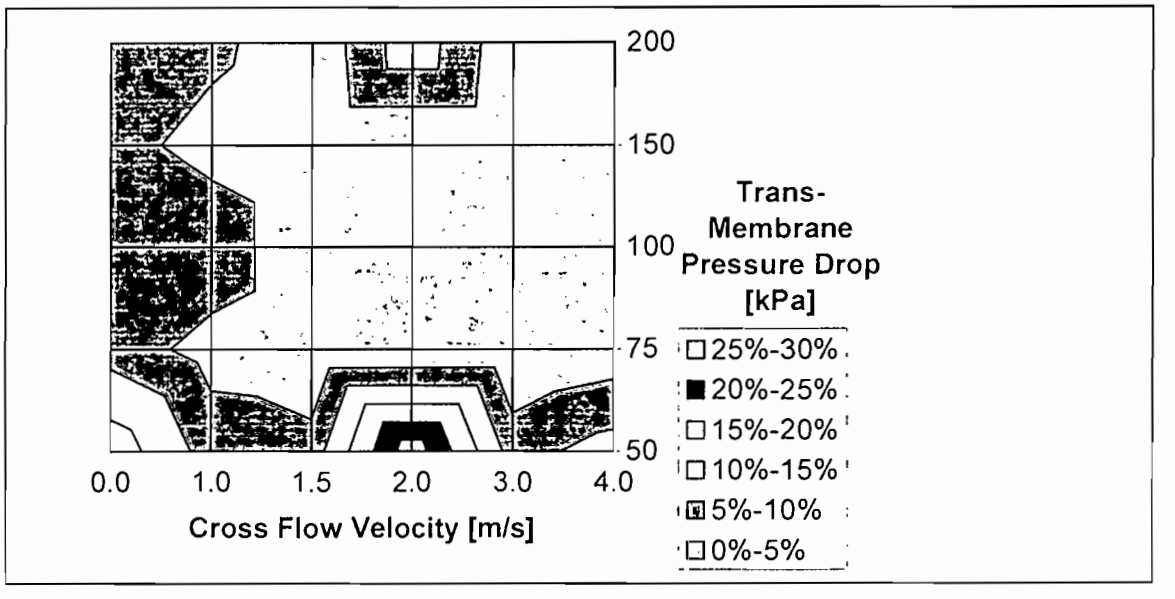

Figure 2-12. Percentage error as a function of the operating conditions for the 150 kD membrane CCRD experiment

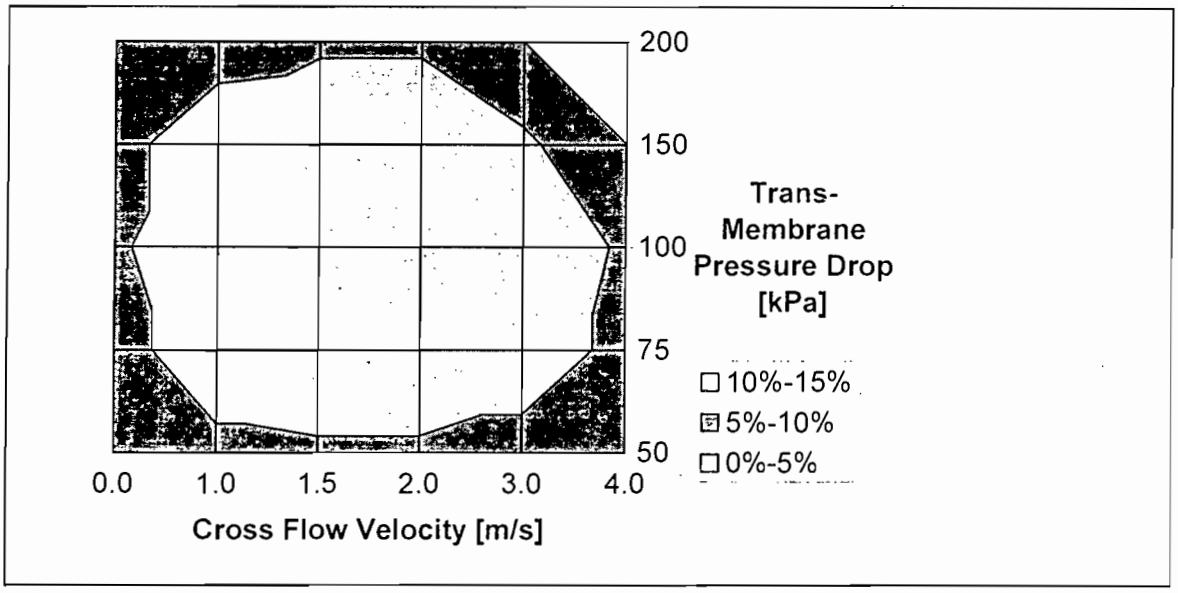

Figure 2-13. Percentage error as a function of the operating conditions for the 0.45-micron membrane CCRD experiment

5.2.1 Discussion

The effect of the trans-membrane pressure drop (ΔP) and the cross-flow velocity (v) depends on the membrane pore size. The effect of these parameters on the flux through the 0.45-μm membrane is more linear and exhibits fewer interactions than the flux through the 150 kD membrane.

For the 150 kD membrane the critical pressure drop or the pressure drop beyond which an increase in pressure drop does not result in a proportional increase in the flux, increases with increasing cross-flow velocities (Figure 2-10). The cross-flow velocity has an almost linear effect on the filtration flux.

There is much less interaction between the cross-flow velocity and the trans-membrane pressure drop for the 0.45-micron MF membrane (Figure 2-11). Furthermore, the non-linear terms in Equation 2-10 are an order of magnitude smaller than the linear terms indicating that the response is largely linear in the tested range. The increased error surrounding the evaluated range of parameter values indicates that beyond the evaluated range the impact cannot be fitted to a quadratic model. Nevertheless, it can still be seen that the critical pressure drop increases at increased cross-flow velocities. Although the effect of the cross-flow velocity is almost linear over the entire range of pressure drops the slope is much reduced at reduced pressure drops. Le *et al.* (1984b), Belfort *et al.* (1994) and Lojinke *et al.* (1992) reported similar phenomena for cross-flow filtration of microbial suspensions.

For both membranes, a critical pressure drop has been defined as the pressure beyond which an increase in the driving force does not result in a proportional increase in flux through the membrane. This has previously been explained by considering that the cake layer on the membrane surface is compressed at higher trans-membrane pressure drops (Belfort *et al.* 1994; Lojinke *et al.* 1992). The more dense cake layer leads to an increase in hydraulic resistance that balances the increased driving force.

Two explanations for the increase in critical pressure with increasing cross-flow velocity will be given:

- It has been recognised by various investigators that the mean particle size of the cake decreases with increasing cross-flow velocity (Wakeman 1994; Belfort 1994; Lojinke *et al.* 1992). Furthermore, cakes comprising smaller particles are less compressible due to their closer approximation of cubic close packing. The reduction in compressibility implies an increased critical pressure drop.

- Tanaka *et al.* (1994) showed that at higher cross-flow velocities rod shaped cells would align towards the direction of flow. This arrangement of the cells increased the specific resistance of the cake and decreased the compressibility thereof. As with the previous explanation the reduced compressibility implies an increased critical pressure drop.

6 Cross-flow filtration fouling mechanisms

In the next section the fouling mechanisms are investigated to attempt an understanding of the impact of the operating parameters on the cross flow filtration flux.

All pressure driven membrane separation processes must follow Darcy's law (Equation 2-1). This law states that the flux is proportional to the driving force and inversely proportional to the hydraulic resistance. The hydraulic resistance is made up of the permeate viscosity and the combined total membrane resistance (R_t). The total membrane resistance can be broken up into the intrinsic membrane resistance (R_m), the pore blocking resistance (R_p) and the cake resistance (R_c).

The intrinsic membrane resistance (R_m) is determined by measuring the pure water flux under a known driving force. The total resistance (R_t) is measured directly during the filtration process. To determine the pore blocking resistance (R_p) the cake layer on the membrane surface is removed physically using cotton wool plungers followed by the measurement of the water flux through the fouled membrane. The cake resistance is then determined by difference. The impact of the membrane pore size, the solvent composition and operating conditions on these resistances are discussed below.

6.1 The intrinsic membrane resistance (R_m)

The intrinsic membrane resistances (R_m) for each of the membranes were determined using pure water flux data. These values are summarised in Table 2-11 below. The intrinsic membrane resistance is independent of the trans-membrane pressure drop and the cross flow velocity.

Table 2-11. Intrinsic membrane resistance

Intrinsic membrane resistance		
300 kD	[1/m]	9.00E+11
150 kD	[1/m]	9.20E+11
0.45 micron	[1/m]	8.00E+10
0.22 micron	[1/m]	9.20E+10

6.2 The hydraulic cake resistance (R_c)

The resistance of the cake layer that forms on the membrane surface is calculated as the difference between the total hydraulic resistance and the pore and intrinsic membrane resistance.

Figure 2-14 shows the effect of the membrane pore size and the solvent composition on the measured cake resistance.

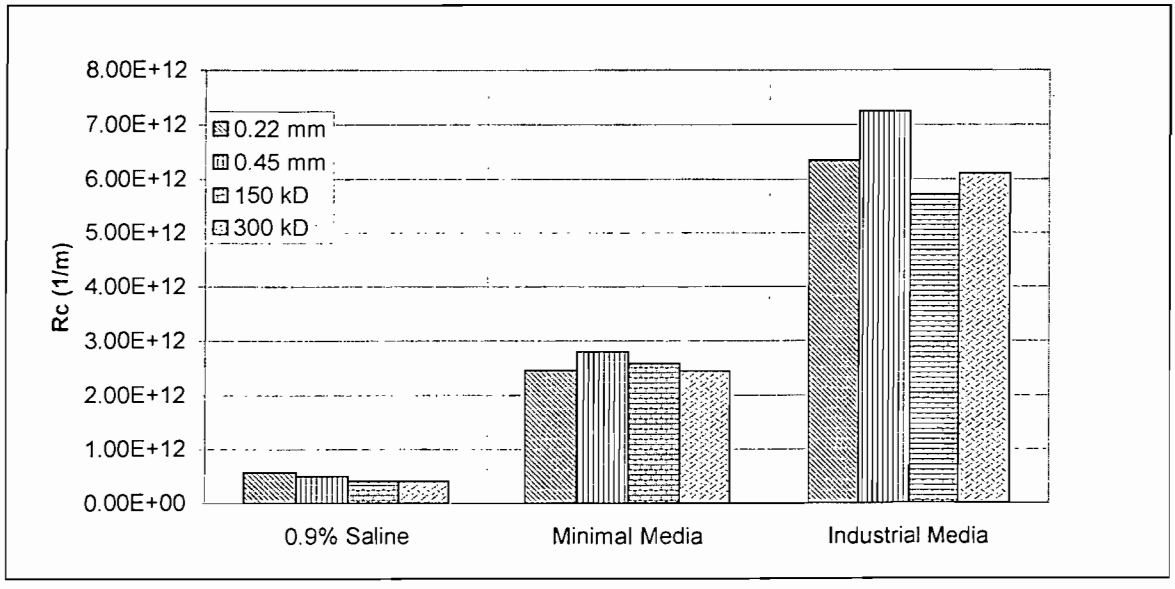

Figure 2-14. Effect of membrane pore size and solvent composition on the cake resistance at a cross flow velocity of 2 m/s, a trans-membrane pressure drop of 100 kPa with 35 g/l of DCW.

The cake resistance depends on the nature of the solvent. This is consistent with the findings published by Hoffman *et al.* (1987); Patel *et al.* (1987); Nipkow *et al.* (1989) and Tanaka *et al.* (1998), who also found that the cake resistance increases with increasing complexity of the media suspension.

For incompressible cakes, the porosity and the resistance are independent of the imposed differential pressure. The specific cake resistance per unit thickness ($\overline{R}_c$ in m^{-2}) may then be estimated by the Carman-Kozeny equation

$$\overline{R}_c = K'(1-\varepsilon_c)^2 \frac{S_c^2}{\varepsilon_c^3} \qquad (2\text{-}11)$$

where ε is the void fraction of the cake and S_c is the solid surface area per unit volume of solids in the cake (m^2/m^3). For rigid spherical particles of radius a (m), the specific surface area $S_c=3/a$, the void fraction of a randomly packed cake is 0.4 and the constant K' is 5.0 (Grace 1953). If these assumptions are used the cake layer thickness is calculated to be 2.2 mm for the saline suspension. This would mean that the entire tube would be one thick cake layer. This is clearly not possible.

Microbial cells are however highly compressible, exhibiting a decrease in void volume and an increase in specific resistance as the differential pressure is increased. The effects of cake compressibility are often estimated by assuming that the specific cake resistance is a power law function of the imposed pressure drop

$$\overline{R}_c = \beta \cdot (\Delta P)^{n_c} \qquad (2\text{-}12)$$

where β is a constant related primarily to the size and shape of the particles forming the cake. The cake compressibility (n_c) varies from zero for an incompressible cake to a value near unity for a highly compressible cake.

These quantities have been measured in dead-end filtration experiments over a trans-membrane pressure drop range of 40 to 300 kPa. The results are reported in Table 2-12. It should be recognised that the resistance as measured in dead-end and cross-flow filtration may differ significantly at high cross flow velocities with non-spherical particles (Xu-Jiang *et al.* 1995). Tanaka *et al.* (1994) however, reported that at modest cross-flow velocities (<3 m/s) the specific cake resistance calculated in dead-end filtration experiments can be used to model the cake resistance of a *Corynebacterium glutamicum* suspension in a complex media formulation. The same assumption did however not hold true for the rod shaped *Bacillus* species.

Table 2-12. Specific cake resistance of *C. glutamicum* cell cakes suspended in various solvents

Nature of the Solvent	n_c	β (m^{-2})	Specific cake Resistance @ 50 kPa (m^{-1})
Cells in 0.9% Saline	0.59	1.98E+10	1.18E+13
Cells in minimal media	0.60	2.68E+10	1.81E+13
Cells in industrial media	0.45	1.98E+11	2.57E+13
Cells in complex media – Tanaka *et al.* (1994)	0.32	1.10E+12	4.33e+13

The specific cake resistance increases as the complexity of the feed stream increases. The macromolecules and smaller particles present in the industrial media allow very dense packing of the cake on the membrane surface (Hoffman *et al.* 1987; Patel *et al.* 1987; Nipkow *et al.* 1989). The macromolecules also act as a binding agent between the cells to reduce the available pore volume (Tanaka *et al.* 1994). It has also been reported that the macromolecules can form a gel layer on the cake surface that is virtually impermeable (Tanaka *et al.* 1998). For the minimal media it has already been shown that struvite precipitation is thermodynamically possible. Choo and Lee (1996) reported that the precipitation of struvite in the cake layer was responsible for hardening the cake layer at the membrane surface where the strong binding and solidification leads to pronounced external fouling.

From Figure 2-14, it is also evident that the membrane pore size has very little impact on the cake resistance. Reismeier *et al.* (1990) found that the specific resistance of the cell layer deposited onto the membrane surface decreased as the pore size of the membrane increased. The did however not distinguish between the pore plugging and the cake resistance and explained this phenomena by stating that the membrane pore size influences the nature of the particles that are retained during the initial stages of the filtration process. In this study these two hydraulic resistances were determined separately and as such this finding does not contradict that of Reismeier *et al.* (1990).

6.3 Pore plugging resistance (R_p)

The pore plugging resistance was determined by physically removing the cake layer from the membrane surface with cotton wool plungers and measuring of the water flux through the fouled membrane. The pore plugging resistances of suspensions of *C. glutamicum* cells in various solvents through tubular ceramic membranes are depicted in Figure 2-15.

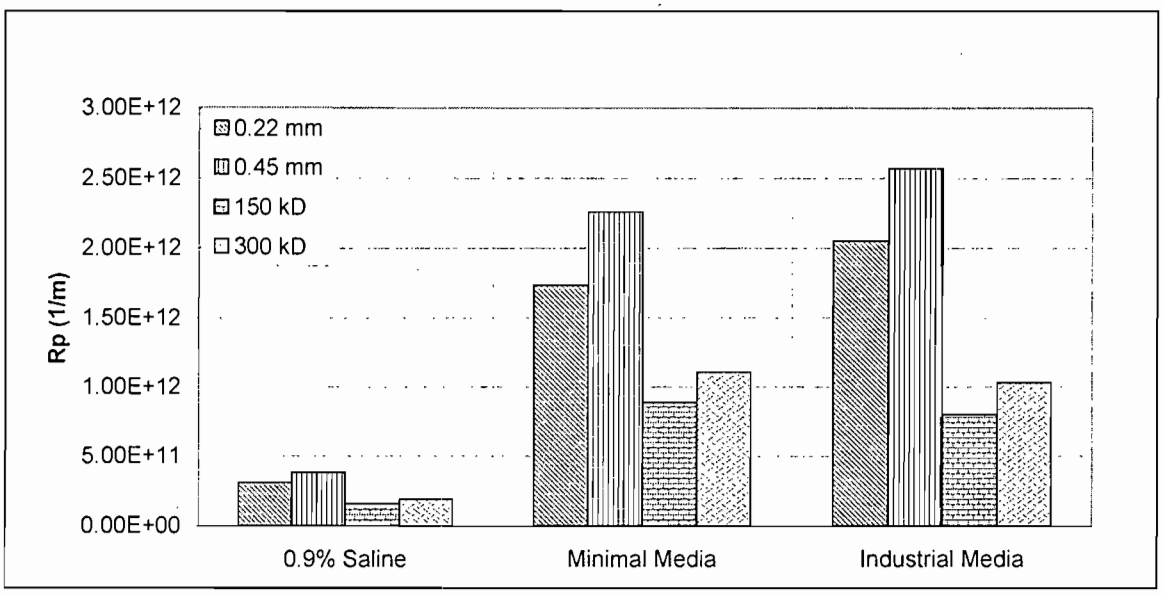

Figure 2-15. Membrane pore plugging resistance for cells suspended in various media formulations, measured at a cross-flow velocity of 2 m/s and a ΔP of 100 kPa

The pore plugging resistance is largely dependent on the membrane pore size. The MF membranes exhibited a much higher pore plugging resistance than the UF membranes. Since the cell size is orders of magnitude larger than the pore size for UF membranes, the internal fouling of the UF membrane should theoretically be zero for cells suspended in saline solution. A non-zero value is however measured. It should be kept in mind that this resistance is measured by physically removing the cake layer with a sponge plunger. The R_p value as reported here therefore represents the internal fouling resistance as well as the external resistance that was not removed by the physical method employed.

6.4 The impact of the operating parameters on the hydraulic resistances

The effect of the operating parameters on the hydraulic resistances for the cells suspended in an industrial media formulation through the 0.45-micron membrane is illustrated in Figures 2-16 and 2-17.

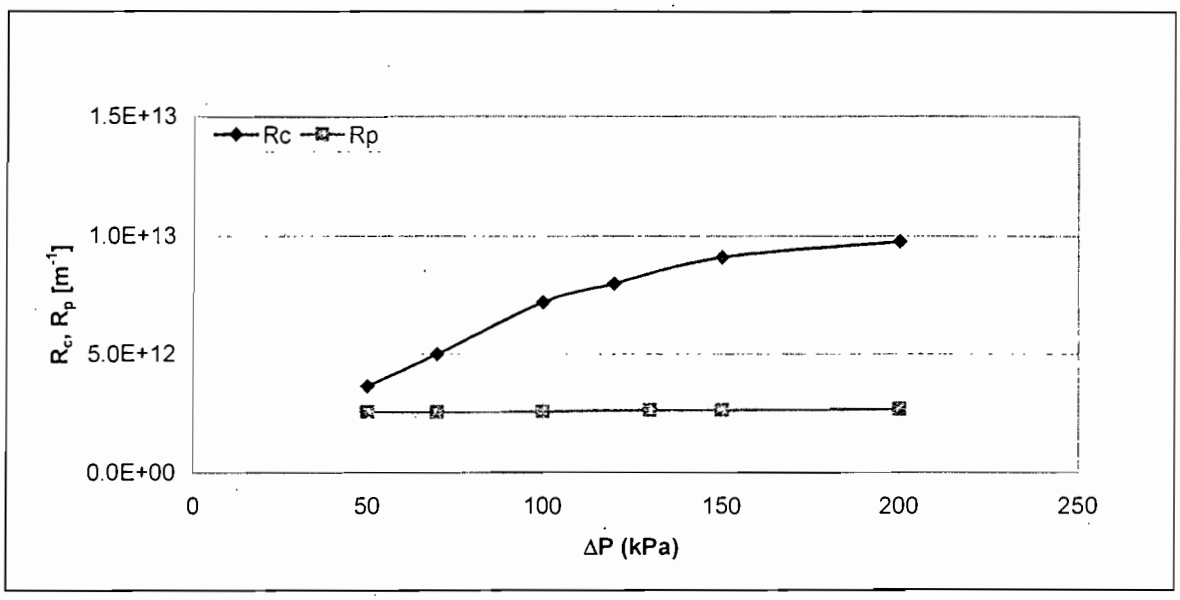

Figure 2-16. The effect of ΔP on the cake and pore resistance through a 0.45-micron MF membrane at a cross flow velocity of 2 m/s

The cake resistance increases with increasing trans-membrane pressure drop until a critical value is reached. The specific cake resistance as measured in dead-end filtration (Table 2-12) is of the same order of magnitude as that measured in cross-flow filtration. If cake compressibility is modelled by a power law (Equation 2-12), the compressibility coefficient of the cross-flow filtration cake is 0.7. This is significantly larger than the compressibility of the cake layer measured during dead-end filtration (0.45). Jiang *et al.* (1995) reported that cakes formed in the cross-flow mode are generally more permeable and more compressible than cakes formed in the dead-end mode. The higher compressibility was ascribed to the open filamentous structure of the cake formed during cross-flow filtration. Houi *et al.* (1986) and Schmitz *et al.* (1993) published computer simulations to illustrate these situations. The deposit formed in dead-end filtration was a compact low permeability cake, which would not be sensitive to pressure. The deposit formed in the cross-flow mode, where particles are captured in an open filamentous structure, was more permeabile but very susceptible to deformation under pressure. SEM photographs as reported by Tanaka *et al.* (1994) did not show this difference as clearly. In fact Tanaka *et al.* (1994) reported that the specific cake resistance measured in dead-end filtration could be used to estimate the cross-flow filtration flux if the cake thickness is known. It should be mentioned however that Tanaka *et al.* (1994) performed experiments at very low pressures (49 kPa) and that the compressibility difference had not been investigated.

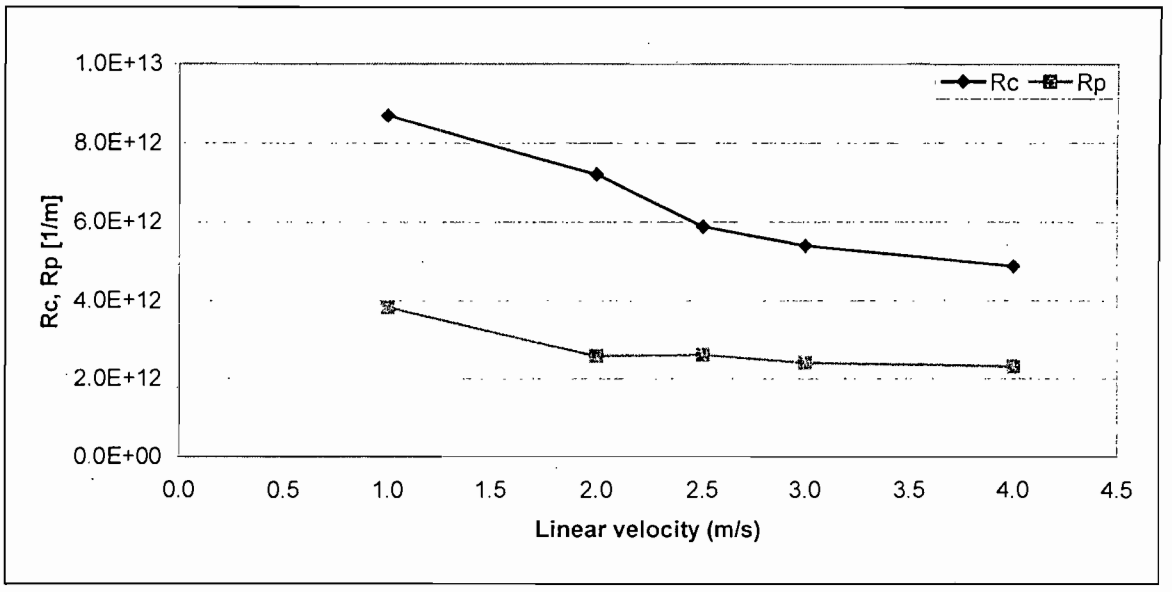

Figure 2-17. The effect of cross-flow velocity on the cake and pore plugging resistance through a 0.45-micon MF membrane, using a industrial media formulation and a trans-membrane pressure drop of 100 kPa.

The cake resistance decreases with increasing cross-flow velocity. Although it is recognised that the specific cake resistance of cross-flow and dead-end filtration cakes might have different compressibility characteristics the absolute values are in the same order of magnitude. If the dead-end filtration resistance is used, the cake weight on the membrane surface can be calculated from the measured flux. The cake weight per unit membrane area as a function of the cross-flow velocity is displayed in Figure 2-18.

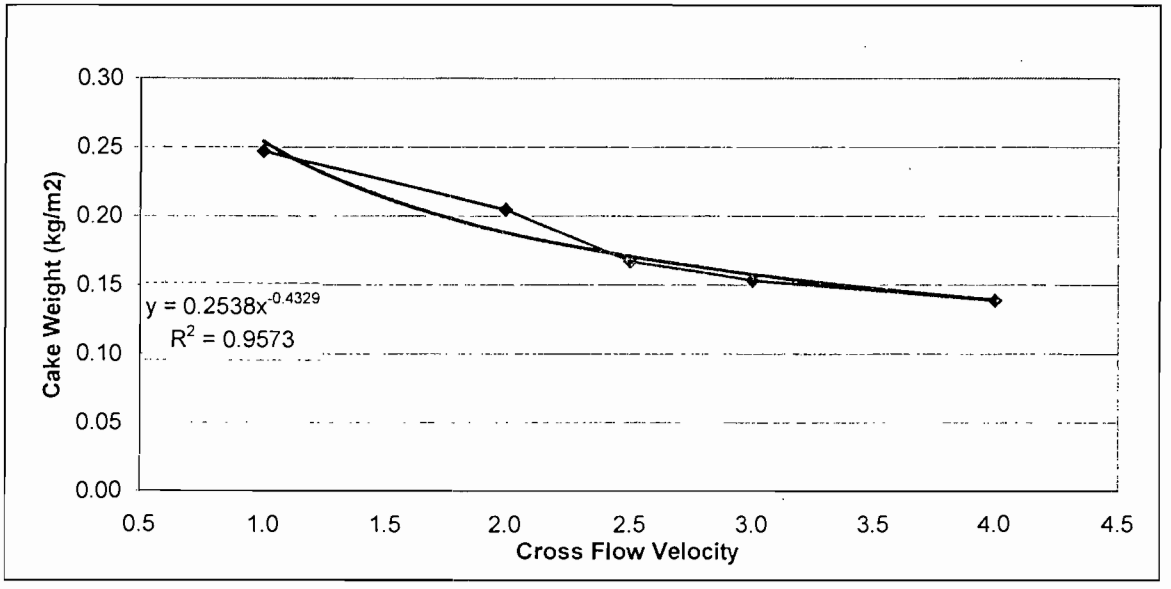

Figure 2-18. Cake weight as calculated using the specific cake resistance measured using dead end filtration as a function of the cross-flow velocity

The cake weight decreases with increasing cross-flow velocity. If it can be assumed that the cake is evenly spread over the membrane surface, this would imply that the cake thickness is reduced by increasing the cross-flow velocity. This is probably due to the larger shear forces experienced at elevated cross-flow velocities. Tanaka *et al.* (1998) reported a similar impact for the weight of *C. glutamicum* cells on the membrane surface as a function of the cross flow velocity.

The pore plugging resistance is largely independent of the cross-flow velocity (Figure 2-17). Although an increase in the cross-flow velocity would result in a flatter trajectory of particles toward the membrane surface (Tarleton & Wakeman 1993), the increase in cross-flow velocity brings smaller particles to the membrane surface that allows for easier internal fouling (Zydney & Colton 1986). Thus although an increased velocity would imply a reduced solid flux toward the membrane surface, there is an increase in the flux of smaller particles to the membrane surface. These two opposing effects could explain the insensitivity of the pore plugging resistance to the cross-flow velocity.

7 The factors that influence the decline of the cross-flow filtration flux of *C. glutamicum* suspensions.

In previous sections, the factors that influence the pseudo-steady state cross-flow filtration flux were investigated. In this section, the flux decline pattern and the factors that influence it are investigated to shed more light on the mechanism of the fouling process. A typical flux decline pattern is illustrated in Figure 2-19 below. The flux declines sharply over the first 200 seconds and then reaches the pseudo steady state value.

Various investigators (Belfort *et al.*1994; Redkar & Davis 1993) have proposed that the flux decline seen in cross-flow filtration can be described by the same fundamental principles used to explain dead-end filtration behaviour. Hermia (1982) developed four constant pressure, blocking laws that are commonly encountered in dead-end filtration applications.

The following characteristic form of the blocking filtration laws was identified

$$\frac{d^2t}{dV_f^2} = k_{BL}\left(\frac{dt}{dV_f}\right)^{n_{DE}} \qquad (2\text{-}13)$$

where t is time in seconds, V_f is the filtrate volume (m^3) and k_{BL} and n_{DE} are constants characteristic to each of the filtration laws (Table 2-13).

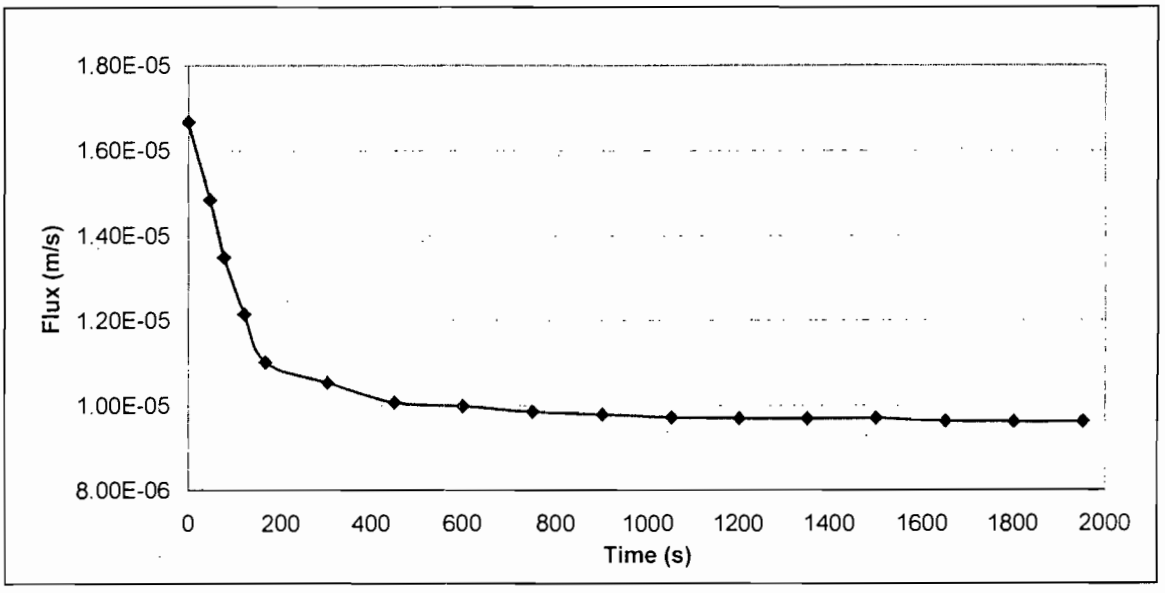

Figure 2-19. Typical cross-flow filtration flux decline pattern, for cells suspended in minimal media, filtered at a cross-flow velocity of 2 m/s, a trans-membrane pressure drop of 100 kPa at 35 g/l DCW through a 0.45-micron tubular ceramic membrane.

Table 2-13. The values of the constants k_{BL} an n_{DE} in Equation 2-13

Law	k_{BL}	n_{DE}
Cake Filtration	$\frac{\overline{R}_c \rho_p s}{AR_m Perm_0 (1 - ms)}$	0
Intermediate	$\frac{\sigma}{A_0}$	1
Standard Law	$\frac{2C_b Perm_0^{0.5}}{L_{mem} A}$	1.5
Complete Blocking	$v\sigma$	2

where $\overline{R}_c$ Specific cake resistance per unit cake thickness (m^{-2})
ρ_p Permeate density (kg/m^3)
s Solid fraction in feed
σ Blocked membrane area per unit permeate volume (m^2/m^3)
R_m Intrinsic membrane resistance (1/m)
$Perm_0$ Permeate volumetric flow rate (m^3/s)
m Mass of cake formed on membrane surface (kg/m^2)
C_b Concentration of foulant species in feed (g/l)
L_{mem} Membrane length (m)
A Membrane area (m^2)
v Cross-flow velocity (m/s)

Factors affecting the cross-flow filtration flux

Cake filtration occurs when the retained solutes accumulate onto the membrane surface in a cake layer that increases the hydraulic resistance to permeate flow. The specific resistance of the cake layer that builds up on the membrane surface is given by the Carman-Kozeny equation. The flux decline is indirectly proportional to the rate of build-up, which is proportional to the rate at which particles reach the membrane surface. This rate is often approximated by the product of the retained solute concentration and the volume of filtrate.

The complete blocking law is based on the assumption that every particle that reaches the membrane participates in the blocking phenomenon by pore sealing, implying that particles are not superimposed. The blocked membrane area is then proportional to the volume of filtrate. The reduced filtrate flow rate is a result of the reduced area available for permeate flow.

The intermediate blocking law allows particles to settle on other particles. The model therefore evaluates the probability of a particle blocking a pore. The probability decreases as the extent of fouling increases due to the reduced availability of unblocked pores.

The standard blocking law assumes that the pore volume decreases proportionally to the filtrate volume by particle deposition on the pore walls. The membrane is assumed to consist of a set of pores of constant diameter and equal length. The decrease of pore volume is then equal to the decrease of pore cross section. Poiseuille's equation is used to find the flow through the membrane.

In Figure 2-21 the derivative of the inverse of the permeate flow rate (G as defined in Equation 2-14) is plotted against the volume of filtrate collected for the experimental data presented in Figure 2-19.

$$G = \frac{d^2t'}{dV'_f{}^2} \qquad (2\text{-}14)$$

where t' is the time (hours) since the start of the filtration process and V'_f is the total permeate volume (in litres) collected at time t'.

Figure 2-20 indicates that there might be two fouling mechanisms at work during the flux decline observed in Figure 2-19. From Equation 2-13 it is clear that if the log of G is plotted against the logarithm of the inverse of the permeate flow rate a straight line would indicate that one of the blocking laws can be used to describe the fouling mechanism at hand. The slope of the line yields the constant n_{DE} as specified in Table 2-13 while the intercept indicates the logarithm of k_{BL} as defined in Equation 2-13.

In Figure 20 the log of G (the inverse of the second derivative of the permeate volume) is plotted against the log of the inverse of the permeate flow rate.

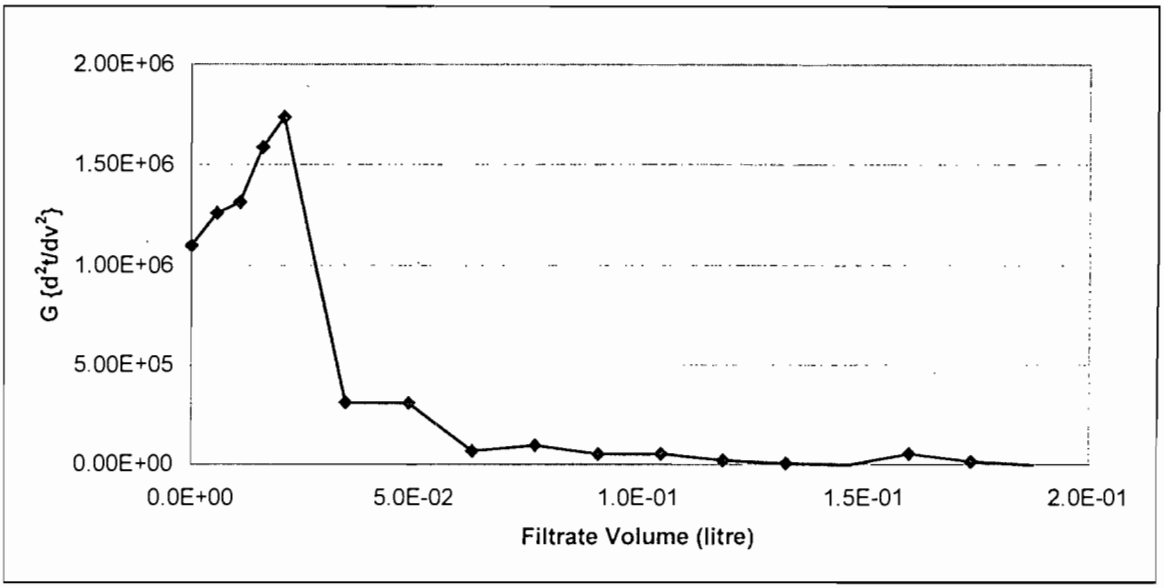

Figure 2-20. Classification of the fouling mechanisms involved during the cross-flow filtration flux decline for cells suspended in minimal media, filtered at a cross-flow velocity of 2 m/s, a trans-membrane pressure drop of 100 kPa at 35 g/l DCW through a 0.45-micron tubular ceramic membrane.

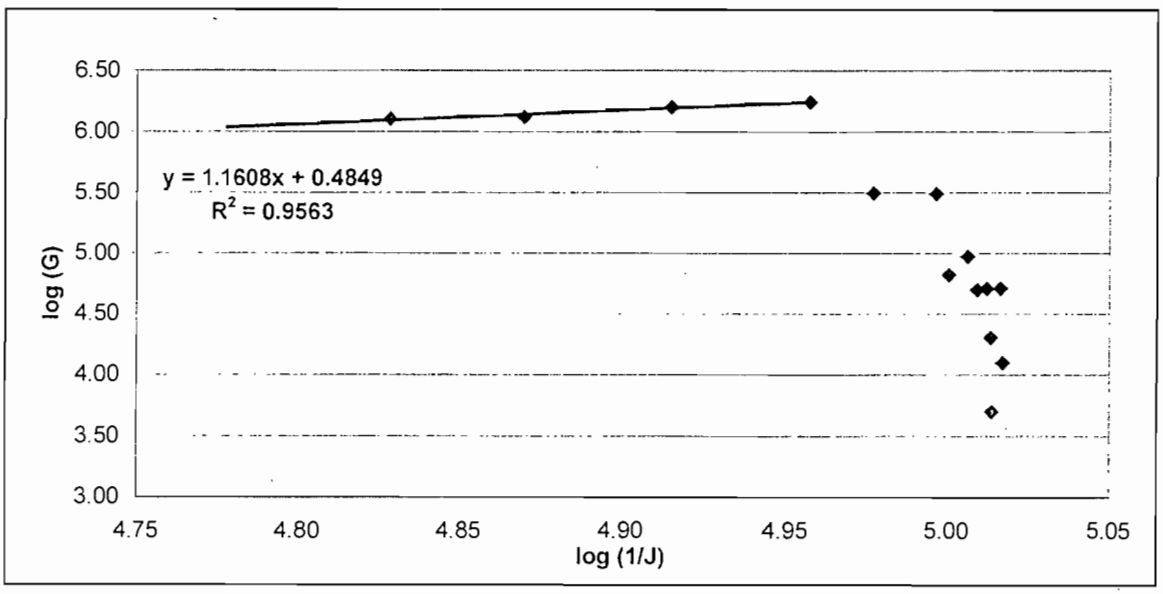

Figure 2-21. A plot of the log of G against the log of the inverse of the permeate flow rate for cells suspended in minimal media, filtered at a cross-flow velocity of 2 m/s, a trans-membrane pressure drop of 100 kPa at 35 g/l DCW through a 0.45-micron tubular ceramic membrane.

The two regions on both sides of the peak in Figure 2-20 represents two different predominating fouling mechanisms. To the left of the peak, Figure 2-21 shows that G vs. the inverse of the permeate flow rate is a straight line with a slope of 1.16. This corresponds to the intermediate blocking filtration law. It should be noted that this is not the only fouling mechanism but merely the predominating fouling mechanism during this period. To the right of the peak the slope of the line for the next two points is zero, corresponding to the cake filtration law. The large negative slope corresponds to the pseudo steady state region.

From the presented graph, it seems that the initial flux decline is governed by the partial blocking of the membrane pores. This period is followed by the build-up of a cake layer on the membrane surface until the pseudo steady state flux is reached.

The values of the "n_{DE}" factor in the constant pressure blocking law (Equation 2-13) and the fouling constant "k_{BL}" as a function of the membrane pore size and the feed suspension are summarised in Figure 2-22 and 2-23.

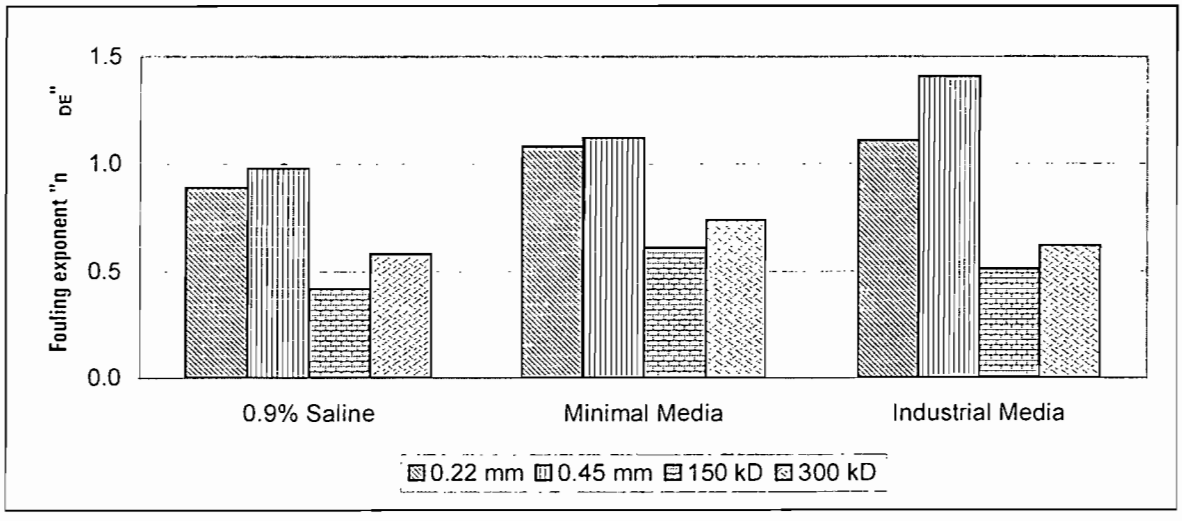

Figure 2-22. Values of the constant "n_{DE}" (as defined in Equation 2-13) as a function of the membrane pore size and the feed media at a cross-flow velocity of 2 m/s, a trans-membrane pressure drop of 100 kPa at 35 g/l DCW.

The values of the constant, "n_{DE}" are all around 1 for the MF filtration membranes while the value decreases to roughly 0.6 for the UF membranes. The n_{DE}-value of 1 corresponds to the intermediate blocking law as defined in Equation 2-13 by Hermia (1982). As the value of n_{DE} decreases, cake filtration becomes more predominant. This implies that the MF filtration membranes are fouled internally following predominantly the intermediate blocking law, while the UF membranes are fouled by cake build-up.

It is interesting to note that the value of n_{DE} for microfiltration membranes increases as the media complexity increases. The standard and the complete blocking laws (Hermia 1982) are based on pore blocking and constriction. Thus as the value of n_{DE} increases, internal

fouling becomes more predominant. The increase in the value of n_{DE} with increasing media complexity could therefore be a result of the larger proportion of fines and macromolecules present in the complex media. These particles cause internal fouling leading to the increased value of n_{DE}. The n_{DE} value of the 300 kD ultrafiltration membrane was larger than that of the 150 kD membrane. Similarly, the value of n_{DE} for the 0.45-micron membrane was larger than that of the 0.22-micron membrane. It would seem that increased membrane pore size leads to an increase in the probability of internal fouling. This is consistent with the findings of Tarleton & Wakeman (1993); Lojinke *et al.* (1992); Le (1987); Haarstrick *et al.* (1991) and Tarleton & Wakeman (1993).

The values of the constant "k_{BL}" in Equation 2-13 as determined for both ultra and microfiltation membranes are shown in Figure 2-21.

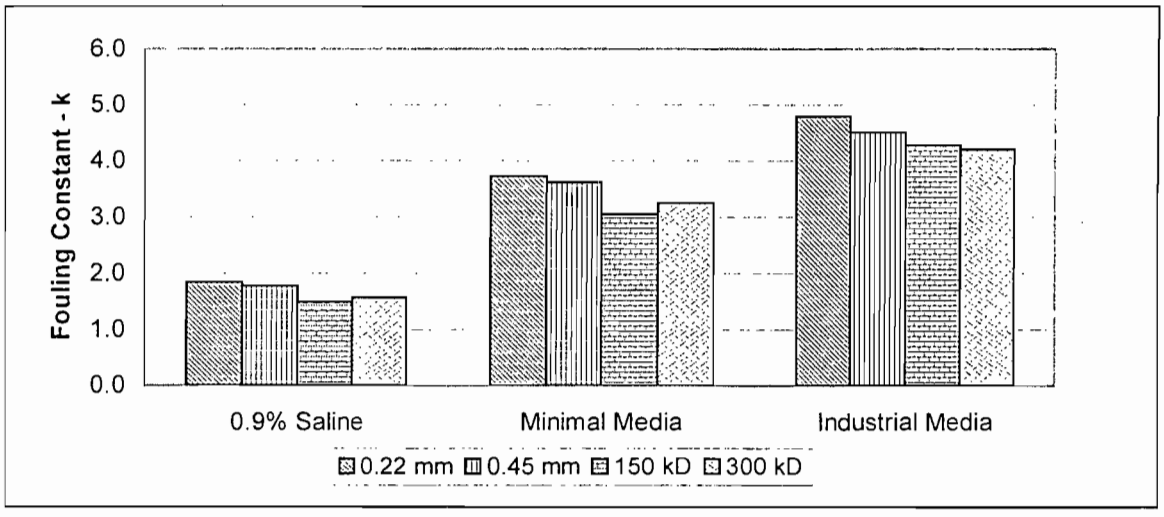

Figure 2-23. Value for the fouling constant, "k_{BL}" (as defined in Equation 2-13) as a function of membrane pore size and solvent composition for cells filtered at a cross-flow velocity of 2 m/s, a trans-membrane pressure drop of 100 kPa at 35 g/l DCW

From Figure 2-23 it seems that the k_{BL} value is a function of the type of solvent. Very little impact of the membrane pore size has been detected on the fouling constant. Shirato *et al.* (1979) has shown that the constants k_{BL} and n_{DE} (as defined in Equation 2-13) are influenced by the composition of the feed. According to Hermia (1982) the cake filtration constant, k_{BL} depends on the specific cake resistance, the thickness of the cake layer and the clean membrane resistance. For the intermediate filtration law the filtration constant (k_{BL}) is a function of a factor, σ depicting the blocked area per unit filtrate volume (m^2/m^3) and the clean membrane area (See Table 2-13). According to the theoretical analysis of Hermia (1982), k_{BL} should increase with increasing complexity (specific cake resistance $\propto$ complexity of media for cake filtration and $\sigma \propto$ complexity of media for the intermediate filtration law) and increase with increasing membrane pore size (decreasing membrane resistance). Both these effects were detected qualitatively in Figure 2-23.

Figure 2-20 showed a local maximum at the point beyond which the straight-line fit of Figure 2-21 could not be extended. This maximum point corresponds to the point when the predominating fouling mechanism changes from internal fouling to cake build-up. The filtrate volumes at which the predominating fouling mechanism changes are summarised in Figure 2-24.

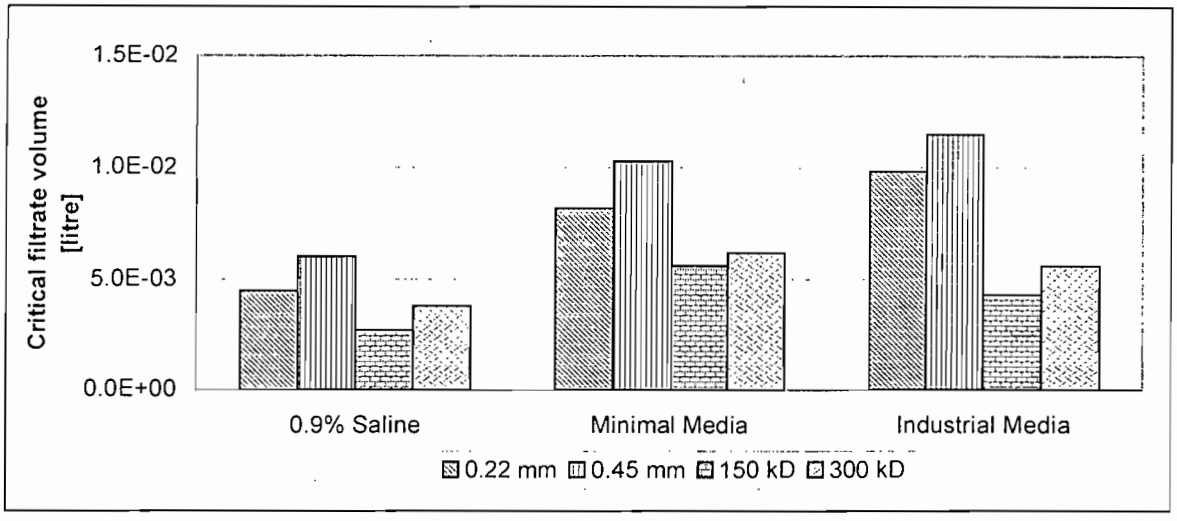

Figure 2-24. The filtrate volume at which the predominating fouling mechanism changes from pore blocking or constriction to cake build-up at a cross-flow velocity of 2 m/s, a trans-membrane pressure drop of 100 kPa at 35 g/l DCW.

The critical filtrate volume at which the dominant fouling mechanism changes is a function of both the membrane pore size and the nature of the solvent (Figure 2-24). Generally, the volume is reduced for the UF membranes compared to MF membranes and increases with increasing solvent complexity. Thus as the complexity of the feed suspension increases more foulant reaches the membrane surface per unit filtrate volume increasing the rate of fouling. Furthermore as the membrane pore size decreases less particles are deposited prior to cake formation and the establishment of the pseudo steady state flux. Belfort *et al.* (1994); Tarleton & Wakeman (1993); Lojinke *et al.* (1992); Ficher and Raasch (1986); Rautenbach (1988); De Balman *et al.* (1990) and Hermia (1982) all suggest that this process is stochastic in nature and depends on the availability of either an open membrane pore or a protrusion on the membrane surface where the particle can be deposited or entrapped. The latter depends to a large extend on the operating parameters that dictates the shear forces experienced by the cells on the cake surface.

8 Conclusions

The membrane pore size and the feed suspension complexity and pore size distribution have an impact on the cross-flow filtration flux. The pseudo-steady state flux decreases as the complexity of the solvent increases. The effect of the membrane pore size on the pseudo steady state flux can largely be ignored for the more complex solutions. Internal

fouling as seen by the values of R_p was more severe for the MF membranes than for the UF membranes.

The flux increased with increasing ΔP (below the critical ΔP) and also with increasing cross-flow velocity. The effect of these operating parameters were predominantly linear for the MF membrane while for the UF membranes the effects were highly non-linear in the tested range. For both MF and UF membranes the critical pressure drop increased with increasing cross-flow velocity.

Membrane fouling has been divided into internal and external fouling phenomena. Internal fouling involves pore plugging and constriction. The extent of the internal fouling was measured as the pore plugging resistance (R_p). The pore plugging resistance depends on the membrane pore size and the fraction of particles of similar size to the membrane pores in the feed. The pore plugging resistance increases with increasing ΔP to a maximum where it remains constant as a pressure independent value. The cross-flow velocity did not significantly influence the pore plugging resistance.

The cake resistance depends on the solvent composition. The resistance increases with increasing complexity of the feed suspension. The cake compressibility is however reduced for the industrial media suspension compared to the minimal and saline solvents. The cake resistance increases with increasing pressure drop until a pressure independent value is reached, while the resistance is reduced with increased cross-flow velocity. It has been found that the cake weight decreases as the cross-flow velocity increases.

The filtration flux typically declines sharply over the first 200 seconds and then reaches a pseudo-steady state value. From a flux decline analysis it has been found that, the initial period of flux decline is predominantly a result of internal fouling. The decrease in flux has been described by Hermia's (1982) intermediate filtration law. The initial flux decline is followed by a period of cake build-up. During this period, the flux decline follows Hermia's (1982) cake filtration law. This is continued until the cake thickness corresponding to the cross-flow velocity is reached. At this point the flux remains relatively constant declining at an almost undetectable rate.

The critical filtrate volume at which the predominate fouling mechanism changes is a function of both the membrane pore size and the nature of the solvent. Generally, this volume is reduced for the UF membranes compared to MF membranes and increases with increasing solvent complexity.

The understanding of the fouling phenomena encountered during the cross-flow filtration of *C. glutamicum* suspensions serves as a basis for the development of a fundamental model describing the system behaviour. This model is discussed in the next chapter.

9 References

Aimar, P., Meireles, P., Bacchin, P. and Sanchez, V. (1994), Fouling and concentration polarisation in ultrafiltration and microfiltration, *NATO ASI Ser. E*, **272**, 27-57

Aptel, P. and Buckley, C. A. (1992), Categories of membrane operations, In "Water Treatment: Membrane Processes", Mallevaille, J., Odendaal, P. E. and Wiesner, M. R. (eds), Chapter 2, McGraw Hill

Arora, N., and Davis, R. H. (1994), Yeast cake layers as secondary membranes in dead-end microfiltration of bovine serum albumin, *Journal of Membrane Science,* **92,** 247-256

Baker, R. J., Fane, A. G., Fell, C. J. D. and Yoo, B. H. (1985), Factors affecting flux in cross-flow filtration, *Desalination,* **53,** 81-93

Bansal, A., Ma, Y. H., Clark, W. M. (1991), A quantitative investigation of membrane fouling by proteins using energy dispersive spectroscopy, *Key Eng. Mat.,* **61,** 505

Bauser, H., Chmiel, H., Stroh, N. and Walitza, E. (1982), Interfacial effects with microfiltration membranes, *Journal of Membrane Science*, **11,** 321-332

Belfort, G., Davis, R. H., Zydney, A. L. (1994), The behaviour of suspensions and macromolecular solutions in cross-flow microfiltration, *Journal of Membrane Science,* **96,** 1-58

Bowen, W. R. and Clark, W. M. (1984), Electro-osmosis at microporous membranes and the determination of zeta potential, *J. Colloid Interface,* **72**(2), 401

Bowen, W. R. and Gan, Q. (1991), Properties of microfiltration membranes: The effect of adsorption and shear on the recovery of an enzyme, *Biotechnology and Bioengineering, **38,** 688*

Cheryan, M. (1986), "The Ultrafiltration Handbook", Technomic, USA

Choo, K. and Lee, C. (1996), Membrane fouling mechanisms in the membrane coupled anaerobic bioreactor, *Water research,* **30**(8), pp 1771-1780

Clark, W. M., Bansal, A. Sontakke, M. and Ma, Y. H. (1991), Protein adsorption and fouling in ceramic ultrafiltration membranes, *Journal of Membrane Science,* **55,** 21-38

Datar, R. (1984), Tangential flow membrane filtration of bacterial cell debris form crude homogenates, *World Biotech Report,* **2,** A15-A30

Davis, R. H. and Birdsell, S. A. (1987), Hydrodynamic model and experiments for crossflow microfiltration, *Chem. Eng. Commun.*, **49,** 217-234

Davis, R. H. (1992), Modelling of fouling of crossflow microfiltration membranes, *Sep. Purif. Methods,* **21,** 75-126

De Balmann, H., Aimar, P. and Sanchez, V. (1990), Membrane partition and mass transfer in ultrafiltration, *Sep. Sci. and Technol.,* **25**(5), 507-534

Defrise, D. and Gekas, V. (1988), Microfiltration membranes and the problem of microbial adhesion, *Process Biochem.* **23**(4), 105-116

Fane, A. G., Fell, C. J. D. and Waters, A. G. (1981), The relationship between membrane surface pore characteristics and flux for ultrafiltration membranes, *Journal of Membrane Science,* **9,** 245-262

Fane, A. G., Jim, K. J., Hodgson, P., Leslie, G., Fell C. D. J., Franken, A. C. M., Chen, V. and Liew, K. H. (1990), Strategies to minimise fouling in the membrane proessing of biofluids, presented at *Frontiers in Bioprocessing II, Boulder, Colorado, June 17-21*

Fischer, E. and Raasch, J. (1985), Cross flow filtration, *Ger. Chem. Eng.,* **8,** 211-216

Fischer, E. and Raasch, J. (1986), Model tests of the particle deposition at the filter medium in cross-flow filtration, *Proc. Fourth World Filtration Conference,* Ostend 1986 (Part II), 11.11-11.17

Forman, S. M., DeBernardez, E. R., Feldberg, R. S. and Swartz, R. W. (1990), Crossflow filtration for the separation of inclusion bodies from soluble proteins in recombinant *Escherichia coli* lysate, *Journal of Membrane Science,* **48,** 263-279

Gabler, R. and Ryan, M. (1985), Processing cell lysate with tangential flow filtration, *Purification of Fermentation Products: Application to Large Scale Processes* (LeRoith D., Schilback T., Leahy T. Eds), 1-20, ACS Symposium Series, 271

Gatenholm, P., Fell, C. J. and Fane, A. G. (1988a), Influence of the membrane structure on the composition of the deposit layer during processing of microbial suspensions, *Desalination,* **70**(1-3), 363-378

Gatenholm, P., Paterson, S., Fane, A. G. and Fell, C. D. J. (1988b), Performance of synthetic membranes during cell harvesting of *E. coli, Process Biochem.,* **23**(3), 79-81

Grabler, F. R. (1985a), Cell processing using tangential flow filtration, In "Comprehensive Biotechnology", Vol. 2, Coeney, Humphrey, Eds., Permagon Press, Oxford, 351-366

Grabler, R. and Ryan, M. (1985b), Processing cell lysate with tangential flow filtration, In "Purification of Fermentation Products: Application to large scale processes", LeRoith, Schilback, Leahy, Eds., ACS Symposium Series, 271

Grace, H. P. (1953), Resistance and compressibility of filter cakes, *Chem. Eng. Prog.,* **49,** 303-318

Green, G. and Belfort, G. (1980), Fouling of ultrafiltration membranes, lateral migration and the particle trajectoy model, *Desalination,* **35,** 129-147

Haaland, P. D. (1989), "Experimental design in biotechnology", Marcel Dekker Inc, NY, pp30-35

Haarstrick, A., Rau, U. and Wagner, F. (1991), Cross-flow filtration as method of separating fungal cells and purifying the polysaccharide produced. *Bioprocess Eng.,* **6,** 179-186

Hadj Sassi, A., Deschamps, A. M. and Lebealt, J. M. (1996), Process analysis of L-lysine fermentation with *Corynebacterium glutamicum* under different oxygen and carbon dioxide supplies and redox potentials, *Process Biotechnology,* **31**(5), 493-497

Harris, T. A. J., Reuben, B. G., Cox, D. J., Vaid, A. K. and Carvell, J. (1988), The cross-flow filtration of an unstable beta-lactum antibiotic fermentation broth, *J. Chemical Technol. and Biotechnol.,* **42 19**-30

Henry, J. D. and Alfred, R. C. (1972), Concentration of bacterial cells by cross-flow filtration, *Develop. In Industrial Microbiol.,* **13,** 177-190

Herak, D. C. and Merrill, E. W. (1989), Affinity crossflow filtration: experimental and modelling work using the system of HAS and Cibacron blue-agarose, *Biotechnol. Progress,* **5**(1), 9-17

Hermia, J (1982) Constant pressure blocking filtration laws: application to power law non-newtonian fluids, *Trans. Inst. Chem., Eng.,* **60,** 183

Hoffman, H., Scheper, T., Schugerl, K. and Schmidt, W. (1987), Use of membranes to improve bioreactor progress, *The Chemical Engineer,* **34**, B13-B19

Houi, D. and Lenormand, R. (1986), Proceedings of the 4th World filtration congress, Ostend, Belgium, Vol. 8, 1.1-3

Howell, J. A., Sanchez, V. and Field, R. W. (1993), "Membranes in Bioprocessing: Theory and Applications", Chapman & Hall, London

Khuri A. I. and Cornell, J. A. (1987), "Response surface: Design and analysis", NY, Marcel Dekker Inc and Milwaukee ASQC Quality Press, pp 45-54

Kroner, K. H. and Nissenen, V. (1985), Dynamic filtration of microbial suspensions using an annular rotating filter, *Journal of Membrane Science,* **36,** 85-100

Kroner, K. H. and Nissinen, V. (1988), Dynamic filtration of suspensions using an axially rotating filter, *Journal of Membrane Science.,* **36,** 85-100

Kroner, K. H., Nissinen, V. and Ziegler, H. (1987), Improved dynamic filtration of microbial suspensions, *Bio/Technology,* **5**, 921-926

Le, M. S. and Atkinson, T. (1985), Cross-flow microfiltration for recovery of intracellular products. *Process Biochem.* **20**(1), 26-31

Le, M. S. and Billet, C. T. (1984) The use of membranes in crossflow mode for the separation of cells and cell product recovery, *Downstream Processing,* **84,** Swansea

Le, M. S. (1987), Recovery of beer from tank bottoms with membranes, *J. Chem. Technol. and Biotechnol.,* **37,** 59-66

Le, M. S., Spark, L. B. and Ward, P. S. (1984a), The separation of acylamidase by crossflow microfiltration and the significance of enzyme/cell debris interaction. *Journal of Membrane Science,* **21**, 219-232

Le, M. S., Spark, L. B., Ward, P. S. and Ladwa, N. (1984b), Microbial asparaginase recovery by membrane processes, *Journal of Membrane Science,* **21,** 307-319

Leonard, E. F. and Vassilieff, C. S. (1984), The deposition of rejected matter in membrane separation processes, *Chem. Eng. Commun.,* **30,** 209-217

Liberge, R., Collinart, P., Fessier, P. and Renon, N. H. (1994), Data and model for progressive fouling in cross flow microfiltration on three industrial mineral membranes, *Ind. Eng. Chem. Res.,* **35,** 1310-1318

Lojinke, M. H., Field, R. W. and Howell, J. A. (1992), Crossflow microfiltration of cell suspensions: a review of models with emphasis on particle size effects, *Trans. Inst. Chem. Eng.,* **70,** 149-164

Lu, W. –M. and Ju, S. –C. (1989), Selective particle deposition in crossflow filtration. *Sep. Sci. Technol.,* **24,** 512-540

Mackley, M. R. and Sherman N. E. (1992), Cross-flow cake filtration mechanisms and kinetics, *Chem. Eng. Sci.,* **47,** 3067-3084

Mateus, M. and Gabral, J. M. S. (1989), Recovery of 6-alpha-methylprednisolone from biotransformation medium by tangential flow filtration, *Bioprocess Eng.,* **4**(4), 160-174

Matsumoto, K., Katsuyama, S. and Ohya, H. (1987), Separation of yeast by cross-flow filtration with backwashing. *J. Fermentation Technol.* **65,** 77-83

Mattiasson, B. and Ramstrop, M. (1984), Ultrafiltration affinity purification: isolation of concanavalin A from seeds of *Canavalia ensiformis, J. Chromatog,* **283,** 323-333

Michaels, A. S. (1968), New Separation Techniques for the CPI, *Chemical Engineering Progress,* **64**(12), 31-43

Michales, A. S. and Matson, S. L. (1985), Membranes in biotechnology: State of the art, *Desalination,* **53,** 231-258

Mochizuki, S. and Zydney, A. L. (1993), Sieving characteristics of albumin deposits formed during microfiltration. *J. Colloid Interface Sci.,* **159,** 136

Mulder, M. (1991), "Basic Principle of Membrane Technology", Kluwer Academic Publishers, Dordrecht

Nagata, N., Herouvis, K. J., Dziewulski, D. M. and Belfort, G. (1989), Crossflow membrane microfiltration of a bacterial fermentation broth, *Biotechnology. Bioengineering.,* **34,** 447-466

Nagata, N., Herouvis, K., Dziewulski, D. M. and Belfort, G. (1989), Cross-flow membrane microfiltration of a bacterial fermentation broth, *Biotechnology. Bioengineering.,* **44,** 161-181

Nipkow, A., Zeikus, J. G. and Gerhardt, P. (1989), Microfiltration cell recycle pilot system for continuous thermoanaerobic production of exo-beta-amylase, *Biotechnology and Bioengineering,* **34,** 1075-1084

Ofsthun, N. J. and Colton, C. K. (1987), Visual evidence of concentration polarization in cross-flow membrane plasmapheresis, *Am. Soc. Artif. Intern. Organs J.,* **10,** 510-517

Ofsthun, N. J. (1989), Crossflow membrane filtration of cell suspensions, PhD Thesis, Massachusetts Institute of Technology, chemical Engineering Department, Cambridge, MA

Opong, W. S. and Zydney, A. L. (1991), Hydraulic permeability of protein layers deposited during ultrafiltration, *J. Colloid Interface Sci.,* **142,** 41

Palacek, S. P. and Zydney, A. L. (1994a) Hydraulic permeability of protein deposits formed during microfiltration: effect of solution pH and ionic strength, *Journal of Membrane Science,* **95,** 71-81

Palacek, S. P. and Zydney, A. L. (1994b), Intermolecular electrostatic interactions and their effect on flux and protein deposition during protein filtration, *Biotechnol. Prog.,* **10,** 207-213

Patel, P. N., Mehaia, M. A. and Cheryan, M. (1987), Crossflow membrane filtration of yeast suspensions, *J. Biotechnology,* **5,** 1-16

Persson, K. M., Capannelli, G., Bottino, A. and Tragardh, G. (1993), Porosity and protein adsorption of four polymeric microfiltration membranes, *Journal of Membrane Science,* **76,** 61-71

Pritchard, M. (1991) *PhD Thesis,* University of Bath, UK

Pritchard, M., Howell, J. A. and Field, R. W. (1992), The concentration of viscous fluids by ultrafiltration, *Engineering of Membrane Processes,* Conference May 1992, Bavaria Germany

Quirck, A. V. and Woodrow, J. R. (1984), Investigation of the parameters affecting the searation of bacterial enzymes from cell debris by tangential flow filtration, *Enzyme Microb. Technol.,* **6**(5), 201-206

Rautenbach, R. and Albrecht, R. (1989), "Membrane Processes", John Wiley, New York

Rautenbach, R. (1988), Ultrafiltration of macromolecular solutions and crossflow microfiltration of colloidal suspensions. A contribution to permeate flux calculations, *Journal of Membrane Science,* **36,** 231-242

Rebsamen, E., Goldinger, W., Scheirer, W., Merten, O. W. and Palfi, G. E. (1987), Use of a dynamic filtration method for the separation of animal cells, *Dev. Biol. Standard,* **66,** 273-277

Redkar, S. G. and Davis, R. H. (1993), Crossflow microfiltration of yeast suspensions in tubular filters, *Biotechnol. Prog.,* **9,** 625-634

Reismeier, B., Kröner, K. H. and Kula, M. R. (1987), Studies on secondary layer formation and its characteristics during crossflow filtration of microbial cells, *Journal of Membrane Science,* **34**(3), 245-266

Reismeier, B., Kröner, K. H. and Kula, M. R. (1989), Tangential filtration of microbial suspensions: filtration resistance and model development, *J. Biotechnol.,* **12,** 153-172

Reismeier, B., Kroner, K. H. and Kula, M. R. (1990), Harvest of microbial suspensions by microfiltration, *Desalination,* **77,** 219-233

Romeo, C. A. and Davis, R. H. (1991), Experimental verification of the shear-induced hydrodynamic diffusion model of cross-flow microfiltration, *Journal of Membrane Science,* **62,** 249-273

Ryder, D. S., Davis, C. R., Anderson, D., Glancy, F. M. and Power, J. N. (1988), Brewing experience with crossflow filtration, *MBAA Technical Quaterly,* **25,** 67-79

Sakai, K., Ozawa, K., Ohashi, K., Yoshida, R. and Sakarai, H. (1989), Low-temperature plasma separation by cross-flow microfiltration with microporous glass membranes, *Ind. Eng. Chem. Res.,* **28,** 57-64

Schmitz, P., Wandelt, B., Houi, D. and Hildebrand, M. (1993), *Journal of Membrane Science,* **84,** 171-183

Schutte, H., Kröner, K. H., Hummel, W. and Kula. (1983), Recent developments in separation and purification of biomolecules, *Annals New York Acad. Sci.,* **413,** 270-282

Scott, J. A. (1988), Application of crossflow filtration to cider fermentations, *Process Biochem,* **23**(5), 146-148

Shimizu, Y., Rokudai, M., Tohya, S., Kayawake, E., Yazawa, T., Tanaka, H. and Eguchi, K. (1989), Filtration characteristics of charged alumina membranes for methonogenic wastes, *J. Chem. Eng. Japan,* **22,** 635-641

Shirato, M., Aragaki, T. and Iritani, E. (1979), *Chem. Eng. J. (Japan)*, **12,** 162

Sieveka E. H. (1966), Reverse osmosis pilot plants in U. Merten (Ed.), Desalination by Reverse Osmosis, The MIT. Press, Cambridge, MA, Chap 7.

Snoeyink, V. L. and Jenkins, D. (1980), "Water Chemistry", John Wiley and Sons, New York, N.Y.

Stamatakis, K and Tien, C. (1993), A simple model of cross-flow filtration based on particle adhesion, *AIChE J.,* **39,** 1293-1302

Stumm, W. and Morgan, J. (1981), "Aquatic Chemistry", 2nd Edn, John Wiley and sons, New York, N.Y.

Taddei, C. and Howel, J. A. (1989), On the effect of membrane conditioning in cell harvesting using microfiltration, *Biotechnol. Techniques,* **3**(3), 155-160

Taddei, C., Aimar, P., Howell, J. A and Scott, J. A. (1990), Yeast harvesting from cider using microfiltration, *J. Chem. Technol. Biotechnol.,* **47,** 365-376

Tanaka, T., Abe, K.I., Asakawa, H., Yoshida, H. and Nakanishi, K. (1994), Filtration characteristics and structure of cake in crossflow filtration of bacterial suspension, *J. Ferment. and Bioeng.,* **78,** 455-461

Tanaka, T., Usui, K. and Nakanishi, K. (1998), Formation of a gel layer of polymers and its effects on the permeation flux in cross flow filtration of *Corynebacterium glutamicum* broth, *Separation Science and Technology,* **33**(5), 707-722

Tanny G. B., Strong D. K., Presswood W. G. and Meltzec T. H., *et al. (*1979), Absortive retention of *Pseudomonas diminuta* by membrane filters, *J. parenteral Drug Association,* **33**(1), 40-51

Tanny, G. B., Mirelmean, P. and Pistole, T. (1980), Improved filtration technique for concentration and harvesting bacteria, *Applied and Environ. Microbiol.* **40,** 269-273

Tarleton, E.S., "The Modelling and Simulation of Solid/Liquid Filtration Processes" 1994, pp 19-20, Particle Technology Subject Group of IChemE, Invited paper .

Tarleton, E. S. and Wakeman, R. J. (1993), Understanding flux decline in crossflow microfiltation – Part I, Effects of particle and pore size, *Trans. IChemE,* **71,** Part A, 399

Tarleton, E. S. and Wakeman, R. J. (1994a), Understanding flux decline in crossflow microfiltration – Part II, Effects of process parameters, *Trans. IChemE,* **72,** Part A, 431

Tarleton, E. S. and Wakeman, R. J. (1994b), Understanding flux decline in crossflow microfiltration – Part III, Effects of membrane morphology, *Trans. IChemE,* **72,** Part A, 521

Wakeman, R. J. (1994), Visualisation of cake formation in cross flow microfiltration, *Trans. IChemE,* **72**, Part A, 530

Wankat, P. C. (1990), Rate Controlled Separations, Elsevier Applied Science

Xu-Jiang, Y., Dodds, J. and Ledere, D. (1995), Cake characteristics in cross flow and dead-end microfiltration, *Filtration and Separation,* September, 795

Zsigmondy, R. (1992) US Patent 1,421,341

Zydney A. L. and Colton C. K. (1986), A concentration polarization model for the filtrate flux in cross-flow microfiltration of particulate suspensions, *Chem. Eng. Commun.*, **47,** 1-21

Modelling of the Cross-Flow Filtration Flux of Suspensions of *Corynebacterium glutamicum* Cells

1 Introduction

The objective of this thesis was to study, understand, model and optimise the performance of the L-lysine fermentation with biomass retention using cross-flow filtration. In the previous chapter the factors that influence the cross-flow filtration flux of suspensions of *Corynebacterium glutamicum* cells were studied. The impact of these factors led to a discussion of the mechanisms involved in flux decline. In this chapter these mechanisms form the basis of a set of mathematical equations to model the flux decline observed experimentally.

Various other attempts to model the cross-flow filtration flux of microbial suspensions have been made. Most of these approaches have been described in review papers (Lojinke *et al.* 1992; Belfort *et al.* 1994). These models were reviewed and tested against the experimental data obtained in this study.

In the next chapter, Bayesian inference was used to select the most appropriate filtration model based on the available experimental data.

2 Review of the existing filtration models

Two approaches have been used to model the filtration process. The first involves empirical correlations of the measured permeate flow rate under different operating conditions. The form of the correlation has no physical meaning and is entirely dictated by the measured data. These models generally predict the experimental data very well but are not suitable for scaling-up and limited to the specific raw material and filter geometry (Liberge *et al.* 1994; Romero & Davis 1990; De Balmann 1988).

On the other hand various investigators have proposed fundamental physical and chemical processes that explained and described the flux decline pattern during filtration of cell suspensions. Unfortunately there are very few, if any models available that accurately describes all the available data (Wakeman 1994; Tarleton & Wakeman 1993; Belfort *et al.* 1994; Zydney & Colton 1994; Lojinke *et al.* 1992).

Some examples of these modelling approaches are discussed in the next two sections. The structure for the discussion of the existing filtration models is depicted in Figure 3-1.

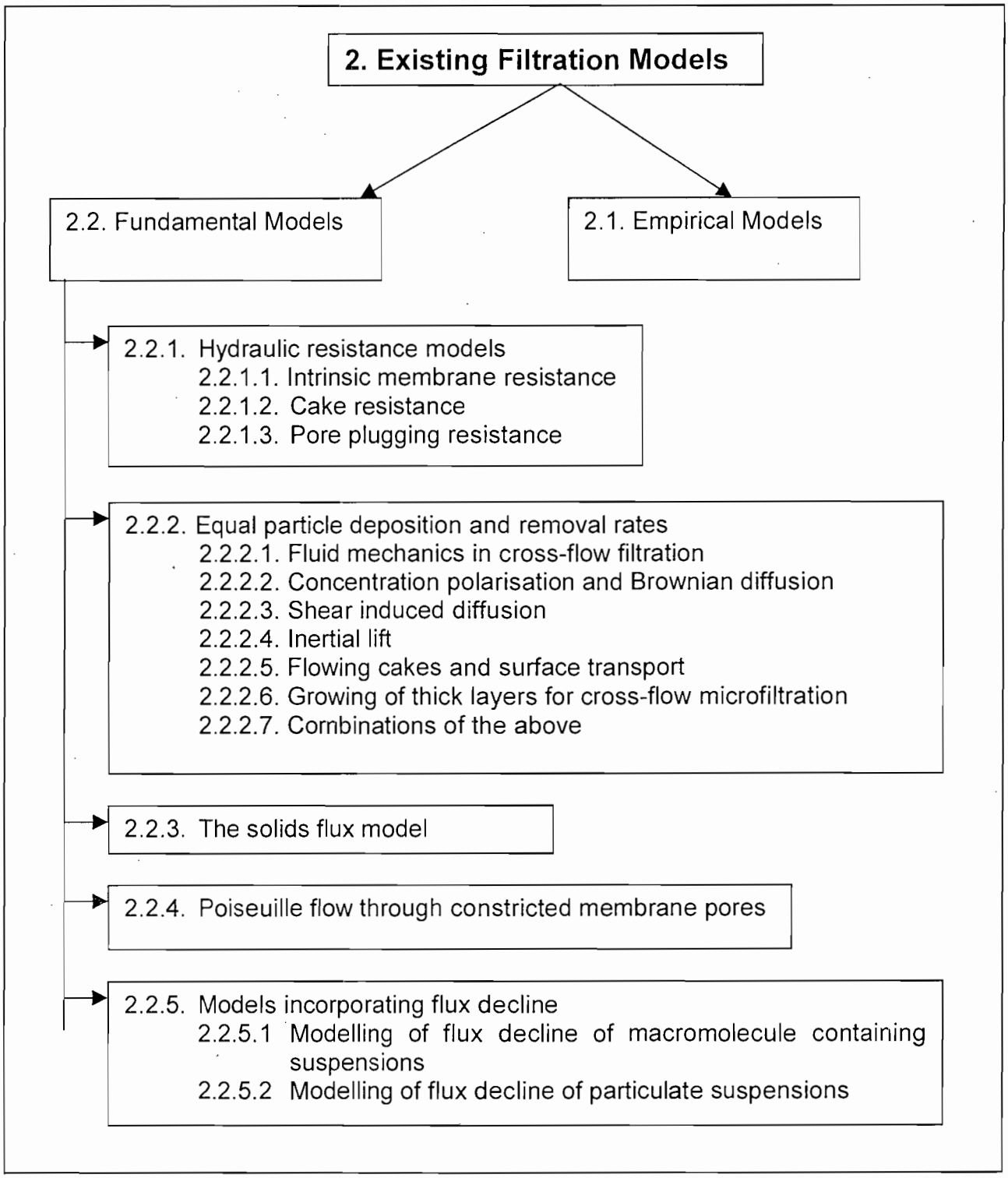

Figure 3-1. Classification of the existing filtration models for the purpose of this discussion

2.1 Empirical Models

Empirical power laws have been suggested by several authors to predict the permeate flux through micro-filtration membranes (de Balmann 1988; Romero & Davis 1990; Liberge *et al.* 1994). Liberge *et al.* (1994) suggested a stepwise multiple regression program to estimate the coefficients of the following equation:

$$Ln(Perm) = a_0 + a_1\bar{x}_1 + a_2\bar{x}_2 + \ldots + a_n\bar{x}_n \qquad (3\text{-}1)$$

where the variables $\bar{x}_i$ were chosen among Z_i; $\ln(Z_i)$; $Z_i\ln(Z_j)$. With Z_i $Z_j \in$ [Parameters that influences the filtration flux] and $i \neq j$

The terms Z or ln Z account for the main influence of the possible operating parameters and the terms Z ln Z test for possible interactions among them. This approach was adapted for the purposes of this study so that Z_i $Z_j \in$ [cell concentration – X in g/l DCW, lysine concentration – Lys in g/l, cross flow velocity – v in m/s, trans-membrane pressure drop - ΔP in Pa and time – t in h] and $i \neq j$. The experimental data obtained in the previous chapter was used together with a multiple regression module in the "STATISTICA" software package to develop a power law prediction of the permeate flux. It was done for suspensions of *C. glutamicum* cells in industrial media formulations through a 150 kD cut-off tubular ceramic membrane.

The multiple regression program uses a least squares method to adjust the coefficients in Equation 3-1. The total variance between the proposed values and the experimental data can be separated into explained (by the model) and the residual variance. The correlation coefficient (R^2) is defined as the ratio of the explained to the total variance. A correlation coefficient close to one indicates that the proposed equation explains the experimental data while values approaching zero would indicate that the variance in the data cannot be explained by the equation.

Using a variance analysis of the regression, the program tests if the proposed variables are significant for each regression. A variable is significant for the regression if it produces a significant increase in the correlation coefficient (R^2). The optimal solution is that with the highest R^2 value with all its coefficients significant at a specific confidence interval (95%).

With all 13 the parameters in place a correlation coefficient of 0.9568 was found, the optimal solution (with the ascending stepwise regression used) had 7 parameters with a correlation coefficient of 0.9429. These solutions are presented below (Equation 3-2 and 3-3).

$$\text{Perm} \times 3.6 \times 10^{9} = e^{7.09+7.42v+0.07t-0.02C}\, t^{0.15-0.01C+0.05v}\, v^{-4.71+0.26C-0.07t}\, X^{0.10-0.01t-2.67v} \quad (3\text{-}2)$$
$$R^2 = 0.9568$$

$$\text{Perm} \times 3.6 \times 10^{9} = e^{10.77}\, t^{-0.01C}\, X^{-1.52}\, v^{-0.58+0.02C+0.01t} \quad (3\text{-}3)$$
$$R^2 = 0.9429$$

where Perm is the permeate flow rate (litre/h); v is the cross-flow velocity (m/s); X is the dry cell weight biomass concentration (g/l); ΔP is the trans-membrane pressure drop (Pa) and t is the time (h).

Each of the coefficients in the optimal solution was found to be significant at a 95% confidence interval. A comparison of the measured versus the predicted data with the optimal empirical solution is presented in Figure 3-2.

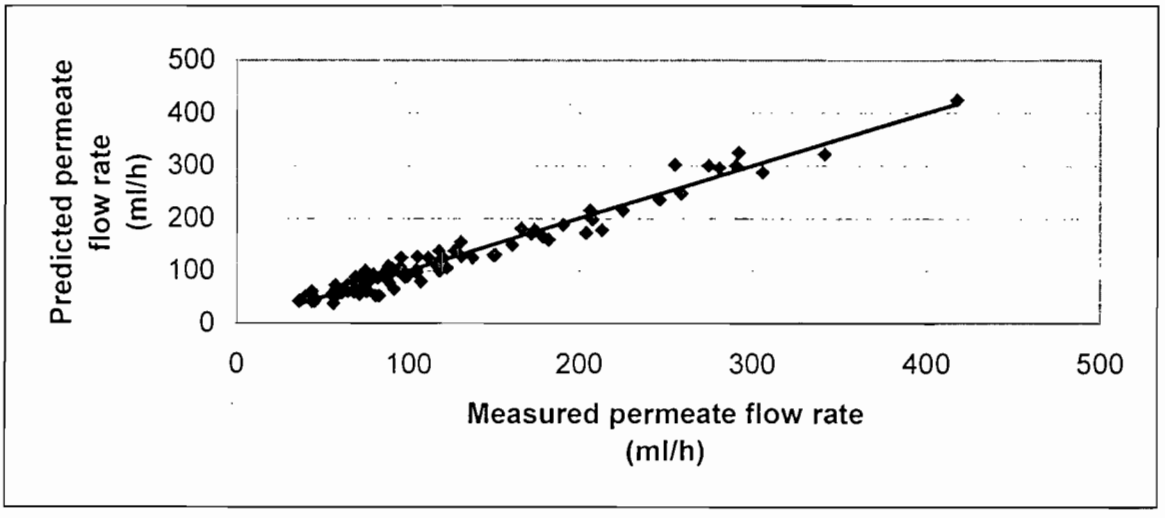

Figure 3-2. Comparison of the measured and predicted permeate flow rate of a 35 g/l (DCW) suspension of *C. glutamicum* cells through a 150 kD, ultrafiltration membrane. The predicted permeate flow rate was determined by using the optimal empirical correlation

From Figure 3-2 it is clear that the empirical model adequately predicts the flux behaviour of a specific fed suspension through a specific membrane. In this case a suspension of *C. glutamicum* cell in an industrial media formulation through a tubular ultrafiltration membrane.
The presented equation would be valid within the tested range of the operating parameters and cannot be extrapolated beyond that range. Therefore the window of operating paramters as well as the spread of data within that window is presented in Table 3-1.

Table 3-1. Operating parameters for cross-flow filtration evaluation

	Time (t) [h]	*Concentration* (X) [g/l]	*Velocity* (v) [m/s]
Average	20.8	40.4	1.9
Standard deviation	17.5	7.3	0.3
Minimum	0	20.7	1.6
Maximum	63.0	53.6	2.4
50% Percentile	16.0	42.3	2.0
10% Percentile	0.3	30.3	1.6
90% Percentile	47.9	48.7	2.4

2.2 Fundamental Models

Most fundamental cross-flow filtration models fall into two main classes: resistance models and particle back-flux models. These models were developed to explain the following phenomena observed experimentally (Tarleton & Wakeman 1993; Belfort *et al.* 1994; Zydney & Colton 1994; Lojinke *et al.* 1992):

- A constant pseudo steady state flux is reached, after an initial sharp decline.
- The steady state flux is not linearly dependent on the trans-membrane pressure drop and under some conditions it is pressure independent.
- The steady state flux has a power law relationship with cross-flow velocity.

2.2.1 Hydraulic resistance models

The hydraulic resistance models are based on Darcy's law (Belfort *et al.* 1992). When a suspension is filtered through a membrane the permeate flux through the membrane is given by the driving force divided by the hydraulic resistance (Equation 3-4). The driving force for ultra and micro-filtration is the pressure drop across the membrane. The hydraulic resistance is made up of the viscosity of the permeate and some hydraulic resistance associated with the membrane and the extent of fouling. This resistance can be considered as a combination of the membrane resistance (R_m), the resistance due to pore blocking (R_p) and the cake resistance (R_c). The flux can therefore be given by:

$$J = \frac{1}{A}\frac{dV_f}{dt} = \frac{\Delta P}{\upsilon(R_m + R_p + R_c)} \qquad (3\text{-}4)$$

where J(t) is the permeate flux (m/s) at time t, V_f the total volume of permeate collected (m^3) at time t, A the membrane area (m^2), t the filtration time (s), ΔP the

trans-membrane pressure drop (Pa), υ the permeate viscosity (Pa·s), R_m the intrinsic hydraulic resistance of the membrane (m^{-1}), R_p is the resistance caused by membrane pore constriction (m^{-1}) and R_c the hydraulic resistance due to the formation of a cake layer on the membrane surface (m^{-1}).

In the next sections the parameters that influence these resistances are discussed as well as the equations that could be used to estimate these resistances.

2.2.1.1 The intrinsic membrane resistance (R_m)

The intrinsic membrane resistance depends on the membrane thickness, its nominal pore size and various morphological features such as the tortuosity, porosity and pore-size distribution. If it is assumed that the membrane pores are cylindrical capillaries of uniform radius perpendicular to the face of the membrane, the membrane resistance can be estimated from Poiseuille's equation.

$$R_m = \frac{8\delta_m}{N_p \pi r_p^4} \tag{3-5}$$

where δ_m is the membrane thickness (m), N_p the number of pores per unit area and r_p the pore radius (m) (Belfort *et al.* 1993; Davis & Grant 1992).

This equation holds when the entrance and exit pressure drops are negligible and porosity is low. For a membrane with uniform cylindrical pores, the void fraction (ε_m) can be estimated by:

$$\varepsilon_m = N_p \pi r_p^2 \tag{3-6}$$

The specific surface area (S_m in m^2/m^3) of the pores is:

$$S_m = \frac{2\pi r_p N_p}{1 - \varepsilon_m} \tag{3-7}$$

The membrane resistance can then be expressed in terms of the void fraction and the specific surface area as:

$$R_m = \frac{2(1 - \varepsilon_m)^2 S_m^2 \delta_m^2}{\varepsilon_m^3} \tag{3-8}$$

For normal membranes, this expression may still be used but the factor 2 should be replaced by a constant, K' which depends on the membrane morphology and pore structure (Gutman 1987). In practise the membrane resistance is often determined form Equation 3-4 using flux measurements obtained with pure water as feed.

2.2.1.2 Cake resistance (R_c)

The cake resistance depends on the nature of the feed solution and the membrane pore size. An incompressible cake is formed on the membrane surface when the porosity and therefore the resistance is independent of the imposed differential pressure drop across the membrane. The specific cake resistance per unit thickness of such a cake can be estimated by the Carman-Kozeny equation (Carman 1938).

$$\bar{R}_c = K'(1-\varepsilon_c)^2 S_c^2 / \varepsilon_c^3 \tag{3-9}$$

where $\bar{R}_c$ is the specific cake resistance per unit cake thickness (m^{-2}); ε_c is the void fraction of the cake and S_c is the solids surface area per unit volume of solids in the cake (m^2/m^3). For rigid spherical particles of radius a (m), the specific surface area is given by $S_c = 3/a$ (m^2/m^3), the void fraction of a randomly packed cake is $\varepsilon_c = 0.4$, and the constant K' is typically 5.0 (Grace 1953). It is often convenient to define:

$$R_c' = \bar{R}_c / (\rho_s \phi_c) \tag{3-10}$$

where ρ_s is the mass density of the solids comprising the cake (kg/m^3), $\phi_c = 1-\varepsilon_c$ is the solids volume fraction of the cake and R'_c is the cake resistance per unit mass deposited per unit area ($m\ kg^{-1}$).

Most materials such as flocculated clays and microbial cells are however highly compressible. They exhibit a decrease in void volume and an increase in the specific resistance as the differential pressure is increased. The effects of cake compressibility can be modelled by a power law function of the imposed pressure drop (Porter 1977; Belter *et al.* 1988)

$$R_c' = \beta'(\Delta P)^{n_c} \tag{3-11}$$

where β' is a constant (m/kg) related primarily to the size and shape of the particles forming the cake, ΔP is the trans-membrane pressure drop in (Pa) and n_c is the cake compressibility which varies from zero for an incompressible cake to a value near unity for highly compressible cakes.

Various investigators have reported that the initial cake build-up and flux decline during cross-flow filtration can be described by the same equations used to describe conventional dead-end filtration (Davis 1992). In this analysis it is assumed that the initial phase of the filtration process starts with a clean membrane on which a cake layer of rejected particles accumulates with time as the filtration proceeds. It is assumed that no internal fouling occurs and therefore the cake resistance and the membrane resistance are the only contributors to the total hydraulic resistance.

Two approaches have been followed to model the growth of the cake layer on the membrane surface during dead-end filtration. In the first approach, the cake mass is determined from a mass balance over the membrane surface to yield:

$$A \cdot m_c = C_b V_f \tag{3-12}$$

where A is the membrane area (m^2), m_c is the total cake mass per unit membrane area (kg/m^2), C_b the bulk concentration of the particles comprising the cake (kg/m^3) and V_f the total volume of permeate collected (m^3).

In this approach it is assumed that all the particles in the bulk that have been associated with the permeate would be deposited onto the membrane surface. For dead-end filtration where the suspension flow is perpendicular to the membrane this is a valid assumption provided that the particles in the feed does not settle faster than the permeate to increase the particle flux to the cake layer. This assumption is not valid for cross-flow filtration where a large portion of the particles is removed with the tangentially flowing retentate.

If R_c' is the specific cake resistance per unit mass (m/kg) then the total hydraulic resistance of the cake layer would be given by:

$$R_c = \frac{R_c' C_b V_f}{A} \tag{3-13}$$

With the membrane resistance known, the flux can be estimated using Darcy's law as described in Equation 3-4.

In the second approach, cake growth during dead-end filtration through a membrane, which completely rejects the particles forming the cake may be determined with the aid of a particle mass balance at the edge of the growing cake layer:

$$(J + \frac{d\delta_c}{dt})C_b = C_c \frac{d\delta_c}{dt} \tag{3-14}$$

where δ_c is the cake thickness (m), Cb is the solid concentration in the suspension (kg/m^3) being filtered, and C_c is the solid concentration in the cake (kg/m^3). Combining Equations 3-4 and 3-14 yields a first order ordinary differential equation for the cake layer thickness on a flat filter:

$$\frac{d\delta_c}{dt} = \frac{C_b J}{(C_c - C_b)} = \frac{C_b \Delta P}{(C_c - C_b)\upsilon(R_m + R_c)} \tag{3-15}$$

subject to the initial conditions of $\delta_c = 0$ at $t = 0$ with ΔP the trans-membrane pressure drop in Pa, and υ the viscosity in Pas.

If the trans-membrane pressure drop (ΔP in Pa) is kept constant, integration of Equation 3-15 yields:

$$R_c = \bar{R}_c \delta_c(t) = R_m \left[\left(1 + \frac{2t\bar{R}_c C_b \Delta P}{(C_c - C_b)\upsilon R_m^2} \right)^{1/2} - 1 \right] \tag{3-16}$$

In performing the integration, it is assumed that R_m (m^{-1}), C_c (kg/m^3), C_b (kg/m^3) and $\bar{R}_c$ (m^{-2}) are constant.

It should be stressed that these equations were developed for dead-end filtration applications. This means that these equations would only be valid for the initial period of cross-flow filtration (Visvanathan & Ben Aim 1989) provided that no internal fouling occurs. Contrary to dead-end filtration a pseudo steady state flux is reached in cross-flow filtration (Baker *et al.* 1985). The existence of a steady state flux is explained by quantitatively assuming that the cake reaches a steady state thickness, controlled by the retentate cross-flow (Schneider & Klein (1982), Reismeier *et al.* (1990)).

2.2.1.3 Pore blocking resistance (R_p)

It is well known that the internal fouling of especially microfiltration membranes occurs when particles and macromolecules partially constrict the flow of permeate through the membrane pores.

Hermia (1982) suggested four blocking laws to describe the reduction in the permeate flux with time for dead-end filtration applications. As mentioned before it has been postulated that the initial period of flux decline observed for cross-flow filtration may be explained by the laws that govern flux decline during dead-end

filtration applications (Davis 1992; Visvanathan & Ben Aim 1989). Hermia (1982) developed four blocking laws that apply to dead-end filtration depending on whether the predominate fouling mechanism is internal or external. Hermia's (1982) "Complete," "Intermediate" and "Standard" blocking laws apply to internal fouling while the "Cake Filtration" law applies to cases where the cake layer forms the predominate hydraulic resistance.

- Complete blocking law

  In the complete blocking law it is assumed that each particle reaching the membrane participates in the blocking phenomenon by pore sealing. This leads to the assumption that particles are not superimposed one upon the other. When a filtrate volume, V_f has been filtered, it has blocked a portion of the membrane area equal to σV_f, where σ (m^2/m^3) is given by:

$$\sigma = 1.5\frac{\rho_f s}{\rho_s d_{eq}\varphi} \tag{3-17}$$

  where ρ_s is the solids density (kg/m^3), ρ_f is the feed suspension density (kg/m^3), d_{eq} is the equivalent sphere diameter (m), s is the solids fraction in the feed and φ is a dimensionless particle shape factor.

  This approach implies that the effective membrane area (m^2) is given by:

$$A = A_0 - \sigma V_f \tag{3-18}$$

  Combining this with Equation 3-4, the permeate flow rate (Perm in m^3/s) can therefore be given by:

$$Perm = \frac{\Delta P}{\upsilon R_m}(A_0 - \sigma V_f) = \frac{\Delta P}{\upsilon(R_m + R_p)}A_0 \tag{3-19}$$

  where A_0 is the clean membrane area (m^2) and Perm is the volumetric permeate flow rate (m^3/s).

  The pore plugging resistance is therefore given by:

$$R_p = R_m\left[\frac{A_0}{A_0 - \sigma V_f} - 1\right] \tag{3-20}$$

- Intermediate blocking law

  As with the complete blocking law, it is still assumed that each time a particle reaches an open pore it seals it. The model is however less restrictive in the sense that particles are allowed to settle on other particles. The probability for a particle blocking a pore is calculated based on the number of pores available to be blocked and the flux of particles toward the membrane surface. The probability of a particle reaching an open pore can be estimated by the ratio of the available membrane area to the total clean membrane area multiplied by the permeate flow rate. The available membrane area at time t+dt is therefore given by:

$$A_{t+dt} = A_t - \sigma(Perm \cdot dt)\left(\frac{A_t}{A_0}\right) \tag{3-21}$$

  Combining this with Equation 3-4 implies that the available membrane area at time t can be estimated by:

$$A = \frac{A_0}{1 + \left(\frac{\sigma \Delta P}{\upsilon R_m}\right) t} \tag{3-22}$$

  The pore plugging resistance (R_p in m^{-1}) is therefore given by:

$$R_p = \frac{\sigma \Delta P}{\upsilon} t \tag{3-23}$$

- Standard blocking law

  In the standard blocking model, particles pass into the filter material and some are deposited or adsorbed to reduce the pore volume and subsequently decrease the filtration flux. The decrease in pore volume is assumed to be proportional to the volume of filtrate that passed through the membrane. From a mass balance on the solid particles the following relation can be derived:

$$N^* \pi \cdot (r_{p,0}^2 - r_p^{\ 2}) \delta_m = \phi_b V_f \tag{3-24}$$

  where N* is the number of pores, δ_m is the pore length (m), $r_{p,0}$ is the clean membrane pore radius (m), r_p is the pore radius (m) and ϕ_b is the volume of particles deposited per unit volume of filtrate.

  Combining Poiseuille's equation with Equation 3-4 yield the initial permeate flow rate:

$$Perm_0 = N^* \left(\frac{\pi}{8} \cdot \frac{r_{p,0}^4 \Delta P}{\upsilon \delta_m}\right) \tag{3-25}$$

If Equation 3-25 is then combined with Equation 3-4, the pore plugging resistance can be estimated by:

$$R_p = R_m \cdot \left(\frac{1}{\left(1 - \frac{KV_f}{2}\right)^2} - 1 \right) \qquad (3\text{-}26)$$

where $K = (2C_b/\delta_m A_0)$ in (kg/m^6)

It should be stressed that these laws were developed for dead-end application and would only be applicable to cross-flow filtration during the initial stages if cake build-up is not the predominating fouling mechanism. Matsumoto *et al.* (1987) tested these laws with yeast suspensions and the standard blocking law explained comparatively well the filtration behaviour over the first ten minutes. Visvanathan & Ben Aim (1989) filtered stable colloids (diameter 12 nm) with a 0.2-μm membrane at a cross-flow velocity of 0.2 m/s. The flux deviated from the standard blocking model for the first five minutes, then appeared to follow the model for 15-20 minutes before deviating again. The results of Tanny *et al.* (1979) were similar. They observed standard blocking behaviour for at least the first ten minutes when filtering *Pseudomonas diminuta* through a 0.45 μm filter.

2.2.2 Equal Particle deposition and removal rate models

The most general approach to model cross-flow filtration is to assume that particle deposition is balanced by another mechanism of particle transport from the membrane surface. At steady state, the flux of particles towards and away from the membrane is assumed to be equal. The mass transfer equations are often solved by simulation of the single-phase flow field in the feed channels and coupling the solution of the flow field to the solute mass transfer balance through convective-diffusive equations. Thus, the continuity equation, the Navier Stokes equation and the initial and boundary conditions are solved for a pre-chosen channel geometry to yield the filtration flux. Kleinsteuer and Belfort (1984) summarised the governing equations and various methods of solution.

In this section fluid mechanics in cross-flow filtration are discussed followed by a discussion of some of the equal particle deposition and removal rate models.

2.2.2.1 Fluid mechanics in cross-flow filtration.

The behaviour of fluid flowing in a porous channel with suction is different from that in a nonporous channel. Mellis *et al.* (1993) have measured axial pressure drops for

water flowing in porous micro-filtration tubes under all regimes of flow as a function of wall suction and axial flow rates. At low axial flow rates (Re < 1000), low values of wall suction ($Re_w = (\rho_p J H_o) / \nu < 0.25$), have a minimal effect on the axial pressure drop, where H_o is the channel half height. At high axial flow rates (Re > 20000), all values of wall suction had minimal effects on the pressure drop. Wall suction has its maximum effect on the axial pressure drop at intermediate flow rates (1000 < Re < 15 000). Moreover, wall suction is stabilising so that the value of Re, for transition to turbulence increases with Re_w. It was therefore concluded that due to the stabilising effect of wall suction the Poiseuille velocity profile relationship remains valid for fully developed laminar flow of Newtonian suspensions in cross-flow applications.

$$u = U_{max}\left(1 - \frac{y^2}{H_0^2}\right) \tag{3-27}$$

where y (m) is the distance from the centre of the tube of inside radius H_o (m) or a slit of half height H_o. For flow in a tube the maximum velocity is twice the average velocity (v in m/s), $U_{max}=2v$, whereas $U_{max}=3v/2$ for a slit.

Based on the velocity profile, the nominal shear rate at the membrane surface $\dot{\gamma}_o$ in s^{-1} can be estimated:

$$\dot{\gamma}_o = \frac{2U_{max}}{H_0} \tag{3-28}$$

A limiting assumption in the analysis above is that this expression neglects the distortion of the flow profiles due to concentration polarisation. In particular the polarisation layer near the membrane surface is likely to have a high viscosity and will flow with a reduced shear rate. For concentrated suspensions of non-colloidal particles in which the particle volume fraction exceeds ~0.1, non-Newtonian effects such as normal stresses and shear thinning are important (Karnis *et al.* 1966).

Davis & Birdshell (1987) developed the following velocity profile to account for the effect of perpendicular permeate flow:

$$u = 2J\left[\frac{y}{H_o} - \frac{1}{2}\left(\frac{y}{H_0}\right)^3\right] \tag{3-29}$$

Theoretical research has focussed primarily on the various mechanisms by which the tangential shear force arrests cake growth. Leading to different models for predicting the permeate flux (Belfort *et al.* 1994). The focus has been on laminar flows with particle transport occurring due to Brownian diffusion, shear induced

transport, inertial lift and surface transport. These mechanisms will be discussed in the following sections.

2.2.2.2 Concentration polarisation and Brownian diffusion

The earliest work in cross-flow micro-filtration (Blatt *et al.* 1970, Porter 1972) was based on the so called classical thin film Fickian diffusion theory. These models assume a balance between convection towards the membrane and molecular back diffusion from the membrane wall. This approach have been successfully applied to the ultrafiltration of macromolecules as well as reverse osmosis applications (Porter 1972; Blatt *et al.* 1970).

The flux is thought to be limited by the formation of a concentration polarisation boundary layer. This layer consists of a large concentration of particles that are retained by the membrane and provides a hydraulic resistance to flow. At steady state, the boundary layer is in dynamic equilibrium. If it is approximated by a stagnant film, the rate of convection of particles normal to the membrane is balanced by back diffusion into the bulk suspension.

$$JC_b = D \times 10^{-4} \cdot \frac{dC_b}{dy} \tag{3-30}$$

where D is the diffusivity in cm^2/s

If this equation is integrated over the boundary layer thickness:

$$100 \cdot J = k_l \ln\left(\frac{C_w}{C_b}\right) \tag{3-31}$$

where J is the permeate flux in m/s, k_l is the local mass transfer coefficient (cm/s) between the bulk suspension and the membrane surface.

The particle concentration at the membrane wall, C_w in the boundary layer immediately above the thin fouling layer on the membrane surface may be determined experimentally from a semi-log plot of flux vs. bulk particle concentration. Alternatively, if the particles are non-adhesive, then C_w can be determined from the maximum random packing density ($1-\varepsilon_c$) of particles in the adjacent cake layer. For rigid spherical particles of equal size, $1-\varepsilon_c=0.6$ and $0.8 < 1-\varepsilon_c < 0.9$ for compressive or poly-disperse particles.

For conditions typical of cross-flow micro-filtration the local mass transfer coefficient for a linear velocity profile within the boundary layer and a constant wall

concentration can be evaluated form the analogous heat transfer problem (Porter 1972; Leveque 1928) as:

$$k_l(x) = 0.537\left(D^2 \frac{\dot{\gamma}_o}{x}\right)^{1/3} \tag{3-32}$$

where x (cm) is the axial co-ordinate along the channel length, $\dot{\gamma}_o$ (s^{-1}) is the wall shear rate, D is the diffusivity in $cm^2\ s^{-1}$, gives k_l in cm s^{-1}.

For turbulent conditions, the mass transfer coefficient can be estimated from the Dittus Boelter equation (Green & Belfort 1980):

$$k_l(x) = 0.023\left[\frac{(v^{-0.8}D^{0.67})}{d_{hyd}^{0.2}(\upsilon')^{0.47}}\right] \tag{3-33}$$

where d_{hyd} is the hydraulic diameter of the channel (cm), D the diffusivity ($cm^2\ s^{-1}$), v the axial velocity (cm s^{-1}) and υ' the cinematic viscosity ($cm^2\ s^{-1}$), gives k_l in (cm s^{-1}).

Porter (1972) claimed that the transition from laminar to turbulent flow occurs at Re = 2000. Schultz & Ripperger (1989) however, noted that while the transition occurs at Re = 2320 in non-permeable tubes, this value can change in the case of permeable tubes, especially with high permeation rates. Belfort & Nagata (1985) found a value of Re = 4000 for conditions typical of microfiltration.

For sub-micron particles Brownian diffusion is important. The Brownian diffusivity, D_{Bo}, of an isolated spherical particle in a fluid of viscosity is given by the Stokes-Einstein relationship:

$$D_{Bo} = \frac{k_B T}{f} \tag{3-34}$$

where D_{Bo} is the diffusivity (m^2/s), k_B is the Boltzman constant (1.380×10^{-23} J/mol K), T is the temperature (K) and f is the frictional coefficient (kg/s.mol). For hydrated flexible macromolecules, obtaining an estimate of f is difficult (Cantor & Schimmel 1980). For rigid colloidal particles of dimensions much larger than the hydrated layer, f can be obtained from the classical Stokes law and the dimensionless Perrin shape factor F,

$$f = 3\pi\upsilon d_{eq} F \tag{3-35}$$

where υ is the liquid viscosity and d_{eq} the diameter of an equivalent sphere with the same volume as the non-spherical solute (m).

$$F = \frac{f}{f_{sph}} = \frac{(1-p_e^{\,2})^{1/2}}{p_e^{\,2/3} H'} \tag{3-36}$$

where for a prolate ellipsoid with $p_e=b_e/c_e$, $H'=\ln\{[1+(1-p_e^{\,2})^{1/2}]/p_e\}$, and for an oblate ellipsoid with $p_e=c_e/b_e$, $H' = \tan^{-1}[(1-p_e^{\,2})^{1/2}]$ and where c_e/b_e is the ratio of the long to the short semi-axis. F has been plotted and tabulated as a function of p_e by Cantor & Schimmel (1980). For a sphere F=1.

Combining all these equations (3-32 to 3-36) for sub micron spherical particles then yields, the following expression for the length averaged permeate flux in m/s.

$$J = 0.81\left(\frac{\overset{o}{\gamma}_o D_{Bo}^2}{L_{mem}}\right)^{1/3} \ln\left(\frac{C_w}{C_b}\right) \tag{3-37}$$

$$J = 0.114\left(\frac{\overset{o}{\gamma}_o k_B^{\,2} T^2}{\upsilon^2 a^2 L_{mem}}\right)^{1/3} \ln\left(\frac{C_w}{C_b}\right) \tag{3-38}$$

where L_{mem} is the membrane length (m).

The predicted flux increases with shear rate, or feed velocity to the 1/3 power and decreases with particle radius to the 2/3 power.

The Leveque solution was derived for linear shear flows near non-porous walls. For porous walls, the concentration dependence of the viscosity causes a non-linear velocity profile in the concentration polarisation layer, and the transverse component of the velocity modifies the mass transfer rate. Trettin and Doshi (1980) used a similar solution to derive numerical and asymptotic results which take the transverse result into account (but not the viscosity variation). Their solution asymptotes to that given by the Stokes-Einstein solution for concentrated suspensions (Eq. 3-41) (C_w-C_b << C_w) whereas for dilute suspensions they showed that:

$$J = 1.31\left(\frac{\overset{o}{\gamma}_o D_{Bo}^{\,2} C_w}{L_{mem} C_b}\right)^{1/3} \tag{3-39}$$

These equations predict the filtration flux very well for ultrafiltration and reverse osmosis applications. Predicted fluxes for micron-sized particles using the Brownian diffusivity given by the Stokes-Einstein relationship were found to be one or more orders of magnitude less than those observed experimentally (Blatt *et al.* 1970; Porter 1972). For micron sized particles, plots of J vs. ln C_b are rarely linear. Green and Belfort (1980) referred to this discrepancy as the "flux paradox for colloidal suspensions". It follows from the fact that the Brownian diffusivities of micron sized particles in water are of the order of 10^{-13} m^2s^{-1}. This diffusivity is three orders of magnitude lower than the molecular diffusivities of typical macromolecules.

Experimental evidence for microfiltration of suspensions shows that the permeate flux increases with particle size and that it increases with shear rate following a power law with powers of 0.8-0.85 (Porter 1972; Taddei *et al.* 1990; Lojinke *et al.* 1992). Both these findings contradict the predictions of the concentration polarisation model with Brownian diffusion.

Blatt *et al.* (1970) argued that this model fails because packed layers of large particles at the membrane provides insufficient hydraulic resistance to account for the dramatic reduction in flux compared to the pure solvent. At least in cross-flow filtration of blood, previous studies of the hydraulic resistance of beds of red blood cells (Zydney *et al.* 1986) indicate that the retained particles can in fact provide the necessary resistance to flow. Porter (1972) added that if the particles did not limit the flux, the flux should increase with increasing pressure, contrary to experimental observations.

Several alternative mechanisms have been proposed to explain the flux paradox for colloidal suspensions. The predictions of models based on the primary mechanisms of shear-induced diffusion, inertial lift and surface transport are summarised in the next sections.

2.2.2.3 Shear induced diffusion

Models based on shear induced diffusion are similar to the original thin film model in that the convective drag of particles towards the membrane surface is balanced by the shear induced diffusion of particles back into the retentate stream. The diffusion coefficient for this process is not that of Brownian motion. Shear induced diffusion results from hydrodynamic interactions of particles in the concentrated layer. A particle in a shear field will tumble over other particles and thereby undergo a series of displacements from the bulk average streamline. The effect of this motion is the net migration of particles from high to low concentration (Zydney & Colton 1986).

Zydney and Colton (1986) proposed that the concentration-polarisation model could be applied to microfiltration provided that the Brownian diffusivity was replaced by the shear-induced hydrodynamic diffusivity as first measured by Eckstein *et al.* (1977) for $0.2 < \phi_b < 0.45$

$$D_s = 0.3\dot{\gamma}^{\circ} a^2 \tag{3-40}$$

The shear-induced hydrodynamic diffusivity (D_s in m^2/s) is proportional to the square of the particle size multiplied by the shear rate, whereas the Brownian diffusivity is independent of shear rate and inversely proportional to particle size. As a result, Brownian diffusion is important for sub-micron particles and low shear rates, whereas it is overshadowed by shear-induced hydrodynamic diffusion in microfiltration applications involving micron-sized particles. Zydney and Colton (1986) used a linear velocity profile with the Leveque mass transfer coefficient to solve for the length-averaged flux:

$$J = 0.078\,\dot{\gamma}_o^{\circ}(a^4 / L_{mem})^{1/3} \ln(C_w / C_b) \tag{3-41}$$

for $C_w - C_b << C_w$

$$J = 0.126\,\dot{\gamma}_o^{\circ}(a^4 C_w / L_{mem} C_b)^{1/3} \tag{3-42}$$

for $C_w >> C_b$

Zydney and Colton (1987) later developed a model accounting for the non-constant viscosity in the boundary layer to compensate for the non-linear velocity profile. The viscosity relationships were however specific to the filtration of blood and fitted plasmaphoresis data quite well.

Leighton and Acrivos (1987a) showed that Eckstein's diffusion coefficient was low due to a wall limitation in the experiments for suspensions more concentrated than 20% (vol). Leighton and Acrivos (1987b) presented a modified expression for the diffusion coefficient that predicted the same dependence on shear rate and particle size as Eckstein (1977), but a stronger dependence on particle volume fraction at high concentrations.

$$D_s = 0.33\,\dot{\gamma}^{\circ} a^2 \phi_b^{\,2}(1 + 0.5e^{8.8\phi_b}) \tag{3-43}$$

where D_s is the shear induced diffusivity in m^2/s, ϕ_b is the particle volume fraction in the feed suspension $\dot{\gamma}^{\circ}$ is the local shear rate (s^{-1}) given by $\dot{\gamma}^{\circ} = \dot{\gamma}_o^{\circ}\upsilon / \upsilon_F$ where $\dot{\gamma}_o^{\circ}$ is the wall shear rate (s^{-1}), υ is the permeate viscosity (Pas) and υ_F is the feed viscosity (Pas).

Davis and Sherwood (1990) described a convective-diffusive equation governing the steady state concentration polarisation boundary layer in cross-flow MF of fine particles, under conditions where shear induced diffusion is the dominant

mechanism of particle transport. Their solution incorporates the concentration dependent effective viscosity and shear-induced hydrodynamic diffusivity for sheared suspensions of spherical particles reported by Leighton and Acrivos (1986,1987). For dilute suspensions ($\phi_b < 0.1$) of monodisperse rigid spheres which are non-adhesive and have a maximum random packing density in the boundary layer of $\phi_w = 0.6$, Davis & Sherwood (1990) found that:

$$J = 0.072\,\gamma_o^{\circ}\left(\frac{\phi_w a^4}{\phi_b L_{mem}}\right)^{1/3} = 0.060\,\gamma_o^{\circ}\left(\frac{a^4}{\phi_b L_{mem}}\right)^{1/3} \qquad (3\text{-}44)$$

The equation is identical to that of Zydney and Colton (1986), except that the value of the leading coefficient is lower. This difference is primarily because the concentration dependency employed by Davis and Sherwood (1990) leads to a lower local shear rate and, hence decreases shear-induced diffusion in the concentration polarisation boundary layer. As with the concentration polarisation model, the analysis of Davis and Sherwood (1990) is restricted to applications where the cake layer remains thin compared to the channel half height or tube radius and has a large resistance which dominates the membrane resistance.

2.2.2.4 Inertial lift

Belfort and coworkers (Green & Belfort 1980; Altena & Belfort 1984; Altena *et al.* 1985; Belfort *et al.* 1985; Otis *et al.* 1986; Drew *et al.* 1991) have proposed that the discrepancy between the predictions of the concentration polarisation models based on Brownian diffusion and the experimental data was due to the augmentation in particle transport due to a hydrodynamic lift force, causing particles to move away from the wall.

The lateral movement of particles across streamlines as they are suspended in a fluid flowing in a tube or slit was observed as early as 1836 (Green & Belfort 1980). In that year, Poiseuille noted that the region immediately adjacent to the walls of the capillaries tend to be free of blood corpses (Segre & Silberberg 1961). An important study following on this discovery was that of Segre and Silberberg (1962), who observed that neutrally buoyant rigid spheres in tube flow, migrated away from both the tube wall and axis, attaining an equilibrium position about 0.6 tube radii from the axis. They also measured the velocities at which, these particles of different sizes and initial radial displacements migrated to this position. Karnis *et al.* (1966) confirmed that non-spherical and non-rigid particles will also undergo lateral migration. These observations stimulated a number of theoretical and experimental papers which attempted to explain and quantify this effect (Brenner 1966)

Theoretical solutions for the lift velocity centre around solution of the Navier-Stokes equation with inertial terms included (Brenner 1966; Rubinow & Keller 1961;

Saffman 1965; Cox & Brenner 1968; Ho & Leal 1974). When these terms are neglected, no lift is predicted. Thus theoretically, this phenomenon is of inertial origin. More simply, lift can be viewed as arising from the pressure difference which in turn arises from the difference in fluid velocity on either side of a particle in a non-constant velocity field.

Virtually all studies of the lift phenomena, whether theoretical (Brenner 1966; Saffman 1965; Cox & Brenner 1968; Ho & Leal 1974) or experimental (Segre & Silberberg 1961; 1962; Thomas 1961; Karnis *et al.* 1966; Theodore 1966; Rakow & Chappell 1987) arrived at the following identical form for the migration velocity expression.

$$v_{l,o} = k_{IL} \cdot v \cdot \mathrm{Re} \left(a/H_o \right)^{n_{IL}} f(y) \tag{3-45}$$

Where a is the particle size (m), v is the average axial cross-flow velocity (m/s) and H_o is the tube radius (m). The value of n_{IL} is close to 3. More recently this equation was refined by Belfort *et al.* (1994) who presented the general form of the equation as:

$$v_{l,o} = \frac{b \rho_F a^3 \dot{\gamma}_o^2}{16 \upsilon} \tag{3-46}$$

where ρ_F is the fluid density, $\dot{\gamma}_o$ is the shear rate at the tube wall and b is a dimensionless function of the dimensionless distance form the wall. For Equation 3-49 to hold $a/(2H) << 1$ and $av/\nu << 1$ are necessary conditions. In the region near the wall, b is positive, indicating that the inertial lift velocity drags the particles away from the wall. Its maximum value near the wall under slow laminar flow conditions (channel Reynolds numbers small compared to unity) is b=1.6 for a slit (Ho & Leal 1974) and b=1.3 for a tube (Ishii & Hasimoto 1980). Particle trajectories calculated from the resultant of axial flow and net lateral flow in the direction of the wall compare very well with measurements over nearly two orders of magnitude in wall flux (Otis *et al.* 1986). However most cross-flow filtration operations are carried out under fast laminar flow conditions (channel Reynolds numbers large compared to unity), for which Drew *et al.* (1991) have shown that the maximum value is given by b=0.577.

The inertial lift velocity for fast laminar flow increases with the cube of the particle size, and the square of the tangential shear rate. So is expected to be significant for large particles and high flow rates. For the typical situation where the permeate flux for a clean membrane exceeds the inertial lift velocity, a concentrated layer of

deposited particles forms on the membrane surface. If this fouling layer has a high resistance then it will reduce the permeate flux until it just balances the inertial lift velocity.

For fast laminar flow with thin fouling layers, the steady-state flux predicted by the inertial lift theory is then (Drew *et al.* 1991):

$$J = v_{l,o} = 0.036 \rho_F a^3 \dot{\gamma}_o^{\,2} / \upsilon \tag{3-47}$$

where J is the permeate flux in m/s, $v_{l,o}$ is the inertial lift velocity in m/s, ρ_F is the feed density (kg/m^3), υ is the permeate viscosity (Pas) and $\dot{\gamma}_o$ is the wall shear rate (s^{-1}).

The flux is therefore inversely proportional to the solution viscosity and independent of the filter length and the concentration of particles in the bulk suspension. For Equation 3-47 to hold α^2 Re << 1, where α = a/2H_o and Re = 2H_o v / υ is a necessary condition. For non-dilute suspensions, however, it is expected that the inertial lift velocity would need to be modified to account for interactions among particles.

Some empirical correlations have also been developed to predict inertial lift velocities (Altena *et al* 1983, Green & Belfort 1980). The most general forms of these equations are:

For laminar conditions:

$$v_{l,o} = K_{lam} C_b^z v / 2H_o \tag{3-48}$$

For turbulent conditions

$$v_{l,o} = K_{tur} C_b^z (v / 2H_o) \cdot \mathrm{Re}^{0.75} \tag{3-49}$$

where K_{lan}, K_{tur} and z are empirical constants for the suspension, v the cross-flow velocity (m/s), 2H_o the inner diameter (m) and Re the Reynolds number.

2.2.2.5 Flowing cakes and surface transport

As an alternative to back transport of particles away from the membrane by mechanisms such as diffusion and inertial lift, it is possible that the particles are carried to the membrane surface by the permeate flow and then roll or slide along the surface due to tangential flow. Both continuum and single particle models have been developed to describe this mechanism.

- Continuum approach

  In the continuum approach, the rejected particles are assumed to form a flowing cake layer. Convective flow, mathematical models describe the simultaneous deposition of particles into the cake layer and the flow of this layer toward the filter exit (Davis & Birdsell 1987; Leonard & Vassilieff 1984). The fully developed laminar flow equations are solved for the velocity profiles in the bulk suspension and in the cake layer from which the steady state cake thickness and permeate flux are determined. In general, the cake thickness increases and the permeate flux decreases with increasing distance from the filter entrance and with decreasing axial flow rate.

  This approach gives rise to some highly empirical models. Fane *et al.* (1982) suggested that the flux enhancement that occurs when particle matter is added to feeds containing dissolved solids might be done due to the scouring effect of the particles on the concentration polarisation layer. By balancing the rate of convective mass transfer towards the membrane against the rate of scour, they derived:

$$J = n_{s,1} C_b^{n_{s,2}} v^{n_{s,3}} \tag{3-50}$$

  where $n_{s,1}$, $n_{s,2}$ and $n_{s,3}$ are unspecified constants.

  This equation predicts a log-log relationship for flux vs. concentration rather than a semi-log relationship as predicted by the conventional concentration polarisation theory. Fane *et al.* (1982) found good correlations between experimental data and the empirical model predictions for suspensions containing rigid and deformable solids and droplets.

  Leonard & Vassilieff (1984) developed a flowing cake model in which the fluid is divided into two regions by a sharp boundary; a close packed region adjacent to the boundary of concentration C_w and a bulk fluid region where the concentration is uniformly fixed at C_b. The close packed region moves along the membrane at a rate depending on the cake rheology. Cakes that behave as Bingham plastics will consist of a stagnant lower layer and a flowing upper layer. The flux prediction equation resulting from these postulations as presented by Zydney and Colton (1986) is:

$$J = \left(\frac{C_w}{C_b} - 1\right)\left(\frac{\overset{o}{\gamma}\,\delta_c}{2L_{mem}}\right) \tag{3-51}$$

  A plasmaphoresis-specific version gave good agreement for plasmaphoresis data (Zydney & Colton 1986). Wakeman (1994) questioned some of the model assumptions:

- An abrupt division between cake and bulk seems unlikely.
- Cell diffusion was neglected entirely and the resistance of a cell layer thicker than a critical value of δ_c was assumed to be infinite, both of which are in conflict with experimental evidence.

- Single particle models

  In single particle models, the basic concept is to consider a spherical particle on the surface of the membrane, or on the surface of a stagnant cake layer and perform force and torque balances on the particle to determine if it will adhere to the surface or to be transported along the surface (Lu & Ju 1989; Stamatakis & Tien 1993). The simplest of these models is that of Fischer & Raasch (1986), who considered a single spherical particle deposited in a sieve mesh, subjected to a drag force parallel to the membrane and a pressure force perpendicular to the membrane. They derived a dimensionless number Q_o, such that:

$$Q_o = \frac{\Delta P}{\overset{o}{\gamma}_o} = f\left(a/r_p\right) \tag{3-52}$$

  where $\overset{o}{\gamma}_o$ is the shear rate at the membrane surface, $f(\frac{a}{r_p})$ is a function of the ratio of the particle size to the membrane pore size.

  For a given geometry, membrane and suspension, there should exist a critical value of Q_o below which particles are swept across the membrane so that a cake does not form.

  Rautenbach (1988) balanced the same forces to give:

$$k_F = 4.7\times10^{-5}\cdot \mathrm{Re}^{1.26}\cdot\left(\frac{\upsilon}{\rho_f d_h}\right) \tag{3-53}$$

  where

$$J = k_f\left(\frac{2a}{d_h}\right)^{0.44} \tag{3-54}$$

  De Balmann *et al.* (1990) extended the force balance model to include the effects of concentration. They suggested that when a particle lands on a pore, it will remain in place if the suction force is strong enough to hold it; otherwise, it will be released due to the tangential feed flow. If the particle is released, another one can replace it. The frequency of replacements depends on the

concentration of particles in the feed, and thus the fraction of the time that the pore is blocked should be proportional to the particle concentration.

De Balman *et al.* (1990) also considered the effect of pore and particle size distributions. When a particle of a given size lands on a pore, three possibilities exist:

- The pore is sufficiently smaller than the particle so that the particle does not stop at the pore entrance; such pores pass a flux equal to that of the pure solvent;
- The pore is large enough for the suction force to arrest but not retain the particle; such pores pass a reduced concentration-dependent flux
- The pore is large enough for the suction force to retain the particle; such pores become blocked.

At a given concentration and pressure, decreasing the cross-flow velocity makes the last two scenarios increasingly likely. There is a similarity between this work and that of Le & Howell (1984) on UF.

More recently, Belfort *et al.* (1994) complied a review on the latest developments regarding single particle force models. Figure 3-3 shows a spherical particle of radius, a, on the edge of a cake which has a non-uniform surface morphology.

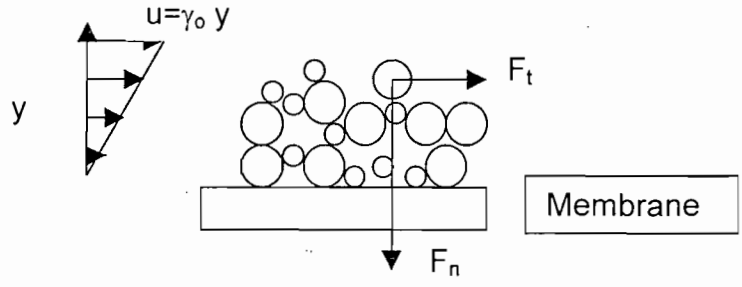

Figure 3-3. Schematic of forces acting on a spherical particle on the surface of the cake.

The tangential drag force due to shear flow may be expressed as:

$$F_t = 3\pi\upsilon a^2 \overset{o}{\gamma}_o C_t \qquad (3\text{-}55)$$

where C_t is a correction factor to the Stokes Law due to the presence of the cake. For a sphere on a smooth impermeable surface O'Neil (1968) found that

C_t = 1.70, but the value is expected to differ for rough filter cakes. The normal drag force due to the permeate flow may be expresses as:

$$F_n = 6\pi\upsilon a J C_n \tag{3-56}$$

where J is the permeate velocity (m/s) at the edge of the cake layer and C_n is a hydrodynamic correction factor to the Stokes law due to the presence of the cake layer. Lu & Ju (1989) used a correction factor from Goren (1979):

$$C_n = \left(\frac{2R_{tot}a}{3} + 1.15 \right)^{1/2} \tag{3-57}$$

where R_{tot} is the total resistance offered by the underlying cake and membrane:

$$R_{tot} = \frac{\Delta P}{\upsilon J} \tag{3-58}$$

The analysis of Goren (1979) is restricted to porous membranes which are thin compared to the sphere radius, or which only permit flow in the direction normal to the membrane surface. Sherwood (1988) considered the drag force on a sphere touching the surface of an isotropic porous medium, which is thick, compared to the sphere radius.

$$C_n = 0.36 \left(\frac{k_p}{a^2} \right)^{-2/5} \tag{3-59}$$

where k_p is the permeability of the porous medium. If there is no cake, then the permeability is that of the membrane ($k_p = \varepsilon_m / R_m$). For the more common situation of a particle at the edge of the cake layer, the permeability is that of the cake ($k_p = \varepsilon_c / R_c$).

Under the simplest situation in which other forces, such as gravitational, lift and adhesive forces, are negligible, the two components of the drag force are balanced by contact forces at the locations where the test sphere is in contact with the cake surface. For the critical condition where the sphere is just able to roll along the surface, the contact forces are zero except at the pivot position. A torque balance about this pivot position gives (Figure 3-4):

$$F_n a \cdot \sin\theta = F_t a \cdot \cos\theta \tag{3-60}$$

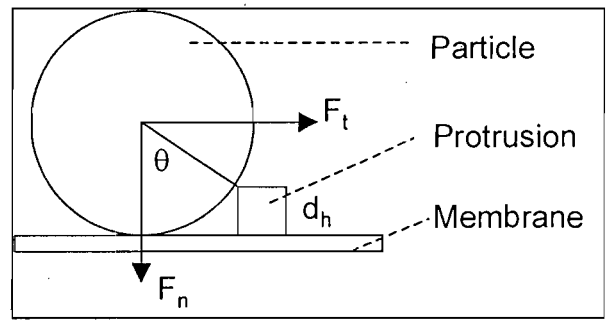

Figure 3-4 Schematic representation of torque balance around a pivot point of a protrusion against a spherical particle

Combining Equations 3-56 to 3-60 for this critical condition yields the predicted permeate flux after the cake layer has reached its steady state thickness:

$$J = 2.4a\dot{\gamma}\left(a^2\overline{R}_c\right)^{2/5}\cot\theta \qquad (3\text{-}61)$$

where cot θ depends on the surface morphology. This equation uses the hydrodynamic correction factors from O'Neil (1968) and Goren (1979) for smooth surfaces, and so the constant value of 2.4 is expected to differ for surface topologies, which are not smooth on the particle length scale.

The surface transport model predicts that the long-term flux increases linearly with shear rate and particle radius. If there is a distribution of particle sizes, then the smaller particles will continue to be captured after the permeate flux is reduced to a value where the larger particles are swept along the surface. Consequently, the cake may become enriched in smaller particles as it grows. Experimental measurements have observed that finer particles selectively deposit in the cake at later times and higher cross-flow velocities (Mackley & Sherman 1992). This causes the specific cake resistance to be cross-flow velocity dependent, and may even lead to decreased steady-state flux with increased shear rate (Mackley & Sherman 1992; Fischer & Raasch 1985; Wakeman & Tarleton 1991). In addition, the cake surface is expected to be inhomogeneous, so that there is a distribution of protuberance heights, resulting in a distribution in θ values. This leads to the possibility of a particle rolling along the cake surface until reaching an obstacle, which is sufficiently high to stop it. This situation has been observed and analysed by Stamatakis & Tien (1993).

2.2.2.6 Combinations of the above

The permeate flux is a function of many variables including time, trans-membrane pressure drop, cross-flow velocity, temperature, membrane pore size, porosity and

surface chemistry and suspension concentration and composition. A universal and comprehensive model for predicting permeate flux should take into account all of these factors, which probably means that the global model needs an expression for fouling, a cake layer sub-model and a back flux sub-model.

Models based on the addition of diffusive and inertial back fluxes over-predicted both the flux at high shear rates, and the shear rate dependency of the flux (Lojinke *et al.* 1992). Madsen (1977) suggested that the lift velocity and the filtration velocity estimated from polarisation theory are additive, with the flux given as:

$$J(x) = v_{l,o} + k_l(x)\ln\left(\frac{C_w}{C_b}\right) \tag{3-62}$$

Altena and Belfort (1984) showed theoretically that this equation is valid under flow conditions typical of cross-flow micro-filtration in the limit of infinitely dilute suspensions.

Davis and Leighton (1987) incorporated the concepts of shear induced hydrodynamic diffusion of particles and the transport along the membrane surface of a fluid like concentrated particle layer whose viscosity is a function of particle volume fraction. This particle layer may impart a hydraulic resistance to permeable flow, which is modelled by standard filtration theory. Their model was a local model – valid at any axial position in a cross-flow micro-filter. Romero and Davis (1988) extended this to a global model by incorporating axial particle convection in the boundary layer. They used acrylic and polystyrene beads filtered through a rectangular glass walled microfilter and a ceramic tube bundle. It was assumed that particle transport towards the membrane results in the formation of a stagnant cake layer and a flowing cake layer, the thickness of both increasing longitudinally. They showed that the stagnant cake forms on the membrane surface only for distances from the filter entrance which exceed a critical value $X_{cr} = \dot{\gamma}_o D_{s2} I_2 / (J^2 C_b)$ where $D_s = \dot{\gamma}_o a^2$ is the characteristic shear induced diffusivity. The presence of the stagnant layer reduces the channel diameter, hence increasing the wall shear stress and facilitating the axial flow of particles. The stagnant layer also provides a hydraulic resistance to permeate flow, and reduces the transverse convection of particles into the flowing layer. The measured steady state fluxes were in good agreement with the theory using independent empirical correlations for the properties (diffusivity, viscosity and specific cake resistance) of rigid non-adhesive spheres.

In 1990, Romero and Davis included the transient behaviour. A transient term describing the increase in particle volume fraction near the membrane surface with time was included in the mass balance for a thin slice of the particlulate layer. The resulting partial differential equation (in the axial co-ordinate, x and in time, t) was

solved. The resulting equation is useful for predicting the effect of material properties and operating parameters on the rate of flux decline and cake layer build-up. In general, more highly concentrated suspensions, higher-pressure drops and larger specific cake resistances result in more rapid flux decline. Romero and Davis (1991) later found experimental verification of their model using acrylic and polystyrene beads filtered through a rectangular glass walled microfilter and a ceramic tube bundle. This experimental work was criticised by Wakeman (1994) who argued that:

- Romero and Davis used oversized particles for the visualisation experiments with respect to those normally encountered in microfiltration
- the operating conditions evaluated fell only within a very limited range of those normally encountered and that
- particle size effects were not evaluated experimentally, and are not interpreted correctly by the model based on other investigator's experimental data.

Schulz and Ripperger (1989) incorporated both back transport and resistance theory. They assumed that membrane resistance can be ignored and back transport of particles is proportional to both shear rate on the membrane and layer thickness. From mass balances at steady state they derived:

$$J = \left[\frac{\kappa_1 \Delta P (\rho_s - C_b) v}{(R_p / \delta_c) C_b \upsilon d_h} \right]^{0.5} \qquad \text{(laminar)} \qquad (3\text{-}63)$$

$$J = \frac{v}{\upsilon} \left[\frac{\kappa_2 \Delta P (\rho_s - C_b) \rho_p}{(R_p / \delta_c) C_b} \right]^{0.5} \qquad \text{(turbulent)} \qquad (3\text{-}64)$$

where κ_1 and κ_2 are empirical constants.

The model is only useful once the constant and the specific hydraulic resistance of the cake are known. Unfortunately, Schulz and Ripperger (1989) did not present any experimental data to support their model.

According to Dharmappa *et al.* (1992) particle transport to and from the membrane surface is equal when the steady state flux is reached. The rate of deposition or particle transport towards the membrane was thought to be a result of convective transport. The rate of re-suspension is a result of the back transport velocity, containing three components, lateral migration, Brownian motion, and shear enhanced diffusion. The significance of these mechanisms depends on the size of the particles.

Dharmappa *et al.* (1992) presented these arguments in a semi-empirical model for the prediction of foulant deposit thickness and concentration that would predict the permeate flux in cross-flow micro and ultrafiltration, for polydispersed colloidal suspensions. The model is based on a mass balance over the fouling layer on the membrane surface, written as:

$$\frac{d}{dt}\left[(1-\varepsilon_c)\delta_c\right] = \sum_j (C_{bj}(J + \frac{d}{dt}((1-\varepsilon_c)\delta_c) - v_{bj}C_{fj} - JC_{ej}) \qquad (3\text{-}65)$$

where ε_c is the porosity of the cake layer, δ_c is the thickness of the cake layer, C_b is the bulk concentration, C_f is the fouling layer concentration, C_e is the permeate concentration, v_b is the backflow velocity and J is the permeate velocity.

Furthermore V_b is comprised of the Brownian diffusion, shear enhanced diffusion and lateral migration velocities as proposed by Wiesner (1989) and Werthle (1990). The growth rate of the fouling layer was estimated using an empirical exponential function.

Some significant deviations from the experimental data of Werthle (1990) and Jang (1987) were observed by Dharmappa *et al.* (1992), especially when the influent concentration was low. The main reasons for these deviations can be attributed to the following factors:

- Negligence of internal membrane fouling
- Limited understanding of back transport velocity
- Consideration of the foulant layer and bulk as completely mixed
- Negligence of concentration polarisation
- Negligence of actual hydraulic conditions

2.2.3 The solids flux model

Nagata *et al.* (1989) postulated that if fouling is severe, then back migration may be irrelevant and the decline in flux may be proportional to the rate of arrival of solids at the surface, i.e. proportional to the flux itself. Such behaviour occurs during micro-filtration of sticky particles (e.g. microbial cells) at high trans-membrane pressure drops and low cross-flow velocities. Nagata *et al.* (1989) modelled this behaviour as a first order feedback inhibition process. For such a process:

$$J = J_o \exp(-b_{sf} C_b) \qquad (3\text{-}66)$$

where J_o is the pure water flux and b_{sf} is a constant describing the characteristics of the sublayer. This suggests that a plot of ln(J) vs. C_b should be linear. The slope gives a value for b_{sf} and the intercept at infinite dilution gives the pure water flux, J_o. The

solids flux to the membrane is the product of the solids concentration and the permeation velocity:

$$S_f = J_o C_b \exp(-b_{sf} C_b) \tag{3-67}$$

A plot of the solids flux against the solids concentration goes through a maximum at $C_b = 1/b_{sf}$, at which the solids flux is equal to $J_o/(C_b\, e)$. (e=2.7218...)

Nagata *et al.* (1989) compared the gel polarisation and the solids flux model, using data for the cross-flow micro-filtration of a phosphate buffer solution containing 3.5 ml/l of 0.5 M HEPES buffer. Nagata *et al.* (1989) reported that the solids flux model describes the data adequately.

2.2.4 Poiseuille flow through membrane pores constricted by particle deposition and intrusion

Most of these models treat the membrane as an array of uniform cylindrical pores of a single pore radius (Blatt *et al.* 1970; Jonsson 1984).

Belfort *et al.* (1993) have extended this analysis to explicitly account for the presence of a pore size distribution on the flux decline associated with pore constriction effects. Following the approach of Meireles *et al.* (1991) assuming a log-normal pore size distribution $n(r_p)$ and assuming that the local flow rate through a pore $j(r_p)$ is given by Poileuille flow, then the solvent flux is given by:

$$J = \int_0^\infty j(r_p) \cdot n(r_p) \cdot dr_p \tag{3-68}$$

where the number of pores of size r_p per unit area is

$$n(r_p) = \frac{\eta_o}{r_p \sqrt{2\pi}} \left[\log\left(1 + \left(r_{p,STDEV} / r_p \right)^2 \right) \right]^{-1/2} \times \exp\left\{ \frac{-\left[\log\left(r_p \sqrt{1 + \left(r_{p,STDEV} / r_p \right)^2} \right) / r_p \right]^2}{2 \log\left(1 + \left(r_{p,STDEV} / r_p \right)^2 \right)} \right\} \tag{3-69}$$

and

$$j(r_p) = \text{velocity} \times \text{area} = \left(\Delta P r_p^{\,2} \Big/ 8\upsilon' \delta_m \right) \pi r_p^{\,2} \tag{3-70}$$

where η_o is the probability density of radius r_p, r_p^* is the mean radius, $r_{p,\,STDEV}$ is the standard deviation of the distribution and υ' is the kinematic viscosity (Zydney *et al.* 1994). If Equations 3-69 and 3-70 are substituted into Equation 3-69, the modified flux would be

$$J' = \frac{J}{\left(\frac{\eta_o}{L}\right)\left(\frac{\pi \Delta P}{8\upsilon}\right)} = \left[2\pi \log\left(1 + \left(r_{p,STDEV} \Big/ r_p^* \right)^2 \right) \right]^{-1/2} \times \int_0^\infty \exp\left\{ \frac{-\left[\log\left(r_p \sqrt{1 + \left(r_{p,STDEV} \Big/ r_p^* \right)^2} \right) / r_p^* \right]^2}{2 \log\left(1 + \left(r_{p,STDEV} \Big/ r_P^* \right)^2 \right)} \right\} r_p^{\,3} dr_p$$

$$= (r_P^*) \left[1 + \left(r_{p,STDEV} \Big/ r_p^* \right)^2 \right]^6$$

(3-71)

Assuming that $k_{thick}=i \bullet \delta_a$ is the thickness of an adsorbed multilayer inside a pore and that δ_a is the thickness of an absorbed layer (a dimension that can be estimated from the molecular structure of a protein or macromolecule), then i is the number of monolayers adsorbed in the pore. To account for the loss in cross sectional area for flow though a pore, r_p is now substituted for by r_p-k_{thick} in Equation 3-70. Since the number of pores per unit area remains the same, Equation 3-69 is unaltered. Explicit expressions for the modified fluxes with and without absorbed solute in the pores are presented by Belfort *et al.* (1993). Their ratio is:

$$\frac{J'_1}{J'_2} = 1 - \frac{4}{q_{pore}^{\,3}} \left(\frac{k_{thick}}{r_p^*} \right) + \frac{6}{q_{pore}^{\,6}} \left(\frac{k_{thick}}{r_p^*} \right)^2 - \frac{4}{q_{pore}^{\,6}} \left(\frac{k_{thick}}{r_p^*} \right)^3 + \frac{1}{q_{pore}^{\,5}} \left(\frac{k_{thick}}{r_p^*} \right) \tag{3-72}$$

The modified flux is given by:

$$J' = \frac{J}{(\eta_o / L)(\pi \Delta P / 8\upsilon)} \tag{3-73}$$

where $q_{pore} = 1+(r_{p,STDEV}/r_p^*)^2$. Equation 3-72 was conveniently used to obtain an estimate for k_{thick} assuming that $r_{p,\ STDEV}$ is the same for the membrane with and without absorbed solute (Belfort *et al.* 1993). The model assumes that on average the absorbed layer is uniform throughout.

Fane *et al.* (1981) developed a similar model for ultrafiltration. The model assumes that the membrane surface is composed of a mosaic of regions of differing solvent permeability. These regions arise from the relatively low free area, and size distribution of open pores, which in turn depends on the manufacturing process, and structural changes caused by usage, damage to the membrane surface, plugging of pores, etc. The conventional concentration polarisation model is assumed to apply to each region.

2.2.5 Models incorporating the flux decline

Most of the models as mentioned above only model the pseudo steady state flux. In the next section some of the models that describe the flux decline will be discussed.

2.2.5.1 Modelling flux decline of protein containing suspensions

Most fundamental flux decline patterns were developed for ultra-filtration and micro-filtration of proteins. The mathematical analysis of the flux decline caused by pore blockage, pore constriction or cake formation is generally performed assuming that the membrane can be described by a single pore size with the details of these analysis discussed by Hermia (1982). The starting point in the development of these models is Darcy's law which, can be written as (Belfort *et al.* 1994):

$$J = \frac{\Delta P - \sigma_o \Delta \pi}{\upsilon \cdot (R_m + R_p + R_c)} \tag{3-74}$$

where σ_o and $\Delta\pi$ are the osmotic reflection coefficient and the osmotic pressure difference across the membrane, respectively.

The reflection osmotic coefficient is a measure of the membrane's ability to retain the macromolecule of interest; it varies from one for a fully retentive membrane to zero for a non-retentive membrane. Particles generally would not have an osmotic pressure due to the increased size thereof. The osmotic reflection coefficient for

ultrafiltration of macromolecules is close to one where for microfiltration it is close to zero.

- Pore blockage

  Chandavarkar (1990) described the early stages of bovine serum albumin (BSA) fouling in microfiltration membranes with a pore blockage model in which the number of blocked pores was assumed to be proportional to the volume of solution filtered through the membrane. The filtrate flux was evaluated as a function of time as:

$$J = J_o \exp\left(-\frac{a_{block} J_o A}{N_p} t\right) \tag{3-75}$$

  where the constant a_{block} is equal to the number of pores that are blocked per unit filtrate volume and A is the area of the upper surface of the membrane.

  Hlavacek and Bouchet (1993) found that a modified form of the pore blockage model referred to as the intermediate blocking law (Hermia 1982) was in good agreement with their data for the increase in pressure required to maintain a constant flux during dead-end filtration of BSA solutions through four different types of 0.2 μm microfiltration membranes.

- Pore constriction

  Bowen and Gan (1991) used the pore constriction model, also referred to as the standard blocking model (Hermia 1982) to describe the flux decline during stirred cell filtration of BSA and YADH through 0.2 μm aluminium oxide membranes. The reduction in pore radius was assumed to be proportional to the filtrate volume with the flux given as:

$$J = \frac{J_o}{\left(1 + \frac{a_{pore} J_o}{N_p \pi r_p^2 \delta_m} t\right)^2} \tag{3-76}$$

  where a_{pore} is the pore volume of protein that deposits on the interior pore walls per volume of filtrate.

  Bowen and Gan (1991) found that the volume of protein that deposited on the interior pore walls per volume of filtrate increased with increasing bulk protein concentration and with increasing pressure drop.

The pore constriction model has also been used by Tracy and Davis (1994) in their analysis of the initial stages of BSA filtration through 0.2 μm polycarbonate membranes. They however also indicated that their flux decline data could be effectively described by the pore blockage model.

- Cake filtration

  The cake filtration model assumes that proteins deposit in a cake on the upper surface of the membrane. The hydraulic resistance of the cake layer is assumed to be proportional to the mass of the deposit analogous to the approach used to develop classical dead end filtration cake resistance, yielding (Belfort *et al.* 1994):

$$J = J_o\left(1+\frac{2a_{deposit}\overline{R}_c C_b A\Delta P}{\upsilon R_m^2}t\right)^{-1/2} \tag{3-77}$$

  where C_b is the mass concentration of protein in the bulk solution, $a_{deposit}$ is the fraction of protein convected to the membrane surface that actually adds to the deposit and R'_m is the specific resistance of the protein cake.

  Tracey and Davis (1995) studied the flux decline associated with protein fouling through 0.05 and 0.2 μm track-etch polycarbonate membranes. Their data indicated that the initial flux decline is generally associated with internal fouling (either pore blockage or pore constriction) while the long term flux decline was due to cake formation, with the transition between these two mechanisms a function of the membrane pore size and bulk protein concentration. Chandavarkar (1990) successfully used a cake filtration model to describe the long term flux decline observed during cross-flow microfiltration of BSA.

  Howell and Velicangil (1980) used a cake filtration model to describe the flux decline during BSA ultrafiltration through fully retentive membranes. Cake growth was assumed to occur via a polymerisation reaction at the membrane surface. The polymerisation reaction was modelled as:

$$\frac{dm_c}{dt} = k_{pd}(C_w)^{n_{pd}} \tag{3-78}$$

  where m_d is the cake mass and C_w is the protein concentration immediately adjacent to the membrane surface.

  Suki *et al.* (1984) used a cake filtration model to describe protein deposition during BSA, ultrafiltration with the growth of the cake layer evaluated using an empirical expression of the form:

$$\frac{dm_c}{dt} = K_{rate}(m_c^{max} - m_c) \tag{3-79}$$

where m_c^{max} is the maximum value of the cake mass at steady state and K_{rate} is an empirical constant describing the rate of cake formation.

This model predicts that the flux attains a steady state value at long filtration times, which is in agreement with much of the available experimental data for both ultrafiltration and microfiltration. Suki *et al.* (1986) subsequently developed a more mechanistic model for the long term flux decline based on the aggregation of proteins due to intermolecular interactions occurring at or near the membrane surface. These models have however only been applied to ultrafiltration.

Palecek and Zydney (1994) developed a simple model whereby protein deposition continues to occur until the drag force on the proteins associated with the filtrate flow is no longer able to overcome the intermolecular repulsive interactions between the proteins in the bulk solution and those already in the protein deposit. The flux was given by:

$$J = J_{ss,iso} + \frac{(\zeta^2 \kappa^{-1}) e^{(-\kappa d_s)}}{(3P_{perm})} \tag{3-80}$$

where κ^{-1} is the Debye length, ζ is the protein surface charge density ($C.m^{-2}$), P_{perm} is the permittivity of the solvent ($=6.95 \times 10^{-10}$ C^2 J^{-1} for water) and d_s is the characteristic separation between the bulk proteins and the deposit at which the proteins are just able to overcome the repulsive interactions and add to the deposit. $J_{ss,\,iso}$ is the steady state flux at the protein iso-electric point.

The equation of Palecek and Zydney (1994) predicts that the steady state flux increases linearly with the square of the protein surface charge density (a function of the solution pH for any given protein). This was shown to be in good agreement with experimental data for BSA, lysozyme hemoglobin and ribonuclease A. This model is also consistent with the observed increase in the steady state flux with decreasing salt concentration (i.e. increasing Debye length).

2.2.5.2 Flux during cross flow filtration of feeds containing particles

The flux decline pattern of suspensions containing particles has in most cases been modelled empirically using equations with the same form as that developed for the filtration of protein containing suspensions.

Redkar and Davis (1993 1995 1996) assumed that flux decline during cross-flow filtration can be modelled using the equations derived for the flux decline in constant pressure dead-end filtration. The flux decline due to cake build-up is therefore given by:

$$J = J_o(1+\frac{t}{k_\tau})^{-0.5} \tag{3-81}$$

where J_o is the initial pure water flux and the time constant k_τ is given by:

$$k_\tau = \frac{(C_c - C_b)R_m}{2R_c C_b J_o} \tag{3-82}$$

where C_b is the volume fraction of cells in the bulk suspension, C_c is the volume fraction of cells in the cake layer. The flux decline curve for an experiment with unwashed yeast cells in water through a ceramic filter corresponded well with the described model.

Mallubhotla and Belfort (1996) later used Redkar and Davis' (1993) model to model cross-flow microfiltration with periodic reverse filtration of a yeast suspension.

Liberge *et al.* (1994), used the generic form of Hermia's filtration laws to model the flux of a yeast suspension through different inorganic membranes.

$$J = J_{ss} + \frac{J_o - J_{ss}}{(1+k_{decline}t')^{n_{decline}}} \tag{3-83}$$

where J_{ss} is the steady state flux.

They found the value of $n_{decline}$ to be close to 1. The value of $k_{decline}$ was modelled empirically using a stepwise multiple regression program to find the impact of the operating parameters. The value of $k_{decline}$ depends on the initial flux, the trans-membrane pressure drop and the cell concentration.

Murase and Ohn (1996) found that for polydisperse suspensions with a concentration below a critical limit two stages of flux decline were observed. The initial stage corresponds to the progressive clogging of the membrane pores. The rate of pore plugging depends on the particle size to pore size ratio, the liquid viscosity and the particle concentration. This initial stage is followed by thin cake filtration, which occurs when a thin cake forms on the initial deposit. The rate of flux decline during thin cake filtration is related to different process conditions expressed in terms of trans-membrane pressure drop, shear stress at the cake surface and the

liquid viscosity. The form of the equations used to predict the flux decline during each of the stages were based on Hermia's (1982) blocking laws.

3 Comparison between models and experimental data

Table 3-2 compares the impact of each parameter on the pseudo steady state cross flow filtration flux as predicted by each of the four transport mechanisms. It is assumed that the feed suspensions are dilute and composed of non-adhesive spherical particles, which form a cake layer, that dominate the membrane resistance. The equations have all been transformed into the form:

$$J = l_0(\Delta P)^{l_1} C^{l_2} u^{l_3} a^{l_4} L^{l_5} \mu^{l_6} \tag{3-84}$$

Table 3-2. Dependence long term flux on the operating parameters for various transport mechanisms

	Brownian Diffusion	Shear-induced diffusion	Inertial lift	Surface transport
Particle concentration	$\ell_1 = -1/3$	$\ell_1 = -1/3$	$\ell_1 = 0$	$\ell_1 = 0$
Cross-flow velocity	$\ell_3 = 1/3$	$\ell_3 = 1$	$\ell_3 = 2$	$\ell_3 = 1$
ΔP	$\ell_2 = 0$	$\ell_2 = 0$	$\ell_2 = 0$	$\ell_2 = 0$
Membrane length	$\ell_5 = -1/3$	$\ell_5 = -1/3$	$\ell_5 = 0$	$\ell_5 = 0$
Particle size	$\ell_4 = -2/3$	$\ell_4 = 4/3$	$\ell_4 = 3$	$\ell_4 = 1$
Suspension viscosity	$\ell_6 = -1$	$\ell_6 = -1/3$	$\ell_6 = -1$	$\ell_6 = 0$

The experimental data obtained by various investigators was grouped according to the impact of each individual parameter.

3.1 Effect of the trans- membrane pressure drop (ΔP)

Although the trans-membrane pressure drop (ΔP) provides the driving force for filtration, increases in ΔP does not always result in increases in the filtration flux. Generally, the flux

increases with ΔP up to a critical value. Above the critical ΔP the rate of flux increase might decrease (Forman *et al.* 1990, Grabler & Ryan 1985; Le *et al.* 1984a; Patel *et al.* 1987; Reismeier *et al.* 1987 and Tanny *et al.* 1980), the flux may be independent of ΔP (Le *et al.* 1984a; Ofsthun & Colton 1987, Sakkai *et al.* 1989 and Taddei *et al.* 1990) or the flux may decease (Forman *et al.* 1990; Sakkai *et al.* 1989). The value of the critical ΔP depends on the cross-flow velocity (Le *et al.* 1984a), pore size (Forman *et al.* 1990; Le 1987) and suspension concentration (Forman *et al.* 1990; Patel *et al.* 1987).

All of the models predicted that the steady state flux would be independent of the applied pressure drop (Table 3-2). This only applies to a portion of the experimental data found in literature. It is therefore not possible to select the most suitable model based on the effect of the ΔP.

3.2 The effect of the cross-flow velocity

The cross-flow velocity directly affects the shear stress and hence the rate of removal of the cake from the membrane surface. Several workers (Bauser *et al.* 1982; Datar 1984; Forman *et al.* 1990; Harris *et al.* 1988; Le & Billiet 1984; Le *et al.* 1984a; Le *et al.* 1984b; Nagata *et al.* 1989; Sakai *et al.* 1989; Scot 1988; Taddei *et al.* 1990 and Tanny *et al.* 1980) found that increasing the cross-flow velocity increases flux. Several workers based on experimental data reported a power law relationship between the flux and cross-flow velocity (Table 3-3).

$$J \propto \text{cross-flow velocity}^{n_v} \qquad (3\text{-}85)$$

Table 3-3. The effect of the cross-flow velocity on the permeate flux.

Organism	Pore size	Value of n_v	Reference
Bakers Yeast spherical 5 μm	0.2	2.59-2.97	Liberge *et al.* 1994
Bovine blood	0.8-1.1	0.90	Sakai *et al.* 1989
Micrococcus sp.	0.22	0.5-0.75	Henry & Alfred 1972
Ps. fluorescens	0.45	0.5	Le *et al.* 1984a
S. cerevisae	0.2-1.2	0.4-0.7	Taddei *et al.* 1990
S. cerevisae	0.22	1.1	Le 1987
Bakers yeast, *Bacillus caldolyticus* M1 and Methanogenic waste	Tubular inorganic [0.1]	1.0	Shimizu *et al.* 1993
Bakers yeast (including broken cells)	0.1	1.0	Shimizu *et al.* 1994
Corynebacterium glutamicum	Flat sheet 0.45μm	0.6	Tanaka *et al.* 1998
Activated sludge	Hollow fibres and tubular ceramic	1.0	Shimizu *et al.* 1996

The experimental data for the coefficient n_v varies over a relatively wide range 0.4 – 3.0. The coefficient is however positive for all cases and are roughly 1.0, for most of the cases. The largest value of n_v (2) is predicted by the inertial lift models while both the surface transport and the shear induced diffusion models predict a value of 1 for the coefficient (Table 3-2).

The only reasonable conclusion that can be drawn from these observations is that a tremendous gulf exists between the complexity of the available models and the complexity of the effect of the cross-flow velocity on the flux. These models are derived for dilute solutions of rigid, spherical, neutrally buoyant particles. This means that several effects are ignored such as:

- Particle interactions
- Particle membrane interactions
- Membrane fouling
- Cake compression
- Concentration dependence of the feed properties especially viscosity

Based on the back transport velocities described by shear induced diffusion and the shear rate dependence of fluxes observed experimentally it seems that shear induced diffusion would be the most accurate model describing the physical phenomena during cross-flow micro-filtration.

3.3 Effect of biomass concentration

The effect of the cell concentration on the cross-flow filtration flux as found from experimental data are shown in Table 3-4.

All the experimental results showed an impact of the biomass concentration on the cross-flow filtration flux. Generally, the flux decreased with increasing concentration. Both the inertial lift and the surface transport models predict that the biomass concentration should not have an impact on the cross-flow filtration flux. These models do however recognise the impact of the cell concentration on the suspension viscosity, which in its part influences the shear force at the membrane surface. Brownian diffusion and shear induced diffusion predict a –0.33 power law coefficient. This is low compared to the experimental values reported in literature (Table 3-4).

Table 3-4. The effect of the biomass concentration on the steady state flux

Organism	Pore size	Value of ℓ_1 in Eq 3-84	Reference
Bakers Yeast spherical 5 μm	LCL tubular ceramic 0.2μm	-0.08v [(1)]	Liberge *et al.* 1994
Bakers Yeast spherical 5 μm	Tech-Sep tubular Ceramic 0.2μm	-0.08v [(1)]	Liberge et al 1994
Bakers Yeast spherical 5 μm	SCT tubular ceramic 0.2μm	-0.11v [(1)]	Liberge et al 1994
Bakers yeast, *Bacillus caldolyticus* M1 and Methanogenic waste	Tubular inorganic membranes [0.1]	-0.5	Shimizu *et al.* 1993
Bakers yeast (including broken cells)	0.1	-0.5	Shimizu *et al.* 1994
Activated sludge	Hollow fibres and tubular ceramic	-0.5	Shimizu *et al.* 1996
Corynebacterium glutamicum	Flat sheet 0.45μm	-0.2	Tanaka *et al.* 1998

[(1)] v is the average cross flow velocity in the tubular membrane

3.4 Other Factors that are modelled and can influence the cross-flow filtration flux

The other factors that were considered in the modelling of the cross-flow filtration flux and compared to the published experimental results included the particle size and the liquid permeate viscosity. These are summarised below:

- Shimizu *et al.* (1993 and 1994) found that the flux was proportional to the particle size to the power 0.67. This corresponds to Brownian diffusion.

- Devereux and Hoare (1986) found that the flux of soya protein precipitates (2.6 to 4.5 μm) through a 50 kD cut-off membrane was proportional to the particle radius.

- McDonogh *et al.* (1988) carried out experiments with two different types of spherical colloids of silica (0.012 – 0.023 μm) and polystyrene latices (0.095 – 0.290 μm). They found that the flux first decreased and then increased with particle radius. On the increasing part of the curve, the flux was proportional to the particle radius raised to the power 0.4. The 0.023 μm spheres gave the lowest flux. They attributed this behaviour to electrokinetic and double layer interactions.

- Vigneswaren & Pandey (1988) microfiltered kaolin clay slurries. Particle radii ranged form 1.5 – 2.5 μm and the flux increased with increasing radius.

- Mateus & Cabral (1989) used anionic and cationic resins to flocculate heat-treated *Arthroacter simplex* cells. Addition of the resins increased the flux 3-10 times. Increased flux was attributed to reduction of the concentration polarisation layer and increased porosity of the cake. This argument was supported by the marked decline in protein retention that occurred when flocculating resins were added.

- In contrast to all the above results, Sims & Cheryan (1986) found that the flux increased when particle size was decreased. During cross-flow filtration of *Aspergillus niger* suspensions, reduction of the particle size distribution from 20-850 to 20-150 μm increased the flux.

Again, there are large deviations between the experimental data and the available models. Microbial cells are not rigid and are generally not spherical. Although not neutrally buoyant in aqueous suspensions, the density difference is not large. More importantly, some species secrete polysaccharides and are surrounded by a slimy gelatinuous capsule. Particle size effects may be obscured by the formation of adherent compressible cakes that are resistant to shear forces. Nagata *et al.* (1989) suspected that compaction of the cake occurred during processing of *B. polymyxa* and Reismeier *et al.* (1987) observed compaction of *E. coli* cakes with time. Ofsthun & Colton (1987) took electron micrographs of the cell layer at the membrane surface and noted that the cells were tightly packed.

3.5 Conclusions

Quantitative comparisons between the modified polarisation model based on shear-induced diffusion and the measured flux for plasmapheresis of whole blood were made by Zydney and Colton (1982). The conventional polarisation model was modified to account for the concentration dependent blood viscosity. The results showed very good agreement between theory and experiment, including verification of the dependence of flux on shear rate, cell concentration and filter length. Close observation of the data shows that each set of measurements has a shallower slope than the diagonal. This suggests that the mean of the data follows the trend but that the individual data do not. Zydney and Colton (1986) also compared the modified concentration polarisation model with data from twelve different studies of cross-flow filtration of suspensions including blood, bacteria, latex, paint, platelets and clay (Zydney & Colton 1986). Good agreement was found over wide ranges of concentrations, particles sizes, filter lengths and shear rates, with the average error being about 40%.

Lojinke *et al.* (1992), concluded that the shear induced diffusion models appear to be the most accurate predictors although there are many complicating features that need further study. These features include the effects of particle adhesion, compressibility, shape and size distribution.

Further support of the shear induced diffusion model has been provided for monodisperse latex beads and for yeast cells by Romero and Davis (1991) and Redkar and Davis (1993).

They showed that the transient flux decline after the start of filtration is well described by the dead-end filtration theory. The long term flux for latex particles of radii, 0.32, 0.47 and 0.70 μm agree with the complete shear induced diffusion theory within an average error of 27%. For unwashed yeast cells with an average radius of 2.1 μm, the long term flux was found to be 2-4 times lower than the predictions of the shear induced diffusion model for non-adhesive rigid spheres.

Because shear induced diffusion models and surface transport models have similar flux dependencies on shear rate and particle size they may provide similar agreement with the data. Indeed Stamatakis and Tien (1993) and Mackley and Sheman (1992) showed that the flux decline could be described by surface transport models. Mackley and Sherman (1992) observed particles rolling along the surface of the cake, with no evidence of back diffusion. Davis and Leighton (1987) showed that the polarisation boundary layer thickness for the relative large particle sizes, high fluxes and low shear rates as used by Mackley and Sherman (1992) for optical observation is only a fraction of the diameter of a single particle.

Although these mathematical models can provide useful descriptions of the decline in flux observed during membrane filtration, it is not currently possible to obtain a priori estimates of the key parameters in these equations. In addition, these models do not provide a quantitative basis for understanding the effects of solution properties or membrane characteristics on the flux decline. These models also provide little insight into the actual physical and chemical mechanisms by which the filtration flux declines during the filtration process (Belfort *et al.* 1994).

3.6 Flux decline data

Most of the flux decline data have been modelled by using Hermia's blocking laws. Expressing the permeate flux as a function of time, three of Hermia's blocking laws may be written in the form:

$$J(t) = \frac{J_o}{(1+k_{declinre}t')^{n_{decline}}} \tag{3-86}$$

where J_0 is the initial flux of the membrane and the choice of ($k_{decline}$, $n_{decline}$) is determined by the predominant fouling mechanism; intermediate blocking (K_i J_o,1), complete blocking cells (1/2 K_s $J_o^{1/2}$; 2) and cake filtration (2 K_c J_o^2;2) with the adjustable parameters K_i, K_s, and K_c depending on the membrane and the solution.

The value of ($k_{decline}$, $n_{decline}$) was determined from the experimental data of various investigators. These values are tabulated in Table 3-5.

Table 3-5. Flux decline experimental data fitted to Equation 3-86

	Liberge *et al.* 1994	Liberge *et al.* 1994	Liberge *et al.* 1994	Redkar & Davis 1995	Mallubhotla & Belfort 1996
Nature of particles	Bakers Yeast spherical 5 μm	Bakers Yeast spherical 5 μm	Bakers Yeast spherical 5 μm	Yeast	
Membrane pore size	LCL tubular ceramic 0.2μm	Tech-Sep tubular Ceramic 0.2μm	SCT tubular ceramic 0.2μm		PES support 0.2μm
Jo/DP (Water) [LMH bar]	1200	600	2500-3000		
$K_{decline}$ [100 kPa, 2 m/s, 0.1%] (1/h)	0.007	0.025	0.004	0.0026	0.0025
$n_{decline}$	1	1	1	0.5	0.5

Most of the experimental data found on flux decline used values of either 0.5 or 1 for $n_{decline}$ (Equation 3-86). This corresponds to either the intermediate blocking law or a hybrid between the intermediate blocking law and cake filtration (Hermia 1982).

4 Development of an empirical correlation of the filtration data

The work of Hermia (1982) serves as a fundamental basis for flux decline modelling. A generic form of the flux decline equation is suggested in this work:

$$J(t) = \frac{J_o}{(1 + k_{decline}\, t)^{n_{decline}}} \tag{3-87}$$

Several authors (Schneider & Klein 1982; Mietton-Peuchot 1992) found that this generic form of Hermia's, (1982) law were well suited to the description of the initial stages of cross-flow micro-filtration. A constant term J_{ss} has been included by Liberge *et al.* (1994) to provide a semi-empirical correlation of the cross-flow filtration flux:

$$J(t) = J_{ss} + \frac{J_o - J_{ss}}{(1 + k_{decline}\, t)^{n_{decline}}} \tag{3-88}$$

where J is the permeate flux in m/s, J_{ss} is the pseudo steady state flux in m/s, J_o is the initial permeate flux in m/s, $k_{decline}$ is the decline constant in h^{-1}, t is the time in h and $n_{decline}$ is a dimensionless constant.

This form should be considered as empirical in its application to cross-flow micro-filtration because it is not based on a flow model and therefore the parameters $k_{decline}$ and $n_{decline}$ have no physical significance.

The steady state flux J_{ss} was estimated based on Darcy' law and a combination between the assumptions of shear induced diffusion models and surface transport models.

$$J_{ss} = \frac{\Delta P}{\upsilon R_t}$$
$$R_t = R_p + R_c + R_m \tag{3-89}$$

where the trans-membrane pressure drop, ΔP is in Pa, the permeate viscosity υ in Pas and the total hydraulic resistance in m^{-1}.

4.1 The intrinsic membrane resistance (R_m)

R_m is the intrinsic membrane resistance in m^{-1}. It is assumed to be a function of the membrane and its properties and not influenced by the operating parameters or the nature of the feed suspension.

4.2 The pore plugging resistance (R_p)

The model predicting the pore plugging resistance at the steady state flux is based on Hagen-Poiseuille flow through an array of uniform cylindrical pores. The equation as proposed by Belfort *et al.* (1993) would be used in this study. This analysis accounts for the impact of a pore size distribution on the flux decline associated with pore constriction effects. The derivation of this law has been discussed in a previous section (2.2.4). Belfort *et al.* (1993) presented the following explicit expression for the ratio of the modified flux with and without constricted pores:

$$\frac{J'_1}{J'_2} = 1 - \frac{4}{q_{pore}^{\,3}}\left(\frac{k_{thick}}{r_p *}\right) + \frac{6}{q_{pore}^{\,6}}\left(\frac{k_{thick}}{r_p *}\right)^2 - \frac{4}{q_{pore}^{\,6}}\left(\frac{k_{thick}}{r_p *}\right)^3 + \frac{1}{q_{pore}^{\,5}}\left(\frac{k_{thick}}{r_p *}\right) \tag{3-90}$$

where J' the modified flux is given by:

$$J' = \frac{J}{(\eta_o / L)(\pi \Delta P / 8\upsilon)} \tag{3-91}$$

J'_2/J'_1 is therefore also proportional to $(R_m+R_p) / R_m$

This means that:

$$R_p = R_m\left(\frac{J'_2}{J'_1} - 1\right) \tag{3-92}$$

where r_p^* (m) is a function of the membrane pore size, q_{pore} (m) is given by $1+(r_{p,STDEV}/r_p^*)^2$ and k_{thick} (m) is the thickness of an absorbent multilayer inside a pore.

In this study it is proposed that the parameter k_{thick} (thickness of the absorbent layer inside a pore) is to be estimated empirically from a least square fit of the experimental data.

4.3 The cake Resistance (R_c)

The cake resistance, R_c is given by the intrinsic cake resistance $\bar{R}_c$ and the thickness of the cake layer, δ_c (m).

$$R_c = \delta_c \bar{R}_c \tag{3-93}$$

The value for $\bar{R}_c$ for compressible cakes is dependent on the trans-membrane pressure drop. This relationship has previously been described in dead-end filtration applications and has been modelled using a power law relationship:

$$\bar{R}_c = \beta' (\Delta P)^{n_c} \tag{3-94}$$

where ΔP, the trans-membrane pressure drop is in Pa and β' is in m^{-2}

The thickness of the cake layer (δ_c) is based on single particle trajectory models (Section 2.2.2.5). In this study it is assumed that the thickness of the cake layer is a power law function of the ratio of the tangential and normal convective forces ($\tan\theta$) multiplied by the cell concentration (X) in the bulk stream:

$$\delta_c = k_t \; X^{p_1} (\tan\theta)^{p_2} \tag{3-95}$$

Although the equations were derived based on the single particle trajectory and solid flux models it is essentially an empirical equation. The factor p_1 compensates for concentration profiles in the broth while the factor p_2 compensates for the stickiness of the particles.

The tangential force (F_t in N) is given by:

$$F_t = 3 \pi \upsilon a^3 \dot{\gamma}_o C_t \quad (3\text{-}96)$$

where C_t is correction factor to Stokes law, υ is the liquid viscosity in Pas, is the wall shear rate (s^{-1}) and a is the particle radius in (m)

The force normal to the membrane surface (F_n in N) is given by:

$$F_n = 6 \pi \upsilon a J_{ss} C_n \quad (3\text{-}97)$$

where C_n is a hydrodynamic correction factor to Stokes law due to the presence of the cake layer.

A torque balance around the protrusion contact point yielded:

$$F_n \sin\theta = F_t \cos\theta \quad (3\text{-}98)$$

from which θ, the angle between the normal force on a particle and the radius to the contact point of the protrusion, could be estimated.

Assuming that $\dot{\gamma}_o$ is proportional to the cross-flow velocity, v and a fixed C_t, Equation 3-95 can be rewritten as:

$$\delta_c = k_t X^{p_1} (\Delta P / R_{tot} v)^{p_2} \quad (3\text{-}99)$$

where δ_c is the cake thickness in (m), k_t is a constant that compensates for the correction factors and the particle size of the suspension, X is the biomass concentration and p_1 and p_2 are empirical constants that compensates for the concentration profiles in the broth and the stickiness of the particles.

From Equation 3-97 and 3-98, the cake resistance then becomes

$$R_c = k_t X^{p_1} (\Delta P / (R_m + R_c + R_p) v)^{p_2} \Delta P^{n_c} \quad (3\text{-}100)$$

or

$$R_c (R_m + R_c + R_p)^{p_2} = k_t X^{p_1} \Delta P^{n_c + p_2} v^{-p_2} \quad (3\text{-}101)$$

The constant k_t (m^{-1}) would take into account the drag coefficients, the value of β' and the viscosity of the permeate.

If p_2 is assumed to be 1 (typical for non-sticky particles) and R_c is significantly larger than R_m and R_p (common for microfiltration), the cake resistance R_c would be given by

$$R_c = \sqrt{(k_t X^{p_1} \Delta P^{1+n_c} v^{-1})} \quad (3\text{-}102)$$

For all other cases, no explicit solution for R_c exists.

5 Experimental estimation of the parameters in the empirical correlation

The parameters in the developed model were determined from experimental data based on a least square fit.

5.1 Predicting the pore plugging resistance

A parity-line for the measured R_p values against the R_p values as calculated by the model is shown in Figure 3-5.

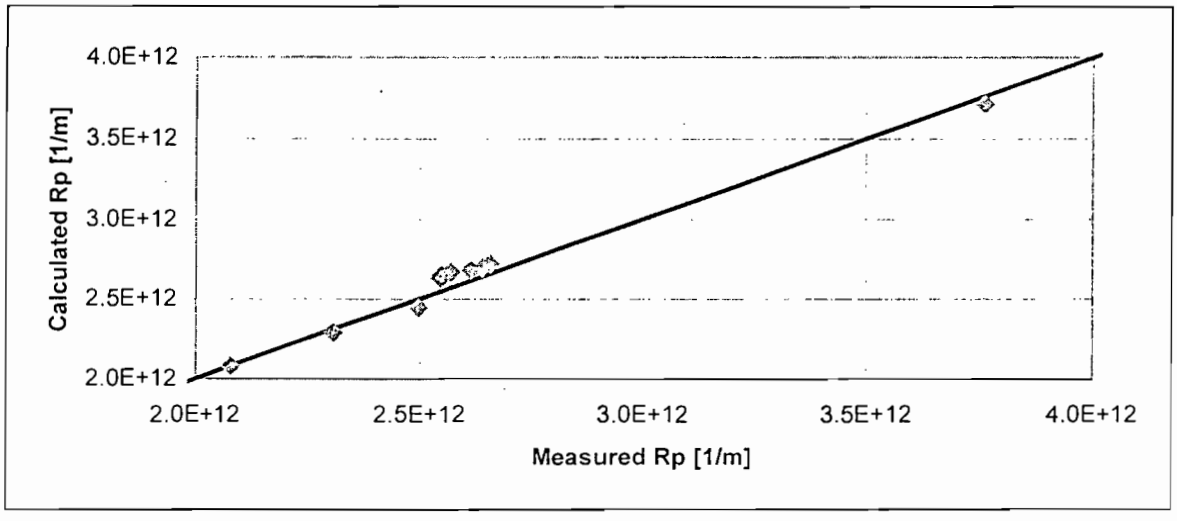

Figure 3-5. Parity-line for the pore-plugging resistance of cells suspended in industrial media though a 0.45-μm membrane.

A correlation coefficient of 0.95 was found for this data set. For all the other data sets an average correlation coefficient of 0.95 and an absolute error of less than 10% was found.

The value of r_p^* of the four membranes tested in the study were obtained from the supplier while $r_{p,STDEV}$ was estimated from pure water flux experiments. The power law parameters that determined the value of k did not show good correlation between the types of feed suspensions or the impact of the operating parameters. Each experimental set (i.e. membrane and feed suspension combination) had its own set of parameters. The

parameters did not seem to be a function of either the membrane type or the feed suspension. The values of these parameters are displayed in Table 3-6 and 3-7

Table 3-6. Values of the pore plugging parameters as determined from experimental results for cells suspended in industrial media formulation, minimal media and a saline solution for the microfiltration membranes.

	Unit	0.45 μm membrane			0.22 μm membrane		
		Industrial	Minimal	Saline	Industrial	Minimal	Saline
Eq. 3-90 – r_p*	(μm)	0.45	0.45	0.45	0.22	0.22	0.22
Eq. 3-90 – $r_{p,\ STDEV}$	(μm)	0.30	0.30	0.30	0.14	0.14	0.14
Eq. 3-90 – q_{pore}	(μm)	**1.44**	**1.44**	**1.44**	**1.40**	**1.40**	**1.40**
Eq 3-90 – k_{thick} [100 kPa, 2 m/s, 35 g/l]	(μm)	**0.42**	**0.41**	**0.23**	**0.20**	**0.20**	**0.14**
Eq. 3-90 – J'_2/J'_1		**0.14**	**0.15**	**0.52**	**0.09**	**0.12**	**0.39**
R_p [100 kPa, 2 m/s, 35 g/l DCW]	(m^{-1})	**2.67E+12**	**2.44E+12**	**4.02E+11**	**2.26E+12**	**1.60E+12**	**3.31E+11**
% Error		4%	8%	5%	10%	8%	8%

Table 3-7 Values of the pore plugging parameters as determined from experimental results for cells suspended in industrial media formulation, minimal media and a saline solution for the ultrafiltration membranes.

		150 kD μm membrane			300 kD μm membrane		
		Industrial	Minimal	Saline	Industrial	Minimal	Saline
Eq. 3-90 – r_p*	(μm)	0.02	0.02	0.02	0.03	0.03	0.03
Eq. 3-90 – $r_{p,\ STDEV}$	(μm)	0.01	0.01	0.01	0.02	0.02	0.02
Eq. 3-90 – q_{pore}	(μm)	**1.44**	**1.44**	**1.44**	**1.44**	**1.44**	**1.44**
Eq 3-90 – k_{thick} [100 kPa, 2 m/s, 35 g/l]	(μm)	**0.0045**	**0.0043**	**0.0011**	**0.0099**	**0.0101**	**0.0025**
Eq. 3-90 – J'_2/J'_1		**0.70**	**0.71**	**0.92**	**0.67**	**0.66**	**0.91**
R_p [100 kPa, 2 m/s, 35 g/l DCW]	(m^{-1})	**8.80E+11**	**8.30E+11**	**1.76E+11**	**9.89E+11**	**1.02E+12**	**2.03E+11**
% Error		10%	7%	10%	4%	8%	7%

5.2 Predicting the cake resistance

A stepwise multiple regression program was used to determine the empirical constants in the cake resistance correlation. The program determined the largest data set that would have a sufficient correlation coefficient with a single set of parameters. The program

calculates the correlation coefficient for a single set of data. For example for the 0.45 membrane and the cells suspended in the industrial media formulation. The number of data sets are then increased using a single set of parameter values until the correlation coefficient is significantly reduced.

From this analysis it was found that $p_2 \approx 1$ (Eq. 3-102) for all the data sets. It was also found that for the simplified equation ($R_t = R_c$) the constant k_t (Eq. 3-102) dependent only on the composition of the feed suspensions and not on the nature of the membrane or the operating parameters. The values of p_1, k_t and n_c for each of the membrane and cell suspension combinations as determined from a least square fit of the experimental data are depicted in Table 3-8

The measured R_c values for the micro-filtration of *C. glutamicum* cells suspended in industrial media through the 0.45μ membrane is plotted against the calculated R_c values. For the first data series it was assumed that the cake resistance is the predominating and that the particles are not adhesive and therefore $p_2 \approx 1$ (Eq. 3-102). The full equation was used for line 2 (Eq. 3-101).

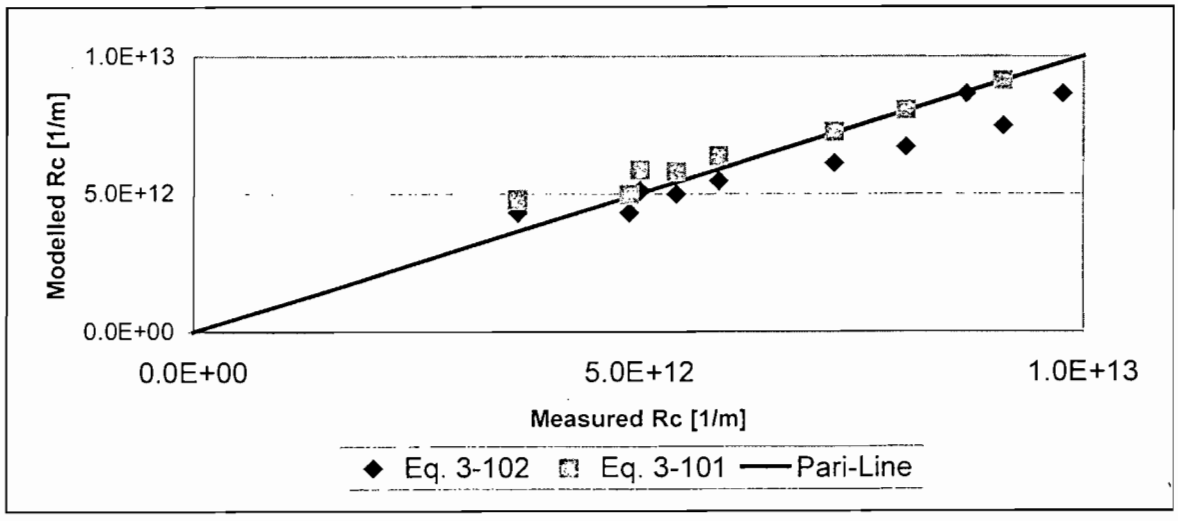

Figure 3-6 Measured vs. Modelled cake resistance (R_c) values

Table 3-8 Values of the cake resistance (Rc) parameters (p_1, n_c and k_t) as defined in Eq. 3-102 as determined from experimental results for cells suspended in industrial media formulation, minimal media and a saline solution for the ultrafiltration membranes.

Symbol	p_1	p_2	n_c	k_t
Unit	[]	[]	[]	[m^{-1}]
Suspension				
Industrial	0.67	0.99	0.45	4.44×10^{12}
Minimal	0.66	1.02	0.60	1.73×10^{12}
Saline	0.65	1.01	0.59	1.18×10^{12}

5.3 Prediction of the rate of flux decline

The model used to estimate the rate of flux decline is depicted in Eq. 3-88.

$$J(t) = J_{ss} + \frac{J_o - J_{ss}}{(1 + k_{decline} t')^{n_{decline}}} \tag{3-88}$$

where $k_{decline}$ and $n_{decline}$ are parameters that depends on the membrane pore size, the operating conditions and the suspension composition

The parameters in Eq. 3-88 ($k_{decline}$ and $n_{decline}$) was determined from a least square fit of the experimental data for each membrane and suspension combination. These values are summarised in Table 3-9.

The value of $n_{decline}$ was close to 1 for all the presented data. If it was assigned a value of one the error of the prediction and the measured data was not significantly impacted. It was therefore assumed that $n_{decline}$ would be 1 for all the membranes and the suspensions.

A multiple regression program was used to find that the flux decline constant $k_{decline}$ in h^{-1} for each suspension can be empirically modelled as a function of the initial flux, the cross flow velocity and the biomass concentration.

$$k_{decline} = m_o J_o^{m_1} v^{m_2} X^{m_3} \tag{3-103}$$

The values of $m_0 \ldots m_3$ was determined from a least square fit of all the experimental data and are presented in Table 3-10.

Table 3-9. Parameters in Eq. 3-88 ($k_{decline}$ and $n_{decline}$) as determined from a least square fit of the experimental data for each membrane and suspension combination.

Membrane	Industrial media		Minimal media		0.9 % Saline	
	$n_{decline}$	$K_{decline}$	$n_{decline}$	$K_{decline}$	$n_{decline}$	$K_{decline}$
	[]	[1/h]	[]	[1/h]	[]	[1/h]
300 kD	0.98	0.013	1.00	0.010	1.01	0.008
150 kD	0.99	0.012	1.00	0.010	1.01	0.008
0.45 μm	0.97	0.051	0.98	0.041	1.04	0.035
0.22 μm	0.98	0.047	0.99	0.038	1.03	0.032

Table 3-10. The values of $m_0 \ldots m_3$, parameters in Eq. 3-103 as determined from a least square fit of all the experimental data and are presented

Parameter	Unit	Industrial	Minimal	Saline
m_0	[1/m]	0.53	0.47	0.43
m_1	[]	0.58	0.60	0.62
m_2	[]	-0.25	-0.28	-0.30
m_3	[]	0.48	0.50	0.52

When the suggested approach (Eq. 3-88) is used to estimate the correlation parameters there is a very good correlation between calculated and measured results for the cross-flow filtration flux. The cross-flow filtration flux obtained when filtering a suspension of *C. glutamicum* cells through the 0.45 μm membrane with an applied trans-membrane pressure drop of 100 kPa at a cross-flow velocity of 1.6 m/s is illustrated below.

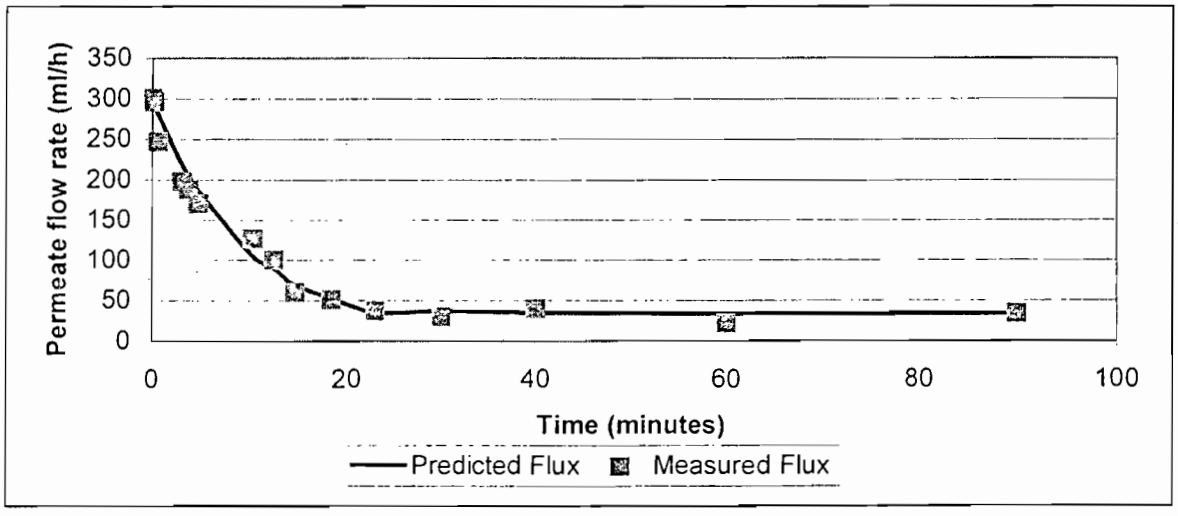

Figure 3-7. The cross-flow filtration flux as a function of time for 30 g/l (DCW) of *Corynebacterium glutamicum* cells in an industrial media formulation through a 0.45 μm tubular ceramic membrane. ΔP = 100 kPa, Cross-flow velocity 1.6 m/s.

5.4 Prediction of the entire cycle of cross-flow microfiltration

A parity-line was constructed for all the data points collected, irrespective of time, operating conditions or membrane pore size.

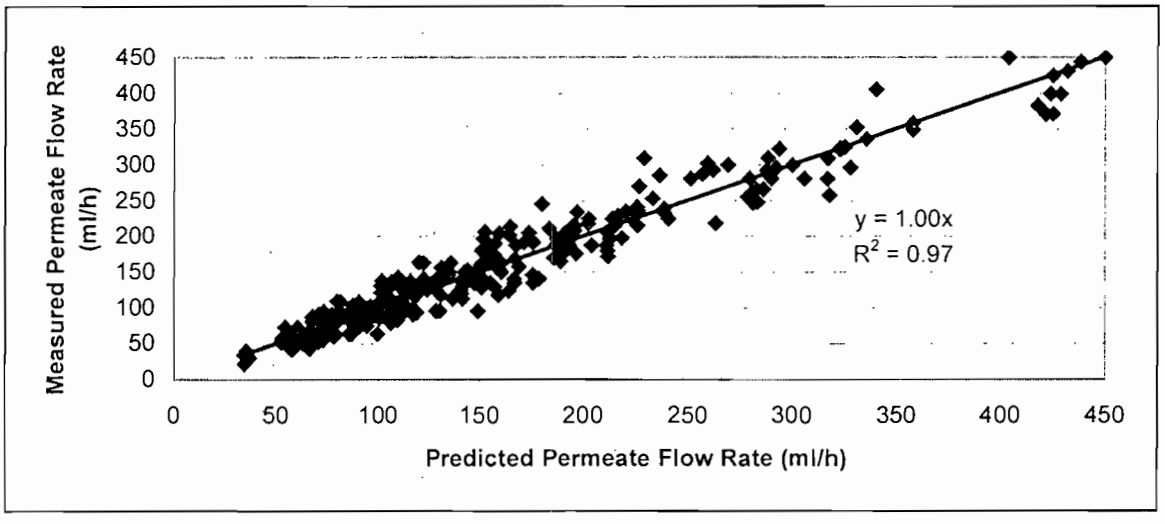

Figure 3-8. Parity-line for the cross-flow filtration flux of cells suspended in industrial media. This represents all the data points for all the operating conditions, membrane pore sizes over the entire flux decline cycle.

This curve shows that the empirical correlation developed above is adequate to describe the cross-flow filtration flux of this specific suspension.

6 Conclusions

Two modelling approaches have been followed to predict the flux behaviour during cross flow filtration. In the first approach the model is based on empirical correlations of the experimental data. The form of the model has in itself no significance and is entirely dictated by the data. On the other hand fundamental models are based on proposed mechanisms of flux decline derived from first principles.

Quantitative comparisons between the modified polarisation model based on shear-induced diffusion and the measured flux data for various systems showed good agreement between theory and experiment. Close observation of the data suggests that the mean of the data follows the trend but that the individual data do not. Because shear induced diffusion models and surface transport models have similar flux dependencies on shear rate and particle size they may provide similar agreement with the data.

It was found that a generic form of Hermia's blocking laws (Equation 3-87) is well suited to the description of the initial stages of cross flow microfiltration. A constant term (the

pseudo steady state flux) has been included to provide a semi-empirical correlation of the cross flow filtration flux (Equation 3-88). The pseudo steady state flux can be estimated based on Darcy's law (Equation 3-89) and a combination of the shear induced diffusion and surface transport models. Darcy's law divides the total resistance to the permeate flux into the mernbrane resistance (or the impact of the membrane on the flitration flux), the pore plugging resistance (or the interaction between the feed suspension and the membrane) and the cake resistance (or the impact of the feed suspension on the filtration flux).

The membrane resistance is estimated from pure water flux data. The pore plugging resistance is based on Hagen-Poiseuille flow through an array of cylindrical pores. The analysis accounts for the impact of a pore size distribution on the flux associated with pore constriction effects (Equation 3-90). The cake resistance is given by the intrinsic cake resistance, which is a function of the applied trans-membrane pressure drop, and the thickness of the cake layer on the membrane surface (Equation 3-94, 3-95). The thickness of the cake layer is based on single particle trajectory models. The thickness of the cake layer is modelled as the product of power law functions of the ratio of the tangential and normal convective forces and the cell concentration in the bulk stream (Equation 3-95) to compensate for concentration profiles in the broth and the stickiness of the particles. The presented model adequately described the experimental data.

Although these mathematical models can provide useful descriptions of the decline in flux observed during membrane filtration, it is not currently possible to obtain a priori estimates of the key parameters in these equations. In addition, these models do not provide a quantitative basis for understanding the effects of solution properties or membrane characteristics on the flux decline. These models also provide little insight into the actual physical and chemical mechanisms by which the filtration flux declines during the filtration process.

7 References

Aimar, P., Meireles, P., Bacchin, P. and Sanchez, V. (1994), Fouling and concentration polarisation in ultrafiltration and microfiltration, *NATO ASI Ser. E*, **272**, 27-57

Altena, F. W. and Belfort, G. (1984), Lateral migration of spherical particles in laminar porous tube flows: application to membrane filtration, *Chem. Eng. Sci.* **39,** 343-355

Altena, F. W., Belfort, G., Otis, J., Fiessinger, F., Rovel, J. M. and Nicoletti, J. (1983), Particle motion in laminar slit flow: a fundamental fouling study, *Desalination,* **47,** 221-232

Altena, F. W., Weigand, R. J. and Mahar, J. J. (1985), Particulate membrane fouling and recent development in fluid mechanics of dilute suspensions, *ACS Symp. Ser.,* **281**

Aptel, P. and Buckley, C. A. (1992), Categories of membrane operations, In "Water Treatment: Membrane Processes", Mallevaille, J., Odendaal, P. E. and Wiesner, M. R. (Eds.), Chapter 2, McGraw Hill

Arora, N., and Davis, R. H. (1994), Yeast cake layers as secondary membranes in dead-end microfiltration of bovine serum albumin, *Journal of Membrane Science,* **92,** 247-256

Baker, R. J., Fane, A. G., Fell, C. J. D. and Yoo, B. H. (1985), Factors affecting flux in cross-flow filtration, *Desalination,* **53,** 81-93

Bansal, A., Ma, Y. H., Clark, W. M. (1991), A quantitative investigation of membrane fouling by proteins using energy dispersive spectroscopy, *Key Eng. Mat.,* **61,** 505

Bauser, H., Chmiel, H., Stroh, N. and Walitza, E. (1982), Interfacial effects with microfiltration membranes, *Journal of Membrane Science*, **11,** 321-332

Belfort, G., Weigand, R. J. and Mahar, J. T. (1985), Particulate membrane fouling and recent development in fluid mechanics of dilute suspensions, *ACS Symp. Ser.,* **281**

Belfort, G. and Nagata, N. (1985), Fluid mechanics and cross-flow filtration: some thoughts, *Desalination,* **53,** 57-79

Belfort, G. (1986), Fluid mechanics and cross-flow filtration, In "Advances in Solid Liquid Separation", H. S. Muralidhara (Ed.), Battelle Press, Columbus, OH, Chapter 7

Belfort, G., Davis, R. H. and Zydney, A. L. (1994), The behavior of suspensions and macromolecular solutions in cross-flow microfiltration, *Journal of Membrane Science,* **96,** 1-58

Belfort, G., Pinbley, J. M., Greiner, A. and Ching, K. A. (1993), Diagnosis of membrane fouling using rotating annular filter. 1. Cell culture media, *Journal of Membrane Science,* **77,** 1-22

Belter, P. A., Cussler, E. L. and Hu, W. S. (1988), Bioseparations, In "Downstream processing for biotechnology", Wiley, NY

Berman, A. S. (1953), Laminar flow in channels with porous walls, *J. Appl. Phys.* **24,** 1232-1235

Blatt, W. F., Dravid, A., Michaels, A. S. and Nelson, L. (1970), Industrial biological waste treament processes, In "Membrane Science and Technology", J. E. Flinn (Ed.), Plenum Press, NY

Bowen, W. R. and Clark, W. M. (1984), Electro-osmosis at microporous membranes and the determination of zeta potential, *J. Colloid Interface,* **72**(2), 401

Bowen, W. R. and Gan, Q. (1991), Properties of Microfiltration membranes. The effect of adsorption and shear on the recovery of an enzyme, *Biotechnology and Bioengineering, **38,** 688*

Brenner, H. (1966), Hydrodynamic resistance of particles at small Reynolds numbers, In "Advances in Chemical Engineering", Drew, T. B., Hoopes, J. W. and Vermuelen, T. (Eds.) (Vol 6), Academic Press, NY, 287-438

Brown, D. E. and Kavanagh, P. R. (1987), Cross-flow separation of cells, *Process Biochem.,* **22**(4), 96-101

Burman, A. S. (1953), Laminar flow in channels with porous walls, *J. Appl. Phys.,* **24,** 1232-1235

Caiman, P. C. (1938), Fundamental principles of industrial filtration, *Trans. Inst. Chem. Eng.* **16,** 168-187

Cantor, C. R. and Schimmel, P. R. (1980), Biophysical Chemistry. Part II, In "Techniques for the Study of Biological Structure and Function", Freeman, San Francisco, CA, pp. 562-565; pp. 581-586

Chandavarkar, A. S. (1990), Dynamics of fouling of microporous membranes by proteins, PhD Thesis, Massachusetts Institute of Technology, Cambridge, MA

Cheryan, M. (1986), "The Ultrafiltration Handbook", Technomic, USA

Choo, K. and Lee, C. (1996), Membrane fouling mechanisms in the membrane coupled anaerobic bioreactor, *Water research,* **30**(8), pp 1771-1780

Clark, W. M., Bansal, A. Sontakke, M. and Ma, Y. H. (1991), Protein adsorption and fouling in ceramic ultrafiltration membranes, *Journal of Membrane Science,* **55,** 21-38

Cox, R. G. and Brenner, H. (1968), The lateral migration of solid particles in Poiseuille flow – I Theory, *Chem. Eng. Sci.,* **23,** 147-173

Datar, R. (1984), Tangential flow membrane filtration of bacterial cell debris form crude homogenates, *World Biotech Report,* **2,** A15-A30

Davis, R. H, and Sherwood, J. D. (1990), A similarity solution for steady–state cross-flow microfiltration, *Chem. Eng. Sci.,* **45,** 3204-3209

Davis, R. H. and Birdsell, S. A. (1987), Hydrodynamic model and experiments for cross-flow microfiltration, *Chem. Eng. Commun.,* **49,** 217-234

Davis, R. H. and Grant, D. C. (1992), Theory of dead-end microfiltration, In "Membrane Handbook", Ho, W. S. and Sirkar, K. K. (Eds.), Van Nostrand Reinhold, NY, pp. 461-479

Davis, R. H. (1992), Modeling of fouling of cross-flow microfiltration membranes, *Sep. Purif. Methods,* **21,** 75-126

Davis, R. H., and Leighton, D. T. (1987), Shear-induced transport of a particle layer along a porous wall, *Chem. Eng. Sci.,* **42,** 275-281

De Balmann, H. (1988), Utilisation de l'Ultrafiltration dans le Traitement de l'Eau, Ph.D Thesis, Universite Paul Sabatier, Toulouse

De Balmann, H., Aimar, P. and Sanchez, V. (1990), Membrane partition and mass transfer in ultrafiltration, *Sep. Sci. and Technol.,* **25**(5), 507-534

Defrise, D. and Gekas, V. (1988), Microfiltration membranes and the problem of microbial adhesion, *Process Biochem.,* **23**(4), 105-116

Devereux, N. and Hoare, M. (1986), Membrane separation of protein precipitates: studies with cross-flow hollow fibres, *Biotechnology and Bioengineering,* **28,** 42-431

Dharmappa, H. B., Verink, J., Ben Aim, R., Yamamoto, K. and Vigneswaran, S. (1992), A comprehensive model for cross flow filtration incorporating polydispersity of the influent, *Journal of Membrane Science,* **65,** 173

Drew, D. A., Schonberg, J. A. and Belfort, G. (1991), Lateral inertial migration of a small sphere in a fast laminar flow through a membrane duct, *Chem. Eng. Sci.,* **46,** 3219-3224

Eckstein, E. C., Bailey, P. G. and Shapiro, A. H. (1977), Self-diffusion of particles in shear flow of a suspension, *J. Fluid Mech.,* **79 19**1-208

Fane, A. G., Fell, C. J. D. and Nor, M. T. (1982), Ultrafiltration in the presence of suspended matter, *IChemE Symp. Ser.,* **73,** C1-C12

Fane, A. G., Fell, C. J. D. and Waters, A. G. (1981), The relationship between membrane surface pore characteristics and flux for ultrafiltration membranes, *Journal of Membrane Science,* **9,** 245-262

Fane, A. G., Jim, K. J., Hodgson, P., Leslie, G., Fell C. D. J., Franken, A. C. M., Chen, V. and Liew, K. H. (1990), Strategies to minimise fouling in the membrane processing of biofluids, presented at *Frontiers in Bioprocessing II,* Boulder, Colorado, June 17-21

Field, R. W. and Aimar, P. (1992), Limiting fluxes in membrane separations, *Engineering of Membrane Processes Conference,* May 1992, Bavaria, Germany

Fischer, E. and Raasch, J. (1985), Cross flow filtration, *Ger. Chem. Eng.,* **8,** 211-216

Fischer, E. and Raasch, J. (1986), Model tests of the particle deposition at the filter medium in cross-flow filtration, *Proc. Fourth World Filtration Conference,* Ostend 1986 (Part II), 11.11-11.17

Forman, S. M., DeBernardez, E. R., Feldberg, R. S. and Swartz, R. W. (1990), Cross-flow filtration for the separation of inclusion bodies from soluble proteins in recombinant *Escherichia coli* lysate, *Journal of Membrane Science,* **48,** 263-279

Gatenholm, P., Fell, C. J. and Fane, A. G. (1988a), Influence of the membrane structure on the composition of the deposit layer during processing of microbial suspensions, *Desalination,* **70**(1-3), 363-378

Gatenholm, P., Paterson, S., Fane, A. G. and Fell, C. D. J. (1988b), Performance of synthetic membranes during cell harvesting of *E. coli, Process Biochem.,* **23**(3), 79-81

Goren, S. L. (1979), The hydrodynamic force resisting the approach of a sphere to a plant permeable wall, *J. Colloid Interface Sci.,* **69,** 78-85

Grabler, F. R. (1985), Cell processing using tangential flow filtration, In "Comprehensive Biotechnology", Coeney, Humphrey (Eds.), Vol 2, Permagon Press, Oxford, 351-366

Grabler, R. and Ryan, M. (1985), Processing cell lysate with tangential flow filtration, In "Purification of Fermentation Products: Application to large scale processes", LeRoith, Schilback, Leahy (Eds.), ACS Symposium Series, 271

Grace, H. P. (1953), Resistance and compressibility of filter cakes, *Chem. Eng. Prog.,* **49,** 303-318

Green, G. and Belfort, G. (1980), Fouling of ultrafiltration membranes: lateral migration and the particle trajectory model, *Desalination,* **35,** 129-147

Gutman, R. G. (1987), Membrane Filtration: the technology of pressure driven cross-flow processes, Adam Hilger, Brisol 19

Haarstrick, A., Rau, U. and Wagner, F. (1991), Cross-flow filtration as method of separating fungal cells and purifying the polysaccharide produced, *Bioprocess Eng.,* **6,** 179-186

Harris, T. A. J., Reuben, B. G., Cox, D. J., Vaid, A. K. and Carvell, J. (1988), The cross-flow filtration of an unstable beta-lactum antibiotic fermentation broth, *J. Chemical Technol. and Biotechnol.,* **42 19**-30

Henry, J. D. and Alfred, R. C. (1972), Concentration of bacterial cells by cross-flow filtration, *Develop. In Industrial Microbiol.,* **13,** 177-190

Herak, D. C. and Merrill, E. W. (1989), Affinity cross-flow filtration: experimental and modelling work using the system of HAS and Cibacron blue-agarose, *Biotechnol. Progress,* **5**(1), 9-17

Hermia, J. (1982), Constant pressure blocking laws – Application to power law non-newtonian fluids, *Trans. IChemE,* **60,** 183-189

Hlavacek, M. and Bouchet, F. (1993), Constant flowrate blocking laws and an example of their application to dead-end microfiltration of protein solutions, *Journal of Membrane Science,* **82,** 285-295

Ho, B. P. and Leal, L. G. (1974), Inertial migration of rigid spheres in two-dimensional unidirectional flow, *J. Fluid Mech.,* **65,** 365-400

Hoffman, H., Scheper, T., Schugerl, K. and Schmidt, W. (1987), Use of membranes to improve bioreactor progress, *Chem. Eng.,* **34**, B13-B19

Houi, D. and Lenormand, R. (1986), Proceedings of the 4th Word Filtration Congress, Ostend, Belgium, 8, 1.1-3.0

Howell, J. A. and Velicangil, O. (1980), Protein ultrafiltration: theory of membrane fouling and its treatment with immobilized proteases, Cooper, A. E. (Ed.), Ultrafiltration Membranes and Applications, Plenum Press, NY, 217-229

Howell, J. A., Sanchez, V. and Field, R. W. (eds) (1993), Membranes in Bioprocessing: Theory and Applications, Chapman & Hall, London

Ishii, K. and Hasimoto, H. (1980), Lateral migration of a spherical particle in flows in a circular tube, *J. Phys. Soc. Jpn.,* **48,** 2144-2153

Jang, C. D. (1987), Effect of different operating parameters and pre-treatment in cross-flow microfiltration, M. Engg at Asian Institute of Technology, Bankok, Thialand

Jonsson, G. (1984), boundary layer phenomena during ultrafiltration of dextran and whey protein solutions, *Desalination,* **51,** 61-77

Karnis, A., Goldsmith, H. L. and Mason, S. G. (1966), The kinetics of flowing dispersions. 1. Concentrated suspensions of rigid particles, *J. of Colloid Interface Sci.,* **22,** 531-553

Kleinstreuer, C and Belfort, G. (1984) Mathematical modeling of fluid flow and solute distribution and pressure-driven membrane modules, In "Synthetic Membrane Processes: Fundamentals and Water Applications", G. Belfort (Ed.), Academic Press, NY, Chapter 5

Kroner, K. H. and Nissinen, V. (1988), Dynamic filtration of suspensions using an axially rotating filter, *Journal of Membrane Science,* **36,** 85-100

Kroner, K. H. and Nissenen, V. (1985), Dynamic filtration of microbial suspensions using an annular rotating filter, *Journal of Membrane Science,* **36,** 85-100

Kroner, K. H., Nissinen, V. and Ziegler, H. (1987), Improved dynamic filtration of microbial suspensions, *Bio/Technology,* **5**, **921-926**

Kroner, K. H., Schütte, H., Hustedt, H., and Kula, M. R. (1984), Cross-flow filtration in downstream processing of enzymes, *Process Biochem. 19,* 67-74

Le, M. S. and Atkinson, T. (1985), Cross-flow microfiltration for recovery of intracellular products, *Process Biochem.,* **20**(1), 26-31

Le, M. S. and Billet, C. T. (1984), The use of membranes in cross-flow mode for the separation of cells and cell product recovery, *Downstream Processing,* **84,** Swansea

Le, M. S. and Howell, J. A. (1984), An alternative model for ultrafiltration, *Chem. Eng. Res. Des.* **64,** 373-380

Le, M. S. (1987), Recovery of beer from tank bottoms with membranes, *J. Chem. Technol. and Biotechnol.,* **37,** 59-66

Le, M. S., Spark, L. B. and Ward, P. S. (1984), The separation of aryl acylamidase by cross-flow microfiltration and the significance of enzyme / cell debris interaction, *Journal of Membrane Science,* **21,** 219-232

Leighton, D. T. and Acrivos, A. (1986), Viscous resuspension, *Chem. Eng. Sci.,* **41,** 1377-1384

Leighton, D. T. and Acrivos, A. (1987a), Measurement of the shear induced coefficient of self diffusion in concentrated suspensions of spheres, *J. Fluid Mech.,* **177,** 109-131

Leighton, D. T. and Acrivos, A. (1987b), The shear induced migration of particles in concentrated suspensions, *J. Fluid Mech.,* **181,** 415-439

Leonard, E. F. and Vassilieff, C. S. (1984), The deposition of rejected matter in membrane separation processes, *Chem. Eng. Commun.,* **30,** 209-217

Levesque, M. A. (1928), *Ann. Mines,* **13,** 201

Liberge, R., Colinart, P., Fessier, P and Renon, N. H. (1994), Data and model for progressive fouling in cross-flow microfltration of yeast on three industrial mineral membranes, *Ind. Eng. Chem. Res,* **33,** 1310-1318

Lojinke, M. H., Field, R. W. and Howell, J. A. (1992), Cross-flow microfiltration of cell suspensions: a review of models with emphasis on particle size effects, *Trans. Inst. Chem. Eng.,* **70,** 149-164

Lu, W. –M. and Ju, S. –C. (1989), Selective particle deposition in cross-flow filtration. *Sep. Sci. Technol.,* **24,** 512-540

Mackley, M. R. and Sherman N. E. (1992), Cross-flow cake filtration mechanisms and kinetics, *Chem. Eng. Sci.,* **47,** 3067-3084

Madsen (1977), Hyperfiltration and ultrafiltration in plate and frame systems, Elsevier Sci. Pub. Co, NY

Mallubhotla, H. and Belfort, G. (1996), Semi-empirical modelling of cross-flow micrfiltration with periodic reverse filtration, *Ind. Eng. Chem. Res.*, **35,** 2920-2928

Mateus, M. and Gabral, J. M. S. (1989), Recovery of 6-alpha-methylprednisolone from biotransformation medium by tangential flow filtration, *Bioprocess Eng.*, **4**(4), 160-174

Matsumoto, K., Katsuyama, S. and Ohya, H. (1987), Separation of yeast by cross-flow filtration with backwashing, *J. Fermentation Technol.*, **65,** 77-83

Mattiasson, B. and Ramstrop, M. (1984), Ultrafiltration affinity purification: isolation of concanavalin A from seeds of *Canavalia ensiformis, J. Chromatog.*, **283,** 323-333

McDonogh, R. M., Welsch, K., Fane, A. G. and Fell, C. J. D. (1988), Flux and rejection in the ultrafiltration of colloids, *Desalination,* **70,** 251-264

Meireles, M., Aimar, P. and Sanchez, V. (1991), Effects of protein fouling on the apparent pore size distribution of sieving membranes, *Journal of Membrane Science,* **56,** 13-28

Mellis, R., Gill, W. N. and Belfort, G. (1993), Fluid dynamics in tubular membrane: theory and experiment, *Chem. Eng. Commun.*, **122,** 103-125

Michaels, A. S. (1968), New Separation Techniques for the CPI, *Chemical Engineering Progress,* **64**(12), 31-43

Michales, A. S. and Matson, S. L. (1985), Membranes in biotechnology: state of the art, *Desalination,* **53,** 231-258

Mietton-Peuchot and Aim, B. (1992), Improvement of cross-flow microfiltration performance with flocculation, *Journal of Membrane Science.*, **68,** 241

Mochizuki, S. and Zydney, A. L. (1993), Sieving characteristics of albumin deposits formed during microfiltration. *J. Colloid Interface Sci.*, **159,** 136

Mulder, M. (1991), Basic Principle of Membrane Technology, Kluwer Academic Publishers, Dordrecht

Murase, T. and Ohn, T. (1996), New decline pattern of filtrate flux in cross-flow microfiltration of dilute suspensions, *AIChE Journal,* **42**(7) 1938-1944

Nagata, N., Herouvis, K., Dziewulski, D. M. and Belfort, G. (1989), Cross-flow membrane microfiltration of a bacterial fermentation broth, *Biotechnolology and Bioengineering,* **44,** 161-181

Nipkow, A., Zeikus, J. G. and Gerhardt, P. (1989), Microfiltration cell recycle pilot system for continuous thermoanaerobic production of exo-beta-amylase, *Biotechnology and Bioengineering,* **34,** 1075-1084

O'Neil, M. E. (1968), A sphere in contact with a plane wall in slow linear flow, *Chem. Eng. Sci.*, **23,** 1293-1297

Ofsthun, N. J. and Colton, C. K. (1987), Visual evidence of concentration polarization in cross-flow membrane plasmapheresis, *Am. Soc. Artif. Intern. Organs J.* **10,** 510-517

Ofsthun, N. J. (1989), Cross-flow membrane filtration of cell suspensions, PhD Thesis, Massachusetts Institute of Technology, Chemical Engineering Department, Cambridge, MA

Opong, W. S. and Zydney, A. L. (1991), Hydraulic permeability of protein layers deposited during ultrafiltration, *J. Colloid Interface Sci.*, **142,** 41

Otis, J. R., Altena, F. W., Mahar, J. J. and Belfort, G. (1986), Measurement of single spherical particle trajectories with lateral migration in a slit with one porous wall under laminar flow conditions, *Experiments Fluids,* **4,** 1-10

Palacek, S. P. and Zydney, A. L. (1994), Intermolecular electrostatic interactions and their effect on flux and protein deposition during protein filtration, *Biotechnol. Prog.*, **10,** 207-213

Patel, P. N., Mehaia, M. A. and Cheryan, M. (1987), Cross-flow membrane filtration of yeast suspensions, *J. Biotechnology,* **5,** 1-16

Persson, K. M., Capannelli, G., Bottino, A. and Tragardh, G. (1993), Porosity and protein adsorption of four polymeric microfiltration membranes, *Journal of Membrane Science,* **76,** 61-71

Phillips, R. J., Armstrong, R. C., Brown, R. A., Graham, A. L. and Abbott, J. L. (1992), A constitutive equation for concentrated suspensions that accounts for shear-induced particle migration, *Phys. Fluids A,* **4,** 30-40

Porter, M. C. (1972), Concentration polarization with membrane ultrafiltration, *Ind. Eng. Chem. Prod. Res. Dev.* **11,** 233-248

Porter, M. C. (1977), What, when and why of membranes – MF, UF and RO, *AICHE Symp. Ser.,* **73,** 83-103

Pritchard, M. (1991) *PhD Thesis,* University of Bath, UK

Pritchard, M., Howell, J. A. and Field, R. W. (1992), The concentration of viscous fluids bt ultrafiltration, *Engineering of Membrane Processes,* Conference May 1992, Bavaria Germany

Quirck, A. V. and Woodrow, J. R. (1984), Investigation of the parameters affecting the searation of bacterial enzymes from cell debris by tangential flow filtration, *Enzyme Microb. Technol.*, **6**(5), 201-206

Rakow, A. L. and Chappell, M. L. (1987), Axial migration of spirulina microalgae in laminar flow tube, *Biorheology,* **24**(6), 763-768

Rautenbach, R. and Albrecht, R. (1989), Membrane Processes, John Wiley, New York

Rautenbach, R. (1988), Ultrafiltration of macromolecular solutions and cross-flow microfiltration of colloidal suspensions. A contribution to permeate flux calculations, *Journal of Membrane Science,* **36,** 231-242

Rebsamen, E., Goldinger, W., Scheirer, W., Merten, O. W. and Palfi, G. E. (1987) Use of a dynamic filtration method for the separation of animal cells, *Dev. Biol. Standard,* **66,** 273-277

Redkar, S. G. and Davis, R. H. (1995), Cross-flow microfiltration with high-frequency reverse filtration, *AIChE Journal,* **41**(3), 501

Redkar, S. G. and Davis, R. H. (1996), Modelling of concentration polarization and depolarization with high-frequency backpulsing, *Journal of Membrane Science.,* **121,** 229-242

Redkar, S. G. and Davis, R. H. (1993) Cross-flow microfiltration of yeast suspensions in tubular filters, *Biotechnol. Prog.,* **9,** 625-634

Reismeier, B., Kröner, K. H. and Kula, M. R. (1987), Studies on secondary layer formation and its characteristics during cross-flow filtration of microbial cells, *Journal of Membrane Science,* **34**(3), 245-266

Reismeier, B., Kröner, K. H. and Kula, M. R. (1989), Tangential filtration of microbial suspensions: filtration resistance and model development, *J. Biotechnol.,* **12,** 153-172

Reismeier, B., Kroner, K. H. and Kula, M. R. (1990), Harvest of microbial suspensions by microfiltration, *Desalination,* **77,** 219-233

Romeo, C. A. and Davis, R. H. (1991), Experimental verification of the shear-induced hydrodynamic diffusion model of cross-flow microfiltration, *Journal of Membrane Science,* **62,** 249-273

Romero, C. A. and Davis, R. H. (1988), Global model of cross-flow microfiltration based on hydrodynamic particle diffusion, *Journal of Membrane Science,* **39,** 157-185

Romero, C. A. and Davis, R. H. (1990), Transient model of cross-flow microfiltration, *Chem. Eng. Sci.,* **45,** 13-25

Romero, C. A. and Davis, R. H. (1991), Experimental verification of the shear induced hydrodynamic diffusion model of cross-flow microfiltration, *Journal of Membrane Science,* **62,** 249-273

Rubinow, S. I. and Keller, J. B. (1961), *J. Fluid Mech.,* **11,** 447

Ryder, D. S., Davis, C. R., Anderson, D., Glancy, F. M. and Power, J. N. (1988) , Brewing experience with cross-flow filtration, *MBAA Technical Quaterly,* **25,** 67-79

Saffman, P. G. (1965), *J. Fluid Mech.,* ***22,*** 385

Sakai, K., Ozawa, K., Ohashi, K., Yoshida, R. and Sakarai, H. (1989), Low-temperature plasma separation by cross-flow microfiltration with microporous glass membranes, *Ind. Eng. Chem. Res.,* **28,** 57-64

Schmitz, P., Wandelt, B., Houi, D. and Hildenbrand, M. J. (1993), *Journal of Membrane Science,* **84,** 171-183

Schneider, K. and Klein, W. (1982), The concentration of suspensions by means of cross-flow microfiltration, *Desalination,* **41,** 263-275

Schultz, G. and Ripperger, S. (1989), Concentration polarisation in cross-flow microfiltration, *Journal of Membrane Science,* **40,** 173-187

Schutte, H., Kröner, K. H., Hummel, W. and Kula. (1983), Recent developments in separation and purification of biomolecules, *Annals New York Acad. Sci.,* **413,** 270-282

Scott, J. A. (1988), Application of cross-flow filtration to cider fermentations, *Process Biochem,* **23**(5), 146-148

Segre, G. and Silberberg, A. (1962), *J. Fluid Mech.,* **14,** 115

Segre, G. and Silberberg, A. (1961), Radal particle displacements in Poiseuille flow of suspensions, *Nature,* **189,** 209-210

Sherwood, J. D. (1988), The force on a sphere pulled away from a permeable half-space, *Physicochem. Hydrodyn.,* **10,** 3-12

Shimizu, Y., Shimodera, K. and Watanabe, A. (1993), Cross-flow microfiltration of bacterial cells, *J. of Ferment. Bioeng.,* **76**(6), 493-500

Shimizu, Y., Okuno, Y., Uryu, K., Ohtsubo, S. and Watanabe, A. (1996), Filtration characteristics of hollow fiber microfiltration membranes used in membrane bioreactor for domestic wastewater treatment, *Wat. Res.,* **30**(10), 2385-2392

Shimizu, Y., Matsushita, K. and Watanabe, A. (1994), Influence of shear breakage of microbial cells on cross-flow filtration flux, *J. Ferment. Bioeng.,* **78,** 170-174

Shirato, M., Aragaki, T. and Iritani, E. (1979), *Chem. Eng. J (Japan),* **12,** 162

Sieveka E. H. (1966), Reverse osmosis pilot plants, In "Desalination by Reverse Osmosis", U. Merten (Ed.), The MIT. Press, Cambridge, MA, Chap 7.

Sims, K. A. and Cheryan, M. (1986), Cross-flow microfiltrarion of *Aspergillus niger* fermentation broth. *Biotechnol. and Bioeng. Symp.,* **17,** 495-505

Snoeyink, V. L. and Jenkins, D. (1980), Water Chemistry, John Wiley & Sons, NY

Stamatakis, K and Tien, C. (1993), A simple model of cross-flow filtration based on particle adhesion, *AIChE J.,* **39,** 1293-1302

Stumm, W. and Morgan, J. (1981), Aquatic Chemistry, 2nd Edn. John Wiley & Sons, NY

Suki, A., Fane, A. G. and Fell, C. J. D. (1984), Flux decline in protein ultrafiltration, *Journal of Membrane Science,* **21,** 269-283

Suki, A., Fane, A. G. and Fell, C. J. D. (1986), Modelling fouling mechanisms in protein ultrafiltration, *Journal of Membrane Science,* **27,** 181-193

Taddei, C. and Howel, J. A. (1989), On the effect of membrane conditioning in cell harvesting using microfiltration, *Biotechnol. Techniques,* **3**(3), 155-160

Taddei, C., Aimar, P., Howell, J. A and Scott, J. A. (1990), Yeast harvesting from cider using microfiltration, *J. Chem. Technol. Biotechnol.,* **47,** 365-376

Tanaka, T., Abe, K.I., Asakawa, H., Yoshida, H. and Nakanishi, K. (1994), Filtration characteristics and structure of cake in cross-flow filtration of bacterial suspension, *J. Ferment. and Bioeng.,* **78,** 455-461

Tanaka, T., Usui, K. and Nakanishi, K. (1998), Formation of a gel layer of polymers and its effects on the permeation flux in cross flow filtration of *Corynebacterium glutamicum* broth, *Separation Science and Technology,* **33**(5), 707-722

Tanny G. B., Strong D. K., Presswood W. G. and Meltzec T. H., et al. (1979), Absortive retention of *Pseudomonas diminuta* by membrane filters, *J. parenteral Drug Association,* **33**(1), 40-51

Tanny, G. B., Mirelmean, P. and Pistole, T. (1980), Improved filtration technique for concentration and harvesting bacteria, *Applied and Environ. Microbiol.* **40,** 269-273

Tarleton, E. S. and Wakeman, R. J. (1993), Understanding flux decline in cross-flow microfiltation – Part I, Effects of particle and pore size, *Trans. IChemE,* **71,** Part A, 399

Tarleton, E. S. and Wakeman, R. J. (1994a), Understanding flux decline in cross-flow microfiltration – Part II, Effects of process parameters, *Trans. IChemE,* **72,** Part A, 431

Tarleton, E. S. and Wakeman, R. J. (1994b), Understanding flux decline in cross-flow microfiltration – Part III, Effects of membrane morphology, *Trans. IChemE,* **72,** Part A, 521

Theodore, L. (1966) Eng. Sc.D Dissertation cited in Green & Belfort (1980)

Thomas, D. G. (1961), *J. AIChE,* **7,** 423

Tracey, E. M. and Davis, R. H. (1995), BSA fouling of track etched polycarbonate microfiltration membranes, *J. Colloid Interface Sci.,* cited in Belfort et al. (1994)

Trettin, D. R. and Doshi, M. R. (1980), Limiting flux in ultrafiltration of maromolecular solution, *Chem. Eng. Commun.,* **4,** 507-522

Vigneswaren, S. and Pandey, J. R. (1988), Assessing the suitability of membranes for microfiltration – an empirical approach, *Filtration and Separation,* **25**(4), 253-255

Visvanathan, C. and Ben Aim, R. (1989), Studies on colloidal membrane fouling mechanisms in cross-flow microfiltration, *Journal of Membrane Science,* **45,** 3-15

Wakeman, R. J. and Tarleton, E. S. (1991), Colloidal foulinhg of microfiltration membranes during the treatment of aqueous feed streams, *Desalination,* **83,** 211-216

Wakeman, R. J. (1994), Visualisation of cake formation in cross flow microfiltration, *Trans. IChemE,* **72**, Part A, 530

Wankat, P. C. (1990), Rate Controlled Separations, Elsevier Applied Science

Werthle, M. (1990), Investigation to fluid mechanics. Pretence Hall, Englewood cliffs, NJ

Whitaker, S. (1968), Introduction to Fluid Mechanics, Prentice Hall, Englewood Cliffs, NJ

Wiesner, M. R., Clark, M. M. and Mallevialle, J. (1989), Membrane filtration of coagulated suspensions, *J. Env. Eng. Div., ASCE,* **115,** 20

Xu-Jiang, Y., Dodds, J. and Ledere, D. (1995), Cake characteristics in cross flow and dead-end microfiltration, *Filtration and Separation,* September, 795

Yuan S. W. and Finkelstein, A. B. (1956), Laminar pipe flow with injection and suction through a porous wall, *Trans. ASME,* **78,** 719-724

Zsigmondy, R. (1992) US Patent 1,421,341

Zydney A. L. and Colton, C. K. (1986), A concentration polarisation model for the filtrate flux in cross flow microfiltration of particulate suspensions, *Chem. Eng. Commun.,* **47,** 1-21

Zydney, A. L. and Colton, C. K. (1987), Fundamental studies and design analysis for cross flow membrane plasmapheresis, Andrade, J. D., Brophy, J. J., Detmer, D. E., Kim, S. W., Narmann, R. A., Olsen, D. B. and Stephen, R. L. (Eds.), Artificial Organs: Proceedings of International Symposium on Artificial Organs, Biomedical Engineering and Transplantation, VCH, NY, 343-358

Zydney, A. L., Aimar, P., Meireles, M., Pimbley, J. M. and Belfort, G. (1994), Use of log-normal probability density function to analyse membrane pore size distributions: functional forms and discrepancies, *Journal of Membrane Science,* **91,**293-298

Selection of the Most Suitable Filtration Flux Estimation Correlation

1 Introduction

There are various correlation's (models) available to predict the cross-flow filtration flux. Due to limited understanding of the complex nature of the fundamental processes that occurs during cross-flow filtration, most models that are entirely based on fundamental principles (i.e. with no parameters that must be estimated from experimental data) does not predict the filtration flux very well.

Therefore, most attempts at modelling the cross-flow filtration flux are hybrids between empirical correlation's and fundamental models. The form of the equation is in most instances determined by some fundamental assumptions about the processes that occur during cross-flow filtration. The parameters in these equations are then estimated from experimental data to yield the final model that can be used for flux estimation for scale-up and design purposes.

Choosing the most suitable model for a specific purpose from the array of different models can be seen as an optimisation problem. The objective would be to find the simplest model (both in concept and in mathematical execution) that adequately describes the filtration flux over the range of conditions of interest.

In this work Bayesian inference would be used to find the functional relationship (model) with the highest probability of predicting the true filtration flux with the least number of parameters.

2 Bayesian Inference

The problem of inference has been the subject of considerable attention since the systematic study of probability theory began in the eighteenth century (O' Hagan 1994). Many different theories of inference have been proposed, and there has hardly been a time when inference was not a matter of controversy. Classical or frequentist inference is well known and was almost uncontested during the middle of the twentieth century. Since about 1960 there has been a steady revival of interest in Bayesian inference to the extent that the Bayesian approach is now a well established alternative to classical inference (O' Hagan 1994).

2.1 Classical vs. Bayesian inference

Classical inference theory is based on the frequency interpretation of probability, which asserts that the probability of an event is the limiting relative frequency of occurrence of the event in an infinite sequence of trials. Classical rules of inference are judged on their long run behaviour in repeated sampling. In this approach, a point estimator has a sampling distribution. The sampling distribution is defined as being unbiased if the mean of that distribution equals the parameter to be estimated. The sampling distribution is composed of frequency probabilities, where the infinite sequence of trials is a sequence of hypothetical repetitions of the sampling process, which generated the data.

In order to follow the Bayesian method it is necessary to adopt a less restrictive interpretation of probability. The principal alternatives to frequency probability are described as logical probability and subjective probability. In both these theories, probability represents a degree of belief in a proposition, based on all the available information.

In the Bayesian approach, some prior probability is given to the event or a prior distribution of the value of a certain parameter. The event is then sampled and a posterior probability calculated from the prior knowledge and the measured information. The posterior distribution is then used to estimate a likelihood of an event or to construct a posterior distribution of the parameter value. The posterior information is then used for inference.

The fundamental distinction between classical and Bayesian inference is that in Baysian inference the parameters are random variables, and therefore have both prior and posterior distributions. In classical inference the parameters has unique values, although these values are unknown, and it is not permitted to be treated as random variables with probabilities (O' Hagan 1994).

2.2 Bayes' Theorem

The Bayesian method of inference is based on Bayes theorem, stated below (O' Hagan 1994)

Consider two events, A and B. From the identity:

$$p(A) \cdot p(B \mid A) = p(A, B) = p(B) \cdot p(A \mid / B) \tag{4-1}$$

The probability of A and B occurring is either the probability of event A multiplied by the probability of event B given that A occurred or the probability of event B multiplied by the probability of event A given that B occurred. The simplest form of Bayes theorem is derived:

$$p(B \mid A) = \frac{p(B) \cdot p(A \mid B)}{p(A)} \tag{4-2}$$

The probability of event B given A is equal to the probability of event B multiplied by the probability of A given B divided by the probability of event B.

2.3 The Bayesian Approach

Assume that an inferences with regard to event B is required, with some initial, prior probability P(B) known. The occurrence of A is then observed. The proper description of how likely B is when A is known to have occurred is the posterior probability P(B | A). Bayes theorem can be understood as a formula for updating from prior to posterior probability, the updating consisting of multiplying by the ratio P(A | B) / P(A). It therefore describes how a probability change as new information becomes known (O' Hagan 1994).

By far the most common inference scenario involves unknown quantities rather than unknown features expressed as a discrete set of hypotheses. Any such unknown quantity in a statistical problem is called a parameter and inference is therefore concerned with statements regarding the values of parameters. Bayes' theorem is therefore restated in terms of random variables:

Consider a general problem in which data x is known and an inference about a parameter θ is required. If in addition, it is assumed that every distribution possess a corresponding density function this can be rewritten as (O' Hagan 1994):

$$f(\psi \mid x) = \frac{f(\psi) \cdot f(x \mid \psi)}{f(x)} \tag{4-3}$$

$f(x)$ can be interpreted as the normalising function, fixing the posterior distribution density to have an unit area under the curve. This equation can therefore be rewritten as:

$$f(\psi \mid x) = \frac{f(\psi) \cdot f(x \mid \psi)}{\int_{-\infty}^{+\infty} f(\psi) \cdot f(x \mid \psi) \cdot d\psi} \tag{4-4}$$

This version of Bayes' theorem is interpreted in the same way as for simpler events. The prior density $f(\psi)$ represents the prior information about ψ. When the data x is observed, Bayes' theorem constructs the posterior density $f(\psi \mid x)$ as proportional to the product of the prior density and the likelihood $f(x \mid \psi)$ (O' Hagan 1994).

Form the posterior density $f(\psi \mid x)$ suitable inference statements can be derived with regard to parameter ψ. The posterior distribution encapsulates all that is known about ψ following the observation of the data x and the prior knowledge about ψ. Unfortunately, the posterior distribution codes this information in a very compact form and therefore it is

helpful to express the properties of this distribution in terms of helpful summaries. These include various statistical operators such as the mode, mean, median, variance skewness and density plots.

In short the Bayesian method comprises the following steps.

- Obtain some prior knowledge with regard to ψ. The prior probability represents the investigators knowledge about ψ before seeing the data. The Baysian method requires prior probabilities to be given explicit values. A logical prior probability must be the unique value logically implied by the available information prior to seeing the data. Unfortunately, in most cases, this value cannot be found; the necessary theory simply does not exist. The exception is the case where prior information is non-existent or, more accurately, where there is no prior information, which is relevant to the parameter ψ. For this case there exists some theory which can be used to construct prior distributions. However, it is a matter of contention whether such a state of complete prior ignorance of ψ can exist. Sufficient prior information always exists to identify ψ as a meaningful quantity in the data generating process, and to have some purpose in requiring inference about it. Nevertheless, logical probabilities are often used as approximations whenever prior information is very weak.

- Obtain the likelihood function $f(x \mid \psi)$. The likelihood function $f(x \mid \psi)$, is regarded as a function of ψ for fixed x. However individual values of this function are obtained form the probability distributions of x for various ψ. For a Gaussian process in which the error is calculated at the difference between the assumed value of ψ and the sampled value is normally distributed with mean zero and standard deviation σ_{STDEV}^2, the likelihood function can be calculated using:

$$f(x \mid \psi) = \prod (2\pi\sigma_{STDEV}{}^2)^{-1/2} e^{(-Error^2/(2\sigma_{STDEV}{}^2))} \qquad (4\text{-}5)$$

- Apply Bayes' theorem to derive the posterior density $f(\psi \mid x)$
- Derive appropriate inference statements from the posterior distribution.

2.4 Model Comparison

The Bayesian method for comparing different models involves the application of Bayes' theorem as explained below.

Consider models H $\in$ {1, 2, 3 ... N} and some observed data D

Then,

$$p(H \mid D) = \frac{p(H) \cdot p(D \mid H)}{C'} \tag{4-6}$$

And for the parameters ψ of H,

$$p(\psi \mid D,H) = \frac{p(\psi \mid D) \cdot p(D \mid \psi,H)}{p(D \mid H)} \tag{4-7}$$

P(D | H) is referred to as the evidence for model H

Therefore,

$$p(H \mid D) \propto p(H) \cdot p(D \mid H) \tag{4-8}$$

where

$$p(D \mid H) = \int_{-\infty}^{+\infty} p(\psi \mid H) \cdot p(D \mid \psi,H) \cdot d\psi \tag{4-9}$$

A Bayesian factor or posterior ratio for model comparison can be defined as:

$$\frac{p(H_i \mid D)}{p(H_j \mid D)} = \frac{p(H_i)}{p(H_j)} \cdot \frac{p(D \mid H_i)}{p(D \mid H_j)} \tag{4-10}$$

Based on these ratios' different models can be compared. Broadly speaking this ratio will increase as the relative fit of model H_i increases compared to model H_j.

2.5 Computational issues in the Bayesian approach

Practical implementation of Bayesian methods requires substantial computation. The computational requirement needs to deal with the large number of multi-dimensional integration steps that are involved in the calculation of the Bayesian factor. For each parameter in the model, calculation of the evidence requires integration of the posterior distribution of the parameter estimation for all possible values of each of the parameters.

2.5.1 Calculation of the likelihood

Assuming a Gaussian process with normal distributions the likelihood can be calculated from:

$$f(x \mid \psi) \prod (2\pi\sigma_{STDEV}{}^2)^{1/2} e^{(-Error^2/(2\sigma_{STDEV}{}^2))} \tag{4-11}$$

where the error is the difference between the measured data value and the value predicted by the model when the parameter has a value ψ.

2.5.2 Calculation of the Evidence

The evidence requires integration of the posterior distribution of the parameter estimator:

$$p(D \mid H) = \int_{-\infty}^{+\infty} p(\psi \mid D) \cdot p(D \mid \psi, H) \cdot d\psi \tag{4-12}$$

Some of the most common estimation techniques would be discussed in the following sections.

2.5.3 Quadrature

Numerical integration, also known as quadrature is directly applicable to the estimation of multidimensional integrals. To illustrate the principle, consider the one-dimensional integral,

$$I = \int f(x) \cdot dx \tag{4-13}$$

Quadrature methods essentially approximate I by calculating f(x) at a number of points, x_1, x_2, x_3... and applying some formula to the resulting values $f(x_1)$, $f(x_2)$, $f(x_3)$...

The simplest and most common form is a weighted average

$$I = \sum w_i f(x_i) \tag{4-14}$$

Different quadrature rules are distinguished by using different sets of design points and/or different sets of weights.

2.5.4 Monte Carlo

A different approach to evaluating an integral, evaluates f(x) at random points. This method is referred to as Monte Carlo integration. Suppose that a series of points x_1, x_2, x_3...are drawn independently from the distribution with density $\eta(x)$.

$$I = \int f(x) \cdot dx = \int \{\frac{f(x)}{\eta(x)}\} \cdot \eta(x) \cdot dx \tag{4-15}$$

$\eta(x)$ must be positive if f(x) is positive. The sample of points x_1, x_2, x_3... drawn independently from η gives a sample of values $f(x)/\eta(x)$. The integral is then estimated from the mean of these values.

$$I = n^{-1} \sum \frac{f(x_i)}{s(x_i)} \tag{4-16}$$

The variance for this estimate depends on how accurately the sampling density $\eta(x)$ mimics f(x). The objective is to obtain a density s such that it is feasible to draw a sample from η and so that η would be approximately proportional to f. For Gaussian processes an obvious choice for s is the normal distribution.

2.5.5 Markov Chain Monte Carlo

A group of methods collectively known as Markov Chain Monte Carlo (MCMC) methods have proved more powerful than either Monte Carlo integration or quadrature and are capable of handling very highly dimensional problems. The essence of these methods involves inference of the posterior distribution from a sample from this distribution.

At least in an asymptotic sense a sample is drawn directly from the normalised density:

$$\eta(x) = \frac{f(x)}{\int f(x) \cdot dx} \tag{3-17}$$

This is not truly possible for the purpose of Monte Carlo integration since numerical integration would then not be possible. The explanation of this apparent contradiction is that in Monte Carlo integration the density $\eta(x) = f(x)/\int f(x)dx$ have to be known explicitly and that implies that $\int f(x)dx$ is known. MCMC methods sample from the normalised density without knowing and without deriving the normalising constant.

Gibbs sampling would be described to illustrate the principles involved in MCMC methods.

Let $g(\mathbf{X}) = f(\mathbf{X})/\int f(x)dx$ be the normalised joint density. Furthermore let:

$f_i(x_i|\mathbf{X}_i) = f(x_i|x_1 \ldots x_{i-1}, x_{i+1}..x_p)$ be regarded as a function of x_i alone with the other components $\mathbf{X}_I$ fixed. In its normalised form $g_i(x_i|\mathbf{X}_i) = f_i(x_i|\mathbf{X}_i)/\int f_i(x_i|\mathbf{X}_i)\, dx_I$ it is the conditional density of x_i given $\mathbf{X}_i$ deriving from the joint density $g(\mathbf{X})$. The Gibbs sampler consists of sampling from these distributions in a cyclical way.

The iterative process starts with an arbitrary point $\mathbf{X}^0 = (x_1 \ldots x_p)$ and generate a series of random points $\mathbf{X}^1, \mathbf{X}^2, \mathbf{X}^3$ where $\mathbf{X}^{m+1}$ is derived from $\mathbf{X}^m$ in the following way:

$\mathbf{X}^{m+1}{}_1$ is randomly drawn from $g(x_1|x_2^m, x_3^m \ldots x_p^m)$
$\mathbf{X}^{m+1}{}_2$ is randomly drawn from $g(x_2|x_1^{m+1}, x_3^m \ldots x_p^m)$
$\mathbf{X}^{m+1}{}_3$ is randomly drawn from $g(x_3|\, x_1^{m+1}, x_2^{m+1}, x_4^m \ldots x_p^m)$

All the random draws are performed independently. This is a stochastic process replacing x_i by a random draw from that conditional distribution. If this procedure is repeated from the same starting point a different sequence of $\mathbf{X}^m$ would be obtained. $\mathbf{X}^m$ can therefore be seen as a random variable whose distribution is determined by the starting point and the distributions $g_i(x_i|\mathbf{X}_i)$. Another important property of the sequence is that the distribution of $\mathbf{X}^m$ given all the previous values $\mathbf{X}^0, \mathbf{X}^1 \ldots$ depends only on $\mathbf{X}^{m-1}$ This is known as the Markov property and the sequence is called a Markov chain. We have a Markov chain with the same transition distribution $f^* = f(\mathbf{X}^1|\mathbf{X}^0)$for every step, which constitutes a homogeneous Markov chain. Markov chains have been extensively studied (Feller (1968) and Grimmett & Stirzaker (1992).

One of the most important properties of Markov chains is that under rather general conditions a homogeneous Markov chain converges. The distribution of $\mathbf{X}^m$ given the starting point converges as $m \rightarrow \infty$ to a limiting distribution f^∞, which is independent of $\mathbf{X}^0$ and depends only on the transition distribution f^*.

Various other sampling techniques are available such as metropolis update, hybrid Monte Carlo and hybrid Monte Carlo with windows techniques.

In essence MCMC techniques comprises selection of $\mathbf{X}^0$, followed by determination of an assumption of $g=f(\mathbf{X})/\int f(x)dx$ by m iterations. This will also yield a corresponding $\mathbf{X}^m$. With $\mathbf{X}^m$ and the approximated g', a single value for $g'/f(\mathbf{X}^m)$ can be calculated. The final estimation of $\int f(x)dx$ can be obtained from the average of several $g'/f(\mathbf{X}^m)$'s.

3 Data acquisition

The filtration models were evaluated by gathering experimental data form a laboratory cross-flow filtration rig. The experimental plan was divided into two main categories. The first evaluated the impact of single parameters on both the steady state flux and the rate of flux decline. These parameters included the biomass concentration, cross-flow velocity and trans-membrane pressure drop.

In the second set of experiments the filtration rig was coupled to a bioreactor and used to recycle biomass to the reactor. The permeate flux through the membrane was measured under different operating parameters. These included cross-flow velocities ranging from 0.5 to 1.2 m/s and transmembrane pressure drops around 100 kPa. Typical lysine and biomass concentrations experienced during the fermentation varied from 0-100 g/l and 0-40 g/l DCW.

It was seen quite clearly form the data that the filtration experiments exhibited higher fluxes at similar operating conditions than the filtration flux measured during the fermentation process with biomass recycling.

The reason for this deviation can ascribed to the effect of cell viability on the hydraulic resistance as well as the effect of by-products on the permeate.

3.1 Parameter Estimation

The experimental data was used to calculate an error defined as the difference between the predicted and the measured flux for each of the data points. These errors were squared and added to present a total square error. This error was minimised by selection of the model parameters. This optimised solution was then used as a starting point for the estimation of the Bayesian factor using MCMC methods.

The models were broadly divided into two groups, models of which the form of the model is based on a fundamental understanding of the system behaviour and empirical models. The model parameters for both these sections of models were however determined using the procedure above. This implies that although the form of some of these equations are dictated by fundamental principles the application of these models are highly dependent on the available experimental data and thus in nature these models are all empirical.

3.1.1 Empirical Models

Empirical power laws have already been used with success by several authors to predict the fouling resistance of permeate flux through micro-filtration membranes (de Balmann 1988; Romero & Davis 1990; Liberge et al. 1994)

A stepwise multiple regression program was used to estimate the coefficients of the following equation:

$$\ln(Perm) = a_0 + a_1 \bar{x}_1 + a_2 \bar{x}_2 + \ldots + a_n \bar{x}_n \qquad (4\text{-}18)$$

where the variables $\bar{x}_i$ were chosen among

Z_i; $\ln(Z_i)$; $Z_i \ln(Z_j)$
With Z_i $Z_j \in |X, Lys; v; t|$ and $i \neq j$

The terms Z or ln(Z) account for the main influence of the possible operating parameters and the terms Z ln Z test for possible interactions among them.

The program uses a least squares method to adjust the coefficients. In multiple regression, the program also tests if the proposed variables are significant for the regression. This is done using the variance analysis of the regression. The total variance can be separated into explained (by the model) and the residual variance. A variable is significant for the regression if it produces a significant increase of the R^2 parameter, which is the ratio of the explained variance to total variance. The best solution is the one with the highest R^2 with as few variables as possible.

3.1.2 Fundamental models

In cross flow filtration the flux typically declines sharply over the first 5-10 minutes, followed by a pseudo steady state flux. This flux is referred to as a pseudo steady state due to the slowly decaying nature thereof.

3.1.2.1 Steady state flux

Contrary to dead-end filtration the cross flow filtration flux does not decline to zero. After some time, a pseudo steady state or slowly declining flux is achieved. Various fundamental mechanisms have been suggested to explain the steady state flux. It is generally believed that the cause of the flux decline is due to either fouling or cake build-up. Fouling is defined as the irreversible internal blocking of membrane pores. Cake build-up refers to a process by which a dense particle layer is formed on the membrane surface increasing the hydraulic resistance to permeate flow.

The most general approach is to assume that particle or foulant deposition onto or drag towards the membrane surface is balanced by some mechanism of back transport from the membrane surface. The mass transfer equations are often solved by simulation of the single-phase flow in the feed channels and coupling the solution of the flow field to the solute mass transfer balance.

The various approaches can be broken down into the following categories:

- Equal rate models
  - Concentration polarisation
  - Shear induced diffusion
  - Inertial lift
- Flowing Cakes
- Solids flux
- Pore constriction

Equal rate models refer to equal particle deposition and removal rates to and from the membrane surface. Concentration polarisation is the oldest and simplest of these models (Blatt et al. 1970 and Porter 1972). In short this model assumes that particle transport to the membrane surface is driven by the convection force caused by the permeate flux. A highly concentrated layer then builds up onto the membrane surface. The solid flux towards the membrane surface is then balanced by diffusion of particles from the membrane surface due to the concentration gradient generated at the cake-feed stream interface. This theory is based on the so-called classical thin film Fickan diffusion theory. This model has been used successfully in reverse osmosis and ultrafiltration applications although it has limited applicability for microfiltration (Blatt et al 1970).

The model is based on the following particle balance:

$$JC_b = D\frac{dC_b}{dy} \tag{4-19}$$

Which can be integrated to give:

$$J = k_l \cdot \ln(\frac{C_w}{C_b}) \tag{4-20}$$

For conditions typical of cross-flow filtration the local mass transfer coefficient has been evaluated by Leveque (1928) and Porter (1972) from the analogous heat transfer problem. The diffusivity was estimated from the Stokes-Einstein relationship for spherical particles. This gives rise to the following expression;

$$J = k_i \cdot u^{0.33} \cdot \mu^{-0.66} \cdot \ln(\frac{C_w}{C_b}) \tag{4-21}$$

with parameters; k_i and C_w.

Zydney and Colton (1986) proposed that the diffusivity used in the concentration polarisation approach is a result of hydrodynamic interaction of particles in a concentrated suspension rather than Brownian motion as suggested by the Stokes-Einstein relationship. A particle in a shear field will tumble over other particles and

thereby undergo a series of displacements from the bulk average streamline. The effect of this motion is the net migration of particles from high to low concentration. From the shear induced diffusivity relationship developed by Eckstein et al. (1977) and the Leveque mass transfer coefficient the flux becomes;

$$J = k_{si} \cdot u^{n_{si}} \cdot \ln(\frac{C_w}{C_b}) \qquad (4\text{-}22)$$

with parameters; k_{si}, n_{si} and C_w

Zydney and Colton (1987) later refined the model to account for the non-constant viscosity in the boundary layer. Their model fitted plasmapheresis data well. This approach was further developed by Leighton & Acrivos (1987) and Davis & Sherwood (1990) with regard to the dependency of the diffusivity on the shear rate at the membrane wall and a concentration dependent viscosity relationship in the boundary layer.

Belfort and coworkers (Green and Belfort 1980; Altena and Belfort 1984; Altena et al. 1983; Belfort et al. 1985; Ottis et al. 1986; Drew et al. 1991) have proposed that the discrepancy between the predictions and the experimental data seen for the concentration polarisation approach were due to the augmentation in particle transport due to a hydrodynamic lift force. The lateral movement of particles across streamlines as they are suspended in a fluid flowing in a tube or slit was observed as early as 1836 (Green and Belfort 1980). Theoretical solutions of this lift velocity centre around solution of the Navier Stokes equations with inertial terms included (Brenner 1966, Rubinow & Keller 1961; Saffman 1965; Cox & Brenner 1968; Ho and Leal 1974) When these terms are neglected no lift is predicted, Thus theoretically this phenomenon is of inertial origin. More simply lift can be viewed as arising from the pressure difference which arises from the difference in fluid velocity on either side of a particle in a non-constant velocity field.

Virually all studies on the lift phenonema, whether theoretical (Brenner 1966; Saffman 1965, Cox & Brenner 1968; Ho & Leal 1974) or experimental (Segre & Silberberg 1961 1962; Thomas 1961; Karnis et al. 1966 Theodore 1966, Ratkow et al. 1987) arrive at the following identical form for the migration velocity expression:

$$J = k_{vl} \cdot u^{n_{vl}} \cdot \rho^{m_{vl}} \cdot \upsilon^{-1} \qquad (4\text{-}23)$$

with parameters, k_{vl}, n_{vl} and m_{vl}.

An alternative to back transport of particles away from the membrane by mechanisms such as diffusion and inertial lift, it is possible that the particles are carried to the membrane surface by the permeate flux and then roll or slide along

the surface due to tangential flow. Both continuum and single particle models have been developed to describe this phenomenon.

In the continuum approach, the rejected particles are assumed to form a flowing cake layer. Davis & Birdsell (1987); and Leonard & Vassilieff (1984) developed mathematical models to describe the simultaneous deposition of particles to the cake layer and the flow of this layer to the filter exit. Leonard & Vassilieff's model divided the fluid above the membrane into two regions. The first a close packed region adjacent to the boundary of concentration Cm and a bulk fluid region where the concentration is uniformly fixed at C_b. The close packed region moves along the membrane at a rate depending on the cake rheology. Cakes that behave as Bingham plastics will consist of a stagnant lower layer and flowing upper layer. This flux was given by Zydney and Colton (1986) as:

$$J = k_{fl} \cdot u^{n_{fl}} \cdot \frac{C_w - C_b}{C_b} \tag{4-24}$$

with parameters, k_{fl}, n_{fl} and C_w.

A plasmapheresis-specific model predicted experimental data adequately. Some of the other assumptions underlying this model is however questionable.

In single particle models, the basic concept is to consider a spherical particle on the surface of the membrane or on the surface of a stagnant cake layer and perform force and torque balances on the paricle to determine if it will adhere to the surface or to be transported along the surface (Lu & Ju 1989 and Stamatakis & Tien 1993, Fischer & Raasch 1986 De Balmann et al. 1990).

The general form of the flux equations for this approach is:

$$J_{ss} = k_{sp} \cdot \mathrm{Re}^{n_{sp}} \cdot \upsilon^{m_{sp}} \cdot \rho^{o_{sp}} \tag{4-25}$$

with parameters, k_{sp}, n_{sp}, m_{sp} and o_{sp}.

If during the microfiltration of certain materials fouling is severe then back migration may be irrelevant and the decline in the flux may be proportional to the rate of arrival of solids at the surface, i.e. proportional to the flux itself. Such behaviour occurs during microfiltration of sticky particles such as microbial cells. Nagata et al. (1989) modelled this behaviour as a first order feedback inhibition process. For such a process,

$$J = J_o e^{-b_{sf} C} \tag{4-26}$$

with parameter, b_{sf}.

The last approach followed is that of particle capture by the membrane, deposition and intrusion. Most of these models treats the membrane as an array of uniform cylindrical pores of a single pore radius (Blatt et al 1970; Jonsson 1984) Belfort et al. (1993) have extended this analysis to explicitly account for the presence of a pore size distribution on the flux decline associated with pore constriction effects. Following the approach of Meirels et al. (1991) assuming a log normal pore size distribution and assuming that the local flow through a pore is given by Poiseuille flow. If the pore diameter is reduced by an absorbed multilayer inside the pore, reducing the available area for permeate flow. The ratio of the clean membrane flux to the fouled membrane flux is given by:

$$\frac{J'_1}{J'_2} = 1 - \frac{4}{q_{pore}^{\ 3}}\left(\frac{k_{thick}}{r_p^{\ *}}\right) + \frac{6}{q_{pore}^{\ 6}}\left(\frac{k_{thick}}{r_p^{\ *}}\right)^2 - \frac{4}{q_{pore}^{\ 6}}\left(\frac{k_{thick}}{r_p^{\ *}}\right)^3 + \frac{1}{q_{pore}^{\ 5}}\left(\frac{k_{thick}}{r_p^{\ *}}\right) \qquad (4\text{-}27)$$

3.1.2.2 Flux decline

In the case of dead-end filtration, the constant pressure blocking laws discussed by Hermia (1982) provide four equations of evolution through simple assumptions on particle deposition. Expressing the permeate flux as a function of time, three of them may be written,

$$J = \frac{J_o}{(1 + k_{decline} t')^{n_{decline}}} \qquad (4\text{-}28)$$

Several authors (Schneider & Klein 1982; Mietton-Peuchot 1984) found these laws were well suited to the description of the beginning of cross flow filtration microfiltration operations. A constant term for the limiting flux J_{ss} reached at the pseudo steady state is added to a transient term, which is initially equal to J_o-J_{ss} and goes to zero according to Equation 4-28. The form of the equation should be considered as empirical in its a application to cross flow filtration because it is not based on a flow model and therefore the parameters $k_{decline}$ and $n_{decline}$ have no physical significance.

$$J = J_{ss} + \frac{J_o - J_{ss}}{(1 + k_{decline} t')^{n_{decline}}} \qquad (4\text{-}29)$$

3.2 The Hybrid approach

This approach is fundamentally based on Hermia's flux decline laws and Darcy's law to estimate the steady state flux. The form of the equation is the same as in Equation 4-29. With $k_{decline}$ and $n_{decline}$ being parameters estimated form the experimental data.

The steady state flux is then estimated using Darcy's law:

$$J_{ss} = \frac{\Delta P}{\mu R_{tot}}$$
$$R_{tot} = R_m + R_c + R_p \quad (4\text{-}30)$$

R_m is estimated from the pure water flux. R_p is determined through the pore plugging equations described before.

$$R_p = R_m\left(\frac{J'_1}{J'_2} - 1\right)$$
$$\frac{J'_1}{J'_2} = 1 - \frac{4}{q_{pore}^{3}}\left(\frac{k_{thick}}{r_p^*}\right) + \frac{6}{q_{pore}^{6}}\left(\frac{k_{thick}}{r_p^*}\right)^2 - \frac{4}{q_{pore}^{6}}\left(\frac{k_{thick}}{r_p^*}\right)^3 + \frac{1}{q_{pore}^{5}}\left(\frac{k_{thick}}{r_p^*}\right) \quad (4\text{-}31)$$

R_c is determined form the intrinsic cake resistance and the thickness of the cake layer, which is assumed to be proportional to a power of the biomass concentration and the angle of the drag force on a particle towards and tangentially across the membrane surface.

$$R_c = \sqrt{k_t \cdot X^{p_1} \cdot \Delta P^{1+n_c} \cdot v^{-1}} \quad (4\text{-}32)$$

with parameters k_t, p_1 and n_c.

3.3 Model selection

Three parameters were calculated from the experimental data points over the entire flux decline cycle under various operating conditions. These parameters included the adjusted sum of squared errors, the correlation coefficient and the Baysian factor relative to the hybrid model developed earlier.

The sum of squared error as well as the correlation coefficient was adjusted for the degrees of freedom to exclude the effect of limited availability of experimental data.

These parameters are summarised in the presented graph below.

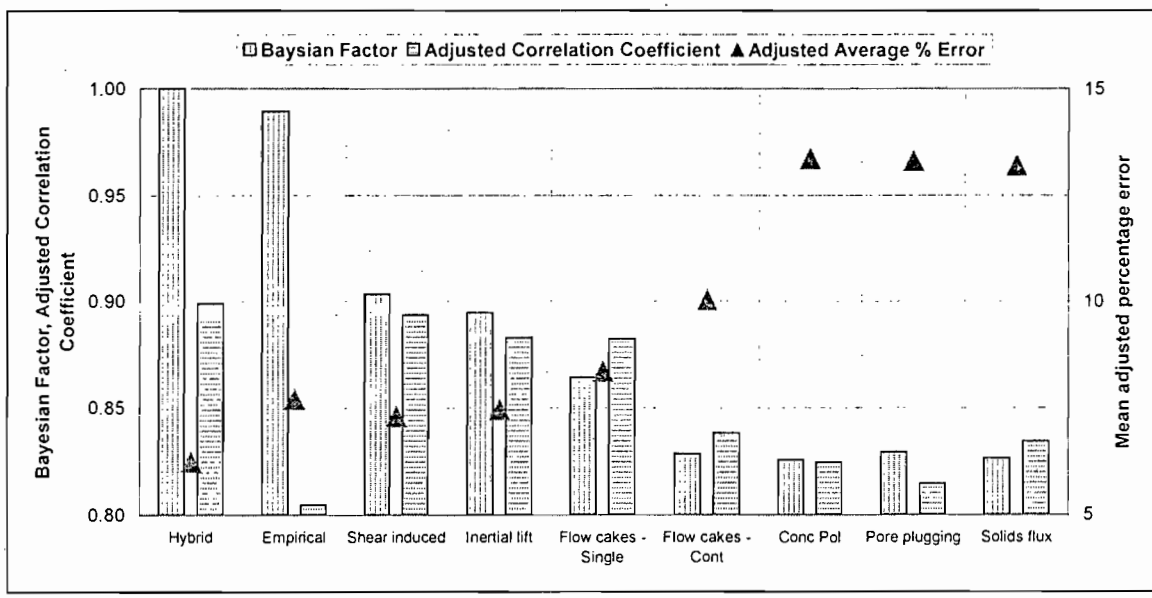

Figure 4-1. Calculated parameters for model comparison

The average percentage error as well as the correlation coefficient was adjusted to represent equal degrees of freedom. This was done to avoid that models with a larger number of parameters would necessarily fit the data better than models with fewer parameters due to the limited availability of data.

The hybrid approach had the lowest adjusted mean error and the highest adjusted correlation coefficient. The hybrid approach was therefore selected as a reference for calculation of the Bayesian factor. As can be seen from the presented graph, all the Bayesian factors were less than one indicating that this model predicts the data better than any of the other models.

4 Conclusions

Choosing the most suitable model for a specific purpose from an array of model can be viewed as an optimisation problem in itself. The objective function is to find the simplest model (both in concept and in mathematical execution) that adequately describes the filtration flux over the range of conditions of interest. In this work Bayesian inference has been used to select the functional relationship with the highest probability of predicting the filtration flux with the least number of parameters.

The hybrid model developed in Chapter 3 was compared against an empirical model derived from a multiple regression approach (Eq. 4-18), concentration polarisation (Eq. 4-21), shear induced diffusion (Eq 4-23), flowing cake layer (Eq. 4-24), single particle models (Eq. 4-25) pore plugging (Eq. 4-27) and the solids flux model (Eq. 4-26).

Bayesian analysis was used to determine the Bayesian factors of the presented model against the hybrid model. All the Bayesian factors were below 1 indicating that these models describe the process less adequately than the hybrid approach. The hybrid approach also showed the lowest adjusted (to compensate for the varying degrees of freedom between models) error (7%) and the highest adjusted correlation coefficient (R^2_{adj} = 0.9950).

The hybrid model was therefore selected as the preferred model to predict the filtration flux as a function of the operating conditions and the feed stream properties.

5 References

Altena, F. W., Belfort, G., Otis, J., Fiessinger, F., Rovel, J. M. and Nicoletti, J. (1983), Particle motion in laminar slit flow: a fundamental fouling study, *Desalination,* **47,** 221-232

Altena, F. W. and Belfort, G. (1984), Lateral migration of spherical particles in laminar purous tube flows: application to membrane filtration, *Chem. Eng. Sci.* **39,** 343-355

Belfort, G., Pinbley, J. M., Greiner, A. and Ching, K. A. (1993), Diagnosis of membrane fouling using rotating annular filter. 1. Cell culture media, *J. Membrane Sci.* **77,** 1-22

Belfort, G., Weigand, R. J. and Mahar, J. T. (1985), Particulate membrane fouling and recent development in fluid mechanics of dilute suspensions, *ACS Symp. Ser.,* **281**

Blatt, W. F., Dravid, A., Michaels, A. S. and Nelson, L. (1970), Industrial biological waste treament processes, J. E. Flinn (Ed.) Membrane Science and Technology, Plenum Press, NY

Brenner, H. (1966), Hydrodynamic resistance of particles at small Reynolds numbers, Drew, T. B., Hoopes, J. W. and Vermuelen, T. (Eds), Advances in Chemical Engineering (Vol 6), Academic Press, NY, 287-438

Cox, R. G. and Brenner, H. (1968), The lateral migration of solid particles in Poiseuille flow – I theory, *Chem. Eng. Sci.,* **23,** 147-173

Davis, R. H, and Sherwood, J. D. (1990), A similarity solution for steady–state crossflow microfiltration, *Chem. Eng. Sci.,* **45,** 3204-3209

Davis, R. H. and Birdsell, S. A. (1987), Hydrodynamic model and experiments for crossflow microfiltration, *Chem. Eng. Commun.,* **49,** 217-234

De Balmann, H. (1988), Utilisation de l'Ultrafiltration dans le Traitement de l'Eau, Ph.D Thesis, Universite Paul Sabatier, Toulouse

De Balmann, H., Aimar, P. and Sanchez, V. (1990), Membrane partition and mass transfer in ultrafiltration, *Sep. Sci. and Technol,* **25**(5), 507-534

Drew, D. A., Schonberg, J. A. and Belfort, G. (1991), Lateral inertial migration of a small sphere in a fast laminar flow through a membrane duct. *Chem. Eng. Sci.,* **46,** 3219-3224

Eckstein, E. C., Bailey, P. G. and Shapiro, A. H. (1977), Self-diffusion of particles in shear flow of a suspension, *J. Fluid Mech.,* **79 19**1-208

Feller, W. (1968), An introduction to probability theory and its applications, Volume 1, 3rd ed. Wiley, NY

Fischer, E. and Raasch, J. (1986), Model tests of the particle deposition at the filter medium in crossflow filtration, *Proc. Fourth World Filtration Conference,* Ostend 1986 (Part II), 11.11-11.17

Green, G. and Belfort, G. (1980), Fouling of ultrafiltration membranes: lateral migration and the particle trajectory model, *Desalination,* **35,** 129-147

Grimmett, G. & Stirzaker, D. (1992), Probability and Random Processes, Clarendon, Oxford

Hermia, J. (1982), Constant pressure blocking laws – Application to power law non-newtonian fluids, *Trans. IchemE,* **60,** 183-189

Ho, B. P. and Leal, L. G. (1974), Inertial migration of rigid spheres in two-dimensional unidirectional flow, *J. Fluid Mech.,* **65,** 365-400

Jonsson, G. (1984), boundary layer phenomena during ultrafiltration of dextran and whey protein solutions, *Desalination,* **51,** 61-77

Karnis, A., Goldsmith, H. L. and Mason, S. G. (1966), The kinetics of flowing dispersions. 1. Concentrated suspensions of rigid particles, *J. of Colloid Interface Sci.,* **22,** 531-553

Leighton, D. T. and Acrivos, A. (1987), Measurement of the shear induced coefficient of self diffusion in concentrated suspensions of spheres, *J. Fluid Mech.,* **177,** 109-131

Leonard, E. F. and Vassilieff, C. S. (1984), The deposition of rejected matter in membrane separation processes, *Chem. Eng. Commun.,* **30,** 209-217

Levesque, M. A. (1928), *Ann. Mines*, **13**, 201

Liberge, R., Colinart, P., Fessier, P and Renon, N. H. (1994), Data and model for progressive fouling in crossflow microfltration of yeast on three industrial mineral membranes, *Ind. Eng. Chem. Res,* **33,** 1310-1318

Lu, W. –M. and Ju, S. –C. (1989), Selective particle deposition in crossflow filtration. *Sep. Sci. Technol.*, **24,** 512-540

Meireles, M., Aimar, P. and Sanchez, V. (1991), Effects of protein fouling on the apparent pore size distribution of sieving membranes, *J. Membrane Sci.*, **56,** 13-28

Mietton-Peuchot and Aim, B. (1992), Improvement of cross-flow microfiltration performance with flocculation, *J. Membrane Sci.*, **68,** 241

Nagata, N., Herouvis, K., Dziewulski, D. M. and Belfort, G. (1989), Cross-flow membrane microfiltration of a bacterial fermentation broth, *Biotechnology and Bioengineering.* **44,** 161-181

O'Hagan, A. (1994), Bayesian Inference, In "Kendall's Advanced Theory of Statistics" Wiley & Sons

Otis, J. R., Altena, F. W., Mahar, J. J. and Belfort, G. (1986), Measuremet of single spehrical particle trajectories with lateral migration in a slit with one porous wall under laminar flow conditions, *Experiments Fluids,* **4,** 1-10

Porter, M. C. (1972), Concentration polarization with membrane ultrafiltration, *Ind. Eng. Chem. Prod. Res. Dev.* **11,** 233-248

Rakow, A. L. and Chappell, M. L. (1987), Axial migration of spirulina microalgae in laminar flow tube, *Biorheology,* **24**(6), 763-768

Romero, C. A. and Davis, R. H. (1990), Transient model of cross-flow microfiltration, *Chem. Eng. Sci.,* **45,** 13-25

Rubinow, S. I. and Keller, J. B. (1961), *J. Fluid Mech.,* **11,** 447

Saffman, P. G. (1965), *J. Fluid Mech.,* ***22,*** 385

Schneider, K. and Klein, W. (1982), The concentration of suspensions by means of crossflow microfiltration, *Desalination,* **41,** 263-275

Segre, G. and Silberberg, A. (1961), Radial particle displacements in poiseuille flow of suspensions, *Nature,* **189,** 209-210

Segre, G. and Silberberg, A. (1962), *J. Fluid Mech.,* **14,** 115

Stamatakis, K and Tien, C. (1993), A simple model of cross-flow filtration based on particle adhesion, *AIChE J.,* **39,** 1293-1302

Theodore, L. (1966) Eng. Sc.D Dissertation cited in Green & Belfort (1980)

Thomas, D. G. (1961), *J. AIChE,* **7,** 423

Zydney A. L. and Colton, C. K. (1986), A concentration polarisation model for the filtrate flux in cross flow microfiltration of particulate suspensions, *Chem. Eng. Commun.,* **47,** 1-21

Zydney, A. L. and Colton, C. K. (1987), Fundamental studies and design analysis for cross flow membrane plasmapheresis, Andrade, J. D., Brophy, J. J., Detmer, D. E., Kim, S. W.,

Narmann, R. A., Olsen, D. B. and Stephen, R. L. (Eds.), Artificial Organs: Proceedings of International Symposium on Artificial Organs, Biomedical Engineering and Transplantation, VCH, NY, 343-358

The Impact of Filtration on Fermentation Performance of *Corynebacterium glutamicum* Cells

1 Introduction

L-Lysine production takes place during the late exponential and stationary metabolic phases, which implies a low biomass growth rate. Therefore, L-lysine production is restricted to either batch or fed batch operated processes. In the fed-batch process, the carbohydrate source is fed continuously to the reactor during the L-lysine production phase, where it is converted to L-lysine. In addition to the increase in reactor volume, caused by the carbohydrate feeding, microbial activity gradually declines. A feed and bleed strategy allows extension of the batch beyond the time taken to reach the working volume of the bioreactor. During the bleed stage, viable biomass is lost, causing a gradual decline in the bioreactor productivity. The fermentation is terminated when the rate of L-lysine production and carbohydrate conversion becomes uneconomical. At this point, the bioreactor is emptied and the spent medium processed for lysine recovery.

A large portion of the production cost is spent on the establishment of the viable cell population. With the feed-and-bleed strategy, up to 50% of the produced biomass can be lost while still viable and capable of L-lysine production. The productivity and conversion of carbohydrates to L-lysine are limited by the reactor volume as well as the inability of the process to retain the microbial population.

The reactor performance can be enhanced by continuously withdrawing microbial culture and recycling of the biomass in the suspension to the reactor. The biomass in the reactor outlet can be separated from the spent medium using cross-flow filtration before being recycled to the reactor.

Cross flow filtration is a pressure driven membrane separation process characterised by the feed suspension flow perpendicular to the permeate flow. The filtration process is essentially based on a sieving mechanism whereby the solvent is forced through the membrane (driven by the pressure difference across the membrane) while the larger solutes (or suspended particles) are retained by the membrane. Compared to other separation techniques cross-flow filtration has several advantages. Separation is based on size difference rather than on the small density differences which centrifuges and settling ponds attempt to exploit (Henry & Alfred 1972). The tangential movement of the process fluid helps to remove most of the rejected material from the membrane surface minimising the accumulation of cells at the filter surface. The beneficial consequence is that the resistance to permeate flow increases at a much slower rate compared with conventional dead-end filtration (Brown & Kavagh 1987). Furthermore, the cell concentrate is not contaminated with flocculents or filter aid. Aerosols are not generated (Kröner *et al.* 1984)

and a contained sterile operation is possible. Under normal operating conditions most investigators including Grabler (1985), Hoffman *et al.* (1987); Le & Atkinson (1985); Ryder *et al.* (1988) and Taddei & Howell (1989), have found that there is generally no loss of viability of bacterial cultures during cross flow filtration. However some viability loss occur under high shear conditions (Nagata *et al.* 1989; Rebsamen *et al.* 1987; Tanny *et al.* 1980).

The effect of the increased hydrodynamic shear stress on the growth, metabolism and morphology of microbial cells have been investigated by various other researchers (Illing 1998; Dunlop & Namdev 1993; Toma *et al.* 1991). Most of these studies were conducted in a stirred tank reactor and the magnitude of shear forces was limited to that caused by the impeller tip speed and the break-up of air bubbles.

In this chapter, the qualitative effect of the shear forces typically encountered in cross-flow micro-filtration applications on the morphology and metabolism of *Corynebacterium glutamicum* cells are investigated. Two extreme sets of fermentations in term of hydrodynamic shear were selected. On the one hand a set of conventional batch fermentatins was performed at mild agiatation conditions, while on the other hand extreme cross flow filtration conditions (cross flow velocity of 7 m/s and trans-membrane pressure drop of 200 kPa) were used.

Image analysis and a bioreaction network model has been used to qualitatively investigate the impact of the hydrodynamic forces on the fermentation performance. Performance was analysed in batch fermentations while continuously filtering the cells. The permeate was returned to the bioreactor to ensure a constant composition. To understand how cells respond to hydrodynamic stress, it is necessary to consider the structure and the functioning of microbial cells (morphology and metabolism) (Section 5-2), the reported response to hydrodynamic conditions (Section 5-3) and the hydrodynamic conditions prevailing in the studied system (Section 5-4). The experimental procedures followed by the results obtained and conclusions drawn are presented in Sections 5-5 to 5-7.

2 The metabolism and morphology of *Corynebacterium glutamicum* cells

2.1 Morphology of C. glutamicum cells

2.1.1 Cell shape and colony forms

Cell morphology can be used as an indication of the physiological state of the cells. Changes in the morphology of the cells can arise from any number of possible changes in the cell's environment. Cells generally change morphology with growth phase. In batch culture, Dean and Hinshelwood (1966) showed that bacterial and

yeast cells are largest at the end of the lag phase while Kjelleberg (1983) showed that starvation following growth can cause dwarf forms. Donachie *et al.* (1976) found that the length of *E. coli* cells increased with increasing growth rate. Furthermore, the cells divided only once they had reached twice the minimum cell length. A characteristic of a successful adaptation after inoculation of yeast cells is a rapid decrease in the production of single cells and an increase in the budding index (Pons *et al.* 1993; Zalewski & Buchholz 1996). *Corynebacterium sp.* generally becomes shorter and more circular when the cells change from lag to the exponential growth phase. During stationary phase *C. glutamicum* is nearly round and much smaller compared to the lag and early growth phase.

Variations in the osmotic pressure of the media can influence the size of microbial cells (Pirt 1975). Srinorakutara *et al.* (1996) showed that *Saccharomyces cerevisae* was smaller in higher osmolarity solutions. Other factors such as pH, dissolved oxygen concentration, media composition and temperature can also influence the morphology of the cells (Illing 1996).

Wase & Patel (1985) showed that the mean cell volume of *Bacillus cereus, Staphylococcus epidermis, Saccharomyces cerevisae* and *Eschericia coli* were directly proportional to the shear stress in a stirred tank reactor. The increase in volume on increased shear stress was attributed to an increase in the water content of the cells. Wase & Ratwatte (1985) showed that the increase in cell volume was accompanied by an accumulation of K^+ and Na^{2+} ions in *E. coli* cells. The excess water was probably required for hydration of these ions. Edwards *et al.* (1989) observed a two fold increase in length of *E. coli* cells when subjected to intense hydrodynamic conditions.

2.1.2 Cell Architecture

To understand how cells respond to hydrodynamic stress, three aspects of the cell anatomy must be considered (Prokop & Bajpai 1992):

- Cell membrane and/or cell wall which forms the physical barrier against the hydrodynamic forces
  All micro-organisms are surrounded by a lipid bilayer membrane, which forms the biological boundary of the cell, through which the cell communicates with the environment. Bacteria, yeast and plant cells have an additional protective cell wall surrounding the cell membrane. In bacteria, the cell wall consists of a thick homogeneous peptidoglycan or murein layer. Peptidoglycan is a polymer consisting of identical sub-units made up of sugar derivatives and amino acids. This forms a rigid barrier between the cell and the extracellular environment. Bacteria may be either Gram positive or Gram negative, depending on the construction of the cell envelope. While the envelope in Gram positive bacteria has a single cell membrane, there are two membranes in Gram negative cells. The outer and inner membrane encloses a region called the periplasmic space. Gram

positive bacteria are generally considered mechanically stronger as they have a thicker peptidoglycan layer. *Corynebacterium glutamicum* cells are gram positive.

- The cell cytoskeleton absorbs the energy generated by turbulence
  The cytoskeleton is a complex network of protein filaments extending throughout the cytoplasm of the cell. There are three types of cytoplasmic fibres that make up the cell cytoskeleton: microtubules, actin filaments and the intermediate filaments. In eucaryotes the cytoskeleton is involved in conducting intracellular transport and enabling cellular movement in an organised fashion. The cytoskeleton is attached to the cell membrane via specialised proteins. In cells that are only surrounded by a cell membrane, the cytoskeleton plays an important role in providing structural support and determining cell shape.

- Receptors in cell envelope which are sensitive to mechanical stress
  Some organisms possess protein receptors in the cell wall or cell membrane, which are sensitive to mechanical stress. Evidence for these receptors has been found in yeast (Gustin *et al.* 1986), plant cells (Falke *et al.* 1986) and animal cells (Stockbridge & Frensch 1988). These cells have evolved a specific regulatory response to mechanical stimuli. The receptors permit rapid adjustments to the changing environment. These receptors are believed to be ion channels, which pass specific ions when mechanically stimulated. The signal is rapidly transmitted throughout the cell by ion channel networking via cytoskeletal elements and the cell may respond accordingly. Ando *et al.* (1991) have shown that hydrodynamic stress induced changes in the Ca^{2+} content of vascular epithelial cells.

2.2 Metabolism of C. glutamicum cells

A living cell is a complex chemical reactor in which enzyme catalysed reactions occur. The total of all reactions occurring in the cell is termed the metabolism. The metabolism may be divided into two distinct parts. Catabolism involves breaking down of larger complex substrate molecules into simpler molecules with the release of energy. Some of this energy is trapped and made available for consumption elsewhere in the cell while the remainder is released as heat. The trapped energy is then used in the second area of the metabolism called the anabolism. Anabolism is the synthesis of complex molecules from simpler ones with the input of energy.

2.2.1 The central carbon flux in *C. glutamicum*

Vallino and Stephanopoulos (1993) constructed a metabolic network for the catabolism of *C. glutamicum* from publications on glutamic acid bacteria. The central carbon flux is depicted in Figure 1-1 repeated below.

A detailed description of the metabolic reactions in *C. glutamicum* is presented in Appendix E.

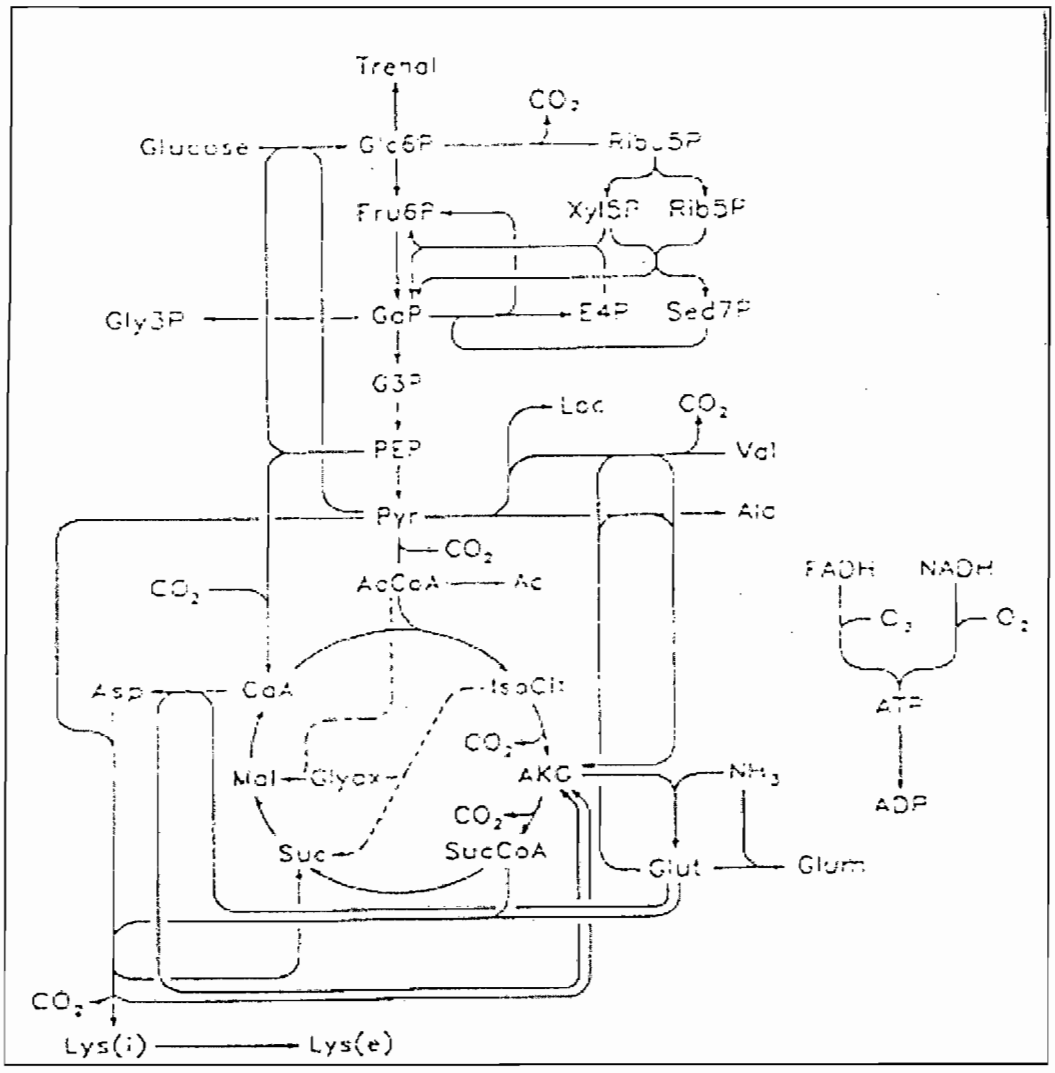

Figure 1-1. Central Carbon flux distribution of *C. glutamicum* as constructed by Vallino & Stephanopoulos (1993)

3 The reported impact of hydrodynamic stress on the growth, metabolism and morphology of cells

The relative differences in the stress sensitivity of different cells are dictated by the biological and physical properties of the cells. Mersmann *et al.* (1990) compared the susceptibility of a range of micro-organisms to rupture in disruption devices. The results are presented in Table 5-1. The shear stress required to rupture bacteria or yeast cells is below 10^8 Nm^{-2}. Plant cells require stresses two orders of magnitude lower while animal cells are ruptured at stress values below 500 Nm^{-2}. It therefore follows that animal cells are

much more susceptible to rupture when compared to bacteria or yeast cells. The stronger cell wall and the smaller size of bacteria or yeast cells yield cells that are more resistant to hydrodynamic stresses when compared to plant or animal cells.

Table 5-1. Susceptibility of micro-organisms to rupture in disruption devices (Mersmann *et al. 1990)*

ORGANISM	SIZE μM	MAX SHEAR STRESS N/M^2	REFERENCE
Bacteria			
Micrococcus luteus	1 × 5	$< 10^8$	Mersmann *et al.* 1990
Synecoccus nidulans		$< 10^7$	Markl *et al.* 1985
Yeast			
Saccharomyces cerevisae	5	$< 8 \times 10^7$	Mersmann *et al.* 1990
Plant cells			
Chlamydomonas reinhardii	4-10 × 100	$< 2 \times 10^6$	Markl *et al.* 1985
Animal cells			
Hela S3		< 500	Augenstein *et al.* 1971
Tetrahymena	10-20	< 4	Midler & Finn 1966
Hybridoma		< 0.005	Mersmann *et al.* 1990

Dunlop *et al.* (1994), studying carrot cells, have shown that hydrodynamic trauma may result in morphological changes, metabolic changers or, in the extreme case, cell rupture. The energy required to induce metabolic changes was several orders of magnitude lower than that required to disrupt cells (Table 5-2).

Table 5-2. Value of the total viscous energy dissipation per unit volume at which 90% ($E_{c,90}$) and 50% ($E_{c,50}$) of the original biological activity of carrot cells are maintained under turbulent conditions in a Haake viscometer (Dunlop *et al.* 1994)

BIOLOGICAL ACTIVITY	$E_{C.90}$ (J/m^3)	$E_{C.50}$ (J/m^3)
Mitochondrial activity	4×10^1	1×10^4
Aggregate breakup	9×10^4	2×10^6
Lysis	3×10^5	1×10^9

3.1 Unicellular organisms

Bacteria are resistant to hydrodynamic conditions due to their small size (0.5 to 3 μm) and strong peptidoglycan cell wall. It is generally accepted that bacteria are unaffected by turbulent eddies, because of their small size with respect to typical eddy size in process equipment (Parker *et al.* 1972; Cherry & Papoutsakis 1986; Ayazi Shamlou & Titchener-

Hooker 1993; Ayazi Shamlou *et al.* 1995). There is however some evidence to the contrary (Table 5-3).

Table 5-3 Effect of hydrodynamic stress on unicellular organisms.

Organism	Impeller Tip Speed [m/s]	Average Energy Dissipation Rate [m^2/m^3]	Nature of the Response to Hydrodynamic Stresses	Reference
Brevibacterium flavum (22LD)	3.11	8-7-11.4	- ATP reduced - Histadine production	Toma *et al.* 1991
Brevibacterium flavum (22LD)	3.46		- Crabtree effect at high sucrose concentration	Rukisha *et al.* 1989
Saccharomyces cerevisae	2.76	6-8	- Optimal growth at the indicated conditions	Toma *et al.* 1991
Saccharomyces cerevisae	12.3		- Mechanical disruption	Virana *et al.* 1982
Eschericia coli			- Catabolic activity increased reversibly	Fowler & Robertson 1991
Bacillus cereus *Stahpylococcus epidermis* *Saccharomyces cerevisae* *Eschericia coli*	1.6-5.3		- Mean cell volume proportional to agitation rate	Wase & Patel 1985
Eschericia coli			- Increase in cell length with increasing shear stress	Edwards *et al.* 1989
Klebsiella pneumonia			- Cells susceptible to ultrasonic stress when grown in intense hydrodynamic conditions	Neseratnam *et al. 1982*
Spirulina platensis			- Decrease in tichome length	Bronnenmeier & Morkel 1982

Toma *et al.* (1991) showed that the growth of Gram positive *Brevibacterium flavum* (22LD) was inhibited at high agitation rates (Impeller tip speed > 3.11 m/s) in a 3-liter stirred tank equipped with two turbine impellers. The sucrose uptake rate, oxygen utilisation rate and specific growth rate peaked at an optimum impeller tip speed of 3.11 m/s and aeration rate

of 3.2 l/min. This corresponds to an average energy dissipation rate as calculated in this study in the range 8.7 to 11.4 m^2/m^3. The ATP level declined sharply at higher impeller tip speeds, indicating a shift in metabolism from the oxidative TCA cycle to the glycolytic pathway. High stirring intensities increased the production of histadine decarboxylase, and hence histamine, a stress indicator. The inhibition of bacterial growth was attributed to the interaction of the cells with turbulent flow in the impeller discharge zone of the stirred tank. A critical zone was considered where the kinetic energy of the medium flow was greater than that required to produce a response on the cell.

Rukisha *et al.* (1989) using the same strain of *Brevibacterium flavum* and experimental apparatus showed that at a high impeller tip speed of 3.46 m/s, increased sucrose concentration induced a Crabtree effect. The appearance of this effect was characterised by an incomplete TCA cycle, increased glutamate dehydrogenase and glycolysis enzyme activities, increase RNA and protein content per cell, a high value of total reducing activity in the cell and increased lactate dehydrogenase activity. The Crabtree effect was not observed at a low impeller tip speed of 1.04 m/s. Analogous changes of metabolic enzyme activity in *Brevibacterium flavum* were observed upon intensive aeration in the fermenter. It was suggested that hydrodynamic stress caused changes in the properties of the cell membrane and damage to the oxidative phosphorylation chain and its functions. The Crabtree effect has been explained by a repression of the phosphorylation site 1 of the electron transport chain, namely $NADH_2$ dehydrogenase and a repression of succinate dehydrogenase (Doelle *et al.* 1983).

Yeast cells (~5 μm) are generally larger than bacteria (~1-2 μm) and they have thick cell walls. Further experiments by Toma *et al.* (1991) showed that the growth of *Saccharomyces cerevisae* was optimal at an impeller tip speed of 2.76 m/s and an aeration rate of 3.2 l/min. This corresponds to an average calculated energy dissipation rate between 6 and 8 m^2/m^3. Virana *et al.* (1982) observed the mechanical disruption of mother *Saccharomyces cerevisae* cells in an airlift reactor fitted with a high-speed motor axle with rotating knives at an impeller tip speed of 12.3 m/s. It was suggested that the multi-budscarred mother cells were less resistant to mechanical strain than the daughter cells as their rigid polysaccharide cell wall was interrupted.

Fowler & Robertson (1991) showed that the catabolic activity of Gram negative *Escherichia coli* increased reversibly with increased hydrodynamic stress in a parallel plate flow chamber. The total acid yield and glucose consumption increased, and the spectrum of organic acids produced changed. It was postulated that the change was due to an osmoregulatory response induced by stressed bacteria to restore cell turgor.

Wase & Patel (1985) showed that the mean cell volume of *Bacillus cereus, Staphylococcus epidermis, Saccharomyces cerevisae* and *Escherichia coli* was directly proportional to the agitation rate of the fermenter. Agitation speed had no effect on cell growth or dry biomass concentration, hence the increased cell volume was due to an increase in the water content of the cells. The impeller speed was varied in the range 1.6 to 5.3 m/s. Edwards *et al.* (1989) observed that *Escherichia coli* cells were twice as long

when grown in a combined type coaxial cylinder and cone and plate viscometer bioreactor at a shear stress of 14.5 Nm^{-2} compared to a shakeflask. Neseratnam *et al.* (1982) showed that *Klebsiella pneumonia* cells grown in intense agitation conditions were more susceptible to ultrasonic disintegration than cells grown at milder conditions. This change in stress sensitivity may be postulated to be attributed directly to a change in cell volume. Larger cells are more susceptible to rupture. Bronnenmeier & Morkel (1982) observed a decrease in the trichome lengths of *Spirulina platensis* at increased levels of hydrodynamic stress. *Spirulina platensis* is approximately 15 μm in diameter, link together by plasmic filaments to form a helical structure called a trichome. The maximum growth rate occurred at an impeller tip speed of 2.35 m/s, which corresponds, to an energy dissipation rate of 3.89 m^2/m^3.

3.2 Filamentous fungi

The impact of hydrodynamic shear stress on filamentous fungi is summarised in Table 5-4.

Table 5-4. Impact of hydrodynamic conditions on filamentous fungi

Organism	Impeller Tip Speed [m/s]	Average Energy Dissipation Rate [m^2/m^3]	Nature of the Response to Hydrodynamic Stresses	Reference
Trichoderma reesei	0.52	0.03-0.05	- Decreased growth rate at increased agitation	Toma *et al.* 1991
Aspergillus niger	600 rpm		- Optimal citric acid production rate	Ujcovo *et al.* 1980
Penicillium chrysogenum	3.33	3.3	- Optimal penicillin production	Smith *et al.* 1990
Ashbya gossypii	0.42	0.0135	- Optimal riboflavin yield and cell concentration	Ozbas & Kutsal 1991
Thermomonospora fusca	1.18-1.60		- Increased protease production with decreased agitation	Gusek *et al. 1991*
Muxor rouxii	2.1-5.8		- Growth and productivity inhibited at increased agitation rates - Morphological changes	Dabee & Harrison 1996

Fungi may grow in a pelleted or mycelial form. The pellet form can vary from being loose and fluffy to being compact and smooth as a function of hydrodynamic conditions. Blanch and Bhavaraju (1976) described two mechanisms of pellet disruption in stirred tanks: the chipping of pellicles from the surface and the direct splitting of the pellets. The mycelial form dominates in stirred tank reactors at higher agitation speeds, due to its mechanically

more resistant morphological structure (Mitard and Riba 1988; Dabee and Harrison 1996). Van Suijdam and Metz (1981) reported shorter, thicker and more branched hyphae at higher agitation rates. The decrease in hyphal length is a direct result of hyphal breakage.

Toma *et al.* (1991) observed a decreased growth rate of *Trichoderma reesei at* an impeller tip speed in excess of 0.52 m/s and an aeration rate of 3.2 l/min. This corresponds to an average energy dissipation rate between 0.03 and 0.05 m^2/s^3.

Ujcovo *et al.* (1980) showed a maximum in citric acid production rate by *Aspergillus niger* at an impeller speed of 600 rpm and an aeration rate of 1 l/min in a 1 litre single turbine stirred tank. The initial decrease in citric acid production resulted on a shift in metabolism, rather than cell damage. Smith *et al.* (1990) reported optimum penicillin production by *Penicillium chrysogenum* at an impeller tip speed of 3.33 m/s and an aeration rate of 5.4 l/min in a 10 litre reactor (average energy dissipation rate of 3.3 m^2/s^3). Higher agitation and aeration rates inhibited production of the metabolite. The specific penicillin production rate was correlated with the product of power input per unit volume and the inverse of the circulation time, $P_g/D_i^3\ t_c$. The greater the frequency of circulation through the impeller discharge zone, the greater the mycelial damage and the lower the rate of penicillin synthesis. Ozbas and Kutsal (1991) found optimum riboflavin yield and *Ashbya gossypii* concentration in a 0.42 litre fermentor fitted with Rushton turbine impellers at an impeller tip speed of 0.42 m/s and an aeration rate of 0.1 litre/min (average energy dissipation rate of 0.0135 m^2/s^3). Disintegration of cells occurred at more extreme conditions. An empirical equation was developed to correlate the riboflavin production rate to gassed power input per unit volume, the superficial gas velocity and the maximum biomass concentration. Gusek *et al.* (1991) showed comparable *Thermomonospora fusca* biomass production in a shake flask and a 10 litre fermenter fitted with two marine impellers, agitated at an impeller speed of 1.6 m/s and aerated at 3 l/min. However, the shake flask culture yielded 30 μg protease/ml compared to 4.6 μg protease/ml in the fermenter. The use of Rushton impeller tip speed of 1.18 m/s produced a five-fold decrease in biomass.

Dabee and Harrison (1996) showed that at an impeller speed of 5.8 m/s in a 5 litre stirred tank reactor, growth and productivity of *Mucor rouxii* were inhibited. After a period of adaptation, the growth and productivity levels recovered. Morphological changes were also observed. At a low impeller speed (2.1 m/s), the morphology of exponentially growing cells was yeast like. At an impeller speed of 5.9 m/s, the mycelial form predominated. The hyphae were thick, short and branched.

The leakage of intracellular nucleotides from the fungi at higher speeds was reported by Tanaka *et al.* (1975). The release was not due to cell disruption. Ujcovo *et al.* (1980) found no correlation between nucleotide release and stirrer speed.

3.3 Animal cells

Animal cells are particularly sensitive to hydrodynamic stresses (Table 5-5). This is mainly because of their large size interacting with a broader range of eddy sizes and the lack of a protective cell wall.

Table 5-5. Impact of hydrodynamic conditions on animal cells

Organism	Impeller Tip Speed [m/s]	Average Energy Dissipation Rate [m^2/m^3]	Nature of the Response to Hydrodynamic Stresses	Reference
TB/C3 Murine hybridomas	6.02	58	- Cell disruption	Zang *et al.* 1995
Hybridomas	60-160 rpm		- Loss of membrane integrity - Reduction in respiratory activity - Cell lysis	Tan *et al.* 1992
Mouse myeloma cells		180 Nm^{-2}	- Cell lysis	McQueen *et al.* 1987
Hybridoma	0.7-2.6		- In absence of vortex formation cell damage occurred at tip speeds > 2.6 - In the presence of vortex, growth inhibited at tip speed > 0.7 m/s	Kunas & Papoutsakis 1990
Murine hybridoma	0.26-1.18		- Cell growth, viability, monoclonal antibody production and metabolic activity was not affected between tip speed of 0.26-1.18 m/s in the absence of entrained air	Oh *et al.* 1989

Moreira *et al.* (1995a) investigated the kinetics and the mechanism of baby hamster kidney cell aggregates in spinner flasks. Disruption of aggregates occurred by two mechanisms: fragmentation and surface erosion of cells from larger aggregates. It was also observed that fluid forces compact cell aggregates. An empirical relationship between the aggregate diameter and the power dissipation per unit volume was developed. Aggregate diameter was dependent on the power per unit volume raised to the power –0.25, suggesting that it

may be related to the critical microscale. Al-Rubeai *et al.* (1990) achieved a lower maximum cell number and growth rate of TB/C3 murine hybridomas at high agitation rates in shaker bottles. The synthesis of DNA was also inhibited. The mitochondrial activity increased as a response to stress, possibly in order to supply energy to repair damage. Nollert *et al.* (1991) showed that endothelial cells respond within minutes of exposure to laminar shear stress by increasing their metabolic rate and increasing the level of secondary messengers; inositol triphosphate and calcium ion concentration.

Zhang *et al.* (1995) observed the total disruption of TB/C3 cells in a standard 2 litre stirred tank reactor fitted with a Rushton turbine impeller at a tip speed of 6.02 m/s in the absence of sparging. This corresponded to an average energy dissipation rate of 58 m^2/s^3. Peterson *et al.* (1990) showed that hybridoma cells (CRL-8018) taken from the lag or stationary phase were more sensitive to shear than those from the exponential phase. In confirmation, Zhang *et al.* (1992a) found that the mechanical strength of TB/C3 hybridomas rose significantly in the exponential phase and fell in the death phase. Further, Lee *et al.* (1998) showed that hybridoma cells (S3H5/γ2bA2) in the stationary and death phase were more sensitive to cell death caused by shear forces, associated with mechanical agitation, than cells in the exponential phase.

Abu-Reesh & Kargi (1989) showed that turbulent shear was more damaging to hybridoma membrane integrity, respiration activity and cell lysis than laminar shear.

Tan *et al.* (1992) observed more cell damage of hybridoma cells when the agitation speed in a 1.3 litre reactor equipped with a cell lift impeller was increased abruptly by a large step change (60-160 rpm) than when agitation speeds were changed gradually by small steps. This indicated that cells were able to acclimatise to hydrodynamic forces.

A fatigue effect that resulted in the loss of hybridoma cell viability when exposed to mild hydrodynamic conditions for long periods have however been observed by Abu-Reesh & Kargi (1989) and Smith *et al.* (1987). Milder and Finn (1966) sheared osmotically shocked protozoa in a coaxial cylindrical viscometer and reported damage in two phases. A rapid initial loss of cell integrity was followed by secondary damage to the cell membrane at lower rates. The latter may result from fatigue effects on repeatedly stressed cells. Al-Rubeai *et al.* (1995b) based on their experimental finding, hypothesised that there are two mechanisms of hybridoma cell destruction by hydrodynamic forces, and that their relative expression is dependent on the energy dissipation rate. A cell will die passively from necrosis as a result of mechanical damage at sufficiently high levels of stress intensity. Active cell suicide, apoptosis, occurs with milder mechanical forces. The cell may initially invoke repair mechanisms but the ongoing stress may eventually cause induction of the apoptotic pathway. The cytoskeleton collapses, causing a rapid decrease in the physical strength of the cell. Exposure to forces, to which it was previously resistant, now results in its complete destruction.

Because the hydrodynamics in stirred tanks are poorly understood, better characterised capillary systems have been used to study shear effects on animal cells. The energy

dissipation rates in capillary flow are several orders of magnitude higher than those found in stirred tank reactors. Al-Rubeai *et al.* (1995a) showed that the exposure of TB/C3 hybridoma cells to turbulent capillary flow resulted in the preferential destruction of older cells. McQueen *et al.* (1987) showed that the probability of mouse myeloma cell lysis per pass through a capillary tube increased with increasing wall stress and with increasing residence time per pass in the tube. Lysis was observed at wall shear stress levels of 180 N/m^2. Augenstein *et al.* (1971) found that the cell damage of mammalian cells in turbulent capillary flow could be characterised by a rate constant which was first order with respect to cell number and dependent on wall shear stress in the capillary section.

Zhang *et al.* (1993) modelled the disruption of TB/C3 hybridoma cells in turbulent capillary flow. It was assumed that cells were deformed by similarly sized eddies. The surface deformations were postulated to increase membrane tension, disrupting the cell wall when the surface energy was exceeded. The animal cell was considered to be an incompressible fluid surrounded by an elastic membrane. This is a gross simplification of the complex structure of a typical cell. The mechanical properties, cell bursting tension, elastic area compressibility modulus and cell size were measured using the micromanipulation method (Zhang *et al.* 1992b). The model was tested in turbulent capillary flow up to an average energy dissipation rate of 2×10^4 m^2/s^3 and found to underestimate cell damage by 15%. The model gave poor estimates of cell damage in a stirred tank reactor (Zhang *et al.* 1995). Born *et al.* (1992) developed a model to predict disruption of animal cells by laminar shear stress. It was assumed that the cells would be disrupted when the bursting membrane tension, as predicted by the micromanipulation technique was overcome.

Cell damage has been attributed to the interaction of cells with similarly sized turbulent eddies in the impeller discharge zone as well as with collapsing air bubbles at the air medium interface. Kunas and Papoutsakis (1990) found that two phenomena participate in cell damage: bulk-liquid turbulence and vortex formation with associated bubble entrapment and bubble break-up. In the absence of vortex formation, hybridoma cells grew at impeller tip speed up to 2.6 m/s. At higher tip speeds the local impeller zone Kolmogorov microscale approached the cell diameter and cell damage occurred. In the presence of a vortex, growth was inhibited at a lower impeller tip speed of 0.7 m/s. In this case, the impeller zone Kolmogorov microscale was larger than the cell diameter. Hydrodynamic forces that accompany gas bubbles collapsing at the air liquid interface were implicated as the source of the cell damage. Oh *et al.* (1989) grew three murine hybridomas in surface aerated 1.4 litre reactors agitated by propellers or Rushton turbine impellers. Cell growth and viability, monoclonal antibody production, glucose and lactate consumption and metabolic activity were unaffected at impeller tip speeds of 0.26 m/s to 1.18 m/s provided no air was entrained at the surface. If air was sparged or entrained, cell growth rates declined with increasing impeller tip speeds across this range. Handa-Corrigan *et al.* (1989) ascribed the damaging effect to mammalian cells in a bubble column to the bubble disengagement zone and not the bubble riser or bubble distributor zone. They found cell viability depended on the cell type, the bubble size and the bubble frequency. Small bubbles at high frequencies resulted in decreased viability.

Protective agents are commonly used to improve the survival of animal cells exposed to hydrodynamic stress. Non-ionic surfactants such as Pluriol PE6800 and Pluronic F68 have a concentration dependent protective effect, as does foetal calf serum. Pluronic F68 has been used to increase the strength of the cells (Zhang *et al.* 1992d). Lee at al. (1989) have suggested that serum can decrease the shear sensitivity of hybridomas by changing the physiological properties of the cells. The surface of bubbles and cells are hydrophobic, hence cells tend to adhere to bubbles as they rise to the surface. Cells in the vicinity of collapsing air bubbles are subjected to rapid accelerations, which may be detrimental to their viability. Pluronic F68 coats the bubble and the cell surface preventing their adhesion thereby protecting the cells. Antifoam on the other hand decreases the degree of cell damage by decreasing the hydrophobicity of the cell and the bubble surfaces (Zhang *et al.* 1992c).

3.4 Plant cells

Single plant cells in suspension can range for 20 – 100 μm in diameter. Plant cells in suspension cultures have a tendency to aggregate primarily due to incomplete cell separation after mitosis. Plant cells are surrounded by a thick rigid cellulose based cell wall. The cytoplasm is highly dense and structured. Plant cells also possess large vacuole compartments, in some cases 80% of the cell volume.

Leckie *et al.* (1991) showed that impeller speed affected the growth and alkaloid accumulation of *Catharanthus roseus* cells. Using two standard 12 cm diameter turbine impellers in a 7.5 litre stirred tank reactor, the growth and alkaloid production decreased with increasing tip speed in the range 1.88 m/s to 4.4 m/s.

Nicotiana tabacum cells were subjected to shear stresses in a Couvette type shearing device and changes in cell viability, cell lysis and the accumulation of secondary metabolites monitored (Hooker *et al.* 1989). Increasing shear stress, caused an increase in cell death, lysis and secretion of phenolics. Cultures in the late exponential and early stationary phase were most susceptible to damage.

The shear susceptibility of *Morinda citrifolia* cultures was investigated in turbulent capillary flow by Kieran *et al.* (1995). Shear stresses were varied from 25 to 350 N/m^2. The relative viability loss was found to conform to a first order model in which the specific death rate constant was observed to increase linearly with the imposed shear stress. Morphological measurements showed that over the course of the shear tests there was a reduction in the mean chain length and in the spread of data.

Experiments conducted in a Couvette viscometer showed that carrot cells exhibit a range of biological responses depending on the magnitude of the applied force (Dunlop *et al.* 1994). In the range 0.5 to 100 N/m^2, carrot cells lost the ability to grow and divide. Intracellular enzyme activity was affected at shear stresses of 750 N/m^2. At 3000 N/m^2,

intracellular enzyme activity was compromised. Membrane integrity was damaged at shear stress levels in the 3000 to 10 000 N/m^2 range. Cell lysis only occurred at stresses in excess of 10 000 N/m^2 applied over an hour period. In each case the loss of the biological response could be characterised by a first order rate constant.

Since cell viability was lost at shear stress levels of two to three orders of magnitude below that required to compromise membrane integrity, it has been presumed that plant cells have a mechanism for sensing the applied force and responding to it. Linthelac and Vasecky (1984) and Pickard (1984) postulated that plant cells possess receptors in the cell membrane or the cell wall which communicate the magnitude of the applied stress to the control centres in the cell via secondary messengers. At shear stresses greater than 10 N/m^2, control pathways are activated to selectively inhibit mitoses without affecting membrane integrity or the electron transport chain activity. Dunlop *et al.* (1994) showed that the intracellular enzyme activity and cell lysis are affected by turbulent stresses lower in magnitude than those required to generate the same degree of damage in laminar flows.

4 Quantification of the hyrodynamic stress in the biomass recycling system

4.1 Basics of fluid mechanics

As a guide to understanding the theory of turbulent flow, some of the basic principles and terminology used in fluid mechanics are described below (Calabrese & Stoots 1989).

The instantaneous velocity at a point (U_i) is the sum of the average velocity ($\overline{U}_i$) and the fluctuating velocity (u_i):

$$U_i = \overline{U}_i + u_i \tag{5-1}$$

For N measurements of the i'th component the average velocity is:

$$\overline{U}_i = \frac{1}{N}\sum_{k=1}^{N} U_{ik} \tag{5-2}$$

The mean square turbulent velocity is the variance of the distribution of the instantaneous velocity:

$$\overline{u_i^2} = \frac{1}{N}\sum_{k=1}^{N} (U_{ik} - \overline{U}_i)^2 \tag{5-3}$$

The magnitude of the mean velocity ($\overline{U}$) and the magnitude of the root mean square (RMS) turbulent velocity ($\overline{U}_{RMS}$) are the vector sum of their three individual components:

$$\bar{U} = [\overline{U_x^2} + \overline{U_y^2} + \overline{U_z^2}]^{1/2} \quad (5\text{-}4)$$

$$\bar{U}_{RMS} = [\overline{u_x^2} + \overline{u_y^2} + \overline{u_z^2}]^{1/2} \quad (5\text{-}5)$$

The total turbulent kinetic energy per unit mass (E_k) is a measure of the strength of turbulence in a velocity field:

$$E_k = \frac{1}{2}\bar{U}_{RMS}^2 \quad (5\text{-}6)$$

To assess the hydrodynamic forces that exist in a flow field, one needs to evaluate the stress caused by the mean velocity gradients as well as the Reynold's stress due to the velocity fluctuations. The stress due to mean velocity gradients is given by Newton's law of viscosity. Each of the three components of velocity can vary in the three co-ordinate directions. There are therefore nine components of stress tensor τ_{ij}.

$$\tau_{ij} = \upsilon\Delta_{ij} \quad (5\text{-}7)$$

where υ is the Newtonian viscosity and Δ are the components of the mean rate of deformation tensor for compressible flows:

$$\Delta_{ij} = \frac{\partial \overline{U_i}}{\partial x_j} + \frac{\partial \overline{U_j}}{\partial x_i} \quad (5\text{-}8)$$

The mean deformation rate ($\overset{o}{\gamma}$) due to normal and shear stresses is given by:

$$\overset{o}{\gamma} = \sqrt{\frac{1}{2}\Delta : \Delta} \quad (5\text{-}9)$$

The rate of energy dissipation ($\bar{e}$) due to mean velocity gradients is a function of the kinematic viscosity (υ') and the mean deformation rate:

$$\bar{e} = \upsilon' \overset{o}{\gamma}^2 \quad (5\text{-}10)$$

Since Reynold's stress (τ') accounts for simultaneous fluctuations in two directions, measurement of this quantity is difficult

$$\tau' = \rho\overline{u_i u_j} \quad (5\text{-}11)$$

It is therefore necessary to relate it to a more readily measured quantity. Turbulent kinetic energy (E_k) is a measure of the Reynold's stress. To obtain an estimate of the turbulent

energy dissipation rate per unit mass (e), the rate of energy dissipation at a point may be assumed equal to the rate of turbulent energy production. The production rate can be related to the RMS turbulent velocity and the resultant length scale of the large energy containing eddies, L_{RES}, which is of the order of the blade width in stirred tanks.

$$e = \frac{A' E_k^{3/2}}{L_{RES}} \tag{5-12}$$

where A' is a constant of typically 0.85 and

$$L_{RES} = \sqrt{L_r^2 + L_z^2 + L_\theta^2} \tag{5-13}$$

The large energy containing eddies decay into smaller eddies. The energy flows continuously from the large macroscale eddies to the smallest microscale eddies where viscous losses convert the kinetic energy into heat. Kolmogorov (1941) suggested that, in fully turbulent conditions, a range of eddy sizes exist in which the turbulence may be considered to be isotropic. This is called the universal equilibrium sub-range and is totally independent of external conditions. The properties of the eddies are determined solely by the energy input and the viscous dissipation. The size of the smallest energy containing eddy (λ) according to Kolmogorov can be estimated as:

$$\lambda = \left(\frac{\upsilon'^3}{e} \right)^{1/4} \tag{5-14}$$

where λ is the Kolmogorov microscale (m), e is the turbulent energy dissipation rate per unit mass (m^2/s^3) and υ' is the kinematic viscosity (m^2s^{-1}).

Local isotropic conditions can usually be assumed in the impeller region of a stirred tank (Kawase & Moo Young 1990). The eddies in the universal equilibrium subrange are subdivided according to whether their size is smaller or larger than the Kolmogorov microscale. Eddies in the viscous dissipation subrange are smaller than the λ. Eddies with sizes greater than λ fall in the inertial convection subrange.

According to the isotropic theory of turbulence the root mean square velocity difference for eddies of diameter d in the viscous dissipation range is given by:

$$\overline{u_1}(d) = \sqrt{\left(\frac{2}{15}\right)\left(\frac{e}{\upsilon'}\right)^{1/2} d} \tag{5-15}$$

where $\overline{u}_1(d)$ is the root mean square velocity for eddies of size d in the viscous dissipation range (m/s), e is the energy dissipation rate per unit mass (m^2/s^3), υ' is the kinematic viscosity and d is the eddy size.

The root mean square velocity difference for eddies of diameter d in the inertial convection subrange is given by:

$$\bar{u}_2(d) = 1.57 e^{\frac{1}{3}} d^{\frac{1}{3}} \tag{5-16}$$

where $\bar{u}_2(d)$ is the root mean square velocity for eddies of size d in the inertial convection sub range (m/s), e is the energy dissipation rate per unit mass (m^2/s^3) and d is the eddy size.

Davies *et al.* (1986) postulated that the fluid mechanical sensitivity of biological cells can be quantified by stating a threshold shear stress for laminar effects and a local Reynolds stress for turbulent effects. This analysis showed cells to be more sensitive to turbulent forces compared to laminar forces when magnitudes of laminar stress and time-averaged turbulent stress were comparable. Another approach compares the turbulent eddy scales with cell size (Croughan *et al.* 1987; Lakhotia & Papoutsakis 1992). Dunlop *et al.* (1994) attempted to integrate both laminar and turbulent effects on plant cells by using the cumulative energy dissipation on the cells during exposure to a particular flow as a common hydrodynamic basis.

Lakhotia & Papoutsakis (1992) modelled the shear damage of animal cells on microcarriers due to eddy-microcarrier and microcarrier-microcarrier interactions as a function of the total energy content of the interacting eddies. Eddies of size comparable to microcarriers or aggregates will dissipate turbulent energy on the cells and thus perform work by deforming the cells in a turbulent flow regime. Sizes of these eddies under typical operating conditions of bioreactors for plant (Dunlop *et al.* 1993) and animal cells (Ho *et al.* 1989; Croughan *et al.* 1987; Lakhotia & Papoutsakis; 1992) were found to be close to Kolmogorov's length scales in corresponding systems. Assuming an isotropic turbulent condition locally, the work performed by these small eddies is given by the flowing equation (Dunlop *et al.* 1993):

$$\frac{\partial}{\partial x_j}\left(\overline{u_i \tau_{ij}'}\right) = \overline{\tau_{ij}' \frac{\partial}{\partial x_j}(u_i)} = e_t \rho \tag{5-17}$$

The above equation shows that the rate of work done by turbulent stresses is equal to the rate of turbulent energy dissipation ($e_t \rho$ - kg / m s^3) and is calculated as the time averaged of the product of the Reynolds stress and the associated frequency.

The rate of work performed by viscous stresses under laminar flow conditions is equal to the rate of viscous energy dissipation ($e_v \rho$ - kg / m s^3) and is calculated as a product of shear stress and shear rate:

$$\frac{\partial}{\partial x_j}\left(\overline{U_i \tau_{ij}}\right) = \tau_{ij} \frac{\partial}{\partial x_j}\left(\overline{U_i}\right) = e_v \rho \tag{5-18}$$

The total rate of work performed on a fluid element will be the sum of the rates of viscous energy dissipation and turbulent energy dissipation.

The total work performed on cells will be a fraction of the total energy dissipation per unit volume ($e\rho$ - kg / m s^3) as the cells occupy a fraction of the total culture volume ϕ_b. At higher cell volume fractions the probability of collision among aggregates will increase and thus contribute to the total energy dissipation.

Unfortunately the impact of hydrodynamic stresses depends on the type of flow as well as the total energy dissipation rate. Provided that a single flow type exists the total energy dissipation rate can be used to quantify the effect of hydrodynamics on metabolic response.

In the system in hand all the flows as well as the conditions inside the stirred tank reactor would be turbulent and therefore the total turbulent energy dissipation rate would be used to quantify the effects of the hydrodynamics on the metabolic response of the organism.

To investigate this hypothesis the hydrodynamic conditions inside the system was characterised by the total turbulent energy dissipation rate. The estimation of the turbulent energy dissipation rate in the stirred tank reactor, the membrane module and the needle valve as illustrated below.

4.2 Calculation of the turbulent energy dissipation rate in the stirred tank reactor

In the stirred and sparged bioreactor the cells would encounter mostly turbulent forces in the impeller region and viscous forces in the bulk region. The mean power input can be calculated from the power correlation:

$$P_0 = N_{power} \cdot \rho \cdot Re v^3 \cdot D_{imp}^{\ 5} \qquad (5\text{-}19)$$

where P_o is the power input into the bioreactor (W), N_{power} is the power number that can be estimated from a correlation developed for 6 bladed Rushton turbines by Bates et al. (1966); ρ is the bulk liquid density (kg/m^3); Rev is the impeller revolutions per second (s^{-1}); D_{imp} is the impeller diameter (m).

It should be noted that the power consumption calculated above is for ungassed single impeller systems. The effect of two impellers on the agitated power drawn was estimated from the correlation developed by Bates et al. (1963). For an impeller spacing of 1.5, the agitator power drawn is double that for a single impeller.

The introduction of air into the stirred tank reduces the medium viscosity and therefore the power drawn by the impeller. For two-impeller, gassed system it has been shown that the

lower impeller draws less power than the upper impeller (Chiampo & Marotto 1995). Since all the gas passes through the lower impeller the power drawn by this impeller can be estimated by gassed power correlations. Michel & Miller (1962) correlated the gassed power drawn by a single impeller:

$$P_g = A_7\left(\frac{P_0^2 \cdot Rev \cdot D_{imp}{}^3}{Air^{0.56}}\right)^{0.45} \quad (5\text{-}20)$$

where A_7 is a function of the impeller geometry.

The gassed power drawn by the upper impeller is always greater than that drawn by the lower impeller and always less than the ungassed power of the upper impeller. Therefore the gassed power drawn by the system would always be between two limits defined by the ungassed power drawn by the top impeller and the gassed power drawn by the lower impeller.

4.3 Calculation of the turbulent energy dissipation rate in turbulent fluid flow through tubular conduits

When a liquid flows in a tubular section under turbulent conditions (Re > 2000), a laminar subsection exists immediately adjacent to the inner wall. The thickness of the sublayer is approximately 3 a, where "a" is the bacterial particle diameter. A negligible fraction of the cells will penetrate this sublayer when passing through the tube. However, significant energy dissipation occurs in this region. This needs to be subtracted from the local energy dissipation to calculate the energy dissipation in the turbulent core.

The pressure drop in developing turbulent flow at the entrance of a tubular conduct can be estimated by flat plate theory. The mean apparent friction factor is given by (Zhang et al. 1993):

$$f_{app} = \frac{0.296}{\left[Re\left(L_p/d_{pipe}\right)\right]^{0.2}} \quad (5\text{-}21)$$

where f_{app} is the mean apparent friction factor, Re is the pipe Reynolds number and L_p/d_{pipe} is the length (L_p in m) to pipe diameter (d_{pipe} in m) ratio. The pressure drop (DP in Pa) is given by:

$$DP = \frac{1}{2} \cdot f_{app} \cdot \rho \cdot \left(L_p/d_{pipe}\right) \cdot U_{max}^2 \quad (5\text{-}22)$$

where ρ is the fluid density and U_{max} is the maximum fluid velocity in the capillary. The total energy dissipation in the tube E_T (m^2/s^3), can be estimated as:

$$E_T = DP\frac{\pi}{4} d_{pipe}{}^2 U_{ave} \quad (5\text{-}23)$$

where U_{ave} is the mean flow velocity (m/s). The energy dissipated in the laminar sublayer (E_L in (m^2/s^3) can be calculated from the fluid viscosity υ in Pas, the wall shear rate $\dot{\gamma}_o$ in s^{-1} and the volume of the laminar sublayer (V_L in m^3).

$$E_L = \upsilon \dot{\gamma}_o^2 V_L \tag{5-24}$$

The wall shear rate is given by the wall stress (τ_0) divided by the fluid viscosity.

$$\dot{\gamma}_o = \frac{\tau_0}{\upsilon} \tag{5-25}$$

The thickness of the sublayer can be estimated as

$$\delta_t = \frac{5\upsilon'}{\left(\frac{\tau_0}{\rho}\right)^{0.5}} \tag{5-26}$$

The volume of the sublayer is therefore:

$$V_L = \frac{\pi}{4}\left[d_{pipe}{}^2 - \left(d_{pipe} - 2\delta_t\right)^2\right] \cdot L_p \tag{5-27}$$

The energy dissipated in the turbulent core can be calculated by subtracting the energy dissipated in the laminar sublayer from the total energy dissipation in the tube. The corresponding energy dissipation rate (e) is determined by dividing the energy dissipation by the product of the turbulent core volume and the fluid density.

$$e = \frac{E_T - E_L}{V_{pipe} - V_L} \tag{5-28}$$

The maximum energy dissipation rate (e_w) was calculated by Laufer (1954) as:

$$e_w = \frac{460u^{*3}}{d_{pipe}} \tag{5-29}$$

where u* is equal to $u^* = \sqrt{\frac{\tau_0}{\rho}}$ and τ_0 is the wall shear stress.

The energy dissipated across the membrane module is also calculated according to the principle above. It has been found that the slip coefficient in a membrane module operated under typical conditions is negligible and therefore it would be assumed that no laminar flow region exists.

4.4 Calculation of the turbulent energy dissipation rate through a needle valve

The flow through a needle valve can be assumed completely turbulent. The volume over which the turbulent energy is dissipated is assumed the valve volume.

The total energy dissipated is then given by the product of the permanent pressure drop over the valve and the average volumetric flow rate.

$$E_T = DP_v \cdot Q_L \tag{5-30}$$

The pressure drop across the valve is given as a function of the valve opening and the liquid flow rate. The characteristic curve for the specific valve used is presented below:

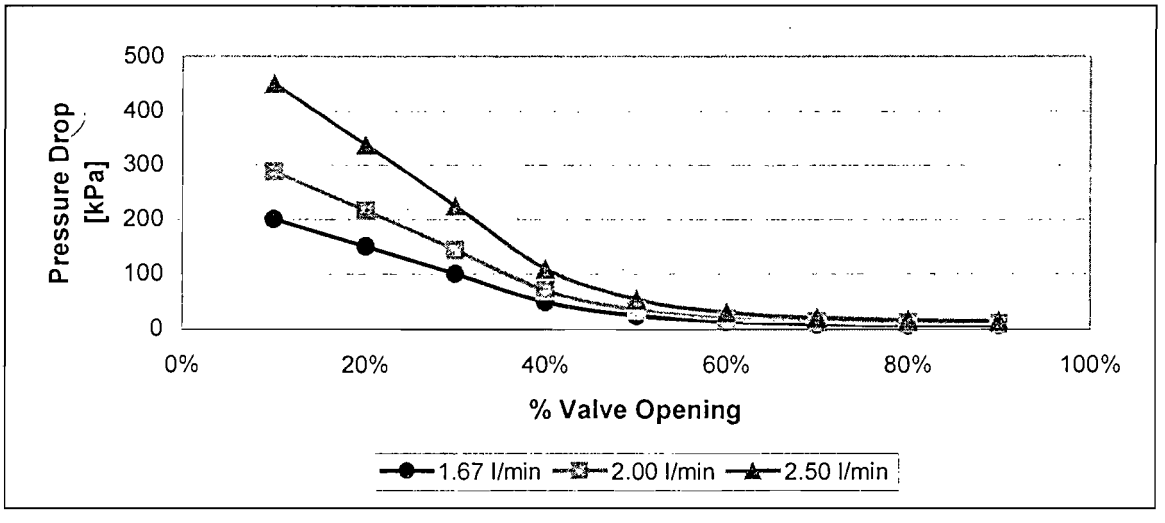

Figure 5-1 Pressure drop across the needle valve as a function of the valve opening and the volumetric flow rate

4.5 Calculation of a parameter to represent the hydrodynamic stress experienced by the cells in the entire system

It has been noted by previous investigators that the effect of the hydrodynamic conditions depends on the intensity of the conditions, the duration of the exposure to the extreme hydrodynamic conditions and the frequency of exposure (Dunlop *et al.* 1994; Maiorella *et al.* 1991; Davies *et al.* 1986; Toma *et al.* 1991; Rukisha *et al.* 1989; Fowler & Robertson 1991). For the biomass recycling system, an average energy dissipation rate has been estimated based on the relative residence time during which the cells are exposed to the different hydrodynamic conditions.

$$e_{ave} = \frac{e_{reac}\frac{V_{reac}}{Q_L} + e_{mem}\frac{V_{mem}}{Q_L} + e_{valve}\frac{V_{valve}}{Q_L}}{\sum\left(\frac{V_{reac}}{Q_L}; \frac{V_{mem}}{Q_L}; \frac{V_{valve}}{Q_L}\right)} \tag{5-31}$$

where e_{reac} represents the average energy dissipation rate in the bioreactor (m^2/s^3); e_{mem} is the average energy dissipation rate in the membrane unit and circulation loop (m^2/s^3); e_{valve} is the average energy dissipation rate in the needle valve (m^2/s^3); V is the corresponding unit volume and Q_L the volumetric flow rate through the circulation loop (m^3/s)

4.6 Evaluation of hydrodynamic stress parameters in biological systems

Using the above mentioned correlations (Section 4.1-4.5), the average and local maximum energy dissipation rates have been estimated for various bioreactor configurations at the operating conditions at which biological response have been reported. This is limited to cases where sufficient specification of the hydrodynamic conditions was given (Table 5-6).

The average energy dissipation rate e_{ave} for all the stirred tank reactors were around 2.5 to 58 m^2/s^3. The maximum energy dissipation rate around the impeller sweep zone was at least one order of magnitude larger around 60 to 1450 m^2/s^3. The reported impact varied from partial inhibition of growth to cell disruption.

Table 5-6. Evaluation of hydrodynamic stress parameters in stirred tank reactors:

Reference	Configuration	Organism	Response	e_{ave} [m^2/s^3]	e_{max} [m^2/s^3]
Toma *et al.* 1991	3-litre Reactor 2 x 6-bladed Rushton 3 baffles D=0.066 m T=0.15 m Q=1 vvm H/T=2 S/D=2 d_b=0.022 m	Brevibacterium flavum d:0.8μm L:1.3μm *Saccharomyces cerevisae* d_{ave}=5μm	• Partial inhibition of growth • Decrease OUR • Decrease sucrose uptake rate • Decreased growth rate • Change in ATP pathway	8.7-11.4 6-8	±250 ±175
Dunlop & Ye 1994	1.45-litre Reactor 1 x 6-bladed Rushton 4 baffles D=0.09 m Q=0.16 vvm	Carrot cells d_{ave}=194μm	• Complete inhibition of mitichondrial activity and growth	2.54	±63.5
Zhang *et al.* 1995	2-litre Reactor 1 x 6-bladed Rushton 4 baffles D=0.0575 m T=0.115 m H/T=2 Q=zero	Hybridoma cells d_{ave}=12μm	• 45% cell disruption • 85% cell disruption	25 58	±625 ±1450

5 The causes of hydrodynamic trauma

In the literature, four mechanisms causing hydrodynamic trauma during have been identified:

- Metabolic inhibition may result on the interaction of the cells with turbulent eddies of similar size (Kunas & Papoutsakis 1990; Smith & Lilly 1990; Toma *et al.* 1991). Maiorella *et al.* (1991) studied the effect of isotropic turbulence in a filtration system by circulating animal cell cultures for 1 hour at several fluid velocities through a 2.44m length of 19.05 mm smooth walled pipe with a single 90° elbow. No cell damage was detected at Reynolds numbers below 71 000 and Kolmogorov eddy lengths greater than 12 micron.

- The interaction of cells with collapsing air bubbles at the medium interface is cited to induce nhibition (Handa-Corrigan *et al.* 1989; Oh *et al.* 1989; Boulton-Stone & Blake 1993; Garcia-Briones & Chalmers 1994).

- Within the filtration module, cells may be damaged by laminar shear stresses. Maiorella *et al.* (1991) studied the effect of laminar shear on cell viability in filtration systems by circulating viable animal cell cultures through selected filter modules at several flow rates for 20 passes and without permeate removal. Viable cells were counted before and after each circulation treatment and their ratio plotted versus the shear rate. Equivalent results were found for all filtration modules (flat plate and hollow fibre) and cell lines. Cells are not damaged in laminar flow at average wall shear rates of up to 3000 s^{-1} but are damaged at higher shear rates. The critical average shear rate of 3000 s^{-1} corresponds to an average shear stress on the cells of 2.5 N/m^2.

- Studies of hemolysis have shown that cells can be damaged by deformation of the cell membrane into a filter pore. For a cell settled on the filter above a pore, the portion of the cell membrane directly above the pore will be deformed under the force of the filter trans-membrane pressure. The cell can be lysed if the strain induced is sufficient to rupture the cell membrane. The strain induced is proportional to the product of the pore diameter and the trans-membrane pressuredrop. This phenomenon has been extensively reported in the plasmapheresis literature (Forstrom *et al.* 1975, Zydney and Colton; 1984). Lysis is a function of both the applied strain and the residence time of the cell above the pore.

6 Materials and Methods

6.1 Production of L-Lysine and Corynebacterium biomass in the bioreactor

The organism used in this study was a *Corynebacterium glutamicum* (ATCC 21253) obtained from the American Type Culture Collection (Rockville). A minimal media formulation as well as a typical industrial media formulation was used. The organism was cultivated in a five litre (working volume) Chemap bioreator equipped with two six bladed Ruston turbine impellers. The biomass was separated from the spent medium using

tubular ceramic membranes contained in a housing especially designed for this purpose. The fermentation recipe and protocol is discussed in Appendix A.

6.2 Quantification of the cell morphology

The image analysis of microbial systems has advanced rapidly over the last few years. Microbial systems in which image analysis has been successfully applied include the study of the morphology of single cell bacteria (James *et al.* 1995; Singh *et al.* 1990; Dickason 1998).

The diluted cell samples were laced on slides covered with a thin layer of agar (2%) to immobilise the cells (Huls *et al.* 1992). The presence of the agar on the slide ensures that the cells all lie in one plane while at the same time keeping the cells hydrated.

Bacteria were viewed using an Olympus BX-40 microscope fitted with bright field, dark field and phase contrast condensers. For the morphological studies all cells were viewed at 1000× magnification under phase contrast. Images from the microscope were acquired in colour using a Panasonic RGB digital camera and an IC-PCI-4× frame grabber. An Intel Pentium-133 PC with 16 Mb Ram was used to process the images using "Optimas" version 5.2.

The macro developed for the quantification of the morphology has been designed to operate semi-automatically (Dickason 1998). Intervention is required to exclude objects that have mistakenly been identified as whole cells or colonies.

The main processing steps are as follows (Dickason 1998):

1. Image capturing is performed by the operator who selects the image field and adjusts the focus. A total of 10 images were taken per sample. This was sufficient to ensure that the standard error in the cell length measurements was less than 5%. A semi-automated image acquisition system was installed which allowed a new image to be acquired every 6 seconds. A first audible tone indicated to the operator to move the stage and focus on a different area of the slide. A second tone indicated that image acquisition would take place within four seconds.

2. The next step in the macro was to binarize the image which meant that the objects of interest were assigned a grey level of 1 and the background grey level was set to 0. Before this could be done a set of filters were applied to the image. Firstly a "median" filter was applied which eliminated noise by replacing each pixel in the original image with the median luminance value of the surrounding pixels in the image. Any small debris in the image was thus erased whilst still preserving the edges. A "sharpen high" filter was then applied. This filter applied a strong edge sharpening grey scale convolution to the image. Edges were highlighted in such a way that the border of dark objects appeared darker and the border of light objects was lighter. The threshold values for binarization of the image were determined automatically such that the dark objects formed the foreground of the image.

3. The purpose of the next stage in the macro was to enhance the binarized image. This included steps to ensure that the cell membrane is closed. For colony

identification, binary "dilate", "fill" and "erode" functions were performed. For identification of single cell area a "fill" function was implemented.

4. To identify single cell areas, it was necessary to separate joined cells. For this the "watershed separation" algorithm was applied to the distance transform on the binary image. The distance transform is the distance between each white pixel in the image and the nearest black pixel. The distance is defined as the chamfer 5-7-11 distance as this is the closest approximation to the Euclidean distance possible while still using integer grey value. The distance transform works by assigning each pixel with a distance value of 5, 7, 11 or the nearest combination of these values. Once the distance transform has been computed the watershed algorithm is applied. A pre-flood of 8 was chosen for the watershed separation. This means that a value of 8 is added to each identified minimum in the inverted distance transform. If this is higher than the watershed separating that minimum from an adjacent watershed area, then that watershed area is eliminated and combined with the adjacent area. The pre-flood of 8 was found to prevent over-separation as a result of irregular cell boundaries. The "ultimate erosion method" was not found to perform well on the binary images of *C. glutamicum* cell needing separation. This was because the number of erosions was globally set and different clumps required a different number of erosions to become separated. Some cell clumps thus remained un-separated while others were over-separated.

5. The final stage in the macro was to assign labels to objects and to extract data to an MS Excel spreadsheet. Only those objects that satisfied the constraints of the object label were marked. In that way any debris left in the image was ignored in the morphology measurement. For colonies, the total tally and the colony areas were evaluated. Area, total tally, length, breadth, circularity and the elliptical fit were calculated for the single cells.

6.3 Metabolic pathway - flux estimation

Metabolic flux analysis have been be used as a technique to determine potential bottlenecks in the lysine production pathway (Vallino & Stephanopoulos 1991; Blumm & Stein 1982; Niranjan & San 1989; Tsai & Lee 1988b). Such bottlenecks can be targeted for further strain development. It can however also be used for metabolic state estimation in both control and optimisation of fermentations.

Although techniques such as metabolic control theory (Delgado & Liao 1991), biochemical systems theory (Sorribas & Savageau 1989), whole cell kinetic models (Jeong *et al.* 1990), stable (Inbar & Lapidot 1987; Marx *et al.* 1996) and ratio (Blumm & Stein 1982) isotope tracers, linear analysis (Palsson & Lightfoot 1985) have been applied to measure metabolic networks, significant information can also be obtained from mass balancing techniques (Niranjan & San 1989; Noorman *et al.* 1991; Papoutsakis 1984, Tsai & Lee 1988; Vallino & Stephanopoulus 1987; 1990; 1994; Verhoff & Spradlin 1976; Takiguchi *et al.* 1997; Gulik & Heijnen 1995). The latter are readily applied and do not require information regarding enzyme kinetics.

The mass balance technique employed by Vallino & Stephanopoulos (1993) to estimate flux distributions during the metabolic phases of *C glutamicum* is discussed here since it

served as the basis for a model used later in this study. The carbon flux through the primary metabolic pathways of *C glutamicum* was estimated from metabolite balances. The approach utilises constraints imposed by the biochemistry, pseudo steady state (PPS) approximation for intracellular metabolites and the measured accumulation rates of extracellular metabolites to generate flux distribution maps during the course of the fermentation. The accumulation rate of a metabolite in a metabolic network is given by the difference between the sum of all reactions producing the metabolite and the summation of all the reactions consuming the metabolite:

$$r_i(t) = \sum_j \alpha_j x_j(t) - \sum_k \alpha_k x_k(t) \qquad (5\text{-}32)$$

where x_i is the rate of flux through reaction j, α_j is the stoichiometric coefficient and r_i is the accumulation rate of metabolite i. The set of equations formed from such balances constructed for each metabolite in the network is represented in matrix notation by:

$$\mathbf{A}\mathbf{x}(t)=\mathbf{r}(t) \qquad (5\text{-}33)$$

where **A** is an m × n matrix of stoichiometric coefficients, **x**(t) an n-dimensional flux vector, and **r**(t) an m-dimensional metabolite accumulation rate vector.

The weighted least square solution to Equation 5-33, provided that m > n and **A** is of full rank, is:

$$\hat{\mathbf{x}}(t) = (\mathbf{A}^T\Psi^{-1}\mathbf{A})^{-1}\mathbf{A}^T\Psi^{-1}\bar{\mathbf{r}}(t) \qquad (5\text{-}34)$$

where Ψ is the measurement noise covariance matrix associated with **r** and the superscripts "^" and "¯" denote estimated and measured quantities respectively. The elements of **r**(t) are divided into two sub-vectors $\mathbf{r}_E(t)$ and $\mathbf{r}_I(t)$ which correspond to extracellular and intracellular metabolites respectively.

Accumulation rates for extracellular metabolites were derived from the slope taken between two consecutive concentration data points. A pseudo steady state approximation is used for intracellular metabolites so that $\mathbf{r}_I(t)$ is set to **0**. This approximation appears to be valid for most intracellular metabolites through the following analysis. To maintain a responsive metabolism, concentrations of intracellular metabolites in a reaction sequence range from 20% to 100% of their respective saturation constants (Atkinson 1977), which are typically less than 1mM and almost never exceed 10 mM (Jeong *et al.* 1990). Because observed metabolic fluxes are typically greater than 1.0 mmol.g $DCW^{-1}.h^{-1}$ and the volume of a cell is approximately 1 $\mu l.mg^{-1}$, fluxes based on intracellular volume are of the order of 1000 mM h^{-1}. Hence, an intracellular metabolite accumulation rate of 1 mM min^{-1}, which would significantly alter enzyme kinetics in less than 1 min, can be achieved with only a 6% difference between flows producing and consuming the metabolite. Consequently, metabolic control directives of the cell can be attained rapidly without significantly violating the PSS approximation (Vallino & Stephanopoulos 1993).

In the full metabolic network it is not possible to determine all the reaction rates solely from measured metabolite accumulation rates, even though there are more equations than unknown fluxes. This occurs when the rank of A is less than the number of unknown fluxes, n in which case A will be referred to as singular. The number of independent

measurements that must be added, or the number of reactions that must be removed or constrained, to render A non-singular is given by the dimension of the null space of A.

Because each of the null space vectors defines a set of fluxes that cannot be uniquely determined, inspection of these vectors identifies the reactions that are affected by introduction of additional constraints. Each of these sets is then referred to as a singular group. A singular group is eliminated by specifying one of the fluxes in the group (typically zero).

Several of these groups were identified from the initial metabolic network for *C. glutamicum* (Vallino & Stephanopoulos 1993):

- Fluxes in the two pathways that lead from meso-DAP to lysine cannot be uniquely determined. The meso-DAP dehydrogenase pathway was removed from the network, which is equivalent to combining the two pathways.
- Several singular groups were associated with the anaplerotic pathways. Vallino and Stephanopoulos (1993) proposed that the TCA cycle was the main oxidative pathway and thereby excluded the glyoxylate shunt from the metabolic network. The only anaplerotic reaction included in the network was the reaction of phosphoenolpyruvate to form oxaloaxetate. The singular group composed by phosphoenolpyruvate carboxylase (PPC), pyruvate kinase (PK) and oxaloacetate decarboxylase (OaADC) was resolved by omitting the reaction involving OaADC. OaADC was removed from the network, because growth could not occur on glucose if OaADC supported a significant flux.

The metabolic network of *C. glutamicum* (Figure 1-1) as constructed by Vallino and Stephanopoulos (1993) was found to be nonsingular. It consisted of 34 unknown fluxes with 37 balance equations. These are summarised in the Appendix F.

6.4 Experimental plan

The aim of the experimental work reported in this section is to investigate the impact of biomass recycling with cross-flow filtration on the fermentation performance of the cells. Two sets of batch fermentations at extreme level of hydrodynamic shear was compared to obtain a qualitative impact of filtration associated shear on fermentation performance. On the one extreme conventional batch fermentations were performed at mild agitated condition while on the other hand extreme filtration conditions was selected. A cross flow velocity of 7 m/s with a trans membrane pressure drop of 200 kPa was used. These conditions represent extreme values of hydrodynamic shear when compared to conventional cross flow filtration applications.

The biological response has been separated into an impact on the metabolism of the cells and an impact on the morphology. Further the impact on the physical properties of the fermentation medium is quantified. Each of these impacts is reported separately and quantified for a well-characterised lysine producing strain of *Corynebacterium glutamicum* (ATCC 21253). Finally, the effect of biomass recycling with cross-flow filtration on the fermentation performance of an industrial strain was investigated.

Batch cultivation of *C. glutamicum* (ATCC 21253) was carried out with and without the filtration loop at two stationary phase biomass concentrations (7 g/l DCW and 23 g/l DCW)

(Table 5-7). The different biomass concentrations were achieved by two initial charge media compositions. The stationary phase biomass concentration of 7 g/l was achieved using 20 g/l of glucose in the initial charge and 230 mg/l of L-threonine, 150 mg/l of L-methionine and 400 mg/l of L-leucine. The increased stationary phase biomass concentration of 23 g/l was achieved using 100 g/l of glucose in the initial charge and 330 mg/l of L-threonine, 750 mg/l of L-methionine and 1300 mg/l of L-leucine. To maintain a constant volume and biomass concentration both the permeate and the retentate from the filtration unit were returned to the bioreactor.

The Rushton turbine impellers in the bioreactor were operated at 800 rpm with 1 vvm of air supplied to the system. The cross flow filtration unit was equipped with a 0.45 micron tubular ceramic membrane with three tubes of 3.2 mm in diameter. The unit was operated at a cross flow velocity of 7 m/s and a trans-membrane pressure drop of 200 kPa.

Table 5-7. Experimental plant for the evaluation of the impact of filtration associated shear stress on the lysine fermentation performance

Designation	Filtration loop	Targeted stationary phase biomass concentration [g/l DCW]
Batch 1	Not running	7.0
Fil 1	Running	7.0
Fil 2	Running	7.0
Batch 3	Not running	23.0
Fil 3	Running	23.0

7 Results and Discussion

7.1 The effect of filtration associated shear stress on the cells morphology

The effect of the hydrodynamic stress generated in the filtration loop on the morphology of the cells throughout the growth cycle is apparent from Figures 5-2 to 5-5 through comparison of cell length, breadth, area and circularity.

At both stationary phase biomass concentrations (Figure 5-2), the cells were longest at the beginning of the cultivation during the lag phase and steadily decreased in length until the late exponential phase from where the cell length remained constant. A comparison of the low and higher biomass concentration shows that the recycled cells are longer throughout the growth cycle at the lower biomass concentrations. The set of fermentations at the increased biomass concentration showed that the recycled cells was longer than the cells cultivated in the conventional batch reactor for the first fifteen hours. From fifteen hours onwards no difference between the stressed and unstressed cells were detected. Wase and Patel (1985) have reported a similar effect of increased cell size under intense agitation conditions for *Bacillus cereus, Staphylocsus epidermis, Saccharomyces cerevisae* and *Eschericia coli.*

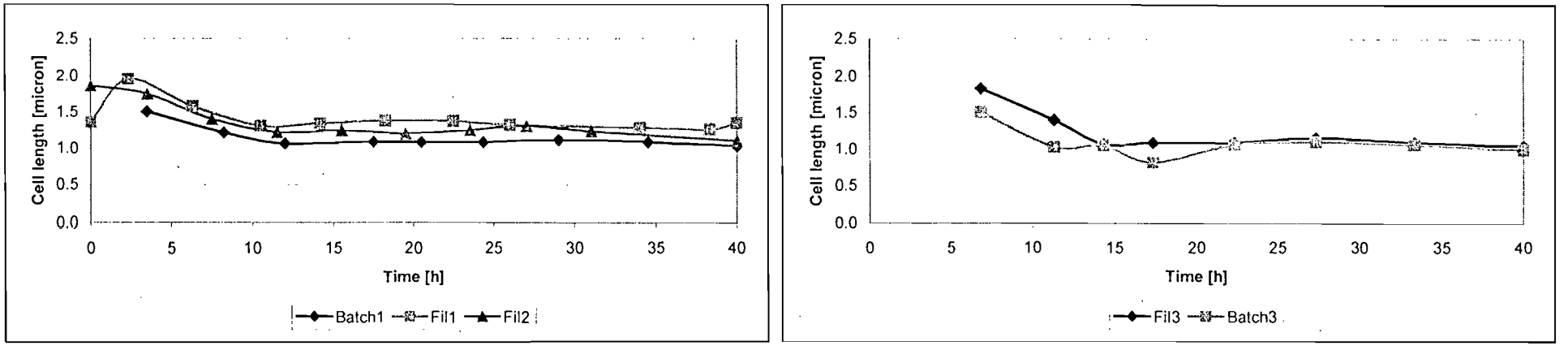

Figure 5-2. Comparison of cell length with cultivation time at different stationary phase biomass concentrations with and without hydrodynamic shear stress experienced by the cells in a tubular flow conduit. (Batch 1 – Conventional batch, 7 g/l DCW at stationary phase; Fil1 and Fil 2 – Batch fermentation with filtration, 7 g/l DCW at stationary phase; Batch 3 – Conventional batch, 23 g/l at stationary phase; Fil3 - Batch fermentation with filtration, 23 g/l DCW at stationary phase) Both the permeate and retentate were returned to the bioreactor.

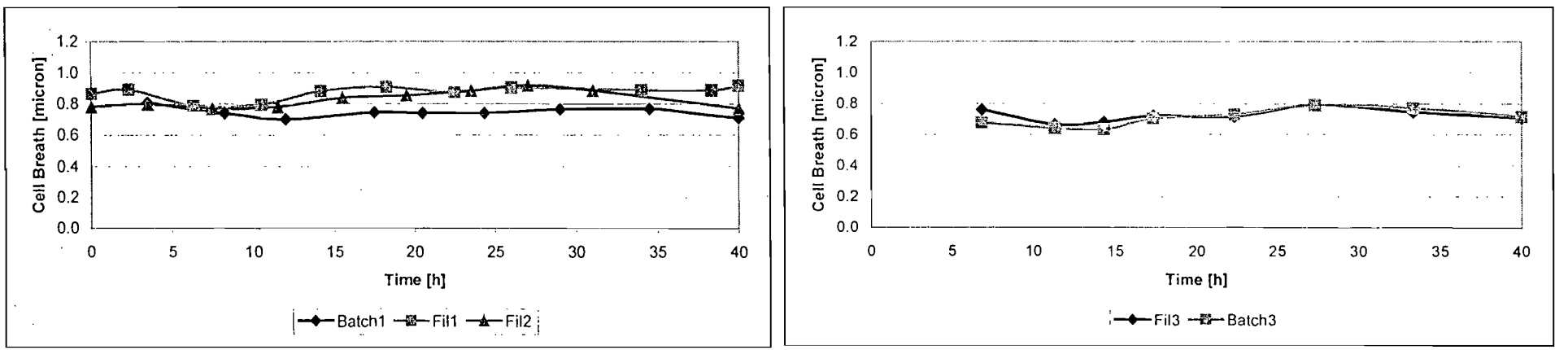

Figure 5-3. Comparison of cell length with cultivation time at different stationary phase biomass concentrations with and without hydrodynamic shear stress experienced by the cells in a tubular flow conduit. (Batch 1 – Conventional batch, 7 g/l DCW at stationary phase; Fil1 and Fil 2 – Batch fermentation with filtration, 7 g/l DCW at stationary phase; Batch 3 – Conventional batch, 23 g/l at stationary phase; Fil3 - Batch fermentation with filtration, 23 g/l DCW at stationary phase) Both the permeate and retentate were returned to the bioreactor.

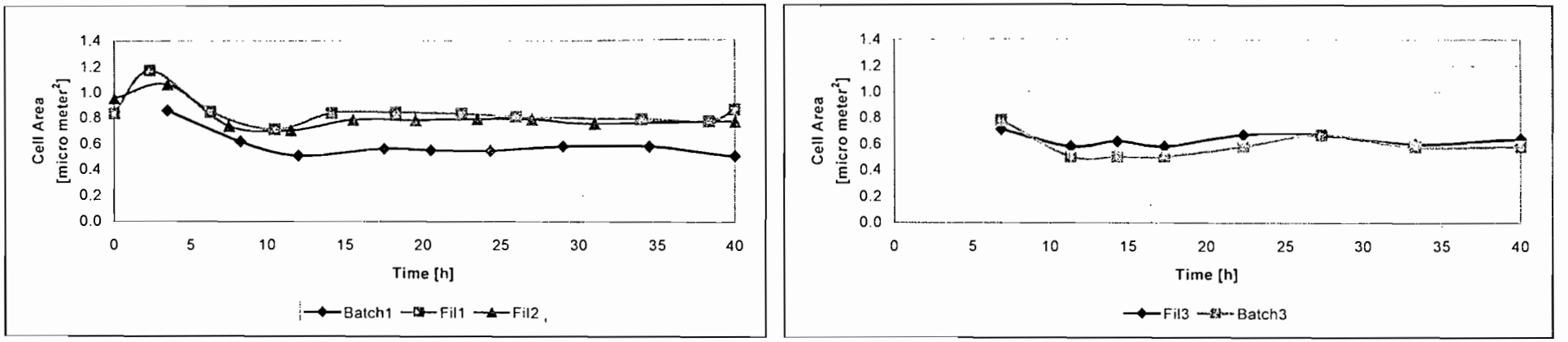

Figure 5-4. Comparison of cell area with cultivation time at different stationary phase biomass concentrations with and without hydrodynamic shear stress experienced by the cells in a tubular flow conduit. (Batch 1 – Conventional batch, 7 g/l DCW at stationary phase; Fil1 and Fil 2 – Batch fermentation with filtration, 7 g/l DCW at stationary phase; Batch 3 – Conventional batch, 23 g/l at stationary phase; Fil 3 - Batch fermentation with filtration, 23 g/l DCW at stationary phase) Both the permeate and retentate were returned to the bioreactor.

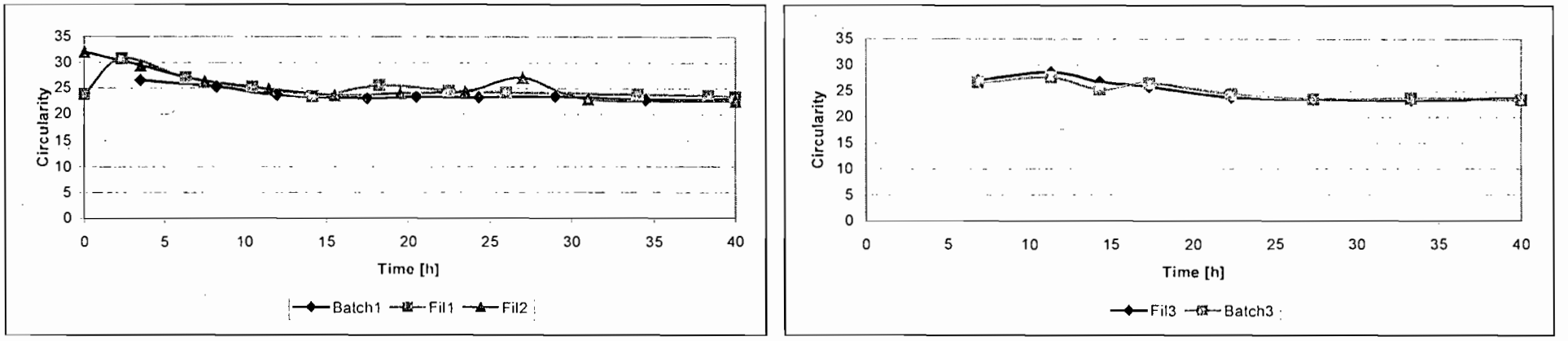

Figure 5-5. Comparison of cell circularity with cultivation time at different stationary phase biomass concentrations with and without hydrodynamic shear stress experienced by the cells in a tubular flow conduit. (Batch 1 – Conventional batch, 7 g/l DCW at stationary phase; Fil1 and Fil 2 – Batch fermentation with filtration, 7 g/l DCW at stationary phase; Batch 3 – Conventional batch, 23 g/l at stationary phase; Fil3 - Batch fermentation with filtration, 23 g/l DCW at stationary phase) Both the permeate and retentate were returned to the bioreactor.

Figure 5-3 shows that cell breath goes through a minimum during exponential growth increasing slightly during the stationary phase. At lower biomass concentrations the recycled cells were wider than the cells cultivated in the stirred tank bioreactor.

The cell area trends (Figure 5-4) are similar to the cell length plots, with a minimum cell area during exponential growth.

The results for the cell circularity index are presented in Figure 5-5. The deviation of the shape of the cell from a perfect circle (Circularity = 12.57) is greatest during the lag phase. No significant difference exists for stressed and unstressed cells.

In conclusion the cell volume increases under increased hydrodynamic stress. Increased shear does not alter the cell shape. It is therefore reasonable to assume that the increased volume may be due to increased water uptake into the cell as suggested by Wase and Patel (1985) rather than alterations in the cytoskeleton or cell wall structure. Furthermore, it can be concluded that the effects of hydrodynamic shear stress are reduced at increased biomass concentrations.

7.2 The effect of filtration associated shear stress on the cells metabolism

To evaluate the effect of the hydrodynamic shear stress caused by the flow of the cell suspension flow through a tubular conduit, two sets of batch fermentation were performed. In each set, the fermentation performance of a conventional batch process was compared to that in which a cross-flow filtration loop was included. Both filtrate and retentate were returned to the reaction vessel to maintain cell concentration and reactor volume. In the first set a stationary phase biomass concentration of 7 g/l DCW was achieved (Batch 1, Fil1, Fil2). In the second set the stationary phase biomass concentration was increased to 23 g/l DCW (Batch3 and Fil3).

7.2.1 Extracellular metabolite consumption and excretion rates

The metabolism of the cells was characterised by dry cell weight measurements, substrate (threonine and glucose) uptake and product (L-Lysine) excretion rates.

Typical profiles for a batch fermentation of ATCC 21253 as published by Kiss and Stephanopoulos (1991) are shown in Figure 5-6.

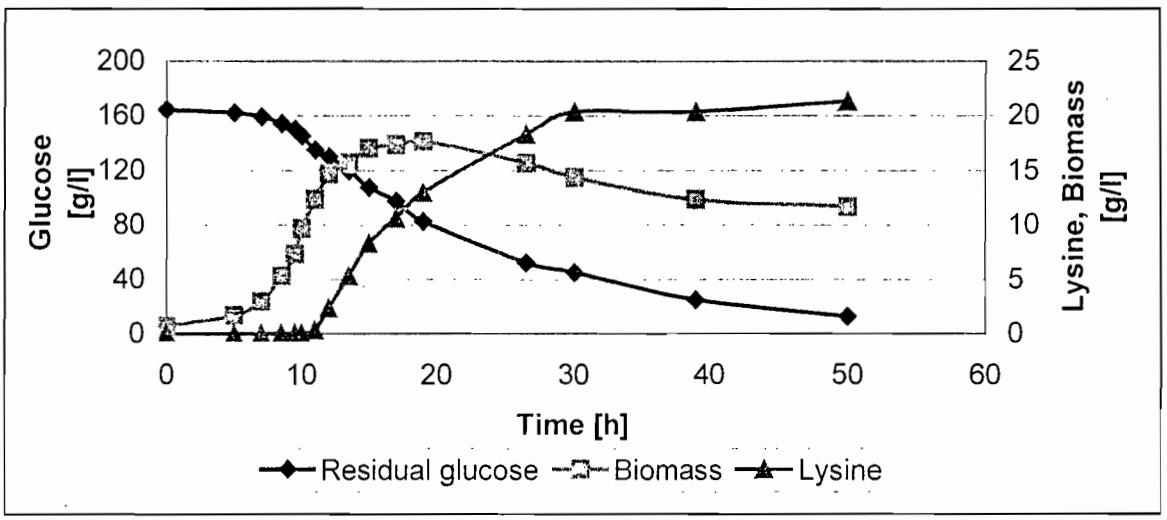

Figure 5-6. Typical batch fermentation profile for *C. glutamicum* (ATCC 21253) as reported by Kiss & Stephanopoulos (1991)

7.2.1.1 Biomass production rate

The biomass profiles for the four fermentations are presented in Figure 5-7. From Figure 5-7, it can be seen that at low biomass concentration, the fermentation with the increased hydrodynamic shear produced more biomass. At the higher biomass concentration (Figure 5-7) increased steady state biomass concentrations, a similar effect was visible in the late exponential and early stationary phase. This difference in biomass concentration disappeared after 25 hours as the cells entered the death phase. There was no difference in the time taken to threonine depletion between the stressed and "conventional" fermentation (Figure 5-8) for both the high and low stationary phase biomass concentrations. The specific growth rate (Table 5-8) of the cells exposed to increased hydrodynamic conditions in the membrane unit was however reduced.

Table 5-8. Maximum specific growth rate of cells cultivated under stressed and unstressed conditions at two stationary phase biomass concentrations using a cross flow filtration unit. (Batch 1 – Conventional batch, 7 g/l DCW at stationary phase; Fil1 and Fil 2 – Batch fermentation with filtration, 7 g/l DCW at stationary phase; Batch 3 – Conventional batch, 23 g/l at stationary phase; Fil3 - Batch fermentation with filtration, 23 g/l DCW at stationary phase) Both the permeate and retentate were returned to the bioreactor.

Fermentation	Stationary phase biomass concentration [g DCW/l]	Time to reach stationary phase [h]	Apparent specific growth rate measured during exponential growth phase [h^{-1}]
Batch 1	6.1 ± 0.5	12 ± 2	0.38 ± 0.2
Fil 1	7.4 ± 0.5	18 ± 2	0.34 ± 0.2
Fil2	7.8 ± 0.5	19 ± 2	0.34 ± 0.2
Batch 3	23.2 ± 0.5	14 ± 2	0.34 ± 0.2
Fil 3	28.0 ± 0.5	18 ± 2	0.28 ± 0.2

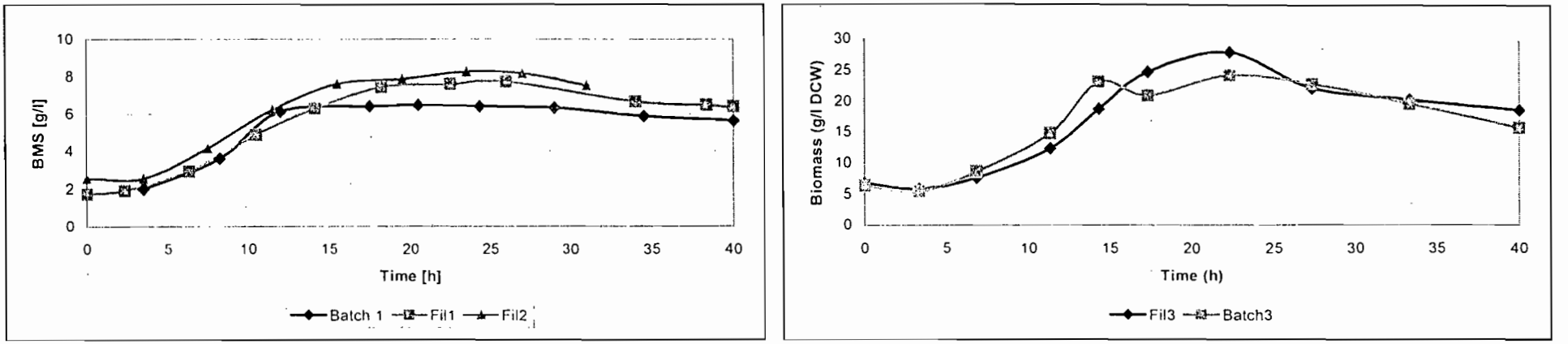

Figure 5-7. Biomass (Dry cell weight) concentration for batch fermentations as a function of time. Batch 1 represents a conventional batch run while Fil1 and Fil2 are repeats of batch fermentations with recycling through the filtration loop. Batch 3 represents a conventional batch fermentation at a higher stationary phase biomass concentration while Fil3 is a batch fermentation at a higher stationary phase biomass concentration with recycling through the filtration loop. For the batches with the recycling loop both the permeate and retentate was returned to the bioreactor

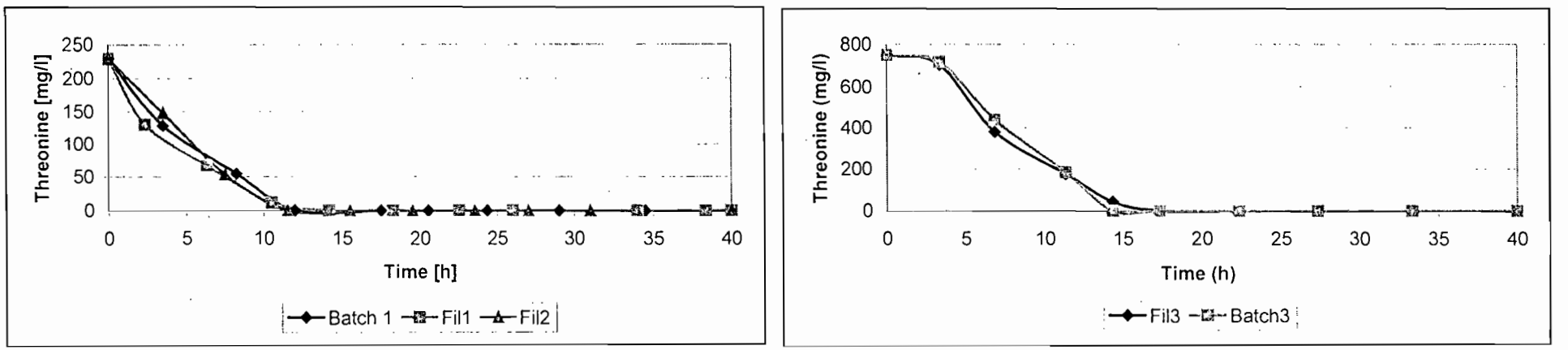

Figure 5-8. Extracellular L-Threonine concentration (g/l) for batch fermentations as a function of time. Batch 1 represents a conventional batch run while Fil1 and Fil2 are repeats of batch fermentations with recycling through the filtration loop. Batch 3 represents a conventional batch fermentation at a higher stationary phase biomass concentration while Fil3 is a batch fermentation at a higher stationary phase biomass concentration with recycling through the filtration loop. For the batches with the recycling loop both the permeate and retentate was returned to the bioreactor.

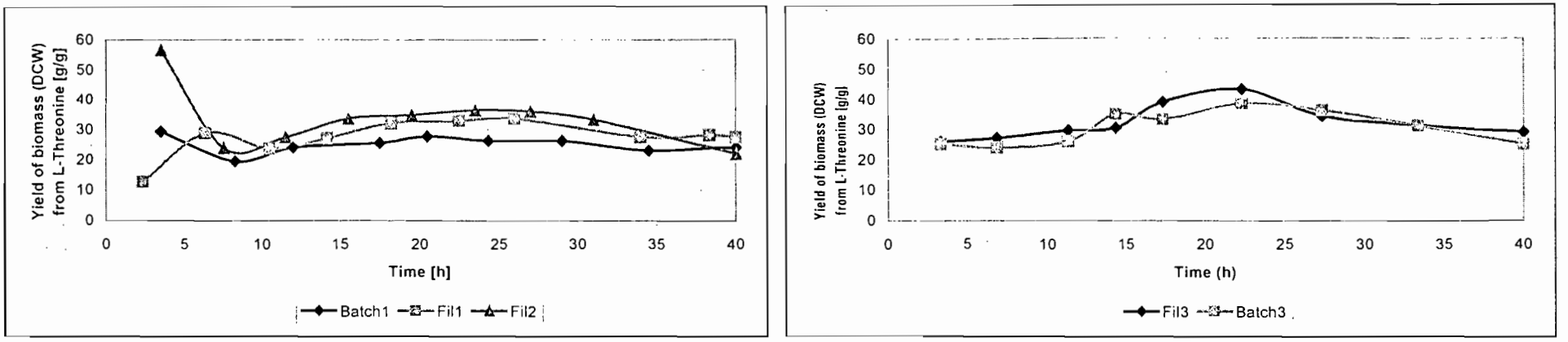

Figure 5-9. The yield of biomass from threonine as a function of batch age. Batch 1 represents a conventional batch run while Fil1 and Fil2 are repeats of batch fermentations with recycling through the filtration loop. Batch 3 represents a conventional batch fermentation at a higher stationary phase biomass concentration while Fil3 is a batch fermentation at a higher stationary phase biomass concentration with recycling through the filtration loop. For the batches with the recycling loop both the permeate and retentate was returned to the bioreactor.

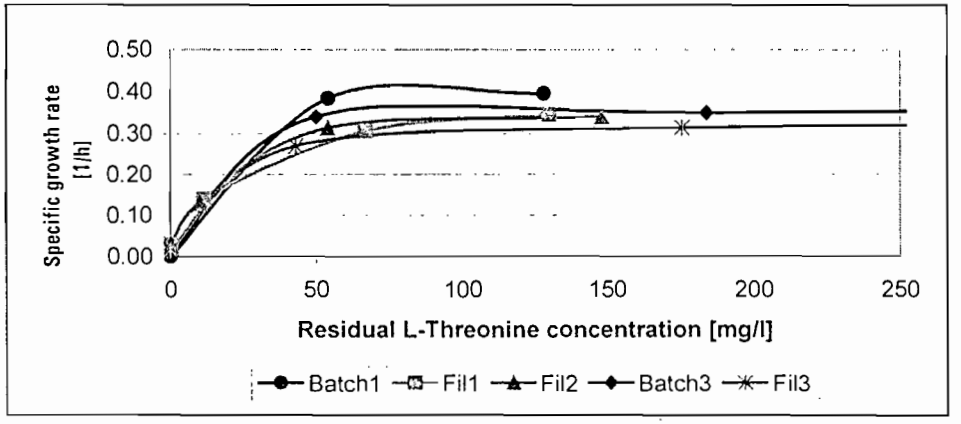

Figure 5-10. The specific growth rate as a function of the residual L-Threonine concentration. Batch 1 represents a conventional batch run while Fil1 and Fil2 are repeats of batch fermentations with recycling through the filtration loop. Batch 3 represents a conventional batch fermentation at a higher stationary phase biomass concentration while Fil3 is a batch fermentation at a higher stationary phase biomass concentration with recycling through the filtration loop. For the batches with the recycling loop both the permeate and retentate was returned to the bioreactor.

Due to the auxothrophy of the cells, biomass production (cell growth) depends on the availability of threonine. This implies that biomass growth is expected to cease on threonine depletion. This can be seen for both the batch runs in the conventional stirred tank reactor. On exposure to the increased hydrodynamic shear, the cells in the flow loop continued to grow beyond the point of threonine depletion. The yield of biomass from threonine was increased in both the cases where the cells on exposure to shear in the filtration loop (Figure 5-9). This effect was more pronounced at low stationary phase biomass concentrations.

Thus, although the apparent specific growth rate of the hydrodynamically stressed cells was reduced, the stationary phase biomass concentration on exposure to increased hydrodynamic stress increased relative to the conventional batch and subsequently the yield of biomass from threonine increased.

There are three possible explanations for these observations:

- Increased hydrodynamic stress causes the cell wall to leak the essential amino acids required for growth and further cell growth occurred. This could lead to an increased yield of biomass from L-Threonine

- Increased hydrodynamic stress could lead to cell lysis. Once again the lysed cells released essential nutrients that allows cell growth beyond the limited supply of the auxothrophic amino acids. In this case the cell debris were also detected by the dry cell weight analysis method

- The third option is that the cell internally strengthened its cell wall with polysaccharides (opposed to protein). This implies that on exposure to increased hydrodynamic stress the cell weight increases although the number of cell remains fixed. It also implies that more carbohydrates would be required to build a unit of cell weight. From Figure 5-12 it can be seen that the yield of biomass from glucose decreased on exposure to increased hydrodynamic stress

When the specific growth rate of the cells is plotted against the residual threonine concentration (Figure 5-10) it becomes evident that the growth rate can be modelled using Monod equation with L-Threonine as limiting substrate.

$$\mu = \frac{1}{X}\frac{dX}{dt} = \frac{\mu_{max}[Thr]}{k_m + [Thr]} \qquad (5\text{-}35)$$

where [Thr] is the extracellular threonine concentration in mg/l. The maximum growth rate (μ_{max} in h^{-1}) and a saturation constant (k_m in mg/l) were determined for each experiment. These results are summarised in Table 5-9.

Table 5-9. Growth parameters of *C. glutamicum* in batch fermentations in the absence and presence of filtration through a tubular ceramic membrane unit. The correlation coefficient indicates the extent to which the data fits the Monod growth model.

Batch	Specific growth rate μ_{max} [h^{-1}]	Saturation constant k_m [mg/l]	Correlation coefficient R^2
Batch1	0.40	2.97	0.997
Fil1	0.32	17.13	0.998
Fil2	0.34	17.85	0.995
Batch3	0.36	3.08	0.962
Fil3	0.30	7.00	0.997

The increased hydrodynamic stress reduced the maximum specific growth rate of the cells. This effect can be explained by incorporation of a death rate constant (k_d) in the range 0.06 to 0.08 h^{-1}. The saturation constant (k_m) increased when the cells were exposed to increased hydrodynamic conditions. This could be due to improved mass transfer characteristics of the recycling bioreactor.

7.2.1.2 Carbohydrate Uptake rate

The glucose uptake rate during the exponential growth phase was increased on cell recycle by cross flow filtration (Figure 5-11). The yield of biomass on glucose during this phase was reduced for cell recycle compared with the standard batch (Figure 5-12). This implied that more glucose was consumed per cell. It can be postulated that the additional glucose is required to repair the cell wall on exposure to hydrodynamic stress or to strengthen the cell wall to withstand the hydrodynamic stress. The carbon to protein ratio of the cell composition is therefore altered by the presence of hydrodynamic stress. This is confirmed by the both the increased yield of biomass from glucose and the biomass from threonine (Figure 5-9)

7.2.1.3 Lysine Production rate

The lysine concentration (Figure 5-13) was lower in batches where cells were exposed to increased hydrodynamic shear than in the conventional batch reactor. At higher biomass concentration, the effect was limited to the initial stages of lysine production. During the latter stages of the fermentation, the lysine concentration of the stressed batch was lower than that of the conventional batch although the rate of lysine production was independent of the hydrodynamic conditions.

The specific lysine productivity (Figure 5-14) of the cells exposed to increased hydrodynamic stress in the flow loop was reduced compared to that of the cells cultivated in the conventional stirred tank reactor. This effect was more pronounced in the low biomass concentration batches. For the conventional fermentation, the maximum specific productivity of the cells was observed around 17 hours after which this declines rapidly. For the higher biomass concentration batch, the

maximum specific productivity was reduced but high levels of specific productivities maintained over a longer period. Lysine production in the conventional batches only commenced after threonine depletion due feedback inhibition of lysine production by threonine. With cell recycle, the start of lysine production was delayed till the completion of cell growth.

The cumulative yield of lysine from glucose (Figure 5-15) for the conventional fermentation increased from zero to a maximum in the late exponential phase, thereafter declining to a fixed value. For the lower biomass concentration batches, the yield of the fermentation with cell recycle did not match the performance of the conventional batch. For the higher biomass case, the cells exposed to increased hydrodynamic stress on cross flow filtration produced lysine at a reduced yield during the initial period of lysine production. During the late stationary and death phase of the fermentation no difference in the yield of lysine from sugar was detected between the conventional batch and the batch with recycle.

During the latter stages of the lysine fermentation, the effect of biomass production on the lysine yield is eliminated and the observed instantaneous yield is closely related to the actual lysine production yield. From the data presented, it is evident that for the lower biomass concentration batches the specific lysine production rate as well as the yield of lysine from sugar was reduced on increased hydrodynamic stress. At the higher stationary phase biomass concentrations, these effects are less marked than at lower concentrations.

In the higher biomass fermentations, the specific biomass growth rate and the yield of biomass on threonine and the yield of biomass from glucose was reduced relative to the control during the initial stages of the fermentation. During the latter half of the fermentation (after establishment of the bulk of the cell population), no effect of increased hydrodynamic stress on the cells were detected.

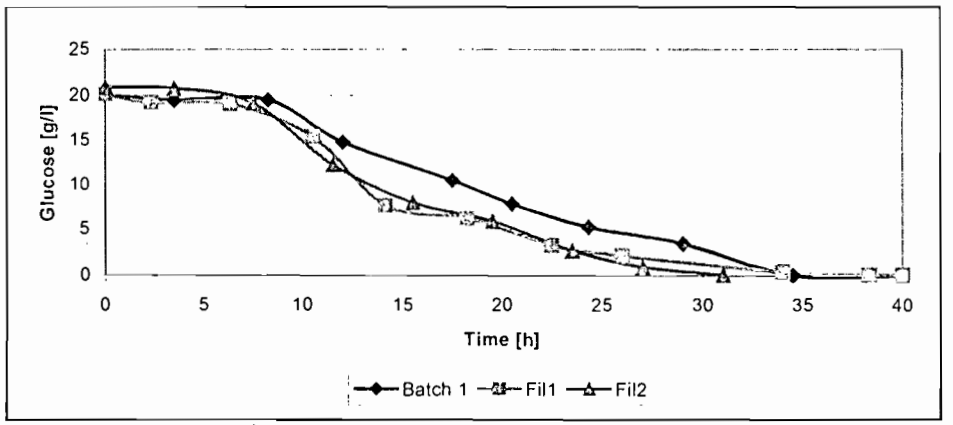

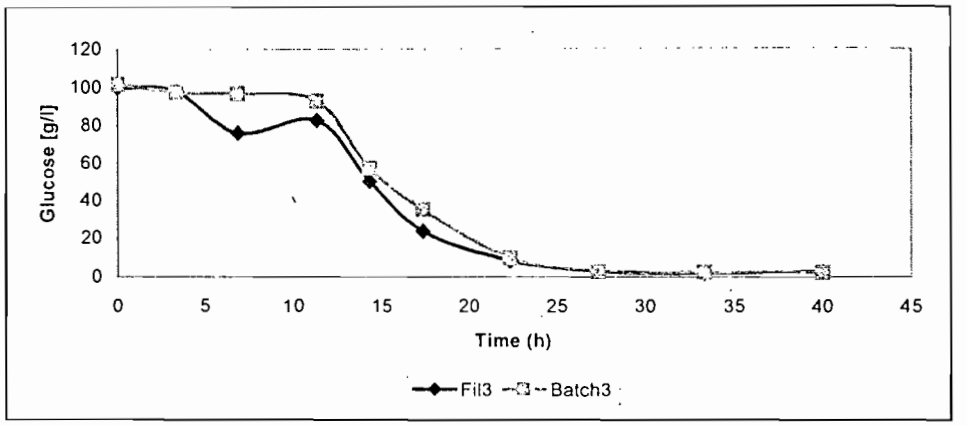

Figure 5-11. The residual glucose concentration for batch fermentations at different stationary phase biomass concentrations with and without filtration. Batch 1 refers to the conventional batch at low stationary phase biomass concentration while Fil1 and Fil2 refer to the batch at low stationary phase biomass concentration with the recycling loop running. Batch 3 refers to the conventional batch at a higher stationary phase biomass concentration while Fil3 refers to the batch at a higher stationary biomass concentration with the filtration unit running. The retentate and the permeate from the filtration unit were returned to the bioreactor.

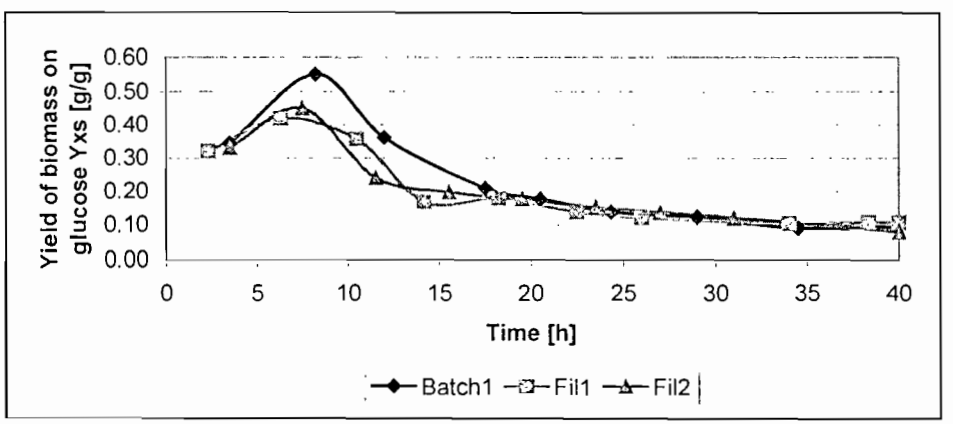

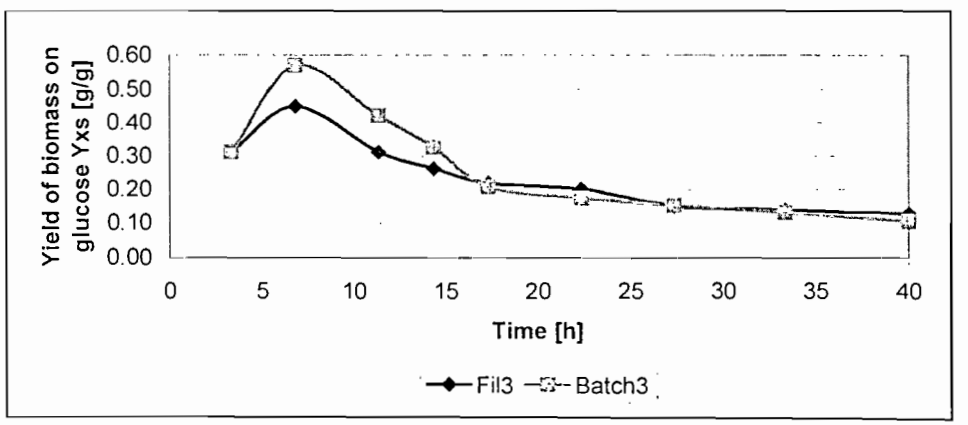

Figure 5-12. The yield of biomass from glucose (m/m) as a function of cultivation time in a bioreactor with and without the filtration loop running. Batch 1 refers to the conventional batch at low stationary phase biomass concentration while Fil1 and Fil2 refer to the batch at low stationary phase biomass concentration with the recycling loop running. Batch 3 refers to the conventional batch at a higher stationary phase biomass concentration while Fil3 refers to the batch at a higher stationary biomass concentration with the filtration unit running. The retentate and the permeate from the filtration unit were returned to the bioreactor.

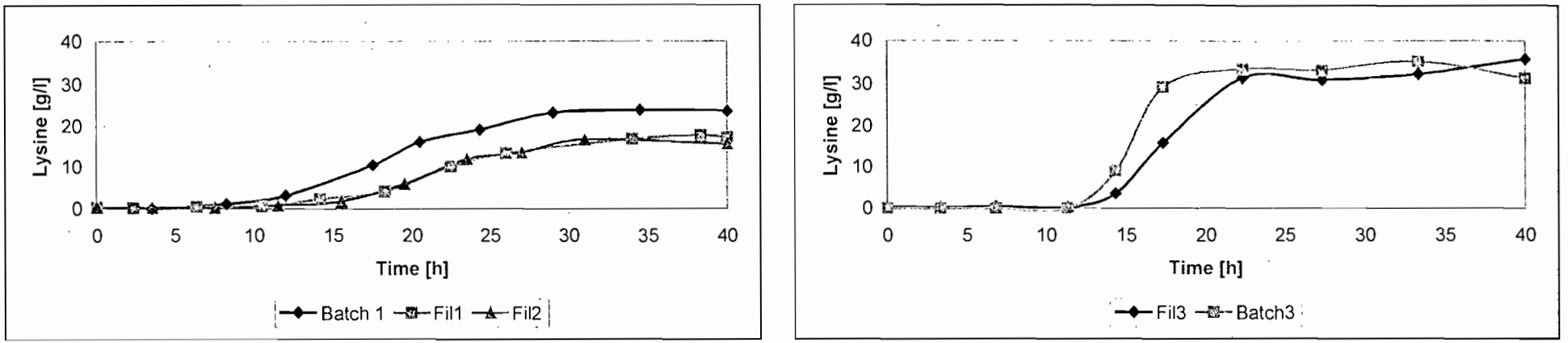

Figure 5-13. The lysine concentration as a function of cultivation time in a bioreactor with and without the filtration loop running. Batch 1 refers to the conventional batch at low stationary phase biomass concentration while Fil1 and Fil2 refer to the batch at low stationary phase biomass concentration with the recycling loop running. Batch 3 refers to the conventional batch at a higher stationary phase biomass concentration while Fil3 refers to the batch at a higher stationary biomass concentration with the filtration unit running. The retentate and the permeate from the filtration unit were returned to the bioreactor.

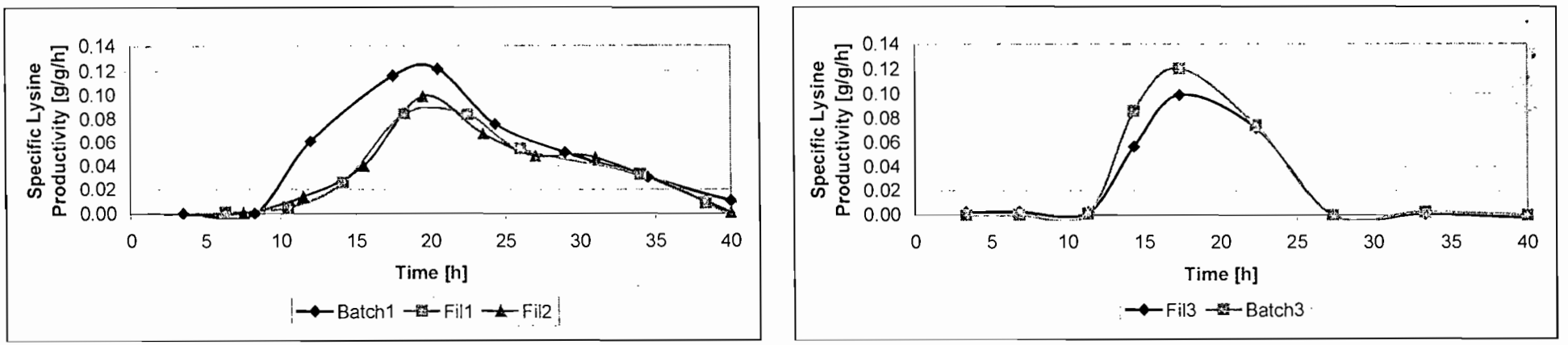

Figure 5-14. The specific lysine productivity (g/g/h) as a function of cultivation time in a bioreactor with and without the filtration loop running. Batch 1 refers to the conventional batch at low stationary phase biomass concentration while Fil1 and Fil2 refer to the batch at low stationary phase biomass concentration with the recycling loop running. Batch 3 refers to the conventional batch at a higher stationary phase biomass concentration while Fil3 refers to the batch at a higher stationary biomass concentration with the filtration unit running. The retentate and the permeate from the filtration unit were returned to the bioreactor.

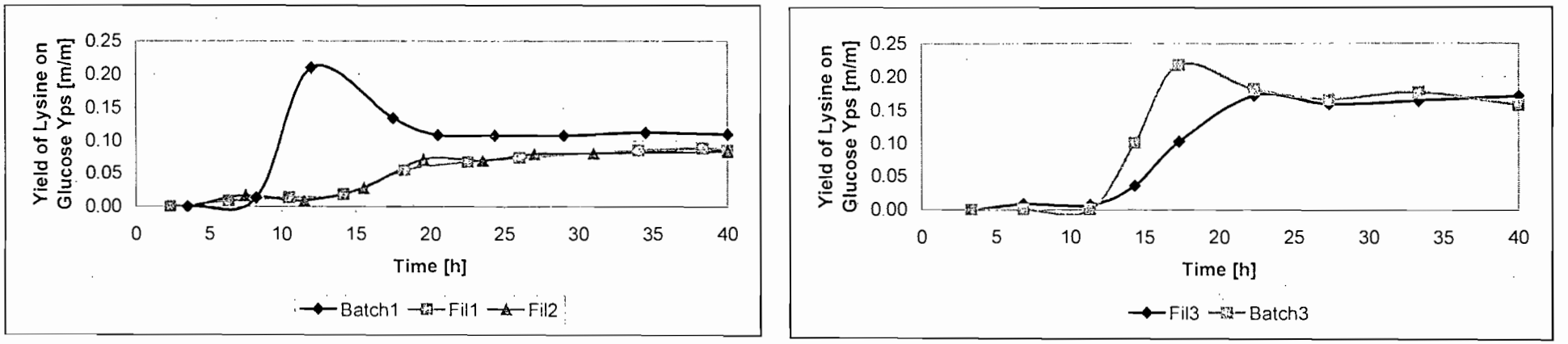

Figure 5-15. The yield of lysine from glucose (m/m) as a function of cultivation time in a bioreactor with and without the filtration loop running. Batch 1 refers to the conventional batch at low stationary phase biomass concentration while Fil1 and Fil2 refer to the batch at low stationary phase biomass concentration with the recycling loop running. Batch 3 refers to the conventional batch at a higher stationary phase biomass concentration while Fil3 refers to the batch at a higher stationary biomass concentration with the filtration unit running. The retentate and the permeate from the filtration unit were returned to the bioreactor.

7.2.2 Distribution of the central carbon flux

The fermentation data provided convenient sets of extracellular flux measurements (glucose, L-lysine, free and saline nitrogen, oxygen and carbon dioxide) to elucidate the impact of increased hydrodynamic stress caused by biomass recycling on the biochemistry of L-lysine synthesis through intracellular flux analysis. This method combines the known metabolic pathways of the organism with a pseudo-steady state approximation for intracellular metabolite concentrations to generate a mathematical representation of the metabolic flows. The equations comprising the network are summarised in Appendix F. The network includes the main energy and metabolite generating bioreactions of glycolysis, the pentose phosphate cycle and the tricarboxylic acid cycle as well as the metabolic pathway via the aspartate family of amino acids leading to lysine.

Biomass synthesis is treated as a lumped reaction drawing energy and metabolites from the main metabolic branches according to the stoichiometry given by Stephanopoulos (1993) (C = 47.6%, H = 6.46%, O = 31.0%, N = 11.8%, Ash = 3.14%). The ATP requirement in the lumped biomass equation is the theoretical amount corresponding to an ATP yield of 28 g of biomass synthesised per mole of ATP consumed and the efficiency of oxidative phosphorylation or P/O ratio, is taken as 2 mol ATP formed per atom of oxygen reduced.

A redundancy analysis, to test the consistency of the measurement set, was carried out in those instances when the number of measurements available rendered the system over-determined. This technique calculates a data set contingency index, which indicates whether the extracellular metabolite flux measurement set satisfies biochemical constraints at a given level of statistical confidence. For three degrees of freedom, the consistency index must be less than the chi-square value of 6.25 at a 90% confidence interval. (Vallino & Stephanopoulos 1994; Vallino & Stephanopoulos 1990; Walker *et al.* 1982).

7.2.2.1 Consistency Index

The distribution of carbon through the central metabolism was determined for five "snap shots" taken during the five metabolic phases: the early logarithmic growth phase, late logarithmic growth, stationary phase and the late stationary or death phase. The phase was determined from the biomass growth curve. The early log phase was identified as being the first three sample points (taken at two hourly intervals) that could be fitted to an exponential expression while the late stationary phase represented the last three sample points (taken at two hourly intervals) during the logarithmic growth phase that could be fitted to an exponential equation. The stationary phase was identified as the period during which the biomass did not change by more than the error associated with the analysis method (0.5 g DCW/l). The point at which the biomass concentration started to decline was defined as the start of the late stationary or death phase. The consistency indices for each of the "snap shots " taken were determined and are presented in Figure 5-16. All the consistency indices were below 6.25, indicating that the balance equations used to describe the observed

measurements were suitable. The larger errors were associated with the late stationary or death phase. The errors for the fermentations exposed to increased hydrodynamic stress were larger than those of the conventional batch fermentations. This could indicate that other metabolic pathways, not described by the suggested profile, could be active when the cells are exposed to hydrodynamic shear.

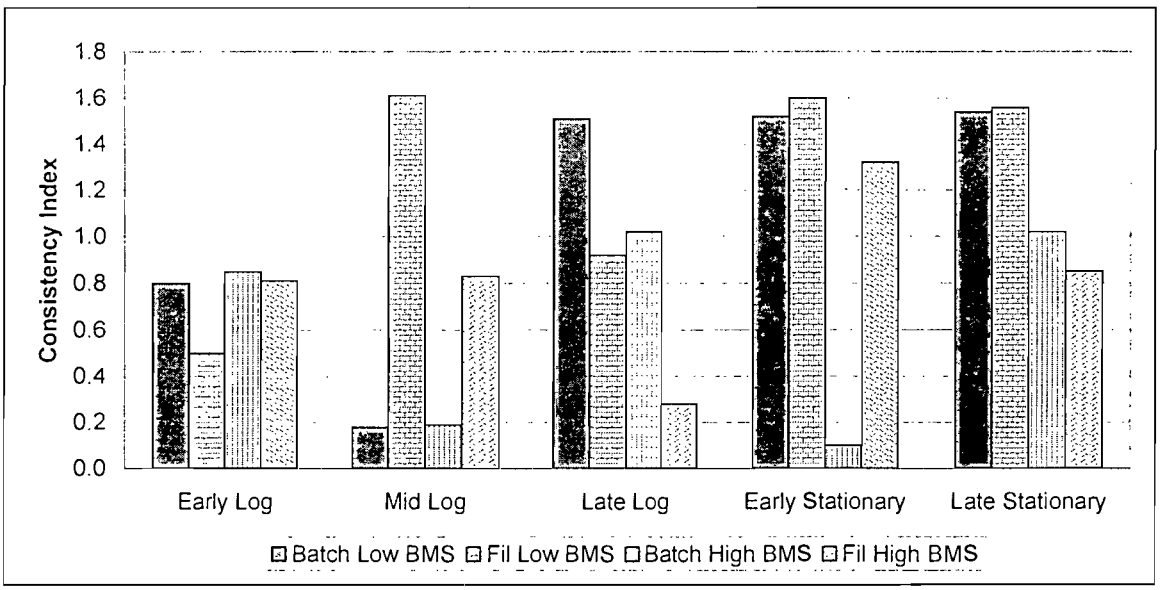

Figure 5-16. Consistency index for the carbon flux distribution through the central metabolism of *C. glutamicum* during the different metabolic phases of a batch fermentation.

7.2.2.2 The availability of ATP

Previous researchers (Toma *et al.* 1991, Ando *et al.* 1991) report that the extracellular hydrodynamic conditions can influence the availability of intra- and extracellular ATP. The aforementioned analysis allows for calculation of the amount of ATP required for biomass synthesis and biomolecule synthesis, as well as the amount of ATP produced by the fuelling reactions. Other ill-defined ATP consumption processes such as maintenance, futile cycles, transport costs or energy required to maintain concentration gradients have not been accounted for in the overall ATP consumption calculation. Instead, an excess of ATP, over the theoretical limit is determined. This excess ATP is then consumed in a virtual reaction to satisfy the pseudo steady state assumptions. The excess ATP removal rate for the four batches as a function of metabolic phase is presented in Figure 5-17. The values of the excess ATP removal rate determined by Vallino & Stephanopoulos (1993) are presented in Table 5-10 below. These rates are very similar to the rates reported for the batch reactions in Figure 5-17 from the results obtained in this study.

Table 5-10. Excess ATP removal rate as reported by Vallino & Stephanopoulos (1993)

Metabolic State	Normalised excess ATP removal rate
Early logarithmic	666
Mid logarithmic	537
Late logarithmic	830
Early Stationary	613

The excess ATP for cells exposed to increased hydrodynamic stress due to cell recycle was reduced relative to that of the "conventional batch" (Figure 5-17). This implies that the increased hydrodynamic conditions reduced ATP generation through the TCA cycle. The reduction in ATP formation has been explained by Toma *et al.* (1991) to be a result of a shift in cellular metabolism from oxidative phosphorylation to substrate level phosphorylation and glycolysis. Toma *et al.* (1991), proposed that this shift in metabolism is induced by turbohypobiosis. This term is used to describe inhibition of microbial growth and inhibition caused by shear forces damaging cell membranes and limited mass transfer in stagnant eddies of microscales of turbulence.

According to Vallino & Stephanopoulos (1991), the true maintenance requirements of ATP can probably best be estimated during rapid growth or product synthesis when futile cycles are expected to be low. Consequently the ATP flux during the mid exponential growth phase should best reflect the maintenance requirements. From a theoretical yield analysis a lysine yield of approximately 65% could be supported (assuming 530 normalised units of ATP for maintenance) while generating sufficient ATP to satisfy maintenance requirements under a zero growth condition. This indicates that for the conventional batch fermentations, the lysine yield was not ATP limited. For the cases where the cells were exposed to increased hydrodynamic stress, a maximum lysine yield of 55% could be expected. Since the observed yield in both the conventional batch fermentation and the fermentation with cell recycle (and increased hydrodynamic stress) was less than the maximum yield that can be supported by the availability of ATP, the yield limitation is expected to result from sub-optimal partitioning of carbon at the principal nodes.

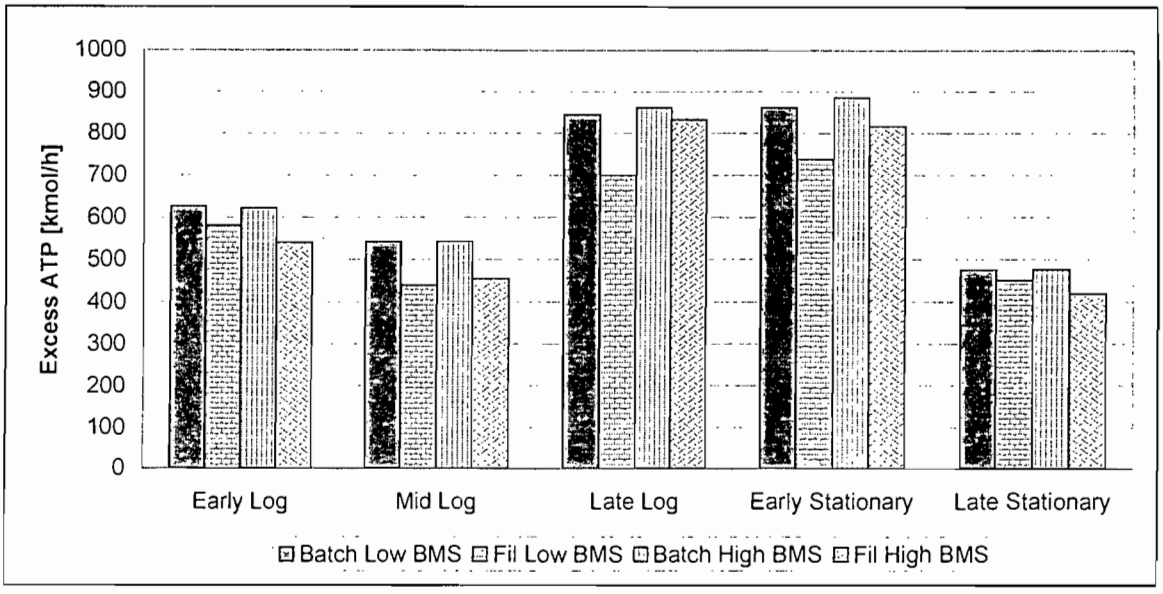

Figure 5-17. Excess ATP removal rate (kmol/h) (normalised by sugar uptake = 100 kmol/h) during different metabolic stages and hydrodynamic conditions.

7.2.2.3 Principle node analysis

The metabolic network contains about 35 nodes or branch points. A theoretical yield analysis reveals that nodal split rations (the carbon flux through a branch normalised by the flux into the node) change at only a few nodes, termed the principle nodes, while partitioning of carbon at all other nodes remains independent of product yield. Partitioning of carbon at the principle nodes must be optimal for maximal lysine yield. Rigid principle nodes, i.e. those principle nodes at which attempts to change the nodal split ratios are resisted by the imposed nodal control architecture, therefore limit the lysine yield.

The carbon split ratios at the following principle nodes (Figure 5-18) were evaluated to determine the impact of biomass recycling on the metabolism of *Corynebacterum glutamicum*: glucose-6-phosphate, phosphoenolpyruvate (PEP), pyruvate (Pyr) and oxaloacetate (OaA).

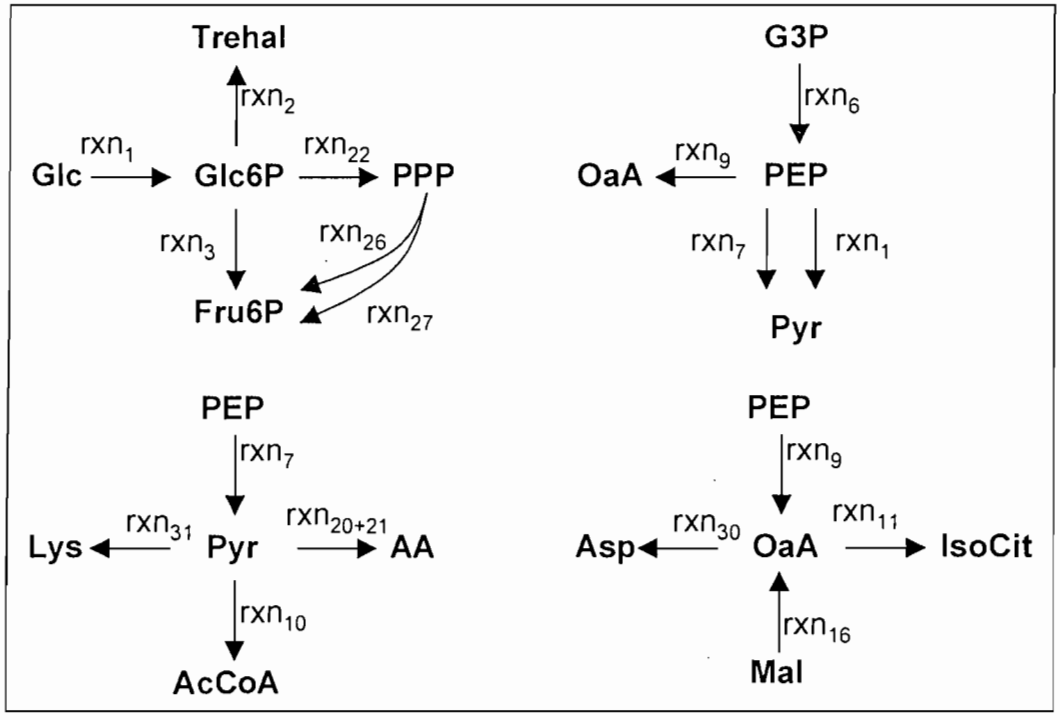

Figure 5-18. Principle nodes for the central metabolism of *C. glutamicum*

- Glucose-6-phosphate (Glc6P)

The carbon split at this node determines the carbon flux through the pentose phosphate pathway (PPP) (Figure 5-18). The carbon flux through PPP generates two NADPH molecules while EMP generates two NADH molecules. This means that the flux of carbon through PPP is driven by the requirement for NADPH which are consumed by ammonia assimilation (NH_3 : NADPH), valine production (Val : NADPH), lysine production (Lys : 3 NADPH) and biomass production (BMS : 0.476 NADPH).

If it is assumed that the fraction of Fru6P recycled back into the PPP equals the fraction of glucose that enters the PPP the fraction of glucose consumed that enters the PPP (f_{PPP}) as a function of the network fluxes is:

$$f_{PPP} = \frac{rxn_{22}}{rxn_1 + rxn_{26} + rxn_{27}} \tag{5-36}$$

where the reactions are presented in Appendix F.

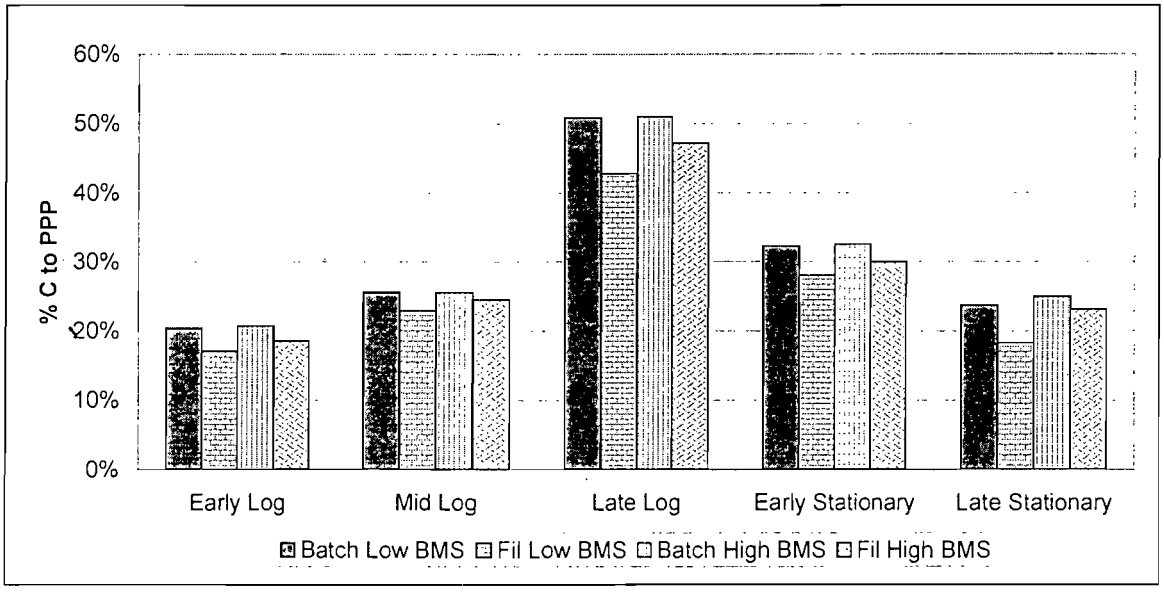

Figure 5-19. Fraction of glucose that enters the PPP (f_{PPP})

The percentage of carbon directed to PPP is presented in Figure 5-19. For quantitative verification, the flux distributions were compared with the radioactive (^{14}C) and stable (^{13}C) isotope tracer measurements cited in the literature for glutamic acid bacteria as well as the data reported by Vallino & Stephanopoulos (1993). Table 5-11 lists the predicted and measured fraction of glucose that entered PPP as a function of metabolic state. From Table 5-11 it is clear that the estimated flux distributions for the conventional batch fermentation are consistent with the data reported in literature

Table 5-11. Measured and reported fraction of glucose that enters PPP as a function of metabolic state.

Reference	Method	Organism	Mid log	Late log	Early Stat	Late Stat
Vallino & Stephanopoulos 1993	Bioreaction network analysis	*C. glutamicum*	23	49	33	27
Oishi & Aida 1965	Radio tracer	*B. ammonigenes*				26
Walker et al. 1982	Stable glucose tracer	*Microbacterium ammoniaphilum*	13			
Ishino et al. 1986	Stable glucose tracer	*C. glutamicum*		44		
Yokota & Shiio 1988	Stable glucose tracer	*C. glutamicum*		44		
This Study	Bioreaction network analysis	*C. glutamicum*	23-26	42-51	28-32	18-25

The transition from mid to late exponential phase corresponds to a marked increase in the flux of carbon through PPP. This is most marked for the

conventional batch fermentations without cell recycle. The shift corresponds to the start of lysine production. The 50% PPP split-ratio at the GLU6P node and the yield of NADPH of (1.38 mol/mol glucose) consumed indicates that a lysine yield of 53% could be supported if biomass synthesis were zero. This potential analysis illustrates that this node is potentially flexible, implying that NADPH availability does not limit the lysine yield.

The flux of carbon through PPP is reduced at increased hydrodynamic stress. In the experiment performed at the lower biomass concentration, a maximum flux of carbon through PPP of about 43% was achieved. This corresponds to a maximum theoretical yield of 42%. As this is still higher than the yield achieved, it can be concluded that the availability of NADPH does not limit the lysine yield for cells exposed to hydrodynamic shear forces experienced in cross flow filtration. It should however be noted that the regulatory mechanism of this node is influenced by the extent of hydrodynamic stress experienced by the cells and that at increased hydrodynamic shear, the NADPH requirement of the cells is either reduced or the production of NADPH is limited.

- Phosphoenolpyruvate (PEP)

The carbon from both PPP and EMP meet at 3-phosphateglycerate (G3P) and is transformed into PEP. PEP then splits into oxaloacetate (OaA) and pyruvate (Pyr). According to Kiss & Stephanopoulos (1992), this node seems to be regulated at a 20-25% split of carbon to OaA. The results from this study for the split ratio of PEP to OaA instead of Pyr are presented in Figure 5-20.

Vallino & Stephanopoulos (1993) reported a slight increase in this split during the transition from growth to lysine production (14% to 28%). In a previous study in continuous culture, Kiss & Stephanopoulos (1992) reported that the split ratio at this node appeared fairly constant over a wide range of specific growth rates. This indicated that the node may be rigid, i.e. the fraction of carbon entering the PEP node, which leaves via a particular branch is strictly regulated at a relatively constant value, and is insensitive to metabolic pertubations. Increased hydrodynamic stress did not have an impact on the split of carbon at this node, supporting the potential rigid nature of the node.

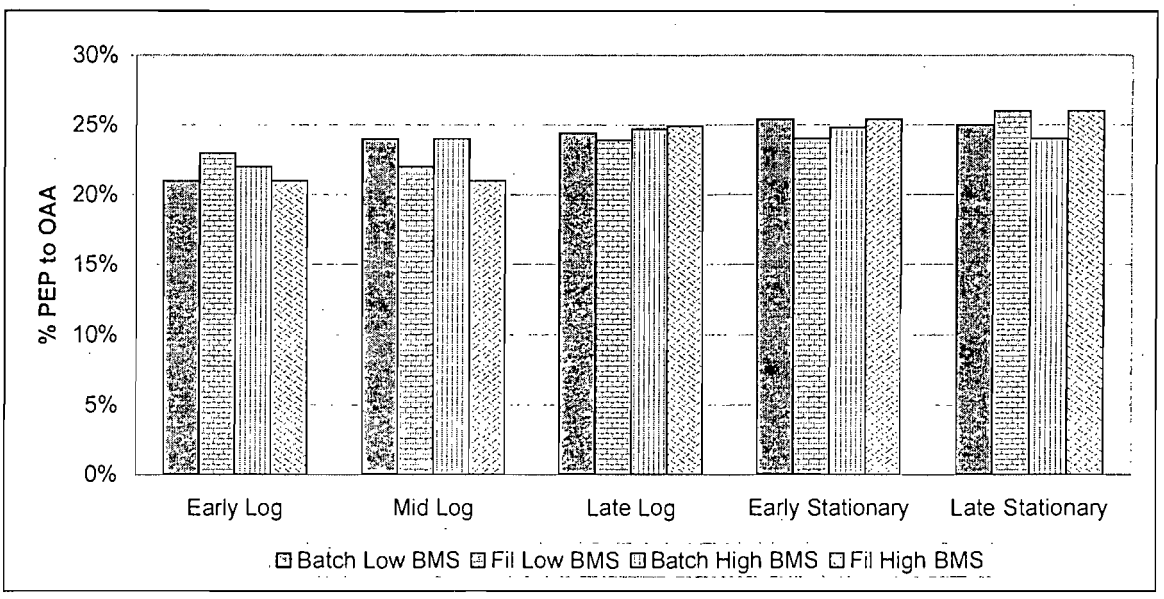

Figure 5-20. PEP principle node split ratios for the lysine fermentation as a function of metabolic phase.

- Pyruvate (Pyr)

At the pyruvate node, a three-way split in the carbon flux is found. In the first branch pyruvate reacts with aspartate (ASP) to form lysine. In the second, pyruvate is converted to Acetyl CoA (AcCoA), and lastly some of the pyruvate is converted into additional amino acids for biomass synthesis. The lysine branch split ratio at the pyruvate principal node shows a maximum of 31% during the late exponential phase (Figure 5-21). The observed yield during that period was 0.22 g/g (Figure 5-15). Although it could seem that the observed yield is limited by the split ratio at the pyruvate node this is not necessarily the case since the flux at the pyruvate node could also be limited by the split ratio at the PEP or the OaA node. The flux of carbon to lysine at the Pyr node (Figure 5-21) and the flux of carbon to AcCoA (Figure 5-22) was reduced at increased hydrodynamic shear, while the flux of pyruvate into other amino acids (Figure 5-23) increased.

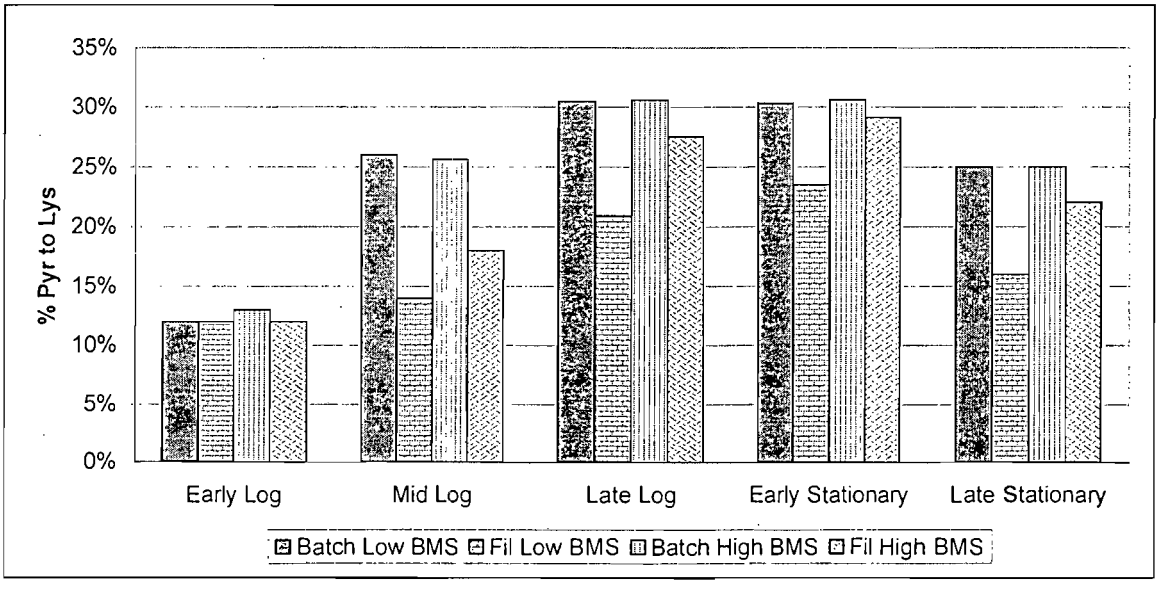

Figure 5-21. Percentage of pyruvate (Pyr) that is converted to Lysine

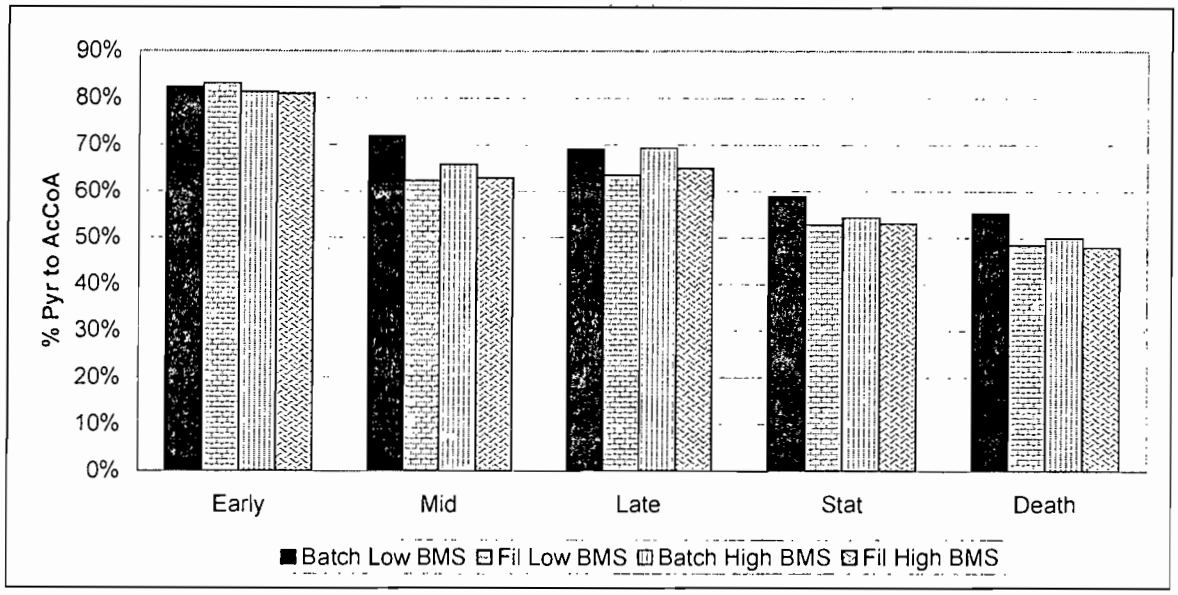

Figure 5-22. Percentage of pyruvate (Pyr) converted into AcetylCoA (AcCoA)

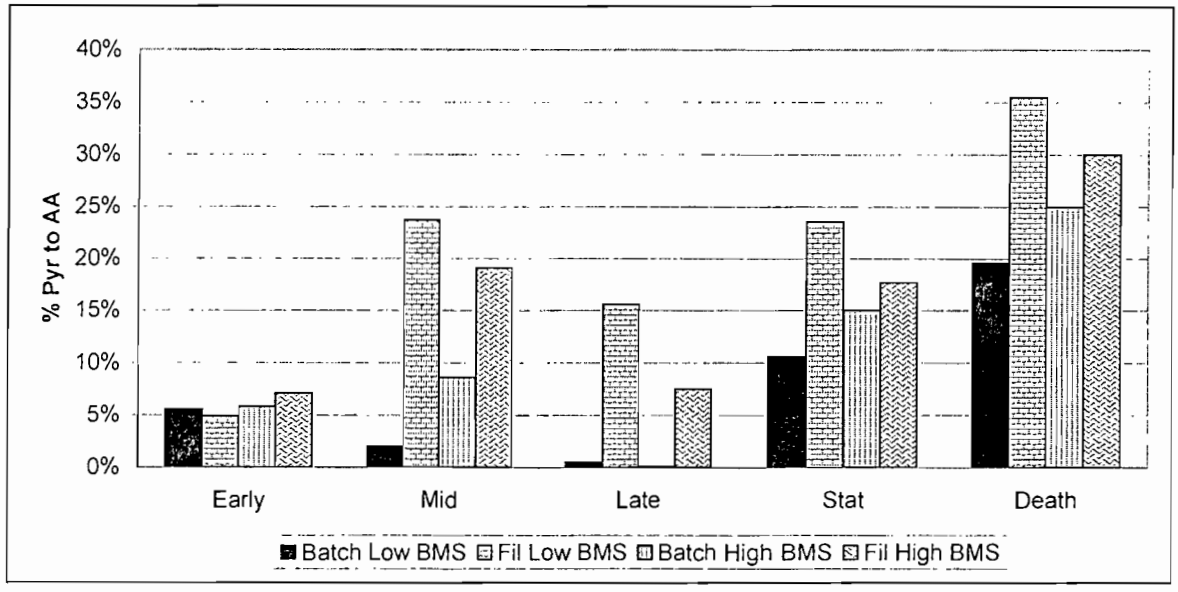

Figure 5-23. Percentage of pyruvate (Pyr) converted into other amino acids (AA) such as valine and alanine

- Oxaloacetate (OaA)

Carbon enters the oxaloacetate (OaA) node from phosphoenolpyruvate (PEP) through an anaplerotic reaction and from malate, a tri-carboxylic acid (TCA) intermediate. Carbon is then distributed to aspartate for lysine synthesis or returned to the TCA cycle. The carbon split ratio at OaA is depicted in Figure 5-24.

During the early and mid logarithmic phase, the split ratio was around 50%. The split ratio of OaA converted to aspartate (Asp) increased during the late logarithmic phase at the onset of lysine production.

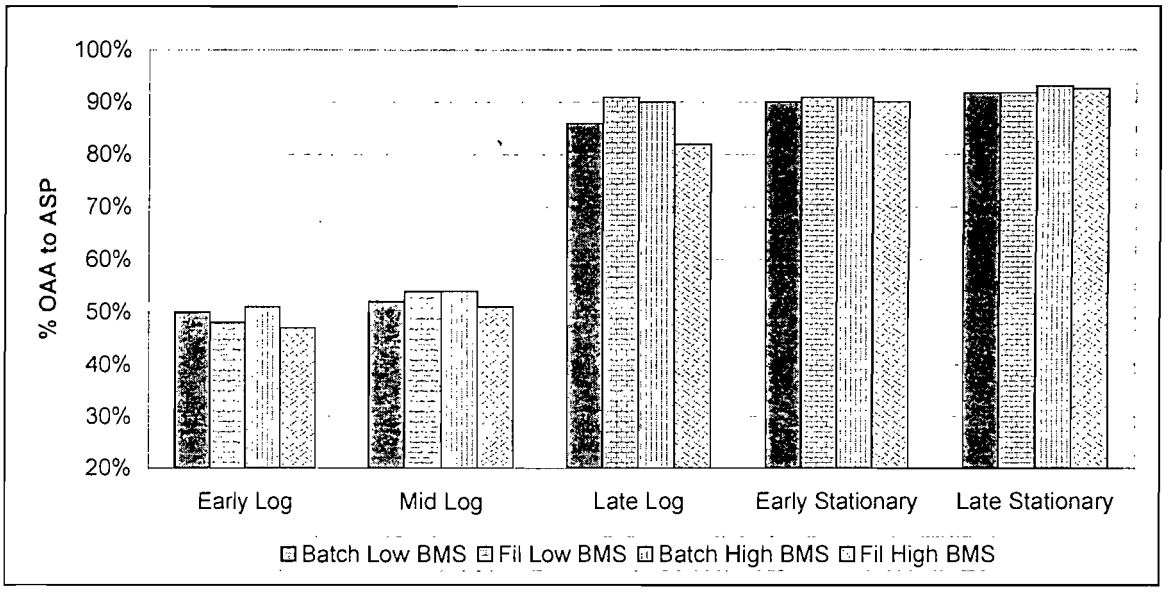

Figure 5-24. Fraction of oxaloacetate (OaA) converted to aspartate (Asp)

Corresponding to the results presented by Vallino & Stephanopoulos (1993), the split between Asp and Glut synthesis is equal on growth in the absence of lysine formation. When lysine synthesis begins, the majority of OaA synthesised from PEP leads to Asp formation. Kiss & Stephanopoulos (1992) studied *C. glutamicum* under continuous growth conditions and found that the fraction of OAA converted to ASP was a function of the specific growth rate. In this study a similar relationship was found as depicted in Figure 5-25. As the specific growth rate increases the fraction of OAA derived from PEP, which ends up as ASP decreases. This result illustrates the increase in the carbon fraction allocated to lysine synthesis as the specific growth rate decreases. This relationship was not influenced by increased hydrodynamic conditions.

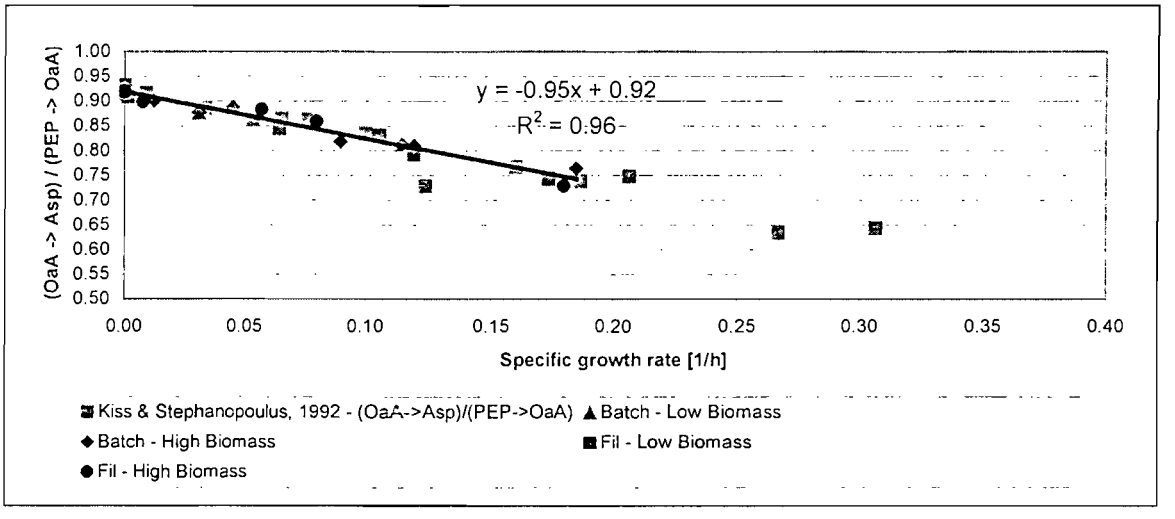

Figure 5-25. Fraction of OaA converted to Asp as a function of the specific growth rate.

The fraction of OAA formed that is converted to ASP (OaA is formed by carboxylation of PEP and by oxidation of malate in the TCA cycle) is approximately constant between 30 and 40% as displayed in Figure 5-26. This implies high TCA activity and subsequently nearly all the PEP carboxylated (to form OaA) is further converted to Asp. Significant quantities of glucose must therefore be oxidised in the TCA cycle to maintain the constant split at the OAA node. This fraction is not influenced by increased hydrodynamic shear experienced in the filtration unit.

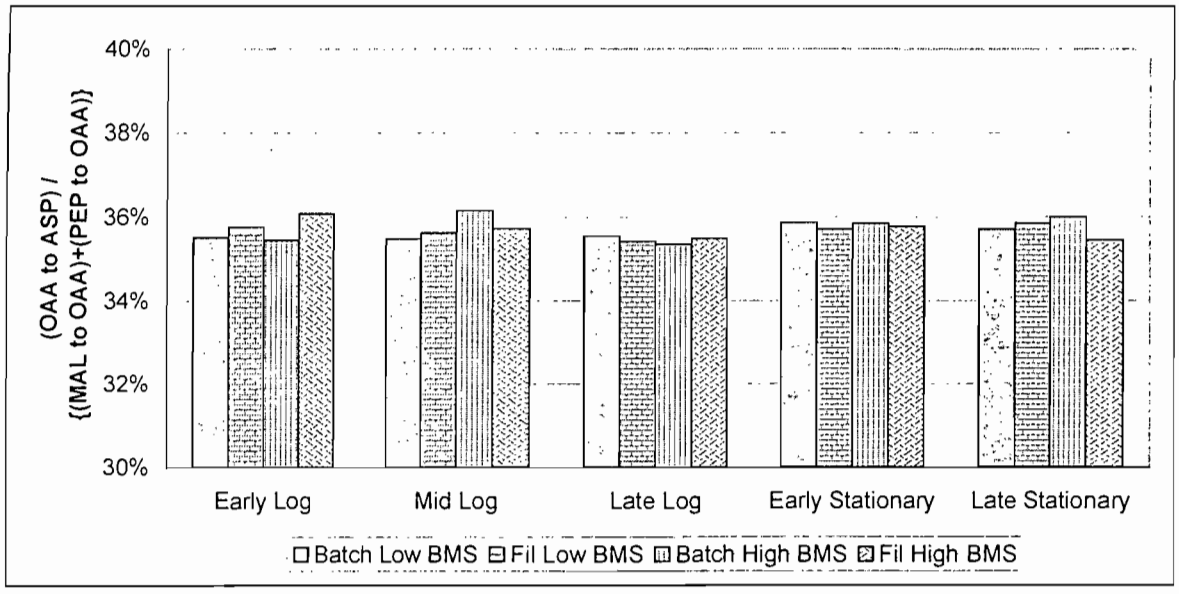

Figure 5-26. Fraction of OAA converted to ASP

7.2.2.4 Discussion

The excess ATP for cells exposed to increased hydrodynamic stress due to cell recycle was reduced relative to that of the "conventional batch" (Figure 5-17). This could either imply that the increased hydrodynamic conditions reduced ATP generation through the TCA cycle or that the usage of ATP as explained by the model increased. The reduction in ATP formation has been explained by Toma *et al.* (1991) to be a result of a shift in cellular metabolism from oxidative phosphorylation to substrate level phosphorylation and glycolysis. Substrate level phosphorylation includes the addition of inorganic phosphate without the respiratory chain.

Although the flux of carbon through PPP is reduced at increased hydrodynamic shear, the flux distribution of 43% could theoretically support a yield of lysine on glucose of 42% (Figure 5-19). Since the observed yield was substantially less than the theoretical maximum as estimated from the carbon split ratio at the Glc6P node it can be concluded that the availability of NADPH does not limit the lysine yield. The regulatory mechanism of this node is influenced by hydrodynamic shear. At increased hydrodynamic shear, the NADPH requirement of the cells is either reduced or the production of NADPH is limited.

It is postulated that the requirement for NADPH of the cells exposed to hydrodynamic shear in the filtration module is reduced. Increased hydrodynamic shear causes an increase in the flux of carbon towards the cell wall to either repair or strengthen the cell wall. The flux of carbon used to build the cell wall is directed through diaminopimelate, an intermediate in the conversion of aspartate into lysine (Figure 1-2).

The initial evidence of the strengthening theory is found in the increase in the yield of biomass on threonine and a reduction in the yield of biomass on glucose. This could support an increase in the carbon to protein ratio of the cells.

Although the specific glucose consumption rate increased on exposure to hydrodynamic shear in the membrane unit, it did not have an impact on the split of carbon at the PEP node. Thus hydrodynamic shear does not influence the ratio of fluxes to Pyr and OaA from PEP. If the total flux of glucose increases (due to increased specific glucose consumption rate), the absolute flux of carbon from PEP to Pyr and OaA increases proportionally. At the Pyr node the (Figure 5-21) flux of carbon to lysine and the flux of Pyr to AcCoA (Figure 5-22) was reduced at increased hydrodynamic shear, while the flux of pyruvate into other amino acids (Figure 5-23) increased. Thus, at increased shear the total flux of carbon toward the TCA cycle decreased. This is confirmed by the reduction in the availability of ATP.

The fraction of oxaloacetate converted to aspartate was however not influenced by increased hydrodynamic shear experienced in the filtration unit. Thus, the flux of carbon to Asp and subsequently Lysine should decrease.

The actual values of the carbon flux through the principle nodes are presented in Table 5-12 for the low biomass concentration fermentation during the late exponential period (between 15 and 20 hours).

Table 5-12. Comparison of the carbon flux through the principle nodes for a conventional batch and a batch reactor coupled to a cross-flow filtration loop, with both the permeate and retentate returned to the Bioreactor

Description	Unit	Conventional Batch	Batch with cross-flow filtration
Specific glucose consumption rate	g/g/h	0.16	0.18
Flux from PEP to Pyr	g/g/h	0.12	0.14
Flux from Pyr to Lys	g/g/h	0.04	0.03
Yield predicted by bioreaction network	g/g	0.24	0.16
Yield as measured (Figure 5-15)	g/g	0.21	0.08
Flux from Asp to Cell wall from measured yield	g/g/h	0.004	0.014

Table 5-12 indicates that the yield predicted by the bioreaction network for the cells exposed to hydrodynamic shear is higher than the actual measured yield. From Figure 5-16 it was found that the consistency index for the sheared

batches were higher (less accurate) than that of the conventional batches. It is postulated that the flux of pyruvate to lysine as predicted by the bioreaction network is an oversimplification. The bioreaction network does not compensate for the conversion of Asp into cell wall material opposed to lysine. The conversion of Pyr to lysine as predicted by the model is therefore increased relative to the actual conversion to compensate for the model's inability to divert carbon from Asp into cell wall material.

7.3 The impact of cell recycling on the physical properties of the fermentation broth

The membrane retains more than 99% of the biomass. The membrane is however permeable to lysine and the other amino acids as well as all the carbohydrates present in the bioreactor. As some of the fermentation broth is removed from the bioreactor without removing the biomass, it follows that the biomass concentration should increase proportionally.

A consequence of the increased biomass concentration is the impact on the dissolved oxygen (DO) concentration in the fermenter. Based on DO measurements a reduction in the available oxygen concentration was seen with increased biomass concentration. Preliminary investigations have shown that this decrease in the oxygen transfer rate is a result of decreased liquid phase mass transfer coefficient ($k_l a$), rather than a decrease in the saturated oxygen concentration of the fermentation broth (Stieger 1998). It was found from a previous study that the increased lysine concentrations attributed to the decrease in $k_l a$ (Stieger 1998).

Mass transfer can be modelled with the following equation:

$$OTR = k_l a(C_{o2,sat} - C_{o2}) \tag{5-37}$$

where OTR is the oxygen transfer rate (mmol/l/h), $k_l a$ is the volumetric mass transfer coefficient in h^{-1}, $C_{o2,sat}$ is the saturation dissolved oxygen concentration (mmol/l) and C_{o2} is the dissolved oxygen concentration (mmol/l).

The saturation dissolved oxygen concentration $C_{o2,sat}$ is a function of the medium composition and can be estimated from Henry's Law:

$$C_{o2,sat} = H \cdot P_{O2} \tag{5-38}$$

where H is Henry's constant which is a function of temperature and medium composition and P_{o2} is the partial pressure of oxygen (kPa).

The volumetric mass transfer coefficient depends on the medium composition, the system geometry, the power input and the air flow rate through the system:

$$k'_l a = a_{media}[\frac{(\mathrm{Re}\, v)^3}{V_{react}}]^{3\alpha_o} Air^{\beta_o} \tag{5-39}$$

The power for a specific system would be proportional to the Rev to the power of 3 where Rev is the impeller speed. Air is the volumetric air flow rate and "a_{media}" is a constant that depends on the composition of the broth

Using Equation 5-37, 5-38 and 5-39, the oxygen transfer rate (OTR) can therefore be expressed as:

$$OTR = k'_la(LMOPP-DO*LMOPP_o) \quad (5\text{-}40)$$

were OTR is the oxygen transfer rate (mmol/l/h), k'_la the mass transfer coefficient compensating for the media dependency of $C_{o2,sat}$, LMOPP the logarithmic mean oxygen partial pressure at the inlet and outlet of the fermenter and $LMOPP_0$ the logarithmic mean oxygen partial pressure at the inlet and outlet of the fermenter with no metabolic activity at the point at which the DO probe was calibrated, DO is the percentage saturation of oxygen in the broth as measured by the DO probe.

In Equation 5-40, the mass transfer coefficient represents a lumped parameter that compensates for the media dependency of the mass transfer coef ficient and the saturation oxygen concentration. Equation 5-39 would still be a valid expression for k'_la (the modified mass transfer coefficient) although the value of a must now compensate for the media dependency of $C_{o2,sat}$ and k'_la.

The parameters in equations were determined by using a least square fit from experimental data for different biomass concentrations, lysine concentrations and recycling flow rates.

For the base case scenario i.e. biomass dry weight concentration of 23 g/l, lysine concentration 30g/l with no biomass recycling the constants had the following values

$a_{media} = 3.51 \times 10^{-4}$ mmol/l/h/kPa
$\alpha_o = 0.66$
$\beta_o = 0.66$

Based on similar method as that used to model the permeate flow rate empirically (See Chapter 3) the following empirical correlation's were established for each of the constants

$a_{media} = 4.16 \times 10^{-4} [Lys]^{-0.04}$ mmol/l/h/kPa
$\alpha_o = 8.31 \times 10^{-1} [v]^{0.02}$
$\beta_o = 4.67 \times 10^{-1} [v]^{-0.03}$

where [v] is the linear velocity through the membrane module. For the base cases where no recycling was employed this term was set to 10^{-6} to approximate zero and avoid a division by zero error. A parity-line for the experimental data against the predicted k_la, presented in Figure 5-27, illustrates the satisfactory description of the data.

It was found that the mass transfer coefficient was influenced significantly by the lysine concentration and cross flow velocity through the membrane module. The cross flow velocity relates to the time, which the organism would spend in the unaerated

recirulation loop. It was found that increased biomass concentrations, up to 50 g/l did not influence the mass transfer coefficient. This was confirmed by the work of Stieger (1998) who found that for lysine broth the impact of the biomass concentration on the volumetric mass transfer coefficient was minimal.

Thus increasing cross flow velocity through the filtration loop implies an increase in the α coefficient. This implies that the impact of the agitation power on the mass transfer coefficient increases at increased cross flow filtration rates. The β coefficient however decreases with increases cross flow velocity. The effect of aeration is therefore reduced at increased cross flow velocities. This implies that if the same oxygen transfer rate is to be maintained, less agitation power and more air would be required at higher cross flow velocities.

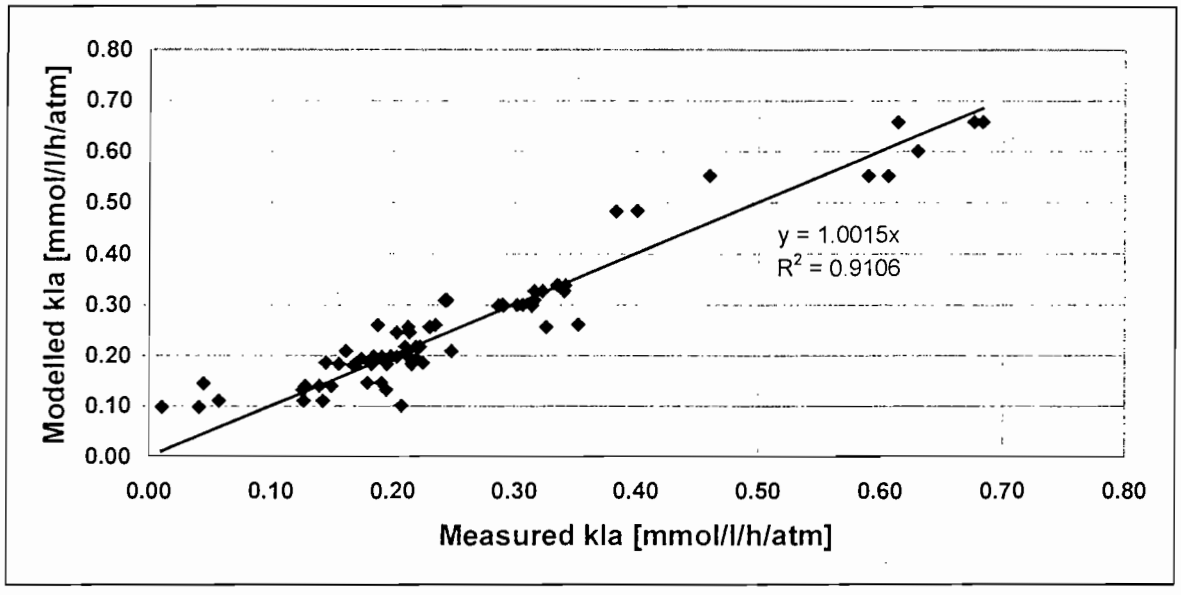

Figure 5-27. Parity-line for estimated and experimentally measured kl_a data.

7.4 The impact of biomass recycling using cross-flow filtration on the fermentation performance of C. glutamicum *cells*

To determine the impact of biomass recycling on the fermentation performance four fermentations were run with different reactor configurations. Batch, conventional fed-batch, continuous and fed-batch with biomass recycling were evaluated on laboratory scale. The runs were based on achieving a maximum biomass concentration of 30 g/l with a maximum initial charge sugar concentration of 100 g/l. At higher biomass concentrations the rheology of the broth alters while osmotic effects retards growth at sugar concentrations that greatly exceed 100 g/l. The continuous fermentation was run at the optimal growth rate for lysine productivity as reported by Kiss & Stephanopoulos (1992), resulting in a continuous specific growth rate of 0.04 g/g/h. The conventional fed-batch fermentation and the fed-batch with biomass recycling was maintained at a specific feed rate of 0.25 g/g/h which was optimal for lysine productivity according to Figure 6-2. The results from these runs are presented in Table 5-13 below.

The duration of the continuous fermentation as well as the fed-batch fermentation with biomass recycling run were limited due to reversion of the strain back to the wild type. Kiss & Stephanopoulos (1992) found that the double-auxothroph, L-lysine producer, *Corynebacterium glutamicum* (ATCC 21253) was susceptible to a back mutation, or reversion. For the growth rate selected for the continuous culture (0.10 h^{-1}), Kiss and Stephanopoulos (1992) reported a 50% decline in auxothrophic population after 4 generations or 77.6 hours. The continuous fermentation was therefore terminated at 80 hours. Based on serial dilutions on plates containing complex medium and medium lacking both L-threonine and L-methionine a 48% decline in the auxothropic population was found after 80 hours. For the fed-batch with biomass recycling a 51 % decline in the auxothropic population was found after 120 hours.

The volumetric productivity as reported in Table 5-13 is based on the working volume of the bioreactor. The specific productivity was based on the overall lysine produced and the total biomass produced during the run and therefore represents and average and not necessarily the maximum instantaneous value. The yield was based on the total lysine produced and the total glucose consumed during the run and represents and cumulative value and not and intrinsic or instantaneous value.

Table 5-13. Fermentation performance for different reactor configurations

	Units	Batch	Conventional Fed-Batch	Continuous	Fed-batch with biomass recycling
IC Volume	[litres]	10	5	10	5
Working volume	[litres]	10	10	10	10
Total biomass	[g]	300	150	178	158
Total lysine	[g]	136	324	160	960
Lysine concentration	[g/l]	14	32	13	48
Y_{ps}	[m/m]	0.14	0.16	0.17	0.16
Duration	[h]	40	60	80	120
Volumetric productivity	[g/l/h]	0.34	0.54	0.20	0.80
Lysine / biomass	[m/m]	0.45	2.16	0.90	6.08
Specific productivity	[g/g/h]	0.01	0.04	0.01	0.05

The batch fermentation produced 136 g of L-Lysine at a yield on sugar of 0.14 g/g in 40 hours. The cumulative specific productivity of 0.01 g/g/h is very low due to the relatively long time required to establish the cell population. Lysine production stopped after the 100 g/l of sugar included in the initial charge was depleted. Only 0.45 g of lysine was produced per gram of biomass, which makes this process very inefficient. A final lysine concentration of 14 g/l was achieved.

In the fed batch fermentation the total biomass was limited by the biomass concentration in the initial charge. The biomass was grown in the batch mode up to 30 g/l in 5 litres of media. Since the biomass concentration was limited to 30 g/l, the total biomass was limited to 150 grams of dry cell weight. The cells were however

maintained in the lysine overproduction metabolic state by feeding sugar at a fixed specific feed rate. The cells were therefore maintained in an optimal condition for lysine production for a proportionally longer time when compared to the batch fermentation. The effective specific productivity was increased from 0.01 g/g/h for the batch fermentation to 0.04 g/g/h for the fed-batch operated fermentation. Subsequently, the total lysine produced to biomass produced ratio increased relative to the conventional batch to 2.16 g/g. Surprisingly the overall yield only increased from 0.14 to 0.16 g/g. The eliminate an excessive increase in volume the glucose concentration in the feed was maintained at 400 g/l which was close to the solubility limit of glucose at 20 °C. The duration of the fed-batch fermantation was limited by the available reactor volume.

At steady state in the continuous fermentation the dilution rate (0.04 h^{-1}) equals the specific growth rate. The sugar concentration in the feed was maintained at 400 g/l. The biomass was initially grown up to 15 g DCW/l in 10 litres. This concentration decreased to 2.5 g DCW/l at steady state. This was the concentration at which the biomass production rate equalled the washout rate. The low specific productivity of 0.01 g/g/h reported was a result of the bulk of the biomass being washed out during the initial stages of the fermentation. At steady state only 28 g DCW of cells was in the reactor. This represents a specific productivity of 0.07 g/g/h, which corresponds to, that reported in Figure 6-2. The rest of the biomass (150 g DCW) was grown initially and washed out. The low total lysine to total biomass ratio (0.90 g/g) reflects this. If the steady state biomass concentration is used this ratio increases to 5.71 g/g.

The fed-batch reactor produced 960 g of Lysine in 120 hours at a yield of lysine on glucose of 0.16 g/g. In this reactor the bulk of the cell population was maintained in the bioreactor, the duration of the batch was not limited by the reactor volume and the cells were maintained in the lysine overproduction state for the bulk of the fermentation time. This results in a total lysine on total biomass ratio of 6.08 g/g. Another advantage of the fed-batch reactor with biomass recycling is the increased final lysine concentration which reduced downstream processing costs.

From the above analysis it is clear that the fed-batch fermentation with biomass recycling outperforms the other reactor configurations based on total lysine produced and the concentration of lysine in the final broth.

8 Conclusions

The qualitative effects of the increased hydrodynamic shear stress typically encountered in cross-flow micro-filtration applications on the growth, metabolism and morphology of *Corynebacterium glutamicum* cells have been investigated. Image analysis and a bioreaction network model has been used to quantify the impact of the hydrodynamic forces on the fermentation performance. Performance was analysed in batch fermentations while continuously filtering the cells. The permeate was returned to the bioreactor to ensure a constant composition.

The cell volume increases under increased hydrodynamic shear although increased shear does not alter the cell shape. It is therefore reasonable to assume that the increased volume may be due to increased water uptake into the cell as suggested by

Wase and Patel (1985) rather than alterations in the cytoskeleton or cell wall structure. It was also found that the effects of hydrodynamic shear stress on the cell's morphology were reduced at increased biomass concentrations.

The apparent specific growth rate of the hydrodynamically sheared cells was reduced, although the stationary phase biomass concentration on exposure to increased hydrodynamic shear increased relative to the conventional batch. The yield of biomass from threonine increased while the yield of biomass on glucose was reduced for cell recycle compared to the conventional batch.

The specific lysine productivity of the cells exposed to increased hydrodynamic stress in the flow loop was reduced compared to that of the cells cultivated in the conventional stirred tank reactor. This effect was more pronounced in the low biomass concentration batches. The cumulative yield of lysine from glucose was reduced on exposure to hydrodynamic shear. At the higher stationary phase biomass concentrations, these effects are less marked than at lower concentrations.

The fermentation data provided convenient sets of extracellular flux measurements (glucose, L-lysine, free and saline nitrogen, oxygen and carbon dioxide) to elucidate the impact of increased hydrodynamic stress caused by biomass recycling on the biochemistry of L-lysine synthesis through intracellular flux analysis. This method combines the known metabolic pathways of the organism with a pseudo-steady state approximation for intracellular metabolite concentrations to generate a mathematical representation of the metabolic flows.

The excess ATP for cells exposed to increased hydrodynamic stress due to cell recycle was reduced relative to that of the "conventional batch". The reduction in ATP formation is believed to be a result of a shift in cellular metabolism from oxidative phosphorylation to substrate level phosphorylation and glycolysis.

The flux of carbon through PPP was reduced at increased hydrodynamic shear due to a reduction in the requirement for NADPH of the cells exposed to hydrodynamic shear in the filtration module. Exposure to hydrodynamic shear in the membrane unit did not have an impact on the split of carbon at the PEP or OaA nodes. At the Pyr node the flux of carbon to lysine and the flux of Pyr to AcCoA was reduced at increased hydrodynamic shear, while the flux of pyruvate into other amino acids increased. Thus, at increased shear the total flux of carbon toward the TCA cycle decreased.

From the qualitative analysis presented it was postulated that increased hydrodynamic shear causes an increase in the flux of carbon towards the cell wall to either repair or strengthen the cell wall.

In the next chapter different level of hydrodynamic shear and its impact on the fermentation performance would be evaluated.

An analysis of the impact of cell recycling on the mass transfer properties of the bioreactor indicated that if the same oxygen transfer rate is to be maintained at increased cross flow velocities, less agitation power and more air would be required at higher cross flow velocities.

It was also shown that the fed-batch fermentation with biomass recycling outperformed the other reactor configurations (batch, fed-batch and continuous) based on total lysine produced and the concentration of lysine in the final broth.

9 References

Abu-Reesh, I., and Kargi, F. (1989), Biological responses of hybridoma cells to defined hydrodynamic stress, *Journal of Biotechnology,* **9,** 167-178

Al-Rubeai, M, Singh, R. P., Emery, A. N. and Zhang, Z., (1995a), Cell recycle and its sixe dependence of susceptibility to hydrodynamic forces, *Biotechnology and Bioengineering,* **46,** 88-92

Al-Rubeai, M, Singh, R. P., Goldman, M. H. and Emery, A. N. (1995b), Death mechanisms of animal cells in conditions of intensive agitation, *Biotechnology and Bioengineering,* **45,** 463-472

Al-Rubeai, M., Oh, S. K. W., Musaheb, R. and Emery, A. N. (1990), <odified cellular metabolism in hybridomas subjected to hydrodynamic and other stresses, *Biotechnology Letters,* **12,** 323-328

Ando, J. T., Kamiya, A., Korenaga, R. and Ohtsuka, A. (1991), Effect of extracellular ATP level on the flow of induced calcium response in cultured endothelial cells, *Biochemical Biophysics Res. Communications,* **179,** 1192-1199

Atkinson, B., Mavituna, F. (1983), Biochemical Engineering and Biotechnology Handbook, Macmillan, NY

Augenstein, D. C., Sinskey, A. J., and Wang, D. I. C. (1971), Effect of shear on the death of two strains of mammalian tissue cells, *Biotechnology and Bioengineering,* **12,** 409-418

Ayazi Shamlou, P. and Titchener-Hooker, N. J. (1993), In "Processing of Solid-Liquid Suspensions", Ayazi Shamlou (Ed.), Academic Press, New York, 1-91

Ayazi Shamlou, P., Siddiqi, S. F. and Titchener-Hooker, N. J. (1995), A physical model of high pressure disruption of baker's yeast cells, *Chemical Engineering Science,* **50,** 1383-1391

Ayazi Shamlow, P. M., Jones, A. G. and Djamarani, K.,(1990), Hydrodynamics of secondary nucleation in suspension crystallisation, *Chemical Engineering Science,* **45,** 1405-1416

Bates, R. L. Fondy, P. L. and Fenic, J. G. (1966), In Mixing: Theory and Practise 1, Uhl, V. W. and Gray, J. B. (Eds.), Academic Press, NY

Bates, R. L., Fondy, P. L. and Corpstein, R. R. (1963), An examination of some geometric parameters of impeller power, *Industrial Engineering Chemical Process Design and Development,* **2,** 310-314

Blanch, H. W. and Bhavaraju, S. M. (1976), Non-newtonian fermentation broths: rheology and mass transfer, *Biotechnology and Bioengineering,* **18,** 745-790

Blumm, J. J. and Stein, R. B. (1982), On the analysis of metabolic networks, Goldberger, R. F. and Yamamoto, K. R. (Eds.), Biological regulation and development, Vol 3A, Plenum Press, NY, 99-125

Born, C., Zang, A., Al-Rubeai, M. and Thomas, C. R. (1992), Estimation of disruption of animal cells by laminar shear stress, *Biotechnology and Bioengineering,* **40,** 1004-1010

Boulton-Stone, J M. and Blake, J. R. (1993), Gas bubble at the free surface, *Journal of Fluid Mechanics,* **254,** 437-466

Bronnenmeier, R. and Märkl, H. (1982), Hydrodynamic stress capacity of microorganisms, *Biotechnology and Bioengineering,* **26,** 553-578

Brown, D. E. and Kavanagh, P. R. (1987), Crossflow separation of cells, *Process Biochemistry,* **22**(4), 96-101

Calabrese, R. V. and Stoots, C. M. (1989), Flow in the impeller region of a stirred tank, *Chemical Engineering Progress,* **85,** 43-50

Charm, S. E. and Wong, B. L. (1970), Enzyme inactivation with shearing, *Biotechnology and Bioengineering,* **12,** 1103-1109

Cherry, R. S. and Papoutsakis, E. T. (1986), Hydrodynamic effects on cells in agitated tissue culture reactors, *Bioprocess Engineering,* **1,** 29-41

Chiampo, F. and Marotto, R. (1995), Flow regimes in gas-liquid reactors stirred with dual Rushton turbines, *The 1995 IChemE Research Event/First European Conference,* 689-691

Croughan, M. S., Hamel, J. F. and Wang, D. I. C. (1987), Hydrodynamic effect on animal cells grown in microcarrier cultures, *Biotechnology and Bioengineering,* **24,** 130-141

Dabee, S. and Harrison, S. T. L. (1996), In *Maximising O_2 transfer and minimising shear damage in the microbial production of GLA by Mucor Rouxii,* Master of Science, Chemical Engineering, University of Cape Town

Davies, P. F., Remuzzi, A., Gordon, E. J., Dewey, C. F., Jr. and Gimbrone, M. A. (1986), Turbulent fluid shear stress induces vascular endothelial cell turnover *in vivo*, *Proc. Natl Acad. Sci.,* **83,** 2114-2117

Dean, A. C. R. and Hinshelwood, C. (1966), *Growth, Function and Regulation in Bacterial cells*, Clarendon Press, Oxford, pp 87-89

Delgado, J. P and Liao, J. C. (1991), Identifying rate controlling enzymes in metabolic pathways without kinetic parameters, *Biotechnology Progress,* **7,** 15-20

Dickason, G. J. (1998), *Image analysis of Bacillus thuringiensis*, MSc Thesis, Chemical Engineering, University of Cape Town

Doelle, H. W., Ewings, K. N. and Hollywood, N. W. (1983), *Advanced Biochemical Engineering,* **23,** 1

Donachie, W. D., Begg, K. J. and Vicente, M. (1976), Cell length, cell growth and cell division, *Nature,* **264,** 328-333

Dunlop, E. H., and Ye, S. J. (1994), Micromixing in fermentors: Metabolic changes in *Saccharomyces cerevisiae* and their relationship to fluid turbulence, *Biotechnol. Bioeng.,* **36,** 854-864

Dunlop, E. H., Namdev, P. K. and Rosenberg, M. Z. (1994), Effect of fluid shear forces on plant cell suspensions, *Chemical Engineering Science,* **49,** 2263-2276

Dunlop, E. H., Namdev, P. K. (1993), Effect of fluid forces on plant cell suspensions. In bioreactor and bioprocess fluid dynamics. Nienow, A. W. (ed.), Cambridge, pp. 447-455

Edwards, N., Beeton, S., Bull, A. T. and Merchuk, J. C. (1989), A novel device for the assessment of shear effects on suspended microbial cultures, *Applied Microbial Technology,* **30 19**0-195

Falke, L., Edwards, K. L., Misler, S. and Pickard, B. G. (1986), A mechanotransductive ion channel in patches from cultured tobacco cell plasmalemma, *Plant Physiology,* **80,** 9

Forstrom, R. J., Bartelt, P. L., Blackshear, Jr. and Wood, T. (1975), *Trans. am. Soc. Artif. Intern. Org.,* **21,** 602

Foster, P. R., Dunnill, P. and Lilly, M. D. (1976), Kinetics of protein salting out, *Biotechnology and Bioengineering,* **18,** 545-580

Fowler, J. D. and Robertson, C. R. (1991), Metabolic behaviour of immobilised aggregates of *Escherichia coli* under conditions of varying mechanical stress, *Applied and Environmental Microbiology,* 93-101

Garcia-Briones, M. A. and Chalmers, J. J. (1994), Flow parameters associated with hydrodynamic cell injury, *Biotechnology and Bioengineering,* **44,** 1089-1098

Glasgow, B. A. (1989), Effect of the physiochemical environment on floc properties, *Chemical Engineering Progress,* **85,** 51-62

Grabler, F. R. (1985), Cell processing using tangential flow filtration in Comprehensive Biotechnology (Vol. 2) (Coeney, Humphrey, Eds.), Permagon Press, Oxford, 351-366

Van Gulik, W.M. and Heijnen, J.J. (1995), A metabolic network stoichiometry analysis of microbial growth and product formation, *Biotechnology and Bioengineering*, **48**, 681-698.

Gusek, T. W., Johnson, R. D., Tyn, M. T., Kinsells, J. E. (1991), Effect of agitational shear on growth and protease production by *Thermomonospora fusca, Biotechnology and Bioengineering,* **37,** 371-374

Gusten, M. C., Martinac, B., Saimi, Y., Culbertson, M. R. and Kung, C. (1986), Ion channels in yeast, *Science,* **233,** 1195-1197

Handa-Corrigan, A., Emery, A. N. and Spier, R. E. (1989), Effect of gas-liquid interfaces on the growth of suspended mammalian cell: mechanisms of cell damage by bubbles, *Enzyme Microbial Technology,* **11,** 230-235

Henry, J. D. and Alfred, R. C. (1972), Concentration of bacterial cells by crossflow filtration, *Develop. In Industrial Microbiol.,* **13,** 177-190

Ho, S. K. W., Nienow, A. W., Al-Rubeai, M. and Emery, A. N. (1989), The effects of agitation intensity with and without continuos sparging on the growth and antibody production of hybridoma cells, *J. Biotechnol.,* **12,** 45-62

Hoffman, H., Scheper, T., Schugerl, K. and Schmidt, W. (1987), Use of membranes to improve bioreactor progress, *Chem. Eng.,* **J34**, B13-B19

Hooker, B. S., Lee, J. M. and An, G. A. (1989), Response of plant tissue culture to a high shear environment, *Enzyme Microbial Technology,* **11,** 484-490

Illing, S. (1986), An investigation of the effect of hydrodynamic stress on the growth, morphology and metabolism of microorganisms, PhD Thesis, Department of Chemical Engineering, University of Cape Town

Inbar, L. and Lapidot, A. (1987), Malic enzyme, *Meth. Enzymol.,* **13,** 230-235

Jeong, J. W., Snay, J. and Ataai, M. M. (1990), A mathematical model for examining growth and sporulation sporulation processes of *Bacillus subtilis, Biotechnology and Bioengineering,* **35,** 160-184

Kawase, Y. and Moo Young, M. (1990) Mathematical models for the design of bioreactors: applications of Kolmogoroff's theory of isotropic turbulence, *Chemical Engineering Journal,* **43 19**-41

Kieran, P. M., O'Donnel, H. J., Malone, D. M. and MacLoughlin, P. F. (1995), Fluid shear effects on suspension cultures of *Morinda citrifolia, Biotechnology and Bioengineering,* **45,** 415-425

Kjelleberg, S. (1983), Bacterial adhesion: mechanisms and physiological sigriificance, Savage, D. C. and Fletcher, M. (Eds.), Plenum, NY, 163-194

Kolmogorov, A. N. (1941), *C.R.Acad. Scie.* URSS 30, 301

Kroner, K. H., Schütte, H., Hustedt, H., and Kula, M. R. (1984), Cross-flow filtration in downstream processing of enzymes, *Process Biochem 19*, 67-74

Kunas, K. Y. and Papoutsakis, E. T. (1990), Damage mechanisms of suspended animal cells in agitated bioreactors with and without bubble entrainment, *Biotechnology and Bioengineering,* **36,** 476-483

Lakhotia, S. and Papoutsakis, E. T. (1992), Agitation induced cell injury in microcarrier cultures: protective effect of viscosity is agitation intensity dependent: experiments and modelling, *Biotechnology and Bioengineering,* **39,** 95-107

Laufer, J. (1954), The structure of turbulence in fully developed pipe flow, *National Advisory Committee for Aeronautics Report 1174,* 1-18

Le, M. S. and Atkinson, T. (1985), Crossflow microfiltration for recovery of intracellular products. *Process Biochem.* **20**(1), 26-31

Leckie, F., Scraggs, A. H. and Cliffe, K. R. (1991), Effects of impeller design on large scale cultivation of suspension cultures of *Caranthus roseus, Enzyme Microbial Technology,* **13,** 801-809

Lee, G. M., Huard, T. K., Kaminski, M. S. and Palsson, B. O. (1998), Effect of mechanical agitation on hybridoma cell growth, *Biotechnology Letters,* **10,** 625-628

Lee, G. M., Savinell, J. M. and Palsson, B. O. (1989), Serum can act as a shear protecting agent in agitated hybridoma cell cultures, *Hybridoma,* **8,** 639-645

Linthelac, P. M. and Vasecky, T. B. (1984), Stress induced alignment of division plane in plant tissue grown in vitro, *Nature,* **307,** 363-364

Logan, B. E. and Wilkinson, D. B. (1991), Fractal dimensions and porosities of *Zoogloea ramigera* and *Saccharomyces cerevisae* aggregates, *Biotechnology and Bioengineering,* **38,** 389-396

Maiorella, B., Dorin, F., Carion, A. and Harano, D. (1991), Crossflow microfiltration of animal cells, *Biotechnology and Bioengineering,* **37,** 121-126

Markl, H. and Bronnenmeier, R. (1985), In "Biotechnology", Vol 2, Rehm, H. J. and Weinheim (Eds.), New York, pp 369-392

M. Marx, Y.N. Chin, F. Zimmer, U. Herbstmeier, U. Mebold (1996), Is the LMC unusually cool?, *AG Abstract Series*, **12**, 212

McQueen, A., Meilhoc, E. and Bailey, J. E. (1987), Flow effect on the viability and lysis of suspended mammalian cells, *Biotechnology Letters,* **9,** 831-836

Mersmann, A., Schneider, G., Voit, H. and Wenzig, E. (1990), Selection and design of aerobic bioreactors, *Chemical Engineering Technology,* **13,** 357-370

Michel, B. J. and Miller, S. A. (1962), Power requirements of gas-liquid agitated systems, *AIChE Journal,* **13,** 262-266

Midler, M. and Finn, R. K. (1966), *Biotechnology and Bioengineering,* **8,** 71

Mitard, A. and Riba, J. P. (1988), Morphology and growth of *Aspergillus niger* ATCC 26036 cultivated at several shear rates, *Biotechnology and Bioengineering,* **32,** 835-840

Moreira, J. L., Cruz, P. E. and Santana, P. C. (1995a), Formation and disruption o animal cell aggregates in stirred vessels: mechanisms and kinetic studies, *Chemical Engineering Science,* **50,** 2747-2764

Moreira, J. L., Alves, P. M., Aunins, J. G. and Carrondo, M. J. T. (1995b), Hydrodynamic effects on BHK cells grown as suspended natural aggregates, *Biotechnology and Bioengineering,* **46,** 351-360

Nagata, N., Herouvis, K. J., Dziewulski, D. M. and Belfort, G. (1989), Crossflow membrane microfiltration of a bacterial fermentation broth, *Biotechnology and Bioengineering,* **34,** 447-466

Neseratnam, S. T., Wase, D. A. J. and Blakebrough, N. (1982), The susceptibility to ultrasonic disentigration of *Klebsiella pneumonia* NCTC 418, *European Journal of Applied Microbiology and Biotechnology,* **15,** 56-58

Niranjan, S. C. and San, K. Y. (1989), Analysis of a framework using mathematical balances in metabolic pathways to elucidate cellular metabolism, *Biotechnology and Bioengineering,* **34,** 496-501

Nollert, M. U. and Diamond, S. L. and McIntre, L. V. (1991), Hydrodynamic shear stress and mass transport modulation of endothelial cell metabolism, *Biotechnology and Bioengineering,* **38,** 588-602

Noorman, H. J., Heijnen, J. J. and Luyben, K. Ch. A, M. (1991), Linear relatins in microbial reaction systems: A general overview of their origin, form and use. *Biotechnology and Bioengineering,* **38,** 603-618

O'Connel, F. P. and Mack, D. E. (1950), Simple turbines in fully baffled tanks, *Chemical Engineering Progress,* **46,** 358-362

Oh, S. K. W., Nienow, A. W., Al-Rubeai, M. and Emery, A. N. (1989), The effects of agitation intensity with and without continuous sparging on the growth and antibody production of hybridoma cells. *Journal of Biotechnology,* **12,** 88-94

Ozbas, T. and Kutsal, T. (1991), Effects of agitation and aeration rates on riboflavin fermentation by *Ashbya gossypii, Biotechnology and Applied Biochemistry,* **13,** 97-105

Palsson, B. O. and Lightfoot, E. N. (1985), Mathematical modelling of dynamics and control in metabolic networks V. Static bioreactions in single biochemical control loops, *J. Theor. Biol.,* **113,** 279-298

Papoutsakis, E. T. (1984), Equations and calculation for fermentation of butyric acid bacteria, *Biotechnology and Bioengineering,* **26,** 174-187

Parker, D. S., Asce, A. M., Kaufman, W. J., Asce, M. and Jenkins, D. (1972), Floc breakup in turbulent flocculation processes, *Journal of Sanitary Engineering Division,* 79-99

Peterson, J. F., McIntire, L. V. and Papoutsakis, E. T. (1990), Shear sensitivity of hybridoma cells in batch, fed-batch and continuous cultures, *Biotechnology Progress,* **6,** 114-120

Pickard, B. G. (1984), Voltage transients elicted by sudden step-up of auxin, *Plant cell Environment,* **7,** 171-178

Pirt, S. J. (1975), Principles of microbe and cell cultivation, Blackwell Scientific Publications, Oxford, Ch 3-15

Pons, M. N., Vivier, H., Remy, J. F and Dodds, J. A. (1993), Morphological characteristics of yeast by image analysis, *Biotechnology and Bioengineering,* **42,** 1352-1359

Prokop, A. and Bajpai, R. K. (1992), The sensitivity of biocatalysts to hydrodynamic shear stress, *Advances in Applied Biochemistry,* **37,** 165-233

Proncelet, D. and Neufeld, R. J. (1989), Turbulent flow in stirred tanks. Part I: Turbulent flow in the turbine impeller region, *AIChE Journal,* **31,** 1113-1120

Rebsamen, E., Goldinger, W., Scheirer, W., Merten, O. W. and Palfi, G. E. (1987) Use of a dynamic filtration method for the separation of animal cells, *Dev. Biol. Standard,* **66,** 273-277

Rukisha, M. P., Vanags, J. J., Rikmanis, M. A., Toma, M. K. and Viesturs, U. E. (1989), Biochemical reactions of *Brevibacterium flavum* depending on the mdeium stirring intensity and flow structure, *Acta Biotechnology,* **9,** 565-575

Ryder, D. S., Davis, C. R., Anderson, D., Glancy, F. M. and Power, J. N. (1988) , Brewing experience with crossflow filtration, *MBAA Technical Quaterly,* **25,** 67-79

Smith, C. G., Greenfield, P. F. and Randerson, D. H. (1987), A technique for determining the shear sensitivity of mammalian cells in suspension culture, *Biotechnology Techniques,* **1,** 39-44

Smith, C. G., Lilly, M. D. and Fox, R. I. (1990), The effect of agitation on the morphology and penicillin production of *Penicillin chrysogenum, Biotechnology and Bioengineering,* **35,** 1011-1023

Sorribas, A. and Savageau, M. (1989), A comparrison of variant theories of intact biochemical systems II. Flux-orientated and metabolic control theories, *Math Biosci.,* **94 19**5-238

Srinorakutara, T., Zhang, Z. and Thomas, C. R. (1996), Osmolarity effect on yeast cell strength and cell size. The 1996 IChemE Research Event. University of Leeds, 2-3 April 1996, Vol. 1, 151-153. IChemE, Rugby, UK.

Stockbridge, L. L. and Frensch, A. S. (1988), Stretch activated carbon channels in human fibroplasts, *Biophysics Journal,* **54,** 187-190

Taddei, C. and Howel, J. A. (1989), On the effect of membrane conditioning in cell harvesting using microfiltration, *Biotechnol. Techniques,* **3**(3), 155-160

Takiguchi, N., Shimizu, H. and Shioya, S. (1997), An on-line physiological state recognition system for the lysine fermentation process based on a metabolic reaction model, *Biotechnolology and Bioengineering*, **55**(1), 170-181

Tan, W. S., Chen, Y. L. and Dai, G. C. (1992), Growth and damage of continuous suspension cultured hybridoma cells in an agitated bioreactor with and without bubble entrainment or sparging. *3rd International Conference on Bioreactor and Bioprocess Fluid Dynamics,* Cambridge, 153-159

Tanaka, H., Semba, H., Jitsufuchi, T. and Harada, H. (1988), the effect of physical stress on plant cells in suspension cultures, *Biotechnology Letters,* **10,** 485-490

Tanny, G. B., Mirelmean, P. and Pistole, T. (1980), Improved filtration technique for concentration and harvesting bacteria, *Applied and Environ. Microbiol.* **40,** 269-273

Tirrel, M. and Middleman, S. (1978), The effect of shearing forces on the catalytic activity of urease, *AIChE Symposium Series,* **744,** 102-107

Toma, M. K., Ruklisha, M. P., Zeltina, M. O., Galinina, N. I., Viesturs, U. E., and Tengerdy, R. P. (1991), Inhibition of microbial growth and metabolism by excess turbulence, *Biotechnology and Bioengineering,* **38,** 552-556

Tsai, S. P. and Lee, Y. H. (1988), Application of Gibb's rule and a simple pathway method to microbial stoiciometry, *Biotechnology Progress,* **4,** 82-88

Tsai, S. P. and Lee, Y. H. (1988), Application of metabolic pathway stoiciometry to statistical analysis of bioreactor measurement data, *Biotechnology and Bioengineering,* **32,** 713-715

Ujcovo, E., Fencl, Z., Musilkova, M. and Seichert, L. (1980), Dependence of release of nucleotides from fungi on fermenter turbinbe speed, *Biotechnology and Bioengineering,* **22,** 237-241

Vallino, J. J. and Stephanopoulos, G. (1993), Metabolic flux distribution in *Corynebacterium glutamicum,* during growth and lysine overproduction, *Biotechnology and Bioengineering,* **41,** 633-646

Vallino, J. J. and Stephanopoulus, G. (1994), Carbon flux distributions at the pyruvate branch point in *Corynebacterium glutamicum* during lysine overproduction, *Biotechnol. Prog.,* **10,** 320-326

Vallino, J. J. and Stephanopoulus, G. (1987), Intelligent sensors in biotechnology applications for the monitoring of fermentations and cellular metabolism, *Am. NY Acad. Sci.* **506,** 415-430

Vallino, J. J. and Stephanopoulus, G. (1989), Flux determination in cellular bioreaction networks: Applications to lysine fermentation, Sikdar, S., Bier, M. and Todd, P. (Eds.), Frontiers in Bioprocessing, CRC Press, Boca Raton, FL

Van Suijdam, J. C. and Metz, B. (1981), Influence of engineering variables upon the morphology of filamentous molds, *Biotechnology and Bioengineering,* **23,** 111-148

Vanags, J. J., Rikmanis, M. A., Ushkans, U. E. and Viesturs, U. E. (1990), Stirring characteristics in bioreactors, *AIChE Journal,* **36,** 1361-1369

Verhoff, F.H. and Spradlin, J.E. (1976), Mass and energy balance analysis of metabolic pathways applied to citric acid production by *Aspergillus niger. Biotechnology and Bioengineering*, **18,** 425-432

Virana, D., Votruba, J. and Placek, J.,(1982), Age related changes in the physiology state of budding cells, *Experimenal Cell Research,* **138,** 57-62

Wase, D. A. J. and Ratwatte, H. A. M. (1985), *Applied Microbial Biotechnology,* **22,** 325

Wase, J. D. A. and Patel, Y. R., (1985), Variations in the volumes of microbial cells with change in the agitation rates of chemostat cultures, *Journal of General Microbiology,* **131,** 725-736

Zalewski, K. and Buchholz, R. (1996), Morphological analysis of yeast cells using an automated image processing system, *Journal of Biotechnology,* **48,** 43-49

Zhang, Z., Al-Rubeai, M. and Thomas C. R. (1992a), Mechanical properties of hybridoma cells in batch culture, *Biotechnology Letters,* **14,** 11-16

Zhang, Z., Al-Rubeai, M. and Thomas, C. R. (1992b), The effect of Pluronic-F68 on the mechanical properties of mammalian cells, *Enzyme Microbial Technology,* **14,** 980-983

Zhang, Z., Al-Rubeai, M. and Thomas, C. R. (1993), Estimation of disruption of animal cells by turbulent capillary flow, *Biotechnology and Bioengineering,* **42,** 987-993

Zhang, Z., Al-Rubeai, M. and Thomas, C. R. (1995), Preliminary modelling of animal cell disruption in a closed stirred tank, *The 1995 Research Event/First European Conference,* 1088-1090

Zhang, Z., Ferenczi, M. A. Thomas C. R. (1992d), A micromanipulation technique with a theoretical cell model for determining mechanical properties of single mammalian cells, *Chemical Engineering Science,* **47,** 1347-1354

Zhang, Z., Handa-Corrigan and Spier, R. E. (1992c), Foaming and media surfactant effects on the cultivation of animal cells ion stirred and sparged bioreactors, *Journal of Biotechnology,* **25,** 289-306

Zydney A. L. and Colton C. K. (1986), A concentration polarization model for the filtrate flux in cross-flow microfiltration of pariculate suspensions, *Chem. Eng. Commun.,* **47,** 1-21

Modelling of the Lysine Fermentation with Biomass Recycling

1 Introduction

Biochemical processes are characterised by a large number of variables that can influence the process outcome. This, combined with the slow nature of fermentation experiments makes optimisation through search plans very tedious and in most cases physically unrealistic and economically unfeasible. It is therefore easily recognised that in the optimisation of biochemical processes, the emphasis falls mainly on the development of accurate relationships between dependent and independent variables.

Unfortunately, due to the complex nature of biochemical processes, fundamental functional relationships are very limited with regard to their ability to predict process performance. Therefore, most attempts at the modelling of biochemical processes are empirical correlations of experimental data that are only valid over the evaluated range. "Hybrid models" use some fundamental understanding of the system behaviour to dictate the form of the empirical correlation. Several of these "hybrid models" exists that describe some aspects of biochemical processes, each with its limitations and defined range of applicability (Luedeking & Piret 1959; Volesky & Votruba 1992; Wang & Cheng 1999; Wang & Stephanopoulos 1983; Büchs 1991).

Choosing the most suitable model for a specific purpose can be seen as an optimisation problem in itself. The objective of the optimisation problem is to find the model or functional relationship that adequately describes the process or the part thereof that the specific purpose at hand requires. In the case of process optimisation, the objective is to find the process model or functional relationship that adequately describes the part of the process that influences the objective function. Bayesian inference (O'Hagan 1994) is a quantitative technique that can be used to find the functional relationship with the highest probability of predicting selected process parameters based on a hybrid of experimental data and some fundamental understanding of the system behaviour.

This concept will be illustrated by optimising the variable cost of production of L-Lysine through the direct fermentation of carbohydrates by an auxothropic mutant of *Corynebacterium glutamicum* in a cell recycle bioreactor. In the cell recycle bioreactor, the biomass is separated from the fermentation broth by using cross-flow microfiltration unit from where the biomass is recycled to the bioreactor and the spent medium processed for lysine recovery (Figure 6-1).

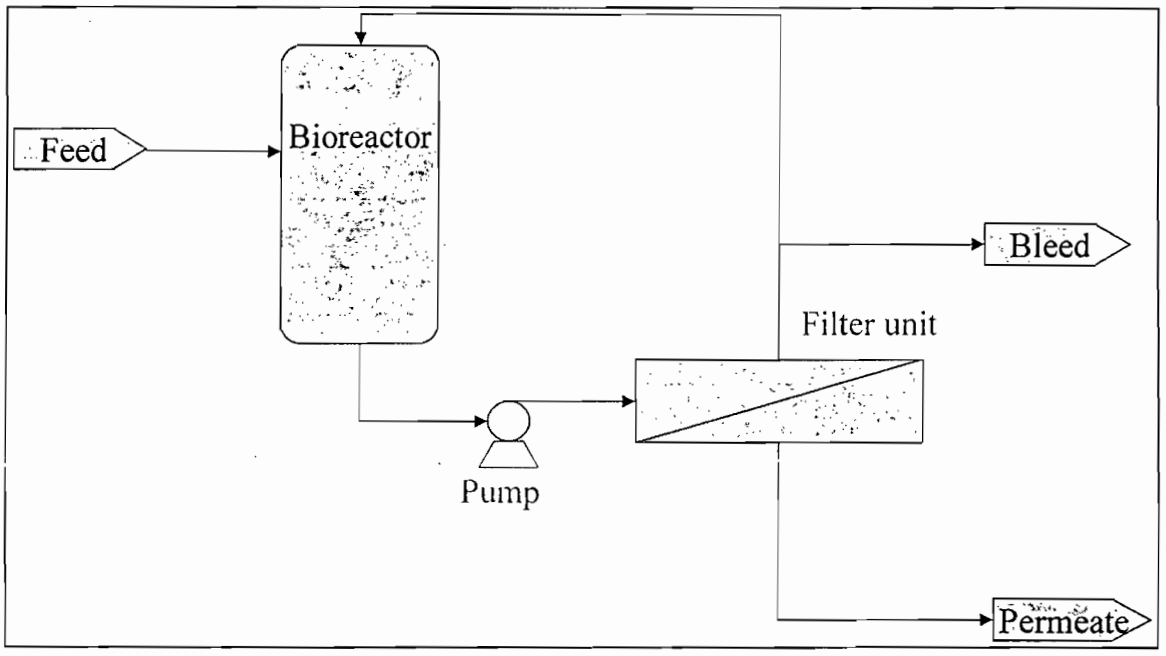

Figure 6-1. The cell recycle bioreactor is used to increase the biomass residence time in the bioreactor. The biomass is separated form the fermentation broth by using cross-flow filtration external to the reactor. The biomass is recycled to the bioreactor and the spent medium processed for lysine recovery.

2 Fermentation models

The following section will give a short overview of the available fermentation modelling approaches:

2.1 Process models with biomass recycling

The biomass recycling process is generally modelled based on component mass balances. These generally include a volumetric balance, a biomass balance, a carbohydrate balance and a product balance. The specific growth rate and specific productivity of the cells are generally modelled by using well known biochemical rate expressions such as the Monod equation.

For example, biomass recycling is a very well studied subject where activated sludge processes are concerned. Ramanathan & Gaudy (1971) modelled the steady state activated sludge process with constant biomass recycle. Most of the biomass recycling models of activated sludge processes are based on Monod growth equations coupled to simple mass balance equations.

Weuster-Botz *et al.* (1997) described a fed-batch process in which nutrient components are continuously fed to the fermenter while the culture liquid is not removed until the end of the fermentation. A quasi-stationary regime is achieved by altering the rate of dilution and composition of the nutrient supplements. In this case the biomass concentration and substrates remain at a constant level.

A mathematical model of one-stage continuous cultivation for producing L-lysine has been presented by Rutkov (1984) using the homoserine deficient mutant ATCC 13286. The model is based on the solution of the basic material macro balances (carbon and nitrogen) of one stage continuous cultivation in accordance with some justified assumptions which reflect the specific peculiarities of the growth and lysine production of the strain used. The adequacy of the model was proven by comparing the experimental data with the model simulations.

Wang & Stephanopoulus (1984), proposed that a time-delay kernel be included in the state equations to compensate for the history of cell behaviour. They also developed a generalised method of transforming the integrodifferential equations to a mathematically equivalent set of first order ordinary differential equations. This allowed the incorporation of the culture's past history in the form of a delay kernel, which greatly enhances the model's predictive capabilities. The transformation then permits the application of a wide variety of analytical techniques. The resulting model effectively combined the simplicity of an unstructured lumped model with the power of a complex structured model.

2.2 Modelling of biomass growth

Most of the modelling of the growth of lysine producing organisms was described with logistic models based on either Malthus or Monod kinetics. For the description of the lag phase, different extensions of kinetics were compared and respectively tested and two new mathematical functions suggested for this purpose by Bona & Moser (1997).

Kiss and Stephanopoulus (1992) studied the long term dynamic characteristics of the L-Lysine producer *Corynebacterium glutamicum* in continuous culture over a range of specific growth rates. The double auxothropic parent strain was found to be susceptible to a back mutation or reversion. They developed a deterministic mathematical model of the culture dynamics, incorporating two limiting substrate balances. The model successfully described the takeover profiles.

Mankad and Nauman (1992) presented several unstructured models for microbial growth under dual substrate limitations. All these models only apply to substrate limitations of the Monod type. They then presented a more general model for microbial growth under any form of dual limitation. Their new model also allows a variable extent of interaction between the two limiting factors.

2.3 Coupling of growth rate and specific amino acid productivity

Luedeking & Piret (1959) suggested that since lysine production by most mutant organisms are only partly growth associated and that the substrate is allocated by the micro-organism mainly for biomass and amino acid production, there should be a relationship between the specific growth rate and the specific lysine productivity. They suggested a linear relationship between the specific growth rate and the specific lysine productivity.

Ohno *et al.* (1976) suggested a model for the lysine fermentation based on Monod kinetics for growth and a second order polynomial relationship between the specific growth rate and the specific lysine productivity instead of the linear relationship suggested by Luedeking & Piret (1959). The result was based on the experimental data reported by Takamatsu *et al.* (1975). This model had various limitations such as the fixed yield of lysine on biomass but was adequate to illustrate the concept to find the optimal feed rate for the lysine fermentation.

Shioya (1992) later revised this model by incorporating a relationship between the specific growth rate and the specific production rate as a function of limiting substrate concentration (L-Leucine). This model was constructed on the assumption that L-leucine repressed the synthetic enzyme for lysine production and that the repression mechanism was regulated by the operator (Shioya *et al.* 1992).

2.4 Intelligent sensors

The concept of using process models to infer data that are difficult or impossible to measure is referred to as intelligent sensoring.

Vallino and Stephanopoulos (1987) developed a model in which the variables that were measured on-line can be fed to a Kalman filter to produce estimates of states that are not directly measurable. Concentrations of substrate, product, biomass and oxygen in the gas and liquid phases as well as the yields, specific growth rate and the $k_l a$ values were estimated from on-line measurements of O_2 and CO_2 in the off gas and the dissolved oxygen concentration.

Both van Gulik and Heijnen (1995) and Vallino and Stephanopoulos (1993) developed an online physiological state recognition system, based on a metabolic reaction model. Here growth, production activity and flux distributions were determined from on-line measurements only.

Neural networks can easily be structured and trained to predict the physiological state of a fermentation at any point in time based on some measured variable inputs. Lui *et al.* (1995) modelled fed batch culture of a *Brevibacterium* for lysine production by combining 3 neural network estimators. The first neural network estimated the consumed sugar

concentration, lysine concentration and cell optical density. The second determined the off gas concentration of CO_2 and O_2 while the third predicted the agitation speed. The model was used for set-point selection for fed-batch fermentation.

Linko *et al.* (1995) programmed well-trained, back propagation multi-layer neural network in MS-Visual C^{++} for Windows and implemented it on a PC. The neural networks were applied to state estimation and multi-step-ahead prediction of sugar consumed and lysine produced based on online measurable variables.

Yet-pole *et al.* (1996) used a moving window neural network for dynamic modelling and on-line estimation of sugar consumed, cell mass and product concentration in a lysine fed batch culture. The reducing sugar concentration was calculated on-line using the estimated sugar consumption rate to determine the sugar concentration. The sugar concentration was maintained at a given value using simple compensatory feeding strategy. The fermenter was controlled to have a constant reduced sugar concentration, by controlling the substrate-feeding rate. Thus, the oxygen uptake rate (OUR), carbon dioxide evolution rate (CER), the respiration quotient (RQ = CER / OUR) and feed rate were fed into a neural network model that predicted the reduced sugar concentration which was controlled with a feedback controller by manipulating the feed rate.

2.5 Modelling of specific metabolic parameters in the lysine fermentation system

Erdmann *et al.* (1992) developed kinetic models for lysine excretion. These models were then further structured by Kelle *et al.* (1996) to represent the lysine excretion system mechanism to determine the activity of the export carrier and to calculate the cell specific concentration of the export carrier.

3 Development of a fermentation model

The lysine fermentation model, developed for this study, is based on general volume and mass balances coupled to expressions that define the excretion and uptake of cellular metabolites as functions of the extracellular component concentrations. The mass and volume balance is based on the system illustrated in Figure 6-1.

Two approaches were followed to model the metabolic behaviour of the strain. In the first approach, the cellular metabolism, i.e. specific growth rate, specific lysine productivity and the specific oxygen utilisation rate were expressed as empirical relationships based on experimental results.

In the second approach a bioreaction network was constructed which represented all the intracellular reactions believed to be active during lysine production. The relative reaction rates were then determined experimentally from batch, fed-batch and continuous experimental results. From these rates, a principle node analysis was done to determine

whether the fluxes through any node were fixed or if the flux through the node could be related to any other metabolic parameter. By fixing or correlating the flux through a number of nodes, the degrees of freedom were reduced to such an extent that the bioreaction network could be used to model the metabolic behaviour of the cell as a function of the extracellular component concentrations.

The two approaches to the modelling of the cell's metabolism was compared using Bayesian inference. The selected model is used in Chapter 7 to optimise the fermentation process performance.

3.1 Volume and mass balances

The volume and mass balance equations that describes the systems state variables are shown below:

$$\frac{dV}{dt} = F_{Gluc} + F_{Thr} + F_{AS} - Bleed - Perm' \tag{6-1}$$

$$\frac{dVX}{dt} = \mu_{obs} VX - X \cdot Bleed \tag{6-2}$$

$$\frac{dVThr}{dt} = \frac{-\mu VX}{Y_{X_{Thr,obs}}} + F_{Thr} \cdot C_{Thr} - Thr(Bleed + Perm') \tag{6-3}$$

$$\frac{dVGluc}{dt} = -q_{Gluc,obs} \cdot XV + F_{Gluc} \cdot C_{Gluc} - Gluc(Bleed + Perm') \tag{6-4}$$

$$\frac{dVLys}{dt} = q_{Lys,obs} VX - Lys(Bleed + Perm') \tag{6-5}$$

where

V is the volume of broth in the bioreactor [litre]
F_{Gluc} is the volumetric glucose feed rate [litre/h]
F_{AS} is the volumetric ammonium sulphate feed rate [litre/h]
F_{Thr} is the volumetric L-threonine feed rate [litre/h]
Bleed is the rate at which the contents of the fermenter is bleed off to maintain a constant maximum volume [litre/h]
Perm' is the permeate flow rate from the filtration unit [litre/h]
X is the biomass concentration [g DCW /l]
μ_{obs} is the specific biomass growth rate [1/h]
Thr is the auxothropic amino acids (threonine) concentration in the fermenter [g/l]
$Y_{x/thr,obs}$ is the yield of biomass from threonine [g/g] this yield was found to be 25.0 g/g. From the data of Kiss & Stephanopoulos (1991) a yield of 24.28 g/g was obtained.
C_{Thr} is the threonine concentration in the threonine feed [g/l]
Gluc is the glucose concentration in the fermenter [g/l]

q_{Gluc} is the specific glucose consumption rate [g/g/h]
C_{Gluc} is the concentration of glucose in the sugar feed [g/l]
Lys is the lysine concentration in the fermenter [g/l]
$q_{Lys,obs}$ is the specific lysine productivity [g/g/h]

3.2 Carbohydrate feed rate

The sugar feed rate F_{Gluc} is initiated at the point of initial charge sugar depletion. This point is generally recognised by an increase in pH and confirmed by spectrophotometric analysis of the residual glucose concentration (Appendix A & C). During the batch phase of the fermentation, the specific glucose consumption rate ($q_{Gluc,obs}$) is equal to the maximum glucose uptake rate of the organism provided that there are no other limiting components such as oxygen, the auxothropic amino acids and co-factors such as Mg^{2+}. Increased osmotic load in the extracellular medium may also reduce the sugar uptake rate (Practical experience at industrial scale lysine producing facility).

The maximum glucose uptake rate has been determined in both continuous and batch experiments by previous investigators under conditions of sufficient oxygen and auxothropic amino acid supply. Lee *et al.* (1995) reported a value of 1.29 g/g/h for *Corynebacterium glutamicum* ATCC 21513 from batch experiments. Oh & Sernetz (1993) conducted several continuous fermentations with *Corynebacterium glutamicum* ATCC 21544 and found a maximum glucose uptake rate of 1.38 g/g/h. The maximum specific glucose consumption rate observed in batch and continuous fermentations for *Corynebacterium glutamicum* ATCC 21253 used in this study was found to be 1.12 ± 0.02 g/g/h in the batch experiments and 1.05 ± 0.02 g/g/h in continuous experiments.

For the purpose of modelling the lysine production fermentation it was however assumed that the maximum specific glucose uptake rate would be limited to 0.4 g/g/h, to prevent overfeeding and a subsequent reduction in lysine on glucose yield (Figure 6-2). It will later be shown that this value adequately modelled both the batch and the fed-batch data generated in this study as well as that of other investigators.

The glucose feed is controlled at a specific glucose feed rate during the feed phase. Generally an increase in the specific feed rate during the lysine production phase results in increased lysine productivity but at the penalty of a reduced yield while a reduced specific feed reduces the specific productivity but brings about a slight increase in the yield of lysine form sugar (Figure 6-2).

This principle was confirmed and quantified by analysing both batch data at the higher biomass concentration as well as running various continuous fermentations at several dilution rates with varying sugar concentrations. The batch sugar, biomass and lysine profiles were analysed and the specific lysine production rate plotted as a function of the specific glucose consumption rate (Figure 6-2). Three continuous fermentations were conducted each at four dilution rates. The initial charge in each case corresponded to the

initial charge media of the batch fermentation (Appendix A). The sugar feed consisted of a mixture of the initial charge media with three sugar concentrations (20 g/l, 40 g/l and 100 g/l). The feed was started at the point of threonine depletion. Four residence times was allowed before steady state measurements were taken. Four different specific growth rates were targeted for each sugar concentration corresponding to dilution times of 0.05; 0.10; 0.20 and 0.30 1/h. Four residence times after increase of the feed rate, the specific glucose consumption rate and the specific lysine productivity were measured. A graph of the specific lysine productivity as a function of the specific glucose consumption rate is plotted in Figure 6-2. Batch data obtained from Lee *et al.* 1995 and continuous data obtained from Oh & Sernetz (1993) are included onto the graph.

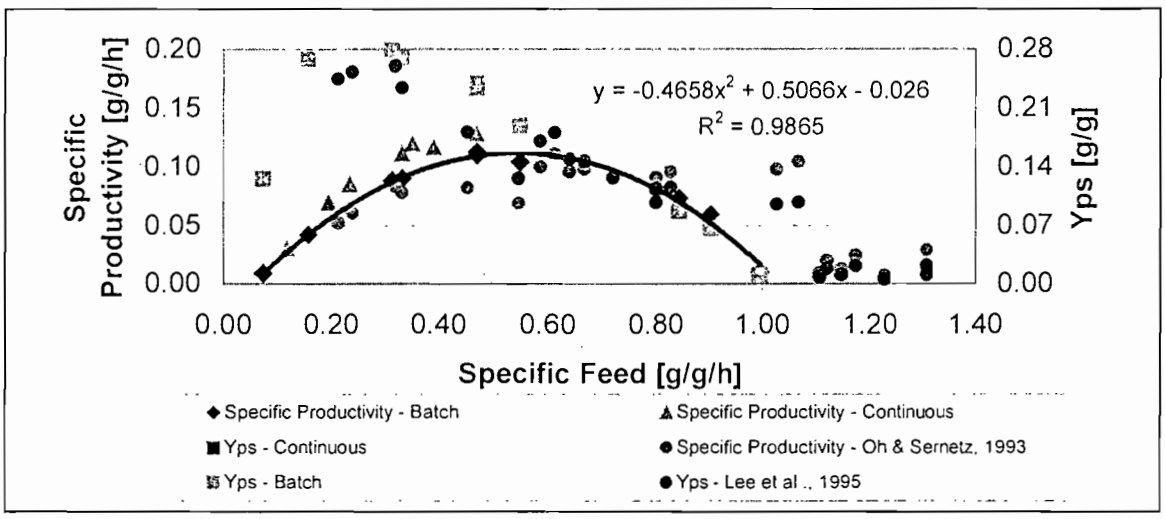

Figure 6-2. The specific lysine productivity as a function of the specific glucose consumption rate as measured in batch and continuous fermentation and compared to published data. The polynomial presented is fitted to the experimental data obtained in this study.

The yield increases sharply with increased specific feed rate, then flattens out over some range of specific feed rates before it decreases until the maximum uptake rate is reached. The specific productivity follows an almost quadratic function of the specific feed rate.

The glucose consumption rate, which maximises productivity and yield, has been determined from experimental results by various investigators. The optimal specific glucose uptake rate under conditions of sufficient supply of oxygen and the auxothropic amino acids reported in the literature are summarised in Table 6-1. From the experimental results presented in Figure 6-2 it was found that the optimal specific glucose uptake rate in the batch, fed batch and continuous fermentations was measured as 0.38 ±0.05 g/g/h. This value was obtained by maintaining the maximum yield and maximising the specific productivity. It corresponds well with the values published in the literature (Table 6-1).

Table 6-1. Maximum glucose uptake rate for lysine producing organisms

Reference	Strain	Maximum glucose uptake rate [1/h]
Kiss & Stephanopoulus (1991)	*C. glutamicum* ATCC 21253	0.46
Hilliger & Hanel (1981)	*C. glutamicum* 9366	0.45
Coello *et al.* (1992)	*C. glutamicum* ATCC 21513	0.42
Vallino & Stephanopoulus (1994)	*C. glutamicum* ATCC 21253	0.40
Lee *et al.* (1995)	*C. glutamicum* ATCC 21513	0.38
Oh & Sernetz 1993	*C. glutamicum* ATCC 21544	0.38

During the feed phase, the specific glucose consumption rate (q_{Gluc}) is equal to the targeted specific feed rate if the feed rate is less than the maximum consumption rate. This implies imply that for the feed phase the residual glucose concentration is either constant or zero depending on the sugar concentration at which the feed was initiated. Because a feed and bleed strategy is generally followed for the fed-batch fermentations, a zero residual sugar concentration will maximise the yield of lysine produced per glucose fed. This is in essence an economic optimum as the fermentation may behave differently under conditions of sufficient glucose supply. For all the fed-batch fermentations, it was therefore ensured that there was no sugar accumulation to ensure that the glucose consumption and feed rates were equal. Hence the feed rate, F_{Gluc} is given by:

$$F_{Gluc} = \frac{Spec_{Gluc} \cdot X \cdot V}{C_{Gluc}} = \frac{q_{Gluc} \cdot X \cdot V}{C_{Gluc}} \qquad (6\text{-}6)$$

where F_{Gluc} is the glucose feed rate (l/h), X is the biomass concentration (g/l DCW), V is the volume of broth in the reactor (l), $Spec_{Gluc}$ represents the specific glucose feed rate (g/g/h which for this model was assumed to be equal to the specific glucose consumption rate q_{Gluc} at a fixed glucose concentration and C_{Gluc} is the concentration of glucose in the feed (g/l).

3.3 Auxothropic amino acid (Threonine) feed rate

C. glutamicum ATCC 21253 is auxothropic for L-threonine, L-methionine and L-leucine. In the absence of these components, cell growth cannot be sustained. The maximum biomass concentration achieved during the batch phase of the fermentation is controlled by the initial charge L-threonine concentration. Experimentally determined cell yields (grams of dry cell weight per milligram of amino acid consumed) from Kiss & Stephanopoulos (1992) were used to determine the required ratio of the auxothropic amino acids both in the initial charge and the threonine feed. The threonine feed therefore represents a feed mixture containing all the initial charge trace salts as well as the desired ratio of the auxothropic amino acids. Addition of the threonine feed results in increased growth due to the increased availability of the auxothropic amino acids. Similar to the

sugar feed the threonine feed rate is maintained at a desired specific threonine consumption rate (q_{Thr} in g/g/h), and is one of the controllable variables.

$$F_{Thr} = \frac{q_{Thr} \cdot X \cdot V}{C_{Thr}} \tag{6-7}$$

where F_{Thr} is the auxothropic amino acid feed rate (l/h), q_{Thr} is the specific threonine consumption rate (g/g/h), X is the biomass concentration (g/l DCW), V is the volume of broth in the bioreactor (l) and C_{Thr} is the concentration of L-threonine in the auxotrophic amino acid feed (g/l).

3.4 Ammonium sulphate (AS) feed rate

L-Lysine is a monovalent cation at pH 7. When lysine is produced from glucose, two ammonium ions are used as source of nitrogen. An H^+ must be excreted with the Lysine to maintain an overall charge balance. The excretion of an H^+ results in a decrease in the fermenter pH. The pH in the fermenter is controlled by the addition of ammonium hydroxide. This results in the next set of reactions:

$$x\ Gluc + y\ O_2 + (NH_4)_2SO_4 \rightarrow Lys^+ + z\ CO_2 + H^+ + SO_4^{2-} \tag{6-8}$$
$$NH_4OH + H^+ \rightarrow NH_4^+ + H_2O \tag{6-9}$$

Nett reaction

$$2x\ Gluc + 2y\ O_2 + (NH_4)_2SO_4 + 2\ NH_4OH \rightarrow 2\ Lys^+ + 2z\ CO_2 + 2\ H_2O + SO_4^{2-} \tag{6-10}$$

The stoichiometric coefficients of the glucose, oxygen and the carbon dioxide depend on the cellular metabolism and therefore only the nitrogen and charge balance is considered in these reactions.

The two nitrogen atoms in the lysine molecule originate from the ammonium sulphate and the ammonium hydroxide used for pH control. It is therefore clear that the requirement for ammonium sulphate depends on the amount of lysine produced. The ammonium sulphate serves to provide a single nitrogen atom to produce lysine but also to supply the sulphate ion that would act as a counter ion for the excreted cationic lysine molecule.

To ensure that there is always an excess of ammonium ions as well as counter ions available, the ammonium sulphate stream are fed to maintain a free and saline nitrogen level in the bioreactor between 1.5 and 2.5 g/l. It is known that increased free and saline nitrogen concentration suppresses biolocical activity due to increased osmotic load. Vallino & Stephanopoulos (1993) used 7 g/l of ammonium sulphate in their growth medium and did not report negative osmotic effect. It was therefore concluded that free and saline levels below 2.5 g/l would not impart negatively on the cells activity.

On a biochemical level the GS/GOGAT ammonium assimilation route (Gottschalk 1986; Vandecasteele *et al.* 1975), does not operate at ammonium ion concentrations above 0.5 g/l. Under these conditions ammonia consumption is catalysed by a single enzyme, glutamate dehydrogenase to produce glutamate from which glutamine is synthesised. Following glutamine synthesis, the newly formed α-amino group can easily be transferred to other carbon skeletons by trans-amination reactions to form, amongst other amino acids L-Lysine. By ensuring that the ammonium ion concentration remains above 0.5 g/l, ammonium uptake is dictated by a single constitutive enzyme and therefore would not limit lysine production by complicated interactive control mechanisms active in the two-enzyme system.

The impact of ammonium sulphate feed rate on the optimisation process is assumed negligible if enough nitrogen and enough sulphate counter ions are available to produce lysine and biomass. The ammonium sulphate flow rate is therefore eliminated as a controllable variable, but is included in the model by the following equation:

$$F_{AS} = \frac{(S_1)q_{Lys,obs}VX + (S_2)\mu_{obs}VX}{C_{AS}} \qquad (6\text{-}11)$$

where F_{AS} is the ammonium sulphate feed rate, S_1 (g Ammonium sulphate / g Lysine) and S_2 (g Ammonium sulphates / g Biomass) are the stoichiometric coefficients for nitrogen uptake for lysine and biomass production respectively, q_{Lys} is the specific lysine production rate (g/g/h), C_{AS} is the concentration of ammonium sulphate in the feed stream.

It has already been shown that one of the nitrogen atoms in the lysine molecule originates from the ammonium sulphate and the other from the ammonium hydroxide used to maintain the fermenter pH. S_1 can there easily be determined by assuming that half a mole of ammonium sulphate would be required to produce one mole of L-Lysine (Equation 6-10).

Ingraham *et al.* (1983) showed that biomass can be synthesised from 12 precursor metabolites. They have calculated the amounts required to form 1 gram dry weight of biomass, as well as the amounts of ATP, $NADH_2$ and $NADPH_2$ required for biosynthesis. Their analysis is similar to that of Stouthamer (1973). Although the reported biomass yields are for *Eschericia coli,* they are adequate for *C. glutamicum.* Vallino & Stephanopoulos (1993), reproduced the biomass yield reported by Ingraham *et al.* (1983) for threonine and methionine to within 5%. From this analysis 0.796 moles of NH_3, 0.025 moles of glutamate and 0.025 moles of glutamine are required to produce one mole of biomass (the molecular weight of the biomass was assumed to be 100 g/gmol). Hence a total of 0.1 g of NH_3 is required to produce 1 gram of dry biomass.

The nitrogen required can be obtained from both the ammonium sulphate feed as well as the ammonium hydroxide solution used for pH control. If it is assumed that all the nitrogen

originates from the ammonium hydroxide feed used for pH control and subsequently none from the ammonium sulphate feed then the factor S_2 would equal zero.

By measuring the amount of biomass formed during the batch phase of the fermentation the amount of ammonia required could be determined through the stoichiometry reported by Ingraham *et al.* (1983). If the ammonium sulphate concentration in the initial charge as well as the amount of ammonium hydroxide fed during this phase is known the total amount of ammonia required for biomass growth can be determined. From a measurement of the free and saline nitrogen concentration at the end of growth, the total amount of ammonia consumed could also be determined. Assuming that all the ammonia present in the fermenter after growth is ammonium sulphate (assuming that no lysine was produced during this phase and therefore all the sulphates would not be used as counter ions but still be attached to ammonium ions) the percentage of the ammonia used for biomass production that originated from the ammonium sulphate in the initial charge can be determined by subtracting the ammonium hydroxide fed from the total ammonia required to form the measured amount of biomass. An example calculation is displayed in Table 6-2.

Table 6-2. Determining the fraction of ammonia in biomass that originates from ammonium sulphate opposed to ammonium hydroxide

	Concentration	Ammonia equivalents
	[g/l]	[g/l]
Ammonium sulphate in initial charge	7.0	1.80
Ammonium hydroxide fed during growth	2.0	0.97
Total ammonia equivalents available		2.77
Residual free and saline N after growth	1.4	1.70
Ammonia used during biomass formation		1.07
Biomass formed during growth	10.7	
% Ammonia that originated from AS		10%

This implies that S_2 should correspond to the ammonium sulphate equivalents of 10% of the amount of ammonia required to constitute 1 gram of biomass which is 0.01 g ammonia / g biomass or 0.04 g ammonium sulphate per gram of biomass.

3.5 Bleed rate

The bleed rate is used to maintain a constant volume in the bioreactor once the maximum volume is reached. Thus during the batch phase as well as during the initial period of the feed phase, before the maximum operating volume is reached, the bleed rate is zero. From the point at which the maximum volume is reached, the bleed rate is calculated from Equation 6-1 by setting the change in volume to zero. Hence

$$\text{if } V < V_{max} \text{ then}$$
$$\text{Bleed} = 0 \tag{6-12}$$
$$\text{if } V \geq V_{max} \text{ then}$$
$$\text{Bleed} = F_{Gluc} + F_{Thr} + F_{AS} - \text{Perm} \tag{6-13}$$

where, Bleed is the bleed rate in (l/h), V_{max} is the maximum working volume of the bioreactor (l).

3.6 Permeate flow rate

The work of Hermia (1982) serves as a fundamental basis for flux decline modelling. A generic form of their equation (Eq. 3-88) was used by several authors (Schneider & Klein 1982; Mietton-Peuchot 1992) found that this generic form of Hermia's laws to be well suited to the description of the initial stages of cross-flow filtration. A constant term J_{ss} has been included by Liberge *et al.* (1994) to provide a semi-empirical correlation of the cross-flow filtration flux.

$$\text{Perm}' = 3.6 \times 10^6 \cdot A\left[J_{ss} + \frac{(J_o - J_{ss})}{(1 + k_{decline} t'_{perm})}\right] \tag{6-14}$$

where Perm' is the permeate flux in (l/h), A is the membrane area (m^2), J_o is the initial flux (m/s) at t = 0, J_{ss} is the steady state flux (m/s), t'_{perm} is the filtration time in h and $k_{decline}$ (1/h) is an empirical functions of the suspension composition and the operating parameters (Eq. 3-103).

The flux decline parameter, $k_{decline}$ is given by:

$$k_{decline} = m_0 J_0^{m_1} v^{m_2} X^{m_3} \tag{6-15}$$

where $m_0 \ldots m_3$ are parameters determined from a least square fit of the experimental data obtained in Chapter 3, J_o is the initial flux (m/s), v is the cross flow velocity (m/s) and X is the biomass concentration (g/l DCW)

In Chapter 3, the parameters in this model have been determined as functions of the broth composition and the membrane operating parameters. Here only the equations would be presented:

The steady state flux, J_{ss}, is estimated based on Darcy's law:

$$J_{ss} = \frac{\Delta P}{\upsilon R_t} \tag{6-16}$$

$$R_t = R_m + R_p + R_c \tag{6-17}$$

where

ΔP is the trans-membrane pressure drop (Pa),
υ is the broth viscosity (Pas)
R_t is the total hydraulic resistance (m^{-1}) made up of the membrane resistance (R_m), cake resistance (R_c) and the pore plugging resistance (R_p).

The intrinsic membrane resistance is assumed to be a function of the membrane properties and is therefore not influenced by the operating parameters or the nature of the feed suspension.

Table 6-3. Intrinsic membrane resistance, determined from pure water flux data in Chapter 2. (Table 2-11)

Membrane type	Pore size	Intrinsic membrane Resistance [m^{-1}]
Micro-filtration membranes	0.45 μm	8.00×10^{10}
	0.22 μm	9.20×10^{10}
Ultra-Filtration membranes	150 kD	9.20×10^{11}
	300 kD	9.00×10^{11}

The determination of the pore-plugging resistance at the steady state flux is based on Hagen-Poiseuille flow through an array of uniform cylindrical pores. Belfort *et al.* (1986) extended this analysis to account for the presence of a pore size distribution. The ratio of the modified flux with and without pore constriction is predicted by:

$$\frac{J_1'}{J_2'} = 1 - \frac{4}{q_{pore}^{\ 3}}\left(\frac{k_{thick}}{r_p^*}\right) + \frac{6}{q_{pore}^{\ 6}}\left(\frac{k_{thick}}{r_p^*}\right)^2 - \frac{4}{q_{pore}^{\ 6}}\left(\frac{k_{thick}}{r_p^*}\right)^3 + \frac{1}{q_{pore}^{\ 5}}\left(\frac{k_{thick}}{r_p^*}\right) \tag{6-18}$$

$$R_p = R_m\left(\frac{J_2'}{J_1'} - 1\right) \tag{6-19}$$

where

k_{thick} is the thickness of an absorbent multilayer inside the pore (micrometer)

q_{pore} is given by $1+(r_{p,STDEV}/r_p^*)^2$ where $r_{p,STDEV}$ is the standard deviation of the pore size distribution (micrometer)

r_p^* is the mean membrane pore size (micrometer)

The values of r_p^* the mean membrane pore size was obtained form the membrane manufacturers. The standard deviation, $r_{p,STDEV}$ for each membrane was estimated from pure water flux data. The value of k_{thick} for each membrane was obtained from a least square fit of the experimentally determined R_p values (Chapter 5, Section 5.1) These values are repeated in Table 6-4.

Table 6-4. Parameters used to estimate the pore plugging resistance for a feed suspension of *C. glutamicum* cells suspended in an industrial media formulation, estimated from the data collected in this study (Chapter 5, Section 5.1)

Parameter Eq. 3-90	Micro-filtration membranes		Ultra-filtration membranes	
Pore size	0.45 μm	0.22 μm	150 kD	300 kD
r_p^* (μm)	0.45	0.22	0.02	0.03
$r_{p,STDEV}$ (μm)	0.30	0.14	0.01	0.02
q_{pore} (μm)	1.44	1.40	1.44	1.44
k_{thick} (μm)	0.42	0.20	0.0045	0.0099
J_2'/J_1'	0.14	0.09	0.70	0.67

The cake resistance is given by the intrinsic resistance of the gel layer formed on the membrane surface during the filtration process. The thickness of the gel or cake layer is determined from a force balance of a single particle flowing in the suspension. The intrinsic resistance of the gel layer depends on the nature of the material retained and the applied pressure. The cake resistance can therefore be estimated from:

$$R_c = \sqrt{k_t \frac{X^{p_1} \Delta P^{1+n_c}}{v}} \qquad (6\text{-}20)$$

where k_t, p_1 and n_c are constants, determined empirically in Chapter 3. X represents the bulk biomass concentration (g/l DCW). ΔP (Pa) and v (m/s) represents the trans-membrane pressure drop and the cross-flow velocity respectively.

These parameters have been determined by a least square fit of experimental data as reported in Chapter 3, Section 5-1. The values of these parameters using an industrial media formulation are presented in Table 6-5.

Table 6-5. Values of the parameters used to estimate the cake resistance for cells suspended an industrial media formulation.

Parameter	Estimated value
p_1	0.67
n_c	0.45
k_t	4.44×10^{12}

The flux decline constant $k_{decline}$ (Equation 6-14) is based on the basic filtration laws developed by Hermia (1982). The flux decline constant, $k_{decline}$ in Equation 6-14 is modelled as a function of the initial flux, the cross-flow velocity and the biomass concentration (Equation 6-15).

The values of the constants m_0 to m_3 were determined by a least squares fit of experimental data (Chapter 3, Section 5.3). The values of these parameters for an industrial media formulation are presented in Table 6-6.

Table 6-6. Values of the parameters in the flux decline equation as determined in Chapter 3, Section 5.3

Parameter	Value
m_0	0.53
m_1	0.58
m_2	-0.25
m_3	0.48

The cleaning of the membrane is modelled as a first order process with constants determined form experimental data using a least square approach. For the industrial media formulation using a 5% Nitric acid solution at 40 °C as cleaning agent the value of k_{clean} was found to be 0.3 h^{-1}.

$$J_i - \frac{Perm_{At\ the\ start\ of\ cleaning}}{A} = \left[J_0 - \frac{Perm_{At\ the\ start\ of\ cleaning}}{A} \right] (1 - \exp(-k_{clean} t_{clean}) \qquad (6\text{-}21)$$

where J_i is the permeate flux (m/s) after the cleaning process, Perm is the volumetric permeate flow rate when the cleaning process is initiated (l/h), k_{clean} is the cleaning time constant (h^{-1}) and t_{clean} is the duration of the nitric acid cleaning process.

3.7 Modelling of the cellular metabolism

The set of equations discussed thus far constitutes the outline of the mass and volume balance. In this section, the microbial metabolism is modelled to obtain relationships between the different components in the mass balance. Two approaches have been followed to model the metabolism. In the first approach, the cell was considered as a

"black box" and empirical correlations developed that simulate the behaviour of the cell with regard to extracellular metabolite consumption and excretion rates. In the second approach the metabolism was modelled as a network of biochemical reactions, by defining certain uptake rates of extracellular metabolites and specifying the flux split ratios at certain critical nodes based on the cellular regulatory system.

3.7.1 Modelling of the cells metabolism through empirical correlations

3.7.1.1 Modelling of microbial growth

The general form of a model for microbial growth under an imposed environmental limitation is:

$$\mu = \mu_{max} G_1 \qquad 0 \le G_1 \le 1 \tag{6-22}$$

where μ_{max} is the maximum specific growth rate under ideal conditions and G_1 represents the limitation imposed by any environmental factor held at a sub-optimum value. Monod substrate limitation is a familiar form of G_1.

$$G_1 = \frac{Sub_1}{k_1 + Sub_1} \tag{6-23}$$

where Sub_1 is the limiting substrate concentration and k_1 is its half-saturation constant, indicating the affinity for the component. Situations are often encountered where the rate of growth is influenced by more than one environmental factor. A general form of the growth model under dual limitation is:

$$\mu = \mu_{max} G_{12} \qquad 0 \le G_{12} \le 1 \tag{6-24}$$

where G_{12} is the combined effect of two limiting factors at sub-optimum values.

Several unstructured models of G_{12} are reported in the literature. These models are characterised by Bader (1982) as non-interactive or interactive. The non-interactive models assume that at any time the specific growth rate is limited by only one substrate. Thus, Ryder & Sinclair (1972) proposed that the growth rate of the micro-organism equals the lowest value predicted from separate single-substrate models under otherwise optimum conditions. Mathematically,

$$G_{12} = \min\left(\frac{Sub_1}{k_1 + Sub_1}, \frac{Sub_2}{k_2 + Sub_2}\right) \tag{6-25}$$

A similar unstructured model was proposed by Baltzis & Fredrickson (1988) wherein the identity of the limiting substrate was determined on the basis of the observed biomass yield coefficient.

The interactive approach assumes that any environmental factor present at other than optimum concentration must affect the overall growth rate. Magee *et al.* (1972) proposed the "double Monod" or factorial model for growth in the presence of two essential substrates:

$$G_{12} = \left(\frac{Sub_1}{k_1 + Sub_1}\right)\left(\frac{Sub_2}{k_2 + Sub_2}\right) \tag{6-26}$$

Tsao & Hansen (1975) extended the above approach to include the effect of growth enhancing substrates.

Mankad & Bungay (1988) expressed the growth rate as a weight average of individual substrate limitations:

$$G_{12} = \left(\frac{k_1/Sub_1}{k_1/Sub_1 + k_2/Sub_2}\frac{Sub_1}{k_1 + Sub_1}\right)\left(\frac{k_2/Sub_2}{k_1/Sub_1 + k_2/Sub_2}\frac{Sub_2}{k_2 + Sub_2}\right) \tag{6-27}$$

Mankad & Nauman (1992) proposed a functional relationship between G_1 and G_2 which takes into consideration the nature of the interaction between the two limitations:

$$G_{12} = \min(G_1, G_2) \cdot \max(G_1, G_2)^{\alpha_{12}} \tag{6-28}$$

where G_1 and G_2 represent the extent of the individual limitations under otherwise optimal conditions and α_{12} is an empirically determined interaction factor. The value of α_{12} depends on the nature of the interaction between the variables on the micro-organism and potentially on the overall fermentation environment.

Büchs (1991) proposed an interactive limitation for the growth of *C. glutamicum* in an industrial medium formulation (Eq. 6-29). The specific growth rate (μ) was limited by the availability of threonine and glucose.

$$\mu = \mu_{max}\left[\frac{Thr}{km_1 + Thr}\right]\left[\frac{Gluc}{km_2 + Gluc}\right] \tag{6-29}$$

Bader (1978) called this the interactive case, as applicable to growth using sub-optimum amounts of two nutrients that are metabolised via independent pathways to give rise to a single product required for growth.

For the system at hand, the glucose limitation term has been ignored. The bulk of the cell growth occurs during the batch phase of the fermentation. During this phase, there is an abundance of glucose, and the growth is limited only by the availability of L-threonine. If growth during the latter stages of the fermentation occurs L-threonine was proportionally more limiting than glucose as a result of the experimental setup used.

The maximum specific growth rate observed in both batch on continuous experiments was 0.52 h^{-1}. Similar values obtained by other investigators are summarised in Table 6-7.

Table 6-7. Literature values of the maximum specific growth rate under ideal conditions

Reference	Strain	μ_{max} [h^{-1}]
Kiss & Stephanopoulus (1991)	*C. glutamicum* ATCC 21253	0.53
Oh & Sernetz (1993)	*C. glutamicum* ATCC 21544	0.49
Lee *et al.* (1995)	*C. glutamicum* ATCC 21513	0.53

The saturation constant determined from the batch experiments was found to be 0.098 ± 0.002 [g/l]. The results found in this study are compared to that of Takamatsu *et al.* (1975) and Kiss & Stephanopoulos (1991). The values obtained in this study is compared with that published in literature can be seen in Figure 6-3.

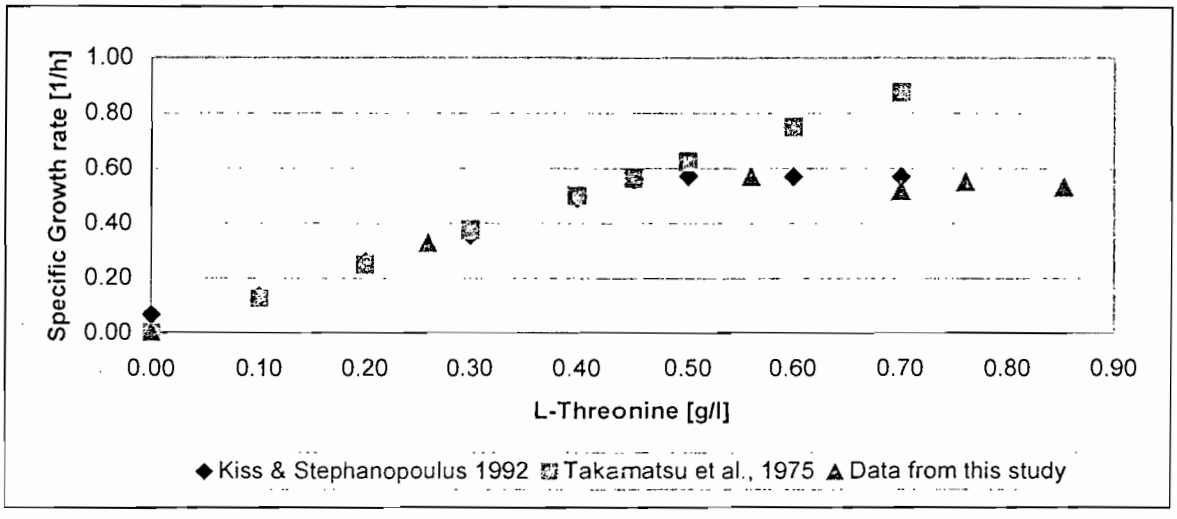

Figure 6-3. The specific growth rate as a function of the L-threonine concentration in the extracellular environment.

3.7.1.2 The specific lysine productivity

It has been shown by previous investigators (Ludeking & Piret 1959, Wang & Stephanopoulos 1984; Büchs 1991) that the specific lysine productivity (q_{Lys}) depends on the specific growth rate and the specific glucose consumption rate. The following equation is proposed to model the specific lysine productivity in this study:

$$q_{Lys} = \left(c_1\mu^2 + c_2\mu + c_3\right)\cdot\left(\frac{q_{Gluc}}{k_{Lys} + q_{Gluc}}\right) \qquad (6\text{-}30)$$

where q_{Lys} is the specific lysine productivity in g/g/h, μ is the specific growth rate in h_{-1}, q_{Gluc} is the glucose feed rate (g/g/h) and c_1 to c_3 and k_{Lys} is constants.

The relationship between the specific growth rate and the specific lysine productivity was determined from continuous fermentation data. This data is compared to that derived by Takamatsu *et al.* (1975), Lee *et al.* (1995) and Kiss & Stephanopoulos (1993) in Figure 6-4.

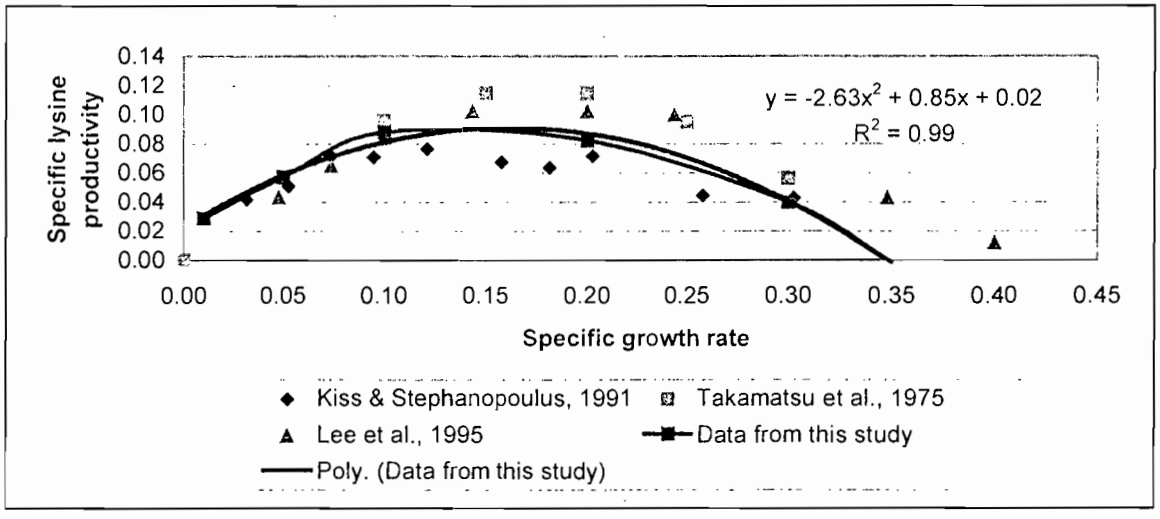

Figure 6-4. The specific lysine productivity as a function of the specific growth rate.

The relationship between the specific glucose feed rate and the specific lysine productivity has already been discussed in Section 3.2 and are illustrated in Figure 6-2. The values of the parameters in the specific lysine productivity equation were determined from a least squares fit of the experimental data and are summarised in Table 6-8.

Table 6-8. Values of the parameters in the specific lysine productivity equation (Equation 6-30) as determined by a least square fit of the experimental data

Parameter	Estimated value
c_1	-2.63 ± 0.005
c_2	0.85 ± 0.005
c_3	0.02 ± 0.005
k_{sp}	0.98 ± 0.01

3.7.1.3 Specific oxygen utilisation rate

Figure 6-5 depicts the measured specific oxygen utilisation rate as a function of the specific growth rate based on continuous experimental data from this study and literature data presented by Kiss & Stephanopoulos (1993).

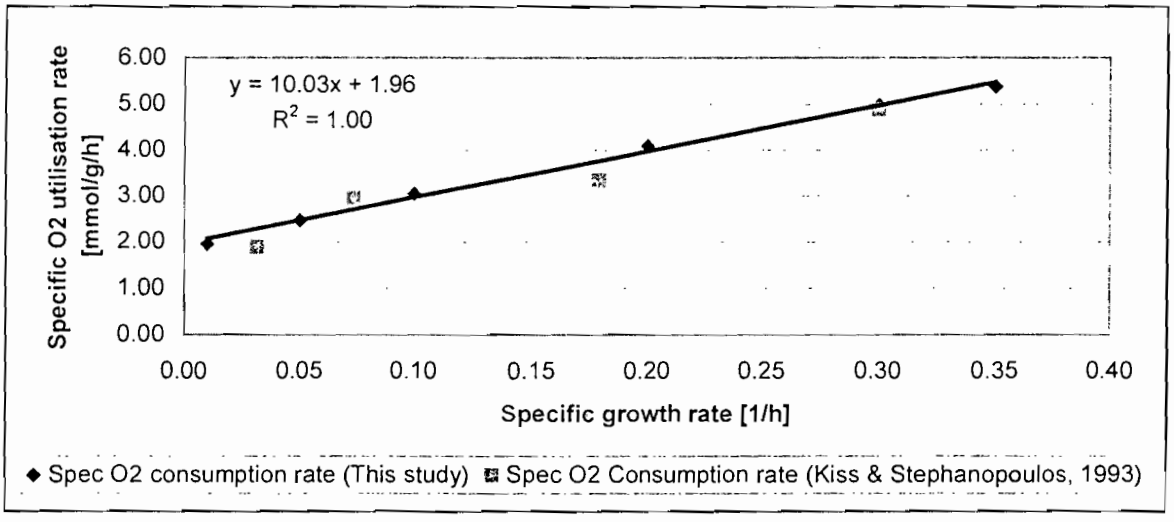

Figure 6-5 Specific oxygen utilisation rate ($Spec_{O2}$ in mmol/g/h) as a function of the specific growth rate (h^{-1}).

A linear equation models the dependency of the specific oxygen consumption rate (mmol/g/h) on the specific growth rate. Viesture *et al.* (1989) suggested the same dependency of specific oxygen consumption on the specific growth rate.

$$OUR = X \cdot q_{O_2} = X \cdot (10.03\mu + 1.96) \qquad (6\text{-}31)$$

where OUR is the oxygen utilisation rate in mmol/l/h, X is the biomass concentration in g/l DCW, q_{o2} is the specific oxygen uptake rate in mmol/g/h and μ is the specific growth rate in h^{-1}.

3.7.2 Modelling of the microbial metabolism using a bioreaction network

In the second approach to model the metabolic behaviour of *C. glutamicum* in the lysine fermentation, a bioreaction network was constructed from published information regarding the biochemistry of lysine producing bacteria. The bioreaction network combines the known metabolic pathways of the organism with a pseudo steady state approximation for intracellular metabolite concentrations to generate a mathematical representation of metabolite flows. Figure 6-6 provides a simplified network for lysine biosynthesis by *C. glutamicum,* including the main energy and metabolite generating bioreactions of glycolysis, the penthose phosphate pathway and the tricarboxylic acid cycle as well as the aspartate family of amino acids leading to L-Lysine (Vallino & Stephanopoulus 1989).

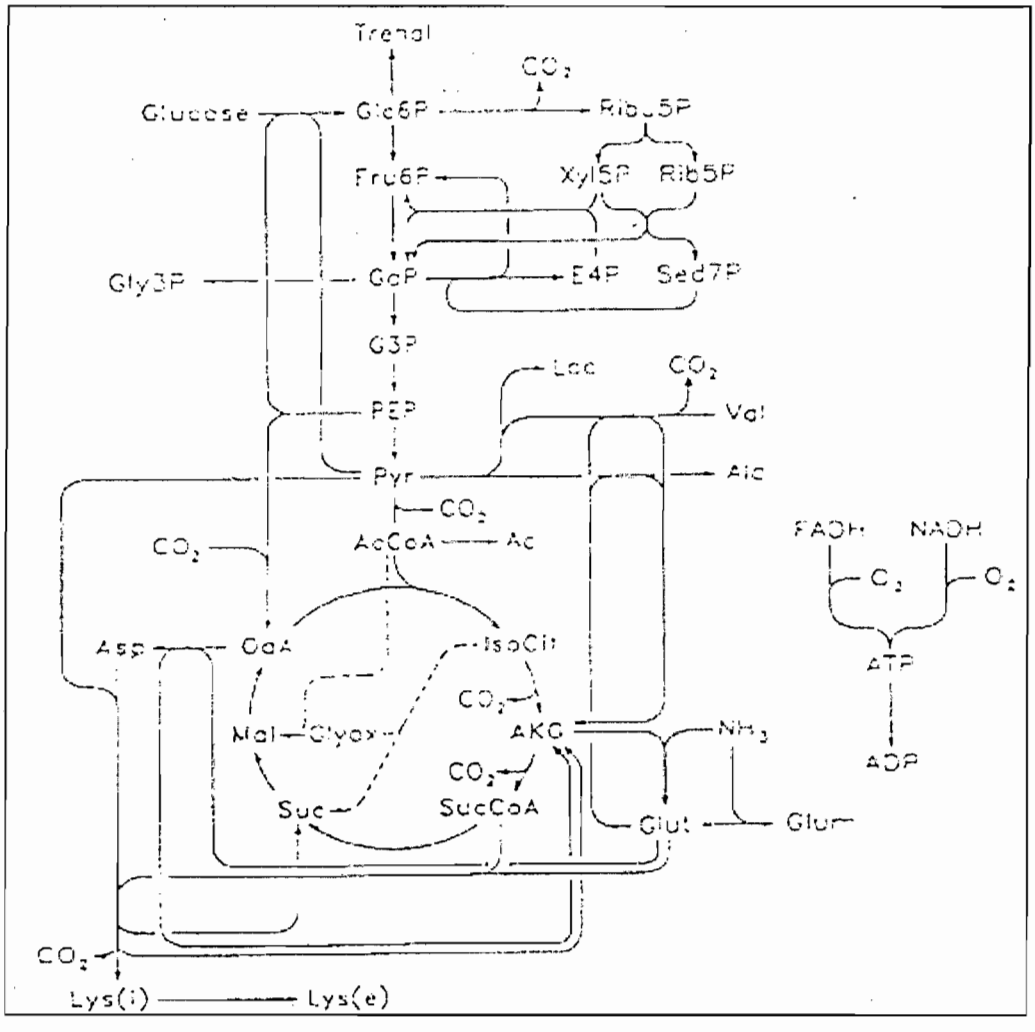

Figure 6-6. Bioreaction network for lysine production by Corynebacterium glutamicum

Biomass synthesis is treated as a lumped reaction which draws energy and metabolites from the main metabolic branches according to the stoichiometry given by Stephanopoulos (1992) (C = 47.6%, H = 6.46%, O = 31.0%, N = 11.8%, Ash = 3.14%).

The ATP requirement in the lumped biomass equation is the theoretical amount corresponding to an ATP yield of 28 g of biomass synthesised per mole of ATP consumed and the efficiency of oxidative phosphorylation or P/O ratio, is taken as 2 mol ATP formed per atom of oxygen reduced (Ingraham *et al.* 1983).

Following the approach of Vallino & Stephanopoulos (1989) a mathematical representation of the metabolic network is constructed by forming a material balance for each metabolite of the network as a function of the reactions producing or consuming that metabolite. The bioreaction network consists of 34 reactions or fluxes and 37 components. Eight extracellular components have been identified: glucose, biomass, lysine, oxygen, carbon dioxide, ammonium, trehalose and valine. On assuming that the concentrations of the intracellular metabolites remain constant, the system consists of 71 unknowns, 29 zero accumulation rates and 37 equations. Thus, five external equations or extracellular metabolites must be specified to yield the intracellular carbon flux distribution.

The carbon flux distribution for both batch and continuous data have been determined using the bioreaction network. For each data point, six extracellular metabolite consumption or excretion rates (glucose, biomass, lysine, oxygen, carbon dioxide, ammonium ion) were determined from the experimental data and normalised using the glucose consumption rate. This data was introduced into the bioreaction network to solve the carbon flux distribution for each case.

Where the number of variables exceeded the degrees of freedom, a least squares solutions rather than an exact solution were obtained. Because the number of variables introduced into the bioreaction network was greater than the degrees of freedom a redundancy analysis could be performed for each data point. The redundancy analysis calculated a consistency index which indicates whether the extracellular metabolite measurement set satisfies the material balance at a given confidence level.

The metabolic network contains some 35 nodes or branch points. However a theoretical yield analysis (Vallino & Atephanopoulus 1989) has revealed that nodal split ratios (the carbon flux through a branch normalised by the flux into the node) change at only a few nodes, while partitioning of carbon at all other nodes remains independent of product yield. Therefore a investigation to determine the characteristic metabolite regulatory constraints need only focus at the principle nodes for L-lysine synthesis: glucose-6-phosphate, phosphenolpyruvate and pyruvate junctions. It has been shown in Chapter 5 as well as by Vallino (1991) that both the glucose-6-phosphate and the pyruvate nodes are flexible, because the nodal split ratios respond to meet metabolic requirements. The PEP node might be rigid.

Kiss & Stephanopoulus (1992) used continuous culture data and the bioreaction network to further understand the PEP node (Figure 6-7). This work has been

repeated in the experimental setup of this study and the results are depicted in Figure 6-8 to 6-10.

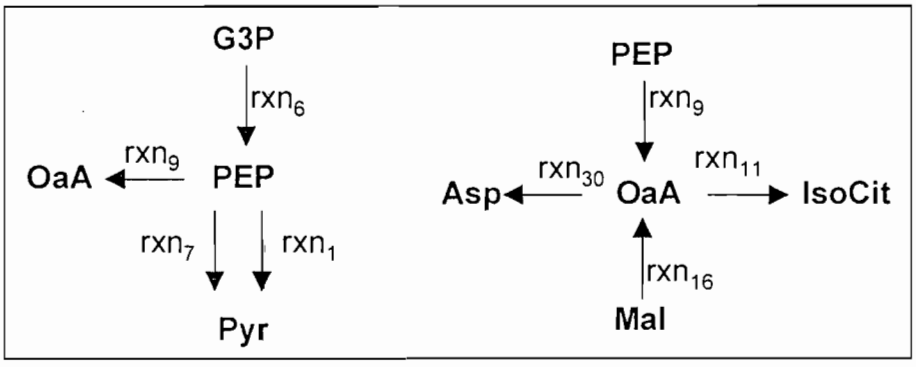

Figure 6-7 Carbon splits around the PEP and OaA principle node. The reactions refer to Appendix E.

Figure 6-8 suggests that the fraction of PEP converted to OaA remains independent of the specific growth rate. This suggests a strong metabolic control around this point pointing to a possible rigidity. The fraction of OaA that was produced from PEP that is converted to Asp (a lysine precursor) depends on the specific growth rate (Figure 6-9). As the growth rate is reduced, a larger portion of the PEP converted into OaA is converted to Asp for lysine formation. This confirms the non-growth-associated nature of lysine production. At reduced growth rates lysine production is favoured. The fraction of OaA converted to Asp is approximately constant (Figure 6-10) between 30 and 40%.

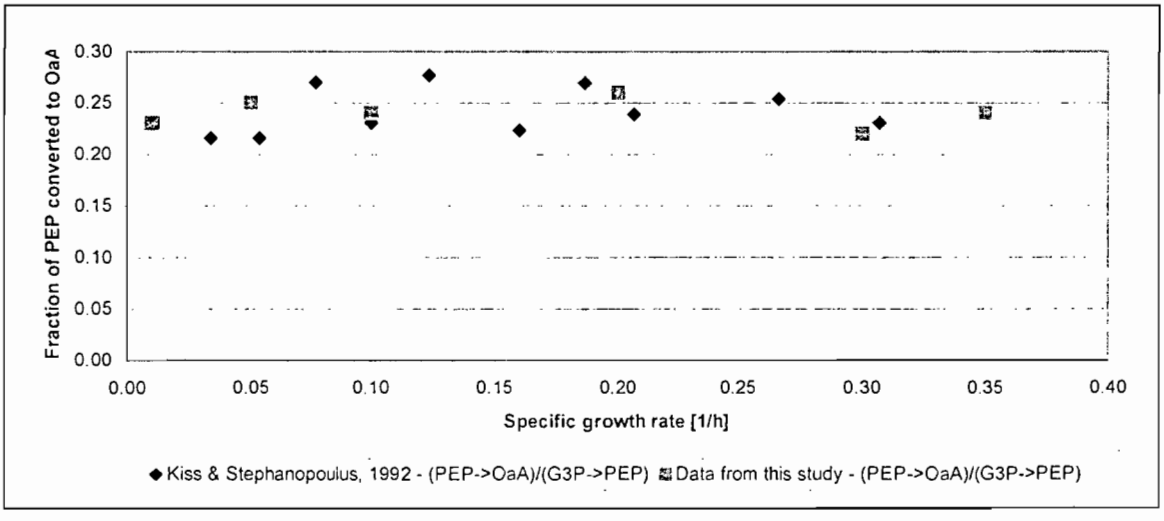

Figure 6-8. Fraction of PEP converted to OaA vs. specific growth rate

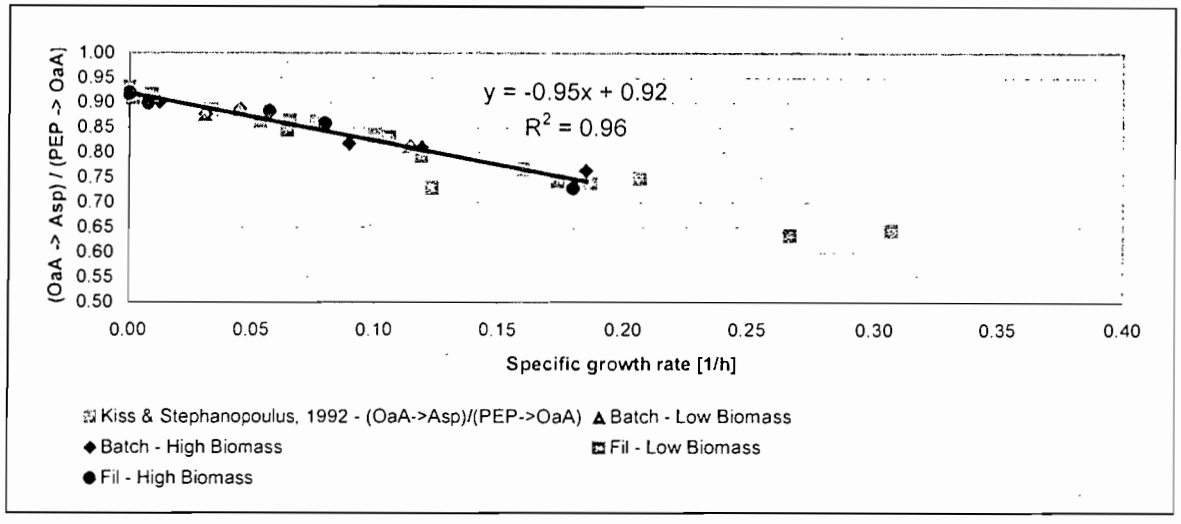

Figure 6-9. The fraction of OaA that originated from PEP that is converted to Asp

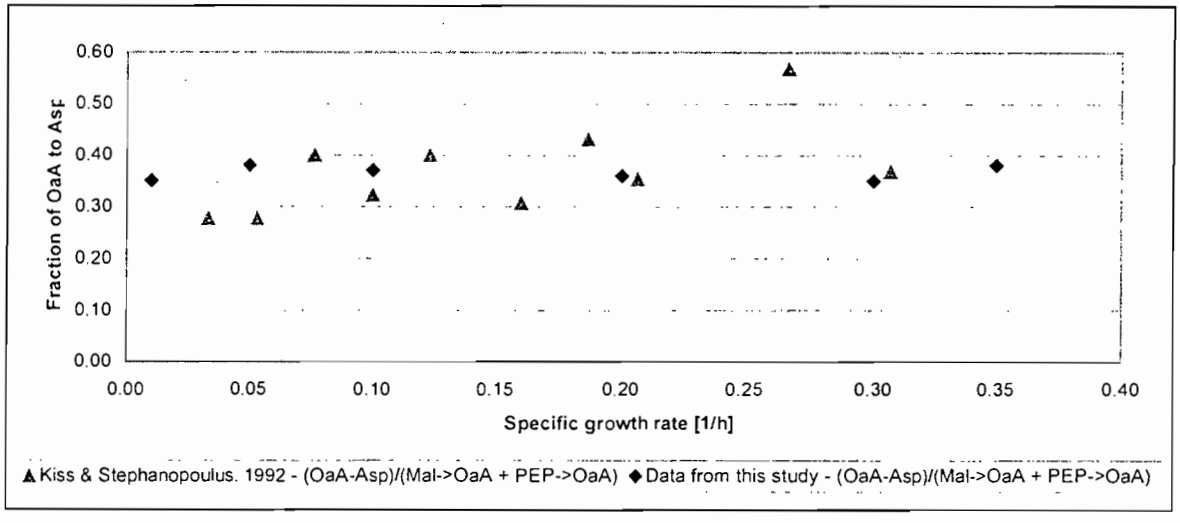

Figure 6-10. The fraction of OaA converted to Asp vs. specific growth rate

The flux analysis around PEP constitutes three additional equations in the bioreaction network. The fraction of PEP converted to OaA is 25% (Equation 6-32); the fraction of OaA that originated from PEP and is converted to Asp is a linear function of the specific growth rate (Equation 6-33) and the fraction of OaA converted to Asp is fixed at 36% (Equation 6-34).

$$\frac{PEP \xrightarrow{rxn_9} OaA}{G3P \xrightarrow{rxn_6} PEP} = 0.25 \tag{6-32}$$

$$\frac{OaA \xrightarrow{rxn_{30}} Asp}{PEP \xrightarrow{rxn_9} OaA} = -0.77\mu + 0.90 \tag{6-33}$$

$$\frac{OaA \xrightarrow{rxn_{30}} Asp}{Mal \xrightarrow{rxn_{16}} OaA + PEP \xrightarrow{rxn_{9}} OaA} = 0.36 \qquad (6\text{-}34)$$

where rxn_x refers to the metabolic reaction as set out in Chapter 5 and Appendix E, μ is the specific growth rate (h^{-1}) and all the metabolite abbreviations (G3P – 3-phosphateglycerate, OaA - oxaloacetate, Asp - aspartate, PEP - phosphoenolpyruvate, Mal - maleate) refer to the molar accumulation rates normalised by the specific glucose uptake rate.

This reduces the degrees of freedom to two. If the biomass growth rate and the specific glucose consumption rate are supplied, the bioreaction network estimates the other extracellular excretion rates based on the known metabolic pathways and the known control strategy around the PEP principle node. It would however not compensate for the impact of increased hydrodynamic shear. The inclusion of the impact of hydrodynamic shear stress on the fermentation performance is discussed in Section 3.10.

The bioreaction network model is therefore constituted by the Monod growth rate equation a coupled to the bioreaction network with the three fixed principle nodes. When the specific glucose consumption rate is specified the specific lysine productivity, the oxygen utilitsation rate, the carbon evolution rate, the trehalose and valine excretion rates are then determined by the bioreation network.

3.8 Aeration and agitation

One of the delimitations of the optimisation process is that the vessel volume and the maximum aeration, agitation and chilling capacity are assumed to be fixed, forming part of the constraints of the optimisation problem. The aeration and agitation required depend on the oxygen utilisation rate of the cells. The following fundamental equation was used to model the oxygen transfer rate.

$$OUR = OTR = k'_l a \cdot (LMOPP - DO \cdot LMOPP_o) \qquad (6\text{-}35)$$

where OUR is the oxygen utilisation rate in (mmol/l/h), OTR is the oxygen transfer rate in (mmol/l/h), $k_l a$ is the mass transfer coefficient in (mmol/h/kPa) that compensates for the media dependency of $C_{O2,sat}$ - the saturation oxygen concentration (mmol/l) in and LMOPP is the log mean partial pressure (kPa) of oxygen in the inlet and outlet air stream.

The volumetric mass transfer coefficient, $k'_l a$, is the product of the mass transfer coefficient k_l the interfacial area a and the media dependency of $C_{O2,sat}$. In a living system, DO (dissolved oxygen concentration – expressed as a fraction of the saturated oxygen

concentration) should exceed some critical dissolved oxygen concentration to prevent oxygen limitation. The dissolved oxygen concentration is dependent on temperature, total head pressure and solution composition (Schumpe *et al.* 1982). The volumetric mass transfer coefficient is a function of both physiochemical and hydrodynamic properties of the fermentation broth (Oolman 1984).

The mass transfer coefficient can be correlated using the following equation:

$$k'_la = a_{media} [(Rev)^3/V]^{3\alpha} Air^{\beta} \quad (6\text{-}36)$$

where a_{media} depends on the composition of the broth and the reactor geometry, Rev is the number of revolutions of the impeller per second, V is the broth volume in the reactor and Air is the volumetric air flow rate through the reactor.

Equation 6-36 will only hold for a specific bioreactor. If scale-up data is required $(Rev)^3/V$ needs to be converted into the power dissipated per unit volume and Air to the superficial air velocity through the bioreactor.

The parameters in this equation were determined experimentally for different biomass concentrations, lysine concentrations and recycling flow rates in Chapter 5.

Based on similar method as that used to empirically model the permeate flow rate (Chapter 5, Section 7.3), the following empirical correlation's were established for each of the constants

$$a_{media} = 4.16 \times 10^{-4} [Lys]^{-0.04} \text{ mmol/h/kPa} \quad (6\text{-}37)$$

$$\alpha_o = 8.31 \times 10^{-1} [v]^{-0.02} \quad (6\text{-}38)$$

$$\beta_o = 4.67 \times 10^{-1} [v]^{-0.03} \quad (6\text{-}39)$$

where v is the linear velocity (m/s) through the membrane module. In the absence of cross flow filtration the value of v is set to 10^{-1}. Figure 6-11 illustrates that equation 6-36 to 6-39 describe k'_la as a function of the agitator speed, the aeration rate and the media composition adequately.

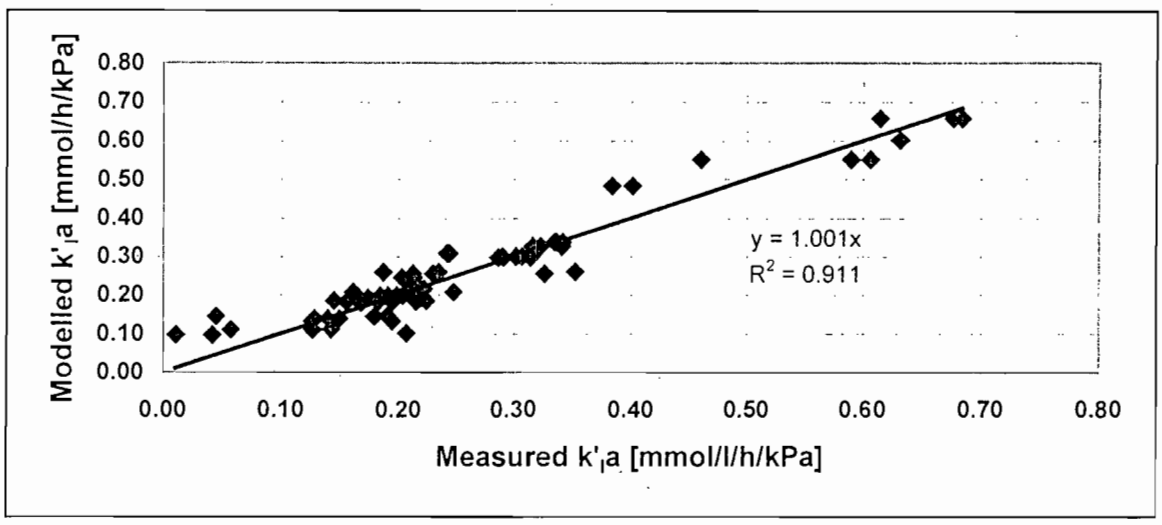

Figure 6-11. Parity chart for oxygen mass transfer coefficient k'$_l$a (mmol/l/h/kPa) predicted by Equations 6-36 to 6-39 and measured in industrial media in the Chemap bioreactor.

3.9 Chilling Capacity

The chilling capacity is determined by the exothermic heat generation of the cells. There is a direct correlation between the exothermic heat generation of the cells and the oxygen utilisation rate (Bailey & Ollis 1977). The energy transferred to the cooling water system in the Chemap bioreactor under temperature control was measured during a fed-batch fermentation. At a constant bioreactor temperature, this energy corresponds to the exothermic heat generation of the cells. The energy transferred was determined from the cooling water flow rate and the change in temperature of the cooling water. Heat losses from the surface of the reactor was minimised by lagging the outer walls of the Chemap bioreactor. Oxygen utilisation rate (mmol/h) as a function of the energy removed to maintain a constant temperature yielded a straight line with a slope of 1.27×10^{-4} kW / (mMol/h). This is equivalent to 454 kJ heat reeased by the uptake of 1 mol of oxygen. (Figure 6-12).

Bailey & Ollis (1977) reported that as a rule of thumb for aerobic growth processes using organic components only the consumption of 1 mol of oxygen would release 460 ± 20 kJ heat. This result originates from combustion data according to which 115 ± 5 kJ of heat are released per electron. Oxygen consumes 4 electrons which gives rise to the above mentioned result. This value closely represents the experimental value.

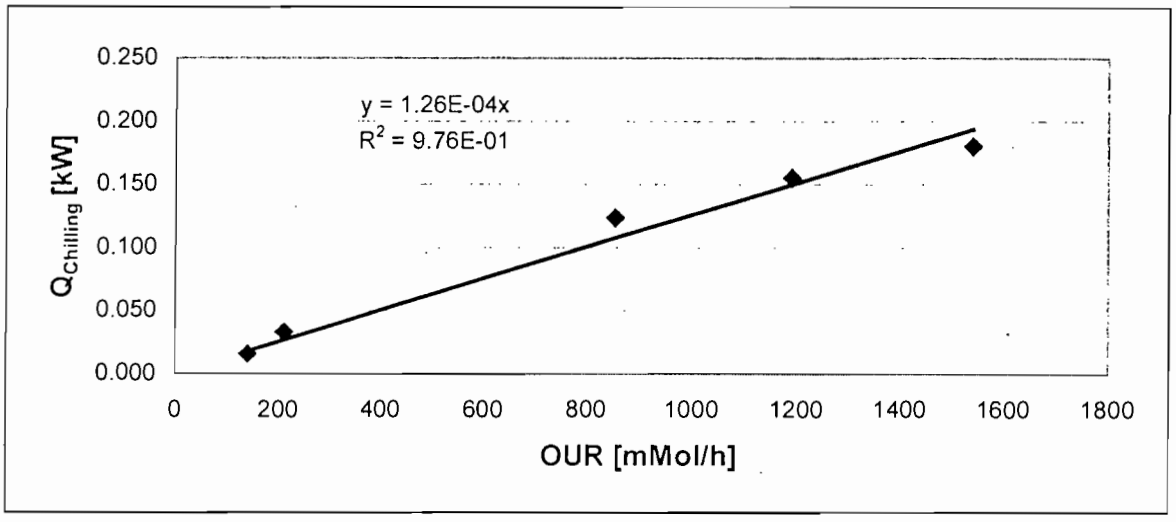

Figure 6-12. A plot of the energy removed for the bioreactor to maintain a constant temperature against the oxygen utilisation rate.

3.10 The effect of biomass recycling on the fermentation performance

The effect of the filtration associated hydrodynamic stress on the cellular metabolism is discussed at length in Chapter 5. The impact of filtration associated hydrodynamic stresses on the metabolism is characterised by a change in metabolite consumption and excretion rates. The magnitude of the change is proposed to be dependent on the turbulent energy dissipation rate (Dunlop *et al.* 1994; Toma *et al.* 1991). Based on the work of previous investigators with regard to the impact of hydrodynamics on the fermentation performance, it is hypothesised that a threshold energy dissipation limit exists below which no impact of hydrodynamic stresses on fermentation performance is observed (Toma *et al.* 1991; Rukisha *et al.* 1989; Fowler & Robertson 1991; Dunlop *et al.* 1994). Further, based on the results of various previous investigators (McQueen *et al.* 1987; Dunlop *et al.* 1994; Toma *et al.* 1991), the effect of hydrodynamic stress is proposed to be proportional to the volumetric energy dissipation rate, the residence time or the duration of the applied stress and the frequency of the stress.

To investigate these hypothesis for this system, the hydrodynamic conditions were characterised by the turbulent energy dissipation rate that was calculated for the stirred tank reactor, the membrane module and the needle valve in the flow loop used to adjust the trans-membrane pressure drop as set out in Chapter 5, Section 4.

To evaluate the impact of hydrodynamic stresses on fermentation performance in the biomass recycle bioreactor, continuos fermentations at a washout rate of 0.10 h^{-1} were conducted at six different shear levels and two maximum biomass concentrations. The washout rate of 0.10 h^{-1} to match the maximum specific lysine productivity at the maximum yield or lowest specific feed. The recycle rate for the lowest cross flow velocity was two orders of magnitude larger than the feed rate (1l/h vs. 108 l/h), which suggests that

equation 6-31 could still be valid to estimate the average energy dissipated in the system. For the fermentations without biomass recycling through the filtration system a steady state was achieved at two biomass concentrations (25 g/l and 7.5 g/l). The specific lysine productivity of 0.08 g/g/h measured corresponds to the data presented in Figure 6-4.

The duration of each experiment was limited by the culture stability. From the data presented by Kiss & Stephanopoulos (1992), the culture starts to revert to the wild type after 5 generations or 97 hours. Each continuous experiment was therefore limited to 72 hours.

Under stressed conditions a decline in the specific growth rate resulted in a decline in the biomass concentration. In some cases, a steady state was not achieved after 72 and the growth rate was calculated from the decline in the biomass concentration. The specific lysine productivity and the yield of biomass on threonine were calculated during the transient period for the stresses fermentations from a mass balance. The average energy dissipation rates (m^2/s^3) as predicted by Equation 5-31 are summarised in Table 6-9.

Table 6-9. Experimental conditions to evaluate the impact of hydrodynamic stress on the fermentation performance

Experiment	TMP [kPa]	Cross-flow velocity [m/s]	e_{reac} [m^2/s^3]	e_{mem} [m^2/s^3]	e_{valve} [m^2/s^3]	e_{max} [m^2/s^3]	e_{ave} [m^2/s^3]
Low BMS	No recycling		11			11	11
	100	2	11	24	86	86	17
	150	2	11	24	129	129	22
	200	2	11	24	172	172	27
	100	1	11	3	21	21	10
	100	3	11	78	141	141	24
	100	5		335	178	335	28
High BMS	No recycling		11			11	11
	100	2	11	42	86	86	18
	150	2	11	42	129	129	23
	200	2	11	42	173	173	28
	100	1	11	8	22	22	11
	100	3	11	123	142	142	24
	100	5	11	496	179	496	29

The presence of shear induced by the filtration unit resulted in a decrease in the specific growth rate as well as a decrease in the specific lysine productivity although an increase in the yield of biomass from L-threonine was observed (Chapter 5, Section 7). The metabolic response was characterised by the reduction in the specific growth rate ($-\Delta\mu$), the reduction in the maximum specific lysine productivity ($-\Delta q_{Lys}$) and the overall increase in

the yield of biomass from threonine ($\Delta Y_{x/thr}$). The absolute values of the changes in the metabolic parameters are presented in Figures 6-14 to 6-16.

For the metabolic network model the impact of shear on the fermentation performance was modelled by the inclusion of an additional principle node at Asp (Figure 6-13). At the Asp node some of the carbon is either converted to lysine or to cell wall material depending on the energy dissipation rate. The percentage of carbon that enters the Asp node that is converted into cellular wall material is presented in Figure 6-17.

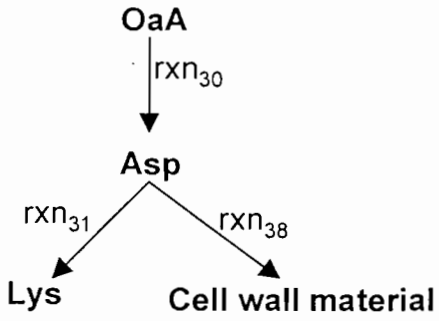

Figure 6-13. The additional node at Asp included in the metabolic network model to compensate for the impact of hydrodynamic shear on the cellular metabolism.

The impact of the effective turbulent energy dissipation rate on the metabolic parameters depends on the biomass concentration. A single relationship between the metabolic response and hydrodynamic stress cannot be establish based on only the effective energy dissipation rate or the maximum energy dissipation rate. When the effective energy dissipation rate is divided by the biomass concentration, a new parameter is derived to model the impact of hydrodynamic stress on the cellular metabolism (Figure 6-18). This parameter represents the turbulent energy dissipated per unit cell mass in the bioreactor. A plot of the non-zero responses against the new parameter is presented in Figure 6-18.

With the introduction of the new parameter (effective turbulent energy dissipation rate / biomass concentration), the impact of the biomass concentration is eliminated from the relationship between the hydrodynamic conditions and the metabolic response. The new parameter takes into account the maximum energy dissipation rate, the number of cycles of exposure to the stress and the impact of biomass concentration.

Figure 6-18 suggests the existence of a critical energy dissipation rate per unit cell mass below which no metabolic response to the hydrodynamic conditions is seen. The impact of hydrodynamic stress on the cell's metabolism was modelled based on the relationship found in Figure 6-8 Although this relationship was only established for a specific washout rate (0.1 h^{-1}), the value of the washout rate approximates the optimal specific growth rate. Optimal is defined as being the maximum yield at which the maximum specific productivity is attained under unstressed conditions. The optimal fed batch fermentation process will attempt to maintain the cells at this specific productivity for the maximum time. The

changes in the metabolic parameters (specific growth rate, specific lysine productivity, the yield of biomass on lysine or the fraction of Asp converted to cell wall material) are therefore applied to the instantaneous values of the metabolic parameters as predicted by the unstressed conditions model in the fed batch fermentation. The metabolic parameters (either the specific growth rate, the specific lysine productivity, the yield of biomass on lysine or the fraction of Asp converted to cell wall material) are estimated using the relationships developed for the unstressed conditions in the preceding sections. The change in the metabolic parameter is the estimated from the analysis in this section and subtracted or added from the unstressed parameter. This is done at all the timepoints in the fermentation.

Although this is a crude approximation, the cells will be maintained around this "optimal" metabolic state for the bulk of the fermentation and subsequently presents a simple yet effective way of modelling the impact of the hydrodynamic stress on the cellular metabolism.

A linear relationship is assumed between the effective energy dissipation rate per unit cell mass and the change in the metabolic response. The following equations are used to estimate this impact:

$$\mu - \mu_{obs} = \max(0;\ 0.031\frac{e_{ave}}{X} - 0.025) \tag{6-40}$$

$$q_{Lys} - q_{Lys,obs} = \max(0;\ 0.006\frac{e_{ave}}{X} - 0.005) \tag{6-41}$$

$$Y_{\frac{X}{Thr},obs} - Y_{\frac{X}{Thr}} = \max(0;\ 1.752\frac{e_{ave}}{X} - 1.304) \tag{6-42}$$

$$\frac{Asp \xrightarrow{rxn_{38}} Cell\ wall}{OaA \xrightarrow{rxn_{30}} Asp} = \max(0;\ \frac{e_{ave}}{X} - 0.031) \tag{6-43}$$

$$Cell\ Wall = -rxn_{38} \tag{6-44}$$

The validity of this approach would is tested based on the ability of the entire models to predict the experimental data. In the next section, a sensitivity analysis is be performed to determine the impact of these assumptions on the ability of the global model to predict the fermentation performance.

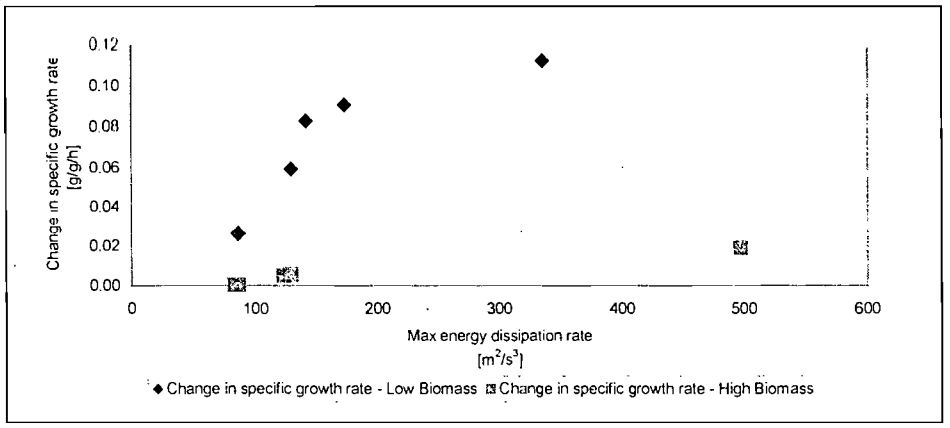

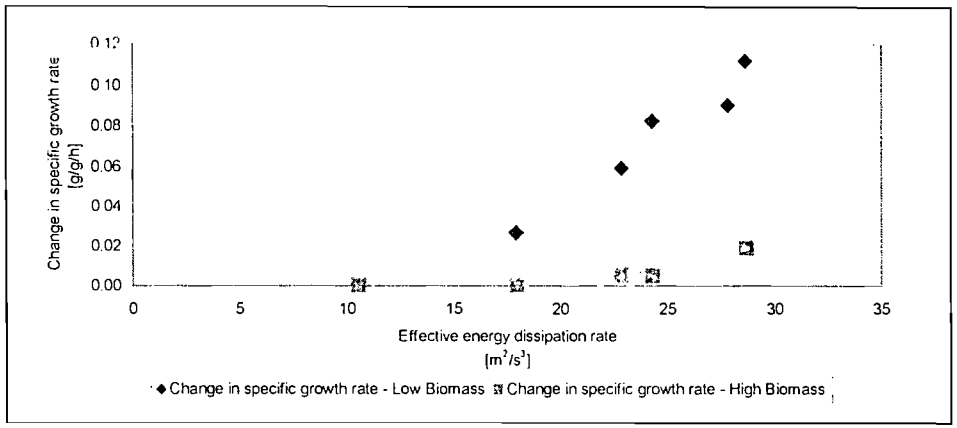

Figure 6-14. Absolute value of the change in the specific growth rate (μ in h^{-1}) plotted against the average energy dissipation rate (Eq. 5-31) and the maximum energy dissipation rate (m^2/s^3)

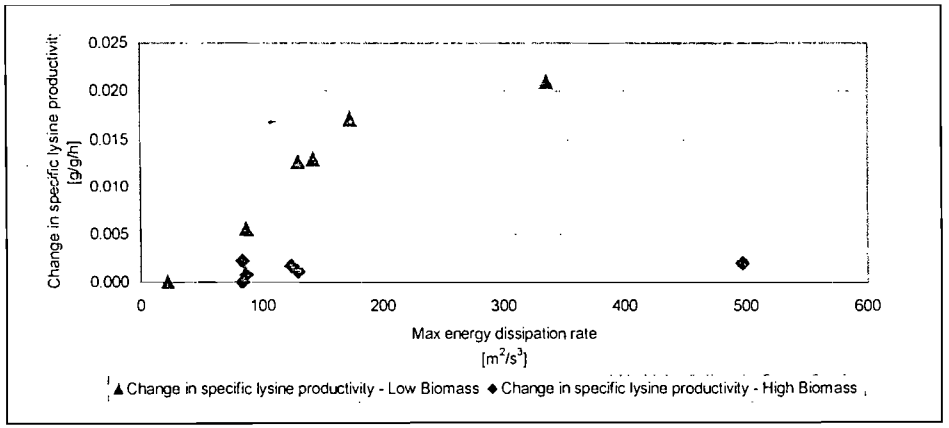

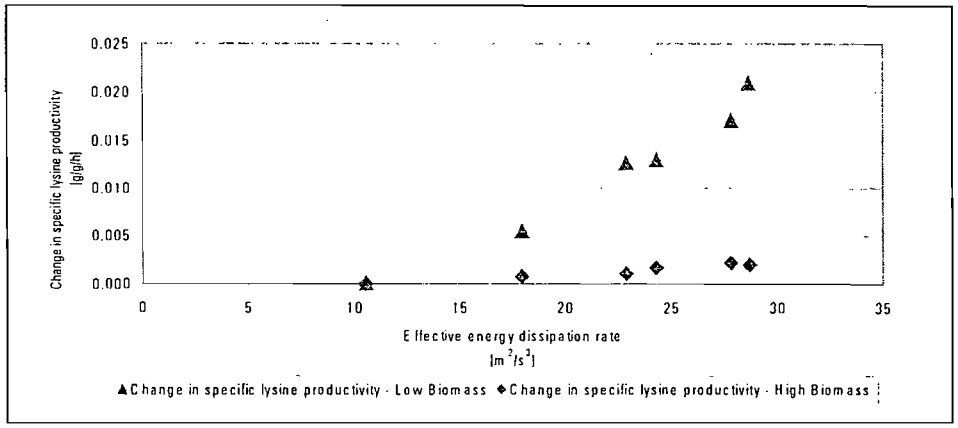

Figure 6-15. Absolute value of the change in the specific lysine productivity (q_{Lys} in g/g/h) plotted against the average energy dissipation rate (Eq. 5-31) and the maximum energy dissipation rate (m^2/s^3)

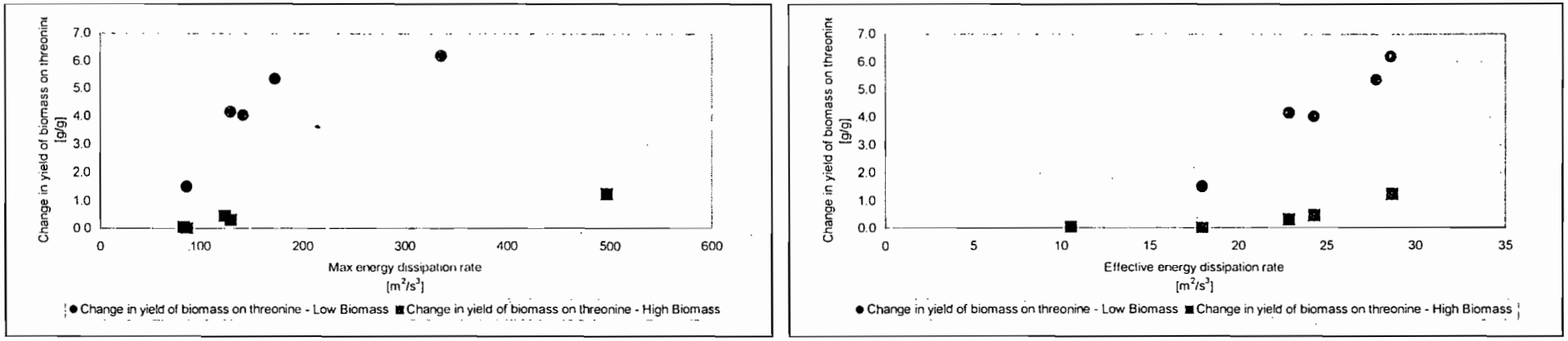

Figure 6-16. Absolute value of the change in the yield of biomass from threonine ($Y_{X/thr}$ in g/g) plotted against the average energy dissipation rate (Eq. 5-31) and the maximum energy dissipation rate (m^2/s^3)

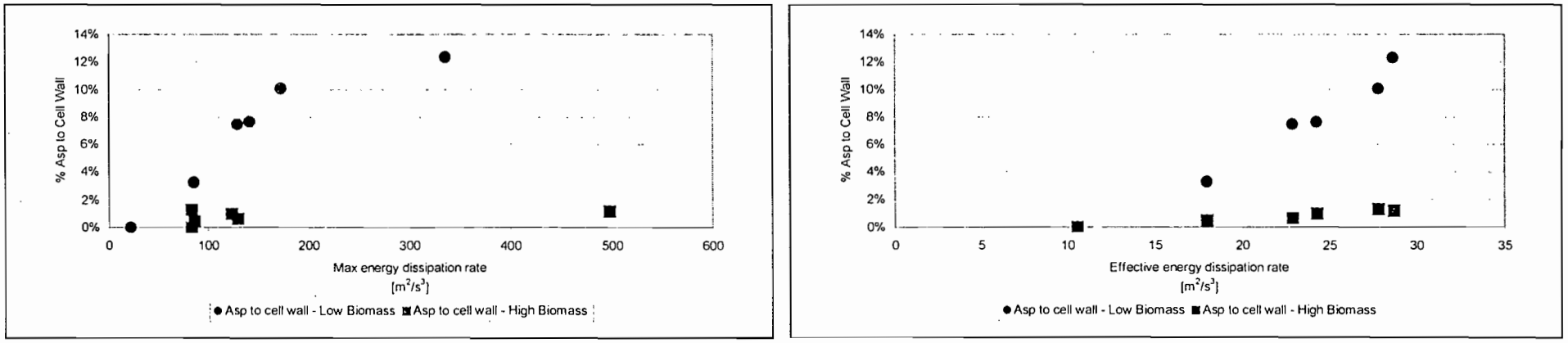

Figure 6-17. Percentage of carbon that enters the Asp node that is converted into cell wall material as a result of increased hydrodynamic stress

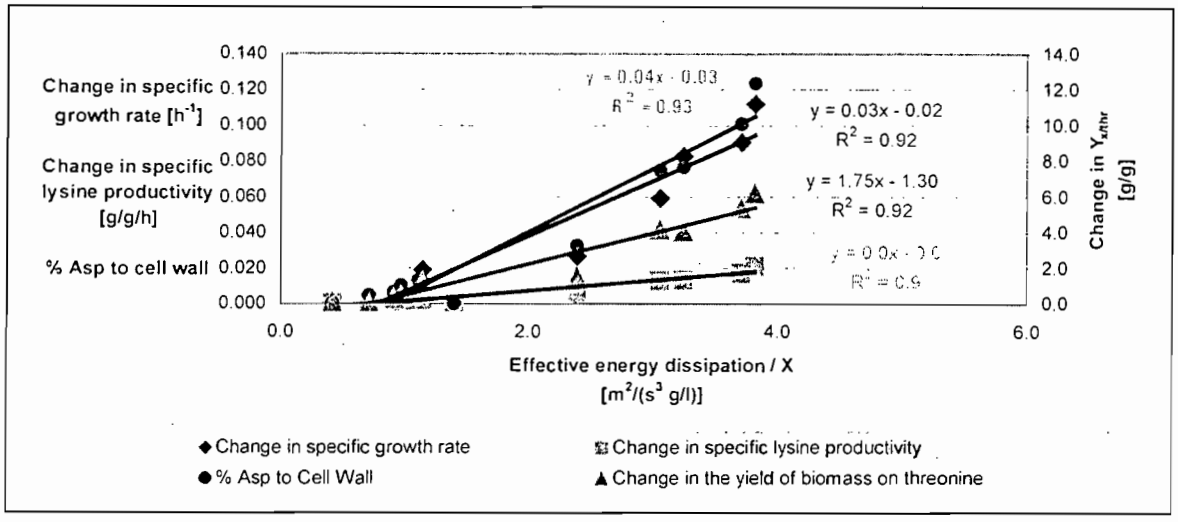

Figure 6-18. The absolute value of the change in the metabolic response (specific growth rate, μ; specific lysine productivity q_{Lys} and the yield of biomass on threonine) for all the data points (both low and high steady state biomass concentrations, plotted against the average energy dissipation rate (Eq. 5-31) divided by the biomass concentration (X in g/l DCW)

4 Analysis and summary of the fermentation models

A summary of the models is presented in Appendix F, including the equations, the parameters and the degrees of freedom. Here it would just be mentioned that the empirical model consists of 45 variables and 36 equations. Nine (9) of the 45 variables are externally specified as controllable variables which implies that the other 36 variable can be solved from the linearly independent set of equations presented.

The model based on the metabolic network has 75 variables, excluding the nine controllable variables and the zero accumulation rates in the bioreaction network. The model consist of 75 equations which implies that for each set of controllable variables a single solution of the 75 variables exists for each point in time.

5 Results and Discussion

The experimental results are compared to the results predicted by the fermentation model suggested. Conventional batches at two different steady state biomass concentrations, batches with biomass recycling at two steady state biomass concentrations, continuous fermentations, fed-batch fermentations and fed-batch fermentations with biomass recycling have been modelled and compared to the experimental data. Model predictions were also compared to literature data for batch, fed batch and continuous fermentations. These results are summarised in Table 10. Only the major performance variables (Y_{ps} and volumetric lysine productivity) are presented. The yield (Y_{ps}) was defined as the mass of lysine produced per mass of glucose consumed, while the volumetric productivity is the lysine produced per unit

time per unit broth volume. Batch fermentations were terminated upon depletion of the initial charge glucose concentration. For the fed-batch and continuous fermentations, the fermentation was terminated when revertant growth was apparent. Revertant growth is therefore ignored for the purpose of this study.

The experimental data for some selected fermentations are presented in Figures 6-19 to 6-23. The experimental data summarised as a yield of lysine in glucose and a volumetric productivity is compared against the model predictions for various reactor configurations in Table 6-10

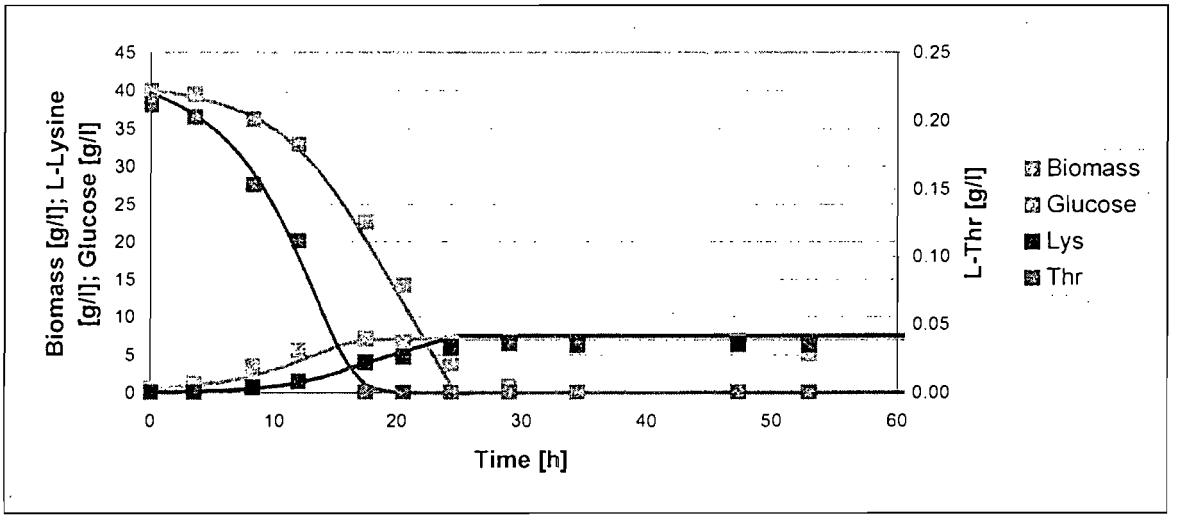

Figure 6-19. Experimentally obtained data for a conventional batch fermentation with a stationary phase state biomass concentration of 7 g/l. The continuous lines represent the empirical model developed in the previous section.

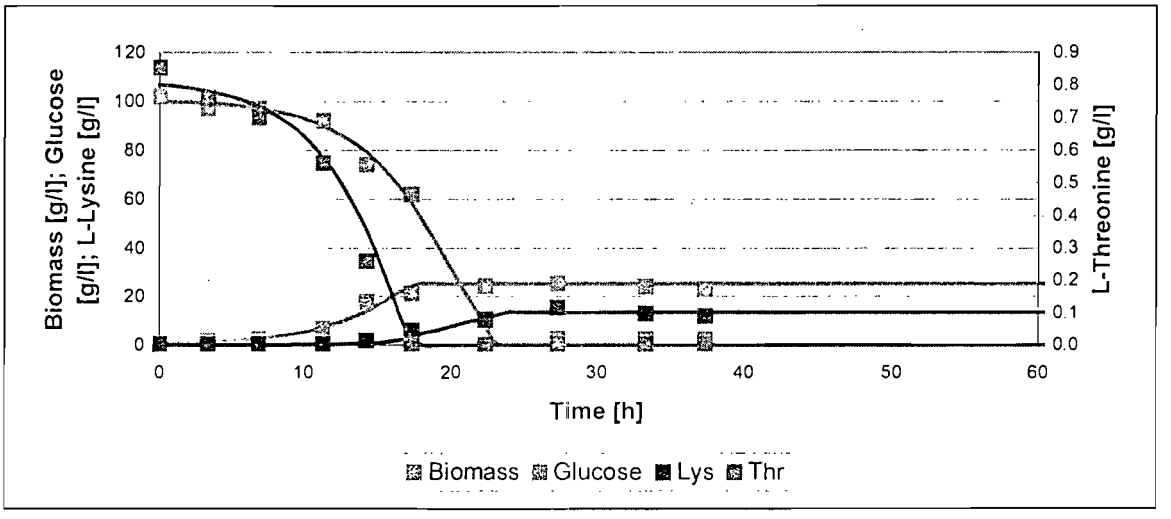

Figure 6-20. Experimental data for a conventional batch fermentation with a stationary phase biomass concentration of 25 g/l. The continuous lines represent the empirical model developed in the previous section

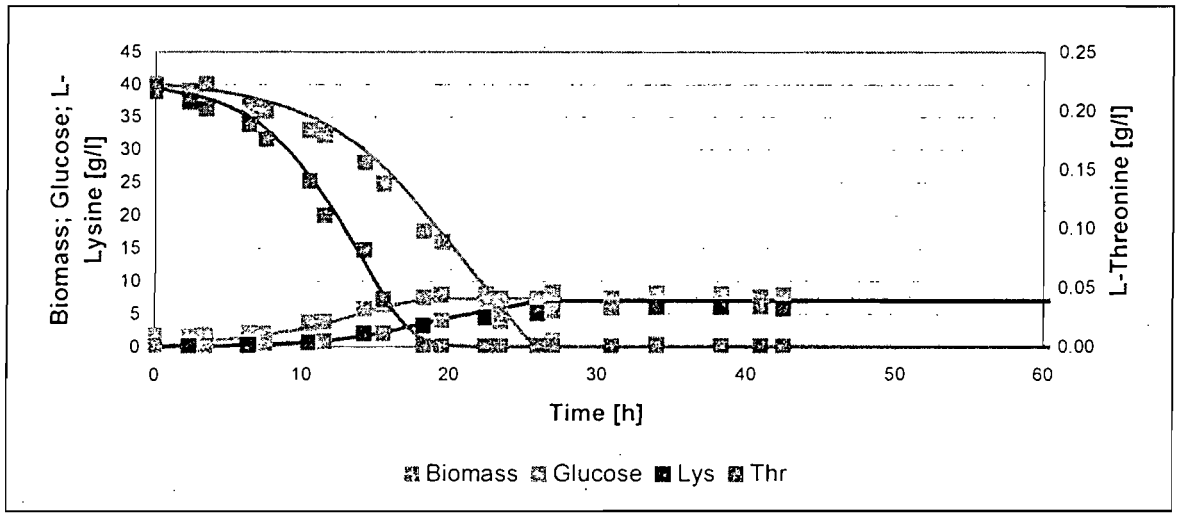

Figure 6-21. Experimental data for a batch fermentation with biomass recycling where the permeate and retentate were recycled to the bioreactor. A stationary phase state biomass concentration of 7.5 g/l was achieved. The continuous lines represent the empirical model developed in the previous section

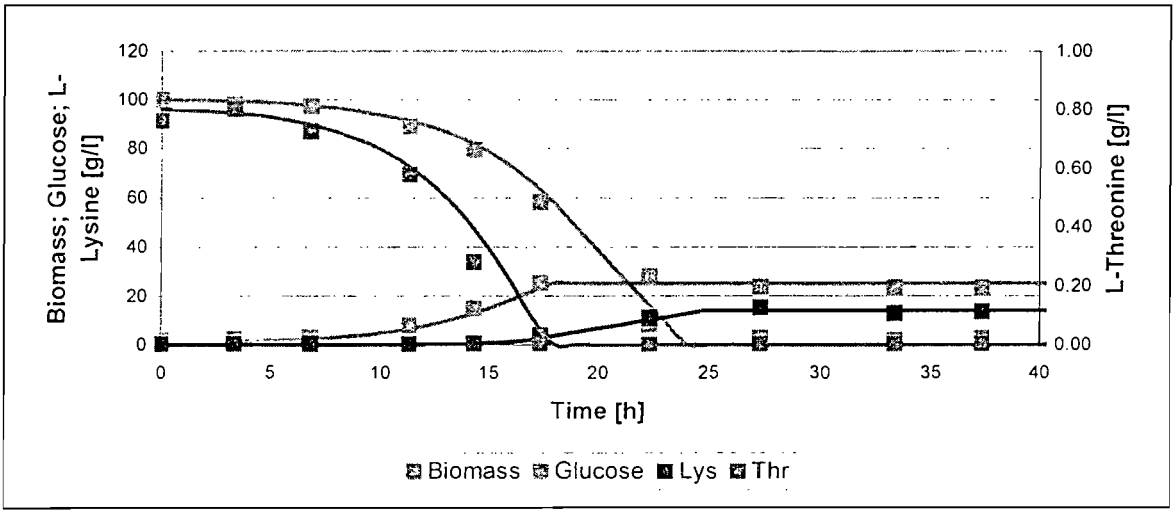

Figure 6-22. Experimental data for a batch fermentation with biomass recycling where the premeate and retentate were recycled to the bioreactor. A stationary phase biomass concentration of 25 g/l was achieved. The continuous lines represent the BRN model developed in the previous section

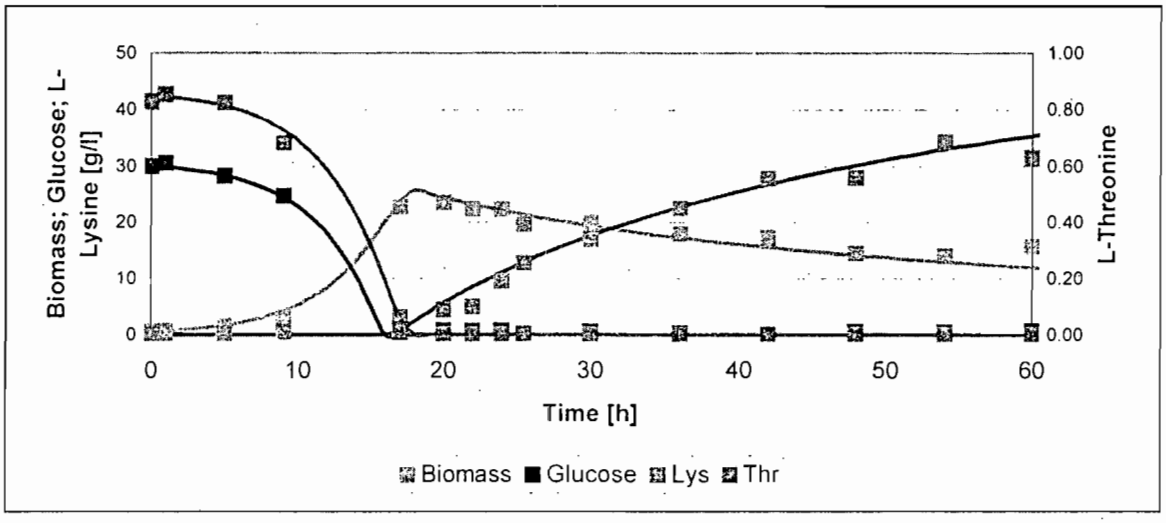

Figure 6-23. Fed-batch fermentation profile without biomass recycling. The continuous lines represent the empirical model prediction.

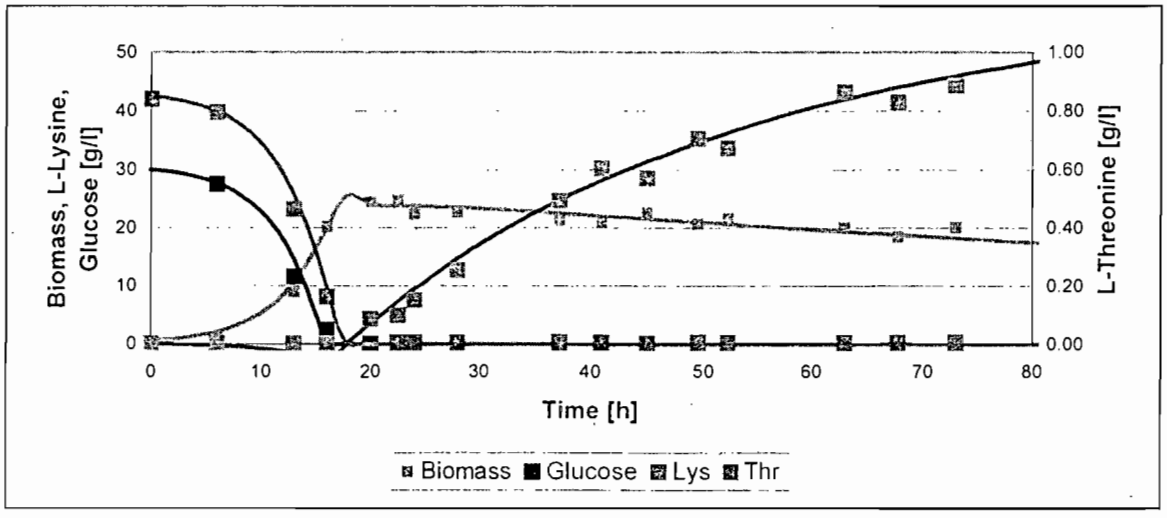

Figure 6-24. Fed-batch fermentation profile with biomass recycling. The continuous lines represent the BRN model prediction.

Table 6-10. Summary of experimental results and model predictions. Only the cumulative yield of lysine from sugar and the lysine productivity is presented. A correlation coefficient for the biomass and lysine profile is also presented.

Fermentation Description	t_{final} [h]	Y_{ps} [g/g]			Productivity [g/lh]			R^2 [Lys]		R^2 [X]		Reference
		Data	Empirical Model	BRN Model	Data	Empirical Model	BRN Model	Empirical Model	BRN Model	Empirical Model	BRN Model	
Conventional Batch -Low BMS	35	0.16	0.18	0.17	0.13	0.14	0.13	0.896	0.837	0.997	0.844	
Conventional Batch -High BMS	35	0.14	0.13	0.14	0.34	0.35	0.36	0.996	0.989	0.994	0.991	
Conventional Batch - Literature	35	0.14	0.13	0.14	0.36	0.35	0.35	0.970	0.997	0.954	0.962	Vallino & Stephanopoulus 1992
Conventional Batch - Literature	40	0.44	0.43	0.42	0.36	0.34	0.35	0.903	0.965	0.983	0.932	Lee *et al.* 1995
Batch with BMS recycling - Low BMS	35	0.15	0.16	0.16	0.11	0.12	0.12	0.867	0.987	0.947	0.944	
Batch with BMS recycling - High BMS	35	0.12	0.12	0.13	0.35	0.35	0.35	0.989	0.906	0.991	0.963	
Conventional Fed Batch	60	0.16	0.16	0.16	0.54	0.54	0.57	0.986	0.974	0.984	0.960	
Conventional Fed Batch - Literature	52	0.15	0.15	0.15	0.44	0.43	0.44	0.903	0.901	0.927	0.912	Kiss & Stephanopoulus 1991
Continuous Fermentation	D=0.10	0.17	0.16	0.16	0.20	0.17	0.17	0.975	0.972	0.982	0.974	
Continuous Fermentation - Literature	D=0.18	0.16	0.16	0.16	0.16	0.17	0.16	0.965	0.955	0.972	0.962	Lee *et al.* 1995
Continuous Fermentation - Literature	D=0.17	0.17	0.16	0.16	0.20	0.20	0.21	0.995	0.985	0.992	0.984	Oh & Sernetz 1993
Continuous Fermentation – Literature	D=0.15	0.13	0.13	0.14	0.18	0.17	0.17	0.975	0.964	0.942	0.933	Kiss & Stephanopoulus 1991
Fed batch with biomass recycling	80	0.16	0.17	0.16	0.80	0.80	0.79	0.996	0.987	0.912	0.902	

The model based on an empirical correlation of the cellular metabolism as well as the bioreaction network (BRN) correlation predict the fermentation profiles of batch, fed-batch, continuous and fed-batch with biomass recycle fermentations well (Figure 6-19 to 6-24 and Table 6-10). In most of the cases above, the empirical model exhibited a slightly higher correlation coefficient than the BRN model (Table 6-10).

It should be noted that neither of the models compensated for cell death during the latter phases of the batch fermentations. Furthermore, revertant growth was ignored in the analysis by terminating the fermentation prior to the start of revertant growth. Revertant growth was estimated from the cell's ability to grow in the absence of L-Threonine.

The batch fermentations were conducted in 10 litre working volume "Chemap" bioreactor. For these fermentations the volume remained constant throughout the run as a neglibile amount of base was added for pH control. The fed batch fermentations were operated in a 10 litre working volume "Chemap". Five litres of initial charge media was used. When the working volume of 10 litres was reached, a feed and bleed strategy was adopted.

Fermentation performance of the different operating strategies - batch, fed-batch, continuous and fed-batch with biomass recycling fermentation is presented in Table 6-11 below. The fermentations were standardised by using the same working volume of the bioreactor The fed-batch fermentations started at an initial charge volume of five litres. This was the minimum volume of the bioreactor that would allow the top impeller to be submerged by one impeller diameter and all the probes to be below the liquid level.

The volumetric productivity depends mainly on the amount and the residence time of biomass in the bioreactor. The total amount of L-threonine fed to the bioreactor (initial charge amount and the total feed quantity) was limited by the maximum biomass concentration of 30 g/l at any point in time. Thus, for the batch fermentation enough threonine was included in the initial charge to produce a stationary phase biomass concentration of 30 g/l, for the fed-batch fermentation thesame philosophy held true although the maximum biomass concentration of 30 g/l was attained at a much lower broth volume of 5 litres. Thus the batch fermentaton produced double the amount of biomass when compared to the fed-batch fermentation.

Table 6-11. Comparison of for operating philosophies for L-Lysine production

Operating philosophy	Yps [g/g]	Volumetric productivity [g/lh]	L-Lysine/ Biomass [m/m]
Batch	0.14	0.34	0.45
Batch with biomass recycling	0.12	0.35	0.40
Fed-Batch	0.16	0.54	2.16
Chemostat	0.17	0.20	0.90
Fed-batch with biomass recycling	0.18	0.80	6.08

Each of the fermentations was operated so as to maximise yield and specific productivity. Thus, the continuous fermentation was operated at a dilution rate of 0.10 h^{-1}, to have a intrinsic yield (Y_{ps}') of 0.28 g/g and a specific productivity of 0.08 g/g/h (Figure 6-2 and 6-4). The fed-batch fermentations was fed to maintain a specific feed of 0.38 g/gh to obtain a intrinsic yield (Y_{ps}') of 0.28 g/g and a specific productivity of 0.10 g/g/h (Figure 6-2).

The cumulative yield is however much less than the intrinsic yield due to the usage of glucose to produce biomass. The longer the fermentation can be extended the less the impact of biomass production. This is seen from the ratio of L-lysine produced per biomass produced. This ratio increases from batch through fed batch and continuous to fed-batch with biomass recycling.

Continuous fermentations are less effective than fed-batch fermentation because a minimal growth rate must be maintained in continuous fermentation. Since some of the glucose fed is used to produce biomass less glucose would be available for lysine production. Furthermore, biomass is continuously removed from the bioreactor at its rate of formation. Thus, viable biomass capable of lysine production is lost without producing lysine and subsequently the glucose investment made to produce this biomass is lost.

Batch fermentations are ineffective because of the constraints on the initial glucose concentration imposed to limit osmotic load imparted on the cells by increased sugar concentration.

Fed batch fermentations allow efficient use of the biomass by glucose addition in the absence of the auxothropic amino acids. This glucose is converted to lysine at an increased intrinsic yield due to the absence of biomass growth. The residence time of the biomass and therefore the cumulative yield in fed-batch fermentations is limited by the total volume available. During the sugar feed phase, the volume in the bioreactor increases until the maximum operating volume is reached. From this point onwards, a feed and bleed strategy is adopted. Thus, some of the fermenter volume is discarded at a set frequency to accomodate the additional sugar fed. Because there is very little biomass growth in fed-batch fermentation during the feed phase owing to auxothropic amino acid limitation and some of the biomass is lost during each bleed step, a decrease in biomass concentration results. The productivity of the fermentation thus declines due to the limited biomass residence time.

The fed-batch fermentation with biomass recycling, however allows some of the liquid within the bioreactor to be removed without loosing biomass. Hence, the volumetric productivity is maintained and the fermentation is terminated when the biomass looses viability, or the membrane is fouled extensively. The longer fermentation time at increased biomass residence time allows the maximum usage of the biomass and therefore an increase in the cumulative yield of lysine from glucose.

6 Comparison of the models using Bayesian inference

This section aims to compare the empirical model of metabolism to the bioreaction network (BRN) approach for the modelling of the cells' metabolism. The experimental work conducted to estimate the parameters is used as a basis for comparison (Appendix G). The yield and the productivity from each experiment (or set of controllable variables) is compared to the yield and productivity predicted by each model.

From this information, the Bayesian approach for model selection was used to compare the ability of each model to predict the experimental data. The error used in the calculation of the likelihood (Eq. 4-5) was the square of the normalised difference between the measured and calculated yield added to the square of the normalised difference between the measured and the calculated productivity.

The Bayesian approach for model comparison involves application of Bayes' theorem as explained below:

Consider models H $\in$ {1, 2, 3 ... N} and some observed data D

Then,

$$p(H \mid D) = \frac{p(H) \cdot p(D \mid H)}{C'} \tag{6-45}$$

and for the parameters ψ of model H;

$$p(\theta \mid D, H) = \frac{p(\theta \mid H) \cdot p(D \mid \theta, H)}{p(D \mid H)} \tag{6-46}$$

p(D | H) is referred to as the evidence for model H

Therefore;

$$p(H \mid D) \propto p(H) \cdot p(D \mid H) \tag{6-47}$$

where

$$p(D \mid H) = \int_{-\infty}^{+\infty} p(\theta \mid H) \cdot p(D \mid \theta, H) \cdot d\theta \tag{6-48}$$

A Bayesian factor or posterior ratio for model comparison can be defined as

$$\frac{p(H_i \mid D)}{p(H_j \mid D)} = \frac{p(H_i)}{p(H_j)} \cdot \frac{p(D \mid H_i)}{p(D \mid H_j)} \tag{6-49}$$

where p(H) is the prior probability of model H. For the current comparison, this has been assumed to be unity. P(D|H) is the evidence for model H and is calculated by integrating the likelihood of each parameter in the model over the entire range of parameters. Basically, a value of a parameter in model H is selected. Then the probability is calculated that this parameter would has specific value given the data. This process is repeated for all possible values of the parameter and added up to give the likelihood. Thereafter the likelihood of all values of all the parameters are calculated and added up to give the evidence. For a detailed explanation of how this is done refer to Chapter 4, Section 2.5.

Based on the ratio of the evidences, different models can be compared. In general, this ratio will increase as the relative fit of model H_i increases compared to model H_j.

The Bayesian approach allows the investigator to include the prior information about the parameter into the comparison. The parameters in empirical correlations have equal priors for all values of parameters used, while the parameters with physical significance have a narrower distribution around the expected values for a variable with physical significance. For example, it is well known that the maximum specific growth rate of the cells should be between 0.30 and 0.60 h^{-1}. Therefore, all the values outside this range will have a zero prior. These limits on the values of parameters increase the probability of the model to predicting the system's performance. It excludes the effects of outliers and weights data points falling within the expected range.

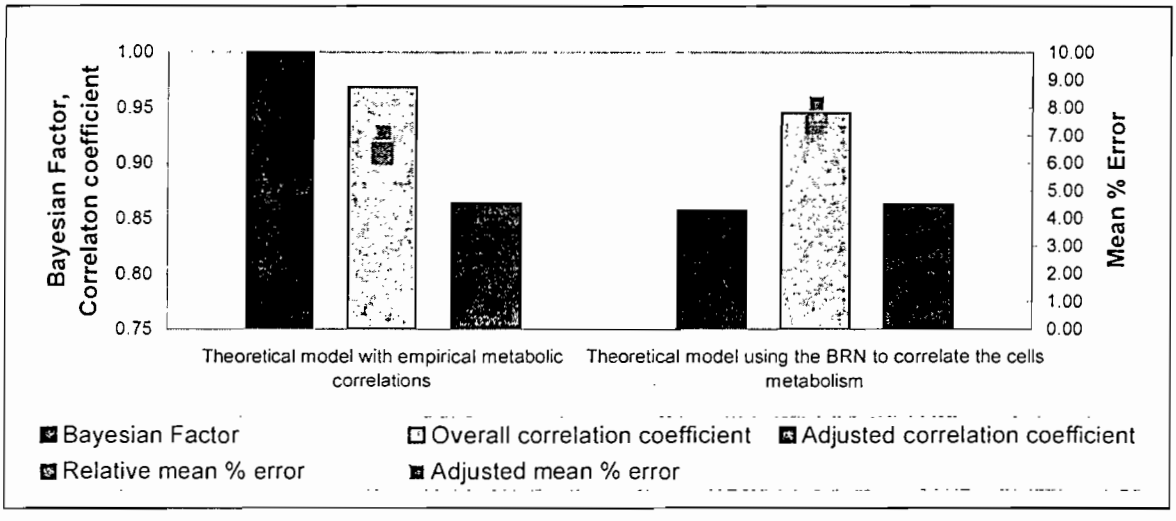

Figure 6-25. Comparison of the different models based on its probability to predict system performance. The correlation coefficient and the root mean square error between the measured and predicted values are included for comparison.

The Bayesian analysis was conducted relative to the model using empirical correlations to model the cells' metabolism. Therefore, the Bayesian factor for this model is one. A reduction in the Bayesian factor for the model based on the bioreaction network (BRN) relative to the empirical model indicates that this model has a reduced likelihood of accurately predicting

system performance (Figure 6-25). This conclusion is confirmed by the mean percentage error between the predicted and measured yield and productivity.

The Bayesian approach compensates for the different degrees of freedom in each model. The likelihood is calculated for each parameter over the entire range of possible values and all these values contribute to the Baysian factor. For every parameter estimated another dimension in the calculation of the likelihood is added. Thus, although the inclusion of an additional parameter increases the degrees of freedom and should therefore also increase the model's ability to predict the data, it adds a dimension to the likelihood calculation. It is therefore not surprising that the adjusted mean percentage error and the adjusted correlation coefficient confirms the finding of the Bayesian analysis (Figure 6-25).

The Bayesian approach also selects the model with least sensitivity to the values of the parameters. Because calculation of the evidence involves finding the probability of the value of the parameter over a wide range of values, the Bayesian approach reports a higher likelihood for models with a wide range for the values of parameters that does not influence the error. Models that contain parameters that are very sensitive to the value of a single parameter would have a reduced likelihood due to the narrow range of permissible values of this parameter.

7 Conclusions

Biochemical processes are characterised by a large number of variables that can influence the process outcome. This, combined with the slow nature of fermentation experiments makes optimisation through search plans very tedious and in most cases physically unrealistic and economically unfeasible. It is therefore easily recognised that in the optimisation of biochemical processes, the emphasis falls mainly on the development of accurate relationships between dependent and independent variables.

Unfortunately, due to the complex nature of biochemical processes, fundamental functional relationships are very limited with regard to their ability to predict process performance. Therefore, most attempts at the modelling of biochemical processes are empirical correlations of experimental data that are only valid over the evaluated range.

The biomass recycling system in this thesis was modelled with adequate accuracy using a mass and volume balance coupled to two types of metabolic equations. In the first approach, the cells metabolism was modelled by approximating the cell as a "black box" and developing empirical correlation's from experimental data to depict the cells response on changes in the extracellular environment. In the alternative approach the metabolism was modelled based on a bioreaction network of the intracellular central carbon distribution. Some critical nodes within this network were identified and the carbon split ratio's around these nodes were fixed or modelled based on extracellular conditions. From this information the cells response to changes in the extracellular environment could be predicted.

The impact of filtration associated hydrodynamic stress on the cells metabolism was modelled based on a linear relationship between the metabolic impact and the average energy dissipation rate per unit cell mass. A critical average energy dissipation rate was identified beyond which no impact on the fermentation performance relative to conventional batch fermentations were detected. Above this critical energy dissipation rate, a reduction in growth rate and specific productivity and an increase in the yield of biomass from threonine can be modelled as linear functions of the turbulent energy dissipation divided by the biomass concentration.

The Bayesian approach was used to determine which model (either the empirical correlation based model or the bioreaction network based model) predicted the fermentation performance with the highest probability. This analysis has shown that the model using empirical correlations to estimate the metabolic behaviour of the cell has a higher probability of predicting the systems performance. Thus although this approach has more degrees of freedom or parameters to estimate from experimental data the ability of this model exceeds that of the more fundamentally based bioreaction network model.

The model with the empirically estimated metabolism would be used in the next chapter to optimise the systems performance.

8 References

Bader, F.G. (1978), Analysis of Double Substrate Limited Growth, *Biotechnology and Bioengineering*, **20**, 183-202

Bader, F.G. (1982), "Kinetics of Double Substrate Limited Growth" in Microbial Population Dynamics, ed. M.J. Bazin, CRC Press, 1-32

Bailey, J. E. and Ollis, D. F. (1977), "Biochemical Engineering Fundamentals", McGraw-Hill Book Company, NY

Baltzis, B. C., Fredrickson, A. G. (1988), Limitation of growth rate by two complementary nutrients: Some elementary but neglected considerations, *Biotechnology and Bioengineering*, **31,** 75-86

Bates, R. L. Fondy, P. L. and Fenic, J. G. (1966), In Mixing: Theory and Practise 1, Uhl, V. W. and Gray, J. B. (Eds.), Academic Press, NY

Bates, R. L., Fondy, P. L. and Corpstein, R. R. (1963), An examination of some geometric parameters of impeller power, *Industrial Engineering Chemical Process Design and Development,* **2,** 310-314

Belfort, G. (1986), Fluid mechanics and cross-flow filtration, H. S. Muralidhara (Ed.), Advances in Solid Liquid Separation, Battelle Press, Columbus, OH, Chapter 7

Bona, R. and Moser, A. (1997), Modelling of growth of *Corynebacterium glutamicum* under biotin limitation, *Bioprocess Engineering*, **17**(2),121-125

Büchs, J. (1991), Kopplung van reactions- und kostenmodell: Der weg zur effizienten prozessoptimierung, *Chem. Ing. Tech.,* **63**(2), 89-98

Chiampo, F. and Marotto, R. (1995), Flow regimes in gas-liquid reactors stirred with dual Rushton turbines, *The 1995 IChemE research Event/First European Conference,* 689-691

Coello, N., Pan, J. G. and Lebeault, J. M. (1992), Physiological aspects of L-lysine production: effect of nutritional limitations on a producing strain of *Corynebacterium glutamicum, Applied Microbiologt and Biotechnology,* **38,** 259-262

Croughan, M. S., Sayre, E. S. and Wang, D. I. C. (1989), Viscous reduction of turbulent damage in animal cell culture, *Biotechnology and Bioengineering.,* **33**, 862-872

Dunlop, E. H. and Namdev, P. K. (1993), Effect of fluid forces on plant cell suspensions, 3rd International Conference on Bioreactor and Fluid Dynamics, Cambridge, September, 447-450

Dunlop, E. H., and Ye, S. J. (1994), Micromixing in fermentors: Metabolic changes in *Saccharomyces cerevisiae* and their relationship to fluid turbulence, *Biotechnol. Bioeng.,* **36,** 854-864

Dunlop, E. H., Namdev, P. K. and Rozenberg, M. Z. (1994), Effect of fluid shear forces on plant cell suspensions, *Chemical Engineering Science,* **49**(14), 2263-2276

Erdmann, A., Weil, B., Kramer, R. (1993), Lysine secretion by *Corynebacterium glutamicum* wild type triggered by dipeptide uptake, *J. Gen. Microbiol.,* **139,** 3115-3122

Fowler, J. D. and Robertson, C. R. (1991), Metabolic behaviour of immobilized aggregates of *Escherichia coli* under conditions of varying mechanical stress, *Applied and Environmental Microbiology,* 93-101

Gottschalk. 1986. Bacterial Metabolism. 2nd ed. Springer-Verlag.

Hermia, J (1982) Constant pressure blocking filtration laws: application to power law non-newtonian fluids, *Trans. Inst. Chem., Eng.,* **60,** 183

Hilliger, M. and Hanel, F., (1981), Process analysis of L-lysine fermentation under different oxygen supply, *Biotechnol. Letters,* **3**(5), 219-224

Ho, B. P. and Leal, L. G. (1974), Inertial migration of rigid spheres in two-dimensional unidirectional flow, *J. Fluid Mech.,* **65,** 365-400

Ingraham, J. L., Maaloe, O. and Neidhardt, F. C. (1983), Growth of the bacterial cell, Sinauer Associates, Sunderland, MA, Chapter 3

Kawase, Y. and Moo Young, M. (1990), Mathematical models for the design of bioreactors: applications of Kolmogoroff's theory of isotropic turbulence, *Chemical Engineering Journal,* **43 19**-41

Kelle, R., Laufer, B., Brunzema, C., Weuster-Botz, D., Krämer, R. and Wandrey, C. (1996), Reaction engineering analysis of L-lysine transport by *Corynebacterium glutamicum. Biotechnology and Bioengineering.* **51,** 40-50

Kiss, R. D. and Stephanopoulus, G. (1991), Metabolic activity control of the L-lysine fermentation by restrained growth fed batch strategies, *Biotechnol. Prog.,* **7,** 501-509

Kiss, R. D. and Stephanopoulus, G. (1992), Metabolic characterization of a L-Lysine producing strain by continuous culture, *Biotechnol. Bioeng.,* **39,** 565-574

Kolmogorov, A. N. (1941), *C.R.Acad. Scie.* URSS 30, 301

Lakhotia, S. and Papoutsakis, E. T. (1992), Agitation induced cell injury in microcarrier cultures: protective effect of viscosity is agitation intensity dependent: experiments and modelling, *Biotechnology and Bioengineering,* **39,** 95-107

Laufer, J. (1954), The structure of turbulence in fully developed pipe flow, *National Advisory Committee for Aeronautics Report 1174,* 1-18

Lee, H. W., Pan, J. G. and Lebeault, M. (1995), Characterisation of Kinetic Parameters and Metabolic Transitions of Corynebacterium glutamicum on L-Lysine Production on Continuous Culture, *Appl. Microbiol. Biot.,* **43**, 1019-1027

Liberge, R., Colinart, P., Fessier, P and Renon, N. H. (1994), Data and model for progressive fouling in crossflow microfltration of yeast on three industrial mineral membranes, *Ind. Eng. Chem. Res,* **33,** 1310-1318

Linko, S., Rajalathi, T. and Zhu, Y. –H. (1995), Neural state estimation and prediction in amino acid fermentation, *Biotechnology Techniques,* **9**(8), 607-612

Luedeking, R. and Piret, E. L. J. (1959), *Biochem. Microbiol. Technol. Eng.,* **1,** 393

Lui, Y. C., Wu, W. T. and Tsao, J. H. (1995), Fed-batch culture for lysine production via online state estimation and control, 1-10

Magee, R. D., Drake, J., Fredrickson, A. G. and Tsuchiya, H. M. (1972), studies in intermicrobillia aymbiosis, *Saccharomyces cerevisae* and *Lactobacillus casei, Can. J. Microbiol.* **18,** 1733-1742

Mankad, T. and Bungay, H. R. (1988) Model for Microbial Growth on More Than One Limiting Nutrient, *Journal of Biotechnology*, **7**, 161-166

Mankad, T., and Nauman, E.B. (1992), Modelling of Microbial Growth under Dual Limitations, *Biochem. Eng. J., 48*, 9-11

McQueen, A., Meilhoc, E. and Bailey, J. E. (1987), Flow effect on the viability and lysis of suspended mammalian cells, *Biotechnology Letters,* **9,** 831-836

Michel, B. J. and Miller, S. A. (1962), Power requirements of gas-liquid agitated systems, *AIChE Journal,* **13,** 262-266

Mietton-Peuchot and Aim, B. (1992), Improvement of cross-flow microfiltration performance with flocculation, *Journal of Membrane Science,* **68,** 241

O'Hagan, A. (1994), Baysian Inference, In "Kendall's Advanced Theory of Statistics", Wiley and Sons

Oh, N. S. and Sernetz, M. (1993), Turnover characteristics in continuous L-Lysine fermentation, *Appl. Microbiol. Biotechnol.,* **39,** 691-695

Ohno, H. and Nakanishi, E. (1976), Optimal control of a semibatch fermentation. *Biotechnol. Bioeng.* **18,** 847-864

Oolman, T. O. (1984), Bubble coalescence and mass transfer in air sparged bioreactors, PhD thesis, University of California, Berkeley, USA

Ramanathan, M. and Gaudy, A. F. (1971), Variability in cell yield for heterogeneous microbial populations of sewage origin grown on glucose, *Biotechnology and Bioengineering,* **13,** 113

Rutkov, A. B. (1984), Microbial production of L-lysine by employing fed batch cultivation, *Bulg. Akad. Nauk.,* **37**(12), 1677-1680

Rukisha, M. P., Vanags, J. J., Rikmanis, M. A., Toma, M. K. and Viesturs, U. E. (1989), Biochemical reactions of *Brevibacterium flavum* depending on the mdeium stirring intensity and flow structure, *Acta Biotechnology,* **9,** 565-575

Ryder, D. N. and Sinclair, C. G., (1972), Model for the growth of aerobic microorganisms under oxygen limiting conditions, *Biotechnology and Bioengineering,* **14,** 787-798

Schneider, K. and Klein, W. (1982), The concentration of suspensions by means of crossflow microfiltration, *Desalination,* **41,** 263-275

Schumpe, A., Quicker, G. and Deckwer, W. D. (1982), Gas solubilities in microbial culture media, *Advances in Biochemical Engineering,* **24,** 1-38

Shioya, S., Yong, Y. K., Omasa, T. and Suga, K. (1992), Maximising lysine production in fed-batch culture by controlling the specific growth rate under oxygen limited conditions, 669-672

Stouthamer, A. H. (1973), A theoretical study on the amount of ATP required for synthesis of microbial cell material, *Antonie van Leeuwenhoek J. Microbiol. Serol.,* **39,** 545

Takamatsu, T., Hashimoto, I., Shioya, S., Mizuhora, K., Koike, T. and Ohno, H. (1975), Theory and practise of optimal control in continuous fermentation process, *Automatica,* **11,** 111

Toma, M. K., Ruklisha, M. P., Zeltina, M. O., Galinina, N. I., Viesturs, U. E., and Tengerdy, R. P. (1991), Inhibition of microbial growth and metabolism by excess turbulence, *Biotechnology and Bioengineering,* **38,** 552-556

Tsao, G. T. and Hansen, T. P. (1975), Extended Monod equations for batch cultures with multiple exponential phases, *Biotechnology and Bioengineering,* **17,** 1591-598

Vallino, J. J. and Stephanopoulus, G. (1994), Carbon flux distributions at the pyruvate branch point in *Corynebacterium glutamicum* during lysine overproduction, *Biotechnol. Prog.,* **10,** 320-326

Vallino, J. J. and Stephanopoulus, G. (1987), Intelligent sensors in biotechnology applications for the monitoring of fermentations and cellular metabolism, *Am. NY Acad. Sci.* **506,** 415-430

Vallino, J. J. and Stephanopoulus, G. (1989), Flux determination in cellular bioreaction networks: Applications to lysine fermentation, Sikdar, S., Bier, M. and Todd, P. (Eds.), Frontiers in Bioprocessing, CRC Press, Boca Raton, FL

Vallino, J. J. and Stephanopoulus, G. (1993), Metabolic flux distributions in *Corynebacterium glutamicum* during growth and lysine overproduction, *Biotechnol. Bioeng.,* **41,** 633-646

Vallino, J. J. (1991), Identification of branch-point restrictions in microbial metabolism through metabolic flux analysis and local network perturbations, PhD Thesis, Massachusetts Institute of Technology, Cambridge, MA, USA

Van Gulik, W.M. and Heijnen, J.J. (1995), A metabolic network stoichiometry analysis of microbial growth and product formation, *Biotechnology and Bioengineering*, **48**, 681-698.

Vandecasteele, J. P., Lemal, J. and Coudert, M. (1975), Pathway and regulation of glutamate synthesis in a *Corynebacterium sp.* overproducing glutamate, *J. Gen. Microbiol.*, **90,** 178-180

Viesturs, U., Ruklisha, M., Krikis, V. Puntse, M. and Shvinka, J. (1989), Microbial synthesis of L-Lysine: problems, bioengergetics, biochemistry, technology, equipment, *Progress in Biotechnology,* **6,** 325-335

Volesky, B. and Votruba, J. (1992), Modelling and optimisation of fermentation processes, Elsevier, 96

Wang, F. S. and Cheng, W. M. (1999), Simultaneous optimisation of feeding rate and operation parameters for fed batch fermentation processes, *Biotechnology Progress,* **15**(5), 949-952

Wang, N. S. and Stephanopoulos, G (1984), Computer Applications to Fermentation Processes, *CRC Critical Reviews in Biotech.*, **2**, 1-103

Wang, N. S. and Stephanopoulos, G. (1983), Applications of macroscopic balances to the identification of gross measurement errors, *Chem. Eng. Sci.*, **36,** 1849

Weuster-Botz, D., Kelle, R., frantzen, M. and Wandrey, C. (1997), Substrate controlled fed-batch production of L-Lysine with *Corynebacterium glutamicum, Bitechnol. Prog.*, **13,** 387-393

Yet-Pole, I., Wu, W-T. and Liu, Y-C. (1996), Neural Network Modelling for On-line State Estimation in Fed-Batch Culture of L-Lysine Production, *The Chemical Engineer Journal*, **61**, 35-40

Zhang, Z., Al-Rubeai, M. and Thomas, C. R. (1993), Estimation of disruption of animal cells by turbulent capillary flow, *Biotechnology and Bioengineering,* **42,** 987-993

Conclusions

L-lysine is an essential amino acid in monogastric animal nutrition. The bulk of L-lysine production throughout the world depends on the direct fermentation of carbohydrates by auxotrophic and regulatory mutants of *Corynebacteria* and *Brevibacteria* species. Amino acid fermentations are intensive in raw material usage. Hence the process yield and productivity are critical measures of performance and economic viability (Kiss & Stephanopoulos 1991).

The overall fermentation performance has been improved by using fed-batch strategies whereby the cells are maintained in the L-Lysine overproduction metabolic state by continuously feeding the substrate to the reactor (Hadj *et al.* 1988; Rutkov 1984, Hirao *et al.* 1989; Kiss & Stephanopoulus 1991). The fermentation is stopped when the bioreactor reaches the maximum volume. A large portion of the production cost is spent to establish a viable biomass population. To maximise the volumetric productivity and reduce production costs, feed and bleed strategies are often employed. However, since L-lysine is predominantly a secondary metabolite, the maximum yield of L-lysine from carbohydrates is achieved at very low growth rates. This implies that viable biomass, still capable of L-lysine production are lost in bleed and not replaced by cell growth. The reactor volume as well as the inability of the process to retain the microbial population limits the productivity and conversion of carbohydrates to L-Lysine.

In this thesis it was demonstrated that the L-Lysine fermentation performance can be enhanced by continuously withdrawing spent medium and recycling of the biomass in the culture suspension to the bioreactor. The biomass in the reactor outlet was separated from the spent medium using cross-flow filtration before being recycled to the reactor. The objective of this thesis was to study, understand, model and optimise the performance of the L-Lysine fermentation with biomass retention using cross flow filtration.

Two L-Lysine producing strains (ATCC 21253 and AEC 94) and two ultrafiltration (150 kD and 300 kD) and two microfiltration (0.22 μm & 0.45 μm) tubular ceramic membranes were used. Fermentations were conducted on 10-litre scale using both a chemically defined and an industrial medium composition.

Cross flow filtration of *C. glutamicum* suspensions

In the second chapter the factors that influence the cross flow filtration flux of suspensions of *C. glutamicum* were investigated. These factors were classified into the impact of the membrane properties, the feed suspension and the operating parameters. It was found that the pseudo-steady state flux decreases as the complexity of the solvent increases. The effect of the membrane pore size can largely be ignored for the more complex solutions although internal fouling was more severe for the MF membranes.

The flux increased with increasing trans-membrane pressure drop (ΔP) until a critical value is reached beyond which an increase in the pressure drop does not result in a proportional increase in the flux. For both MF and UF membranes the critical pressure drop increased with increasing cross-flow velocity. An increase in flux was also reported on increasing cross-flow velocity. The effect of the operating parameters (trans-membrane pressure drop and cross flow velocity) were mostly linear for the MF membranes while for the UF membranes the effects were highly non-linear over the range tested.

Membrane fouling can be divided into internal and external fouling phenomena. Internal fouling involves pore plugging and constriction. The hydraulic resistance that results from pore plugging was found to depend on the membrane pore size and the fraction of near sized particles. The pore plugging resistance increases with increasing trans-membrane pressure drop to a maximum and then decays to a pressure independent value. The cross-flow velocity did not significantly influence the pore plugging resistance.

External fouling is mainly due to the build-up of a fouling cake layer on the membrane surface. The hydraulic resistance caused by the cake layer increases with increasing complexity of the feed suspension and increasing trans-membrane pressure drop. A decrease in the cake resistance was found with increasing cross-flow velocity. This reduction has been attributed to a decrease in cake weight with increasing cross-flow velocity.

The filtration flux typically declines sharply over the first 200 seconds and then reaches a pseudo-steady state value. From a flux decline analysis it has been found that, the initial period of flux decline is predominantly a result of internal fouling. The initial flux decline is followed by a period of cake build-up. Cake build-up is continued until the cake thickness corresponding to the cross-flow velocity is reached. At this point the flux remains relatively constant declining at an almost undetectable rate.

The critical filtrate volume at which the predominate fouling mechanism changes from internal to external fouling is a function of both the membrane pore size and the nature of the solvent. Generally, this volume is reduced for the UF membranes compared to MF membranes and increases with increasing solvent complexity.

The understanding of the fouling phenomena encountered during cross-flow filtration of *C. glutamicum* suspensions served as a basis for the development of a semi-empirical model describing the system behaviour. A generic form of Hermia's blocking laws (Equation 3-90) was found to be well suited to the description of the initial stages of cross-flow microfiltration. A constant term (the pseudo steady state flux) has been included to provide a semi-empirical correlation of the cross flow filtration flux (Equation 3-91). The pseudo steady state flux is based on Darcy's law (Equation 3-92) and a combination of the shear induced diffusion and surface transport models. Darcy's law divides the total hydraulic resistance into the membrane resistance (or the impact of the membrane on the filtration flux), the pore plugging resistance (or the interaction between the feed suspension and the

membrane) and the cake resistance (or the impact of the feed suspension on the filtration flux).

The membrane resistance can be estimated from pure water flux data. The pore plugging resistance was estimated based on Hagen-Poiseuille flow through an array of cylindrical pores. The analysis accounts for the impact of a pore size distribution on the flux associated with pore constriction effects (Equation 3-93). The cake resistance is given by the intrinsic cake resistance, which is a function of the applied trans-membrane pressure drop, and the thickness of the cake layer on the membrane surface (Equation 3-97, 3-98). The thickness of the cake layer is based on single particle trajectory models and is modelled as the product of power law functions of the ratio of the tangential and normal convective forces and the cell concentration in the bulk stream (Equation 3-99). The model presented adequately described the experimental data.

Although these mathematical models can provide useful descriptions of the decline in flux observed during membrane filtration, it is not currently possible to obtain a priori estimates of the key parameters in these equations. In addition, these models do not provide a quantitative basis for understanding the effects of solution properties or membrane characteristics on the flux decline. These models also provide little insight into the actual physical and chemical mechanisms by which the filtration flux declines during the filtration process.

In Chapter 4, the model developed in Chapter 3 was compared against previously developed models (a multiple regression approach (Eq. 4-18), concentration polarisation (Eq. 4-21), shear induced diffusion (Eq 4-23), flowing cake layers (Eq. 4-24), single particle models (Eq. 4-25) pore plugging (Eq. 4-27) and the solids flux model (Eq. 4-26) using Bayesian inference. Bayesian analysis was used to determine the Bayesian factors of the model presented against the hybrid model. All the Bayesian factors were below 1 indicating that these models describe the process less adequately than the hybrid approach. The hybrid approach also showed the lowest adjusted error of 7% (to compensate for the varying degrees of freedom between models) and the highest adjusted correlation coefficient (R^2_{adj} = 0.9950).

The hybrid model was therefore selected as the preferred model to predict the filtration flux as a function of the operating conditions and the feed stream properties. This model was combined with the fermentation model (developed in Chapter 5 and 6) and used in Chapter 7 for the optimisation of the entire system.

The impact of hydrodynamic stress generated in filtration on the fermentation performance of *C. glutamicum*

The qualitative effects of the increased hydrodynamic shear stress typically encountered in cross-flow micro-filtration applications on the growth, metabolism and morphology of *Corynebacterium glutamicum* cells have been investigated. It was found that the cell volume increases under increased hydrodynamic shear although increased shear does not

alter the cell shape. It is therefore reasonable to assume that the increased volume may be due to increased water uptake into the cell as suggested by Wase and Patel (1985). It was also found that the effects of hydrodynamic shear stress on the cell's morphology were reduced at increased biomass concentrations.

The apparent specific growth rate of the cells exposed to hydrodynamic shear in the filtration system decreased although the stationary phase biomass concentration increased relative to the conventional batch. Similarly the yield of biomass from threonine increases while the yield of biomass on glucose decreases when the cells are passed through the filtration system. The specific lysine productivity of the cells exposed to increased hydrodynamic shear was reduced compared to that of the cells cultivated in the conventional stirred tank reactor. The reduced specific lysine productivity and the increased glucose uptake rate of the cells exposed to increased shear in the filtration loop implies a reduced cumulative yield of lysine from glucose. These effects were less pronounced at the higher biomass concentrations (25 g/l DCW).

The fermentation data provided convenient sets of extracellular flux measurements (glucose, L-lysine, free and saline nitrogen, oxygen and carbon dioxide) to elucidate the impact of increased hydrodynamic stress caused by biomass recycling on the biochemistry of L-lysine synthesis through intracellular flux analysis. This method combines the known metabolic pathways of the organism with a pseudo-steady state approximation for intracellular metabolite concentrations to generate a mathematical representation of the metabolic flows.

The excess ATP for cells exposed to increased hydrodynamic stress due to cell recycle was reduced relative to that of the "conventional batch". The reduction in ATP formation is believed to be a result of a shift in cellular metabolism from oxidative phosphorylation to substrate level phosphorylation and glycolysis. The flux of carbon through PPP was reduced at increased hydrodynamic shear due to a reduction in the requirement for NADPH of the cells exposed to hydrodynamic shear in the filtration module. Exposure to hydrodynamic shear in the membrane unit did not have an impact on the split of carbon at the PEP or OaA nodes. At the Pyr node the flux of carbon to lysine and the flux of Pyr to AcCoA was reduced at increased hydrodynamic shear, while the flux of pyruvate into other amino acids increased. Thus, at increased shear the total flux of carbon toward the TCA cycle decreased. From the qualitative analysis presented it was postulated that increased hydrodynamic shear causes an increase in the flux of carbon towards the cell wall to either repair or strengthen the cell wall.

An analysis of the impact of cell recycling on the mass transfer properties of the bioreactor indicated that if the same oxygen transfer rate is to be maintained at increased cross flow velocities, less agitation power and more air would be required at higher cross flow velocities.

It was also shown that the fed-batch fermentation with biomass recycling outperformed the other reactor configurations (batch, fed-batch and continuous) based on total lysine produced and the concentration of lysine in the final broth.

The effect of exposing the cells to increased hydrodynamic shear in the cross flow filtration system was quantified in Chapter 6 and two fermentation models were developed to predict the fermentation performance as a function of the controllable variables. The models consist of a mass and volume balance coupled to two sets of metabolic equations. In the first approach, the cellular metabolism is modelled by approximating the cell as a "black box" and using empirical correlations developed from experimental data to depict the cells' response on changes in the extracellular environment. In the alternative approach the metabolism is modelled based on a bioreaction network of the intracellular central carbon distribution. Some critical nodes within this network were identified and the carbon split ratios around these nodes were fixed or modelled based on extracellular conditions. From this information the cells response to changes in the extracellular environment could be predicted.

The impact of filtration associated hydrodynamic stress on the cellular metabolism was modelled based on a linear relationship between the metabolic impact and the average energy dissipation rate per unit cell mass. A critical average energy dissipation rate was identified below which no impact on the fermentation performance relative to conventional batch fermentations were detected. Above this critical energy dissipation rate, reduction in growth rate and specific productivity and an increase in the yield of biomass from threonine were modelled as linear functions of the turbulent energy dissipation divided by the biomass concentration.

The Bayesian approach was used to illustrate that the model using empirical correlations to estimate the metabolic behaviour of the cell exhibits a higher probability of predicting the performance of the system. The model with the empirically estimated metabolism was used to optimise the entire system's performance.

Optimisation of the bioreactor system with cell recycle using cross flow filtration for lysine production

The fed batch fermentation with biomass recycling using cross flow filtration for the production of L-Lysine was optimised using an equation-based dynamic simulation package (gPROMS). The variable cost of production (VCOP) defined as the cost to produce a kilogram of lysine was used as the objective function for the optimisation process. The predicted optimum represented a 26% reduction in variable cost compared to the conventional fed-batch fermentation technology (R14.50/kg vs R10.65/kg).

The predicted optimum was physically achievable and the experimental results obtained when a fermentation was conducted at the optimal conditions corresponded with that predicted by the proposed model (Figure 7-4 to 7-9). This indicated that the fermentation

model as proposed was accurate enough, with enough resolution for optimisation of the fermentation process.

The VCOP of the lysine fermentation can be minimised by maximising the biomass in the bioreactor and retaining all the produced biomass in the bioreactor, while feeding at a rate close to the maximum glucose uptake rate. The specific sugar feed rate represents a trade-off between increased yield at lower feed rates and increased productivity at higher feed rates. None of the auxotrophic amino acids are to be included in the feed for minimal VCOP.
The permeate flow rate from the cross flow filtration system matched the total feed rate, thus maintaining a zero or minimal bleed rate.

During the lysine production phase, the total biomass in the bioreactor remains virtually constant. Furthermore, it was evident that at optimal conditions the fermentation is to be conducted at virtually zero residual sugars. Since spent medium is continuously withdrawn from the bioreactor, a zero residual sugar concentration would maximise the yield of lysine from the sugar fed. The duration of the fermentation process is limited by the ability of the strain to sustain its performance and not by the residence time of the biomass in the bioreactor.

The model parameters were re-established for the industrial lysine producing strain (AEC94). The model was then used to optimise the fermentation performance of a conventional fed-batch process with a feed and bleed strategy as well as that of a fed-batch process with biomass recycling using cross flow filtration. The model predicted a 12% improvement in VCOP while a 14% improvement was realised from experimental data.

The linear approximation used to model the impact of filtration on fermentation performance is limited to application of hydrodynamic shear experienced in cross flow filtration systems and cannot be transferred to other hydrodynamic stress impacts. The model parameters are empirical in nature and must therefore be redeveloped for each strain. Although this is a tedious process the methodology allows for process optimisation that produces a physically realisable optimum. Biomass recycling using cross flow filtration improves the variable cost of production of the lysine fermentation process by at least 12% compared to the current fed-batch technology.

Optimisation of the Performance of the Biomass Recycling System for L-Lysine Production

1 Introduction

Optimisation involves the process of finding the extreme (minimum or maximum) value of a certain criterion by selection of a set of values for the adjustable or control variables. Optimisation methods are generally classified based on whether a functional relationship between the criteria and the adjustable or control variables are known. Where no functional relationship is known, optimisation generally involves "search plans" - a set of n experiments with different values for the independent variables in an attempt to find the optimum value of the criterion or selected dependent variable. When a functional relationship between the independent variables and the criterion is known, there are various mathematical methods from which the optimum can be predicted.

For the latter group of methods, the success of the optimisation process as well as the physical reliability of the predicted optimum depends on the quality of the functional relationship and to a lesser extent on the optimisation technique used. The success of the optimisation technique depends on the rate of convergence and the probability of reaching a global rather than a local extreme value. The physical reliability of the predicted optimum indicates to what extent the predicted optimum can be achieved experimentally. This depends on the quality of the model and the imposed constraints.

Biochemical fermentation processes are characterised by a large number of variables that can influence the process outcome. The large number of degrees of freedom in these processes combined with their slow nature makes optimisation through search plans very tedious and in most cases physically unrealistic and economically unfeasible. It is therefore easily recognised that, in the optimisation of fermentation processes, the emphasis falls mainly on the development of accurate relationships between dependent and independent variables.

Due to the complex nature of fermentation processes, fundamental functional relationships are limited with regard to their ability to predict process performance. Therefore, most attempts at the modelling of biochemical processes use empirical correlations of experimental data that are only valid over the range evaluated. There are however "hybrid models" that use some fundamental understanding of the system's behaviour to dictate the form of the empirical correlation. Several of these "hybrid models" exist that describe some aspects of biochemical processes, each with its limitations and defined range of applicability (Shioya 1992; Weuster-Botz *et al.* 1997; Büchs 1991; Ohno & Nakanishi 1976; Modak *et al.* 1986; San & Stephanopoulus 1984; Wang and Cheng 1999).

In the Chapter 6, a "hybrid" model was developed that effectively described the performance of the bioreactor with biomass recycling. In this chapter, a broad overview of optimisation techniques is given, followed by the optimisation of the biomass recycling process for the production of L-Lysine using an equation-based dynamic simulation package. The results from the optimisation process are then compared to experimental data.

The chapter is concluded by the optimisation of an industrial scale fermentation process with biomass recycling to indicate the economic value of biomass recycling and the realising of the true potential of the system through effective process optimisation.

2 Background on the optimisation of fed-batch fermentation processes

Various fermentation processes are operated on a fed-batch mode. The nutrients are fed continuously into a bioreactor over the fermentation period with or without partial withdrawal of fermentation broth. Determining the optimal control policy to produce the maximum yield is a challenging task, since the dynamic governing equations are frequently non-linear and include some physical constraints. Therefore it is not surprising that the dynamic optimisation of fed-batch fermentation processes is an active area of research (San and Stephanopoulos *1989*; Banga & Seider *1995*).

Ultimately the objective function of any industrial process should be expressed in monetary gain. The optimisation then attempts to minimise cost and maximise throughput. Weuster-Botz *et al.* (1997) proposed an economic model for the production of L-isoleucine by coupling the mass balance and energy balance with the semi-empirical models of the unit operations. This model was used to minimise the production cost of the fermentation process (Weuster-Botz *et al.* 1997). Büchs (1991) developed a cost model coupled with a fermentation model. He proposed a systematic and efficient method of process development that can be achieved when experimental work is accompanied and guided by mathematical modelling. The advantage of a complete and verified process model coupled to an economic cost model was illustrated by optimising an industrial L-lysine production process.

Various optimisation methods or approaches have been developed to yield the optimal settings of the control variables.

2.1 Surface response methods

Surface response methods form part of the first class of optimisation problems. In these methods, no fundamental understanding of the system's behaviour is required and the optimum settings are achieved by constructing a surface response of various settings of the control variables. The major limitation of this method is that it requires large amounts of

experiments. Therefore, this approach is generally only suitable for the optimisation of time independent variables and optimal control profiles cannot be achieved.

Surface response methods are therefore most commonly used to optimise medium composition. Udeh & Acremovicz (1993) and Hadj Sassi *et al.* (1990) optimised the fermentation medium composition by using surface response methods. Weuster-Botz *et al.* (1997) obtained the optimal medium composition for the lysine fermentation by using a genetic evolutionary algorithm.

2.2 Substrate controlled fermentations

A second approach is to convert the optimal control problem into a problem with time independent variables. One of the time independent variables can be the substrate concentration in the bioreactor. In this approach the feed rate is adjusted to maintain a specific extracellular substrate concentration. For example, Weuster-Botz *et al.* (1997) reported that a constant set-point of 10-100 mM glucose as well as a variable set point within this range has no effect on the specific lysine production rate and the differential lysine selectivity. This was confirmed by Kelle *et al.* (1996). They therefore derived a feed profile that would maintain the extracellular glucose concentration at 10 mM to maximise the yield.

Another approach is to convert the optimal feed problem into a problem of finding the optimal extracellular substrate concentration. As an example Guthke and Knorre (1981) used optimal control theory based on a fermentation model to find the optimal extracellular substrate concentration from which the optimal feed profile was derived.

2.3 Control of metabolic activity

The third general approach to fermentation optimisation is to manipulate the extracellular environment to maintain a specific metabolic state.

Firstly, measurable indicators are derived that would identify or characterise the metabolic state of the cells. For example, Kiss and Stephanopoulos (1991) used respiratory measurements to indicate the metabolic activity of the cells. Using these, the relationship between the controllable variable, in most cases the feed rate, and the metabolic state is derived. From this information a control philosophy can be determined to maintain the metabolic state and activity of the cells by manipulating the feed rate. Kiss and Stephanopoulos (1991) illustrated this by deriving two control schemes for maximising the fermentation yield and productivity. They suggested an algorithm to control the feed rate based on measurements of the respiration quotient as an indication of the cells metabolic activity. They proved that proper environmental control (control of the availability of substrate) is an effective method for manipulating the microbial metabolism (respiration

quotient and thus the lysine yield from carbohydrate or the cells specific lysine productivity) to favour metabolite overproduction.

Shioya (1992) identified the relationship between the specific growth rate and the specific lysine production rate for *C. glutamicum.* This was represented by a mathematical model. The optimal strategy that allows for the maximisation of the specific productivity by manipulating the specific feed rate was then obtained from a relationship between the specific feed and growth rates. Yamane *et al.* (1977) converted the problem of obtaining an optimal feed rate strategy into one involving the determination of the optimal specific growth rate which corresponds to a specific metabolic state.

2.4 Mathematical optimisation methods

Where a simple but effective process model of the fermentation process is available, there are various numerical techniques available for process optimisation. A number of numerical techniques have been suggested for the determination of optimal feed rate profiles, such as gradient methods, a differential dynamic program approach, multiple shooting methods and quasi-linearisation methods (Stutts 1983).

Optimal control theory can be used to predict the optimal feed rate profile during fed-batch fermentations (Ohno & Nakanishi 1976; Modak *et al.* 1986). Moda *et al.* (1986) considered the optimal glucose feed strategy for penicillin fermentations from the standpoint of singular control theory. Modak & Lim,(1986) formulated the problem of feedback optimisation of the feed rate for fed-batch fermentation processes in the framework of singular control theory and switching hypersurfaces. The method is based on four differential equations (mass balances) that describe a general class of fed batch processes. Modak & Lim (1986) have shown that, under certain restrictions, the feedback optimisation of the feed rate can be realised as a nonlinear function of the state variables, such as the concentrations of cell mass, substrate and product as well as fermenter volume.

Weigand *et al.* (1979) and San and Stephanopoulos (1984) considered the problem of optimal feed strategies for fed-batch fermentation processes for cell production described by three or fewer mass balance equations.

Wang and Cheng (1999) used optimal control theory and optimal parameter selection for selection of the optimal fed-batch feed profile. The optimisation problem is converted into the finite dimensional problem using a control parameterisation technique. A hybrid differential evolution is introduced to solve the converted problem.

Ohno and Nakasaki (1976) developed a model using Kelley's transformation method with Pontryagin's maximum principle to optimise fermentations with regard to mode of operation (batch, fed-batch or continuous). Kelly's transformation method is a device, to

avoid the singular situation which occurs when the usual procedure of selecting the optimal control function by the maximum principle breaks down.

Ohno and Nakasaki (1976) also optimised the lysine fed-batch fermentation by applying Green's theorem to the maximisation problem proposed. This approach succeeded in determining the feed rate of the substrate that maximises the production rate of the desired product.

It can be seen that most attempts at dynamic optimisation of the fed-batch fermentation centre on optimal control theory. In the next section a brief overview of optimal control will be given.

3 Background on Optimal Control

In this section, the basic principles behind optimisation and optimal control theory are introduced. A general statement of the optimal control problem is given, and some approaches to its solution are described. The fundamental mathematical principles of the calculus of variations are essential in the formulation and solution of optimal control problems. Assuming that the dynamics of a system are known and the state can be measured instantaneously, the theory of optimal control may be regarded as a generalisation of the problem of Lagrange in the calculus of variations. This involves the minimisation of an integral, subject to side conditions which may be ordinary or differential equations.

Optimal control theory originated from wave propagation and variational principles in physics, beginning with Huygens, continuing with Bernulli and finally achieving its maturity with the work of Hamilton, Jacobi and Lie in the nineteenth century. Johann Bernulli challenged his contemporaries with the *"Brachystochrone problem"* (BP). The objective was to find the orbit AMB of a movable point M along which starting from A and under the influence of its own weight arrives at B in the shortest possible time; given that A and B are in the same vertical plane. Bernulli's BP problem was a true minimum time problem. The BP was the first problem to deal with a dynamic behaviour and explicitly ask for the optimal selection of the path. Such minimum time problems predominantly influenced the development of modern optimal control and at the same time most clearly demonstrate the difference between optimal control and the classical formulation of the calculus of variations.

Optimal control in its modern sense began in the 1960's with the formulation of two design optimisation techniques, both relying on the calculus of variations:

- *Pontryagin Minimum Principle* (PMP)
- *Dynamic Programming* (DP).

The minimum principle represents a generalisation of the Euler-Lagrange equations from the classical calculus of variations. This may be viewed as an outgrowth of the Hamiltonian approach to variational problems. The method of dynamic programming may be viewed as an outgrowth of the Hamilton-Jacobi approach to variational problems. A large part of the history of the calculus of variations can best be understood as the search for the simplest and most general statement of the necessary conditions for optimality. This is best provided by the minimum principle of optimal control theory.

The rapid development of control theory was simultaneously followed by a continuous revolution in computer technology. Computers provided computational facilities and simulation tools that greatly reduced the need for closed form solutions. New computational techniques in the area of optimal control were introduced. Other techniques have been rendered obsolete while at the same time, other previous impractical methods have become feasible and efficient.

3.1 Optimal Control Problem

The basic control problem may be subdivided into the following interrelated parts:

- Problem statement
- State estimation problem
- Modelling and system identification
- Optimisation

The problem statement is a definition of the goal or objective of the optimisation problem. The state estimation problem relates current measurements to the current state of the system. Knowledge of how the environment affects the past, present and future states of the system is modelled and used to find the extreme value of the goal or objective.

To state the control problem in its simplest form it is assumed that physical measurements are available giving the exact numerical value of the state at every instant of time. It should be pointed out that optimal control does not necessarily have to involve feedback. This form does, however result from the solution of the LQ optimal control problem which is a simplified case of optimal control. Additionally it is assumed that the system model describes the true system without error. These assumptions are large idealisations from the engineering point of view.

3.1.1 System description

Consider the general non-linear system:

$$\dot{x} = f(x, u_c(t), t), \qquad x_0 = x(t_0) \tag{7-1}$$

Here $x \in \Re^n$ represents the state vector of the system, $u_c(t) \in \Re^m$ is the input vector and f denotes the system vector that is continuously differentiable in all arguments. The couple (x, t) is referred to as a phase. The phase space is given by the Cartesian product of the state space X ($=\Re^n$) with the space T ($\Re^1$) of all the values of time t.

The input function $u_c(t)$ represents an admissible control if it is piecewise continuous in t and its values belong to a given closed subset $U_c(t)$ of $\Re^m$, for each t. For any admissible control u_c and any initial phase (x_0, t_0), there exists a unique absolutely continuous function $\eta(t)$ denoted by:

$$\eta(t) = \eta_u(t; x_0, t_0) \tag{7-2}$$

that satisfies the system equation and has the property:

$$\eta(t_0) = \eta_u(t; x_0, t_0) = x_0 \tag{7-3}$$

Here $\eta_u(t_0; x_0, t_0)$ denotes the motion of the system passing through x_0 at time t_0 under the action of the control u_c. The value of η at some fixed t is the state of the system.

3.1.2 Problem statement

Consider the system discussed above for an arbitrarily selected initial phase (x_0, t_0). Let S be a surface in the phase space. The following scalar functional of motions defines the performance index:

$$V_c(x_0, t_0, S, u_c) = \varphi(\eta_u(t_f; x_0, t_0), t_f) + \int_{t_0}^{t_f} L(x(\tau), u_c(\tau), \tau)d\tau \tag{7-4}$$

L and φ are scalar functions, continuously differentiable in all arguments, which denote the Lagrangian and the terminal cost, respectively, with $L(0,0,\tau)=0$ and $\varphi(o,t_f)=0$. The terminal time t_f describes the first instant of time after t_0 when the motion enters the set S. Therefore, it suffices for φ to be defined only on S. To reflect some physical quantity for the minimisation which is desired, $L(x(\tau), u_c(\tau),\tau)$ and $\varphi(x(t_f))$ are chosen to be nonnegative functions of x and u. As the notation implies, the performance index depends on the initial state x_0 and time t_0, and the control variable $u_c(t)$ for all $t \in [t_0,t_f]$.

An optimal control problem is given by specification of the system dynamics, the Lagrangian (L), the terminal function (φ), the target (S), the cost function (V_c) and can be defined as follows:

"Given any initial phase (x_0,t_0), find a corresponding admissible control (u_c^*) in the interval ($[t_0,t_f]$) at which the cost function assumes its extreme value with regard to the set of all admissible control laws."

For technology reasons an equivalent definition of optimal control can be formulated as:

"Find a state-feedback control law $u_c^* = \phi(x)$, such that the performance objective assumes its infinum with regard to the set of all admissible control laws, given the nonlinear system dynamics."

If the system's description (Equation 7-1) depends on stochastic factors, the extreme value of the cost function with respect to the control laws will usually be lower than with respect to all admissible controls that are uniquely determined by the initial phase. This is a result of the fact that the control law that is determined *a priori* as a function of only the initial phase must, in some sense, be a design that accounts for all possible trajectories that can result depending on the stochastic factors. On the other hand, if the control takes into account not only the initial state, but all successive states as well, the added information so obtained may result in a better optimum.

3.1.3 Typical control problems

A number of typical control problems can be put into the optimal control formulation stated above:

- *Terminal control*

The problem is to bring the state of the system as close as possible to a given terminal state x_f at a given terminal time t_f. At L=0, $\varphi(x)$ is the distance of x from x_f and $S = X \times \{t_f\}$.

- *Minimal-time control*

The goal is to reach a state x_f from (x_0, t_0) in the shortest possible time. Then L=1, φ = 0 and $S = \{x_f\} \times T$. This problem ordinarily has a solution only if $U_c(t)$ is a bounded set for all $t \geq t_0$.

- *Regulator problem*

Assuming that the system is in some initial phase (x_0, t_0), the goal is to return it to an equilibrium state x^0 in such a way that some integral of the motion is minimised. In this case L and φ are usually taken to be nonnegative. The dependence of L on u_c is needed because otherwise the problem may not have a solution. The set S is $X \times \{t_f\}$.

- *Pursuit problem*

Given a moving target $\xi(t)$, the problem is to bring the motion to the phase $(\xi(t),t)$ as soon as possible. This is a generalisation of the minimal time problem $S = \{(\xi(t), t); t \in T\}$.

- *Tracking problem*

This is a generalisation of the regulator problem. Given a desired state $\xi(t)$, the problem is to cause the phase of the controlled motion to be as close as possible to $(\xi(t), t)$ on the interval $[t_0, t_f]$. The instantaneous distance between $(x(t), t)$ and $(\xi(t), t)$ is measured by L.. The set S is the same as in the regulator problem.

- *Minimum energy problem*

The goal is to transfer from an initial phase (x_0, t_0) to a final phase (x_f, t_f) with the expenditure of a minimal amount of control energy. In this case L is taken to be a nonnegative function of u_c, independent of φ; S is the set consisting of the single phase (x_f, t_f).

3.2 Solution of the optimal control problem

There are basically two different approaches to solving the optimal control problem:

- *Dynamic programming (DP)*

(Hamilton-Jacobi-Bellman (HJB) approach)

- *Classical Variational Approach*

(Pontryagin Minimum Principle (PMP), Euler-Lagrange (EL) equations)

Dynamic programming is founded on the so-called principle of optimality, which characterises global optimality in a local sense, utilising the concept of an optimal value function. Techniques based on classical variational methods view optimality from a global perspective by studying optimal trajectories.

3.2.1 Dynamic Programming

Using the principle of optimality to derive optimisation equations was first proposed by Bellman (1957) and it is commonly referred to as the dynamic programming approach. In the context of optimal control it can be used to derive the well-known Hamilton-Jacobi-Bellman partial differential equation.

The basic assumption underlying the optimality principle is that the system can be characterised by its state x(t) at time t, which completely summarises the effect of all inputs $u_c(\tau)$ prior to time t. This allows for a local characterisation of optimality as given by the optimality principle. The optimality principle states that if $u_c^*(\tau)$ is optimal over the interval $[t, t_f]$, starting at state x(t) then $u_c^*(\tau)$ is necessarily optimal over the subinterval $[t + \Delta t, t_f]$ for any Δt such that $t_f - t \geq \Delta t > 0$. More details as well as a proof of the optimality principle can be found in many references (Sage & White 1977).

Dynamic programming is the concept of using the optimality principle to formulate an optimisation problem as a recurrence relation, i.e. the remaining sub-problem has precisely the same structure as the previous sub-problem. In this way, a particular optimisation problem is solved by studying a family of problems, which contain the particular problem as a member. For instance, in the optimal control problem, if one considers a function which associates to every point in the state space, the optimal cost starting from that point (such a function is often called a value function), then it is possible to write a recurrence relation in terms of the optimal value function which is valid for the entire state space. If this relation can be solved, the value function obtained is associated with an entire family of optimal control problems, each with a different initial point. Knowledge of the optimal value associated with a particular initial condition provides no way of determining the minimising trajectory itself. Knowledge of the value function on the entire state space does allow one to determine the minimising trajectory of any particular member of the family of problems.

3.2.2 Classical Variational Calculus

The classical variational calculus methods lead to the derivatisation of the Euler-Lagrange equations, which give a necessary condition for optimality. The Euler-Lagrange equation results by considering the optimal control problem in the framework of constrained optimisation. Lagrange multipliers are used to adjoin the constraints to the performance index. Since the constraints are determined by the system differential equation and represent equality constraints that must hold at each instant in time, an associated multiplier is a function of time.

According to the theory of Lagrange multipliers, the problem of determining the control function $u_c(t)$ that minimises the original performance index subject to the constraints has been converted to the problem of minimising the Hamiltonian. The Hamiltonian is the scalar function representing the adjointed performance index and the original constraint functions. The Euler-Lagrange equations are derived from the Hamiltonian and define the necessary conditions for optimality.

3.3 Dynamic optimisation of differential algebraic systems through a dynamic simulation package

gPROMS is an equation-orientated software package for dynamic simulation, parameter estimation and optimisation of various chemical processes. The package was developed by Imperial College, London and is marketed by Process Systems Enterprise, an UK based company founded in 1997 (Pantelides & Barton 1993; Vassiliadis *et al.* 1994a 1994b).

A chemical process in the gPROMS language is represented by a set of differential-algebraic equations (DAE). These equations generally describe the process mass and

energy balances as well as all physical and chemical laws that are used to model the system behaviour.

Another package called DYNSIM has been developed by Sorensen (1991) which behaves very similarly to gPROMS. DYNSIM is also an equation-orientated process simulator that can be employed for simulation problems related to design and analysis of complex chemical processes.

3.3.1 Dynamic simulation of chemical processes in the dynamic optimisation packages

The dynamic simulator is particularly suitable for simulation of complex chemical processes which can be highly integrated and can involve non-ideal mixtures or operate at extreme conditions. A chemical process in either DYNSIM or gPROMS is represented by the following set of differential-algebraic equations in a sequence of stages k = 1,2...

$$f((x(t), \dot{x}(t), y(t), u_c(t), v_t) = 0 \qquad t \in [t_{k-1}, t_k] \qquad (7\text{-}5)$$
$$k = 1,...NS-1; \qquad t \in [t_{NS-1}, t_f] \qquad k = NS$$

where t is time, $x(t) \in \mathbf{X} \in \Re^n$, $y(t) \in \mathbf{Y} \in \Re^m$ are sets of differential and the algebraic variables respectively. $\dot{x}(t)$ denotes the time derivative of x(t). Also, $u_c(t)$ and v_c are sets of time-varying control variables and time invariant parameters. The time horizon of interest $[t_o; t_f]$ is partitioned into NS stages.

In the above equations the ordinary differential equations (ODE) represents the balance equations, the implicit algebraic equations resulting from thermodynamic properties, phase equilibrium calculations and other explicit algebraic equations relating to the systems behaviour. Accordingly, **Y** is the vector of differential variables and **X** the vector of implicit algebraic variables.

The features of gPROMS such as switching between ODE and DAE simulation mode, using stiff or non-stiff integration methods and employing dense, sparse or partitioned solution techniques have been described and illustrated (Pantelides & Barton 1993; Vassiliadis *et al.* 1994a 1994b). The features of DYNSIM are reported by Gani *et al.* (1990a and b), Sorensen (1991) and Sorensen *et al.* (1991).

Problem specific simulation strategies have been developed (Gani *et al.* 1990) and a robust procedure for consistent initialisation of the differential-algebraic equations has been proposed. Sorensen *et al.* (1991) developed an efficient coupling to a large range of thermodynamic models and an algorithm has been suggested to determine an optimal calculation sequence and analyse the process flowsheet with respect to feasibility of partitioning.

The DYNSIM simulation package consists of a main program called DYNSIM, an input file generator called DYNDAT and a program, DYNSET for setting the memory requirements of the simulator. The structure of the simulator is discussed in the user manual (Sorensen 1991).

The gPROMS package consists of a main program called gPROMS, which receives an input file written in FORTRAN and then produces an output file with the dynamic simulation results. Other features of the gPROMS package include gEST, a parameter estimation program and gOPT the dynamic optimisation package.

3.3.2 Solution of dynamic optimisation problems

In gOPT some of the design variables on the dynamic simulation model are considered as control variables and are determined by applying an optimal control algorithm. DYNSIM uses a similar approach to dynamic optimisation. In the rest of the chapter gOPT would be discussed although it should be kept in mind that essentially the same would apply in DYNSIM.

Here a mathematical statement of the class of dynamic optimisation problems solved by gPROMS is provided.

3.3.2.1 The Process Model

Processes described by mixed differential and algebraic equations of the following form are considered

$$f((x(t), \dot{x}(t), y(t), u_c(t), v_t) = 0 \tag{7-6}$$

Here x(t) and y(t) are the differential and algebraic variables in the model while $\dot{x}(t)$ is the time derivative of the x(t). $u_c(t)$ is the control variable and v_t the time invariant parameters to be determined by the optimisation.

3.3.2.2 The initial conditions

The initial conditions are described in terms of a set of non-linear relations of the form:

$$I(x(0), \dot{x}(0), y(0), u_c(0), v_t) = 0 \tag{7-7}$$

Once the time variation of the control variable $u_c(t)$ and the value of any time invariant parameter, v_t, is fixed, the modelling equations together with the initial conditions completely determine the transient response of the system.

3.3.2.3 The objective function

The general optimal control problem to be solved for a process described by the system equations (Eq. 7-5), is to find values of the control variable $u_c(t)$ such that the performance measure given in equation (7-8) has a maximal value taking into account the constraints.

$$I[u_c(t)] = G[y(t_f)] + \int_0^{t_f} f_0(y, x, u_c)dt \rightarrow \max \tag{7-8}$$

Dynamic optimisation in gPROMS seeks to maximise the performance measure through determining:

- The time horizon t_f
- The values of the time invariant parameters v_t
- The time variation of the control variables $u_c(t)$ over the entire time horizon

3.3.2.4 Constraints

The time horizon is often subject to certain lower and upper bounds:

$$t_f^{min} \leq t_f \leq t_f^{max} \tag{7-9}$$

In some applications it is necessary to impose certain conditions that the system must satisfy at the end of the operation. There are called end-point constraints:

$$w^{min} \leq w(t_f) \leq w^{max} \tag{7-10}$$

GPROMS also allows for some constraints that must hold at one or more distinct times during the time horizon. These are referred to as interior-point constraints:

$$w_I^{min} \leq w(t_I) \leq w_I^{max} \tag{7-11}$$

Path constraints must be satisfied at all times during the system operation.

3.3.2.5 Solving the dynamic optimisation problem

The solution of the optimisation problem comprises three key elements:

- The value of the time horizon
- The values of the time invariant parameters
- The variation of the control variable u(t) over the time horizon

Various types of control variables can be defined. These include:

- Piecewise constant controls
  These remain constant at a certain value over a certain part of the time horizon before jumping discretely to a different value over the next interval.
- Piecewise linear controls
  These take a certain linear time variation over a certain part of the time horizon before jumping discretely to a different linear variation over the next interval
- Piecewise linear continuous controls
  These are similar to the piecewise linear controls described above, with the additional requirement that their values be continuous at the interval boundaries
- Controls that vary smoothly over time
  These can be polynomials of any given degree.

It is important to realise that the choice of the form of control is an engineering rather than a mathematical issue. It depends on the capabilities of the actual control system.
gPROMS supports direct specification of piecewise constant and piecewise linear controls, but can support other function input types via a simple construct, described by Vassiliadis et al. (1994).

3.3.2.6 Algorithm for optimal control computation

A number of approaches have been developed to solve dynamic optimisation problems for processes described by a set of differential-algebraic equations. One such approach involves the use of dynamic programming techniques (Bellman 1957; Jacobson and Mayne 1970; Luus 1990a,b 1993; Luus and Rosen 1991). A second class is based on the solution of the necessary optimality conditions expressed as a two point boundary value problem. These approaches include the quasilinearisation approach proposed by Miele et al. (1970 1974 and Miele 1975) and the use of multiple shooting algorithms (Bulirsch 1971) as well as other shooting algorithms such as that proposed by Dixon and Bartholomew-Biggs (1981).

A different approach is based on converting the dynamic optimisation problem to a finite dimensional nonlinear program (NLP) through discretization of all variables. Initial work was based on finite difference approximations to the system constraints (Canon et al. 1970), but later global orthogonal collocation (Tsang et al. 1975; Biegler 1984), global approximation using Chebyshev series expansions (Vlassenbroeck and van Dooren 1988) and orthogonal collocation on finite elements (Renfro 1986; Renfro et al. 1987; Cuthrell and Biegler 1987) were also used. The use of approximations over finite elements, the size and the number of which can be determined automatically, allows some control over the error of discretization (Logsdon & Biegler 1989; Vasantharanjan & Biegler 1990).

In the complete discretization approach, optimisation is carried out in the full space of the discretized variables and the discretized constraints are only satisfied at the solution of the optimisation problem. This is often called an infeasible path approach.

An alternative approach is to carry out the optimisation in the space of the decision variables ($u_c(t)$) only. For a given $u_c(t)$, it is then possible to integrate the underlying DAE system using standard integration algorithms to evaluate the objective function and other constraints that have to be satisfied by the solution. This control vector parameterisation corresponds to a "feasible path" approach since the DAEs are satisfied at each step of the optimisation algorithm (Pollard & Sargent 1970; Sullivan 1977; Sargent & Sullivan 1977 1979; Morison 1984; Morison & Sargent 1979; Gritsis 1990).

In the gPROMS package, Vassiliadis et al. (1994) have proposed a method which employs a control parameterization approach coupled with a backward-difference formula method for the integration of the DAEs (Gear 1971). The duration of each stage is divided into a number of control intervals.

A low order polynomial form is assumed for the control variable, $u_c(t)$ over each stage. The same polynomial is employed for each control variable over all stages. The control variables are expressed in terms of a set of Lagrange polynomials. This effectively expresses the control variables in terms of a finite vector of parameters ($u_{c,i,j,k}$) to be determined by the optimisation:

$$u^{(k)}_{c,j}(t) = \sum_{i=1}^{M_j} u^{(k)}_{c,i,j} \Phi_i^{(M_j)}(\tau^{(k)}_n) \qquad j = 1...\text{No of control variables}$$
$$t \in [t_{k-1}, t_k], \qquad k = 1...NS \tag{7-12}$$

where $u^{(k)}_{c,j}$ is control variable j during stage k, M_j is the polynomial order used for control $u_{c,j}$, $\tau^{(k)}_n$ is the normalised time over stage k given by:

$$\tau_n^{(k)} = \frac{t - t_{k-1}}{t_k - t_{k-1}} \qquad k = 1...NS \tag{7-13}$$

The Lagrange polynomials $\Phi^{(M)}$ of order M are defined as:

$$\Phi_i^{(M)}(\tau_n) \equiv 1 \text{ if } M = 1$$
$$\Phi_i^{(M)}(\tau_n) \equiv \prod_{\substack{i'=1 \\ i' \neq i}}^{M} \frac{\tau_n - \tau_{n,i'}}{\tau_{n,i} - \tau_{n,i'}} \text{ if } M \geq 2 \tag{7-14}$$

The choice of the set of normalised time points τ_n used for the construction of the polynomials does not affect the solution obtained. It may be desirable to enforce some degree of continuity in the control variable profiles across stage boundaries. Continuity can be achieved simply by constraints of the form:

$$u_{c,M,j,k-1} = u_{c,j,k} \qquad k = 2...NS \tag{7-15}$$

Higher order continuity can be obtained by linear constraints derived by differentiating the polynomials defined in Equation 7-15 to 7-17 with respect to time for the requisite number of times and enforcing equality of the first and higher order derivatives of $u_c(t)$ at the stage boundaries.

By applying a degree of freedom analysis as described by Vassiliadis *et al.* (1994), any variable values at the start of the first or subsequent stages that must be treated as optimisation decision variables can be identified and new time invariant parameters and initial or junction conditions can be introduced. Similarly, any of the original initial and junction conditions that are redundant in the context of the DAE integration are identified and are treated as point equality constraints to be enforced by the optimisation at the start of individual stages.

The optimisation problem therefore comprises:

- a multistage DAE system with a complete and non-redundant set of initial and junction conditions
- a set of point equality and inequality constraints
- a set of point equality constraints at the start of individual stages, arising in the manner detailed above
- bounds and constraints on the stage durations, constraints on the time-invariant parameters and bounds on the control variable discretization parameters
- continuity relations expressed in terms of the control variable discretization parameters and
- an objective function.

Given the values of the optimisation parameters $[u_{c,i,j,k}, v_c, t_k]$, the initialization problem at time t_0 involves solving simultaneously the DAE equations for k=1 and the initial conditions. Then the first stage DAEs are integrated from t_0 to t_1. The values of the variables at the start of the second stage can be determined by simultaneous solution of the DAE equations for k=1 and the first set of junction conditions. By proceeding in the same manner, the final time is reached, thus obtaining the solution over the entire time domain. From this solution and the values of the optimisation parameters, the constraints and the objective function can be readily evaluated. Overall then the original infinite dimensional optimisation problem

has been converted to a finite dimensional non-linear programming problem (NLP) (Vassiliadis *et al.* 1994).

In addition to values of the objective function and the constraints, most efficient NLP algorithms require their gradients with respect to the optimisation decision variables. The gPROMS package uses the sensitivity equation approach as discussed by Rosen and Luus (1991).

The algorithm presented has been implemented as DAEOPT, a code for the solution of large-scale dynamic optimisation problems. The solution of the DAE system is performed using the DASOLV code (Jarvis & Pantelides 1992) which implements of BDF algorithm for large sparse systems of DAEs and incorporates efficient sensitivity evaluation and discontinuity handling. The optimisation is carried out using the SRQPD code (Chen & Macchietto 1989) which implements a reduced quadratic programming algorithm.

DAEOPT allows control variables of up to fifth polynomial order, with or without continuity at the control interval boundaries. The lengths of the control intervals may be fixed or variable. However, the choice of the number of the control intervals and the order of the polynomial representation of the controls is left to the user. More details on the DAEOPT code are given by Vassiliadis (1993).

3.4 Optimisation of the L-Lysine fermentation processes

In this section the optimisation of the L-lysine fermentation process with biomass recycling using the gPROMS package is described. The optimisation problem is stated with particular emphasis on how the problem is translated in gPROMS. This is followed by various optimisation scenarios and an experimental verification of the predicted optimum. In the last section the combined process model and optimisation approach is used to optimise the performance of industrial scale fermentation processes.

3.4.1 The optimisation problem

The optimisation problem consists of a process model that would simulate the dynamic behaviour of the system, an objective function and constraints on the state and controllable variable ranges.

3.4.1.1 The dynamic simulation model

The lysine fermentation model has been discussed at length in the Chapter 6. In essence the model consists of four component mass balance equations and a volume balance with a set of metabolic interactions and equations relating the

physical properties of the broth. The following state variables are identified from the system model:

- V - the volume of broth in the bioreator (litre)
- X - the biomass concentration in the bioreactor (g/l DCW)
- Thr - the Threonine or auxothrophic amino acid concentration in the bioreactor (g/l)
- Gluc - the glucose concentration in the bioreactor (g/l)
- Lys - the L-Lysine concentration in the bioreactor (g/l)
- $Spec_{Gluc}$ - the specific glucose feed rate which is assumed to be equal to the specific consumption rate q_{Gluc} (g/g/h)
- $Spec_{Thr}$ - the specific auxotropic amino acid feed rate (g/g/h)

The model is summarised in Appendix F.

3.4.1.2 The objective function

Ultimately the objective function of any industrial optimisation process should be based on process economics. The objective function selected for this process is the variable cost of production (VCOP) of L-lysine via a fermentation process with biomass recycling using cross flow filtration. The variable cost is made up from raw material cost and energy cost used to produce 1 kg of L-lysine. It should be noted that although the prices are typical of the South African process industry, they are by no means exact and do not represent the financial condition of any particular industrial plant.

The variables cost is made up of the following components:

1. Raw material costs
   - Glucose
   - Threonine representing the stoichiometric mixture of auxotropic amino acids

   The other raw materials are assumed to have a negligible impact on the variable cost.

2. Energy Cost
   - Electricity usage in the fermentation process

     The electricity usage in the fermentation process is made up from the power input through agitation, the power required for aeration and the power required for cooling of the bioreactor to maintain a constant temperature. The power for aeration and cooling is estimated from air compressor and chiller efficiencies.

$$\begin{aligned} \text{Electricity}_{\text{Ferment}} = {} & \text{Agitation power} \\ & + \text{Air} \times (\text{Air compressor efficiency}) \\ & + \text{Cooling duty} \times (\text{Chiller efficiency}) \end{aligned} \tag{7-16}$$

- Electricity usage in the biomass separation process

$$\text{Electricity}_{Recycle} = \alpha \times (\text{Linear Velocity} \times \text{Pressure Drop} \times \text{Membrane Area} \times D_{mem}) \quad (7\text{-}17)$$

where a is an efficiency factor typical of membrane applications, and D_{mem} is the cross sectional diameter of the membrane.

3. Downstream processing cost
The downstream processing cost includes effluent treatment and lysine recovery through the downstream processing (DSP) unit operations.

The variable cost of production (VCOP) is therefore given by:

$$\begin{aligned}\text{Cost per Batch} = {} & \text{Electricity Cost} \times (t_{f,Ferment} \cdot \text{Electricity}_{Ferment} + t_{f,perm} \cdot \text{Electricity}_{Re\ cycle}) \\ & + \text{Sugar Cost} \times (\text{Total Glucose used per batch}) \\ & + \text{Threonine Cost} \times (\text{Total Threonine used per batch}) \\ & + \text{DSP Cost} \times (\text{Lysine produced per batch})\end{aligned} \quad (7\text{-}18)$$

$$\text{VCOP} = \frac{\text{Cost per Batch}}{\text{Lysine produced per batch}} \quad (7\text{-}19)$$

where $t_{f,Ferment}$ is the total fermentation time (h) and $t_{f,perm}$ is the total run time of the filtration loop. The numerical values used for the parameters are displayed in Table 7-1.

Table 7-1. Economic parameters used in the optimisation process

Description	Unit	Value
Electricity Cost	R/Wh	0.45
Sugar Cost	R/kg	1.80
Threonine Cost	R/kg	294
DSP Cost	R/kg	1.50
Recycle Variables		
a	1/m	1.24×10^4
Air Compressor Efficiency	kW/Nm^3/h	1.8
Chiller Efficiency	kW/kW	0.25

3.4.1.3 Classification of the control variables

The control variables or the variables that can be selected to minimise the VCOP are summarised in Table 7-2.

Table 7-2. Control variables used for the optimisation of the lysine fermentation process with biomass recycling

Description	Symbol	Unit	Minimal Value	Maximur Value
Time Independent Variables				
Initial state variables				
Initial Volume	V_o	[litre]	4	10
Initial Threonine Concentration	Thr_o	[g/l]	0	2.50
Initial Glucose concentration	$Gluc_o$	[g/l]	10	100
Filtration properties				
Membrane Area	A	[m^2]	0	0.028
Time dependent Variables				
Specific feeds				
Specific glucose feed rate, assumed to be equal to the specific consumption rate (q_{Gluc})	$Spec_{Gluc}$	[g/g/h]	0	0.40
Specific threonine feed rate	$Spec_{Thr}$	[g/g/h]	0	0.017
Agitation power input	P_g	[W]	0	100
Membrane operating conditions				
Cross-flow velocity	v	[m/s]	0.5	7.0
Trans membrane pressure drop	ΔP	[kPa]	50	250
Runtime of filtration unit	t_{perm}	[h]	0	180
Duration of the fermentation	$t_{Ferment}$	[h]	0	180

3.4.1.4 Process and control constraints

The process constrains are imposed on the system to ensure that the values of the state variables remain physically realisable. The minimum broth volume in the bioreactor is limited by the upper impeller and the height of the instrumentation (pH, Temperature and DO probes) in the bioreactor. For the Chemap bioreactor used the minimum volume that would ensure that the top impeller and all the probes (pH and DO) are submerged is 4 litres. The maximum working volume of the bioreactor is 10 litres. This sets the limits for the optimisation problem.

The broth rheology is strongly dependent on the biomass concentration. It has been determined experimentally that the broth starts to exhibit non-Newtonian behaviour at biomass concentrations exceeding 30 g/l. Since all the hydrodynamic and mass transfer relationships have been developed for Newtonian fluids, the biomass

concentration is limited to a maximum value of 30 g/l DCW. No lower limit is imposed on the biomass concentration.

There are two limits on the fermentation power required for agitation (P_g). The power required for agitation is determined by the oxygen mass transfer dependency on the power input and the air flow rate. In the fermentation model the oxygen demand is determined through the metabolic governing equations. From a specified power consumption the air flow rate is determined using the mass transfer correlations. The first limitation on the airflow rate is that a minimum air flow rate of 0.2 vvm must be maintained at all times. The second limitation is that a maximum of 30% of the oxygen in the inlet air is to be consumed by the fermentation process to prevent CO_2 toxicity. Both the air flow rate and the agitation require power and impact significantly on the process economics. There will therefore be a trade off between the air and power requirements both in terms of process economics and oxygen requirements.

The maximum initial charge threonine concentration (Thr_o) is limited to 2.5 g/l in accordance with the maximum allowable biomass concentration. With an initial charge of 4 litres, 10 g of L-threonine is added. It is known that the yield of biomass from threonine is 30 g/g (Chapter 5-5). Thus, 300 g of biomass DCW is subsequently produced. At a final volume of 10 litres this equates to 30 g/l the maximum limit on biomass.

The initial charge glucose concentration is limited between 10 and 100 g/l. It was found that the maximum biomass growth rate is reduced due to osmotic loading at initial charge glucose concentrations in excess of 100 g/l. The lower bound of 10 g/l was determined to be the minimum glucose concentration not limiting biomass growth if all other substrates were available in abundance (Weuster-Botz *et al.* 1997).

The specific glucose feed rate ($Spec_{Gluc}$) is assumed to be equal to the specific glucose consumption rate (q_{Gluc}) and is limited to 0.40 g/g/h. As shown in Chapter 6, this corresponds to the maximum glucose uptake rate.

The specific threonine feed rate ($Spec_{Thr}$) is limited by the maximum growth rate and the yield of biomass from threonine. The maximum biomass growth rate is 0.52 h^{-1}. This implies an upper limit of 0.017 g/g/h for the specific threonine feed rate.

The membrane area (A) is limited to 0.028 m^2. This represents the maximum area that is available for the filtration equipment used.

The filtration operating parameters, the trans-membrane pressure drop (ΔP) and the cross-flow velocity (v) are limited by the filtration equipment. The cross-flow filtration pump can deliver a maximum cross-flow velocity of 7 m/s at a head of 2.5 bar. The

corresponding trans-membrane pressure drop that can be attained is 250 kPa. The duration of the filtration process is limited to 180 hours.

3.4.2 Optimisation of the fed-batch biomass recycling fermentation process for L-Lysine production

The initial estimate of the control variables is given in Table 7-3.

Table 7-3. Initial estimate of control variable values

Controllable Variable	Unit	Initial
Base Case		
$Gluc_o$	[g/l]	30
Thr_o	[g/l]	1.7
V_o	[l]	4
q_{Gluc}	[g/g/h]	0.4
$Spec_{Thr}$	[g/g/h]	0
Area	[m^2]	0
ΔP	[kPa]	100
v	[m/s]	2
P_g	[kW]	30
t_{perm}	[h]	20
$t_{,f,recycle}$	[h]	160
t_{dur}	[h]	180
$t_{Ferment}$	[h]	180

where

- t_{dur} is the cleaning frequency. Thus, a value of 180 h for t_{dur} implies that the membrane is cleaned once every 180 hours of operation.
- $t_{,perm}$ refers to the time relative to $t_{ferment}$ when the filtration loop was started
- $t_{,f,Recycle}$ refers tot the total time for which the filtration loop ran per batch
- $t_{f,Ferment}$ refers to the total fermentation time

The predicted variable cost of production under these conditions was R14.50/kg.

The initial optimisation experiment was aimed at optimising the initial charge glucose concentration and the specific glucose feed.

Table 7-4. Optimisation results for Experiment 1.

Controllable Variable	Unit	Initial	Minimum	Maximum	Time Interval	Optimal Value
Experiment 1						
$Gluc_o$	[g/l]	30	10	100		100
q_{Gluc}	[g/g/h]	0.4	0	0.4	115.3	0.27
$t_{f,Ferment}$	[h]					115.3
VCOP	[R/kg]					14.26

- Experiment 1 (Table 7-4)
  In the first case study, the final fermentation time ($t_{,f,Ferment}$), the initial charge glucose concentration ($Gluc_o$) and the specific glucose feed (or consumption) rate ($spec_{Gluc}$) were optimised as time independent parameters. The glucose, threonine and ammonium sulphate feed rate were initiated at the point of glucose depletion. The glucose feed rate was then calculated from the biomass concentration and the desired specified specific feed rate (Equation 6-6). The other parameters were fixed to the values specified in Table 7-3.

  From the results presented in Table 7-4, the initial charge glucose concentration should be a maximum to minimise the VCOP while an intermediate value of 0.27 g/g/h was selected for the specific glucose feed rate. A VCOP of R14.26 / kg was achieved after 115.3 hours of fermentation in the absence of biomass recycling.

  In this optimisation case, the initial charge threonine concentration was fixed. This implies that the total biomass produced during the run was also fixed. Therefore, to maximise the lysine produced while minimising the cost, not only must the biomass residence time be maximised but the cells must also be kept at a metabolic state that maximises yield of lysine on sugar. To maximise the biomass residence time, the total volume of the feed should be minimised. Since all the feeds are initiated on glucose depletion, the duration of the feed and therefore the volume fed can be minimised by increasing the initial charge glucose concentration. Furthermore there is a relationship between the specific glucose feed, the specific productivity and the yield of lysine from sugar (Figure 6-2). As the specific feed rate increases, the specific productivity increases but the yield is reduced. Therefore there is a trade off between good productivity and an optimal yield when the VCOP is concerned (Figure 7-1 and 7-2).

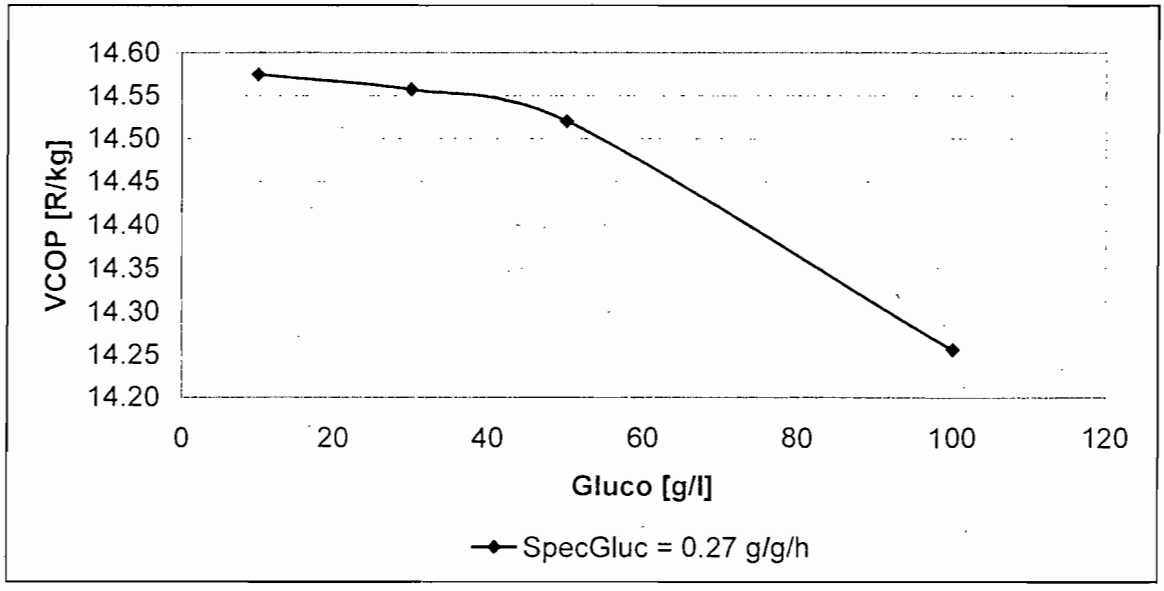

Figure 7-1. Single parameter effect of the initial charge glucose concentration on the VCOP after 120 hours of fermentation time with all the other parameters fixed to the values as specified in Table 7-3.

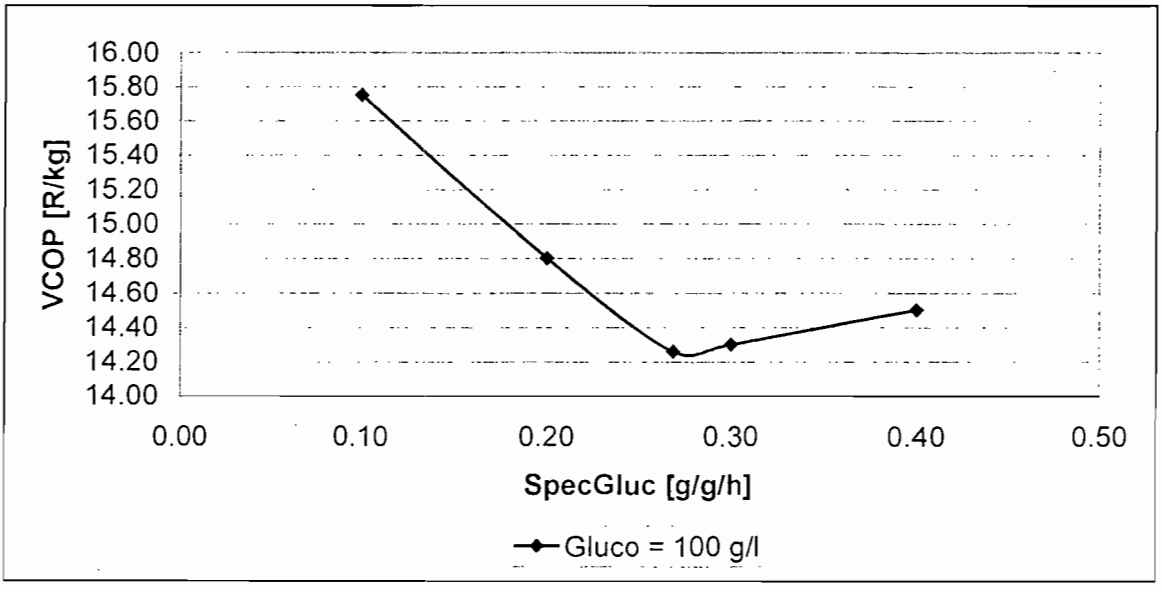

Figure 7-2. The effect of the specific glucose feed rate as a time independent parameter on the VCOP after 120 hours of fermentation time. The other parameters have the values as specified in Table 7-3.

Table 7-5. Optimisation results for Experiment 2

Controllable Variable	Unit	Initial	Minimum	Maximum	Time Interval	Optimal Value
Experiment 2						
$Gluc_o$	[g/l]	30	10	100		100
$Spec_{Gluc}$	[g/g/h]	0.4	0	0.4	12.15	0.02
$Spec_{Gluc}$	[g/g/h]	0.4	0	0.4	29.70	0.19
$Spec_{Gluc}$	[g/g/h]	0.4	0	0.4	19.46	0.26
$Spec_{Gluc}$	[g/g/h]	0.4	0	0.4	18.38	0.31
$Spec_{Gluc}$	[g/g/h]	0.4	0	0.4	40.04	0.40
$t_{f.Ferment}$	[h]					119.73
VCOP	[R/kg]					14.00

- Experiment 2 (Table 7-5)
  In the next case study the specific glucose feed rate was considered as a piece-wise constant controllable variable. The fermentation was divided into five intervals of varying length, each with a separate specific feed rate. The resulting optimal specific feed rate profile is shown in Figure 7-3.

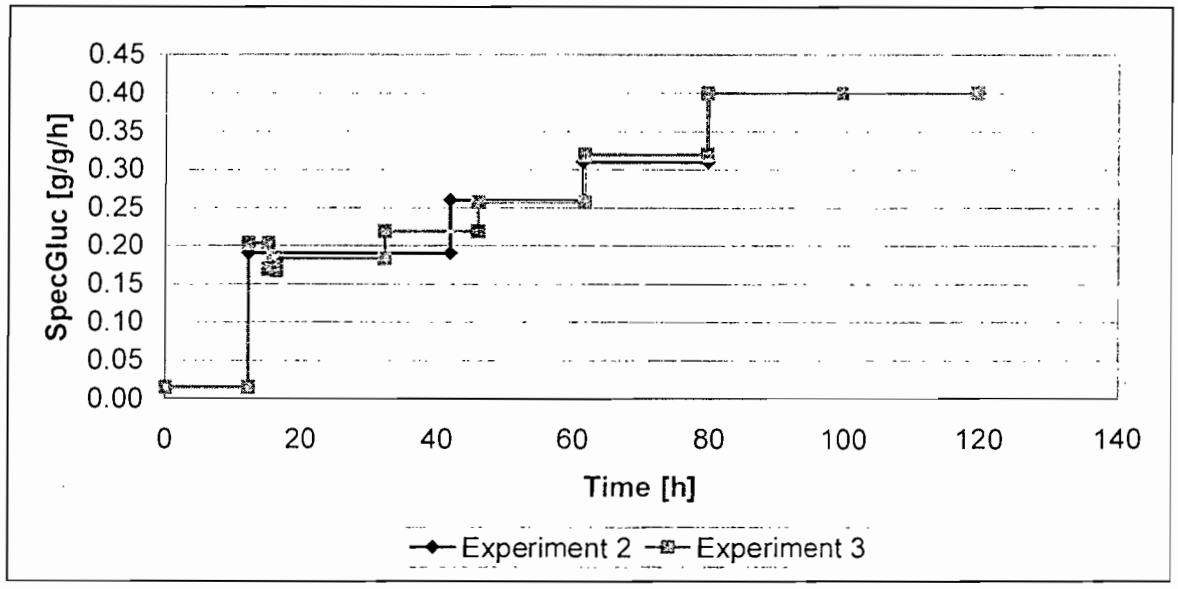

Figure 7-3. Optimal specific glucose feed rate for Experiment 2 and 3.

This approach reduced the optimal VCOP to R14.00/kg and increased the optimal time to 140 hours. The increasing specific feed rate profile attempts to maximise yield and productivity. While the yield increases with decreasing specific feed rate the specific productivity increases (Figure 6-2). As the fermentation proceeds, biomass is lost from the bioreactor. With the reduction in biomass, the specific feed

rate increases to increase the specific productivity in an attempt to maintain the overall productivity.

Table 7-6. Optimisation results for Experiment 3

Controllable Variable	Unit	Initial	Minimum	Maximum	Time Interval	Optimal Value
Experiment 3						
$Gluc_o$	[g/l]	30	10	100		100
$Spec_{Gluc}$	[g/g/h]	0.4	0	0.4	12.22	0.01
$Spec_{Gluc}$	[g/g/h]	0.4	0	0.4	2.86	0.20
$Spec_{Gluc}$	[g/g/h]	0.4	0	0.4	1.24	0.17
$Spec_{Gluc}$	[g/g/h]	0.4	0	0.4	0.00	0.17
$Spec_{Gluc}$	[g/g/h]	0.4	0	0.4	16.00	0.18
$Spec_{Gluc}$	[g/g/h]	0.4	0	0.4	13.59	0.22
$Spec_{Gluc}$	[g/g/h]	0.4	0	0.4	15.76	0.26
$Spec_{Gluc}$	[g/g/h]	0.4	0	0.4	17.92	0.32
$Spec_{Gluc}$	[g/g/h]	0.4	0	0.4	20.02	0.40
$Spec_{Gluc}$	[g/g/h]	0.4	0	0.4	20.02	0.40
$t_{f,Ferment}$	[h]					119.66
VCOP	[R/kg]					14.00

- Experiment 3 (Table 7-6)

In the third experiment the number of intervals was increased to 10. The specific feed rate profile was very similar to that of Experiment 2 (Figure 7-3), and the minimum VCOP was still R14.00 /kg.

Table 7-7. Optimisation results for Experiment 4

Controllable Variable	Unit	Initial	Minimum	Maximum	Time Interval	Optimal Value
Experiment 4						
$Gluc_o$	[g/l]	30	10	100		18.59
Thr_o	[g/l]	1.7	0	2.5		0.29
$Spec_{Gluc}$	[g/g/h]	0.4	0	0.4		0.4
$Spec_{Thr}$	[g/g/h]	0	0	0.017		1.16E-03
$t_{f,Ferment}$	[h]					180
VCOP	[R/kg]					12.15

- Experiment 4 (Table 7-7)

The initial charge threonine concentration and the specific threonine feed rate were included as time independent control variables. The threonine feed was also initiated on depletion of the glucose concentration. The absolute flow rate of this stream would be so small that it would not be possible to add independently. Therefore it was

considered as if the threonine would be mixed with the glucose stream and that the two feeds be added as one, that is initiated on glucose depletion.

The optimal conditions are set out in Table 7-7. The initial charge glucose concentration dropped to 18.59 g/l and the initial charge threonine concentration to 0.29 g/l. This threonine was depleted at the same time as the glucose. The maximum biomass in the fermentation was 8.0 g/l and this was maintained for the bulk of the fermentation time. This is less than the maximum allowable biomass concentration of 30 g/l.

With the initiation of the threonine feed, the fermentation starts to approximate a continuous fermentation mode. The specific threonine feed rate combined with the biomass in the fermentation sets the specific growth rate. From the model equations the specific growth rate combined with the glucose feed rate determines the specific productivity which eventually determines the lysine production rate. In the optimal case the specific growth rate was maintained at 0.0348 1/h. This represented the economic optimum between the specific productivity (0.12 g/g/h) and the yield of 0.30 g/g.

Table 7-8. Optimisation results for Experiment 5

Controllable Variable	Unit	Initial	Minimum	Maximum	Time Interval	Optimal Value
Experiment 5						
$Gluc_o$	[g/l]	30	10	100		18.59
Thr_o	[g/l]	1.7	0	2.5		0.29
$Spec_{Gluc}$	[g/g/h]	0.4	0	0.4		0.4
$Spec_{Thr}$	[g/g/h]	0	0	0.017		1.16E-03
Power	[W]	30	0	100		30
$t_{f,Ferment}$	[h]					180
VCOP	[R/kg]					12.15

- Experiment 5 (Table 7-8)
  The agitation power is included as a time independent variable in this experiment. The agitator power is independent of the other control variables in this experiment. It was found that a fixed agitation power consumption of 30 W minimised the variable cost of production.

Table 7-9. Optimisation results for Experiment 6

Controllable Variable	Unit	Initial	Minimum	Maximum	Time Interval	Optimal Value
Experiment 6						
$Gluc_o$	[g/l]	30	10	100		10
Thr_o	[g/l]	1.7	0	2.5		0.15
$Spec_{Gluc}$	[g/g/h]	0.4	0	0.4	21.1	0.4
$Spec_{Gluc}$	[g/g/h]	0.4	0	0.4	124	0.4
$Spec_{Gluc}$	[g/g/h]	0.4	0	0.4	69.9	0.4
$Spec_{Gluc}$	[g/g/h]	0.4	0	0.4	67.1	0.4
$Spec_{Gluc}$	[g/g/h]	0.4	0	0.4	17.68	0.4
$Spec_{Thr}$	[g/g/h]	0	0	0.017	21.1	2.94E-03
$Spec_{Thr}$	[g/g/h]	0	0	0.017	124	1.20E-03
$Spec_{Thr}$	[g/g/h]	0	0	0.017	69.9	1.21E-03
$Spec_{Thr}$	[g/g/h]	0	0	0.017	67.1	1.07E-03
$Spec_{Thr}$	[g/g/h]	0	0	0.017	17.68	0
$t_{f,Ferment}$	[h]					180
VCOP	[R/kg]					12.94

- Experiment 6 (Table 7-9)
  In this experiment the specific glucose and the specific threonine feed rates were considered to be time dependent control variables. The results obtained were very similar to that obtained for the time independent case. The fermentation approaches continuous operation maintaining the biomass concentration at 8 g/l with a specific growth rate of 0.0348 1/h, similar to the values obtained with time independent variables. The specific glucose feed rate did not vary with time. During the initial stages more threonine was fed (higher specific threonine feed rate) to reach the required biomass concentration in a shorter period of time and during the latter stages the specific threonine feed rate was reduced to limit threonine losses through washout.

Table 7-10. Optimisation results for Experiment 7

Controllable Variable	Unit	Initial	Minimum	Maximum	Time Interval	Optimal Value
Experiment 7						
$Gluc_o$	[g/l]	30	10	100		10.05
Thr_o	[g/l]	1.7	0	2.5		2.00
$Spec_{Gluc}$	[g/g/h]	0.4	0	0.4		0.32
$Spec_{Thr}$	[g/g/h]	0	0	0.017		0.00E+00
Area	[m2]	30	0	100		2.40E-04
$t_{f,Ferment}$	[h]					180
VCOP	[R/kg]					10.60

- Experiment 7 (Table 7-10)
  In this experiment all the control variables were considered to be time independent. The membrane area was included with the initial charge and feed properties. The membrane was operated at a trans-membrane pressure drop of 100 kPa with a cross-flow velocity of 2m/s. The minimum variable cost was reduced from R12.95/kg to R10.60/kg. The bulk of the cost saving is due to the reduction in the threonine usage per unit lysine produced. The biomass is to be produced as fast as possible during the initial stages of the fermentation process. The maximum biomass (30 g/l) is maintained for the duration of the batch. The specific threonine feed rate is zero with a specific glucose feed rate of 0.32 g/g/h. The membrane area is sized so that the permeate flow matches the glucose feed flow. This would imply a zero or a minimal bleed flow rate and would ensure maximum biomass retention.

Table 7-11. Optimisation results for Experiment 8

Controllable Variable	Unit	Initial	Minimum	Maximum	Time Interval	Optimal Value
Experiment 8						
$Gluc_o$	[g/l]	30	10	100		10.05
Thr_o	[g/l]	1.7	0	2.5		2.00
$Spec_{Gluc}$	[g/g/h]	0.4	0	0.4		0.34
$Spec_{Thr}$	[g/g/h]	0	0	0.017		0.00E+00
Area	[m^2]	30	0	100		2.65E-04
ΔP	[Pa]	100	50	250		9.72E+04
v	[m/s]	2	0.5	7		1.00E+00
$t_{,f,Ferment}$	[h]					180
VCOP	[R/kg]					10.65

- Experiment 8 (Table 7-11)
  The membrane operating parameters did not significantly reduce the VCOP. The membrane area increased slightly with the reduction in flux, which was a result of the decrease in cross-flow velocity compared to Experiment 7. The trans-membrane pressure drop did not change significantly from 100 kPa. The permeate flow rate was equal to the sum of the glucose and threonine feed rates respectively and therefore eliminated the loss of biomass from the bioreactor.

Table 7-12. Optimisation results for Experiment 9.

Controllable Variable	Unit	Initial	Minimum	Maximum	Time Interval	Optimal Value
Experiment 9						
$Gluc_o$	[g/l]	30	10	100		10.67
Thr_o	[g/l]	1.7	0	2.5		2.00
$Spec_{Gluc}$	[g/g/h]	0.4	0	0.4		0.32
$Spec_{Thr}$	[g/g/h]	0	0	0.017		0.00E+00
Area	[m^2]	30	0	100		1.53E-04
DP	[Pa]	100	50	250		1.57E+05
v	[m/s]	2	0.5	7		1.00E+00
t_{perm}	[h]	20	0	300		1.60E+01
$t_{dur(1)}$	[h]	20	0	300		2.09E+01
$t_{f,Ferment}$	[h]					180
VCOP	[R/kg]					10.65

- Experiment 9
  In the last experiment the start and stop times of the membrane system were included as variables in the optimisation process. This implied that it would be possible to stop the filtration system during the run, and clean the membrane. The cleaning time was fixed by the actual duration of the cleaning process and the sterilisation procedure required. The motivation of the start-stop operated system is to attain a higher average flux by stopping the membrane system to allow for frequent cleaning.

  In the optimal case, the filtration system was started after the start of the sugar feed (20.9 hours after inoculation). The start time of the filtration system is influenced by various factors. Delaying the start of filtration would imply that the starting flux is lower due to the increased biomass concentration while starting too early had a negative impact on the cellular metabolism and may also lead to a violation of the minimum volume constrains. In the optimal solution, the membrane unit is cleaned after 20.9 hours of usage and then only at the end of the run.

  Experiment 9 represents the global optimum for the entire system, when all the control variables are taken into account. The VCOP of R10.65/kg represents the minimal variable cost that can be achieved with the biomass recycling system. This represents a 12% improvement on the R12.15/kg that can be attained with semi-continuous technology and a 24% improvement on conventional fed-batch technology. This optimisation can however only be realised in practise if it can be proven that the parameters that influence the cost structure as predicted by the model can be attained. In the next section it will be validated that the suggested optimum performance can be attained on laboratory scale.

4 Evaluating the predicted optimum on laboratory scale

Laboratory scale fermentations were run with the optimal set of parameters as found in Experiment 9. The specific glucose feed rate of 0.32 g/g/h was maintained by analysis of the biomass concentration on an hourly basis followed by adjustment of the feed rate. The predicted and the measured fermentation performance are presented in Figure 7-4 to 7-7 below.

The predicted and measured yield of lysine from glucose as well as the lysine productivity is presented in Figure 7-4.

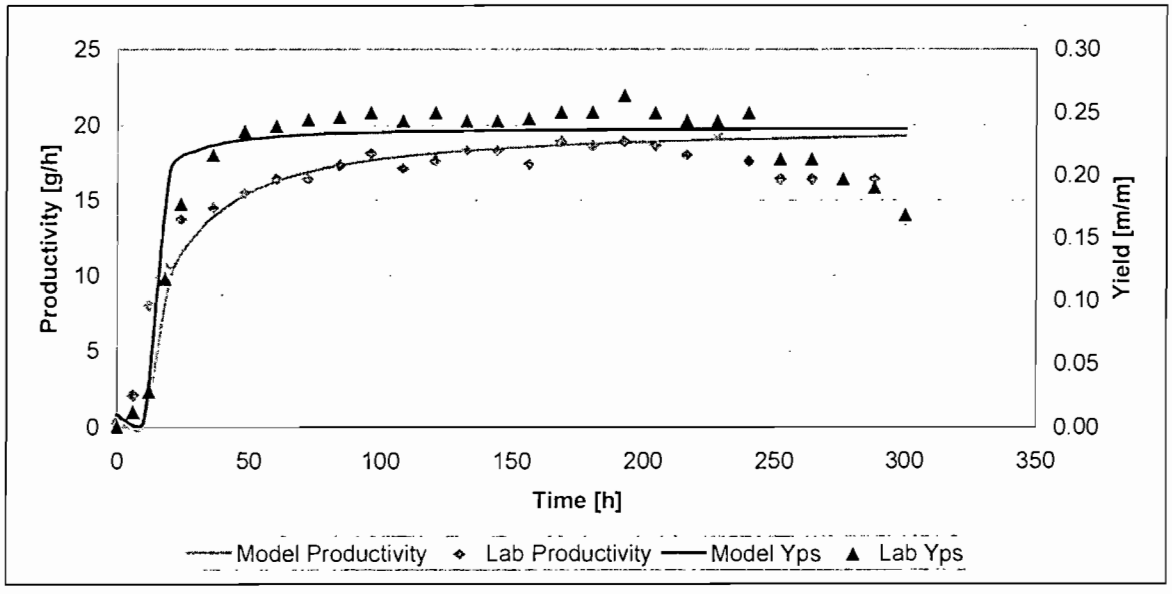

Figure 7-4. The predicted and the measured yield of Lysine from glucose and the lysine productivity in a 10 litre working volume bioreactor.

The biomass and Lysine concentration profiles are presented in Figure 7-5. The residual glucose and threonine concentration profiles are presented in Figure 7-6. It is evident that, especially during the early stages of the fermentation, the model adequately describes the fermentation performance. During the latter stages of the process, the model's ability to predict the fermentation performance is reduced. This is attributed to reversion of the strain to the wild type and cell death which are not accounted for in the model.

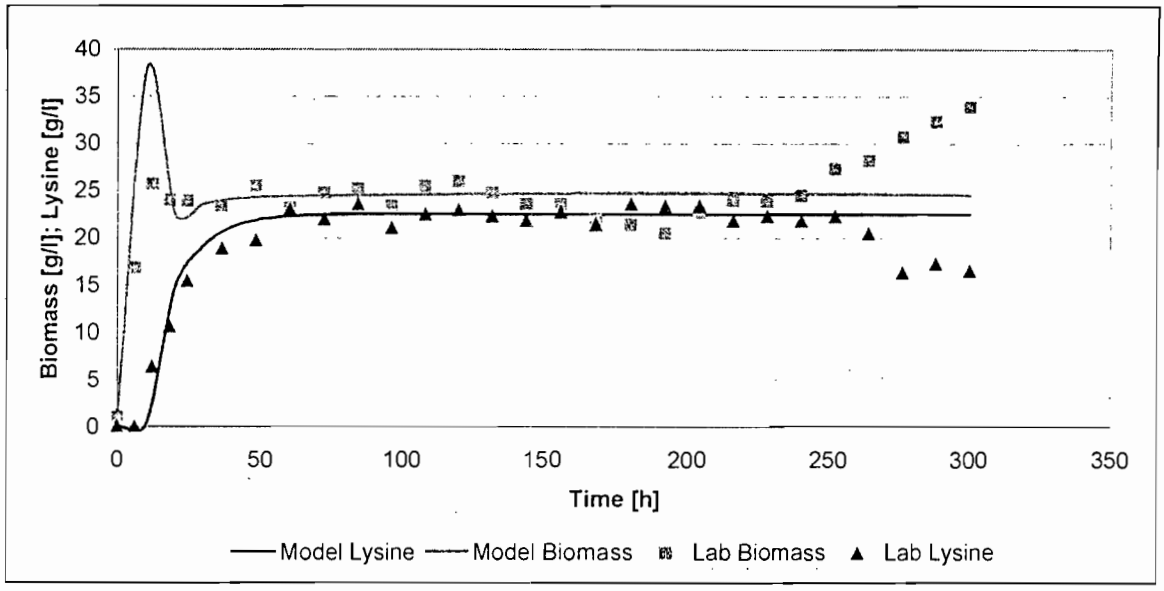

Figure 7-5. The predicted and the measured Lysine and Biomass concentration profiles

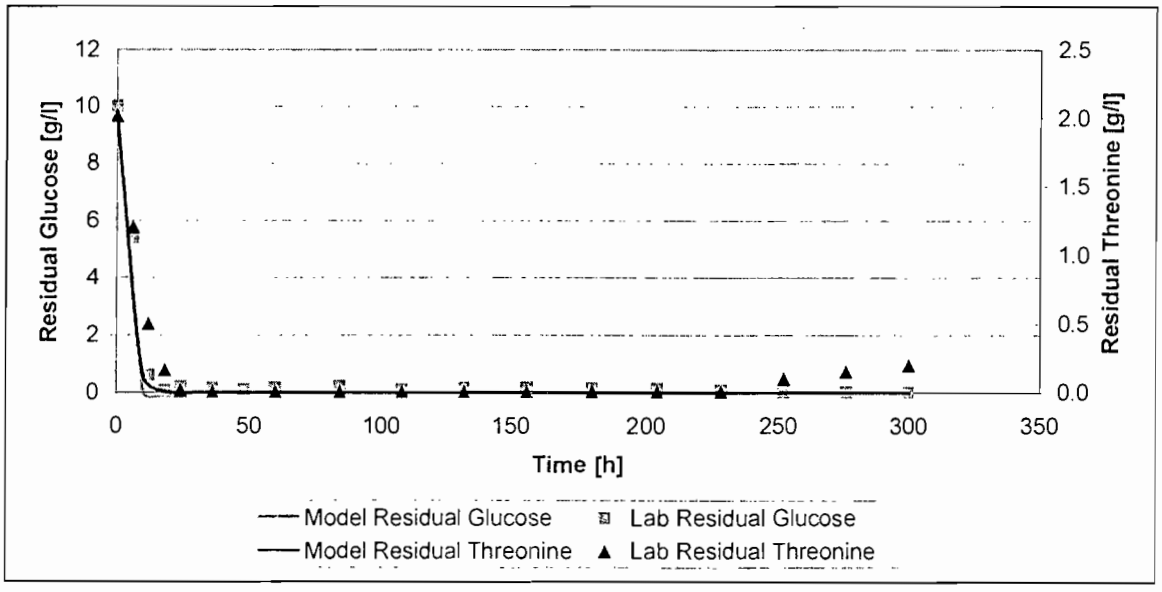

Figure 7-6. Residual glucose and threonine concentration profiles for the laboratory fermentation run at optimal conditions.

The predicted optimum can be achieved on laboratory scale. Furthermore, the presented data once again illustrates the ability of the models to predict the fermentation performance accurately.

The fermentation is driven towards a zero residual sugar concentration by feeding just below the maximum consumption rate. The biomass is retained by increasing the cross-flow filtration area and subsequently the permeate flow rate. To retain all the biomass

implies that the permeate flow rate should equal the total flow rate of feeds into the fermenter.

The glucose feed flow rate and the permeate flow rate, as prescribed by the model and executed during the experimental evaluation are depicted in Figure 7-7. The offset between the permeate flow rate and the glucose flow rate is due to the ammonium sulphate and the ammonium hydroxide solutions fed. The reactor volume of the run was maintained at the maximum operating volume of 10 litres after 50 hours.

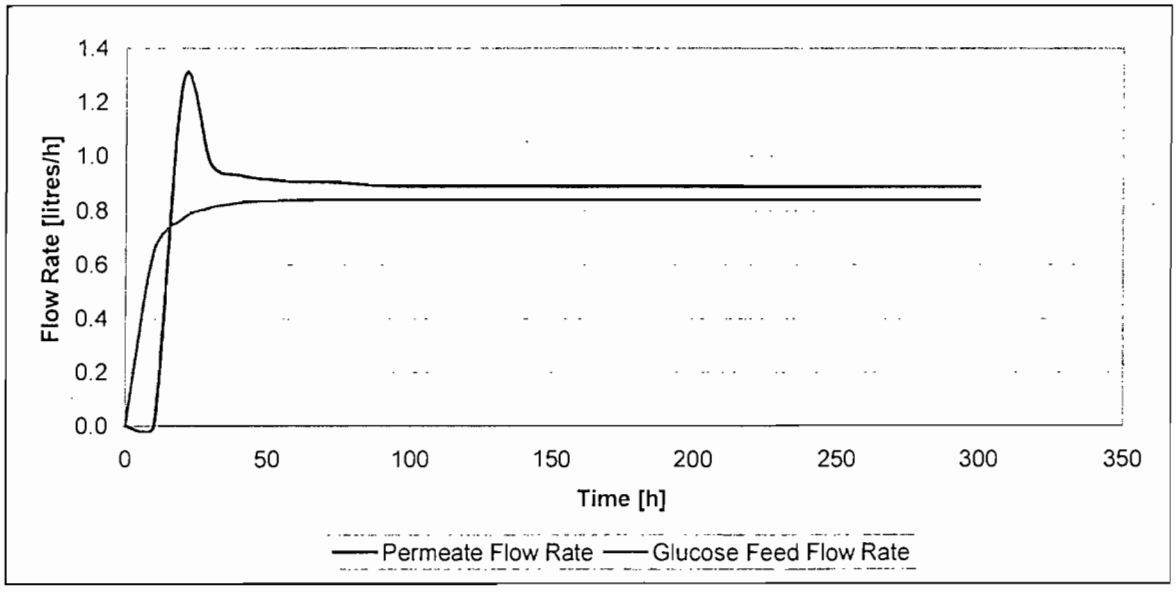

Figure 7-7. Glucose feed rate and permeate flow rate as a function of time

The philosophy used to minimise the VCOP of the Lysine fermentation is to retain all the biomass produced in the bioreactor, while feeding at a rate close to the maximum glucose uptake rate. The sugar feed rate represents a trade-off between increased yield (Y_{ps}) at lower feed rates and increased productivity at higher feed rates. This optimum is influenced by the sugar price, which determines the gearing ratio between yield (Y_{ps}) and productivity. The specific feed rate of 0.32 g/g/h represents an optimal between yield and productivity for the sugar price specified. Furthermore it is evident that the fermentation is conducted at residual sugar concentration approximating zero. Since spent medium is continuously withdrawn from the bioreactor, a zero residual sugar concentration maximises the yield of lysine from the sugar provided.

5 Application of biomass recycling on industrial scale

The concept of biomass recycling to increase the residence time of the biomass in a feed and bleed operated L-Lysine fermentation was evaluated using an industrial mutant of *Corynebacterium glutamicum* (AEC94) at industrial scale.

The values of the empirical parameters in the fermentation model were obtained from continuous Chemostat experiments conducted at 10 litre scale. These experiments were similar to those used to derive the filtration model for ATCC 21253. The results from these experiments are confidential and are therefore not presented.

The fermentation model and the gPROMS optimisation package was then used to optimise the fermentation performance of two types of fermentation. In the first approach, a feed rate and bleed fed-batch strategy was adopted. In this approach the specific feed as predicted in the optimisation process was maintained. The feed was started on depletion of the initial charge of glucose and maintained at the specific level using hourly biomass analysis. When the working volume of the bioreactor was reached the bleed was initiated to match the total volumetric feed rate. This led to a reduction in biomass, and subsequently a reduced feed rate (to maintain a fixed specific feed) and a reduced productivity.

The second approach involved biomass recycling through cross flow filtration. The specific sugar feed rate predicted by the optimisation approach was maintained. The membrane area was selected to prevent loss of biomass. Thus the permeate flow rate matched the total volumetric flow rate of the different feed streams.

The performance of the fed-batch with biomass recycling is presented relative to the fed-batch operated using a feed and bleed approach. For example, if the specific lysine productivity were compared, it would be calculated by:

$$\overline{q_{Lys}} = \frac{q_{\text{Lys, Recycle}}}{q_{\text{Lys,Feed and bleed}}} \tag{7-20}$$

where $\overline{q_{Lys}}$ is the relative specific lysine productivity of the biomass recycling fed-batch to the feed and bleed fed batch operated bioreactors.

The optimal fermentation time was the time predicted by the fermentation model that would minimise the VCOP. For the fed-batch operated bioreactor using a feed and bleed strategy this time was dependent on the biomass concentration and the duration of the fermentation was limited by washout of the biomass. For the fed-batch bioreactor with biomass recycling the fermentation time was limited by reversion of the strain to the wild type. In the actual experiments conducted the fermentations were extended beyond the predicted optimal fermentation times. The VCOP was then calculated at each time point an the minimum VCOP dictated the optimal fermentation time.

The total biomass produced as presented in Table 7-13 represents the total biomass that was produced during the run. The yield of lysine on sugar (Y_{ps}) represents the cumulative yield of lysine from glucose achieved during the entire run. The productivity represents the total lysine production rate and can be viewed as the product of the total biomass in the bioreactor and the specific lysine productivity. The experimental results as well as the

performance as predicted by the fermentation system model is presented in Table 7-13 below

Table 7-13. Experimental results obtained with Industrial organism. The results for the fed-batch process with biomass recycling are presented as a percentage of fed-batch process operated using a feed and bleed approach after 168 hours.

	Model prediction	Experimental results
e_{ave} (m^2/s^3)	25	
Optimal Fermentation time		
Feed and Bleed	138	145
Biomass recycling	180	174
Total biomass produced	101%	108%
Y_{ps}	90%	95%
Specific lysine productivity	98%	100%
Total productivity	118%	122%
VCOP	88%	86%

The optimal fermentation time predicted by the model for the feed and bleed strategy was lower than that found experimentally. This extension could mainly be attributed to the underprediction of the total biomass produced. Since more biomass was produced than anticipated by the fermentation model, the productivity could be sustained for a slightly longer period increasing the optimal fermentation time.

The total amount of biomass produced for the fermentation with biomass recycling exceeded that produced using the feed and bleed approach. This corresponds to the findings of Chapter 5 for the ATCC 21253 strain. The reduced biomass concentration predicted by the model was a result of the lower effective yield of biomass from threonine that was estimated by the model.

The reduction in yield predicted by the model was observed for the biomass recycling case. The prediction of the magnitude of the decrease in yield depends on the impact of hydrodynamic stress on fermentation performance. A similar approach to that discussed in Chapter 6. Section 3-10 was used. Thus the magnitude of the change in the metabolic variable was assumed to depend linearly on the quotient of the average effective energy dissipation rate (e_{ave}) and the biomass concentration. This approach also predicted a reduction in specific lysine productivity, which was not observed experimentally. This resulted in an under prediction of the total productivity and the cumulative yield of lysine on sugar.

Thus, the linear approximation of the impact of hydrodynamic shear on the cellular metabolism reduced the accuracy of the model when applied to the industrial strain. The model is however still sufficiently accurate to show that biomass recycling reduces the

VCOP of the fermentation process. The model predicted a 12% improvement in VCOP while a 14% improvement was realised.

6 Conclusions

In this chapter, the fed batch fermentation with biomass recycling using cross flow filtration for the production of L-Lysine was optimised using an equation-based dynamic simulation package (gPROMS). The fermentation process model developed in Chapter 6 was used for the optimisation of the fermentation process according to the defined economic parameters. The variable cost of production (VCOP) defined as the cost to produce a kilogram of lysine was used as the objective function for the optimisation process. The predicted optimum represented a 26% reduction in variable cost compared to the conventional fed-batch fermentation technology (R10.65/kg vs R14.50/kg).

Achievement of the predicted optimum experimentally was validated. The experimental at the optimal conditions corresponded with that predicted by the proposed model (Figure 7-4 to 7-9). This indicated that the fermentation model as proposed was sufficiently accurate, with enough resolution for optimisation of the fermentation process.

The philosophy to minimise the VCOP of the lysine fermentation is to retain all the biomass produced in the bioreactor, while supplying glucose at a rate close to the maximum glucose uptake rate. The specific sugar feed rate represents a trade-off between increased yield at lower feed rates and increased productivity at higher feed rates. None of the auxotrophic amino acids are included in the feed. Thus, during the lysine production phase, the total biomass in the bioreactor remains virtually constant. This also reduced the rate of reversion of the strain to the wild type.

Furthermore, the fermentation is to be conducted at a residual sugars concentration approaching zero. Since spent medium is continuously withdrawn from the bioreactor, a zero residual sugar concentration maximises the yield of lysine from the sugar fed. The duration of the fermentation process is limited by the strain's ability to sustain its performance and not by the residence time of the biomass in the bioreactor.

The model parameters were re-established for the industrial lysine-producing strain. This model was then used to optimise the fermentation performance of a conventional fed-batch process with a feed and bleed strategy as well as that of a fed-batch process with biomass recycling using cross flow filtration. The model predicted a 12% improvement in VCOP while a 14% improvement was realised.

The linear approximation used to model the impact of filtration on fermentation performance is limited to application of hydrodynamic shear experienced in cross flow filtration systems and cannot be transferred to other hydrodynamic stress impacts. The model parameters are empirical in nature and must therefore be redeveloped for each

strain. Although this is a tedious process, the methodology allows for process optimisation that produces a physically realisable optimum.

A rigorous optimisation approach allowed improvement in the variable cost of production by some 26% over the conventional fed-batch technology. Biomass recycling using cross flow filtration improves the variable cost of production of the lysine fermentation process by at least 12% compared to the current feed and bleed technology.

7 References

Banga, J. R., and Seider, W. D. (1995), global optimisation of chemical processes using stochastic algorithms, In C. A. Floudas & P. M. Poralos, Nonconvex optimisation and its applications, Dortrecht, Kluwer

Bellman, R. (1957), *Dynamic Programming,* Princeton University Press: Princeton, NJ

Biegler, L. T. (1984), Solution of dynamic optimisation problems by successive quadratic programming and orthogonal collocation, *Comput. Chem. Eng.,* **8,** 243-248

Brenan, K. E., Campbell, S. L. and Petzold, L. R. (1989), *Numerical Solution of Initial Value Problems in Differential-Algebraic Equations,* North-Holland, Elsevier Scientific Publishing Co. NY

Büchs, J. (1991), Kopplung van reactions- und kostenmodell: Der weg zur effizienten prozessoptimierung, *Chem. Ing. Tech.,* **63**(2), 89-98

Burlirsch, R. (1971), *Die Mehrzielmethode zur numerischen Losung von nichtlinearen Randwertproblemen un Aufgaben der optimalen Steuerung,* Deutche Forschungs und Versuchsanhalt fur Luft und Raumfahrt, Oberpfaffenhofen, Federal Republic of Germanay, Carl-Cranz Gesellschaft

Canon, M. D., Cullum, C. D. and Polak, E. (1970), *Theory of Optimal Control and Mathematical Programming,* McGraw-Hill, NY

Chen, C. L. and Macchietto, S. (1989), *Successive Reduced Quadratic Programming Code – User;s guide,* Technical Report, Centr for Process Systems Engineering, Imperial College, London

Cuthrell, J. E. and Biegler, L. T. (1987), On the optimisation of differential algebraic process systems, *AIChE J.,* **33,** 1257-1270

Dixon, L. C. W. and Bartholomew-Biggs, M. C. (1981), Adjoint-control transformations for solving practical optimal control problems, *Optim. Control Appl. Methods,* **2,** 365-381

Gani, R., Sorensen, G. and Perregaard, J. (1990a), *AIChE Annual Meeting,* Chicargo, November 1990

Gani, R., Perregaard, J. and Johansen, H. (1990b), *Trans. I. ChemE.,* **60,** A, 407-417

Gear, C. W. (1971), Simultaneous numerical solution of differential algebraic equations. *IEEE Trans. Circuit Theory,* **CT-18,** 89-95

Gritsis, D. M. (1990), The dynamic simulation and optimal control of systems described by index two differential algebraic equations, Ph.D Thesis, University of London

Guthke, R. and Knorre, W. A. (1981), Optimal substrate profiles for antibiotic fermentations, *Biotechnology and Bioengineering,* **23,** 2771-2777

Jacobson D. H. and Mayne, D. W. (1970), *Differential Dynamic Programming,* Americal Elsevier, NY

Jarvis, R. B. and Pantelides, C. C., (1992), *DASOLV – a Differential Algebraic Equation Solver,* Technical Report, Centre for Process Systems Engineering, Imperial College, London 1992

Kelle, R., Laufer, B., Brunzema, C., Weuster-Botz, D., Krämer, R. and Wandrey, C. (1996), Reaction engineering analysis of L-lysine transport by *Corynebacterium glutamicum. Biotechnology and Bioengineering.* **51,** 40-50

Kiss, R. D. and Stephanopoulos, G. (1991), Metabolic activity control of the L-lysine fermentation by restrained growth fed batch strategies, *Biotechnol. Prog.,* **7,** 501-509

Logsdon, J. S. and Biegler, L. T. (1989), Accurate solution of differential algebraic optimisation problems, *Ind. Eng. Chem. Res.,* **28,** 1628-1639

Luus, R. and Rosen, O. (1991), Application of dynamic programming to final state constrained optimal control problems, *Ind. Eng. Chem. Res.,* **30,** 1525-1530

Luus, R. (1990a), Optimal control by dynamic programming using systematic reduction in grid size, *Int. J. Control,* **51,** 995-1018

Luus, R. (1990b), Application of dynamic programming to high dimensional non-linear optimal control problems, *Int. J. Control,* **52,** 239-250

Luus, R. (1993), Piecewise linear continuous optimal control by iterative dynamic programming, *Ind. Eng. Chem. Res.,* **32,** 859-865

Miele, A., Pritchard, R. E. and Damoulakis, J. N. (1970), sequential gradient restoration algorithm for optimal control problems, *JOTA*, **5,** 235-282

Miele, A., Damoulakis, J. N. Cloutier, J. R. and Tietze, J. L. (1974), Sequential gradient restoration algorithm for optimal control problems with nondifferential constraints, *JOTA,* **13,** 218-225

Miele, A. (1975), Recent advances in gradient algorithms for optimal control problems, *JOTA,* **17,** 361-430

Modak, J. M., Lim, H. C. and Tayeb, Y. J. (1986), General characteristics of optimal feed rate profiles for various fed-batch fermentation processes. *Biotechnology and Bioengineering.* **28,** 1396-1407

Morison, K. R. (1984), Optimal control of processes described by systems of differential algebraic equations, PhD Thesis, University of London

Morison, K. R. and Sargent, R. W. H. (1979), Optimisation of multistage processes described by differential algebraic equations, *Lect. Notes Math.,* **1230,** 86-102

Ohno, H. and Nakanishi, E. (1976), Optimal control of a semibatch fermentation. *Biotechnology and Bioengineering.* **18,** 847-864

Ohno, H., Nakamishi, E., Takamatzu, T. (1976), Optimal control of a semibatch fermentation, *Biotechnology and Bioengineering,* **11,** 141

Ohno, H. Nakamishi, E., Takamatzu, T. (1978), Optimum operating mode for a class of fermentations, *Biotechnology and Bioengineering, **20,** 625*

Pantelides, C. C. and Barton, P. I. (1993), Equation orientated dynamic simulation: Current status and future perspectives, *Comput. Chem. Eng.,* **17**S, S268-S285

Pollard, G. P and Sargent, R. W. H. (1970), Off line computation of optimum control for a plate distillation column, *Automatica,* **6,** 59-76

Renfro, J. G., Morshedi, A. M. and Asbjornsen, O. A. *(*1987), Simultaneous optimisation and solutioon of systems described by differential algebraic equations, *Comput. Chem. Eng.,* **11,** 503-517

Renfro, J. G. (1986), Computational studies in the optimisation of systems described by differential algebraic equations, PhD Thesis, University of Houston

Rosen, O. and Luus, R. (1991), Evaluation of gradients for piecewise constant optimal control, *Comput. Chem. Eng.,* **15,** 273-281

Sage, A. P. and White C. C. (1977), Optimal systems control, 2nd Ed. Pretence Hall, Englewood Cliffs, NY

San, K. Y. and Stephanopoulos, G. (1984), Studies on On-Line Bioreactor Identification. II. Numerical and Experimental Results. *Biotechnology and Bioengineering:* 26, 1189 - 1197.

San, K. Y. and Stephanopoulos, G. (1989), Optimisation of fed-batch penicillin fermentation: A case of singular control with state constraints, *Biotechnology and Bioengineering,* **34,** 72-78

Sargent, R. W. H. and Sullivan, G. R. (1977), The development of an efficient optimal control package, *Proc. IFIP Conf. Optim, Tech.* **8th**, Part 2

Sargent, R. W. H. and Sullivan, G. R. (1979), Development of feed change-over policies for refinery distillation units, *Ind. Eng. Chem. Process Des.*, **18,** 113-124

Hadj Sassi, A., Coello, N., Deschamps, A. M. and Lebeault, J. M. (1990), Effect of medium composition of lysine production by a variant strain of *Corynebacterium glutamicum* ATCC 21513, *Biotechnology Letters,* **12**(4), 295-298

Shioya, S. Yang, Y. K., Omasa, T. and Suga, K. (1992), Maximising lysine production in a fed-batch culture by controlling the specific growth rate under leucine limited condition, 669-672

Sorensen, E. (1991), Dynamic process simulation using accurate thremodynamic modelling, PhD. Thesis, University of Denmark

Sorensen, E., Johansen, H. and Gani, R. (1991), MAN 9101, Manual for DYNSIM version 1.1

Stutts, B. E. (1983), An improved algorithm for singular control problems, Application to the optimisation of semi-batch reactors, PhD Thesis, Purdue University, Indiana, USA

Sullivan, G. R. (1977), Development of feed change-over policies for refinery distillation units, PhD Thesis, University of London

Tsang, T. H., Himmelblau, D. M. and Edgar, T. F. (1975), Optimal control via collocation and nonlinear programming, *Int. J. Control,* **21,** 763-768

Udeh, K; Achremowicz, B. (1993), Optimization of cultivation medium composition of an L-lysine producing mutant: The use of response surface methodology, *Acta Microbiologica Polonica*, **42**(2), 171-180.

Vasantharanjan, S. and Biegler, L. T. (1990), Simultaneous strategies for the optimisation of differential algebraic systems with enforcement of error criteria, *Comput. Chem. Eng.*, **14,** 1083-1100

Vassiliadis, V. S. (1993), DAEOPT – A differential algebraic dynamic optimisation code vs. 2.0, *Technical Report,* Centre for Process Systems Engineering, Imperial College, London

Vassiliadis, V. S., Sargent, R. W. H. and Pantelides, C. C. (1994), Solution of a class of multistage dynamic optimisation problems. 2. Problems with path constraints, *Ind. Eng. Chem. Res.*, **33,** 2123-2133

Vassiliadis, V. S., Sargent, R. W. H. and Pantelides, C. C. (1994), Solution of a class of multistage dynamic optimisation problems. 1. Problems without path constraints, *Ind. Eng. Chem. Res.*, **33,** 2111-2122

Vassiliadis, V. (1991), A differential algebraic optimal control problem solver, Centre for Process Systems, Engineering, Imperial College, London

Vlassenbroeck, J. and van Dooren, R. A. (1988), Chebyshev Techniques for solving nonlinear optimal control problems, *IEEE Trans. Autom. Control,* **33,** 333-340

Wang, F. S. and Cheng, W. M. (1999), Simultaneous optimisation of feeding rate and operation parameters for fed-batch fermentation processes, *Biotechnology Progress,* **15**(5), 949-952

Weigand, W. A., Lim, H. C., Creagan, C. C. and Mohler, R. D. (1979), Optimisation of a repeated fed-batch reactor for maximising cell productivity, *Biotechnol. Bioeng. Symp.*, **9,** 335-348

Weuster-Botz, D., Kelle, R., Frantzen, M. and Wandrey, C. (1997), Substrate controlled fed-batch production of L-lysine with *Corynebacterium glutcamicum, Biotechnol. Prog.* **13,** 387-393

Yamane, T., T. Kume, E. Sada and T. Takamatsu (1977), A simple optimization technique for fed-batch culture, *J. Ferment. Technol.*, **55**, 587-593

Fermentation Methodology

1 Micro-organisms used

The organism, *Corynebacterium glutamicum,* ATCC 21253, obtained from the American Type Culture Collection (ATCC, Rockville MD) was used in all the experiments described in this thesis. *C. glutamicum* (ATCC 21253) requires biotin, L-Homoserine (L-Threonine plus L-Methionine) and L-Leucine for growth and produces L-lysine under L-Threonine limitation due to the bypass of aspartate kinase inhibition by L-Threonine plus L-Lysine. The gram-positive bacteria are ellipsoidal in shape with dimensions of 0.7μm by 1.4μm. They may occur singly, in pairs or in irregular aggregates.

Limited experimental work was also performed using *Corynebacterium glutamicum*, (AEC 94). This organism was obtained from AECI Bioproducts (Pty) Ltd and is used in their industrial process and therefore no metabolic information could be disclosed.

2 Medium Composition

2.1 Defined Medium composition

The medium composition, the storage of stock cultures and the inoculation procedure used is described by Kiss & Stephanopoulos (1991).

Complex medium used for initial seed cultures was modified Luria-Bertani broth: 5 g yeast extract, 10 g NaCl, and 5 g glucose per litre of distilled water. Defined, L-Threonine growth-limiting media was used for inoculum as well as for fermentation medium. It consisted of (per litre of distilled water):

- 20 g glucose
- 0.4 g $MgSO_4 \bullet 7H_2O$
- 75 mg $Na_2EDTA \bullet 2H_2O$
- 25 mg $FeSO_4 \bullet 7H_2O$
- 0.1 g NaCl
- 50 mg $CaCl_2 \bullet 2H_2O$
- 7 g $(NH_4)_2SO_4$
- 3 g K_2HPO_4
- 1 g KH_2PO_4
- 100 mg L-Threonine
- 150 mg L-Methionine
- 400 mg L-Leucine

- 1 mg Biotin
- 1 mg Thiamine
- 10 ml trace salts
- 1 ml poly(propylene glycol) MW 2000 antifoam

The trace salt solution consisted of (per litre of distilled water):

- 200 mg $MnSO_4$
- 6 mg H_3BO_3
- 4 mg $(NH_4)_6Mo_7O_{24}•4H_2O$
- 100 mg $FeCl_3•6H_2O$
- 1 mg $ZnSO_4•7H_2O$
- 30 mg $CuSO_4•5H_2O$

2.2 Complex fermentation medium

The complex fermentation medium consisted of (per litre of IC medium):

- 0.125 kg of Corn Steep Liquor at 35% total solids obtained from African Products (Pty) Ltd. (RSA)
- 0.4 g $MgSO_4•7H_2O$
- 25 mg $FeSO_4•7H_2O$
- 3 g K_2HPO_4
- 1 mg Biotin
- 1 mg Thiamine
- 1 ml poly(propylene glycol) MW 2000 antifoam

2.3 Carbohydrate source

Two feed streams were used in the fed-batch fermentations. The sugar feed consisted of a 60% (m/m) glucose solution with varying amounts of L-Threonine, L-Methionine and L-Leucine (added in the same ratio as in the initial charge).

The second feed was a 40% (m/m) ammonium sulphate solution.

The pH was controlled using a 25% Ammonium hydroxide solution.

3 Cultivation Conditions

The inoculation procedure began by the transfer of a loop-full of the organism from a complex media plate (24h of growth) to a 250 ml flask containing 25 ml of LB media. The flask is incubated for 8 hours at 30 °C and 180 rpm. The flask contents were transferred to

a 1 litre flask containing 250 ml of the defined medium. This flask is incubated for 12 hours under the same conditions.

The broth from the larger flask is then transferred to the 10 litre working volume Chemap fermenter.

The temperature was maintained at 30±0.5 °C using internal heating and cooling coils. The reactor was fitted with sterilisable Ingold pH (model 764-31) and Mettler Toledo dissolved oxygen (model 4100) electrodes. The pH was controlled by a UCT pH controller driving a UCT peristaltic dosing pump. The base reservoir was positioned on a scale pan interfaced to a data logger for continuous monitoring of base consumption. The DO probe was linked to a UCT amplifier and the dissolved oxygen concentration was recorded continuously.

The air supply to the vessel was passed through a pressure regulating unit, an oil filter, a rotameter and a sterile carbon filter before entering the reactor. The exhaust gasses passed through a sterile carbon filter and a condenser cooled with tap water.

Broth samples were taken aseptically using a steam sterilisable sample port at the base of the vessel.

For continuous culture, the reactor feed was added at a constant flow rate using a peristaltic pump. The feed bottle was placed on a load cell to facillitate measurement of the flow. The bioreactor rested on a sensitive load cell. The output of the load cell was linked to the output pump flow controller. The controller switched the output pump on when the mass of the fermenter exceeded the setpoint mass.

4 Fermentation protocol

4.1 Batch fermentations

The batch fermentations were conducted in a 7.3 litre Chemap stirred tank reactor fitted with Rushton turbine impellers. A 0.5 litre inoculum was transferred into 4.5 litres of medium. In these fermentations pH was controlled at 7.0 with sulphuric acid and 25% ammonium hydroxide. Temperature was controlled at 30°C. Aeration and agitation was controlled to maintain a DO in excess of 30%.

4.2 Fed-batch fermentations

The fed-batch fermentations were conducted in the same bioreactors as the batch fermentations. pH and temperature was controlled at the same values as that of the batch fermentations The initial starting volume was however reduced to 2.7 litres and the inoculum to 0.3 litres. Feed was started at glucose depletion, which was detected, from the sudden increase in pH and subsequent acid demand. Glucose depletion was confirmed by

analysis of the glucose concentration. The feed rate was controlled at a certain specific feed by measuring the biomass by optical density and adjusting the absolute feed rate accordingly. When the reactor volume reached 8 litres the sample volume was increased to maintain the liquid volume at 8 litres.

4.3 Continuous fermentations

For the continuous culture, the reactor feed was added at a constant flow rate using a Watson Marlow (model 313S) peristaltic pump. The feed bottle was placed on a 60 kg load cell to allow measurement of flow rate. The bioreactor rested on a sensitive load cell. The output from the load cell was linked to the output pump flow controller. The controller switched the output pump on when the mass of the fermenter overshot the setpoint mass.

5 Reactor Configuration

5.1 Chemap stirred tank reactor

The Chemap stirred tank reactor was operated at 30 °C at a pH of 7.0. Three molar NH_4OH was used to maintain the neutral pH. The reactors were fitted with sterilisable Ingold pH (model 764-31) and Mettler Toledo dissolved oxygen (model 4100) electrodes. The pH was controlled by a UCT pH controller driving a UCT peristaltic dosing pump. The base reservoir was positioned on a scale pan interfaced to a data logger for continuous monitoring of base consumption. The dissolved oxygen probe was linked to a Mettler Toledo transmitter (4100) and the dissolved concentration was recorded continuously. The air to supply to the reactor was passed through a pressure regulating unit, an oil filter, rotameter and a sterile carbon filter before entering the reactor. The exhaust gasses passed through a sterile carbon filter and a condenser cooled with tap water. The temperature of the vessel was maintained to within 5 °C by heating a water stream that passed through two stainless steel coils situated near the baffle cage. Bacterial samples were taken aseptically using a steam sterilisable sample port at the base of the culture vessel.

The 7.3 liter Chemap stirred tank (5 liter working volume) reactor fitted with Rushton turbine impellers of the following dimentions: diameter 0.08 m, width 0.02 m and length 0.02 m. Two impellers was used with an impeller clearance of 0.04m and an impeller spacing of 0.12 m. The diameter of the tank was 0.2 m. The reactor was fitted with four baffles of 0.03 m width. In continuous culture a 3.5 liter working volume was used with a single impeller set at an impeller clearance one third of the liquid height.

5.2 Filtration flow loop

The purpose of the cross-flow filtration unit is to separate the biomass from the spent medium. The biomass is then recycled to the bioreactor while the spent medium is processed for lysine recovery.

The biomass recycling system is illustrated in Figure 1.

- The holding vessel was a "Chemap" bioreactor with agitation, temperature and pH control. The broth was cultivated in the bioreactor. A positive pressure was maintained by sparging filtered air through the broth. The temperature was maintained at 30°C and the pH at 7.2.
- From the holding vessel the broth was pumped to the membrane module using a peristaltic pump. The peristaltic pump was rated to deliver a head of 3 bar. The pressure at the inlet of the membrane module was measured using a electronic pressure transducer. The pressure was continuously logged using a stand alone PC.
- The membrane is situated in the membrane module held between the two screw heads resting on o-rings to prevent leaking. The permeate is collected in the outer housing and diverted to a closed permeate collection vessel. The permeate collection vessel is placed on a three decimal scale connected to the PC that logs the weight every 10 seconds.

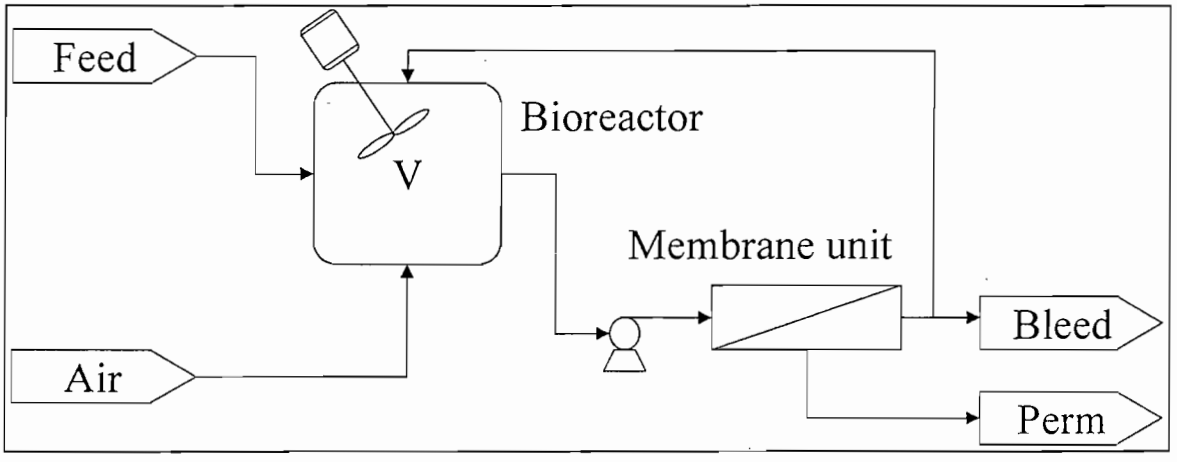

Figure A-1. Experimental set up to evaluate the impact of the operational parameters on the cross-flow filtration flux. "Feed" is the carbohydrate feed, "Bleed" is the bleed of broth from the reactor while "Perm" is the permeate flow rate from the membrane unit

Cross-Flow Filtration Rig and Flux Estimation

1 Cross-flow filtration flow loop

The objective of the cross-flow filtration unit is to separate the biomass from the spent medium. The biomass is then recycled to the bioreactor while the spent medium is processed for lysine recovery.

The biomass recycling system is illustrated in Figure B.1.

- The holding vessel was a "Chemap" bioreactor with agitation, temperature and pH control. The broth was cultivated in the bioreactor. A positive pressure was maintained by sparging filtered air through the broth. The temperature was maintained at 30°C and the pH at 7.2.
- From the holding vessel the broth was pumped to the membrane module using a peristaltic pump. The peristaltic pump was rated to deliver a head of 3 bar. The pressure at the inlet of the membrane module was measured using a electronic pressure transducer. The pressure was continuously logged using a stand alone PC.
- The membrane is situated in the membrane module held between the two screw heads resting on o-rings to prevent leaking. The permeate is collected in the outer housing and diverted to a closed permeate collection vessel. The permeate collection vessel is placed on a three decimal scale connected to the PC that logs the weight every 10 seconds.

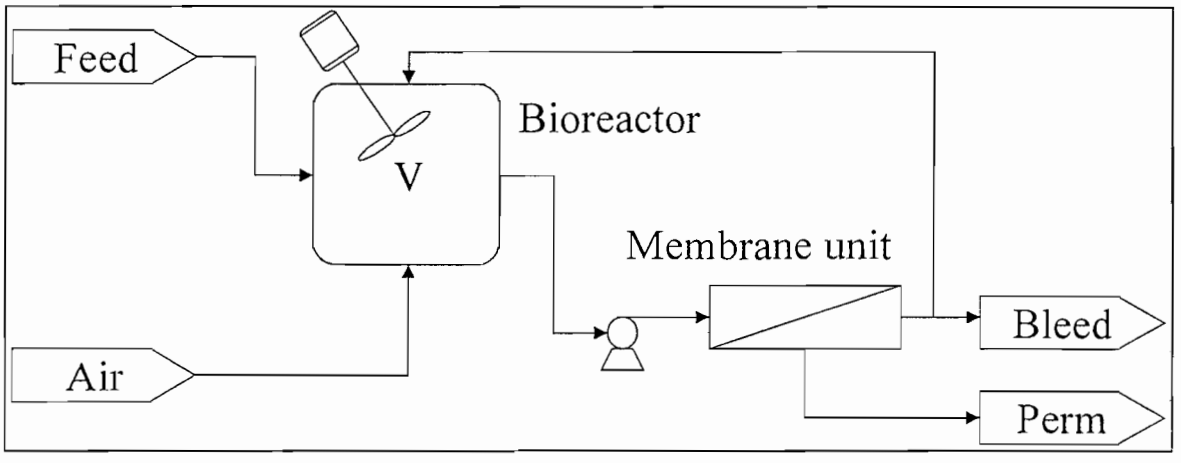

Figure B.1. Experimental set up to evaluate the impact of the operational parameters on the cross-flow filtration flux. "Feed" is the carbohydrate feed, "Bleed" is the bleed of broth from the reactor while "Perm" is the permeate flow rate from the membrane unit

2 Membrane housing

A mechanical drawing of the membrane housing is shown in Figure B.2.
The housing was machined in-house by the UCT Workshop from 316 SS and polished to a 0.64 micron surface finish.

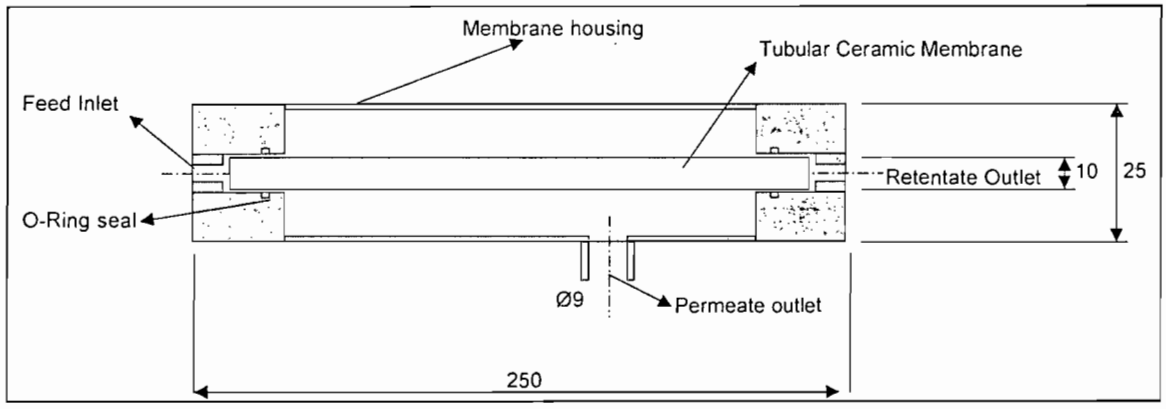

Figure B.2 Mechanical drawing of the membrane housing. All units are in mm

3 Operational and control velocity around the filtration loop

The filtration loop is equipped with a peristaltic pump, two pressure transducers and a needle valve as shown in Figure B.3. The peristaltic pump is equipped with a variable speed drive that can be used to set the re-circulation rate and subsequently the cross-flow velocity. The needle valve is used to set the mean trans-membrane pressure drop across the membrane as measured by the pressure transducers.

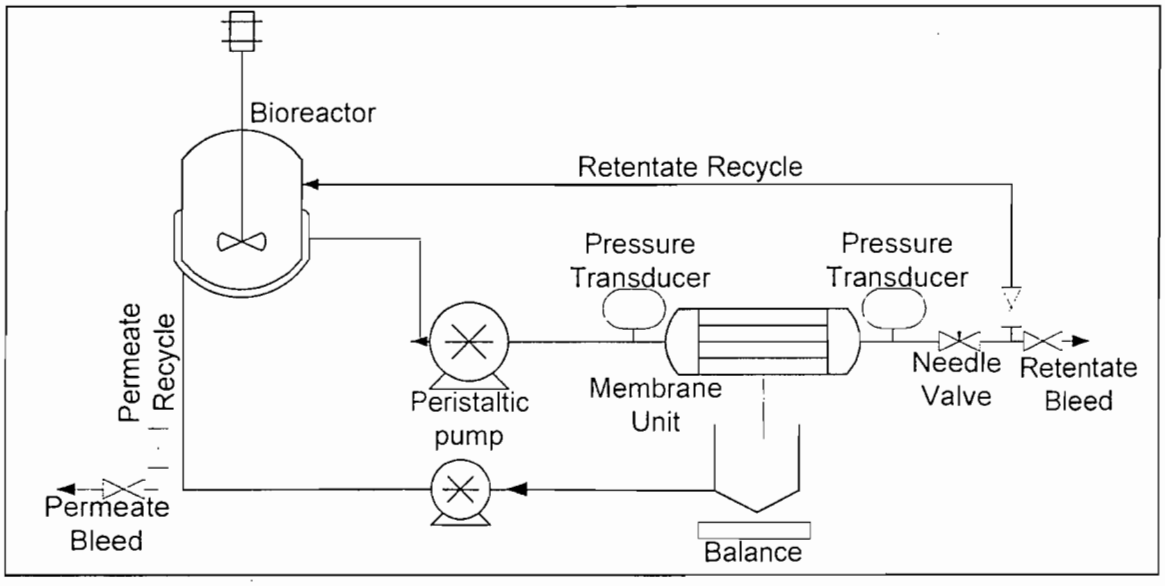

Figure B.3. P&ID of the cross-flow filtration loop

The piping in the filtration loop were all 25 NB, 316 SS tubing with a 0.64 micron surface finish. All the welds conformed to the AECI Bioproducts Pty (Ltd) sterile welding specification with a weld finish of 1.6 microns.

4 Measuring of the cross flow filtration flux

The permeate is collected in the outer housing and diverted to a closed permeate collection vessel. The permeate collection vessel is placed on a three decimal scale connected to the PC that logs the weight every 10 seconds. The permeation rate is calculated from the slope of the weight curve.

For the batch fermentations where the permeate was recycled to the bioreactor, the permeate collection flask was emptied in ten minute intervals. The filtration flux was then estimated from the slope of the weight of permeate collected during ten minute periods.

5 Estimation of the hydraulic resistances

The filtration flux through any system follows

All pressure driven membrane separation processes must follow Darcy's law (See Equation B.1). This law states that the flux is proportional to the driving force and inversely proportional to the hydraulic resistance. The hydraulic resistance is made up of the permeate viscosity and the additional resistance (R_t). The additional resistance can be broken up into the intrinsic membrane resistance (R_m), the pore blocking resistance (R_p) and the cake resistance (R_c).

$$J = \frac{\Delta P}{\upsilon R_t} \qquad (B.1)$$

$$R_t = R_m + R_p + R_c$$

The intrinsic membrane resistance (R_m) is measured by measuring the pure water flux under a known driving force. For this case the pore plugging resistance and the cake resistance would be zero. The intrinsic membrane resistance can therefore be obtained from the measured flux and a known pure water viscosity.

The total resistance (R_t) is measured directly during the filtration process. To determine the pore blocking resistance (R_p) the following procedure is followed:

- Weight out 1.5 g of cotton wool. The cotton wool is attached to a plunger and forced down each of the membrane tubes. The cotton wool fits very tightly in the tube and a large portion of the cake layer on the membrane surface is removed.
- The water flux through the fouled membrane is then measured.

- The resistance calculated from the water flux through the fouled membrane is the sum of the intrinsic membrane resistance and the pore plugging resistance

The cake resistance (R_p) is then determined by difference.

6 Membrane cleaning procedures

The membranes were cleaned according to the following procedure

- 10-litres of warm water (60 °C) is circulated through the membrane unit for 30 minutes
- This is followed by a hot (60°C) caustic (10% m/m) rinse with 10 litres of caustic solution for 45 minutes
- After the caustic rinse the membrane is washed with clean water by circulating fresh water through the control loop until the bleed pH is neutral
- The membrane is then rinsed with 10 litres of 5% nitric acid at 60 °C for 45 minutes
- The membrane is then washed with clean water until the bleed pH is neutral
- The pure water flux is measured and compared to the new pure water flux. If this value is not within 10% of the new membrane pure water flux the cleaning procedure is repeated.

Analysis of the Biological Response

A micro-organism uses its available resources, such as carbohydrates and oxygen, to products various products, maintain intracellular functioning and for repair mechanisms. Changes in the mass flux through the cellular metabolic pathways can be measured through analysis of extracellular production and substrate consumption rates.

1 Cell viability

Plate counts were performed as a measure of cell viability. The latter was defined as the ability of a single cell or aggregate to reproduce. In the plate count, 0.1ml of diluted cell sample (to count between 10 and 300 colonies) was spread on the agar plates with a sterile glass rod. The colonies were counted after 2 day incubation in a 30 °C oven.

The agar media contained (per liter): 10 g tryptone, 10 g yeast extract, 5 g NaCl and 15 g bacteriological agar.

Due to the clumping of the cells, the method was altered by dividing this number by the dry biomass. Thus, the specific plate count is a measure of the number of viable colonies per gram of dry biomass.

Other viability techniques included:

- Inoculation of a defined media shake flask and then measuring the final biomass, glucose consumption and lysine production yield after a defined time-period. This gives an indication of the ability of the cells to reproduce and produce lysine.
- Staining the cell population with acrodine orange and measuring the ratio of red to green dots as a measure of RNA and DNA activity. This ration gives an indication of the intracellular activity and protein production.

2 Rate of Metabolism and metabolic pathway analysis

The rate of metabolism and possible metabolic pathway fluxes were measured in terms of biomass formation (dry biomass), substrate utilisation (residual glucose, ammonium, phosphate) oxygen utilisation rate and product formation (amino acid production)

2.1 Dry Cell Weight

Dry cell weight was determined by centrifuging 2 ml samples at 6000g for 15 min, washing the pellet twice with water and drying it for 30 hours at 80 °C.

Two different dry weight analysis methods were evaluated:

2.1.1 Eppendorf micro-centrifuge tubes

Empty 1.5 ml micro-centrifuge tubes were dried for 72 hours at 80° C and weighed to 4 decimal places. Then 1ml of sample was pipetted into the pre-weight centrifuge tubes. The tubes were then centrifuged and the supernatant poured off. The residue was washed twice with distilled water before being dried at 80° C for 70 hours. The difference between the weight of the empty tube and sample tube divided by the volume would the give the dry weight per unit volume.

To evaluate the accuracy of this method the following experiments were performed. A large sample from the Chemap fermentation was taken and 20 centrifuge tubes pre-weight and the dry cell weight determined. From this it was found that the average dry weight analysis gave a standard deviation of 2.13×10^{-1} (measured in g/l) resulting in a error less than 8% for a single tube. This error would be reduced even more if the analysis is performed in triplicate.

Then the sample was diluted with distilled water and after each dilution the dry weight determined in triplicate. The average weight was then plotted against the dilution factor. The data fits a straight line trough the origin with a correlation coefficient of 0.98.

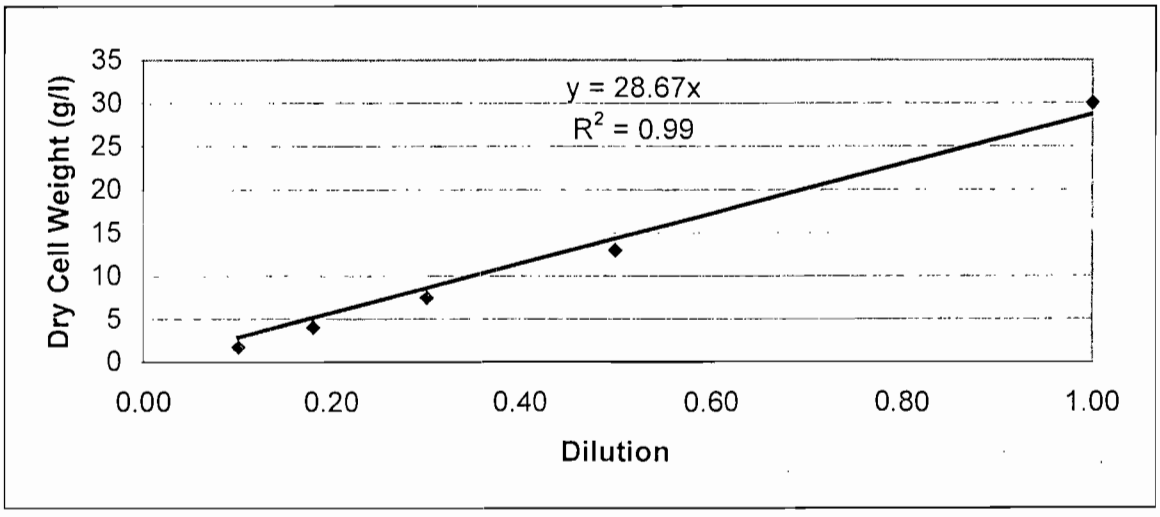

Figure C-1. A plot of the dry weight determined using the micro-centrifuge tubes vs. the dilution factor. The dilution factor is defined as the ratio of the volume of the original sample to the total volume analysed.

2.1.2 Filtration paper

0.22 micron Millipore filtration paper discs were dried at 80° C for 72 hours and pre-weight to 4 decimal places. Then 10 ml of sample were filtered through these filters using the Millipore vacuum filtration system. The filters were washed with 5 ml of distilled water before being dried at 80° C for 72 hours. The weight difference of the sample and pre weighed filter divided by the sample volume (10 ml) would yield the dry weight per unit volume. The accuracy of this analysis technique was determined by analysing the same sample as used for the Eppendorf tube dry weight determinations.

Thirty filters gave a standard deviation of 2.51 (measured in g/l). This resulted in an error of 22% for a single filter.

The plot of dry weight (determined in triplicate) against the dilution factor yielded a straight line through the origin with a correlation coefficient of 0.91.

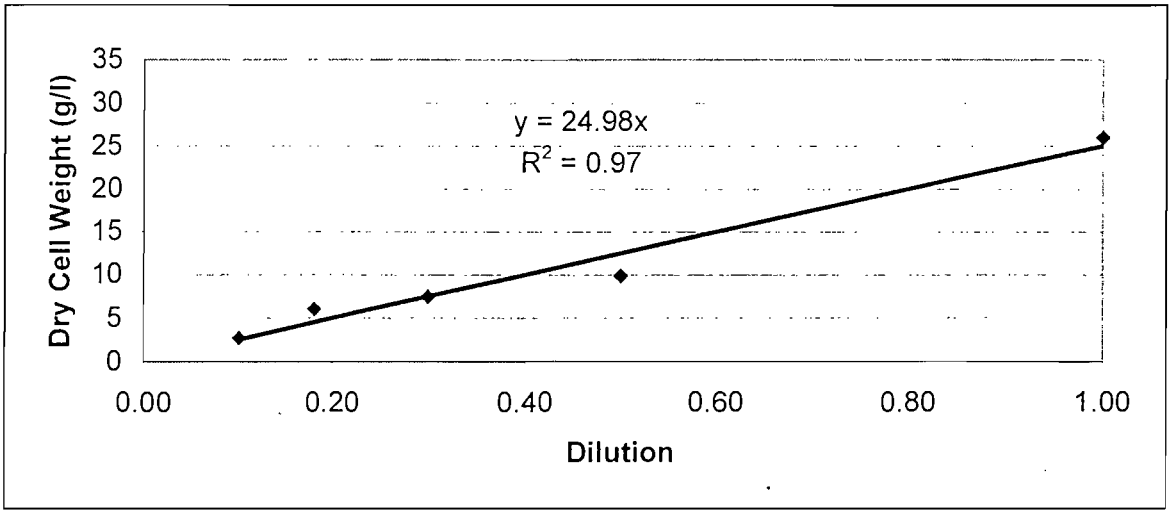

Figure C-2. A plot of the dry weight determined using Millipore filtration paper vs. the dilution factor. The dilution factor is defined as the ratio of the volume of the original sample to the total volume analysed.

From this can be concluded that the Eppendorf method is more reproducible.

2.2 Turbidity

Samples were placed in plastic cuvettes and the absorbance at 660nm determined against distilled water. The samples were diluted so that the absorbance read was less than 2. The same sample used for the dry weight analysis verification experiment were used to determine the reproducibility and range of the turbidity measurements. A plot of the absorbance at 660 nm against the dilution factor yielded a straight line with a correlation

coefficient of 0.93, while a plot of the turbidity against the dry weight yielded a straight line with a correlation coefficient of 0.97.

The error of each turbidity reading was less than 5%. This was determined by taking 30 readings of the same sample at 2 min intervals and obtaining the mean and the standard deviation.

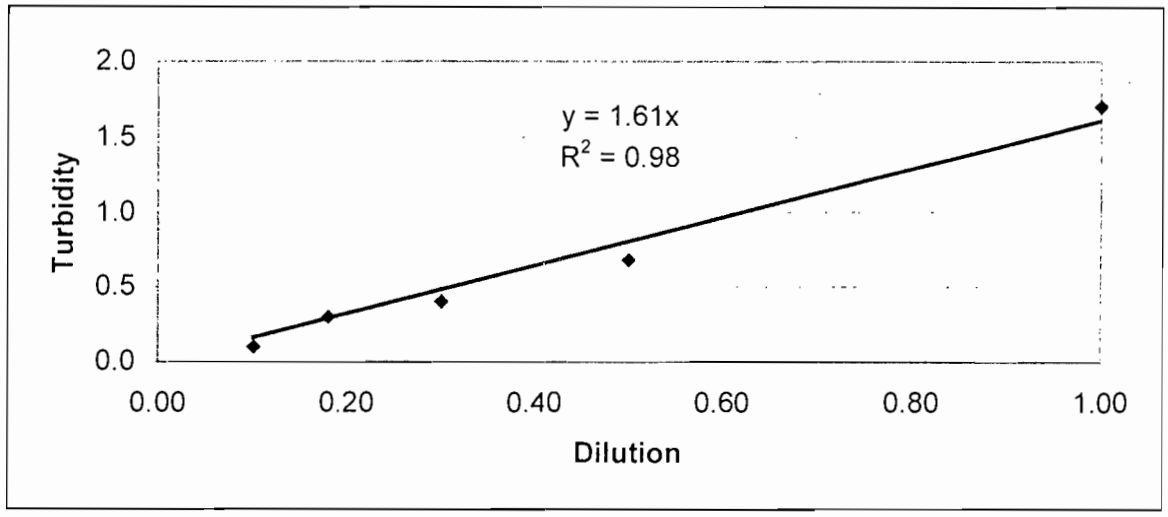

Figure C-3. A plot of turbidity vs. dilution factor where dilution factor is defined as the fraction of the original sample in the volume analysed.

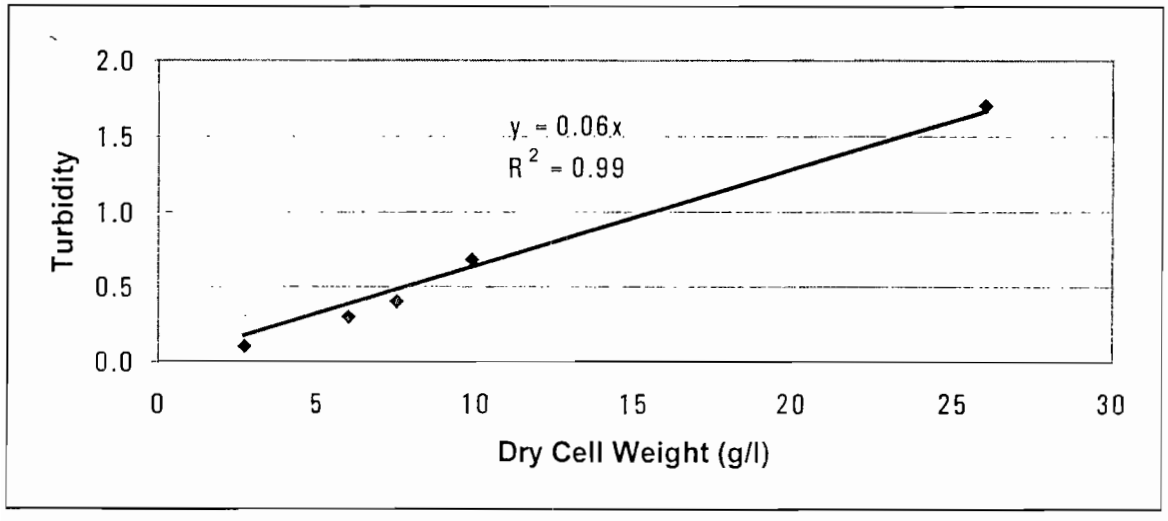

Figure C-4. A plot of turbidity vs. dry weight as determined by the Eppendorf method. The correlation coefficient was 0.97

2.3 Cell counts

The same sample as used for the turbidity and dry weight experiments were used to determine the reproducibility of cell counts. Due to the high degree of clumping observed for the cells, counting of the cells was not possible. The samples were however sonicated at 350 Hz for 4 min. The samples were diluted in the same ratios as before and counted in a Hawksley counting chamber. At least 100 cells were counted in each sample. Cells on the line were counted as "in". A plot of the cell number against the dilution factor yielded a straight line with a correlation coefficient of 0.94.

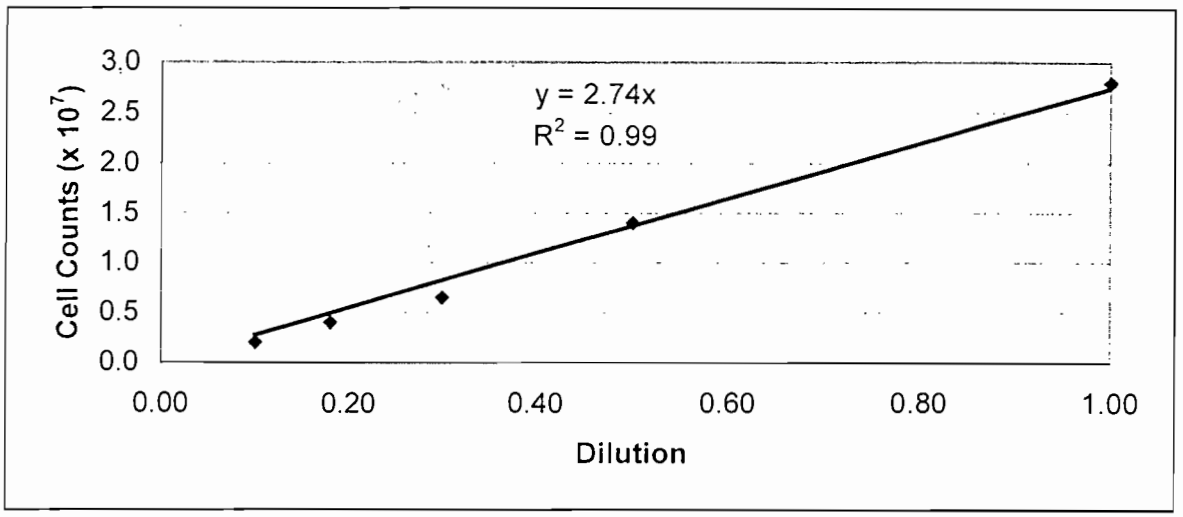

Figure C-5. A plot of the counted cells vs. the dilution factor. Where the dilution factor is defined as the fraction of the original sample in the volume analysed.

2.4 Glucose

The residual glucose concentration was measured colorimetrically following its stoichiometric reaction to gluconate and H_2O_2 in the presence of glucose oxidase. The equilibrium of this reaction was maintained towards gluconate by constant removal of H_2O_2 by reaction with di-ammonium 2,2-azino-bis(3-ethylbenzothiazoline-6-sulphonate) (ABTS) to form a coloured complex:

$$\text{glucose} + O_2 + H_2O \xrightarrow{\text{glucoseoxidase}} \text{gluconate} + H_2O \qquad \text{(C-1)}$$

$$H_2O_2 + \text{ABTS} \xrightarrow{\text{operoxidase}} \text{coloured complex} + H_2O \qquad \text{(C-2)}$$

The coloured complex was quantified spectrophotometrically at 610 nm and is directly proportional to the glucose concentration. Cell samples were centrifuged and the supernatant analysed using the Boehringer Mannheim kit, cataloque number 124 036. In

the assay procedure, 0.06 ml of diluted sample was mixed in a test tube with 3 ml of reagent solution and incubated at 25° C for 20 min. The absorbance was read at 610 nm against the blank. The method error was less than 5%.

Residual glucose was measured colorimetrically based on the oxidation of glucose to gluconic acid and H_2O_2.

2.5 Amino Acids

L-Lysine, L-Threonine and the other amino acids were analysed using a reverse phase HPLC column as described by Nakatani et al. (1972).

2.6 Morphology

Use the phase contrast light microscope at 1000 fold magnification. Methyl violet staining can be used.

The image analysis of microbial systems has advanced rapidly over the last few years. Microbial systems in which image analysis has been successfully applied include the study of the morphology of single cell bacteria (James *et al.* 1995; Singh *et al.* 1990; Dickason, 1998).

The diluted cell samples were laced on slides covered with a thin layer of agar (2%) to immobilise the cells (Huls *et al.* 1992). The presence of the agar on the slide ensures that the cells all lie in one plane while at the same time keeping the cells hydrated.

Bacteria were viewed using an Olympus BX-40 microscope fitted with bright field, dark field and phase contrast condensers. For the morphological studies all cells were viewed at 1000× magnification under phase contrast. Images from the microscope were acquired in colour using a Panasonic RGB digital camera and an IC-PCI-4× frame grabber. An Intel Pentium-133 PC with 16 Mb Ram was used to process the images using "Optimas" version 5.2.

The macro developed for the quantification of the morphology has been designed to operate semi-automatically (Dickason 1998). Intervention is required to exclude objects that have mistakenly been identified as whole cells or colonies.

The main processing steps are as follows (Dickason 1998):

1. Image capturing is performed by the operator who selects the image field and adjusts the focus. A total of 10 images were taken per sample. This was sufficient to ensure that the standard error in the cell length measurements was less than 5%. A semi-automated image acquisition system was installed which allowed a new image to be acquired every 6 seconds. A first audible tone indicated to the operator to move the

stage and focus on a different area of the slide. A second tone indicated that image acquisition would take place within four seconds.

2. The next step in the macro was to binarize the image which meant that the objects of interest were assigned a grey level of 1 and the background grey level was set to 0. Before this could be done a set of filters were applied to the image. Firstly a "median" filter was applied which eliminated noise by replacing each pixel in the original image with the median luminance value of the surrounding pixels in the image. Any small debris in the image was thus erased whilst still preserving the edges. A "sharpen high" filter was then applied. This filter applied a strong edge sharpening grey scale convolution to the image. Edges were highlighted in such a way that the border of dark objects appeared darker and the border of light objects was lighter. The threshold values for binarization of the image were determined automatically such that the dark objects formed the foreground of the image.

3. The purpose of the next stage in the macro was to enhance the binarized image. This included steps to ensure that the cell membrane is closed. For colony identification, binary "dilate", "fill" and "erode" functions were performed. For identification of single cell area a "fill" function was implemented.

4. To identify single cell areas, it was necessary to separate joined cells. For this the "watershed separation" algorithm was applied to the distance transform on the binary image. The distance transform is the distance between each white pixel in the image and the nearest black pixel. The distance is defined as the chamfer 5-7-11 distance as this is the closest approximation to the Euclidean distance possible while still using integer grey value. The distance transform works by assigning each pixel with a distance value of 5, 7, 11 or the nearest combination of these values. Once the distance transform has been computed the watershed algorithm is applied. A pre-flood of 8 was chosen for the watershed separation. This means that a value of 8 is added to each identified minimum in the inverted distance transform. If this is higher than the watershed separating that minimum from an adjacent watershed area, then that watershed area is eliminated and combined with the adjacent area. The pre-flood of 8 was found to prevent over-separation as a result of irregular cell boundaries. The "ultimate erosion method" was not found to perform well on the binary images of *C. glutamicum* cell needing separation. This was because the number of erosions was globally set and different clumps required a different number of erosions to become separated. Some cell clumps thus remained un-separated while others were over-separated.

5. The final stage in the macro was to assign labels to objects and to extract data to an MS Excel spreadsheet. Only those objects that satisfied the constraints of the object label were marked. In that way any debris left in the image was ignored in the morphology measurement. For colonies, the total tally and the colony areas were evaluated. Area, total tally, length, breadth, circularity and the elliptical fit were calculated for the single cells.

Analytical Procedures

1 Malvern Particle Sizer

Particle size analysis by laser light diffraction of bacterial samples was carried out in a Malvern 3600Ec particle sizer fitted with a 63 mm lens. The particle size distribution and relative increase in the total particle count of samples were determined. The principle of operation of the particle sizer was based on conventional Fourier optics. A beam of light from a low power Helium-Neon laser was scattered by particles in its path. The scattered light was incident on a Fourier transform lens which formed a diffraction pattern of the scattered light on a detector. The scattering angle was related to the particle diameter. Large particles had peak energies at low angles of scatter and *vice versa.*

Phosphate buffered saline (PBS) was used as background medium for particle size analysis. The medium contained (per litre): 0.800 g NaCl, 0.200 g KI, 2.254 g Na_2HPO_4 and 0.200 g KH_2PO_4. The saline was passed through a 0.22 μm filter.

Before measurements were taken, the laser beam was aligned by manipulation of the x and y alignment screws. Samples were analysed using the magnetically stirred stationary cell. The particle size analyser was zeroed with PBS at ambient temperature. 5000 measuring sweeps were chosen to ensure significant results. Using a pipette, a few drops of bacterial sample were added to the PBS in the agitated sample cell so that the concentration was between 0.2 and 0.3 vol %. The particle size distribution was measured. Experiments showed that the morphology remained stable for 20 minutes after sampling. Special care was therefore taken to analyse bacteria immediately after sampling. Repeated analysis of samples showed that the method was reproducible.

2 Zeta Potential

Cells were diluted in 0.05 M phosphate and citrate-phosphate buffers made up to specific pH's in the range 3 to 8.

For the preparation of the 0.05M phosphate buffer, 1.78 g Na_2HPO_4 and 1.38 NaH_2PO_4 were dissolved in 200 ml distilled water. The buffers in the pH range between 6 and 8 contained x ml Na_2HPO_4 solution, (50-x) ml NaH_2PO_4 and 50 ml distilled water (Table C.1)

Table C.1 Preparation of phosphate buffers

pH	x
6.0	6.15
6.5	15.75
7.0	30.50
7.5	42.00
8.0	47.35

For the preparation of the citrate-phosphate buffer, 4.2 g of citrate and 3.56 g Na_2HPO_4 were each dissolved in 200 ml distilled water. The buffers contained x ml citric acid, (50-x) ml Na_2HPO_4 and 50 ml distilled water (Table C.2).

Table C.2 Preparation of citrate-phosphate buffers

pH	x
3.0	39.80
4.0	30.70
5.0	24.30
6.0	17.90
7.0	6.50

Metabolic pathways in Corynebacterium glutamicum

Vallino & Stephanopoulos (1993) constructed the metabolic network of *C. glutamicum* from publications on glutamic acid bacteria. Most of the enzymes of the Embden-Meyerhof-Parnas (EMP) pathway, the tricarboxylic acid cycle and the pentose phosphate pathway have been detected in *C. glutamicum* or related strains.

The EMP pathway involves the conversion of glucose into pyruvate with the production of ATP. The carboxylic acid cycle oxidised acetyl CoA to CO_2.

In this appendix general cell metabolism is discussed with typical reactions depicted for each of the characteristic pathways.

1. The glycolytic pathway

The glycolytic pathway, also referred to as the Embden-Meyerhof-Parnas pathway is responsible for the conversion of glucose into pyruvate with the production of ATP. The pathway as a whole may be divided into two parts. In the initial six-carbon (C-6) stage, glucose is phosphorylated twice and eventually converted to fructose 1,6-bisphosphate (Fru6P). Other sugars are often fed into the pathway by conversion to glucose 6-phosphate or fructose 6-phosphate. This preliminary stage does not yield energy. These initial steps prime the pump by adding phosphates to each end of the sugar. The phosphates will be used to make ATP.

$$Glc + PEP \rightarrow Glc6P + Pyr \quad \text{(E-1)}$$
$$Glc6P \rightarrow Fru6P \quad \text{(E-2)}$$

The three-carbon stage of glycolysis begins when the enzyme, fructose 1,6-bisphosphate aldolase catalyses the cleavages of fructose 1,6-bisphosphate (Fru6P) into two halves, each with a phosphate group.

$$Fru6P + ATP \rightarrow GaP + DaP + ADP \quad \text{(E-3)}$$

One of the products, glyceraldehyde 3-phosphate (GaP) is converted directly into pyruvate (Pyr) in a five-step process. Because the other product dihydroxyacetone phosphate (DaP) can be easily changed to glyceraldehyde 3-phosphate (GaP), both halves of fructose 1,6-bisphosphate are used in the three-carbon stage.

$$DaP \rightarrow GaP \quad \text{(E-4)}$$

Glyceraldehyde 3-phosphate (GaP) is first oxidised with NAD+ as the electron acceptor and a phosphate is simultaneously incorporated to give a high-energy molecule called 1,3-bisphosphoglycerate (G3P). The high-energy phosphate on carbon one is subsequently donated to ADP to produce ATP. This synthesis of ATP is called substrate level phosphorylation because ADP phosphorylation is coupled with the exergonic breakdown of a high-energy substrate molecule.

$$GaP + NAD + ADP \rightarrow G3P + ATP + NADH \quad \text{(E-5)}$$

A somewhat similar process generates a second ATP group by substrate level phosphorylation. The phosphate group on 3-phosphoglycerate (G3P) shifts to carbon two and 2-phosphoglycerate is dehydrated to form a second high-energy molecule phosphoenolpyruvate (PEP). This molecule donates its phosphate to ADP forming a second ATP and pyruvate (Pyr), the final product of the pathway.

$$G3P \rightarrow PEP + H_2O \quad \text{(E-6)}$$
$$PEP + ADP \rightarrow Pyr + ATP \quad \text{(E-7)}$$

In some instances pyruvate (Pyr) will react with NADH to form lactate (Lac) and NAD to control the availability of pyruvate.

$$Pyr + NADH \rightarrow Lac + NAD \quad \text{(E-8)}$$

2. Pentose phosphate pathway

The enzymes of a second pathway, the pentose phosphate or hexose monophosphate pathway have also been detected in *C. glutamicum* (Vallino & Stephanopoulos 1993).

The pentose phosphate pathway begins with the oxidation of glucose 6 phosphate (Glc6P) to 6-phosphogluconate followed by the oxidation of 6-phosphogluconate to the pentose ribulose 5-phosphate (Ribu5P) and CO_2. NADPH is produced during these oxidations.

$$Glc6P + 2NADP \rightarrow Ribu5P + 2\,NADPH + CO_2 \quad \text{(E-9)}$$

Ribulose 5-phosphate (Ribu5P) is then converted to a mixture of three through seven-carbon sugar phosphates. Two enzymes unique to this pathway play a central role in these transformations: (1) transketolase catalyses the transfer of two carbon ketol groups and (2) transaldolase transfers a three carbon group from sedoheptulose 7-phosphate to glyceraldehyde 3-phosphate.

$$Ribu5P \rightarrow Rib5P \quad \text{(E-10)}$$
$$Rib5P + Xyl5P \rightarrow Sed5P + GaP \quad \text{(E-11)}$$
$$Sed5P + GaP \rightarrow Fru6P + E4P \quad \text{(E-12)}$$
$$Xyl5P + E4P \rightarrow Fru6P + GaP \quad \text{(E-13)}$$

These intermediates are used in two ways. The fructose 6-phosphate (Fru6P) can be changed back to glucose 6-phosphate (Glu6P) while glyceraldehyde 3-phosphate (GaP) is converted to pyruvate (Pyr) by glycolytic enzymes. The glyceraldehyde 3-phosphate also may be returned to the pentose phosphate pathway through glucose 6-phosphate formation. This results in the complete degradation of glucose 6-phosphate to CO_2 and the production of a great deal of NADPH.

3. The tricarboxylic acid cycle (TCA)

Although some energy is obtained from the breakdown of glucose (Glc) to pyruvate (Pyr) by the pathways previously described, much more energy is released when pyruvate (Pyr) is degraded aerobically to CO_2 in stage three of the catabolism. The multi-enzyme system called the pyruvate dehydrogenase complex first oxidises pyruvate to form CO_2 and acetyl coenzyme A (AcCoA), an energy rich molecule composed of coenzyme A and acetic acid joined by a high energy thiol ester bond. Acetyl CoA arises from the catabolism of many carbohydrates, lipids and amino acids.

$$Pyr + CoA + NAD \rightarrow AcCoA + CO_2 + NADH \qquad (E\text{-}14)$$

In the first reaction of the TCA cycle acetyl CoA is condensed with a four carbon intermediate, oxaloacetate (OaA) to form citrate and to begin the six carbon stage. Citrate (a tertiary alcohol) is rearranged to give iso-citrate (IsoCit), a more readily oxidised secondary alcohol. Iso-citrate (IsoCit) is subsequently oxidised and then decarboxilated twice to yield α-ketogluteraldehyde (AKG), then succinyl-CoA (SucCoA). At this point two NADH's are formed and two carbons are lost from the cycle as CO_2. Because two carbons were added as acetyl CoA at the start, balance is maintained and no net carbon is lost. The cycle now enters the four-carbon stage, during which two oxidation steps yield one $FADH_2$ and one NADH per acetyl CoA. In addition GTP (a high-energy molecule equivalent to ATP) is produced from succinyl CoA by substrate level phosphorylation. Eventually oxaloacetate (OaA) is reformed and ready to join with another acetyl CoA.

$$OaA + AcCoA \rightarrow IsoCit + CoA \qquad (E\text{-}15)$$
$$IsiCit + NADP \rightarrow AKG + NADPH + CO_2 \qquad (E\text{-}16)$$
$$AKG + COA + NAD \rightarrow SucCoA + NADH + CO_2 \qquad (E\text{-}17)$$
$$SucCoA + ADP \rightarrow Suc + ATP + CoA \qquad (E\text{-}18)$$
$$Suc + FAD \rightarrow Mal + FADH \qquad (E\text{-}19)$$
$$Mal + NAD \rightarrow OaA + NADH \qquad (E\text{-}20)$$

4. Anaplerotic reactions

The TCA cycle intermediates are used to synthesise pyrimidines as well as a variety of amino acids. There is a heavy demand upon the TCA cycle to supply carbon for

biosynthesis and cycle intermediates could be depleted if nothing were done to maintain their levels. Reactions that replace these cycle intermediates are called anaplerotic reactions. Most organisms replace TCA cycle intermediates by CO_2 fixation. CO_2 is added to an acceptor molecule; either pyruvate (Pyr) or phosphoenolpyruvate (PEP) to form the TCA intermediate oxaloacetate (OaA). The enzyme mediation CO_2 fixation, pyruvate carboxylase requires the cofactor biotin.

$$PEP + CO_2 \rightarrow OaA \qquad \text{(E-21)}$$

Another major group of anaplerotic reactions is called the glyoxylate cycle. In this cycle isocitrate lyase and malate synthase catalyse the following reactions:

$$Isocit \rightarrow Suc + Gly \qquad \text{(E-22)}$$
$$Gly + AcCoA \rightarrow Mal + CoA \qquad \text{(E-23)}$$

The glyoxylate cycle is a modified TCA cycle. The two decarboxylations of the latter pathway are bypassed, making possible the conversion of acetyl CoA to oxaloacetate (OaA) without the loss of acetyl CoA carbon as CO_2. In this fashion acetate can contribute carbon to the cycle.

Other anaplerotic pathways detected in gluctamic acid bacteria include phosphoenolpyruvic acid carboxykinase (PPC), pyruvic carboxylase (PC) and malic enzyme (Vallino & Stephanopoulos, 1993). Although some evidence exists that PEP carboxylase and PEP carboxytransphophorylase are present in *B. ammoniagenes* the findings are not well supported, so these reactions are not considered in this study. (OAA – Oxalacetic acid, PEPA - Phosphoenol pyruvic acid, PYRA - pyruvic acid)

$$PPC: \quad PEPA + CO_2 + GTP \rightarrow OAA + GTP \qquad \text{(E-24)}$$
$$PC: \quad PYR + CO_2 + ATP \rightarrow OAA + ADP \qquad \text{(E-25)}$$
$$PEP: \quad PEP + CO_2 \rightarrow OAA \qquad \text{(E-26)}$$
$$Malic: \quad PyrA + CO_2 + NADPH \rightarrow Mal + NADP \qquad \text{(E-27)}$$
$$ICLY: \quad Isocit \rightarrow Suc + Gly \qquad \text{(E-28)}$$

5. Electron transport and oxidative phosphorylation

Little ATP has been synthesised up to this point. Only the equivalent of four ATP molecules are directly synthesised when one glucose molecule is oxidised to six CO_2 molecules by way of glycolysis and the TCA cycle.

The electron transport chain is composed of a series of electron carriers that operate together to transfer electrons from donors like NADH and $FADH_2$, to acceptors such as O_2. The electrons flow from carriers with more negative reduction potentials to those with more positive potentials. The difference in reduction potential between NADH and the final

electron acceptor (usually O_2) is large and allows for the release of a large amount of energy.

The process by which energy from electron transport is used to make ATP is called oxidative phosphorylation. As many as three ATP, molecules may be synthesised from ADP and phosphate when a pair of electrons passes through the electron transport chain. This is the same thing as saying that the phosphorous to oxygen (P/O) ratio is equal to 3. Because electrons from $FADH_2$ can only pass through two oxidative phosphorylation points the maximum P/O ratio for $FADH_2$ is 2.

6. Catabolism of Carbohydrates and Intracellular reserve polymers

6.1. Carbohydrates

Other mono-saccharides such as fructose (Fru), mannose (Man) and galactose (Gal) can also enter the glycolytic pathway. The first two are phosphoryated and easily enter the glycolytic pathway. In contrast, galactose must be converted to uridine diphosphate galactose (UDP-Gal) after initial phosphorylation, then changed into glucose 6-phosphate in a three-step process.

Fru + PEP → Fru6P + Pyr	(E-29)
Man + PEP → Man6P + Pyr	(E-30)
Man6P → Fru6P	(E-31)
Gal + ATP → GalP + ADP	(E-32)
GalP + UTP → UDP-Gal + PP	(E-33)
UDP-Gal → UDP-Glc	(E-34)
UDP-Glc + PP → UTP + GlcP	(E-35)
GlcP → Glc6P	(E-36)

The common disaccharides are cleaved to mono-saccharides by at least two mechanisms. Maltose, sucrose and lactose are hydrolysed to their constituent sugars. Many disaccharides are split by phosphate attack on the glycosidic bond, a process called phosphorolysis. Polysaccharides, like disaccharides are cleaved by both hydrolysis and phosphorolysis.

6.2. Reserve polymers

Microorganisms often survive for long periods in the absence of exogeneous nutrients. Under such circumstances they catabolise previously accumulated intracellular stores of glycogen, starch, poly-β-hydroxybutyrate and trehalose. For example glucose 6-phosphate (Glc6P) can be converted to trehalose (Trehal) to act as internal storage of the carbon source.

$$Glc6P + 0.5\ ATP \rightarrow 0.5\ Trehal + 0.5\ ADP \quad (E\text{-}37)$$

7. Protein and amino acid catabolism

Some bacteria use proteins as a source of carbon and energy. They secrete protease enzymes that hydrolyse proteins and polypeptides to amino acids. The latter are transported into the cell and catabolised.

The first step in amino acid use is de-amination, the removal of the amino group from the acid. This is often accomplished by trans-amination. The amino group is transferred from an amino acid to a α-keto acid acceptor. The organic acid resulting from de-amination is converted to pyruvate (Pyr), acetyl CoA (AcCoA) or a TCA cycle intermediate and oxidised in the TCA cycle to release energy. It can also be used as a source of carbon for the synthesis of cell constituents. Excess nitrogen from de-amination may be excreted as ammonium ions, increasing medium alkalinity.

8. Assimilation of inorganic phosphorous

Phosphorous is found in nucleic acids, proteins, phospholipids, ATP and coenzymes like NADP. The most common phosphorous sources are inorganic phosphate and organic phosphate esters. Inorganic phosphate is incorporated through the formation of ATP by oxidative phosphorylation and substrate level phosphorylation.

9. Assimilation of inorganic nitrogen

Nitrogen is a major constituent of proteins, nucleic acids and coenzymes. Most organisms incorporate either ammonia or nitrate as nitrogen source.

Ammonium nitrogen can be incorporated into organic material directly because it is more reduced than other forms of inorganic nitrogen. Some micro-organisms form the amino acid alanine (Ala) in a reductive amination reaction catalysed by alanine dehydrogenase.

$$Pyr + NH_4^+ + NADH\ (NADPH) \rightarrow Ala + NAD^+(NADP^+) \quad (E\text{-}38)$$

The major route for ammonia incorporation is the formation of glutamate (Glut) from α-ketoglutarate (a TCA cycle intermediate). When the ammonia concentration is high, glutamate dehydrogenase is employed.

$$AKG + NH_4^+ + NADH\ (NADPH) \rightarrow GLUT + NAD^+(NADP^+) \quad (E\text{-}39)$$

Once either alanine or glutamate has been synthesised, the newly formed α-amino group can be transferred to other carbon skeletons by transamination reactions to form different amino acids.

A second route of ammonia assimilation involves two enzymes acting in sequence, glutamine synthetase and glutamate synthase. Ammonia is used to synthesise glutamine (Glum) from glutamate (Glut), then the amide nitrogen of glutamine is transferred to α-ketoglutarate (AKG) to generate new glutamate molecules.

Because glutamate acts as an amino donor in transaminase reactions, ammonia may be used to synthesise all common amino acids when suitable transaminases are present. Both ATP and a source of electrons such as NADPH are required. The two enzymes acting in sequence operate very effectively at low ammonia concentrations, unlike the glutamate dehydrogenase pathway which has a low affinity for ammonia.

10. Amino acid synthesis

Besides assimilation of inorganic nitrogen in the ammonia form, amino acid synthesis also requires the construction of the proper carbon skeletons. These skeletons are derived from acetyl CoA (AcCoA) and intermediates of the TCA cycle, glycolysis and the pentose phosphate pathway. To maximise efficiency and economy, the precursors for amino acid biosyntheis are provided by a few major amphibolic pathways. Sequences leading to individual amino acids branch off from these central routes. Alanine (Ala), aspartate (Asp) and glutamate (Glut) are made by transamination directly from pyruvate (Pyr), oxaloacetate (OaA) and α-ketoglutarate (AKG) respectively. Most biosynthetic pathways are more complex. Common intermediates are used to synthesise families of related amino acids. L-Lysine (Lys), L-Threonine (Thr), Isoleucine (Ileu) and L-Methionine (Met) are synthesised from oxaloacetate (OaA) by such a branching anabolic route.

The following sequence of reactions is hypothesised to account for L-Lysine (Lys), Glutamine (Glut), L-Alanine (Ala) and Valine (Val) synthesis in *C. glutamicum*.

$$\text{Glut} + NH_4 + \text{ATP} \rightarrow \text{Glum} + \text{ADP} \quad \text{(E-40)}$$

$$\text{Pyr} + \text{Glut} \rightarrow \text{Ala} + \text{AKG} \quad \text{(E-41)}$$

$$2\,\text{Pyr} + \text{NADPH} + \text{Glut} \rightarrow \text{Val} + CO_2 + H_2O + \text{NADP} + \text{AKG} \quad \text{(E-42)}$$

$$\text{OaA} + \text{Glut} \rightarrow \text{Aap} + \text{AKG} \quad \text{(E-43)}$$

$$\text{Asp} + \text{Pyr} + 2\text{NADPH} + \text{SucCoA} + \text{Glut} + \text{ATP} \rightarrow \text{Lys} + \text{SucC} + \text{AKG} + O_2 + 2\text{NADP} + \text{CoA} + \text{ADP} \quad \text{(E-44)}$$

11. Biomass generation

Biomass generation can be approached in two separate ways. The first and most fundamental way includes the anabolism or generation of complex molecules within the

cells. This includes metabolic reactions for amino acid polymerisation, nucleotide synthesis, RNA synthesis, fatty acid synthesis and synthesis of glycogen and polysaccharises.

The second approach uses the precursors of the complex molecules and incorporates the total anabolism into a singe reaction that yields biomass based on the chemical biomass composition:

0.021 Glc6P + 0.007 Fru6P + 0.09 Rib5P + 0.036 E4P + 0.013 GaP + 0.15 G3P + 0.052 PEP + 0.03 Pyr + 0.332 AcCoA + 0.08 Asp + 0.033 Lys + 0.416 Glut + 0.025 Glum + 0.054 Ala + 0.04 Val + 0.052 Thr + 0.015 Met + 0.043 Leu + 3.82 ATP + 0.476 NADPH + 0.312 NAD → BMS + 3.82 ADP + 0.364 AKG + 0.476 NADP + 0.312 NADH + 0.443 CO_2 (E-45)

12. The Metabolic Pathway used in intracellular flux analysis

Vallino and Stephanopoulos (1993) constructed the following carbon flux distribution for *Corynebacterium glutamicum* ATCC 21253.

The resulting network containing 34 reactions and 37 metabolites were found to be non-singular.

PEP: glucose phosphotransferase system

GLUC + PEP → GLUC6P + PYR (E-46)

Storage compound: trehalose

GLC6P + 0.5ATP → 0.5TREHAL +0.5ADP (E-47)

EMP pathway

GLUC6P → FRUC6P (E-48)
FRUC6P + ATP → 2GAP + ADP (E-49)
GAP + ADP + NAD → NADH + G3P + ATP (E-50)
G3P → PEP + H2O (E-51)
PEP + ADP → ATP + PYR (E-52)
PYR + NADH → LAC + NAD (E-53)

Anapletrotic reaction: PEP carboxylase

PEP + CO_2 → OAA (E-54)

Tricarboxylic acid cycle

PYR + COA + NAD → ACCOA + CO_2 + NADH (E-55)
OAC + ACCOA → ISOCIT + COA (E-56)
ISOCIT + NADP → AKG + NADPH + CO_2 (E-57)
AKG + COA + NAD → SUCOA + NADH + CO_2 (E-58)

$$SUCCOA + ADP \rightarrow SUC + ATP + COA \quad \text{(E-59)}$$
$$SUC + FAD \rightarrow MAL + FADH \quad \text{(E-60)}$$
$$MAL + NAD \rightarrow OAC + NADH \quad \text{(E-61)}$$

Acetate production or consumption

$$ACCOA + ADP \rightarrow AC + COA + ATP \quad \text{(E-62)}$$

Amino acid synthesis

$$NH4 + AKG + NADPH \rightarrow GLUT + NADP \quad \text{(E-63)}$$
$$GLUT + NH_4 + ATP \rightarrow GLUM + ADP \quad \text{(E-64)}$$
$$PYR + GLUT \rightarrow ALA + AKG \quad \text{(E-65)}$$
$$2PYR + NADPH + GLUT \rightarrow VAL + CO_2 + H_2O + NADP + AKG \quad \text{(E-66)}$$
$$OAA + GLUT \rightarrow ASP + AKG \quad \text{(E-67)}$$
$$ASP + PYR + 2NADPH + SUCCOA + GLUT + ATP \rightarrow LYSI + SUCC + AKG + O_2 + 2NADP + COA + ADP \quad \text{(E-68)}$$
$$LYSI \rightarrow LYSE \quad \text{(E-69)}$$

Oxidative phosphorylation

$$2\ NADH + O_2 + 4\ ADP \rightarrow 4\ ATP + 2\ NAD \quad \text{(E-70)}$$
$$2\ FADH + O_2 + 2\ ADP \rightarrow 2\ ATP + 2\ FAD \quad \text{(E-71)}$$

Penthose phosphate pathway

$$GLUC6P + 2NADP \rightarrow RIBU5P + CO_2 + 2NADPH \quad \text{(E-72)}$$
$$RIBU5P \rightarrow RIB5P \quad \text{(E-73)}$$
$$RIBU5P \rightarrow XYL5P \quad \text{(E-74)}$$
$$RIB5P + XYL5P \rightarrow SED5P + GAP \quad \text{(E-75)}$$
$$SED5P + GAP \rightarrow FRUC6P + E4P \quad \text{(E-76)}$$
$$XYL5P + E4P \rightarrow FRUC6P + GAP \quad \text{(E-77)}$$

Biomass synthesis

$$0.021GLC6P + 0.007FRU6P + 0.09RIB5P + 0.036E4P + 0.013GAP + 0.15G3P + 0.052PEP + 0.03PYR0.332ACCOA + 0.08ASP + 0.033LYS + 0.416GLUT + 0.025GLUM + 0.054ALA + 0.04VAL + 0.052THR + 0.015MET + 0.043LEU + 3.82ATP + 0.476NADPH + 0.312NAD \rightarrow BMS + 3.82ADP + 0.364AKG + 0.476NADP + 0.312NADH + 0.443CO_2 \quad \text{(E-78)}$$

Excess ATP removal

$$ATP \rightarrow ADP \quad \text{(E-79)}$$

Modelling of the biomass recycling system

The lysine fermentation model, developed for this study, is based on general volume and mass balances coupled to expressions that define the excretion and uptake of cellular metabolites as functions of the extracellular component concentrations. The mass and volume balance is based on the system illustrated in Figure 6-1.

Two approaches were followed to model the metabolic behaviour of the strain. In the first approach, the cellular metabolism, i.e. specific growth rate, specific lysine productivity and the specific oxygen utilisation rate were expressed as empirical relationships based on experimental results.

In the second approach a bioreaction network was constructed which represented all the intracellular reactions believed to be active during lysine production. The relative reaction rates were then determined experimentally from batch, fed-batch and continuous experimental results. From these rates, a principle node analysis was done to determine whether the fluxes through any node were fixed or if the flux through the node could be related to any other metabolic parameter. By fixing or correlating the flux through a number of nodes, the degrees of freedom were reduced to such an extent that the bioreaction network could be used to model the metabolic behaviour of the cell as a function of the extracellular component concentrations.

1. Empirical Model of the Lysine Fermentation with Biomass Recycling

1.1. Volume and mass balances

$$\frac{dV}{dt} = F_{Gluc} + F_{Thr} + F_{AS} - Bleed - Perm' \qquad (F\text{-}1)$$

$$\frac{dVX}{dt} = \mu_{obs} VX - X \cdot Bleed \qquad (F\text{-}2)$$

$$\frac{dVThr}{dt} = \frac{-\mu VX}{Y_{X_{Thr},obs}} + F_{Thr} \cdot C_{Thr} - Thr(Bleed + Perm') \qquad (F\text{-}3)$$

$$\frac{dVGluc}{dt} = -q_{Gluc} \cdot XV + F_{Gluc} \cdot C_{Gluc} - Gluc(Bleed + Perm') \qquad (F\text{-}4)$$

$$\frac{dVLys}{dt} = q_{Lys,obs} VX - Lys(Bleed + Perm') \qquad (F\text{-}5)$$

1.2. Carbohydrate feed rate

$$F_{Gluc} = \frac{q_{Gluc} \cdot X \cdot V}{C_{Gluc}} \tag{F-6}$$

1.3. Auxotropic amino acid (Threonine) feed rate

$$F_{Thr} = \frac{q_{Thr} \cdot X \cdot V}{C_{Thr}} \tag{F-7}$$

1.4. Ammonium sulphate (AS) feed rate

$$F_{AS} = \frac{(S_1)q_{Lys,obs}VX + (S_2)\mu_{obs}VX}{C_{AS}} \tag{F-8}$$

1.5. Bleed rate

$$\begin{aligned} &\text{if } V < V_{max} \text{ then} \\ &\quad \text{Bleed} = 0 \\ &\text{if } V \geq V_{max} \text{ then} \\ &\quad \text{Bleed} = F_{Gluc} + F_{Thr} + F_{AS} - \text{Perm}' \end{aligned} \tag{F-9}$$

1.6. Permeate flow rate

$$\text{Perm}' = 3.6 \times 10^6 \cdot A\left[J_{ss} + \frac{(J_i - J_{ss})}{(1 + k_{decline} t_{perm})}\right] \tag{F-10}$$

$$k_{decline} = m_0 J_0^{m_1} v^{m_2} X^{m_3} \tag{F-11}$$

$$J_o = \frac{\Delta P}{\upsilon R_m} \tag{F-12}$$

$$J_{ss} = \frac{\Delta P}{\upsilon R_t} \tag{F-13}$$

$$R_t = R_m + R_p + R_c \tag{F-14}$$

$$\frac{J_1'}{J_2'} = 1 - \frac{4}{q_{pore}^{\ 3}}\left(\frac{k_{thick}}{r_p^*}\right) + \frac{6}{q_{pore}^{\ 6}}\left(\frac{k_{thick}}{r_p^*}\right)^2 - \frac{4}{q_{pore}^{\ 6}}\left(\frac{k_{thick}}{r_p^*}\right)^3 + \frac{1}{q_{pore}^{\ 5}}\left(\frac{k_{thick}}{r_p^*}\right) \tag{F-15}$$

$$R_p = R_m\left(\frac{J_2'}{J_1'} - 1\right) \tag{F-16}$$

$$q_{pore} = 1 + (r_{p,STDEV}/r_p^*)^2 \tag{F-17}$$

$$R_c = \sqrt{k_t \frac{X^{p_1} \Delta P^{1+n_c}}{v}} \tag{F-18}$$

$$J_i - \frac{Perm_{At\ the\ start\ of\ cleaning}}{A} = \left[J_0 - \frac{Perm_{At\ the\ start\ of\ cleaning}}{A}\right](1 - \exp(-k_{clean} t_{clean}) \tag{F-19}$$

1.7. Modelling of the cellular metabolism

1.7.1. Modelling of the cellular growth

$$\mu = \mu_{max}\left[\frac{Thr}{km_1 + Thr}\right] \tag{F-20}$$

1.7.2. The specific lysine productivity

$$q_{Lys} = \left(c_1\mu^2 + c_2\mu + c_3\right) \cdot \left(\frac{q_{Gluc}}{k_{sp} + q_{Gluc}}\right) \tag{F-21}$$

Modelling of the biomass recycling system

1.7.3. Specific oxygen utilisation rate

$$OUR = X \cdot q_{O_2} \quad \text{(F-22)}$$

$$q_{o_2} = (10.03\mu + 1.96) \quad \text{(F-23)}$$

1.8. Aeration and agitation

$$OUR = k'_la \cdot (LMOPP\text{-}DO \cdot LMOPP_o) \quad \text{(F-24)}$$

$$k'_la = a_{media}\,[(Rev)^3/V]^{3\alpha}\,Air^{\beta} \quad \text{(F-25)}$$

$$a_{media} = 4.1F \times 10^{-4}\,[Lys]^{-0.04}\ mmol/h/kPa \quad \text{(F-26)}$$

$$\alpha = 8.31 \times 10^{-1}\,[v]^{-0.02} \quad \text{(F-27)}$$

$$\beta = 4.F7 \times 10^{-1}\,[v]^{-0.03} \quad \text{(F-28)}$$

1.9. Chilling Capacity

$$Q_{chilling} = 1.25x10^{-4}\,(OUR \cdot V) \quad \text{(F-29)}$$

1.10. The effect of biomass recycling on the fermentation performance

$$\mu - \mu_{obs} = \max\left(0;\ 0.031\frac{e_{ave}}{X} - 0.025\right) \quad \text{(F-30)}$$

$$q_{Lys} - q_{Lys,obs} = \max\left(0;\ 0.006\frac{e_{ave}}{X} - 0.005\right) \quad \text{(F-31)}$$

$$Y_{\frac{X}{Thr},obs} - Y_{\frac{X}{Thr},0} = \max\left(0;\ 1.752\frac{e_{ave}}{X} - 1.304\right) \quad \text{(F-32)}$$

$$e_{ave} = \frac{e_{reac}\frac{V_{reac}}{Q_L} + e_{mem}\frac{V_{mem}}{Q_L} + e_{valve}\frac{V_{valve}}{Q_L}}{\sum\left(\frac{V_{reac}}{Q_L};\frac{V_{mem}}{Q_L};\frac{V_{valve}}{Q_L}\right)} \quad \text{(F-33)}$$

Modelling of the biomass recycling system

$$e_{react} = f(Re\, v) \quad \text{(F-34)}$$
$$e_{mem} = f(v, \Delta P) \quad \text{(F-35)}$$
$$e_{valve} = f(v, \Delta P) \quad \text{(F-36)}$$

1.11. Analysis of the variables and the parameters in the model

A distinction is made between model parameters and model variables. Parameters refer to values such as physical properties and empirically determined constants. The values are fixed for each model and are not predicted by the model. The value of a parameter must therefore be externally specified.

The variables in the model can be divided into controllable variables, that must be specific externally for a solution of the model to exist and internal variables that are solved for by using an equal number of linearly independent equations.

1.11.1.Variables

1.11.1.1.Controllable variables

All the controllable variables are listed in Table F-1 below.

Table F-1. List of the controllable variables in the empirical biomass recycling system model

Symbol	Unit	Description
t	h	Time
t_{perm}	h	Duration of the filtration process in the cell recycling
t_{clean}	h	Duration of the membrane cleaning process
q_{Thr}	g/g/h	Specific threonine feed rate
q_{Gluc}	g/g/h	Specific glucose feed rate
Rev	s^{-1}	Bioreactor impeller speed
Air	SLPM	Air flow rate to bioreactor
V	m/s	Cross flow velocity through membrane module
ΔP	Pa	Trans-membrane pressure drop

1.11.1.2.Internal variables

The internal variables that are determined from the linearly independent equations are listed in Table F-2

Table F-2. List of the internal variables in the empirical biomass recycling system model

No	Symbol	Unit	Description
1	V	litre	Broth volume
2	F_{Gluc}	l/h	Glucose feed rate
3	F_{Thr}	l/h	Threonine feed rate
4	F_{AS}	l/h	AS feed rate
5	Bleed	l/h	Bleed rate
6	Perm'	l/h	Permeate flow rate
7	X	g/l	Biomass concentration in the bioreactor
8	Thr	g/l	Threonine concentration in the bioreactor
9	Gluc	g/l	Glucose concentration in the bioreactor
10	Lys	g/l	Lysine concentration in the bioreactor
11	q_{o2}	mmol/g/h	Specific oxygen uptake rate
12	μ_{obs}	h^{-1}	Observed specific growth rate
13	$q_{Lys,obs}$	g/g/h	Observed specific lysine productivity
14	$Y_{X/Thr,obs}$	g/g	Observed yield of biomass on threonine
15	μ	h^{-1}	Specific growth rate for unstressed conditions
16	q_{Lys}	g/g/h	Specific lysine productivity for unstressed conditions
17	J_{ss}	m/s	Pseudo steady state flux
18	J_o	m/s	Clean membrane flux
19	J_l	m/s	Permeate flux after cleaning
20	R_t	m^{-1}	Total hydraulic resistance to permeate flow
21	R_p	m^{-1}	Pore plugging resistance
22	R_c	m^{-1}	Cake resistance
23	$k_{decline}$	h^{-1}	Flux decline constant
24	J_1'/J_2'	-	Ratio of clean membrane and fouled membrane modified fluxes
25	q_{pore}	μm	Pore size distribution
26	OUR	mmol/l/h	Oxygen uptake rate
27	k'_la	mmol/h/kPa	Volumeteric mass transfer coefficient
28	α	-	Variable in mass transfer equation
29	β	-	Variable in mass transfer equation
30	a_{media}	-	Variable in mass transfer equation
31	$Q_{chilling}$	W	Heat to be removed from bioreactor
32	e_{ave}	m^2/s^3	Average energy dissipated in the bioreactor system including the recycle loop
33	e_{react}	m^2/s^3	Average energy dissipated in the bioreactor
34	e_{mem}	m^2/s^3	Average energy dissipated in the membrane unit
35	e_{valve}	m^2/s^3	Average energy dissipated in the valve controlling the trans-membrane pressure drop
36	DO	%	Percentage of the saturation dissolved oxygen concentration

1.12. Parameters

The model parameters are divided into physical properties and empirical constants.

1.12.1.Physical properties

The physical properties are summarised in Table F-3.

Table F-3. List of the physical properties in the empirical biomass recycling system model

Symbol	Unit	Description	Value
C_{Thr}	g/l	Threonine concentration in the threonine feed stream	0.73
C_{Gluc}	g/l	Glucose concentration in the glucose feed stream	600
C_{AS}	g/l	Ammonium sulphate concentration in the AS feed stream	400
V_{max}	litre	Maximum bioreactor volume	10
A	m^2	Membrane area	0.00952
R_m	m^{-1}	Intrinsic membrane resistance	9.20×10^{10}
r_p*	µm	Mean membrane pore size	0.22
$r_{p,STDEV}$	µm	Standard deviations in the membrane pore size	0.14
υ	Pas	Permeate viscosity	5×10^{-3}
μ_{max}	h^{-1}	Maximum specific growth rate	0.52
LMOPP	KPa	Log mean oxygen partial pressure	21.27
$LMOPP_o$	kPa	Log mean oxygen partial pressure when the DO probe is calibrated	21.27

1.12.2.Empirical constants

The empirical constants that was determined from experimental data are presented in Table F-4

Table F-4. List of the empirical constants in the biomass recycling system model

Symbol	Unit	Description	Value
$Y_{x/Thr}$	g/g	Yield of biomass on threonine for unstressed conditions	28
S1 and S2	g/g	Stoichiometric constant in AS feed rate	0.1 and 0.01
k_{clean}	h^{-1}	Membrane cleaning constant	0.30
km_1	g/l	Saturation constant for cell growth under threonine limited conditions	0.098
c_1 to c_3		Constants in the specific lysine productivity equation	
k_{sp}		Saturation constant for the specific lysine productivity under sugar limited conditions	
m_0 to m_3		Empirical constants used to estimate $k_{decline}$ as a function of J_o, v and X	
k_{thick}		Thickness of fouling layer inside a membrane pore	
k_t		Constant in cake resistance estimation	
p_1		Constant in cake resistance estimation	
n_c		Fouling cake layer compressibility	

2. Bioreaction network based model of the Lysine Fermentation with Biomass Recycling

The major difference in the metabolic network model is in the modelling of the cellular metabolism. Equation F-1 to F-7; F-9 to F-20, F-22, F-24 to F-30 and F-32 to F-36 remains exactly the same as for the empirical model.

2.1. Modelling of the cellular metabolism

2.1.1. Modelling of the distribution of the central carbon flux

$$\mathbf{A}\cdot\mathbf{x}(t) = \mathbf{r}(t) \qquad \text{(F-37)}$$

where **A** is an 37 by 34 matrix of stoichiometric coefficients as specified in Appendix E, **x** is a 34-dimensional flux vector and **r** is a 37-dimensional metabolite accumulation rate

vector. Eight external metabolites have been identified; glucose, biomass, ammonia, trehalose, oxygen, valine, carbon dioxide and lysine.

This system constitutes 71 (34+37) unknowns and 37 equations. Of the 37 metabolites, 29 have a zero accumulation rate, and can be subtracted from the unknowns. Thus this set of equations have five degrees of freedom or variables that must be specified externally.

Once of these degrees of freedom is taken up by the external specification of the specific glucose feed rate. The other four are taken up by the next set of equations,

$$\mu = \mu_{max}\left[\frac{Thr}{km_1 + Thr}\right] \tag{F-20}$$

$$\frac{PEP \xrightarrow{rxn_9} OaA}{G3P \xrightarrow{rxn_6} PEP} = 0.25 \tag{F-38}$$

$$\frac{OaA \xrightarrow{rxn_{30}} Asp}{PEP \xrightarrow{rxn_9} OaA} = -0.77\mu + 0.90 \tag{F-39}$$

$$\frac{OaA \xrightarrow{rxn_{30}} Asp}{Mal \xrightarrow{rxn_{16}} OaA + PEP \xrightarrow{rxn_9} OaA} = 0.36 \tag{F-40}$$

Thus the bioreactor network model receives as input the specific glucose feed rate as well as the specific growth rate from Eq. F-20. Then by using equations (F-21 to F-23) it calculates the specific lysine productivity q_{Lys}, the specific oxygen uptake rate q_{o2} and the specific ammonium consumption q_{NH4} rate.

The ammonium sulphate feed rate is then given by

$$F_{AS} = \frac{q_{NH4} V X}{C_{AS}} \tag{F-41}$$

2.2. The effect of biomass recycling on the fermentation performance

$$\text{Cell wall} = -rxn_{38} \tag{F-42}$$

$$\frac{Asp \xrightarrow{rxn_{38}} \text{Cell wall}}{OaA \xrightarrow{rxn_{30}} Asp} = \max(0; \frac{e_{ave}}{X} - 0.031) \tag{F-43}$$

2.3. Analysis of the variables and the parameters in the model

The physical properties for the bioreaction network model are the same as that for the empirical model. The following empirical constants do not form part of the bioreaction network problem: S_1 and S_2, c_1 to c_3 and k_{sp}. All the other parameters are similar to those listed in Table F-4.

The controllable variables correspond to that of the empirical model discussed in Section F-1 and listed in Table F-2.

The internal variables for the bioreaction network model is summarised in Table F-5

Table F-5 Internal variable analysis of the bioreaction network based model

Internal Variables from the empirical model (Excl q_{Lys} which becomes redundant)	35
Variables in the bioreaction network (34 reactions and 37 component accumulation rates)	71
Duplicate variables in empirical model and bioreaction network ($q_{Lys,obs}$, q_{O2}, μ_{obs},)	3
Controllable variable in bioreaction network (q_{gluc})	1
Zero accumulation rates	29
Variables from impact of shear on BRN (rxn_{38} and Cell wall accumulation rate)	2
Total number of internal variables	**75**

Extra equations from bioreaction network	37
Equations from empirical model	32
Extra equations used in bioreaction network model:	6
Total number of equations	**75**

The number of internal variables (75) equals the number of equations (75) which implies that this model has a single solution for each set of controllable variables.

Summary of all experimental fermentation work conducted in this study

Experimental Designation		Controllable variables													
	Configuration	$Gluc_o$ [g/l]	Thr_o [mg/l]	V_o [litre]	D [1/h]	C_{Gluc} [g/l]	q_{Gluc} [g/g/h]	q_{Thr} [g/g/h]	A [cm2]	ΔP [kPa]	v [m/s]	Power [W]	T_{start} [h]	CF [h-1]	Time [h]
Batch 1	Batch	20	230	5	-	-	-	-	-	-	-	30	-		60
Batch 3	Batch	100	750	5	-	-	-	-	-	-	-	30	-		60
Fil1	Batch	20	230	5	-	-	-	-	-	100	2	30	-		60
Fil2	Batch	20	230	5	-	-	-	-	-	100	2	30	-		60
Fil3	Batch	100	750	5	-	-	-	-	-	100	2	30	-		60
Con1	Continuous	100	750	5	0.01	100	-	-	-	-	-	30	-		200
Con2	Continuous	100	750	5	0.05	20	-	-	-	-	-	30	-		200
Con3	Continuous	100	750	5	0.05	40	-	-	-	-	-	30	-		200
Con4	Continuous	100	750	5	0.05	100	-	-	-	-	-	30	-		200
Con5	Continuous	100	750	5	0.1	20	-	-	-	-	-	30	-		200
Con6	Continuous	100	750	5	0.1	40	-	-	-	-	-	30	-		200
Con7	Continuous	100	750	5	0.1	100	-	-	-	-	-	30	-		200
Con8	Continuous	100	750	5	0.2	20	-	-	-	-	-	30	-		200
Con9	Continuous	100	750	5	0.2	40	-	-	-	-	-	30	-		200
Con10	Continuous	100	750	5	0.2	100	-	-	-	-	-	30	-		200
Con11	Continuous	100	750	5	0.3	20	-	-	-	-	-	30	-		200
Con12	Continuous	100	750	5	0.3	40	-	-	-	-	-	30	-		200
Con13	Continuous	100	750	5	0.3	100	-	-	-	-	-	30	-		200
Con14	Continuous	100	750	5	0.35	100	-	-	-	-	-	30	-		200
CR1	Continuous	20	230	5	0.1	100			95.2	100	2	30	20		200
CR2	Continuous	20	230	5	0.1	100			95.2	150	2	30	20		200
CR3	Continuous	20	230	5	0.1	100			95.2	200	2	30	20		200
CR4	Continuous	20	230	5	0.1	100			95.2	100	1	30	20		200
CR5	Continuous	20	230	5	0.1	100			95.2	100	3	30	20		200
CR6	Continuous	20	230	5	0.1	100			95.2	100	5	30	20		200
CR7	Continuous	100	750	5	0.1	100			95.2	100	2	30	20		200
CR8	Continuous	100	750	5	0.1	100			95.2	150	2	30	20		200
CR9	Continuous	100	750	5	0.1	100			95.2	200	2	30	20		200

Summary of fermentation experiments

Experimental Designation		Controllable variables													
	Configuration	$Gluc_o$	Thr_o	V_o	D	C_{Gluc}	q_{Gluc}	q_{Thr}	A	ΔP	v	Power	T_{start}	CF	Time
		[g/l]	[mg/l]	[litre]	[1/h]	[g/l]	[g/g/h]	[g/g/h]	[cm2]	[kPa]	[m/s]	[W]	[h]	[h-1]	[h]
CR10	Continuous	100	750	5	0.1	100			95.2	100	1	30	20		200
CR11	Continuous	100	750	5	0.1	100			95.2	100	3	30	20		200
CR12	Continuous	100	750	5	0.1	100			95.2	100	5	30	20		200
FB1	Fed-batch	100	1.7	5			0.4	0	-	-	-	30	20		200
FB2	Fed-batch	50	1.7	5			0.4	0	-	-	-	30	20		200
FB3	Fed-batch	30	1.7	5			0.4	0	-	-	-	30	20		200
FB4	Fed-batch	10	1.7	5			0.4	0	-	-	-	30	20		200
FB5	Fed-batch	30	1.7	5			0.2	0	-	-	-	30	20		200
FB6	Fed-batch	30	1.7	5			0.3	0	-	-	-	30	20		200
FB7	Fed-batch	30	1.7	5			0.4	0	-	-	-	30	20		200
FB8	Fed-batch	30	1.7	5			0.4	0.002	-	-	-	30	20		200
FB9	Fed-batch	30	1.7	5			0.4	0.005	-	-	-	30	20		200
FB10	Fed-batch	30	1.7	5			0.4	0.01	-	-	-	30	20		200
FB11	Fed-batch	30	1.7	5			0.4	0	-	-	-	50	20		200
FB12	Fed-batch with biomass recycle	30	1.7	5			0.4	0	95.2	100	2	30	20		200
FB13	Fed-batch with biomass recycle	30	1.7	5			0.4	0	190.4	100	2	30	20		200
FB14	Fed-batch with biomass recycle	30	1.7	5			0.4	0	258.6	100	2	30	20		200
FB15	Fed-batch with biomass recycle	30	1.7	5			0.4	0	95.2	50	2	30	20		200
FB16	Fed-batch with biomass recycle	30	1.7	5			0.4	0	95.2	100	2	30	20		200
FB17	Fed-batch with biomass recycle	30	1.7	5			0.4	0	95.2	150	2	30	20		200
FB18	Fed-batch with biomass recycle	30	1.7	5			0.4	0	95.2	200	2	30	20		200
FB19	Fed-batch with biomass recycle	30	1.7	5			0.4	0	95.2	100	1	30	20		200
FB20	Fed-batch with biomass recycle	30	1.7	5			0.4	0	95.2	100	2	30	20		200
FB21	Fed-batch with biomass recycle	30	1.7	5			0.4	0	95.2	100	4	30	20		200

Summary of fermentation experiments

Experimental Designation		Controllable variables													
	Configuration	$Gluc_o$	Thr_o	V_o	D	C_{Gluc}	q_{Gluc}	q_{Thr}	A	ΔP	v	Power	T_{start}	CF	Time
		[g/l]	[mg/l]	[litre]	[1/h]	[g/l]	[g/g/h]	[g/g/h]	[cm2]	[kPa]	[m/s]	[W]	[h]	[h-1]	[h]
FB22	Fed-batch with biomass recycle	30	1.7	5			0.4	0	95.2	100	2	30	5		200
FB23	Fed-batch with biomass recycle	30	1.7	5			0.4	0	95.2	100	2	30	20		200
FB24	Fed-batch with biomass recycle	30	1.7	5			0.4	0	95.2	100	2	30	60		200
FB25	Fed-batch with biomass recycle	30	1.7	5			0.4	0	95.2	100	2	30	20	20	200
Optimal1	Fed-batch with biomass recycle	10	2	5			0.32	0	190.4	160	1	30	16	20.9	300
Optimal2	Fed-batch with biomass recycle	10	2	5			0.32	0	190.4	160	1	30	16	20.9	300
Optimal3	Fed-batch with biomass recycle	10	2	5			0.32	0	190.4	160	1	30	16	90.9	300

Summary of fermentation experiments